PolyPublie
Polytechnique Montréal

POLYTECHNIQUE MONTRÉAL
UNIVERSITÉ D'INGÉNIERIE

Titre: Title:	Innovative Numerical Modeling and Experimental Simulation of the Seismic Response of Structure-Water Systems and their Appurtenant Structures
Auteur: Author:	Ramtin Kouhdasti
Date:	2024
Type:	Mémoire ou thèse / Dissertation or Thesis
Référence: Citation:	Kouhdasti, R. (2024). Innovative Numerical Modeling and Experimental Simulation of the Seismic Response of Structure-Water Systems and their Appurtenant Structures [Thèse de doctorat, Polytechnique Montréal]. PolyPublie. https://publications.polymtl.ca/62515/

Document en libre accès dans PolyPublie
Open Access document in PolyPublie

URL de PolyPublie: PolyPublie URL:	https://publications.polymtl.ca/62515/
Directeurs de recherche: Advisors:	Najib Bouaanani
Programme: Program:	Génie civil

Ce fichier a été téléchargé à partir de PolyPublie, le dépôt institutionnel de Polytechnique Montréal
This file has been downloaded from PolyPublie, the institutional repository of Polytechnique Montréal

https://publications.polymtl.ca

POLYTECHNIQUE MONTRÉAL
affiliée à l'Université de Montréal

Innovative numerical modeling and experimental simulation of the seismic response of structure-water systems and their appurtenant structures

RAMTIN KOUHDASTI
Département de génies civil, géologique et des mines

Thèse présentée en vue de l'obtention du diplôme de *Philosophiæ Doctor*
Génie civil

December 2024

© Ramtin Kouhdasti, 2024.

POLYTECHNIQUE MONTRÉAL
affiliée à l'Université de Montréal

Cette thèse intitulée :

Innovative numerical modeling and experimental simulation of the seismic response of structure-water systems and their appurtenant structures

présentée par **Ramtin KOUHDASTI**
en vue de l'obtention du diplôme de *Philosophiæ Doctor*
a été dûment acceptée par le jury d'examen constitué de :

Mahdi BEN FTIMA, président
Najib BOUAANANI, membre et directeur de recherche
Pierre LÉGER, membre
M. Amin HARIRI-ARDEBILI, membre externe

DEDICATION

To my wife, my parents, and my sister,
for their unwavering support, love,
and encouragement throughout
this journey!

ACKNOWLEDGEMENTS

First and foremost, I would like to express my deepest gratitude to my supervisor, professor Najib Bouaanani, for his invaluable guidance, unwavering support, and constant encouragement throughout this research. His expertise and insight have been essential in shaping this thesis, and I am forever grateful for his mentorship. To show my sincere appreciation, I would like to share this Persian poem with him:

گرچه ای استاد به پای تو نمی رسم،
هر چه از تو آموختم، جهان گشود در برم

This journey would not have been the same without the help and collaboration of the incredible team members I had the privilege of working with. From Ph.D. students to interns, each one played a vital role in the success of this research. I would like to extend my special thanks to Mr. Ehsan Rowzeh for his hard work and expertise, especially during the experimental phase. His dedication provided peace of mind throughout the testing process, ensuring everything ran smoothly, even during the more challenging moments.

I am deeply appreciative of the technicians and researchers at the structural laboratory and the staff of Groupe de Recherche en génie des Structures (GRS). Their professionalism, patience, and readiness to assist during every meeting and lab test ensured that each phase of the experimental work could be completed successfully. I would especially like to acknowledge Mr. Martin Leclerc, whose expertise gained over many years was an invaluable asset during the shaking table experiments. His extensive experience and tireless efforts in meticulously preparing all the equipment, particularly the shaking table, played a pivotal role in overcoming the challenges we faced.

I sincerely thank my evaluation committee members, Professors Pierre Léger, Mahdi Ben Ftima, and Dr. M. Amin Hariri-Ardebili, for accepting to read and evaluate this thesis. I deeply appreciate their time, dedication, and willingness to provide valuable insights.

I would like to extend my gratitude to the Natural Sciences and Engineering Research Council of Canada (NSERC), the Quebec Fund for Research on Nature and Technology (FRQNT) and

Translation of the poem: Though I may never reach your stature, dear professor, everything I have learned from you has broadened my world.

the Canada Research Chairs for their generous financial support, which made this research possible.

I would also like to express my deepest gratitude to my wife, Razieh Anari, whose unwavering support, patience, and encouragement have been the greatest source of strength throughout this research. Special thanks are extended to my parents, Mehdi and Mehri, and my sister, Maryam, for their constant love, belief, and encouragement, which have provided the foundation for all achievements. Their presence has been invaluable, and this accomplishment would not have been possible without their unwavering support.

Ramtin Kouhdasti

Montréal, QC, Canada

September 2024

RÉSUMÉ

Les systèmes structure-eau, tels que les barrages, les éoliennes en mer et leurs structures annexes, jouent un rôle clé à la fois économiquement et socialement dans les sociétés modernes. Alors que le monde se tourne vers les énergies propres en réponse au changement climatique, l'importance de ces systèmes se trouve amplifiée. Assurer leur sécurité et leur fiabilité, notamment dans les régions à forte activité sismique, est essentiel. Ces dernières années, de nombreux barrages et leurs structures annexes ont subi des dommages variés en raison des charges sismiques. Une analyse dynamique précise des systèmes eau-structure est donc cruciale pour concevoir de nouvelles structures et évaluer la performance sismique des structures existantes. Ces analyses se répartissent en deux catégories : les analyses robustes et les méthodes simplifiées. Les analyses robustes, les plus précises, utilisent des formulations analytiques avancées ou des méthodes couplées par éléments finis, mais nécessitent des logiciels spécialisés et un haut niveau d'expertise pour modéliser précisément les interactions fluide-structure. Les ingénieurs praticiens trouvent souvent ces méthodes complexes en raison de la difficulté des modèles par éléments finis. En revanche, les méthodes simplifiées reposent sur des hypothèses qui simplifient le processus d'analyse. Le concept de masse ajoutée, une méthode simplifiée couramment utilisée, suppose que la structure est rigide lors du calcul des forces hydrodynamiques. Bien que cette approche présente des limites et ne fournisse pas toujours des résultats précis, elle reste largement utilisée en ingénierie en raison de sa simplicité. Une autre méthode courante est l'analyse spectrale, qui prend en compte principalement le mode fondamental du système tout en incluant les effets des modes supérieurs par une correction statique. Cependant, pour les systèmes flexibles, négliger les contributions dynamiques des modes supérieurs peut entraîner des erreurs significatives. Il existe donc un besoin pour une méthode simplifiée mais efficace permettant de modéliser les interactions dynamiques structure-eau, tout en étant facile à mettre en œuvre et permettant des analyses sismiques complexes sans compromettre la précision des paramètres critiques.

L'évaluation expérimentale des systèmes structure-eau, via des essais sur table vibrante, offre une alternative interessante pour étudier leur réponse sismique. Ces essais sont particulièrement utiles pour valider des modèles numériques complexes nécessitant des vérifications expérimentales supplémentaires. Cependant, ils présentent des défis importants lorsqu'il s'agit d'intégrer les effets hydrodynamiques. Les essais sur table vibrante dans ce cas sont souvent limités à l'utilisation de tables immergées ou de méthodes simplifiées, comme la distribution de masses ajoutées le long de la hauteur de la structure, ou encore à l'emploi d'une longueur de réservoir réduite. Dans certains cas, les forces hydrodynamiques sont exclues pour des

raisons de sécurité ou de coûts élevés. Par conséquent, une approche expérimentale intégrant de manière sûre les effets hydrodynamiques est nécessaire.

Cette thèse de doctorat comble ces lacunes en proposant des solutions innovantes dans la modélisation numérique et les essais expérimentaux. La recherche débute par le deéveloppement d'une méthode numérique pour l'analyse par superposition modale en régime transitoire et l'analyse spectrale de réponse des systèmes barrage-réservoir. Cette méthode transfère les effets induits par les séismes dans des accélérations modifiées du sol et des spectres de réponse. Contrairement à l'analyse spectral traditionnelle, cette approche intègre directement les effets des modes supérieurs dans l'analyse, sans recourir à une correction statique. La réponse sismique totale peut ensuite être obtenue par des règles de combinaison telles que la racine carrée de la somme des carrés (SRSS) ou la combinaison quadratique complète (CQC).

Suite au développement de cette méthode numérique, la recherche a étendu l'approche d'accélération du sol modifiée à d'autres systèmes eau-structure, offrant une alternative pour les tests expérimentaux. Une analyse approfondie a montré qu'en raison de limitations opérationnelles, un prototype de barrage à l'échelle n'était pas optimal pour des essais sur table vibrante. Il était donc nécessaire d'identifier un système alternatif pouvant être testé selon les contraintes de la table vibrante.

Enfin, cette recherche a permis le développement d'une méthodologie novatrice pour réaliser des essais sur table vibrante intégrant les effets hydrodynamiques par des accélérations modifiées. Cette technique élimine la nécessité de la présence "réelle" d'eau dans le montage expérimental, répondant ainsi aux défis importants associés aux tables immergées. De plus, elle offre une alternative pour intégrer les effets de masse ajoutée hydrodynamique directement dans les accélérations modifiées, évitant ainsi la distribution de masse le long de la hauteur de la structure, un processus souvent difficile à contrôler.

ABSTRACT

Structure-water systems, such as dams, offshore wind turbines, and their appurtenant structures, play an important role both economically and socially in modern societies. As the world shifts towards clean energy in response to climate change, the importance of these systems is further magnified. Ensuring their safety and reliability, particularly in seismically active regions, is essential. In recent years, numerous dams and their appurtenant structures have experienced different levels of damage due to earthquake loads. Consequently, accurate dynamic analysis of structure-water systems is vital for designing new structures and assessing the seismic performance of existing ones. These analyses can be categorized into two main types: advanced and simplified methods. Advanced methods are generally more comprehensive, using advanced analytical formulations or coupled finite element methods, but they require specialized software and a high level of expertise to model fluid-structure interactions accurately. Practicing engineers often find these methods difficult to implement due to the complexity of finite element models and analytical formulations. On the other hand, simplified methods rely on assumptions to ease the analysis process. The added mass concept is a widely used simplified approach that assumes the structure is rigid for hydrodynamic force calculations. Although this method has limitations and may not always provide highly accurate results, it remains a common practice in everyday engineering due to its simplicity and ease of application. Another commonly used method for analyzing structure-water systems in day-to-day engineering practice is the Response Spectrum Analysis (RSA) method. This approach primarily considers the fundamental mode of the structure-water system while incorporating the effects of higher modes through a static correction technique. However, for flexible systems, neglecting the dynamic contributions of higher modes can result in significant inaccuracies in the analysis. Therefore, there is still a demand for a simplified yet effective method that models dynamic structure-water interactions while maintaining ease of implementation, enabling complex seismic analyses to be performed more efficiently without compromising the accuracy of critical response parameters.

Experimental seismic evaluation of structure-water systems provides a valuable alternative approach for studying the seismic response of these systems. Experimental methods, such as shaking table tests, are particularly valuable for validating complex numerical models, especially when robust analytical or finite element methods require additional experimental verification. However, available shaking table tests face challenges when incorporating hydrodynamic effects into the experimental setup. Shaking table tests of structure-water systems are typically limited to the use of underwater shaking tables or simplified methods, such as

distributing added masses along the structure's height or employing a limited reservoir length to approximate hydrodynamic effects. In some cases, experiments have completely excluded hydrodynamic forces due to safety concerns and the high costs associated with specialized facilities. Consequently, there is a clear need for an experimental approach that can safely and effectively integrate hydrodynamic effects into the seismic testing of structure-water systems and their appurtenant structures.

This Ph.D. thesis addresses these gaps by proposing innovative solutions in both numerical modeling and experimental testing of structure-water systems. The research first proposes a numerical procedure for time-history modal superposition and response spectrum analyses of gravity dam-reservoir systems. This method effectively transfers earthquake-induced reservoir effects into modified ground motion accelerations and response spectra. Unlike the traditional RSA method, this approach directly includes higher mode effects into the response spectrum analysis of dam-reservoir systems, in lieu of using the static correction method. The total seismic response, including higher modes, can then be obtained using combination rules such as the Square Root of the Sum of the Squares (SRSS) or the Complete Quadratic Combination (CQC) method.

Following the development of the numerical procedure for gravity dam-reservoir systems, the research extended the modified ground acceleration approach to other structure-water systems. This extension provides an alternative structure-water system for experimental testing.

The final part of this research focused on developing a novel methodology for conducting shaking table tests of water structure system and its appurtenant structures, incorporating hydrodynamic effects through modified ground accelerations. This innovative approach eliminates the need for the presence of water in the experimental setup, addressing the significant challenges associated with underwater shaking tables. Additionally, the method provides an alternative way of incorporating hydrodynamic added mass effects directly into the modified ground motion acceleration, eliminating the need to distribute the mass along the structure's height, a process that can be both difficult to implement and challenging to control during shaking table tests.

TABLE OF CONTENTS

DEDICATION iii

ACKNOWLEDGEMENTS iv

RÉSUMÉ vi

ABSTRACT viii

TABLE OF CONTENTS x

LIST OF TABLES xiv

LIST OF FIGURES xv

LIST OF SYMBOLS AND ACRONYMS xxx

CHAPTER 1 INTRODUCTION 1
1.1 Background 1
1.2 Problem Statement 3
1.3 Objectives and scope 5
1.4 Methodology 6
1.4.1 Time-History modal superposition and response spectrum analysis including higher modes effects 7
1.4.2 Extension of modified ground acceleration method to other type of structures 7
1.4.3 Simplified alternative implementing added masses to representing hydrodynamic effect 8
1.4.4 Development of innovative shaking table test of structure-water supported appurtenant structures 8
1.4.5 Implementation of the proposed method and validation using any standard engineering software 9
1.5 Main contributions and their originality 9
1.6 Organization of this thesis 10

CHAPTER 2 LITERATURE REVIEW 12
2.1 Introduction 12

2.2 Seismic analysis of dam-reservoir systems 13
2.2.1 Analytical methods 13
2.2.2 Finite Element Methods 19
2.2.3 Simplified Methods 25
2.3 Seismic analysis of axisymmetric structures surrounded by water 35
2.3.1 Analytical methods 35
2.3.2 Numerical methods 39
2.3.3 Simplfiied method 41
2.4 Shaking table test of structure-water system and its appurtenant structure . 46
2.4.1 Underwater shaking table tests 46
2.4.2 Experimental tests using simplified hydrodynamic representation . . . 55
2.4.3 Experimental tests neglecting hydrodynamic effects 65

CHAPTER 3 ARTICLE 1: RESPONSE SPECTRUM AND MODAL DYNAMIC ANALYSES OF GRAVITY DAMS USING GROUND MOTION ACCELERATIONS MODIFIED TO ACCOUNT FOR HYDRODYNAMIC EFFECTS 68
3.1 Abstract 68
3.2 Introduction 73
3.3 Theoretical background and proposed methods 75
3.3.1 Basic assumptions 75
3.3.2 Equations of motion 75
3.3.3 Fundamental mode analysis 75
3.3.4 Effects of higher modes 81
3.3.5 Summary of proposed procedures 85
3.4 Numerical examples, results and discussion 86
3.4.1 Case studies 86
3.4.2 Modified ground motion accelerations, response spectra and seismic demands 90
3.4.3 Seismic response of the dams 99
3.5 Conclusions 108

CHAPTER 4 ARTICLE 2: AN EFFICIENT PROCEDURE FOR MODAL SEISMIC RESPONSE ANALYSIS OF AXISYMMETRIC STRUCTURES SURROUNDED BY WATER 117
4.1 Abstract 117
4.2 Introduction 117
4.3 Theoretical background and proposed methods 119

4.3.1 Basic assumption and governing equations 119
4.3.2 Proposed formulations 122
4.4 Numerical examples, results and discussion 127
4.4.1 Case studies 127
4.4.2 Original and modified ground motions used 130
4.4.3 Seismic response of the water-surrounded axisymmetric structures . . 138
4.5 Conclusions 143

CHAPTER 5 INNOVATIVE SHAKING TABLE TEST FOR EVALUATING THE SEISMIC RESPONSE OF STRUCTURE-WATER SYSTEMS AND THEIR APPURTENANT STRUCTURES USING MODIFIED GROUND MOTION ACCELERATION 149
5.1 Introduction 149
5.2 Shaking table test 151
5.2.1 Single-axis shaking table facility at Polytechnique Montréal 151
5.2.2 Primary structure and appurtenant secondary structure 153
5.2.3 Instrumentation and data acquisition 154
5.2.4 Determination of the dynamic properties of the tested structure . . . 156
5.3 Finite Element Models 160
5.4 Shaking table test of structure-water system 164
5.4.1 Original and modified ground motions 170
5.5 Experimental and numerical results 171
5.6 Summary and Conclusions 181

CHAPTER 6 DISCUSSION 187
6.1 Objectives of the discussion 187
6.2 Numerical validation of proposed method 187
6.2.1 Frequency effects on the modified ground acceleration 187
6.2.2 Dam-reservoir case study: Pine Flat dam 200
6.2.3 Structure surrounded by water case study: San Bernardino intake tower 206
6.3 Application of the proposed method using general purpose structural analysis software 213
6.3.1 Dam-reservoir system 214
6.3.2 Axisymmetric structures surrounded by water 223
6.4 Experimental consideration for shaking table test of water structure system . 227
6.4.1 Shaking table test of axisymmetric structure surrounded by water . . 227

6.4.2 Experimental considerations for applying the proposed method for low-damping systems 236
6.5 Conclusion of discussion 240

CHAPTER 7 CONCLUSION AND RECOMMENDATIONS 242
7.1 Conclusions 242
7.1.1 Development of a numerical method for time-history modal superposition and response spectrum analyses of gravity dam-reservoir systems 243
7.1.2 Extension of the modified ground acceleration method to other types of structure-water systems 244
7.1.3 Development of an innovative shaking table test of structure-water systems and their appurtenant structures using modified ground acceleration 245
7.1.4 General conclusions 246
7.2 Recommendations 247
7.2.1 Numerical modeling 247
7.2.2 Experimental tests 248

REFERENCES 249

LIST OF TABLES

Table 2.1	Operating parameters of the underwater shaking table of Hohai University [1]	52
Table 3.1	Hydrodynamic modification factors obtained for the first five vibration modes of dams D35 and D90 subjected to the ground motion accelerations considered.	116
Table 4.1	Constitutive materials of the axisymmetric structures (Fig. 4.2)	128
Table 4.2	Hydrodynamic modification factors obtained for the six vibration modes of towers Cases nos. 1, 2, and 3 subjected to the ground motion accelerations considered.	131
Table 5.1	Material properties of the tower and the apartment structure	158
Table 6.1	Harmonic ground motion excitation with forcing frequencies as a function of the fundamental natural frequency of dams D35 or D90	197
Table 6.2	Material properties used for the Pine Flat dam model	200
Table 6.3	First six natural frequencies of the axisymmetric structure using different section materials (steel vs. aluminum) and geometries (hollow vs solid)	228
Table 6.4	First six natural frequencies of the aluminum material axisymmetric structure using different sections available in the market	234

LIST OF FIGURES

Figure 2.1 Gravity dam-reservoir-foundation system. 15

Figure 2.2 Dam-reservoir system and boundary conditions used for pressures: (a) p_0; (b) p_j. 18

Figure 2.3 Finite element models of the dam-reservoir systems and corresponding boundary conditions [2]. 20

Figure 2.4 Dam retaining a truncated-length reservoir. 23

Figure 2.5 Representation of hydrodynamic effects using simplified Westergaard's added mass: (a) hydrodynamic pressure or added mass per unit height of the dam; (b) distribution of concentrated masses at the nodes of the dam-reservoir interface. 26

Figure 2.6 Approximation of the fundamental mode shape of a gravity dam [3]. . 30

Figure 2.7 Gravity dam subjected to: (a) original ground acceleration which is applied to the dam-reservoir system; (b) modified ground acceleration which is applied to the dry dam [4]. 31

Figure 2.8 Boundary conditions for evaluating hydrodynamic pressure FRF p_0 at *rigid* structure-water interface due to horizontal ground motion $\ddot{x}_{\mathrm{g}}$. . 37

Figure 2.9 Boundary conditions for evaluating hydrodynamic pressure FRF p_j at *flexible* structure-water interface due to horizontal acceleration $\psi_j^{(x)}(R_{\mathrm{s}}, 0, z)$, $j = 1 \ldots N_{\mathrm{s}}$. 38

Figure 2.10 Finite element models of 3D coupled axisymmetric structures surrounded by water with required boundary conditions. 40

Figure 2.11 Representation of hydrodynamic effects using simplified added mass. 42

Figure 2.12 Representation of hydrodynamic effects using Morsion's added mass. 43

Figure 2.13 Comparison of the distribution of added mass (adapted from [5]). . . 44

Figure 2.14 Approximation of parameters $\mathcal{D}_n(\kappa_n R_{\mathrm{s}})$, $\mathcal{E}_n(\kappa'_n R_{\mathrm{s}})$, and $\tau_n R_{\mathrm{s}}$ (adapted from [6]). 45

Figure 2.15 Underwater shaking tables in the world [7]: (a) Port and Airport Research Institute (PARI) in Japan; (b) Dalian University of Technology in China; (c) Large Hydro-Geo Flume (LHGF) in PARI, Japan; (d) Hohai University in China; (e) underwater shaking table array system at Tianjin University in China; (f) National Facility for Earthquake Engineering Simulation in China. 47

Figure 2.16 Overviews of test setup: (a) dry condition; (b) with water at a depth of 0.65 m [8]. 48
Figure 2.17 Overviews of test setup using water tank on shaking table facility at SERVOTEST Testing Systems Ltd in Beijing [9]: (a) overview of water tank and shaking table; (b) and (c) overview of specimens and instrumentation. 49
Figure 2.18 Overview of the test setup using the underwater shaking table facility at Tianjin University [9]: (a) shake table in dry condition; (b) shake table in wet condition with the specimen installed; (c) 351 mm diameter specimen mounted on the shaking table in wet condition. 50
Figure 2.19 View of experimental tests [10]: (a) no water, (b) a water depth of 1.6 m, and (c) a water depth of 2.0 m. 51
Figure 2.20 View of the specimen and instrumentation [1]. 53
Figure 2.21 View of underwater shaking table test [1]. 53
Figure 2.22 Segmented arch model on shaking table [11]. 56
Figure 2.23 Koyna dam model with reservoir tank [11]. 56
Figure 2.24 Experiment set-up showing a 1/115-scaled Pine Flat dam on the shaking table adjacent to the reservoir [12]. 57
Figure 2.25 Experimental simulation of hydrodynamic pressure [13]. 58
Figure 2.26 Experiment setup [13]. 59
Figure 2.27 Experiment setup [14]: (a) and (b): elevation and plan view of the system; (c) experimental setup with instrumentation; (d) crack pattern in dam model. 60
Figure 2.28 The model for the dam-reservoir coupling system [15]: (a) the model cured for 24 h; (b) the model of full reservoir. 61
Figure 2.29 Comparison of the the experimenal results with numerical models (adapted from [15]): (a) the distributions of acceleration amplification factors along the model height; (b) the distributions of hydordynamic pressure along the model height. 61
Figure 2.30 Experimental setup [16]: (a) concrete gravity dam model along with loading arrangements; (b) load pattern applied over the model for the hydrostatic and coupled-dynamic loads. 62
Figure 2.31 Models used in the experimental test and numerical validation of the pseudo-dynamic test [17]: (a) prototype dam; (b) scaled dam model/specimen; (c) and (d) sketch and experimental test setup. 63

Figure 2.32 Dimensions and details of the experimental setup [18]: (a) dimensions of the rigid brick basin and specimen; (b) global view of the specimen and testing setup. 65
Figure 2.33 Experimental set up and residual deformation of the model system at the end of the experiment [19]. 67
Figure 3.1 Geometry of typical dam-reservoir system studied. 76
Figure 3.2 Proposed procedures: (a) Reference method; (b) THMSA of the dam-reservoir system including only the contribution of the vibration mode j; (c) THMSA of SDOF systems; (d) RSA of the dam-reservoir system including higher modes effects. 87
Figure 3.3 Flowchart of the proposed procedures. 88
Figure 3.4 Dimensions and solid finite element meshes of the studied dam-reservoir systems: (a) 35-m height gravity monolith dam (D35), (b) 90-m height gravity dam monolith (D90). 89
Figure 3.5 Five first mode shapes and corresponding vibration periods of the 35 m high gravity dam monolith (D35). 90
Figure 3.6 Five first mode shapes and corresponding vibration periods of the 90 m high gravity dam monolith (D90). 90
Figure 3.7 Time-history accelerations, pseudo-acceleration response spectra and Fourier amplitudes of the ground motions selected for this study: (a) to (c) Imperial Valley (1940) earthquake; (d) to (f) Loma Prieta (1989) earthquake; Parkfield (1966) earthquake; and Nahanni (1985) earthquake. 91
Figure 3.8 Original and modified ground motion accelerations $a_g^{(1)}$ to $a_g^{(5)}$ corresponding to the first five mode shapes of the 35 m high dam (D35) and the ground motions considered: (a) to (d) $a_g^{(1)}$; (e) to (h) $a_g^{(2)}$; (i) to (l) $a_g^{(3)}$; (m) to (p) $a_g^{(4)}$; (q) to (t) $a_g^{(5)}$. 92
Figure 3.9 Original and modified ground motion accelerations $a_g^{(1)}$ to $a_g^{(5)}$ corresponding to the first five mode shapes of the 90 m high dam (D90) and the ground motions considered: (a) to (d) $a_g^{(1)}$; (e) to (h) $a_g^{(2)}$; (i) to (l) $a_g^{(3)}$; (m) to (p) $a_g^{(4)}$; (q) to (t) $a_g^{(5)}$. 93

Figure 3.10 Modified ground motion accelerations $a_g^{(1)}$ to $a_g^{(5)}$ corresponding to the first five mode shapes of the 90 m high dam (D90) subjected to two ground motion accelerations, and obtained for fully reflective reservoir bottom(i.e. $\alpha = 1.00$) and absorptive reservoir bottoms with $\alpha = 0.85$ and $\alpha = 0.65$: (a), (c), (e), (g), and (i) Imperial Valley (1940) earthquake; and (b), (d), (f), (h), and (j) Nahanni (1985) earthquake. . . . 94

Figure 3.11 5%-damped pseudo-acceleration response spectra of the original ground motions and those of the modified ground motions corresponding to each of the first five vibration modes obtained assuming compressible water in the reservoir: (a), (c), (e), (g) dam D35; (b), (d), (f), (h) dam D90. 95

Figure 3.12 5%-damped pseudo-acceleration response spectra of the original ground motions and those of the modified ground motions corresponding to each of the first five vibration modes obtained assuming incompressible water in the reservoir: (a), (c), (e), (g) dam D35; (b), (d), (f), (h) dam D90. 96

Figure 3.13 5%-damped pseudo-acceleration response spectra of the original ground motions and those of the modified ground motions corresponding to each of the first five vibration modes obtained using Westergaard added-masses: (a), (c), (e), (g) dam D35; (b), (d), (f), (h) dam D90. 97

Figure 3.14 Absolute values of maximum relative horizontal displacements along the height of the upstream face of the 35 m high dam (D35) determined for each vibration mode using modified ground motion accelerations $a_g^{(1)}$ to $a_g^{(5)}$ and then combined to obtain total dam response: (a) Imperial Valley (1940) earthquake; (b) Loma Prieta (1989) earthquake; (c) Parkfield (1966) earthquake; and (d) Nahanni (1985) earthquake. 100

Figure 3.15 Absolute values of maximum relative horizontal displacements along the height of the upstream face of the 90 m high dam (D90) impounding a reservoir determined for each vibration mode using modified ground motion accelerations $a_g^{(1)}$ to $a_g^{(5)}$ and then combined to obtain total dam response: (a) Imperial Valley (1940) earthquake; (b) Loma Prieta (1989) earthquake; (c) Parkfield (1966) earthquake; and (d) Nahanni (1985) earthquake. 101

Figure 3.16 Heightwise distribution of the equivalent lateral static forces, including hydrodynamic effects, computed for each of the first vibration modes of dam D35 considering empty reservoir and reservoir modeling assumptions of compressible water, incompressible water and Westergaard added-masses: (a) Imperial Valley (1940) earthquake; (b) Loma Prieta (1989) earthquake; (c) Parkfield (1966) earthquake; and (d) Nahanni (1985) earthquake. 103

Figure 3.17 Heightwise distribution of the equivalent lateral static forces, including hydrodynamic effects, computed for each of the first vibration modes of dam D90 considering empty reservoir and reservoir modeling assumptions of compressible water, incompressible water and Westergaard added-masses: (a) Imperial Valley (1940) earthquake; (b) Loma Prieta (1989) earthquake; (c) Parkfield (1966) earthquake; and (d) Nahanni (1985) earthquake. 104

Figure 3.18 Time-histories of relative horizontal displacements at the crest of the 90 m high dam (D90) with impounded reservoir obtained for each vibration mode using modified ground motion accelerations $a_g^{(1)}$ to $a_g^{(5)}$ and then combined to obtain total dam response. 105

Figure 3.19 Time-histories of the totals of relative horizontal displacements at the crest of the 35 m and 90 m high dams (D35 and D90) with empty reservoir and including compressible water effects: (a) and (b) Imperial Valley (1940) earthquake; (c) and (d) Loma Prieta (1989) earthquake; (e) and (f) Parkfield (1966) earthquake; (g) and (h) Nahanni (1985) earthquake. 106

Figure 3.20 Maximum shear stresses τ_{xy} developing within dam D90 subjected to the four earthquakes considered as obtained using proposed methods A or B for each of the first five vibration modes as well as the total dam response. 107

Figure 3.21 Generation of modified ground motion acceleration $a_g^{(1)}$ for the 90 m high dam (D90) subjected to Imperial Valley (1940) earthquake: (a) Dynamic properties of the dam with an empty reservoir; (b) Initial ground motion acceleration; (c) Interpolated and zero-padded ground motion acceleration; (d) DFFT of the interpolated original ground motion acceleration; (e) Evaluation of $\vartheta_{0,1}(\omega)$; (f) Evaluation of $\vartheta_{1,1}(\omega)$; (g) Evaluation of modified ground motion acceleration $a_g^{(1)}(\omega)$ in the frequency domain; (h) IDFFT of the modified ground motion acceleration $a_g^{(1)}(\omega)$ to obtain its time-domain representation $a_g^{(1)}(t)$. 113

Figure 4.1 Proposed procedures. 124

Figure 4.2 Dimensions, materials and finite element meshes of the studied water-surrounded axisymmetric structures: (a) Case no. 1 - 42-m height tower; (b) Case no. 2 - 56-m height tower; (c) Case no. 3 - 70-m height tower. 125

Figure 4.3 Finite element mode shapes and corresponding vibration periods of the towers, as well as the modal mass participation factors: (a) Case no. 1; (b) Case no. 2; (c) Case no. 3. 127

Figure 4.4 Frequency response functions for horizontal acceleration $\ddot{\widehat{u}}$ and $\ddot{u}$ at point A of the tower-water systems studied: (a) and (b): Tower Case no. 1 assuming water level to be H_w and $0.5H_w$, respectively; (c) and (d): Tower Case no. 2 assuming water level to be H_w and $0.5H_w$, respectively; (e) and (f): Tower Case no. 3 assuming water level to be H_w and $0.5H_w$, respectively; 129

Figure 4.5 Time-history accelerations, pseudo-acceleration response spectra and Fourier amplitudes of the ground motions selected for this study: (a) to (c) Imperial Valley (1940) earthquake; (d) to (f) Loma Prieta (1989) earthquake. 130

Figure 4.6 Original and modified ground accelerations $a_g^{(1)}$ to $a_g^{(6)}$ corresponding to the six mode shapes of the 42 m (Case no. 1), 56 m (Case no. 2) and 70 m (Case no. 3) high towers, subjected to Imperial Valley (1940) earthquake with compressible water assumption. 132

Figure 4.7 Original and modified ground accelerations $a_g^{(1)}$ to $a_g^{(6)}$ corresponding to the six mode shapes of the 42 m (Case no. 1), 56 m (Case no. 2) and 70 m (Case no. 3) high towers, subjected to Loma Prieta (1989) earthquake with compressible water assumption. 133

Figure 4.8 Modified ground accelerations $a_g^{(1)}$ to $a_g^{(6)}$ corresponding to the selected six vibration modes of the studied towers subjected to Imperial Valley (1940) earthquake considering different water assumptions. 134
Figure 4.9 5%-damped pseudo-acceleration response spectra of the original ground motions and those of the modified ground motions corresponding to each of the selected six vibration modes assuming compressible water. 135
Figure 4.10 5%-damped pseudo-acceleration response spectra of the original ground motions and those of the modified ground motions corresponding to each of the six selected vibration modes obtained assuming simplified added mass formulation for the water surrounding the towers. 136
Figure 4.11 5%-damped pseudo-acceleration response spectra of the original ground motions and those of the modified ground motions corresponding to each of the six selected vibration modes obtained assuming Morison's added mass formulation for the water surrounding the towers. 137
Figure 4.12 Absolute maximum relative displacements along the height of the face of towers determined for each vibration mode using modified ground accelerations $a_g^{(1)}$ to $a_g^{(6)}$ and then combined to obtain total response: (a) Imperial Valley (1940) earthquake; (b) Loma Prieta (1989) earthquake obtained assuming compressible water in the reservoir. 139
Figure 4.13 Time-history horizontal relative displacements at point A of studied towers with hydrodynamic effects obtained for each vibration mode using modified ground accelerations $a_g^{(1)}$ to $a_g^{(6)}$ subjected to Imperial Valley (1940) earthquake assuming compressible water, and then combined to obtain total seismic response. 140
Figure 4.14 Time-history horizontal relative displacements at point A of studied towers with hydrodynamic effects obtained for each vibration mode using modified ground accelerations $a_g^{(1)}$ to $a_g^{(6)}$ subjected to Loma Prieta (1989) earthquake assuming compressible water, and then combined to obtain total seismic response. 141
Figure 4.15 Time-history of total horizontal relative displacements at point A of the studied towers including hydrodynamic effect considering Imperial Valley (1940) and Loma Prieta (1989) earthquakes obtained for different water assumptions. 142

Figure 4.16 Time-history shear force at the base of studied towers with surrounding water obtained for each vibration mode using modified ground accelerations $a_g^{(1)}$ to $a_g^{(6)}$ under the effect of Imperial Valley (1940) earthquake assuming compressible water, and then combined to obtain total seismic response. 144
Figure 4.17 Maximum shear stresses τ_{xz} and σ_{zz} developing within towers Case no. 1 and Case no. 2 subjected to Imperial Valley (1940) earthquake assuming compressible water. 145
Figure 5.1 Experimental facilities at Polytechnique Montréal (adopted from [20]): (a) structural laboratory; (b) detail of the shaking table. 153
Figure 5.2 Test setup: (a) specimen fixed on the shaking table; (b) dimensions and details of the primary structure. 155
Figure 5.3 Details of the apartment structure fixed at the top of the tower. . . . 156
Figure 5.4 Instrumentation layout for the experimental test. 157
Figure 5.5 Input harmonic excitation and acceleration response of the studied tower at point A: (a) and (b) 5 Hz excitation frequency; (c) and (d) 7 Hz excitation frequency; (e) and (f) 15 Hz excitation frequency; (g) and (h) 40 Hz excitation frequency. 159
Figure 5.6 Normalized frequency response function of the tower at point A without surrounded-water due to harmonic horizontal excitation: (a) first four natural frequencies; (b) first two natural frequencies. 160
Figure 5.7 Free vibration test with instrumentation: (a) the studied tower subjected to an initial displacement at 0.70% of its total height; (b) two string pot displacements used to capture the initial displacement. . . 161
Figure 5.8 Free vibration response of the studied tower with and without appurtenant structure subjected to an initial displacement: (a) and (b) time history and FFT of the normalized displacement applied at 0.70 height of the tower, respectively; (c) and (d) time history and FFT of the normalized acceleration of the tower at point A, respectively; (e) and (f) time history and FFT of the normalized acceleration of the tower at point B, respectively. 162
Figure 5.9 Finite-element model of the tower and the appurtenant structure. . . 163
Figure 5.10 Details of finite-element model of the appurtenant structure. 164
Figure 5.11 Different water levels surrounding the structure: (a) assuming water level to be $0.5H_w$; (b) assuming water level to be $0.75H_w$; (c) assuming water level to be H_w. 165

Figure 5.12 Finite-element model of coupled structure-water system. 166
Figure 5.13 First six lateral mode shapes and corresponding vibration periods of the tower. 167
Figure 5.14 Flowchart of the proposed procedures. 169
Figure 5.15 Time-history accelerations, pseudo-acceleration response spectra and Fourier amplitudes of the ground motions selected for this study: (a) to (c) Nahanni (1985) earthquake; (d) to (f) El Salvador (2001) earthquake. 171
Figure 5.16 Original and modified ground accelerations generated for the tower with different water levels subjected to Nahanni (1985) and El Salvador (2001) earthquakes with compressible water assumption: (a) and (b) assuming water level to be $0.5H_{\mathrm{w}}$; (c) and (d) assuming water level to be $0.75H_{\mathrm{w}}$; (e) and (f) assuming water level to be H_{w}. 172
Figure 5.17 Original and modified ground accelerations generated for the tower subjected to Nahanni (1985) and El Salvador (2001) earthquakes with Morison's added mass formulation assuming water level to be H_{w}: (a) Nahanni (1985) earthquake; (b) El Salvador (2001) earthquakes. . . . 173
Figure 5.18 Comparison of modified ground accelerograms generated for the tower under two different water assumptions for the surrounding water, subjected to: (a) Nahanni (1985) earthquake; (b) El Salvador (2001) earthquake. 173
Figure 5.19 Time-histories of relative horizontal accelerations at point A of studied tower without water subjected to Nahanni (1985) and El Salvador (2001) earthquakes: (a) and (b) using 25% scaled factor; (c) and (d) using 50% scaled factor. 175
Figure 5.20 Time-histories of relative horizontal accelerations at point B of the appurtenant structure without water subjected to Nahanni (1985) and El Salvador (2001) earthquakes: (a) and (b) using 25% scaled factor; (c) and (d) using 50% scaled factor. 176
Figure 5.21 Time-histories of relative horizontal accelerations at point A of studied tower including hydrodynamic effects subjected to Nahanni (1985) earthquake considering compressible water assumption with different water levels: (a), (d) and (g) water level selected to be $0.5H_{\mathrm{w}}$; (b), (e) and (h) water level selected to be $0.75H_{\mathrm{w}}$; (c), (f) and (i) water level selected to be H_{w}. 177

Figure 5.22 Time-histories of relative horizontal accelerations at point A of studied tower including hydrodynamic effects subjected to El Salvador (2001) earthquake considering compressible water assumption with different water levels: (a), (d), (g) and (j) water level selected to be $0.5H_{\mathrm{w}}$; (b), (e), (h) and (k) water level selected to be $0.75H_{\mathrm{w}}$; (c), (f), (i) and (l) water level selected to be H_{w}. 178

Figure 5.23 Time-histories of relative horizontal accelerations at point B of studied tower including hydrodynamic effects subjected to Nahanni (1985) earthquake considering compressible water assumption with different water levels: (a), (d) and (g) water level selected to be $0.5H_{\mathrm{w}}$; (b), (e) and (h) water level selected to be $0.75H_{\mathrm{w}}$; (c), (f) and (i) water level selected to be H_{w}. 179

Figure 5.24 Time-histories of relative horizontal accelerations at point B of studied tower including hydrodynamic effects subjected to El Salvador (2001) earthquake considering compressible water assumption with different water levels: (a), (d), (g) and (j) water level selected to be $0.5H_{\mathrm{w}}$; (b), (e), (h) and (k) water level selected to be $0.75H_{\mathrm{w}}$; (c), (f), (i) and (l) water level selected to be H_{w}. 180

Figure 5.25 Strain-acceleration curve and maximum shear stress developed at notch location subjected to Nahanni (1985) earthquake: (a) strain measured using the strain gauged installed at the notch location; (b) strain-acceleration curve; (c) maximum shear stresses τ_{xy} developing within the notch of the appurtenant structure. 182

Figure 5.26 Strain-acceleration curve and maximum shear stress developed at notch location subjected to El Salvador (2001) earthquake: (a) strain measured using the strain gauged installed at the notch location; (b) strain-acceleration curve; (c) maximum shear stresses τ_{xy} developing within the notch of the appurtenant structure. 183

Figure 5.27 Time-histories of relative horizontal accelerations at points A and B of studied structure including hydrodynamic effects subjected to Nahanni (1985) earthquake considering added mass formulation and assuming full water level of H_{w}: (a) and (c) acceleration response at point A; (b) and (d) acceleration response at point B. 184

Figure 5.28 Time-histories of relative horizontal accelerations at points A and B of studied structure including hydrodynamic effects subjected to El Salvador (2001) earthquake considering added mass formulation and assuming full water level of H_w: (a), (c) and (e) acceleration response at point A; (b), (d) and (f) acceleration response at point B. 185
Figure 6.1 Dimensions of the studied dam-reservoir systems having three water levels H_w, $0.75H_w$, and $0.5H_w$. 190
Figure 6.2 Variation of absolute value of $a_g^{(1)}(\omega)$ for studied dams D35 and D90 considering compressible water assumption with water level assumed to be: (a) and (b) H_w; (c) and (d) $0.75H_w$; and (e) and (f) $0.5H_w$. . . 191
Figure 6.3 Modifying original ground motion acceleration in the frequency domain for studied dams D35 and D90 assuming water level to be H_w considering compressible water assumption: (a) and (b) normalized FFT of Imperial Valley (1940) and Nahanni (1985) earthquakes, respectively; (c) and (d) variation of absolute value of $a_g^{(1)}(\omega)$ calculated using Equation (6.13); (e) and (f) normalized $a_g^{(1)}(\omega)$ calculated using Equation (6.16); (g) and (h) time histories of original and modified ground accelerograms. 194
Figure 6.4 Modifying original ground motion acceleration in the frequency domain for studied dams D35 and D90 assuming water level to be $0.75H_w$ considering compressible water assumption: (a) and (b) normalized FFT of Imperial Valley (1940) and Nahanni (1985) earthquakes, respectively; (c) and (d) variation of absolute value of $a_g^{(1)}(\omega)$ calculated using Equation (6.13); (e) and (f) normalized $a_g^{(1)}(\omega)$ calculated using Equation (6.16); (g) and (h) time histories of original and modified ground accelerograms. 195
Figure 6.5 Modifying original ground motion acceleration in the frequency domain for studied dams D35 and D90 assuming water level to be $0.5H_w$ considering compressible water assumption: (a) and (b) normalized FFT of Imperial Valley (1940) and Nahanni (1985) earthquakes, respectively; (c) and (d) variation of absolute value of $a_g^{(1)}(\omega)$ calculated using Equation (6.13); (e) and (f) normalized $a_g^{(1)}(\omega)$ calculated using Equation (6.16); (g) and (h) time histories of original and modified ground accelerograms. 196
Figure 6.6 Original harmonic ground motion accelerations. 198

Figure 6.7 Time-history relative horizontal displacements at the crest of dams D35 and D90 subjected to harmonic excitation case 1 to case 5 according to two different approaches: Red curves, proposed method for each vibration mode using modified ground accelerations $a_g^{(1)}$ to $a_g^{(5)}$ and then combined to obtain total dam response; Blue curves, dam-reservoir system based on analytical formulation. 199
Figure 6.8 Studied dam-reservoir system and original ground acceleration: (a) dimensions of Pine Flat dam; (b) time-history accelerations and Fourier amplitudes of Imperial Valley (1940) and Nahanni (1985) earthquakes. 200
Figure 6.9 Five first mode shapes, corresponding vibration periods and effective modal masses of the studied Pine Flat dam monolith. 201
Figure 6.10 Original and modified Imperial Valley (1940) and Nahanni (1985) ground motion accelerations corresponding to Pine Flat dam assuming compressible water in the reservoir. 202
Figure 6.11 5%- damped pseudo-acceleration response spectra of the original ground motion and the modified ground motions of Pine Flat dam assuming water to be compressible in the reservoir. 203
Figure 6.12 Absolute maximum displacements along the height of the upstream face of Pine Flat dam. 204
Figure 6.13 Time-histories of total relative horizontal displacements at the crest of Pine Flat dam. 205
Figure 6.14 Maximum stresses σ_{yy} and σ_{xy} developing within Pine Flat dam subjected to the two earthquakes considered as obtained using proposed method: (a) and (b) Imperial Valley (1940) earthquake; (c) and (d) Nahanni (1985) earthquake. 205
Figure 6.15 Dimensions and finite element meshes of San Bernardino intake tower. 206
Figure 6.16 Finite element mode shapes and corresponding vibration periods of San Bernardino intake tower, as well as the modal mass participation factors. 207
Figure 6.17 Original and modified ground accelerations $a_g^{(1)}$ to $a_g^{(6)}$ corresponding to the six mode shapes of San Bernardino intake tower, subjected to Imperial Valley (1940), Loma Prieta (1989), and Nahanni (1985) earthquakes considering compresssible water assumption and add added mass formulation.. 208

Figure 6.18 5%-damped pseudo-acceleration response spectra of the original ground motions and those of the modified ground motions corresponding to each of the selected six vibration modes assuming compressible water and added mass formulation. 209
Figure 6.19 Time-histories of total relative horizontal displacements at top the top of San Bernardino intake tower including hydrodynamic effect considering Imperial Valley (1940) and Loma Prieta (1989) earthquakes obtained assuming compressible water in the reservoir. 210
Figure 6.20 Maximum stresses σ_{xz} developing within San Bernardino intake tower subjected to Imperial Valley (1940) earthquake assuming compressible water. 210
Figure 6.21 Absolute maximum relative displacements along the height of the face of San Bernardino intake tower determined for each vibration mode using modified ground accelerations $a_g^{(1)}$ to $a_g^{(6)}$ obtained assuming compressible water in the reservoir and then combined to obtain total response. 212
Figure 6.22 Five first mode shapes both gravity dam monoliths: (a) the 35 m height dam (D35); (b) the 90 m height dam (D90). 214
Figure 6.23 Modified ground motion accelerations $a_g^{(1)}$ to $a_g^{(5)}$ corresponding to the first five mode shapes of dams D35 and D90 both subjected to Imperial Valley (1940) earthquake and considering compressible water assumption. 215
Figure 6.24 Steps for setting up and executing the modal time history analysis of dam D35 in SAP2000 including hydrodynamic effects. 216
Figure 6.25 Steps for setting up and executing the modal time history analysis of dam D90 in SAP2000 including hydrodynamic effects. 217
Figure 6.26 Time-history horizontal relative displacements (for the first 5 modes and the total) at the crest of dams D35 and D90 subjected to Imperial Valley (1940) earthquake obtained using to SAP2000 and ADINA. . . 218
Figure 6.27 Maximum stresses σ_{xx} and σ_{zz} developing within dams D35 and D90 subjected to Imperial Valley (1940) earthquake. 220
Figure 6.28 Coupled finite element dam-reservoir system. 221

Figure 6.29 Time-history horizontal relative displacements at the crest of dams D35 and D90 subjected to Imperial Valley (1940) earthquake according to three different approaches: blue curve, proposed method using ADINA or SAP2000; green curve, dam-reservoir system based on analytical formulation; red curve, coupled dam-reservoir system using potential-based fluid elements. 221

Figure 6.30 Maximum stresses σ_{xx} and σ_{zz} developing within dams D35 and D90 subjected to Imperial Valley (1940) earthquake: (a) and (c) coupled dam-reservoir system using potential-based fluid element; (b) and (d) proposed method using ADINA or SAP2000. 222

Figure 6.31 Six first lateral mode shapes of San Bernardino intake tower modeled using 3D beam elements and 3D-solid elements. 224

Figure 6.32 Modified ground motion accelerations $a_g^{(1)}$ to $a_g^{(6)}$ corresponding to the first six lateral mode shapes of San Bernardino intake tower subjected to Imperial Valley (1940) earthquake and considering compressible water assumption. 224

Figure 6.33 Time-history total relative horizontal displacements at the top of the San Bernardino intake tower subjected to the Imperial Valley (1940) earthquake, according to two different approaches: blue curves represent the proposed method using SAP2000 with beam and 3D-solid elements; red curves represent the coupled structure-water system using potential-based fluid elements modeled in ADINA software. . . . 225

Figure 6.34 Procedural steps for setting up and executing the modal time history analysis of San Bernardino intake tower in SAP2000 including hydrodynamic effects: (a) natural frequencies highlighting the first six lateral modes; (b) combination of defined load cases; (c), (f), and (i) modal load cases with appropriate frequency shifts applied; (d), (g), and (j) linear modal history load cases; (e), (h), and (k) defining modified ground accelerations as time history functions. 226

Figure 6.35 Dimensions of circular hollow sections using HSS 127×9.5 and solid sections of the same diameter mounted on the shaking table. 229

Figure 6.36 Frequency response function (FRF) of relative horizontal acceleration at the top of the axisymmetric tower, comparing the effects of hollow and solid sections and materials: (a) and (b) steel material; (c) and (d) aluminum material. 230

Figure 6.37 Frequency response function (FRF) of relative horizontal acceleration at the top of the axisymmetric tower, comparing the effects of different tower heights: (a) FRF for the 4.3 m tower; (b) FRF for the 3 m tower; (c) FRF for the 2 m tower; and (d) FRF for the 1.75 m tower. 232
Figure 6.38 Dimensions of circular hollow sections using HSS 127 × 9.5 for towers of varying heights mounted on the shaking table: (a) 4.3 m; (b) 3 m; (c) 2 m; and (d) 1.75 m. 233
Figure 6.39 Frequency response function (FRF) of relative horizontal acceleration at the top of the axisymmetric tower, comparing the effects of different tower heights: (a) HSS 76 × 6.4; (b) HSS 89 × 6.4; (c) HSS 89 × 8.0; (d) HSS 102 × 6.4; (e) HSS 102 × 8.0; (f) HSS 127 × 9.5. 234
Figure 6.40 Fabricated aluminum tower with HSS 76 × 6.4 cross section, including detailed views of the design features. 235
Figure 6.41 Damping effect on the FRF of acceleration at the top of the tower as well as on the modified ground motion acceleration. 237
Figure 6.42 Effects of different zero padding lengths on modified ground acceleration: (a), (c), (e), and (g) zeros added with the same length as the original signal; (b), (d), (f), and (h) zeros added with four times the original signal length. 239

LIST OF SYMBOLS AND ACRONYMS

Acronyms

ADINA	Automatic dynamic incremental nonlinear analysis
ESDOF	Equivalent single degree of freedom
FEA	Finite element analysis
DFFT	Discrete fast Fourier transform
IDFFT	Inverse discrete Fourier transform
FRF	Frequency response function
HMF	Hydrodynamic modification factor
RSA	Response spectrum analysis
SDOF	Single degree of freedom
SRSS	Square root of the sum of the squares
THMSA	Time-history modal superposition analysis

Roman symbols

$a_{\mathrm{g}}^{(j)}$	Modified horizontal ground motion acceleration corresponding to vibration mode j
$\widetilde{a}_{\mathrm{g}}$	Mode- and coordinate-independent modified horizontal ground motion acceleration
$C_{\mathrm{f}}\,;C_{\mathrm{w}}$	Velocity of pressure waves in the foundation and water, respectively
C_{e}	Modification factor for Westergaard's added masses to include compressibility effects given by Eq. (2.38)
$\mathbf{C}_{\mathrm{ss}}\,;\mathbf{C}_{\mathrm{ww}}$	Structural damping matrix and damping due to energy dissipation at the reservoir bottom, respectively
$\mathbf{C}_{\mathrm{sw}}$	Matrix that Couples the velocity potential to displacements on the water-structure interface
$C_{\mathrm{D}}\ ;C_{\mathrm{M}}$	Drag and inertia coefficients
$\mathbf{D}_{\mathrm{s}}\,;\mathbf{B}_{\mathrm{w}}$	elasticity matrix for the solid and fluid elements, respectively
$\mathcal{D}_n\,;\mathcal{E}_n\,;\tau_n R_{\mathrm{s}}$	Parameter to caccluate hydrodynamic pressure around an axisymmetric structures surrounded by water
$\mathbf{F}_{\mathrm{h}}$	Earthquake-induced lateral hydrodynamic forces
$\widehat{f}_j(y)$	Equivalent lateral static force on the structure with water subjected to original horizontal ground motion acceleration $\ddot{x}_{\mathrm{g}}$, and considering only the contribution of vibration mode j

$\widetilde{f}_j(y)$	Equivalent lateral static force on the structure without water subjected to modified horizontal ground motion acceleration $a_{\rm g}^{(j)}$, including hydrodynamic effects and considering only the contribution of vibration mode j
$f_j(y)$	Equivalent lateral static force on the structure without water subjected to original horizontal ground motion acceleration $\ddot{x}_{\rm g}$ considering only the contribution of vibration mode j
$\widehat{f}_{sc}(y)$	Equivalent lateral earthquake forces associated with the higher vibration modes of dams using static correction method given by Eq. (2.42)
$\mathbf{F}_{\rm M}$	Morison's hydrodynamic force
$f_{\rm D}$; $f_{\rm I}$	Drag and inertia forces
$H_{\rm s}\,;H_{\rm w}$	Structure and water heights, respectively
$I_{0,n}\,;I_{j,n}$	Integral terms given by Eqs. (2.23) and (2.24), respectively
$K_j\,;C_j$	Stiffness and viscous damping of the SDOF systems corresponding to vibration mode j
K_ℓ	Modified Bessel function of order ℓ
$\mathrm{J}_\ell\,;\mathrm{Y}_\ell$	Bessel functions of order ℓ of the first and second kind, respectively
$L_{\rm w}$	Length of the water domain
$\mathbf{M}\,;\mathbf{C}\,;\mathbf{K}$	Mass, damping, and stiffness matrices of the structure without water, respectively
$\mathbf{M}_{\rm ww}\,;\mathbf{K}_{\rm ww}$	Potential and kinetic energy matrices of the impounded water, respectively
$\mathbf{M}_{\rm ss}\,;\mathbf{K}_{\rm ss}$	Structural mass and stiffness matrices of the impounded water, respectively
$M_j\,;L_j$	Generalized modal mass and force of the structure without water corresponding to vibration mode j
$m_a(y)$	Added mass per unit height of the dam given by Eq. (2.36)
$\widehat{M}_i(y)$	Lumped added masses on the nodes of the dam's face using the tributary method given by Eq. (2.37)
$N_{\rm P}=2^k$	Number of excitation frequencies for DFFT and IDFFT with k integer
$N_{\rm s}$; $N_{\rm w}$	Number of structural and water (i.e. acoustical) modes, respectively
p_0	FRF of hydrodynamic pressure at rigid water-structure interface due to horizontal ground motion acceleration $\ddot{x}_{\rm g}$
p_j	FRF of hydrodynamic pressure at water-structure interface due to horizontal ground motion acceleration corresponding to the x–component of structural mode shape $\psi_j^{(x)}$

p	FRF of total hydrodynamic pressure
q	Damping coefficient accounting for reservoir bottom wave absorption due to sedimentation given by Eq. (2.17)
$\widehat{\mathbf{Q}}\,;\widehat{Q}_m$	Matrix and its elements to solve coupled water structure system given by Eq. (2.6)
$\left\lvert \tilde{r} \right\rvert^{(\max)}$	Maximum absolute total seismic response including hydrodynamic effects
$\left\lvert \tilde{r}_j \right\rvert^{(\max)}$	Maximum absolute modal seismic response including hydrodynamic effects
R_{s}	Radius of axisymmetric structures surrounded by water
$\widehat{\mathbf{S}}\,;\widehat{S}_{j,m}(\omega)$	Vector and its elements to solve coupled water structure system given by Eq. (2.5)
$S_{\mathrm{A}}^{[a_{\mathrm{g}}^{(j)}]}\,;\,S_{\mathrm{D}}^{[a_{\mathrm{g}}^{(j)}]}$	Pseudo-acceleration and displacement response spectra of modified ground motion acceleration $a_{\mathrm{g}}^{(j)}$, respectively
$S_{\mathrm{A}}^{[\ddot{x}_{\mathrm{g}}]}$	Pseudo-acceleration response spectrum of the original ground motion acceleration $\ddot{x}_{\mathrm{g}}$
T_j	Vibration period of the structure without water corresponding to mode j
t_a	Duration of the applied accelerogram
$\ddot{\mathbf{U}}\,;\dot{\mathbf{U}}\,;\mathbf{U}$	Vectors of nodal relative accelerations, relative velocities, and relative displacements of the structure without water subjected to original ground motion acceleration $\ddot{x}_{\mathrm{g}}$, respectively
$\ddot{\widehat{\mathbf{U}}}\,;\dot{\widehat{\mathbf{U}}}\,;\widehat{\mathbf{U}}$	Vectors of nodal relative accelerations, relative velocities, and relative displacements of the structure with water and subjected to original ground motion acceleration $\ddot{x}_{\mathrm{g}}$, respectively
$\mathbf{U}\,;\boldsymbol{\Phi}$	Vectors containing nodal relative displacements and fluid potentials, respectively
$\widehat{u}\,;\,\ddot{\widehat{u}}\,;\,u\,;\,\ddot{u}$	Total of relative horizontal displacements and accelerations of the water-structure system, and total of relative horizontal displacements and accelerations of the structure without water subjected to original ground motion acceleration $\ddot{x}_{\mathrm{g}}$, respectively
$\widetilde{u}\,;\,\ddot{\widetilde{u}}$	Total of relative horizontal displacements and accelerations of the structure without water subjected to modified ground motion acceleration, respectively
$u_j\,;\ddot{u}_j$	Relative horizontal displacement and relative horizontal acceleration of the structure without water subjected to original ground motion acceleration $\ddot{x}_{\mathrm{g}}$ considering only the contribution of vibration mode j, respectively

$\widehat{u}_j$; $\ddot{\widehat{u}}_j$ — Relative horizontal displacement and relative horizontal acceleration of the water-structure system subjected to original ground motion acceleration $\ddot{x}_{\mathrm{g}}$ considering only the contribution of vibration mode j, respectively

$\widetilde{u}_j$; $\ddot{\widetilde{u}}_j$ — Relative horizontal displacement and relative horizontal acceleration of the structure without water subjected to modified ground motion acceleration $a_{\mathrm{g}}^{(j)}$ considering only the contribution of vibration mode j, respectively

$\left|u_j(x,y,t)\right|^{(\max)}$ — Maximum (i.e. peak) absolute value of seismic relative horizontal displacement of a point of coordinates (x,y) of the structure without water subjected to the original ground motion acceleration $\ddot{x}_{\mathrm{g}}$ considering only the contribution of mode j

$\left|\widehat{u}_j(x,y,t)\right|^{(\max)}$ — Maximum (i.e. peak) absolute value of seismic relative horizontal displacement of a point of coordinates (x,y) of the water-structure system subjected to the original ground motion acceleration $\ddot{x}_{\mathrm{g}}$ considering only the contribution of mode j

$\left|\widetilde{u}_j(x,y,t)\right|^{(\max)}$ — Maximum (i.e. peak) absolute value of seismic relative horizontal displacement of a point of coordinates (x,y) of the structure without water subjected to the modified ground motion acceleration $a_{\mathrm{g}}^{(j)}$ considering only the contribution of vibration mode j

$\left|u_j(y,t)\right|^{(\max)}$ — Maximum (i.e. peak) absolute value of seismic relative horizontal displacement of a point of coordinate y at the upstream face of the structure without water subjected to the original ground motion acceleration $\ddot{x}_{\mathrm{g}}$ considering only the contribution of mode j

$\left|\widehat{u}_j(y,t)\right|^{(\max)}$ — Maximum (i.e. peak) absolute value of seismic relative horizontal displacement of a point of coordinate y at the upstream face of the structure with water and subjected to the original ground motion acceleration $\ddot{x}_{\mathrm{g}}$ considering only the contribution of mode j

$\left|\widetilde{u}_j(y,t)\right|^{(\max)}$ — Maximum (i.e. peak) absolute value of seismic relative horizontal displacement of a point of coordinate y at the upstream face of the structure without water subjected to the modified ground motion acceleration $a_{\mathrm{g}}^{(j)}$ considering only the contribution of vibration mode j

v_i — Tributary volume of water at node i

$\ddot{x}_{\mathrm{g}}$; $\dot{x}_{\mathrm{g}}$ — Original horizontal ground motion acceleration and velocity, respectively

$\ddot{Z}_j\,;\dot{Z}_j\,;Z_j$	Relative acceleration, relative velocity, and relative displacement of the SDOF system equivalent to the structure without water subjected to original ground motion acceleration $\ddot{x}_{\mathrm{g}}$ considering only the contribution of vibration mode j, respectively
$\ddot{\widehat{Z}}_j\,;\dot{\widehat{Z}}_j\,;\widehat{Z}_j$	Relative acceleration, relative velocity, and relative displacement of the SDOF system equivalent to the water-structure system subjected to original ground motion acceleration $\ddot{x}_{\mathrm{g}}$ considering only the contribution of vibration mode j, respectively
$\ddot{\widetilde{Z}}_j\,;\dot{\widetilde{Z}}_j\,;\widetilde{Z}_j$	Relative acceleration, relative velocity, and relative displacement of the SDOF system equivalent to the structure without water subjected to modified ground motion acceleration $a_{\mathrm{g}}^{(j)}$ considering only the contribution of vibration mode j, respectively

Greek symbols

α	Wave reflection coefficient at reservoir bottom
$\beta_n\,;\,\kappa_n$	Parameters given by Eq. (2.22)
$\Delta t^{(\mathrm{init})}$	Initial time interval of the original ground motion acceleration
$\Delta t^{(\mathrm{new})}$	New time interval of the original ground motion acceleration
$\psi_j^{(x)}\,;\psi_j^{(y)}$	x- and y-components of structural mode shape j, respectively
ξ_j	Viscous damping ratio corresponding to vibration mode j
η_{s}	Hysteretic damping
θ	Transmitting boundary conditions (TBCs)
$\widehat{\omega}_1$	Fundamental vibration frequency of the dam-reservoir system
ω_j	Vibration frequency of the structure without water corresponding to mode j
ω_0	Reservoir's resonance frequency
$\vartheta_{0,m}\,;\,\vartheta_{j,m}$	Integral terms for analytical formulation of hydrodynamic pressure, or simplified added-mass formulation
$\rho_{\mathrm{f}}\,;\,\rho_{\mathrm{s}}\,;\,\rho_{\mathrm{w}}$	Mass densities of foundation, structure, and water, respectively
μ_{s}	Mass of the structure per unit height
ω	Exciting frequency
$\lambda_n\,;\,Y_n$	Reservoir eigenvalue and eigenvector corresponding to water (i.e. acoustical) mode n, respectively

CHAPTER 1 INTRODUCTION

This chapter introduces the subject of the thesis by framing the research context and defining the core problem under investigation. It outlines the research objectives and explains the methodology employed. Additionally, the chapter highlights the scope of the study and its novel contributions. The structure of the thesis is also summarized at the end of the chapter.

1.1 Background

The seismic response of structure-water systems, including their appurtenant structures, is a critical area of study within structural engineering. Earthquakes can induce significant forces and displacements in structure-water systems, leading to potential failures and substantial economic losses. The complex interaction between water and structural elements under seismic loading generally necessitates advanced numerical modeling and/or experimental techniques to predict and mitigate these effects with a sufficient level of accuracy. Additionally, the flexibility of the primary structure and the earthquake-induced hydrodynamic forces can significantly affect the seismic response of appurtenant structures or equipment generally fixed at the top of the primary structure. Understanding these interactions is vital for ensuring the safety and resilience of such systems.

Dam-reservoir systems are the first type of structure-water systems examined in this thesis. These structures have been in the center of both human and environmental challenges for over a century as the second-largest source of renewable energy in the world. The safety of dams during earthquakes is extremely important because the failure of such a structure can have catastrophic consequences on life and property. Therefore, investigating the dynamic behavior of dam-reservoir systems and evaluating their seismic safety have been major research and engineering concerns for the last several decades. These systems are subjected to hydrodynamic effects induced by the impounded reservoir during earthquakes. Appropriate modeling of such effects can be achieved using a variety of analytical and numerical methods. In the seventies, a two-stage procedure was proposed for the elastic analysis phase of seismic design and safety evaluation of concrete gravity dams. This procedure includes: (i) response spectrum analysis (RSA), where the peak response value is estimated directly from the earthquake design spectrum; and (ii) response history analysis (RHA) of a finite element idealization of the dam monolith. Initially, these procedures either ignored the hydrodynamic effects or used simplified added masses to represent the hydrodynamic effects. In the mid-1980s, these procedures were extended to consider the full effects of dam-water interaction,

dam-foundation interaction, and reservoir bottom absorption, all of which significantly influence a dam's response to earthquake ground motion. Appropriate modeling of such effects can be achieved using a variety of analytical and numerical methods (e.g. [2–4, 21–40]). Dynamic time history modal superposition and response spectrum analyses are popular among the broad range of available numerical tools, as they allow the dissection of a structure's response into the contributions of multiple vibration modes. For a dam-reservoir system, such analyses can be conducted using finite element methods that couple solid and fluid elements to model earthquake-induced responses of the dam and the reservoir, respectively. Alternative approaches include modeling water effects analytically, either through the formulation of added masses attached to the dam's upstream face or by considering hydrodynamic pressures acting at the dam-reservoir interface. The added masses concept remains widely used in practice for its simplicity, although it has been shown to be potentially inaccurate depending on the type of ground motion and the specific dam studied. A more accurate alternative is the implementation of earthquake-induced hydrodynamic forces acting on the upstream face of a gravity dam modelled using solid finite elements, i.e. sub-structuring dynamic analysis (e.g. [27, 41]). Another approach to analyzing dam-reservoir systems is the use of semi-analytical techniques. Although these methods are limited by the simple geometry of the reservoir and water modeling assumptions, they can still provide useful insights into the seismic response of gravity dams, especially in the initial phases of design or safety assessments.

The second type of structure-water systems considered in this study are axisymmetric structures surrounded by water. These structures are critical components of modern infrastructure, playing a important role in energy generation and transportation, such as intake towers, offshore wind turbines, and deep-water bridge piers. They are subjected to hydrodynamic forces during seismic events and their stability and functionality are critical to maintaining essential services. The analysis of these structures follows a similar pattern to that of dam-reservoir systems. A simplified method widely used for analyzing these structures is based on Morison's equation, which has gained widespread acceptance for evaluating hydrodynamic effects on slender cylinders due to its simplicity [42–46]. Originally proposed by Morison et al. [47] for calculating wave loads, this semi-empirical formula was later modified by Penzien and Kaul [48] to account for hydrodynamic forces on cylindrical structures during earthquakes. In addition to Morison's equation, numerical techniques such as finite element, boundary element, and scaled boundary element methods are also commonly used to investigate earthquake-induced hydrodynamic effects on axisymmetric water-surrounded structures (e.g. [49–59, 59–61]).

In addition to numerical studies on the seismic response of structures, experimental methods

like shaking table tests have been widely used to examine the dynamic behavior of structures. However, due to complexity of structure-water systems, particularly the challenges of incorporating hydrodynamic effects and handling the large scale of test specimens, makes such experiments difficult to perform. As a result, experimental tests on structure-water systems are relatively limited compared to the extensive testing performed on structures in dry conditions, such as buildings and bridges, despite the long-standing research interest in testing structure-water systems, particularly dam-reservoir systems.

Existing experimental tests on structure-water systems that incorporate hydrodynamic effects can be classified into three main categories: (i) utilizing underwater shaking tables, which provide high accuracy but come with significant challenges such as the need for expensive facilities and the risk of water leakage, posing safety concerns [7, 8, 62–64]. (ii) A second approach simplifies the complexity of the tests by using added masses or a limited reservoir length to simulate hydrodynamic effects during experimental tests, but this method lacks the accuracy necessary for comprehensive seismic studies [13–15, 18]. (iii) The third approach ignores hydrodynamic effects entirely in the experimental setup, primarily due to the high costs of required facilities and associated safety concerns [19, 65–67].

As mentioned earlier, incorporating hydrodynamic effects into the numerical and experimental study of the seismic response of structure-water systems is essential. However, these studies face challenges due to the complexities of incorporating hydrodynamic effects and the constraints of existing experimental methods. This research aims to overcome these obstacles by proposing innovative numerical and experimental methods, offering engineers and researchers alternative, accurate, and simplified approaches for analyzing and testing structure-water systems and their appurtenant structures.

1.2 Problem Statement

Despite extensive research and available methods to study the seismic response of structure-water systems and their appurtenant structures, both numerical and experimental approaches have significant shortcomings. Coupled finite element methods require specialized software and a high level of expertise. They demand consideration of several parameters that affect the response of a structure-water system, such as the flexibility of the structure, the compressibility of water, and the fluid-structure interaction boundary conditions. Because the water is practically infinite in length, virtually cutting off the water domain at a certain distance from the structure is necessary. An appropriate boundary condition must then be applied to prevent wave reflection at the cut section of the reservoir. Additionally, to reduce computation time, it is desirable to minimize this length. Indeed, appropriate modeling of

the reservoir domain, fluid-structure interaction, and relevant boundary conditions can be challenging in day-to-day engineering practice. Simplified methods are often used to calculate hydrodynamic loads generated by fluid-structure interaction, which are then introduced into finite element models to simulate the hydrodynamic effects of water. Most existing simplified methods, such as Westergaard added masses [21] or the Morison method [47], are derived from analytical formulations that include several simplified assumptions to manage the complexity of fluid-structure interaction. However, it has been shown that many of these simplifications can significantly impact the response of the structure. Therefore, while these methods are useful, they may not always provide the precision needed for analysis and design of water structure system.

To further enhance the implementation of earthquake analysis of structure-water systems, specifically for dam-reservoir systems, on a routine basis in engineering practice, Fenves and Chopra [29] proposed a simplified method that can be used to estimate a gravity dam's peak seismic response directly from an earthquake design spectrum. This technique consists of modeling a gravity dam as an equivalent single degree of freedom (ESDOF) system used to evaluate the fundamental mode response of the dam through equivalent lateral static forces and response spectrum analysis. The effects of higher vibration modes are accounted for approximately through a static correction method [29, 68].

Although simplified methods are necessary for day-to-day engineering practice, they must be accurate enough when compared to more comprehensive analysis procedures and need continuous improvement. Therefore, alternative simplified methods are still required for practical applications. In RSA including hydrodynamic effects, it is crucial to include the flexibility of higher modes in the analysis, especially for flexible systems. Additionally, it is necessary to use the standard finite element method to analyze structure-water systems with hydrodynamic effects without being restricted to specific software. This also avoids the need for high expertise to accurately model the fluid domain in such softwares. Reducing the complexity and size of the computational domain to include only the structural domain significantly saves computational resources.

In the context of experimental studies on structure-water systems, each available method has specific objectives and relies on distinct assumptions to incorporate hydrodynamic effects. However, all these methods encounter challenges due to the inherent complexity of accurately simulating these effects in experimental setups. Additionally, distributing the added masses along the height of the structure and maintaining stability during dynamic tests presents significant challenges. Underwater shaking table tests, on the other hand, require costly and large-scale laboratory facilities, along with specialized instrumentation to accurately capture

structural responses beneath the water, making them resource-intensive and challenging to conduct. Additionally, the presence of water during seismic shaking table tests poses safety concerns, such as water leakage that can endanger equipment. Furthermore, when similitude laws are applied to scale down a prototype structure, adjusting the density of the water typically used in underwater shaking tables becomes challenging, often resulting in distortions of the similitude laws [64]. Another challenge associated with the presence of water in experimental tests is the difficulty in achieving accurate boundary conditions, which are important for accurately simulating wave propagation effects. Due to these challenges, there are many research in this filed that simply neglect the fluid-structure interaction effects during the experimental tests [19]. Therefore, alternative approaches that accurately incorporate dynamic fluid-structure interaction into experimental tests are highly needed and can pave the way for numerous future experimental studies in this field.

In summary, this thesis seeks to address the following issues:

- How can higher mode effects be directly included in the response spectrum analysis of dam-reservoir systems, in lieu of static correction methods?
- How can an alternative simplified approach be used to perform modal time history analysis of dam-reservoir system and axisymmetric water-surrounded structures, including earthquake-induced hydrodynamic effects, to enable a comprehensive understanding of each mode's impact on the total seismic response?
- How can coupled fluid-structure interaction analysis of structure-water systems be accurately performed using any standard structural engineering software, while incorporating hydrodynamic effects and reducing computational demands?
- How can the seismic response of structure-water-system be experimentally investigated using standard shaking table facilities without the need for specific facilities?
- How can the proposed procedures for response spectrum analysis and modal time history analysis, be extended to other types of structure-water systems?

1.3 Objectives and scope

The overall objectives of this research are to propose innovative methods for numerical modeling and experimental simulation of the seismic response of structure-water systems and their appurtenant structures. The main novelty lies in the concept of transferring earthquake-induced hydrodynamic pressure into modified versions of the original ground motion acceleration and its response spectrum, which can be directly applied to the dry structure

(i.e., without water). These modified ground accelerations can then be used in experimental tests, specifically as input signals for shaking table tests of structure-water systems and their appurtenant structures, eliminating the need for water in the laboratory while effectively incorporating hydrodynamic effects into the linear seismic response of the system.

In particular, the main objectives of this thesis are:

- Extend the modified ground acceleration method to other types of structure-water systems.
- Provide an innovative approach for conducting time-history modal superposition and response spectrum analyses of dam-reservoir systems and axisymmetric water-surrounded structures, directly accounting for higher mode effects in lieu of static correction.
- Provide an alternative method for incorporating hydrodynamic added mass effects into the dynamic analysis of structure-water systems by transferring these effects into modified ground motion accelerations, rather than applying them as lumped masses at each node along the structure-water interface.
- Validate the accuracy of the proposed analysis procedure by comparing it against analytical, semi-analytical, and coupled structure-water finite element models.
- Develop an innovative shaking table test for evaluating the seismic response of structure-water systems and their appurtenant structures using modified ground motion accelerograms.
- Validate the effectiveness of the proposed shaking table test by comparing the experimental results with coupled structure-water finite element models.
- Demonstrate the usefulness of the proposed analysis procedure for conducting time-history modal and response spectrum analyses of dam-reservoir systems and axisymmetric water-surrounded structures using any standard structural engineering software, such as SAP2000.

1.4 Methodology

This section outlines the approaches and procedures used to achieve the objectives of this research. The study involves both numerical and experimental investigations to develop and validate innovative methods for analyzing the seismic response of structure-water systems and their appurtenant structures.

1.4.1 Time-History modal superposition and response spectrum analysis including higher modes effects

A simplified approach is proposed to conduct time-history modal superposition and response spectrum analyses of a dam-reservoir system while directly accounting for higher mode effects instead of using static correction techniques. The proposed method incorporates earthquake-induced reservoir effects into modified versions of the original ground motion acceleration and its response spectrum, which can be applied directly to the dam with an empty reservoir (i.e., without water). This approach allows the dam-reservoir system to be uncoupled into multiple modal coordinates, each subjected to modified ground motion acceleration considering the corresponding mode. By enabling a comprehensive understanding of each mode's impact on the total seismic response, this technique allows for the inclusion of higher vibration modes in the response spectrum analysis of dam-reservoir systems, thereby enhancing the accuracy and reliability of the seismic response assessment. This method eliminates the need for specialized software to account for fluid-structure dynamic interaction, making it more accessible for practical engineering applications. By applying these modified ground motion accelerations, the dynamic response of the dam can be accurately assessed without the complexities associated with traditional fluid-structure interaction models. This approach not only simplifies the analysis but also maintains the accuracy required for reliable seismic evaluation. A similar methodology was developed by Miquel and Bouaanani [4], but their focus was on direct integration time-history dynamic analysis of dam-reservoir systems rather than response spectrum and modal superposition analyses. The current study extends this concept to provide a comprehensive solution for evaluating the seismic response of gravity dams using standard structural engineering software, thus broadening its applicability and ease of use. Additionally, the proposed method includes a thorough validation process, comparing the results obtained using this approach with those from more complex coupled structure-water finite element models. This validation ensures that the proposed method provides results that are both accurate and reliable, making it a valuable tool for engineers and researchers working on the seismic analysis of gravity dams.

1.4.2 Extension of modified ground acceleration method to other type of structures

An efficient procedure for modal seismic response analysis of axisymmetric structures surrounded by water is developed by extending the modified ground acceleration method. The modified ground acceleration method was extended to other types of structure-water systems, specifically axisymmetric water-surrounded structures, liquid storage tanks, and navigation lock chambers in contact with water.

The classical approach for dynamic analysis of axisymmetric water-surrounded structures, such as intake towers and offshore wind turbines, typically involves 3D coupled fluid-structure finite element models. Due to the large fluid domain and the need for refined mesh around the structure and surrounding water, these models are computationally demanding. Additionally, they require specialized software and expertise to ensure accurate and reliable results. By using modified ground motion accelerations, the seismic response of axisymmetric water-surrounded structures can be analyzed without the complexities associated with classical methods. This approach simplifies the analysis while maintaining the accuracy required for reliable seismic evaluation of such structures, reducing computational demands and eliminating the need for specialized software. The proposed method is validated by comparing its results with those obtained from 3D coupled fluid-structure finite element models.

1.4.3 Simplified alternative implementing added masses to representing hydrodynamic effect

A simplified alternative approach is proposed for representing hydrodynamic added masses for both dam-reservoir systems and axisymmetric water-surrounded structures. This method involves transferring the effects of added masses directly into the modified ground motion time-history or spectral accelerations. The methodology utilizes the analytical Westergaard added mass formulation for dam-reservoir systems. For axisymmetric water-surrounded structures, the effects of added masses can be included based on two theories: (i) added masses derived from radiation wave theory and (ii) added masses based on Morison's formulation. By incorporating the effects of these added masses into the modified version of the ground acceleration, the seismic response of the structure can be analyzed without the need to implement added masses on each node of the structure-water interface. Additionally, the issue of whether damping should be applied only to the structure or also to the water can be resolved through this technique, as the modified ground acceleration can be implemented to incorporate the effects of hydrodynamic damping.

1.4.4 Development of innovative shaking table test of structure-water supported appurtenant structures

In this study, an innovative approach for shaking table tests is proposed to evaluate the seismic response of structure-water systems and their appurtenant structures. As mentioned, one of the main challenges in conducting shaking table tests of structure-water systems is incorporating hydrodynamic effects into the experimental setup in a safe and controlled environment. Developing an alternative method that accurately represents these hydrodynamic forces without the need for specialized or expensive facilities can greatly benefit researchers

and engineers, allowing them to perform these tests using commonly available shaking tables and facilities. Additionally, the method must be easy to implement and manage, especially during rapid dynamic tests like shaking table experiments.

The proposed method is based on the concept of transforming hydrodynamic effects into modified ground motion acceleration, which is then used as the input signal for shaking table tests. This approach utilizes analytical formulations of earthquake-induced hydrodynamic pressures within the fluid domain, allowing for the consideration of both compressible and incompressible water behavior in the experiments. Furthermore, the use of the added mass concept to represent hydrodynamic effects in the reservoir is also feasible, providing flexibility in modeling structure-water interaction. Additionally, it enables the inclusion of various water level assumptions for experimental tests, enhancing the method's adaptability to different scenarios.

1.4.5 Implementation of the proposed method and validation using any standard engineering software

The application of the proposed methods for seismic analysis of dam-reservoir systems and axisymmetric structures surrounded by water, utilizing modal time history and response spectrum analyses, is demonstrated using any standard structural engineering software. The process includes applying the modified ground motion accelerations and conducting time history modal superposition and response spectrum analyses and provide a guideline for setting up numerical models of dam-reservoir systems and axisymmetric structures. The accuracy and effectiveness of these methods are validated by comparing the obtained results from the software with those from more complex coupled structure-water finite element models. A series of numerical case studies on different types of structure-water systems are conducted to ensure comprehensive validation, focusing on key response indicators such as displacements, stresses, and modal contributions. The case studies are documented to highlight procedures, findings, and comparisons, demonstrating the feasibility and efficiency of using the proposed methods with any standard structural engineering software. This approach significantly reduces computational demand and eliminates the need for specialized software, making the simplified methods readily adoptable in day-to-day engineering practice.

1.5 Main contributions and their originality

This research makes several contributions in the fields of numerical modeling and experimental simulation of structure-water systems and their appurtenant structures. These contributions are both novel and important, filling crucial gaps in the seismic analysis of these

systems. The key contributions are summarized as follows:

Firstly, a simplified approach for conducting time-history modal superposition and response spectrum analyses of dam-reservoir systems is proposed. This method directly accounts for higher mode effects, eliminating the need for static correction and specialized software. Secondly, the modified ground acceleration method is extended to axisymmetric water-surrounded structures such as intake towers and offshore wind turbines. An alternative approach for representing hydrodynamic added masses is also developed. This method incorporates added masses directly into the modified ground motion time-history or spectral accelerations for both dam-reservoir systems and axisymmetric structures, simplifying the analysis process. Additionally, the proposed methods are integrated into standard structural engineering software like SAP2000. This integration includes creating user-friendly guidelines and validating the methods through comprehensive case studies, ensuring practical applicability and reliability.

A new approach for conducting shaking table tests of structure-water systems and their appurtenant structures is introduced, using modified ground motion acceleration to assess the seismic response of these structures. This method allows for safe and effective testing on standard shake table facilities without the need for water or specialized equipment. The proposed methods are validated through comparative analysis with more complex coupled structure-water finite element models.

1.6 Organization of this thesis

Following this introduction, a comprehensive literature review is presented, updating the current state of research on the seismic response of structure-water systems and their appurtenant structures. This review covers existing analytical, finite element, and experimental methods, highlighting their strengths and limitations. This study aims to address the shortcomings in existing numerical and experimental methods. The following two chapters contain work that was published in international peer-reviewed journals: Journal of Earthquake Spectra (Chapter 3), published on June 16, 2024, and Journal of Ocean Engineering (Chapter 4), published on July 15, 2024. Chapter 3 presents the proposed method, detailing the procedures for time-history modal superposition and response spectrum analyses that account for higher mode effects for dam-reservoir systems. Chapter 4 extends this method to axisymmetric structures surrounded by water. Chapter 5 introduces an innovative shaking table test for evaluating the seismic response of an axisymmetric structure-water system and its appurtenant structure using modified ground motion acceleration. Additionally, another peer-reviewed journal paper is in press in the Journal of Engineering Structure but is not in-

cluded in this thesis. This paper extends the proposed modified ground acceleration method to liquid storage tanks and navigation lock chambers. Furthermore, three conference papers (12NCEE, USSD2023, and WCEE2024) have been published based on the proposed methods. These papers are not included in this thesis. Chapter 6 provides a comprehensive discussion of the proposed seismic analysis method for structure-water systems using modified ground motion acceleration. It focuses on the numerical validation of the method, its practical application with general-purpose structural engineering software, and experimental considerations for shaking table tests on structure-water systems. The chapter validates the method by examining how structural flexibility and water levels influence and amplify the modified ground acceleration, altering its frequency content. A detailed mathematical derivation of the closed-form equation for modified ground acceleration, considering the fundamental mode, is included. Practical applications of the method are demonstrated using general-purpose software, such as SAP2000, to conduct seismic analyses of dam-reservoir systems and axisymmetric structures surrounded by water. These examples showcase how hydrodynamic effects can be effectively incorporated without requiring a fluid domain. The experimental considerations for shaking table tests are addressed, focusing on an axisymmetric structure surrounded by water as the primary structure. The rationale for selecting an axisymmetric structure, the effects of low damping on modified ground acceleration, and critical factors for achieving accurate results under these conditions are thoroughly discussed. The thesis concludes with a summary of the key findings, contributions, and potential directions for future research.

CHAPTER 2 LITERATURE REVIEW

2.1 Introduction

Structure-water systems, such as dam-reservoir systems and axisymmetric structures surrounded by water, play a vital role in energy production, water management, transportation. The failure of these structures as a result of seismic events can lead to catastrophic consequences, highlighting the critical need for reliable analysis and design to ensure public safety and environmental protection.

Two types of structure-water systems are the focus of this research: dam-reservoir systems and axisymmetric structures surrounded by water. Dam-reservoir systems are critical for water storage, flood control, and hydroelectric power generation, while axisymmetric structures, including intake towers, offshore wind turbines, and bridge piers, are integral to various engineering applications, including wind energy production and transportation infrastructure. Both types of structures are subjected to complex interactions between the water and the structure during seismic events, necessitating advanced numerical and experimental techniques to accurately analyze and design such structures.

While numerical methods for analyzing structure-water systems have significantly advanced with the increase in computational power, simplified methods remain popular among engineers due to their ease of use, particularly in the early design stages or when assessing existing structures. Aside from numerical analyses, experimental investigations are equally important, particularly for understanding the behaviour of structure-water systems and their appurtenant structures fixed on the top of primary structure-water systems. These appurtenant structures, can experience significant amplified seismic responses due to the flexibility of the primary structure and the influence of hydrodynamic effects. Therefore, it is essential to incorporate both the flexibility of the primary structure and the hydrodynamic effects in experimental tests to accurately assess the seismic response of these appurtenant structures.

In this section, a comprehensive review of the seismic analysis of dam-reservoir systems and axisymmetric structures surrounded by water will be presented, including robust analysis techniques and simplified methods. Additionally, a literature review of experimental studies focusing on shaking table tests for these systems will be provided. This review section aims to highlight the current state of research, identify gaps in knowledge, and underscore the need for the innovative and alternative approaches proposed in this thesis.

2.2 Seismic analysis of dam-reservoir systems

The potential failure of dam-reservoir systems poses a significant threat to populations, leading to the establishment of federal or provincial agencies worldwide to ensure the safe construction and operation of these structures. In Canada, the responsibility for dam management falls to the provinces, many of which have enacted legislative measures to regulate dam safety, such as Quebec's regulations in effect since April 2002. Ministerial agencies, such as the Centre d'expertise hydrique de Québec (CEHQ), oversee the compliance of structures with safety standards. In the United States, the Federal Emergency Management Agency (FEMA) aims to mitigate the risks associated with dam failure. To support these agencies and structure owners, several guidelines have been developed (e.g. ACB [69]; FEMA [70]; FERC [71]; Hydro-Québec [72]; CSB [73]; USBR [74]) based on extensive research.

Earthquakes pose a significant risk to dam-reservoir systems, prompting extensive research since the 1930s to understand the dynamic behavior of these type of structures. Various analytical and numerical methods, both frequency domain-based and time domain-based, have been developed to account for the flexibility of structures, the compressibility of water, and energy dissipation due to sediment deposition. Some methods have been validated through in situ forced vibration tests [75] or laboratory simulations [76]. Research has explored several nonlinear phenomena affecting seismic behavior, including the effect of cracking during earthquakes [77, 78], the variation of uplift pressures in seismic cracks [76], and cavitation caused by hydrodynamic pressure [79, 80].

While the literature is rich with publications and studies on these systems, this chapter will focus only on the most relevant aspects for the studies presented in the following sections. First, a review of research on the analytical approach will be presented, followed by a detailed discussion of the finite element approach, which serves as one of the primary method used as a reference solution in this study. Finally, simplified methods will be discussed, highlighting their importance and ongoing development in making seismic analysis more accessible and reliable for practical applications.

2.2.1 Analytical methods

Analytical methods are generally constrained by the complexity of the geometry and the governing equations of the study domain. This limitation often restricts these methods to two-dimensional (2D) analyses, which are justified when the dimensions of the problem and its behavior comply with plane stress or plane strain conditions. The first notable analytical method was developed by Westergaard in 1933 [21], who explicitly considered the

effect of hydrodynamic pressure acting on a dam subjected to an earthquake. His pioneering research introduced the concept of added masses, which simplifies the problem by considering the inertia of the water mass as an added load on the dam. This concept has become a foundational element in the study of dam-reservoir interactions and will be reviewed in detail later in this chapter [21].

Since Westergaard's initial work, significant advancements have been made to incorporate additional parameters that affect hydrodynamic pressure and, consequently, the dynamic response of dams. For instance, Chopra's studies in the late 1960s provided analytical solutions that considered the compressibility of water, highlighting that neglecting this factor could introduce errors in seismic response of the dam [22, 81]. These studies paved the way for more sophisticated analyses that account for various dynamic interactions within the dam-reservoir system. Further developments include the work of Chakrabarti and Chopra in 1973, who incorporated hydrodynamic interaction into the earthquake analyses of gravity dams, using analytical methods to represent the dam and treating the reservoir as a continuum governed by the wave equation [23].

In the 1980s, Liu and Cheng improved boundary solutions for fluid-structure interaction, addressing infinite reservoir boundary conditions. Their work provided a more realistic representation of the dam-reservoir interaction by considering the effects of sediment layers and slight desaturation of pore water on hydrodynamic response curves [28]. Additionally, Fenves and Chopra contributed notably during this period. They developed analytical formulations for the seismic analysis of concrete gravity dams and implemented these formulations into computer programs, facilitating practical application for engineers. Their work also included the development of simplified methods based on these analytical formulations, which streamlined the process of evaluating dam safety under seismic loads [26, 29].

In the 1990s and 2000s, analytical methods continued to evolve with contributions from researchers like Maity and Bhattacharyya, who introduced far-boundary conditions for time-domain analyses [82], and Bouaanani et al., who developed models to account for the effects of ice covers [83–85] and proposed closed-form formulations for computing earthquake-induced hydrodynamic pressure on gravity dams [86].

In the 2010s, there was a focus on simplifying analytical formulations for day-to-day engineering practice. Bouaanani and Miquel [87] developed simplified evaluation methods for the vibration period and seismic response of gravity dam-water systems, aiming to make seismic analysis more practical without sacrificing accuracy. Miquel and Bouaanani proposed a method to transfer hydrodynamic pressure into a modified version of original ground acceleration based on analytical formulations, focusing on direct integration time-history dynamic

analysis of dam-reservoir systems [4].

All the analytical approaches mentioned above, are based on a substructure technique, where the fluid and structure domains interact at dam-foundation interface. In these methods, the flexibility of the dam, the compressibility of water, dam-foundation interaction, and wave absorption at the bottom of the reservoir are considered in the analysis (as illustrated in Figure 2.1). The equations governing the behavior of the dam-foundation system are obtained by writing the force equilibrium and displacement compatibility at the interface. To reduce the number of degrees of freedom, and thus the number of equations to solve, the approach based on the Ritz concept is used.

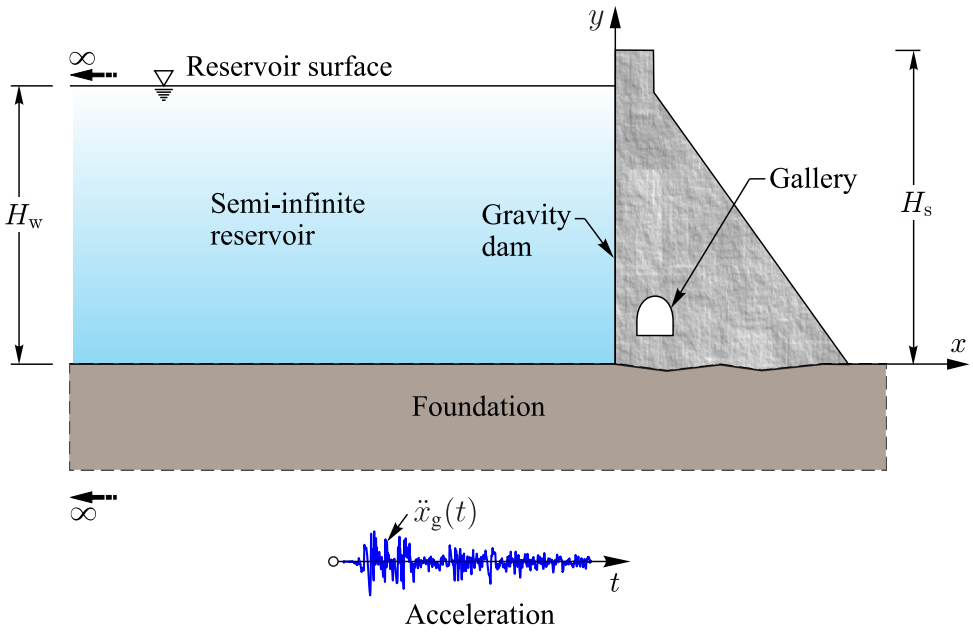

Figure 2.1 Gravity dam-reservoir-foundation system.

Assuming rigid and massless foundation, the equations of motion of a dam-reservoir system subjected to horizontal ground motion acceleration $\ddot{x}_g(t)$ can be expressed as [2, 26]

$$\mathbf{M}\,\ddot{\widehat{\mathbf{U}}}(t) + \mathbf{C}\,\dot{\widehat{\mathbf{U}}}(t) + \mathbf{K}\,\widehat{\mathbf{U}}(t) = -\mathbf{M}\,\mathbf{1}^{(x)}\,\ddot{x}_g(t) + \mathbf{F}_h(t) \tag{2.1}$$

in which $\ddot{\widehat{\mathbf{U}}}(t)$, $\dot{\widehat{\mathbf{U}}}(t)$ and $\widehat{\mathbf{U}}(t)$ are column-vectors containing the time-history nodal accelerations, velocities and displacements of the structural nodes of relative to the ground, respectively. $\mathbf{M}$, $\mathbf{C}$ and $\mathbf{K}$ are the structure's mass, damping and stiffness matrices, respectively, $\mathbf{1}^{(x)}$ is a column-vector containing zeros except along horizontal degrees of freedom corresponding to earthquake direction, and $\mathbf{F}_h(t)$ is a column-vector representing earthquake-induced hydrodynamic forces on the structure. Using modal analysis including N_s structural modes,

the horizontal relative displacement and acceleration at a point of coordinate (x, y) of the structure can be approximated as

$$\widehat{u}(x,y,t) = \sum_{j=1}^{N_\mathrm{s}} \widehat{u}_j(x,y,t) = \sum_{j=1}^{N_\mathrm{s}} \widehat{Z}_j(t)\, \psi_j^{(x)}(x,y) \tag{2.2}$$

$$\ddot{\widehat{u}}(x,y,t) = \sum_{j=1}^{N_\mathrm{s}} \ddot{\widehat{u}}_j(x,y,t) = \sum_{j=1}^{N_\mathrm{s}} \ddot{\widehat{Z}}_j(t)\, \psi_j^{(x)}(x,y) \tag{2.3}$$

where $\psi_j^{(x)}(x,y)$ denotes the x–component of the fundamental structural mode shape and $\widehat{Z}_j$ the associated generalized modal coordinate. modal coordinates $\widehat{Z}_j$ corresponding to the dam-reservoir system is obtained by solving the system of equations [26, 41]

$$\widehat{\mathbf{S}}\, \widehat{\mathbf{Z}} = \widehat{\mathbf{Q}} \tag{2.4}$$

in which the elements of the matrix $\widehat{\mathbf{S}}$ and vector $\widehat{\mathbf{Q}}$ are given for $m = 1 \ldots N_\mathrm{s}$ and $j = 1 \ldots N_\mathrm{s}$ as [26, 41]

$$\widehat{S}_{j,m}(\omega) = \Big(-\omega^2 + 2\,\mathrm{i}\,\xi_j\,\omega\,\omega_j + \omega_j^2 \Big)\, M_j\, \delta_{j,m} + \omega^2 \int_0^{H_\mathrm{w}} p_j(0,y,\omega)\, \psi_m^{(x)}(0,y)\, \mathrm{d}y \tag{2.5}$$

$$\widehat{Q}_m = -L_m + \int_0^{H_\mathrm{w}} p_0(0,y,\omega)\, \psi_m^{(x)}(0,y)\, \mathrm{d}y \tag{2.6}$$

where ξ_j and ω_j are the fraction of critical damping and the natural vibration frequency at mode j of the dam with empty reservoir, respectively. $\psi_j^{(x)}(0,y)$ is the x–component of the structural mode shape at the dam-reservoir interface. The generalized modal mass M_j and modal participation factor L_j of the dam with empty reservoir are given by [26, 41]

$$M_j = \iint \rho_\mathrm{s}(x,y) \left\{ \Big[\psi_j^{(x)}(x,y)\Big]^2 + \Big[\psi_j^{(y)}(x,y)\Big]^2 \right\} \mathrm{d}x\, \mathrm{d}y \approx \int_0^{H_\mathrm{s}} \mu_\mathrm{s}(y)\, \Big[\psi_j^{(x)}(0,y)\Big]^2\, \mathrm{d}y \tag{2.7}$$

$$L_j = \iint \rho_\mathrm{s}(x,y)\, \psi_j^{(x)}(x,y)\, \mathrm{d}x\, \mathrm{d}y \approx \int_0^{H_\mathrm{s}} \mu_\mathrm{s}(y)\, \psi_j^{(x)}(0,y)\, \mathrm{d}y \tag{2.8}$$

with p_0 denoting the hydrodynamic pressure FRF at *rigid* dam-reservoir interface due to horizontal ground motion $\ddot{x}_\mathrm{g}$ and p_j the hydrodynamic pressure FRF at *flexible* dam-reservoir interface due to horizontal acceleration $\psi_j^{(x)}(0,y)$ of the structure [26, 41]. The hydrodynamic pressure is obtained by solving wave equation [3, 26]

$$\nabla^2 p = \frac{1}{C_\mathrm{w}^2} \frac{\partial^2 p}{\partial t^2} \tag{2.9}$$

where ∇^2 denoting the Laplace differential operator, t the time variable, ρ_w the mass density of water and C_w is compression wave velocity within the reservoir (i.e. $C_\mathrm{w} = \sqrt{\mu_\mathrm{w}/\rho_\mathrm{w}}$, with

μ_{w} denoting the bulk modulus of water). Considering a unit harmonic horizontal ground motion $\ddot{x}_{\mathrm{g}}(t) = \mathrm{e}^{\mathrm{i}\omega t}$, the displacements and hydrodynamic pressures can be expressed in terms of the complex Frequency Response Functions (FRF), $\widehat{u}(x, y, \omega)$ and $p(x, y, \omega)$: $\widehat{u}(x, y, t) = \widehat{u}(x, y, \omega)\, \mathrm{e}^{\mathrm{i}\omega t}$ and $p(x, y, t) = p(x, y, \omega)\, \mathrm{e}^{\mathrm{i}\omega t}$. By introducing this transformation into equation (2.9), Helmholtz equation can be obtained as [26, 41]

$$\nabla^2 p(x, y, \omega) + \frac{\omega^2}{C_{\mathrm{w}}^2}\, p(x, y, \omega) = 0 \tag{2.10}$$

$$\frac{\partial^2}{\partial x^2}\, p(x, y, \omega) + \frac{\partial^2}{\partial y^2}\, p(x, y, \omega) + \frac{\omega^2}{C_{\mathrm{w}}^2}\, p(x, y, \omega) = 0 \tag{2.11}$$

One of the features of this analytical method is the coupling of the hydrodynamic pressure $p(x, y, \omega)$ to the generalized coordinates $\widehat{Z}_j(\omega)$, $(j = 1, \ldots, N_s)$ [26, 41]

$$p(x, y, \omega) = p_0(x, y, \omega) - \omega^2 \sum_{n=1}^{N_{\mathrm{s}}} \widehat{Z}_j(\omega)\, p_j(x, y, \omega) \tag{2.12}$$

The boundary conditions illustrated in Figure 2.2 are used for solving the Helmholtz equation to obtain the expressions for the pressures p_0 and p_j. The complex FRFs p_0 and p_j can be expressed as [26, 41]

$$p_0(0, y, \omega) = -2\rho_{\mathrm{w}} H_{\mathrm{w}} \sum_{n=1}^{N_{\mathrm{w}}} \frac{\lambda_n(\omega)^2\, I_{0,n}(\omega)}{\beta_n(\omega)\, \kappa_n(\omega)}\, Y_n(y, \omega) \tag{2.13}$$

$$p_j(0, y, \omega) = -2\rho_{\mathrm{w}} H_{\mathrm{w}} \sum_{n=1}^{N_{\mathrm{w}}} \frac{\lambda_n(\omega)^2\, I_{j,n}(\omega)}{\beta_n(\omega)\, \kappa_n(\omega)}\, Y_n(y, \omega) \tag{2.14}$$

where N_{w} is the number of water (i.e. acoustical) modes included in the analysis, and λ_n and Y_n are complex-valued frequency-dependent eigenvalues and orthogonal eigenfunctions satisfying for each reservoir acoustical mode n

$$\mathrm{e}^{2\mathrm{i}\lambda_n(\omega) H_{\mathrm{w}}} = -\frac{\lambda_n(\omega) - \omega q}{\lambda_n(\omega) + \omega q} \tag{2.15}$$

$$Y_n(y, \omega) = \frac{\Big[\lambda_n(\omega) - \omega q\Big]\mathrm{e}^{-\mathrm{i}\lambda_n(\omega)\, y} + \Big[\lambda_n(\omega) + \omega q\Big]\mathrm{e}^{\mathrm{i}\lambda_n(\omega)\, y}}{2\lambda_n(\omega)} \tag{2.16}$$

in which q is a damping coefficient defined at reservoir bottom as

$$q = \frac{\rho_{\mathrm{w}}}{\rho_{\mathrm{f}}\, C_{\mathrm{f}}} = \frac{1}{C_{\mathrm{w}}} \frac{1 - \alpha}{1 + \alpha} \tag{2.17}$$

where ρ_{f} and C_{f} denote the mass density and the compression wave velocity within the reservoir bottom foundation, respectively, C_{w} is compression wave velocity within the reservoir,

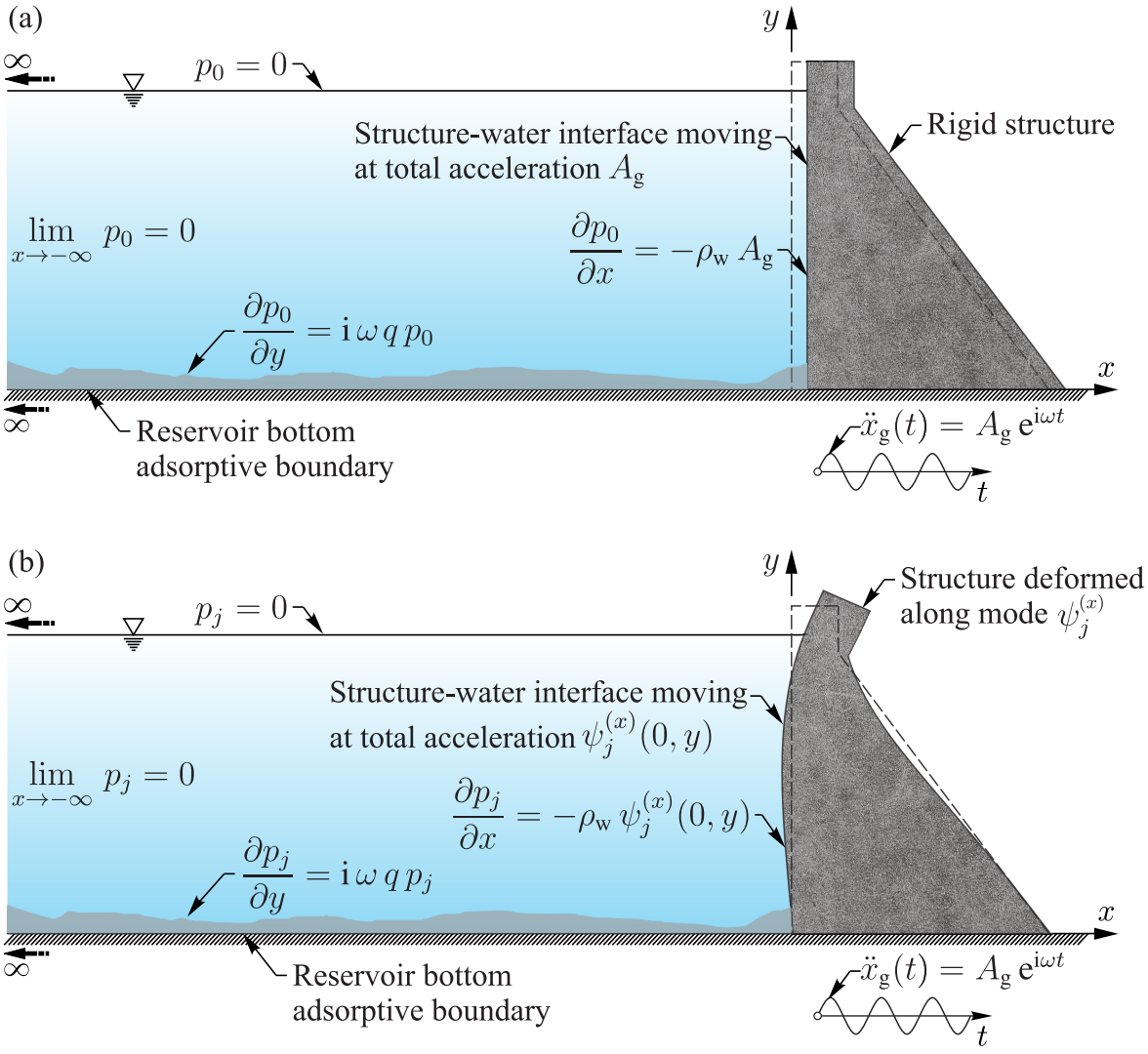

Figure 2.2 Dam-reservoir system and boundary conditions used for pressures: (a) p_0; (b) p_j.

and α is the wave reflection coefficient representing the portion of the wave amplitude reflected back to the reservoir. Instead of solving the transcendental equation (2.15), the eigenvalues λ_n can be approximated using the closed-form expression developed by Bouaanani and Perrault [41] for moderately to highly reflective reservoir bottoms, i.e. $\alpha \geqslant 0.65$

$$\lambda_n(\omega) = \frac{(2n-1)\pi}{4H_w} + \sqrt{\frac{(2n-1)^2\pi^2}{(4H_w)^2} + i\,\frac{\omega q}{H_w}} \tag{2.18}$$

If full wave reflection at reservoir bottom is assumed (i.e. $\alpha = 1$), the reservoir eigenvalues λ_n

are frequency-independent, simplifying to

$$\lambda_n = \frac{(2n-1)\,\pi}{2H_{\mathrm{w}}} \tag{2.19}$$

In this case, hydrodynamic pressure FRFs p_0 and p_j are expressed as

$$p_0(y,\omega) = \frac{-4\rho_{\mathrm{w}}}{\pi} \sum_{n=1}^{N_{\mathrm{w}}} \frac{(-1)^n}{(2n-1)} \frac{\cos(\lambda_n\, y)}{\sqrt{\lambda_n^2 - \dfrac{\omega^2}{C_{\mathrm{w}}^2}}} \tag{2.20}$$

$$p_j(y,\omega) = 2\rho_{\mathrm{w}} \sum_{n=1}^{N_{\mathrm{w}}} \frac{I_{j,n}(\omega)}{\sqrt{\lambda_n^2 - \dfrac{\omega^2}{C_{\mathrm{w}}^2}}} \cos\left(\lambda_n\, y\right) \tag{2.21}$$

The parameters β_n, κ_n, $I_{0,n}$, and $I_{j,n}$ in Eqs. (2.13) and (2.14) are given by [26, 41]

$$\beta_n(\omega) = H_{\mathrm{w}} \left[\lambda_n(\omega)^2 - \omega^2\, q^2\right] + \mathrm{i}\,\omega q\,; \qquad \kappa_n(\omega) = \sqrt{\lambda_n(\omega)^2 - \frac{\omega^2}{C_{\mathrm{w}}^2}} \tag{2.22}$$

$$I_{0,n}(\omega) = \frac{\mathrm{i}\,\mathrm{e}^{-\mathrm{i}\,\lambda_n(\omega) H_{\mathrm{w}}}}{\lambda_n(\omega)^2 H_{\mathrm{w}}} \left[\lambda_n(\omega) - \omega q + \omega q \mathrm{e}^{\mathrm{i}\lambda_n(\omega) H_{\mathrm{w}}}\right] \tag{2.23}$$

$$I_{j,n}(\omega) = \frac{1}{H_{\mathrm{w}}} \int_0^{H_{\mathrm{w}}} \psi_j^{(x)}(y)\, Y_n(y,\omega)\, \mathrm{d}y \tag{2.24}$$

Chopra and his collaborators demonstrated that the compressibility of water must be included if the ratio of the reservoir's resonance frequency ($\omega_0 = \pi\, C_{\mathrm{w}}/2H_{\mathrm{w}}$) to the resonance frequency of the structure is greater than 2, with H_{w} denoting the height of the reservoir [88]. This was further confirmed by Proulx and Paultre by comparing the results of in situ forced vibration tests to the predictions of the analytical method described here. They also validated the necessity of accounting for energy absorption due to sediment deposition at the bottom of the reservoir [75].

Solving the dynamic equation provides the expression for the generalized coordinate, which gives the Frequency Response Function (FRF) for the hydrodynamic pressure or displacement. By applying a Fourier transform, the time-domain response of the dam-reservoir system subjected to an earthquake can be obtained [26, 41].

2.2.2 Finite Element Methods

The Finite Element Method (FEM) has become increasingly popular for modeling the dynamic interaction of dam-foundation-reservoir systems. This approach discretizes the dif-

ferent substructures (domains) into solid or fluid finite elements, with interaction interfaces placed between these domains. FEM allows for detailed and accurate representation of the complex behaviors and interactions within the system. Since this technique is one of the most important methods used as a reference solution in this study, a more detailed description of these methods is provided in this section. Figure 2.3 illustrates a FEM of a dam-reservoir system, including the consideration of energy absorption at the bottom of the reservoir.

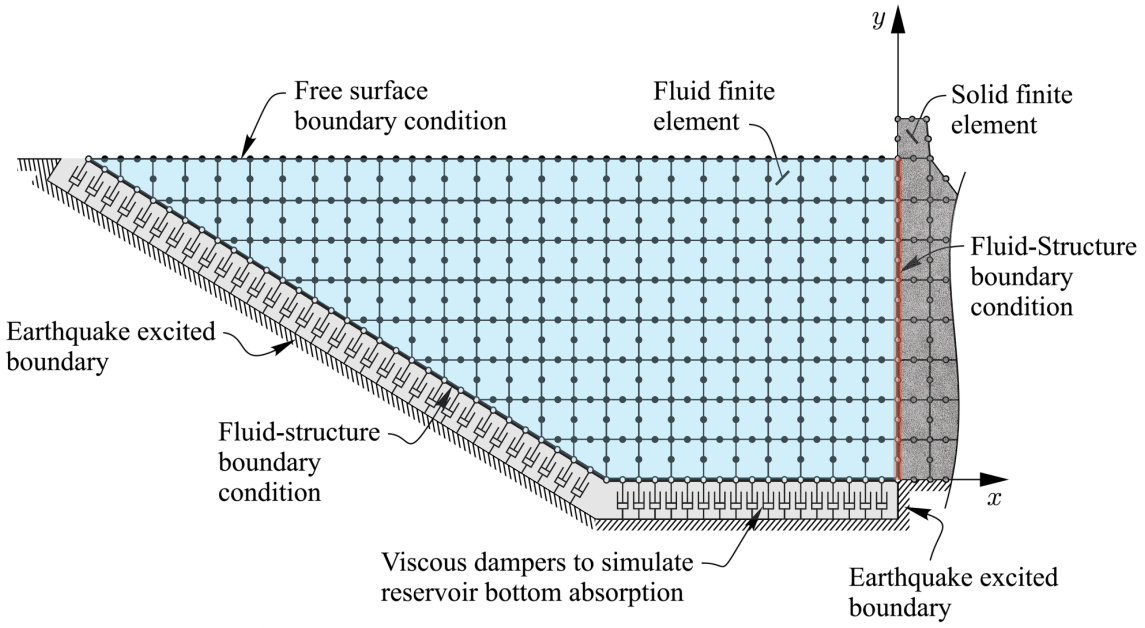

Figure 2.3 Finite element models of the dam-reservoir systems and corresponding boundary conditions [2].

Extensive research has been dedicated to formulate the fluid finite elements, distinguishing between the Lagrangian and Eulerian approaches. The Lagrangian formulation is an extension of the classical displacement-based finite element formulation developed for solid elements, meaning that the degrees of freedom for the fluid elements are the same as those for solid elements. However, fluid elements are characterized by a bulk modulus equal to the compressibility modulus of the fluid and a zero shear resistance to simulate inviscid flow. Compatibility at the fluid-structure interface is achieved by imposing the same normal displacements on the fluid and solid nodes superimposed at the fluid-structure interface. The Eulerian formulation, also known as the potential-based or pressure-based formulation, utilizes only one degree of freedom per element, thus significantly reducing the number of degrees of freedom in the system [89]. However, interface elements are necessary to ensure compatibility and equilibrium conditions at the fluid-structure interface, as shown by the red

line in Figure 2.3. These elements connect the fluid elements to the adjacent solid elements. Each node of these elements has a potential degree of freedom as well as displacement degrees of freedom. The Eulerian formulation (or potential-based approach) is particularly attractive in this field of study due to its ease of use, especially for complex problems. Many researchers have validated this approach through numerous numerical and experimental studies. In this study, potential-based elements are used for finite element models of coupled structure-water systems.

Potential-based formulation

In this method, the seismic response of the dam, including displacements and accelerations, is known as the $\phi - U$ formulation, where U represents displacements in the solid domain and ϕ denotes velocity potentials in the fluid domain. Assuming an irrotational water motion and infinitesimal velocity and density changes, implies the existence of a velocity potential ϕ satisfying the equations of continuity and energy conservation [50, 89]

$$\boldsymbol{\nabla}\phi = \mathbf{v}\,; \qquad \nabla^2\phi = -\frac{1}{\rho_{\mathrm{w}}}\frac{\partial p}{\partial t}\,; \qquad \frac{\partial p}{\partial t} = -\frac{p}{\rho_{\mathrm{w}}} \tag{2.25}$$

with $\boldsymbol{\nabla}$ is the vector gradient and $\mathbf{v}$ is the velocity vector of fluid particles. Then, the the wave equation transfers to

$$\nabla^2\phi = \frac{1}{C_{\mathrm{w}}^2}\frac{\partial^2\phi}{\partial t^2} \tag{2.26}$$

The velocity potential ϕ satisfies several boundary conditions: a free surface boundary condition, a compatibility boundary condition at the vibrating dam-reservoir interface [2, 29], and a radiation boundary condition to prevent wave reflection at the far upstream end of the reservoir [2, 90–92], which can be modeled using infinite fluid elements placed at the upstream end of the reservoir. Additionally, there is a boundary condition that accounts for energy dissipation at the reservoir bottom through one-dimensional partial wave absorption of incident compression waves normal to the reservoir-foundation interface [2, 25, 26], which can be achieved using viscous dampers placed at the reservoir bottom, as shown in Figure 2.3. Using the classical Galerkin discretization and other standard techniques, the coupling between the dam and reservoir substructures results in the following system of equations [2, 50, 91]

$$\begin{bmatrix} \mathbf{M}_{\mathrm{ss}} & \mathbf{0} \\ \mathbf{0} & -\mathbf{M}_{\mathrm{ww}} \end{bmatrix} \begin{bmatrix} \ddot{\mathbf{U}} \\ \ddot{\boldsymbol{\Phi}} \end{bmatrix} + \begin{bmatrix} \mathbf{C}_{\mathrm{ss}} & \mathbf{C}_{\mathrm{sw}} \\ \mathbf{C}_{\mathrm{ws}} & \mathbf{C}_{\mathrm{ww}} \end{bmatrix} \begin{bmatrix} \dot{\mathbf{U}} \\ \dot{\boldsymbol{\Phi}} \end{bmatrix} + \begin{bmatrix} \mathbf{K}_{\mathrm{ss}} & \mathbf{0} \\ \mathbf{0} & -\mathbf{K}_{\mathrm{ww}} \end{bmatrix} \begin{bmatrix} \mathbf{U} \\ \boldsymbol{\Phi} \end{bmatrix} = \begin{bmatrix} -\mathbf{M}_{\mathrm{ss}}\,\mathbf{1} \\ -\mathbf{C}_{\mathrm{sw}}\,\mathbf{1} \end{bmatrix} \begin{bmatrix} \ddot{x}_{\mathrm{g}}(t) \\ \dot{x}_{\mathrm{g}}(t) \end{bmatrix} \tag{2.27}$$

where $\mathbf{U}$ and $\boldsymbol{\Phi}$ are vectors containing nodal relative displacements and fluid potentials, $\mathbf{M}_{\mathrm{ss}}$ and $\mathbf{K}_{\mathrm{ss}}$ are the structural mass and stiffness matrices, respectively. $\mathbf{C}_{\mathrm{ss}}$ is a damping matrix

for the structure, which can be determined using Rayleigh damping, equivalent to a modal damping ξ_{s}, or hysteretic damping η_{s}. $\mathbf{M}_{\mathrm{ww}}$ and $\mathbf{K}_{\mathrm{ww}}$ are the potential and kinetic energy matrices of the impounded water, respectively. $\mathbf{C}_{\mathrm{sw}}$ is a matrix that couples the velocity potential to displacements on the structure-water interface. The matrix $\mathbf{C}_{\mathrm{ww}}$ accounts for damping due to energy dissipation at the reservoir bottom or at the far upstream boundary of the reservoir. $\ddot{x}_{\mathrm{g}}$ and $\dot{x}_{\mathrm{g}}$ are prescribed ground accelerations and velocities, and $\mathbf{1}$ is a column vector with the same dimension as $\mathbf{U}$, containing ones when a translational degree of freedom corresponds to the direction of earthquake excitation, and zero otherwise. These matrices can be calculated as [2]

$$\mathbf{M}_{\mathrm{ss}} = \rho_{\mathrm{s}} \int_{V_{\mathrm{s}}} \mathbf{N}_{\mathrm{s}}^{\mathsf{T}} \mathbf{N}_{\mathrm{s}} \, \mathrm{d}V \, ; \qquad \mathbf{M}_{\mathrm{ww}} = \frac{\rho_{\mathrm{w}}}{C_{\mathrm{w}}^2} \int_{V_{\mathrm{w}}} \mathbf{N}_{\mathrm{w}}^{\mathsf{T}} \mathbf{N}_{\mathrm{w}} \, \mathrm{d}V \tag{2.28}$$

$$\mathbf{K}_{\mathrm{ss}} = \rho_{\mathrm{s}} \int_{V_{\mathrm{s}}} \mathbf{N}_{\mathrm{s}}^{\mathsf{T}} \mathbf{D}_{\mathrm{s}}^{\mathsf{T}} \mathbf{N}_{\mathrm{s}} \, \mathrm{d}V \, ; \qquad \mathbf{K}_{\mathrm{ww}} = \rho_{\mathrm{w}} \int_{V_{\mathrm{w}}} \mathbf{B}_{\mathrm{w}}^{\mathsf{T}} \mathbf{B}_{\mathrm{w}} \, \mathrm{d}V \tag{2.29}$$

$$\mathbf{C}_{\mathrm{sw}} = -\rho_{\mathrm{w}} \int_{S_{\mathrm{s}}} \mathbf{N}_{\mathrm{s}}^{\mathsf{T}} \mathbf{n} \, \mathbf{N}_{\mathrm{w}} \, \mathrm{d}S \, ; \qquad \mathbf{C}_{\mathrm{ws}} = \mathbf{C}_{\mathrm{sw}}^{\mathsf{T}} \tag{2.30}$$

$$\mathbf{C}_{\mathrm{ss}} = \alpha \, \mathbf{M}_{\mathrm{ss}} + \beta \, \mathbf{K}_{\mathrm{ss}} \, ; \qquad \mathbf{C}_{\mathrm{ww}} = \rho_{\mathrm{w}} \, \hat{q} \int_{\hat{S}_{\mathrm{w}}} \mathbf{N}_{\mathrm{w}}^{\mathsf{T}} \mathbf{N}_{\mathrm{w}} \, \mathrm{d}S \tag{2.31}$$

in which $\mathbf{N}_{\mathrm{s}}$ and $\mathbf{N}_{\mathrm{w}}$ represent the standard isoparametric shape function matrices for the solid and fluid elements, respectively. V_{s} and V_{w} denote the volumes of the structure and the fluid, respectively. The matrix $\mathbf{D}_{\mathrm{s}}$ is the elasticity matrix for the solid elements, while $\mathbf{B}_{\mathrm{w}}$ for the fluid elements can be calculated as follows:

$$\mathbf{B}_{\mathrm{w}} = \begin{bmatrix} \dfrac{\partial N_{\mathrm{w}}^{(1)}}{\partial x} & \dfrac{\partial N_{\mathrm{w}}^{(2)}}{\partial x} & \cdots & \dfrac{\partial N_{\mathrm{w}}^{(n_{\mathrm{w}})}}{\partial x} \\ \dfrac{\partial N_{\mathrm{w}}^{(1)}}{\partial y} & \dfrac{\partial N_{\mathrm{w}}^{(2)}}{\partial y} & \cdots & \dfrac{\partial N_{\mathrm{w}}^{(n_{\mathrm{w}})}}{\partial y} \end{bmatrix} \tag{2.32}$$

where n_{w} denotes the number of nodes per fluid element. Earthquake loading can be applied either as a mass-proportional body force or as prescribed displacements imposed at the boundaries excited by the earthquake, as indicated in Figure 2.3. For reservoir bottom absorption, $\hat{S}_{\mathrm{w}}$ denotes the reservoir bottom boundary, and the damping coefficient $\hat{q}$ is set equal to q as given by Equation (2.17). The solution of Equation (2.27) yields the time-history response of the structure. Bouaanani and Lu evaluated the efficacy of potential-based fluid elements programmed in ADINA software [92] and compare the results with analytical formulation [2].

Transmitting Boundary Conditions (TBCs)

Due to the nearly infinite length of the reservoir, it is virtually truncated at a finite distance from the upstream face of the dam. A Transmitting Boundary Condition (TBC) must then be applied at this distance (i.e. L_{w}) to simulate the infinity of the reservoir, as shown in Figure 2.4. Correctly applying the boundary condition at the truncated location prevents the reflection of waves towards the dam. In practice, it is highly advantageous to minimize this truncation distance to limit the number of elements in the finite element model, thereby increasing the calculation speed. However, if the performance of the TBC is insufficient, using a truncation distance that is too short may introduce significant errors into the results. These

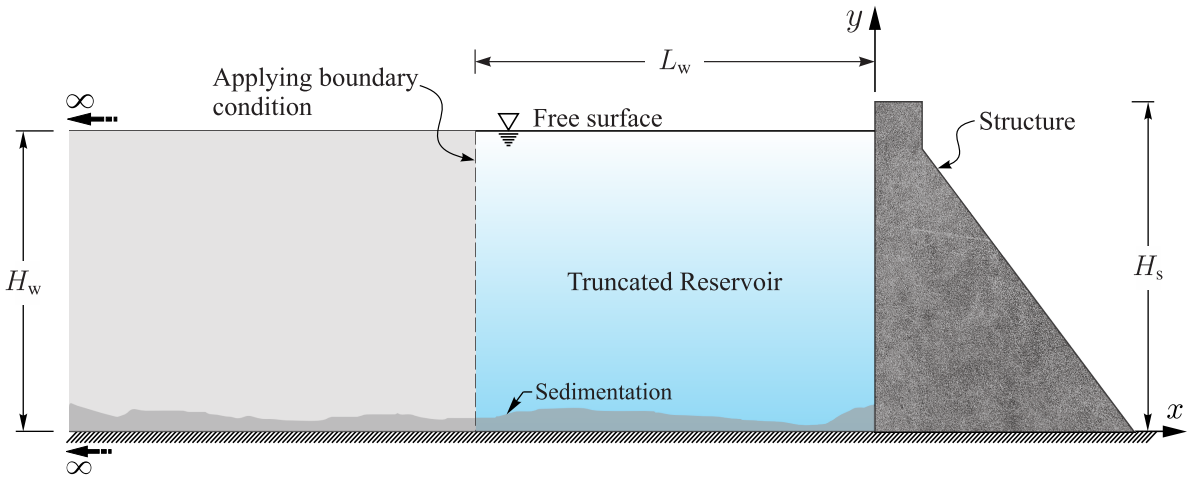

Figure 2.4 Dam retaining a truncated-length reservoir.

Transmitting Boundary Conditions (TBCs), denoted as θ, are mathematically defined by the relationship that links the hydrodynamic pressure to its normal gradient at the truncation boundary and can be expressed as [93]

$$\frac{\partial}{\partial x} p_0^{(\infty)}(-L_{\mathrm{w}}, y, \omega) = \theta_0^{(L_{\mathrm{w}})}(y, \omega)\, p_0^{(\infty)}(-L_{\mathrm{w}}, y, \omega) \tag{2.33}$$

$$\frac{\partial}{\partial x} p_j^{(\infty)}(-L_{\mathrm{w}}, y, \omega) = \theta_j^{(L_{\mathrm{w}})}(y, \omega)\, p_j^{(\infty)}(-L_{\mathrm{w}}, y, \omega) \tag{2.34}$$

where $\theta_0^{(L_{\mathrm{w}})}(y, \omega)$ and $\theta_j^{(L_{\mathrm{w}})}(y, \omega)$ represent the TBCs related to the rigid and flexible motion of the structure, respectively. Among the various TBCs documented in the literature, the Sommerfeld boundary condition is frequently employed, defined by [90]

$$\theta_0^{(L_{\mathrm{w}})}(y, \omega) = \theta_j^{(L_{\mathrm{w}})}(y, \omega) = \frac{\mathrm{i}\omega}{C_{\mathrm{w}}} \tag{2.35}$$

It can be readily implemented in finite element programs, as demonstrated by Bouaanani and Lu [2], and yields satisfactory results when positioned at a considerable distance from the dam. Humar and Jablonski developed a boundary condition assuming an infinitely rigid dam, which modifies Sommerfeld's condition and incorporated it into finite element software. The expression of their TBC varies depending on the excitation frequency [31]: (i) For $\omega = 0 \ldots \omega_0; \rightarrow \theta_0^{(L_\mathrm{w})} = 0$. This condition is equivalent to placing a rigid wall at the truncation boundary, or it can also be seen as Sommerfeld's condition where the compressibility of water is neglected. (ii) For $\omega = \omega_0 \ldots 3\,\omega_0; \rightarrow \theta_0^{(L_\mathrm{w})} = \mathrm{i}\omega/C_\mathrm{w}\sqrt{1-\omega_0^2/\omega}$. (iii) For $\omega > 3\,\omega_0$; $\theta_0^{(L_\mathrm{w})} = \mathrm{i}\omega/C_\mathrm{w}$, like Sommerfeld's condition. They showed that the proposed condition provides better results than Sommerfeld's for excitation frequencies between the first and second natural frequencies of the reservoir. In their study, the effect of wave absorption at the bottom of the reservoir was neglected. By neglecting the compressibility of water, Sharan developed a condition based on the analytical expression of hydrodynamic pressure in a reservoir in contact with a rigid dam and proposed a method to implement it in finite element software. the condition expressed $\theta_0^{(L_\mathrm{w})} = \pi/2H_\mathrm{w}$ [94]. He improved the method to include the compressibility of water, still neglecting wave absorption at the bottom of the reservoir. He confirmed that Sommerfeld's condition provides good results only if it is placed very far from the dam wall and if the excitation frequencies do not exceed the first natural frequency of the reservoir. Sharan extended the applicability his method to a flexible dam by dividing the reservoir into a near-field part close to the dam with arbitrary geometry and a far-field part of rectangular shape [95]. The dam and reservoir were modeled using finite elements, and his TBC, developed for a rigid dam, is applied at the far end of the reservoir. Finally, Sharan in later researches included the effect of wave absorption at the bottom of the reservoir and demonstrated that his new TBC provides excellent results for short truncation distances and a wide frequency range, except when the frequencies are close to the second and third natural frequencies of the reservoir [96].

All the previously mentioned conditions overlook the dam's flexibility and, consequently, do not consider its height. Maity and Bhattacharyya proposed a TBC that considers dam flexibility, making it dependent on the dam's height [82]. This approach assumes the bottom of the reservoir to be fully reflective and was implemented into finite element software. Gogoi and Maity later improved this formulation to include energy dissipation at the reservoir bottom based on a simplified analytical method developed by Bouaanani and Paultre [86,97]. TBCs are generally applied with approximations and only partially absorb spurious waves, thereby introducing an error in the dynamic response of the system. This error must be minimized using the analyst's experience and judgment. Bouaanani and Miquel proposed error estimators to validate TBCs in fluid-structure interaction problems [93]. These error

estimators are based on a formulation of the dynamic response of fluid-structure systems that include TBCs and take into account several factors, such as the structure's flexibility, fluid compressibility, energy dissipation at fluid boundaries, fluid domain truncation length, and excitation frequency [93] .

Noble conducted an in-depth study on various methods for modeling fluid-structure and soil-structure interaction using the Finite Element Method [80]. A comprehensive guide discussing nonlinear dynamic finite element modeling approaches and analysis procedures for concrete gravity dams is also available in the literature [35, 79, 98, 99].

2.2.3 Simplified Methods

Finite element models of structure-water system can be computationally intensive and time-consuming, particularly when considering the effects of fluid-structure interaction and soil-structure interaction. For practical engineering applications, simplified procedures are often preferred to evaluate the seismic response of concrete gravity dams, especially in the preliminary design phase. Simplified methods aim to reduce the complexity and computational demand while maintaining reasonable accuracy in calculating the dam's seismic response.

Pseudo-static method or added mass method

One commonly used approach is the added mass method, which approximates the hydrodynamic effects of the reservoir. This method, initially proposed by Westergaard, remains popular due to its simplicity and effectiveness for preliminary design and assessments. Westergaard proposed a simplified formula for calculating the maximum hydrodynamic pressure, acting as added mass per unit height of the dam that can be expressed as [21]

$$m_a(y) = \frac{7}{8}\,\rho_{\mathrm{w}}\,\sqrt{H_{\mathrm{w}}(H_{\mathrm{w}} - y)} \tag{2.36}$$

This added mass can be lumped on the nodes of the dam's face using the tributary method, as shown in Figure 2.5:

$$\widehat{M}_i(y) = v_i \times m_a = \frac{7}{8}\,\rho_{\mathrm{w}}\,v_i\,\sqrt{H_{\mathrm{w}}(H_{\mathrm{w}} - y)} \tag{2.37}$$

where v_i represents the tributary volume of water at node i. This method neglects the hydrodynamic pressure due to the flexibility of the structure and assumes water to be incompressible. However, water compressibility can be included in this method by introducing

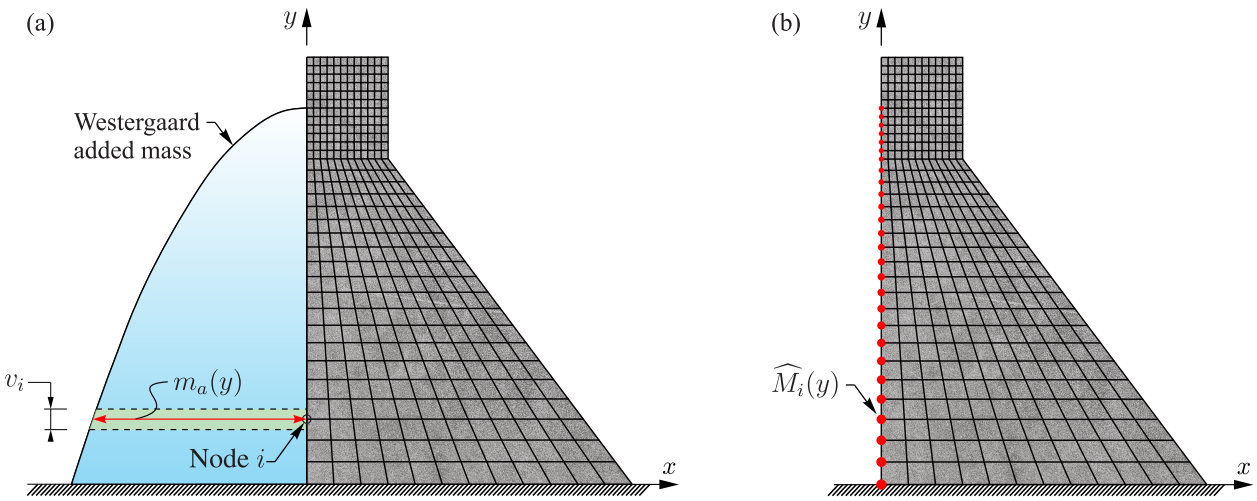

Figure 2.5 Representation of hydrodynamic effects using simplified Westergaard's added mass: (a) hydrodynamic pressure or added mass per unit height of the dam; (b) distribution of concentrated masses at the nodes of the dam-reservoir interface.

the parameter C_e into the Equation (2.37)

$$\widehat{M}_i(y) = v_i \times m_a = \frac{7}{8}\,\rho_w\, C_e\, v_i \sqrt{H_w(H_w - y)}\,; \qquad C_e = \frac{1}{\sqrt{\left[1 - 7.75\left(\frac{H_w}{1000\,T}\right)^2\right]}} \tag{2.38}$$

with T is the excitation period. One of the major advantages of the added mass method is that these masses are independent of the vibration period. Therefore, when applying the correction for the compressibility of water, the value of T is set to the average period of the design accelerogram. Although these developments are based on very simplified assumptions, this method remains widely used due to its simplicity. Several researchers, such as Corns and his colleagues have proposed other correction factors to approximately account for the compressibility of water and to consider a non-zero slope of the upstream face of the dam [100].

It should be noted that while this technique is well-developed and easy to use, there are important aspects that require careful consideration. The lumping process involves extracting nodes and their coordinates at the dam's face and applying the tributary method. However, employing consistent mass matrices to transfer hydrodynamic added masses might yield more accurate results and should be addressed. Additionally, in modal time history analysis, modal damping should only apply to the structural mass and not to those hydrodynamic masses added on the face of the dam. Therefore, an alternative method that applies the same principles while avoiding these challenges can simplify the process, offering greater ease of use when employing such approaches.

Pseudo-dynamic method or response spectrum analysis

To further enhance the implementation of earthquake analysis of gravity dams on a routine basis in engineering practice, Fenves and Chopra proposed a simplified method to estimate a gravity dam's peak seismic response directly from an earthquake design spectrum [29, 101]. This technique models a gravity dam as an equivalent single degree of freedom (ESDOF) system to evaluate the fundamental mode response of the dam through equivalent lateral static forces and response spectrum analysis. This approach, also known as pseudo-dynamic analysis, is conceptually similar to pseudo-static analysis but includes the flexibility of the dam and the compressibility of water [29, 34, 88, 101]. They implemented a standard mode shape into the modal analysis, including only the fundamental mode. They observed that separating the effects of reservoir-dam and dam-foundation interactions does not significantly affect the results. They demonstrated that fluid-structure interaction and the effect of the foundations independently modify the vibration period and damping of the dam on a rigid foundation.

$$\widehat{T}_1 = R_{\mathrm{w}}\, R_{\mathrm{f}}\, T_1; \quad \widehat{\xi}_1 = \frac{1}{R_{\mathrm{w}}} \frac{1}{R_{\mathrm{f}}^3}\, \xi_1 + \xi_{\mathrm{w}} + \xi_{\mathrm{f}} \tag{2.39}$$

with $\widehat{T}_1$ and $\widehat{\xi}_1$ are the fundamental period and damping ratio of the dam-reservoir-foundation system, respectively. ξ_1, ξ_{f}, and ξ_{w} are the damping ratios of the dam, the foundations, and the added damping due to fluid-structure interaction, respectively. T_1 is fundamental period of the dam, R_{w} is a factor dependent on the properties of the dam, the water height, and energy absorption due to sediments, while R_{f} is a factor dependent on the properties of the dam and foundations. The peak response of the dam in its fundamental vibration mode, including dam-water-foundation interaction effects, can be estimated by static analysis of the dam alone subjected to equivalent static lateral forces acting on the upstream face of the dam [3, 29, 34, 88, 101]

$$\widehat{f}_1(y) = \frac{\widehat{L}_1}{\widehat{M}_1}\, S_{\mathrm{A}}^{[\ddot{x}_{\mathrm{g}}]}(\widehat{T}_1, \widehat{\xi}_1) \left\{ \mu_{\mathrm{s}}(y)\, \psi_1^{(x)}(0, y) - \mathrm{Re}\left[p_1(0, y, \widehat{T}_1) \right] \right\} \tag{2.40}$$

where $\widehat{M}_1$ and $\widehat{L}_1$ are the generalized mass and force of the dam-reservoir system, respectively. $S_{\mathrm{A}}^{[\ddot{x}_{\mathrm{g}}]}(\widehat{T}_1, \widehat{\xi}_1)$ is the pseudo-acceleration obtained from the design spectrum for the fundamental period and damping coefficient of the dam-reservoir-foundation system. $\mu_s(y)$ is the mass per unit height of the dam, $\psi_1^{(x)}(0, y)$ is the fundamental vibration mode the dry dam along excitation direction, and $\mathrm{Re}\left[p_1(0, y, \widehat{T}_1) \right]$ is the real-valued component of the complex-valued frequency response function (FRF) for the pressure due to the deformation of the dam in the shape of the fundamental mode shape at the dam-reservoir interface. The generalized mass

and force of the dam-reservoir system (i.e. $\widehat{M}_1$ and $\widehat{L}_1$) can be expressed as [3,29,34,86,88,101]

$$\widehat{M}_1 = M_1 + \int_0^{H_\mathrm{w}} \mathrm{Re}\left[p_1(0,y,\widehat{T}_1)\right] \psi_1^{(x)}(0,y)\,\mathrm{d}y\,; \quad \widehat{L}_1 = L_1 + \int_0^{H_\mathrm{w}} \mathrm{Re}\left[p_1(0,y,\widehat{T}_1)\right] \mathrm{d}y \quad (2.41)$$

with M_1 and L_1 representing the generalized mass and force of the dry dam, respectively. These can be calculated using Equations (2.7) and (2.8), considering only the fundamental mode (i.e., $j = 1$).

The effects of higher vibration modes were incorporated into the analysis using the static correction method [68]. This method approximates the pseudo-acceleration design spectrum ordinates at the higher mode periods by the zero-period ordinate, which corresponds to the peak ground acceleration. Based on these principles, the equivalent lateral earthquake forces associated with the higher vibration modes of dams, accounting for the presence of impounded water, can be expressed as [3, 29, 34, 86, 88, 101]

$$\begin{aligned}\widehat{f}_{sc}(y) = &\left|\ddot{x}_\mathrm{g}(t)\right|^{(\max)} \left\{\mu_s(y)\left[1 - \frac{L_1}{M_1}\psi_1^{(x)}(0,y)\right] - \right. \\ &\left. \left[p_0(0,y) + \frac{\mu_s(y)}{M_1}\,\psi_1^{(x)}(0,y) \int_0^{H_\mathrm{w}} \mathrm{Re}\left[p_0(0,y)\right]\,\psi_1^{(x)}(0,y)\mathrm{d}y\right]\right\}\end{aligned} \quad (2.42)$$

where $|\ddot{x}_\mathrm{g}(t)|^{(\max)}$ and $\mathrm{Re}[p_0(0,y)]$ are maximum absolute value of the ground acceleration and the real-valued component of the complex-valued hydrodynamic pressure due to the rigid motion of the dam, respectively.

Miquel and Bouaanani introduced a closed-form technique for accurately estimating the fundamental vibration period of gravity dams, including for hydrodynamic effects [3]. Their method involved simplifying analytical expressions and providing a systematic procedure to determine the fundamental period, as well as the corresponding added damping, force, and mass for vibrating dam-reservoir systems. This approach considered factors such as dam geometry and flexibility, water compressibility, and varying reservoir levels. Formulations were developed for both incompressible and compressible impounded water. They approximated the fundamental vibration frequency of the dam-reservoir system ($\widehat{\omega}_1$) by solving the eigenvalue equation as [3]

$$\widehat{\omega}_1^2\left[M_1 + B_1(\widehat{\omega}_1)\right] - K_1 = 0 \quad (2.43)$$

with

$$B_1(\widehat{\omega}_1) = B_{1,1}(\widehat{\omega}_1) + 4\rho_{\mathrm{w}} H_{\mathrm{s}}^2 \left\{ \widehat{\phi}(\frac{H_{\mathrm{w}}}{H_{\mathrm{s}}}) - \frac{1}{\pi^3}(\frac{H_{\mathrm{w}}}{H_{\mathrm{s}}})^2 \Big[2F_1(\frac{H_{\mathrm{w}}}{H_{\mathrm{s}}}) + \pi\, G_1(\frac{H_{\mathrm{w}}}{H_{\mathrm{s}}}) \Big]^2 \right\} \tag{2.44}$$

$$B_{1,1}(\widehat{\omega}_1) = 4\rho_{\mathrm{w}} H_{\mathrm{w}}^2 \frac{\Big[2F_1(\frac{H_{\mathrm{w}}}{H_{\mathrm{s}}}) + \pi\, G_1(\frac{H_{\mathrm{w}}}{H_{\mathrm{s}}}) \Big]^2}{\pi^2 \sqrt{1 - \widehat{\omega}_1^2/\omega_0^2}}\,; \qquad \omega_0 = \frac{\pi\, C_{\mathrm{w}}}{2H_{\mathrm{w}}} \tag{2.45}$$

$$\widetilde{\phi}(\frac{H_{\mathrm{w}}}{H_{\mathrm{s}}}) = (\frac{H_{\mathrm{w}}}{H_{\mathrm{s}}})^4 \Big\{ \gamma_1\, a_1^2 + \gamma_2\, a_1\, a_2 \frac{H_{\mathrm{w}}}{H_{\mathrm{s}}} + (\gamma_3\, a_2^2 + \gamma_4\, a_1\, a_3)(\frac{H_{\mathrm{w}}}{H_{\mathrm{s}}})^2 + \tag{2.46}$$

$$\gamma_5\, a_1\, a_3 (\frac{H_{\mathrm{w}}}{H_{\mathrm{s}}})^3 + \gamma_6\, a_3^2 (\frac{H_{\mathrm{w}}}{H_{\mathrm{s}}})^4 \Big\} \tag{2.47}$$

with coefficients γ_1 to γ_6 which can be find in [3].

a_1, a_2 and a_3 are coefficients of a cubic polynomial function that was defined to approximate the x-component of the dam fundamental mode shape $\psi_1^{(x)}$

$$\psi_1^{(x)}(0, y) = a_1 \frac{y}{H_{\mathrm{s}}} + a_2 \left(\frac{y}{H_{\mathrm{s}}} \right)^2 + a_3 \left(\frac{y}{H_{\mathrm{s}}} \right)^3 \tag{2.48}$$

where y is a coordinate varying along the height of the structure measured from its base. The coefficients a_1, a_2 and a_3 can be determined based on a finite element analysis (as illustrated in Figure 2.6) or fundamental mode shape of a standard gravity dam section proposed by Fenves and Chopra [101]. If water compressibility is neglected, the fundamental resonant frequency and period of the dam-reservoir system can be calculated as follows [3]

$$\widehat{\omega}_1 = \frac{\omega_1}{\sqrt{1 + \dfrac{4\rho_{\mathrm{w}}\, H_{\mathrm{s}}^2 \widehat{\phi}(H_{\mathrm{w}}/H_{\mathrm{s}})}{M_1}}}\,; \qquad \widehat{T}_1 = T_1 \sqrt{1 + \frac{4\rho_{\mathrm{w}}\, H_{\mathrm{s}}^2 \widehat{\phi}(H_{\mathrm{w}}/H_{\mathrm{s}})}{M_1}} \tag{2.49}$$

For the case of compressible water, they demonstrated that the fundamental vibration period could be calculated by solving a cubic equation. Simplified expressions to compute the equivalent lateral earthquake forces and the static correction forces were also provided, based on this simplified methods. Both the Response Spectrum Analysis methods proposed by Fenves and Chopra [101] and Miquel and Bouaanani [3] have been incorporated into CADAM software [102,103]. Developed by Martin Leclerc and Pierre Léger, CADAM is a user-friendly tool grounded in the gravity method and has been widely used for stability analyses of concrete hydraulic structures. The latest version, CADAM3D, is now available for use.

Although these methods have been widely used for many years in the elastic analysis phase of seismic design and safety evaluation of concrete gravity dams, there remains a need for

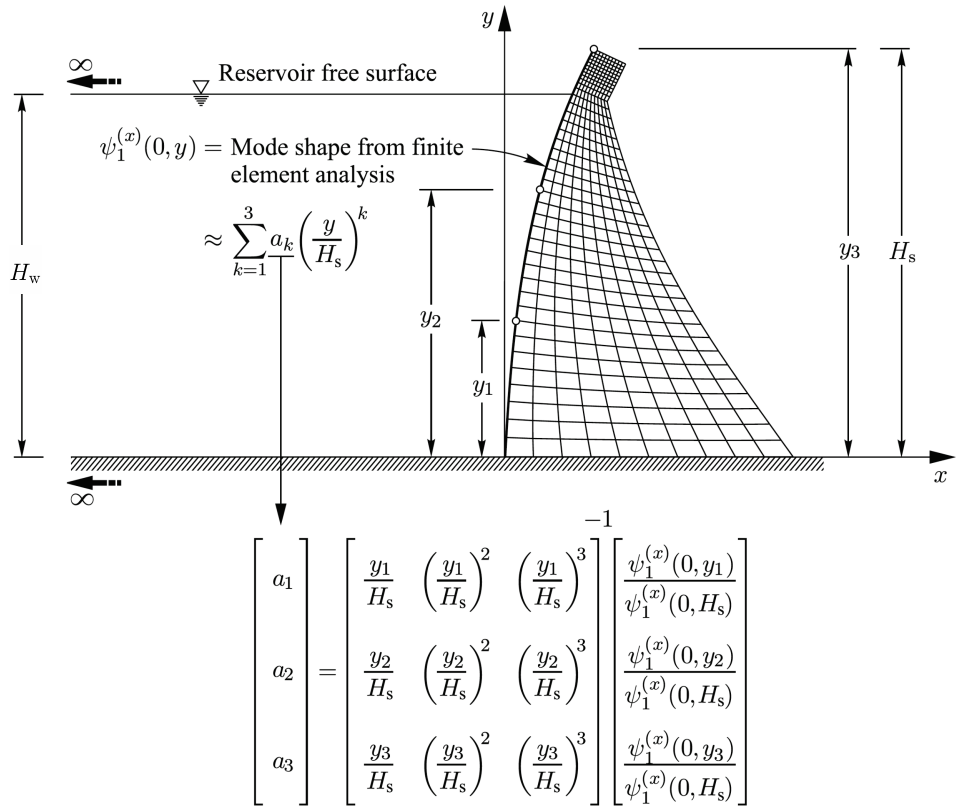

Figure 2.6 Approximation of the fundamental mode shape of a gravity dam [3].

improvement. Specifically, it is essential to incorporate the flexibility of higher modes in the response analysis, including hydrodynamic effects, rather than using static correction methods. This highlights that while current methods are effective, there is still considerable potential for improvement to better capture the complex dynamics of dam-reservoir systems using response spectrum method.

Time history dynamic analysis

Pseudo-dynamic analyses do not account for the oscillatory nature of the dynamic behavior of structures. If a pseudo-dynamic analysis indicates that certain locations of the structure may be subjected to internal forces exceeding allowable stresses, it is recommended to perform a dynamic analysis. Additionally, existing pseudo-dynamic analyses do not consider the dynamic effect of higher modes, which is particularly important for flexible structures that require proper consideration of these higher modes. In a pseudo-dynamic analysis, the direction of forces due to each mode is ignored. The response of the fundamental mode and that due to higher modes are combined using modal combination techniques (CQC, SRSS)

to calculate the total response, which introduces errors.

A time history dynamic analysis addresses these shortcomings and provides detailed information about the seismic response of the system. In practice, Westergaard's added masses are often used to perform this type of analysis by lumping hydrodynamic added masses on the dam-reservoir interface and performing time history analysis. However, this technique can lead to errors because these masses were developed without considering the compressibility of water and the flexibility of the structure. Therefore, using these added masses for a higher-level analysis is not justified. Time history analysis of dam-foundation-reservoir systems can also be performed using coupled finite element models through time history modal dynamic analysis or direct integration time history analysis. The dam-foundation-reservoir system, assumed to remain in the linear elastic domain, is subjected to ground seismic excitation based on the site-specific design spectrum, which may include horizontal and vertical components. However, such solutions generally require specialized software and a high level of expertise to obtain valid results. Proper modeling of the reservoir domain, fluid-structure interaction, and relevant boundary conditions can be challenging.

Miquel and Bouaanani proposed a simplified method to conduct time history analysis using a dry system (i.e. without water) to get the dam-reservoir responses [4]. This technique involves modifying the original ground acceleration to account for hydrodynamic effects, allowing for a more practical application of time history analysis in engineering practice (Figure 2.7). They

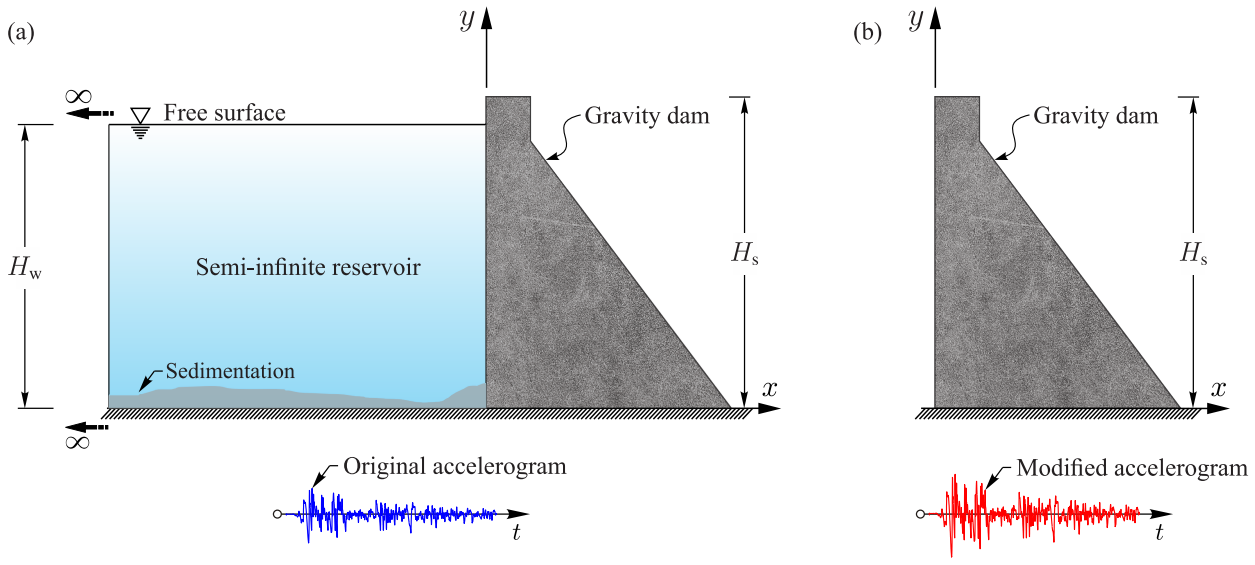

Figure 2.7 Gravity dam subjected to: (a) original ground acceleration which is applied to the dam-reservoir system; (b) modified ground acceleration which is applied to the dry dam [4].

proposed a mode- and coordinate-independent accelerogram $\widetilde{a}_g(\omega)$ by modifying the original

input ground acceleration $\ddot{x}_{\mathrm{g}}(\omega)$ as [4]

$$\widetilde{a}_{\mathrm{g}}(\omega) = \ddot{x}_{\mathrm{g}}(\omega)\, \frac{\sum_{j=1}^{N_{\mathrm{s}}} \widehat{Z}_j(\omega)}{\sum_{j=1}^{N_{\mathrm{s}}} Z_j(\omega)} \tag{2.50}$$

where the $\ddot{x}_{\mathrm{g}}(\omega)$ is Fourier transform of ground motion acceleration $\ddot{x}_{\mathrm{g}}(t)$ and given by

$$\ddot{x}_{\mathrm{g}}(\omega) = \int_0^{t_a} \ddot{x}_{\mathrm{g}}(t)\, \mathrm{e}^{-\mathrm{i}\omega t}\, \mathrm{d}t \tag{2.51}$$

in which t_a is the time duration of the applied accelerogram. In equation (2.50), $\widehat{Z}_j$ denoted the generalized coordinates of structure-water system and can be calculated using Equations (2.4). Z_j is the generalized coordinates of the structure without water and can be calculated as [4, 26, 41]

$$Z_j(\omega) = -\frac{L_j}{M_j} \times \frac{1}{\left(-\omega^2 + 2\,\mathrm{i}\,\xi_j\,\omega\,\omega_j + \omega_j^2 \right)} \tag{2.52}$$

Applying Fourier inverse transform to $\widetilde{a}_{\mathrm{g}}(\omega)$ yields the following modified time-history ground acceleration [4]

$$\widetilde{a}_{\mathrm{g}}(t) = \frac{1}{2\pi} \int_{-\infty}^{\infty} \widetilde{a}_{\mathrm{g}}(\omega)\, \mathrm{e}^{\mathrm{i}\omega t}\, \mathrm{d}\omega \tag{2.53}$$

To increase computational efficiency, a simplified method was proposed by their work to calculate generalized modal coordinate corresponding to each structural mode as [4]

$$\widehat{Z}_1(\omega) = \frac{\widetilde{S}_{2,2}(\omega)\, \widetilde{Q}_1(\omega) - \widetilde{S}_{1,2}(\omega)\, \widetilde{Q}_2(\omega)}{\widetilde{S}_{1,1}(\omega)\, \widetilde{S}_{2,2}(\omega) - \widetilde{S}_{1,2}^2(\omega)} \tag{2.54}$$

$$\widehat{Z}_j(\omega) = \frac{\widetilde{S}_{j-1,j-1}(\omega)\, \widetilde{Q}_j(\omega) - \widetilde{S}_{j-1,j}(\omega)\, \widetilde{Q}_{j-1}(\omega)}{\widetilde{S}_{j-1,j-1}(\omega)\, \widetilde{S}_{j,j}(\omega) - \widetilde{S}_{j-1,j}^2(\omega)} \qquad \text{for } j = 2 \ldots N_{\mathrm{s}} \tag{2.55}$$

Equations (2.54) and (2.55) are exact when only two modes are included in the analysis and approximations otherwise [4]. The technique used is based on the approach proposed by Bouaanani and Perrault [41].

They illustrated the application of this method by utilizing the modified ground accelerogram to perform a direct integration time history dynamic analysis, incorporating Rayleigh damping.Although using the modified accelerogram avoids the finite or boundary element discretization of the fluid domain and the direct modeling of related fluid-structure interaction forces and boundary conditions, this technique needs to be expanded to perform modal time history analysis to evaluate the effects of each mode on the total response of the sys-

tem. Since modified ground acceleration incorporates the effects of hydrodynamic pressure, including period elongation and damping in the dam-reservoir system, using it for response spectrum analysis offers a practical advantage. It eliminates the need to separately evaluate the vibration period and damping associated with the dam-reservoir system, which differ from those of a dam without a reservoir. Furthermore, extending this method to other types of structure-water systems is required to broaden its applicability and usefulness in practical engineering scenarios.

Other simplified methods

In the literature, several other simplified methods exist, particularly for calculating different hydrodynamic parameters. Hatanaka developed simplified expressions to estimate the fundamental frequency of a dam with an empty reservoir [104]. By considering beam theory, Okamoto proposed a simplified method to estimate the fundamental period of a dam-reservoir system [105]. Jafari and Khiavi conducted a parametric study on the modal behavior of concrete gravity dams using the finite element method [106]. Their study aimed to calculate natural frequencies and understand the first mode period of dams. Mohammadnezhad and his colleagues examined the seismic analysis of dam-foundation-reservoir systems, including the effects of foundation mass and radiation damping [107]. Their study highlighted the limitations of assuming a massless foundation in commercial software, emphasizing the need for more comprehensive modeling approaches. Løkke and Chopra introduced a direct finite element method for nonlinear earthquake analysis of concrete dams, focusing on simplification, modeling, and practical application [35]. Aldemir proposed prediction equations that include the effects of the dam body and valley geometry, utilizing a large database of numerical models. This study aimed to enhance the accuracy of predicting the fundamental period and mode shape of roller-compacted concrete gravity dams [108]. Qu and his colleagues presented a direct time-domain procedure for the seismic analysis of dam-foundation-reservoir systems using the scaled boundary finite element method [109]. Their method enhanced the accuracy and efficiency of seismic analyses by addressing the interactions between the dam, foundation, and reservoir within a single computational framework.

Hariri-Ardebili and Pourkamali-Anaraki proposed an automated machine learning engine with inverse analysis for the seismic design of dams [110]. Their approach aimed to optimize the dam cross-section, enhancing the efficiency and accuracy of seismic design processes through machine learning techniques. Guo and his colleagues combined ambient vibration measurements, advanced fluid-element methods, and modified engineering approaches for the modal analysis of an arch dam [111]. Their comprehensive approach provided detailed in-

sights into the dynamic characteristics of arch dams, including natural frequencies and mode shapes. Filho and his colleagues developed a polynomial response surface-based transformation function for improving the performance of low-fidelity models for concrete gravity dams [112]. Their probabilistic methods aimed to enhance the accuracy of seismic response predictions by refining low-fidelity models. The simplified methods also served as the basis for several investigations of the behavior of dam-reservoir systems. For example, Hariri-Ardebili and Saouma introduced a random simplified response spectrum method for gravity dams, utilizing equivalent static lateral forces to assess the seismic risk associated with these structures [39]. The authors also employed a numerical technique to assess the effects of uncertainties in input parameters on the results. Kita and his colleagues used Chopra's simplified method to investigate the effects of selecting a seismic hazard model on the assessment of the structural integrity of an existing dam ("Le Grazie") located in the high seismic risk region of Central Italy [113].

The development of simplified methods remains an active field of study, as researchers continue to improve techniques to simplified seismic evaluation of dam-reservoir systems for practical applications, especially in the early phases of the design of new dams or the assessment of existing dams. This ongoing effort highlights the necessity of developing more simplified techniques that not only provide easy-to-follow steps for performing analysis but also ensure accurate and reliable results.

2.3 Seismic analysis of axisymmetric structures surrounded by water

Axisymmetric structures surrounded by water are commonly found in various civil engineering applications, such as intake towers, offshore wind turbines, and bridge piers. When these systems are subjected to earthquake loads, the dynamic interaction between the structure and the surrounding water generates hydrodynamic loads, impacting the structural dynamic properties, including natural periods. The seismic analysis of axisymmetric structures involves additional complexity due to the geometry of the structure and the hydrodynamic pressure exerted all around the structure during an earthquake. In contrast to analysis of dam-reservoir system, there is no widely accepted method for response spectrum or pseudo-dynamic analysis using an Equivalent Single Degree of Freedom (ESDOF) system for axisymmetric structures surrounded by water that accurately incorporates hydrodynamic effects. Instead, the dynamic properties of these structures are typically calculated using the added mass method based on wave radiation theory or Morison's added mass formulation [47, 48, 114]. These techniques are then applied in response spectrum analysis to assess the seismic response of the system.

The seismic analysis of axisymmetric structures surrounded by water has been extensively studied in the literature. These studies can be broadly classified into three categories based on the modeling approach adopted for hydrodynamic loads: (i) analytical solutions using continuum-based methods, (ii) numerical methods involving finite element, boundary element, or scaled boundary finite element approaches, and (iii) simplified methods. This section reviews the significant contributions in each category and highlights the need for simplified and alternative methods that can be practically implemented in engineering practice.

2.3.1 Analytical methods

The early seismic analyses of structure-water systems, including axisymmetric structures surrounded by water, were based on the assumption of rigid body motion of structures in incompressible water [115, 116]. These studies introduced the concept of "added mass" of water, which moves with the structure during an earthquake, representing the hydrodynamic effects.

After systematic studies conducted on dam-reservoir systems during the 1960s, it became evident that the dynamic interaction between a flexible structure and the surrounding fluid can significantly influence the seismic response of the structure. It was also demonstrated that the impact of water compressibility on the system is important and depends on the dynamic properties of the structure relative to the reservoir [22, 23, 81].

Analytical solutions for hydrodynamic pressure that account for both water compressibility and dynamic interaction between a flexible structure and the surrounding fluid were proposed by Liaw and Chopra based on radiation wave theory [114]. The frequency response function for radial hydrodynamic pressure exerted at a point with coordinates $(r = R_\mathrm{s}, \theta = 0, z)$ at the outer surface of the structure, including higher vibration mode effects, can be decomposed as [6, 114]

$$p(R_\mathrm{s}, 0, z, \omega) = p_0(R_\mathrm{s}, 0, z, \omega) - \omega^2 \sum_{j=1}^{N_\mathrm{s}} \widehat{Z}_j(\omega)\, p_j(R_\mathrm{s}, 0, z, \omega) \tag{2.56}$$

with p_0 denoting the hydrodynamic pressure FRF at *rigid* structure-water interface due to horizontal ground motion $\ddot{x}_\mathrm{g}$ and p_j the hydrodynamic pressure FRF at *flexible* structure-water interface due to horizontal acceleration $\psi_j^{(x)}(R_\mathrm{s}, 0, z)$, $j = 1 \ldots N_\mathrm{s}$, with R_s representing the radius of the structure. $\widehat{Z}_j$ is the corresponding generalized coordinate of structure water system, and N_s is the total number of structural mode shapes along the x-direction which are included in the analysis. The radial hydrodynamic pressure responses in time and frequency domains at a point with coordinates $(r = R_s, \theta, z)$ on the exterior surface of the immersed structure can be derived from the radial hydrodynamic pressure as [6, 114]

$$p(R_\mathrm{s}, \theta, z, t) = p(R_\mathrm{s}, \theta = 0, z, t)\, \cos(\theta)\,; \qquad p(R_\mathrm{s}, \theta, z, \omega) = p(R_\mathrm{s}, \theta = 0, z, \omega)\, \cos(\theta) \tag{2.57}$$

The FRFs p_0 and p_j can be evaluated respecting the boundary conditions illustrated in Figures 2.8 and 2.9 and as [6, 114]

$$\begin{aligned} p_0(R_\mathrm{s}, \theta, z, \omega) = \frac{4\rho_\mathrm{w}}{H_\mathrm{w}} \Bigg[& -\sum_{n=1}^{\bar{n}-1} \frac{I_{0n}}{\kappa_n}\, \mathcal{D}_n(\kappa_n\, R_\mathrm{s}) \cos(\lambda_n z)\, \mathrm{e}^{\mathrm{i}\,\tau_n R_\mathrm{s}} \\ & + \sum_{n=\bar{n}}^{N_\mathrm{w}} \frac{I_{0n}}{\kappa'_n}\, \mathcal{E}_n(\kappa'_n\, R_\mathrm{s}) \cos(\lambda_n z) \Bigg] \cos(\theta) \end{aligned} \tag{2.58}$$

$$\begin{aligned} p_j(R_\mathrm{s}, \theta, z, \omega) = \frac{4\rho_\mathrm{w}}{H_\mathrm{w}} \Bigg[& -\sum_{n=1}^{\bar{n}-1} \frac{I_{jn}}{\kappa_n} \mathcal{D}_n(\kappa_n\, R_\mathrm{s}) \cos(\lambda_n z)\, \mathrm{e}^{\mathrm{i}\,\tau_n R_\mathrm{s}} \\ & + \sum_{n=\bar{n}}^{N_\mathrm{w}} \frac{I_{jn}}{\kappa'_n}\, \mathcal{E}_n(\kappa'_n\, R_\mathrm{s}) \cos(\lambda_n z) \Bigg] \cos(\theta) \end{aligned} \tag{2.59}$$

where N_w is the number of considered acoustical water modes, and the parameters λ_n, κ_n,

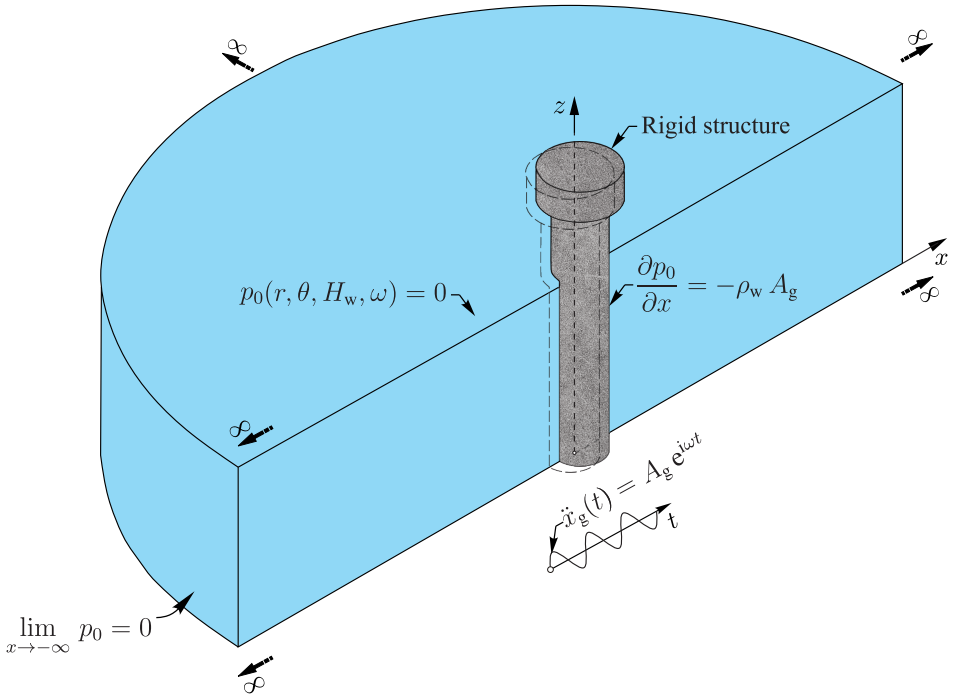

Figure 2.8 Boundary conditions for evaluating hydrodynamic pressure FRF p_0 at *rigid* structure-water interface due to horizontal ground motion $\ddot{x}_g$.

κ'_n, I_{0n}, I_{jn}, $\mathcal{D}_n$, $\mathcal{E}_n$ and τ_n are given by [6, 114]

$$\lambda_n = \frac{(2n-1)\,\pi}{2H_w}\,; \qquad \kappa_n = \sqrt{\frac{\omega^2}{C_w^2} - \lambda_n^2}\,; \qquad \kappa'_n = -\mathrm{i}\,\kappa_n \tag{2.60}$$

$$I_{0n} = -\frac{2H_w(-1)^n}{\pi(2n-1)}\,; \qquad I_{jn} = \int_0^{H_w} \psi_j^{(x)}(z)\,\cos(\lambda_n z)\,\mathrm{d}z \tag{2.61}$$

$$\mathcal{D}_n(\kappa_n R_s) = \sqrt{\frac{[\mathrm{J}_1(\kappa_n R_s)]^2 + [\mathrm{Y}_1(\kappa_n R_s)]^2}{[\mathrm{J}_0(\kappa_n R_s) - \mathrm{J}_2(\kappa_n R_s)]^2 + [\mathrm{Y}_0(\kappa_n R_s) - \mathrm{Y}_2(\kappa_n R_s)]^2}} \tag{2.62}$$

$$\mathcal{E}_n(\kappa'_n R_s) = \frac{\mathrm{K}_1(\kappa'_n R_s)}{\mathrm{K}_0(\kappa'_n R_s) + \mathrm{K}_2(\kappa'_n R_s)} \tag{2.63}$$

$$\tau_n R_s = \tan^{-1}\left\{\frac{[\mathrm{Y}_0(\kappa_n R_s) - \mathrm{Y}_2(\kappa_n R_s)]\,\mathrm{J}_1(\kappa_n R_s) - [\mathrm{J}_0(\kappa_n R_s) - \mathrm{J}_2(\kappa_n R_s)]\,\mathrm{Y}_1(\kappa_n R_s)}{[\mathrm{J}_0(\kappa_n R_s) - \mathrm{J}_2(\kappa_n R_s)]\,\mathrm{J}_1(\kappa_n R_s) + [\mathrm{Y}_0(\kappa_n R_s) - \mathrm{Y}_2(\kappa_n R_s)]\,\mathrm{Y}_1(\kappa_n R_s)}\right\} \tag{2.64}$$

in which K_ℓ is the modified Bessel function of order ℓ of the second kind and J_ℓ and Y_ℓ are the Bessel functions of order ℓ of the first and second kind, respectively. The integer $\bar{n}$ in the

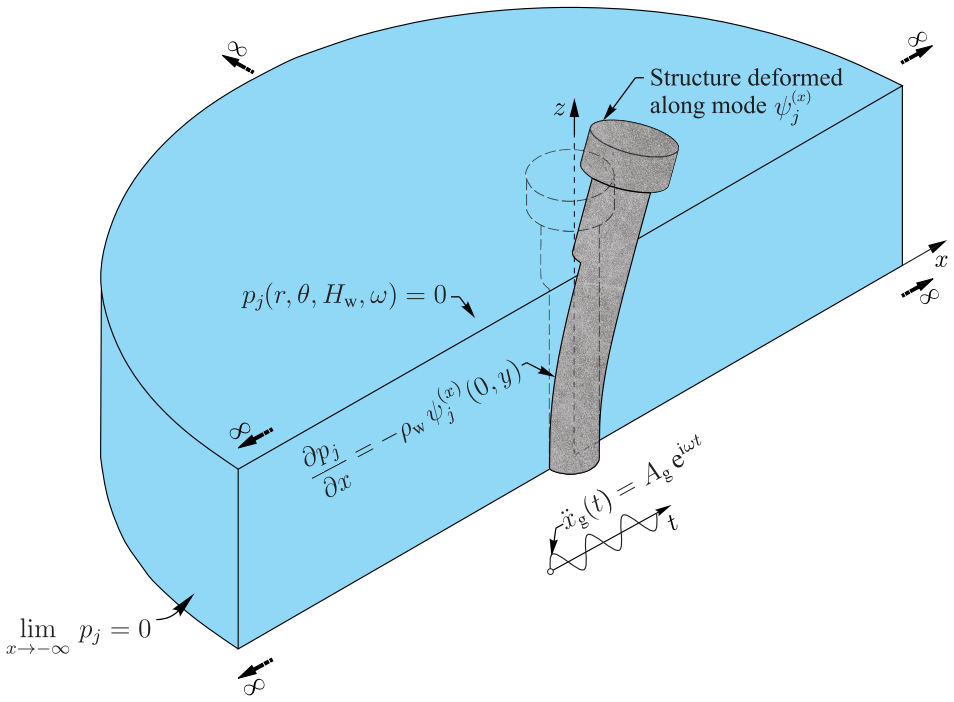

Figure 2.9 Boundary conditions for evaluating hydrodynamic pressure FRF p_j at *flexible* structure-water interface due to horizontal acceleration $\psi_j^{(x)}(R_s, 0, z)$, $j = 1 \ldots N_s$.

first sums of Eqs. (2.58) and (2.59) is the smallest value of integer n such that $\lambda_n > \dfrac{\omega}{C_w}$. We note that the first series in Eqs. (2.58) and (2.59) vanishes if $\bar{n} = 1$. If water compressibility is neglected, the frequency-independent hydrodynamic pressure solutions p_0 and p_j given by Eq. (2.58) and (2.59) can be simplified to [6, 114]

$$p_0(R_s, z, \theta) = \sum_{n=1}^{N_w} \frac{4\rho_w}{H_w} \frac{I_{0n}}{\kappa'_n} \mathcal{E}_n(\kappa'_n R_s) \cos(\lambda_n z) \cos(\theta) \tag{2.65}$$

$$p_j(R_s, z, \theta) = \sum_{n=1}^{N_w} \frac{4\rho_w}{H_w} \frac{I_{jn}}{\kappa'_n} \mathcal{E}_n(\kappa'_n R_s) \cos(\lambda_n z) \cos(\theta) \tag{2.66}$$

in which λ_n, I_{0n}, I_{jn} and $\mathcal{E}_n(\kappa'_n R_s)$ are given by Eqs. (2.60), (2.61) and (2.63), respectively, and

$$\kappa'_n = \frac{(2n-1)\,\pi}{2H_w} \tag{2.67}$$

It has been demonstrated that surface waves have minimal impact on hydrodynamic pressure, except at low frequencies [6, 114]. This effect becomes significant on the structural response only if the structure's fundamental natural frequency falls within or below $18/H_w$ Hz. It was also found that, for slender structures, neglecting water compressibility has minimal impact on hydrodynamic pressure, thus simplifying the analytical expressions. Additionally,

for squat axisymmetric structures, water compressibility has a more pronounced effect on the structural response, particularly in the fundamental modes, while its influence on the higher modes remains relatively small [114].

This method delivers excellent results, even when water compressibility is ignored, and is recognized as a robust analysis procedure for axisymmetric structures surrounded by water. However, it is often impractical for routine engineering applications, highlighting the need for more convenient alternative methods [117].

2.3.2 Numerical methods

Numerous numerical methods, including finite element, boundary element, and scaled boundary finite element approaches, have been developed to discretize the surrounding water and model fluid-structure interaction. Among these, the Finite Element Method (FEM) has gained significant popularity for modeling dynamic interactions in structure-water systems, particularly those involving axisymmetric structures surrounded by water. FEM offers a detailed and accurate representation of the complex behaviors and interactions within the system, including three-dimensional effects and energy absorption at the bottom of the reservoir.

For the seismic analysis of axisymmetric structures surrounded by water, coupled 3D finite element analyses can be conducted using 3D solid elements for the structure and potential-based fluid finite elements for the fluid domains. A more detailed explanation of the coupled fluid-structure interaction finite element model using the potential-based formulation is presented in subsection 2.2.2. The primary difference lies in the use of 3D solid and potential-based fluid elements instead of 2D elements. This introduces an additional translational degree of freedom for each node in the solid elements, while each node in the fluid elements still has one degree of freedom, representing the velocity potential. As previously mentioned, to simulate the infinity of the fluid domain, a Transmitting Boundary Condition (TBC) must be applied at a certain distance, L_{w}. In practice, minimizing this truncation distance is advantageous to limit the number of elements in the finite element model, especially since 3D analysis demands high computational resources. Earthquake loading can be applied either as a mass-proportional body force or as prescribed displacements imposed at the boundaries excited by the earthquake along the x-direction. The finite element models of 3D coupled axisymmetric structures surrounded by water, with proper boundary conditions, are illustrated in Figure 2.10. In general, advancing numerical methods to model fluid-structure interactions has seen significant contributions from various researchers over the years. Everstine pioneered the development of a symmetric potential formulation for fluid-structure interac-

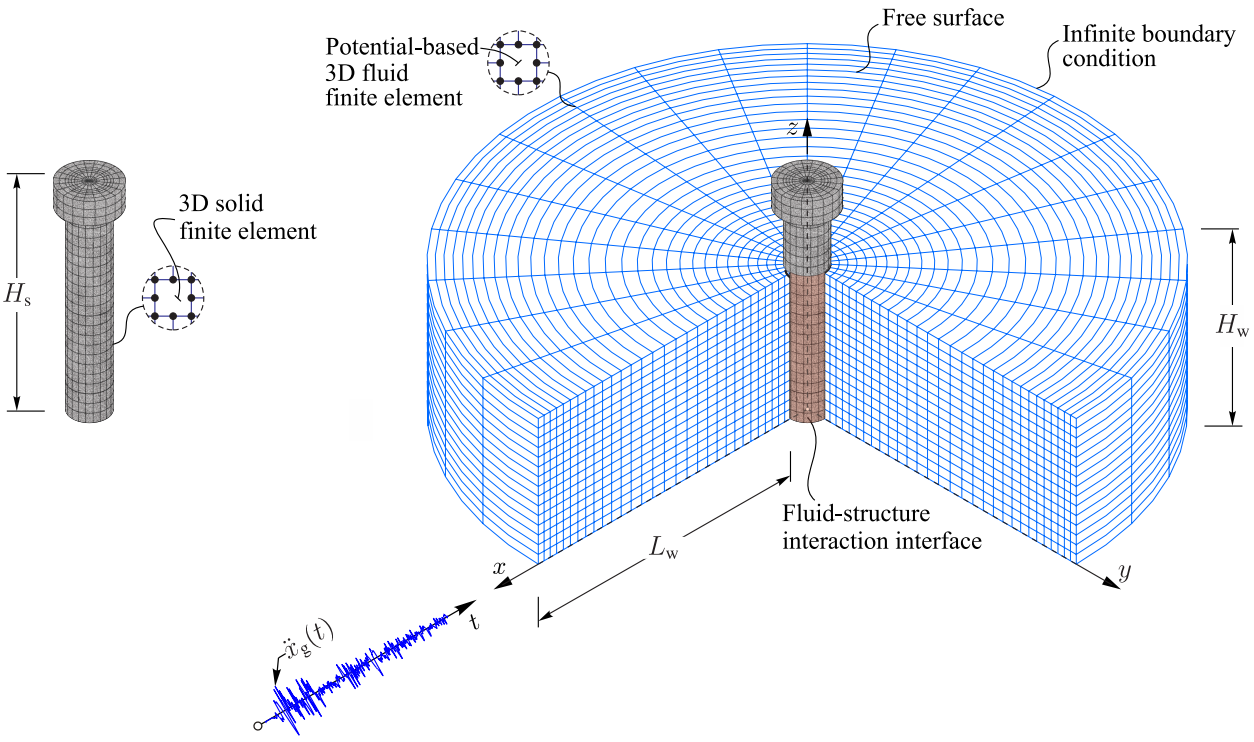

Figure 2.10 Finite element models of 3D coupled axisymmetric structures surrounded by water with required boundary conditions.

tion, providing detailed mathematical models and simulations for improved understanding of hydrodynamic load modeling [49]. Olson and Bathe advanced this work by applying a direct symmetric coupled formulation based on fluid velocity potential, thereby enhancing computational techniques for analyzing fluid-structure interactions [50]. This foundation was extended by Sigrist and his colleagues, who analyzed dynamic problems using pressure-based fluid finite elements with modal methods, incorporating both theoretical developments and practical simulations [53]. Similarly, Czygan and Von Estorff combined the boundary element method (BEM) with nonlinear finite element method (FEM) for a more robust analysis, enhancing the accuracy and efficiency of fluid-structure interaction models [52]. These advancements provided a robust framework for further studies, such as those by Chen, who investigated the dynamic responses of coastal structures during earthquakes [51], and Millan and his colleagues, who focused on the seismic responses of intake towers, including dam-tower interaction [54]. These studies, along with others by researchers like [55] and [56], have collectively enhanced the understanding and application of numerical methods in the seismic analysis of structure-water systems, particularly those involving axisymmetric structures surrounded by water.

2.3.3 Simplfiied method

Robust analysis procedures, even neglecting water compressibility, remain inconvenient for practical applications. Finite element methods require specialized software, a high level of expertise, and significant computational resources to yield valid results. Therefore, alternative simplified methods are essential for routine engineering practice. Simplified methods can be categorized into several approaches. The first is based on the added mass concept.

The concept of added mass has been applied for many years across various fields of engineering, including ship vibrations [118] and earthquake effects on dams [21, 114]. This approach typically assumes the structure to be rigid and calculates an added mass to replicate the hydrodynamic pressures on the vibrating structure. For axisymmetric structures, this method results in a hydrodynamic added mass that can be expressed as the added mass per unit height of the structure [6, 114]

$$m_a(\theta, z) = p_0(R_\mathrm{s}, \theta, z)\,; \qquad p_0(R_\mathrm{s}, \theta, z) = \sum_{n=1}^{N_\mathrm{w}} \frac{4\rho_\mathrm{w}}{H_\mathrm{w}} \frac{I_{0n}}{\kappa'_n}\, \mathcal{E}_n(\kappa'_n\, R_\mathrm{s}) \cos(\lambda_n z) \cos(\theta) \tag{2.68}$$

Therefore, the modal equation of motion, including the fundamental mode, can be expressed as [6, 114]

$$\Big[M_1 + B_1\Big]\, \ddot{\widetilde{Z}}_1(t) + 2\, M_1\, \xi_1\, \omega_j\, \dot{\widetilde{Z}}_1(t) + M_1\, \omega_1^2\, \widetilde{Z}_j(t) = -\Big[L_1^{(x)} + B_0\Big]\, \ddot{x}_\mathrm{g}(t) \tag{2.69}$$

with

$$B_0 = R_\mathrm{s} \int_0^{H_\mathrm{w}} \int_0^{2\pi} m_a(\theta, z)\, \cos(\theta)\, \psi_1^{(x)}(R_\mathrm{s}, 0, z)\, \mathrm{d}\theta\, \mathrm{d}z \tag{2.70}$$

$$B_1 = R_\mathrm{s} \int_0^{H_\mathrm{w}} \int_0^{2\pi} m_a(\theta, z)\, \cos(\theta) \Big[\psi_1^{(x)}(R_\mathrm{s}, 0, z)\Big]^2\, \mathrm{d}\theta\, \mathrm{d}z \tag{2.71}$$

Liaw and Chopra incorporated the flexibility of the structure in its fundamental mode shape into the added mass concept and redefined the added masses as [114]

$$m_a(\theta, z) = \frac{p_1(R_\mathrm{s}, \theta, z)}{\psi_1^{(x)}(R_\mathrm{s}, 0, z)}\,; \qquad p_1(R_\mathrm{s}, z, \theta) = \sum_{n=1}^{N_\mathrm{w}} \frac{4\rho_\mathrm{w}}{H_\mathrm{w}} \frac{I_{1n}}{\kappa'_n}\, \mathcal{E}_n(\kappa'_n\, R_\mathrm{s}) \cos(\lambda_n z) \cos(\theta) \tag{2.72}$$

This added mass can be lumped on the nodes of the dam's face using the tributary method

$$\widehat{M}_i(y) = v_i \times w_i \times m_a \tag{2.73}$$

with $v_i \times w_i$ represents the tributary area of water at node i as shown in Figure 2.11.

Another approach focuses on how the structure's frequency changes due to the effects of

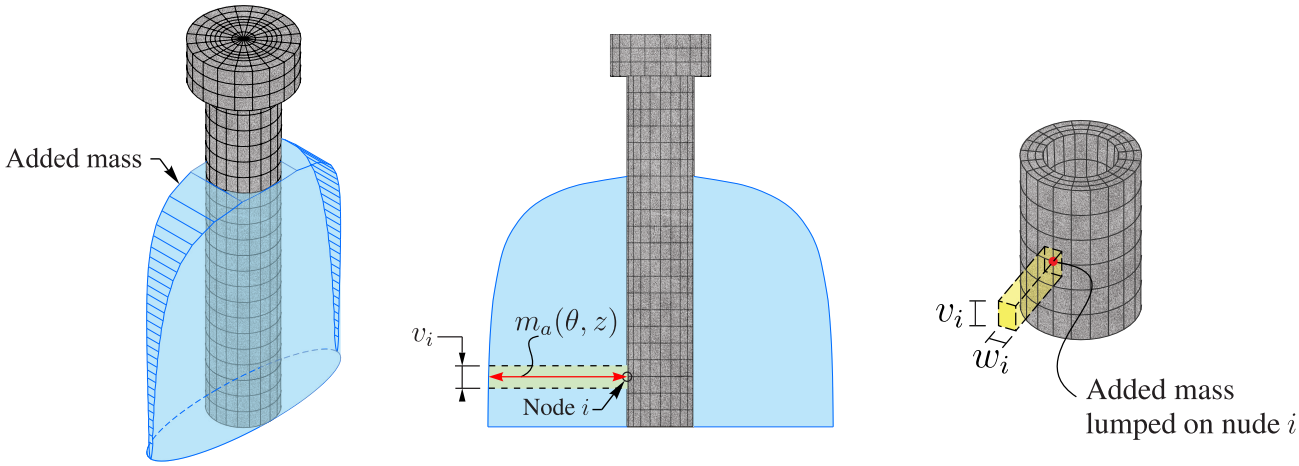

Figure 2.11 Representation of hydrodynamic effects using simplified added mass.

hydrodynamic added mass. By analyzing the altered ratio of the fundamental frequency and assuming the added mass is uniformly distributed along the depth in incompressible water, the magnitude of the added mass can be determined [119]. Yang and Li developed an added mass formula for circular cylinders with diameters ranging from 1 m to 20 m and water depths from 20 m to 140 m. The expression for the added mass is as follows [120]

$$m_a(z) = \pi\,\rho_{\mathrm{s}}\,R_{\mathrm{s}}^2\,C_{m2} \tag{2.74}$$

where $C_{m2} = [0.0133 \ln H_{\mathrm{w}} - 0.112] \ln(2R_{\mathrm{s}}) + 0.0002\,H_{\mathrm{w}} + 0.4$, ρ_{s} is the mass density of concrete, R_{s} is the radius of the circular cylinder, and H_{w} is the water level [120].

Apart from the above appraches, the Morison equation is widely used for assessing hydrodynamic effects on slender cylindrical structures. Morison and his colleagues introduced a semi-empirical formula to calculate wave loads on slender structures with minimal impact on the wave field [47]. This equation was later refined by Penzien and Kaul to account for hydrodynamic forces caused by earthquakes [48]. Due to simplicity, the Morison method has become extensively used for evaluating hydrodynamic forces on slender cylindrical structures [43, 121, 122]. The equation of motion including hydrodynamic force can be written as

$$\mathbf{M}\,\ddot{\widehat{\mathbf{U}}}(t) + \mathbf{C}\,\dot{\widehat{\mathbf{U}}}(t) + \mathbf{K}\,\widehat{\mathbf{U}}(t) = -\mathbf{M}\,\mathbf{1}^{(x)}\,\ddot{x}_{\mathrm{g}}(t) + \mathbf{F}_{\mathrm{M}} \tag{2.75}$$

with $\mathbf{F}_{\mathrm{M}}$ denotes the hydrodynamic force. Based on Morison's method, the hydrodynamic force exerted at depth z, in unit length can be expressed as [5, 47, 48]

$$f_{\mathrm{M}} = f_{\mathrm{D}} + f_{\mathrm{I}} = \frac{1}{2}\rho\,A\,C_{\mathrm{D}}\,(v_z - \dot{u})\,|v_z - \dot{u}| + \rho\,\bar{V}_0\,C_{\mathrm{M}}\,(\ddot{v}_z - \ddot{u}) + \rho\,\bar{V}_0\,\ddot{v}_z \tag{2.76}$$

where f_{D} and f_{I} are the drag and inertia forces, respectively. A is the projected area of the cylinder per unit length in the vertical direction of the wave. The coefficients C_{D} and C_{M}, representing the drag and inertia forces, respectively, are determined using experimental data. Sarpkaya demonstrated that these coefficients depend on the Keulegan-Carpenter number, Reynolds number, and surface roughness [123]. For circular cylinders, C_{M} has a value of 1 [123]. v_z is the horizontal velocity of a water particle at depth z, while $\dot{u}$ and $\ddot{u}$ are the absolute velocity and acceleration of the cylinder at depth z, respectively. $\bar{V}_0$ is the volume of water displaced by the structure per unit length. $\ddot{v}_z$ is the local acceleration of the fluid. In this equation, if the water is initially at rest, both v_z and $\ddot{v}_z$ can be considered zero.

Other researchers showed that the drag force is significantly less than the inertia force under earthquake excitation [124, 125]. Additionally, it can be shown that fluid damping has a negligible contribution to the seismic response of the cylinders and can be ignored [126]. Therefore, Equation (2.76) can be simplified as

$$f_{\mathrm{M}} = f_{\mathrm{I}} = -\rho \bar{V}_0 C_{\mathrm{M}} \ddot{u} \tag{2.77}$$

Therefore, $\mathbf{F}_{\mathrm{M}}$ in Equation (2.75) represents the total contribution of these added masses along the length of the structure. Figure 2.12 depicts the representation of hydrodynamic effects using Morison's added mass. It is equivalent to having a column of water with a radius of R_{s} and a height of H_{w} attached to the structure.

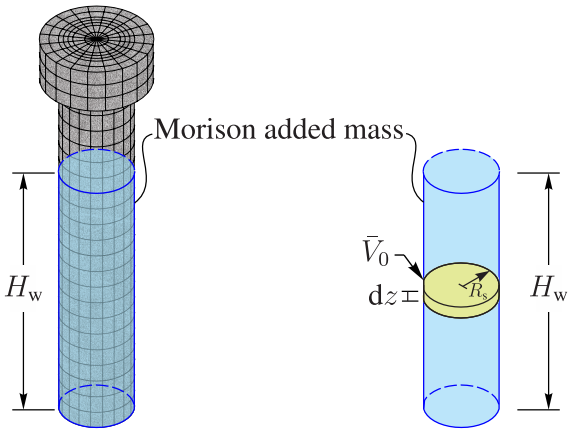

Figure 2.12 Representation of hydrodynamic effects using Morsion's added mass.

Guo and his colleagues conducted a comparative study of simplified methods for assessing cylindrical hydrodynamic forces [5]. They constructed relative errors of structural elastic peak responses to measure the accuracy of these simplified methods under various cylindrical cases. The study compared the added masses based on radiation wave theory using Eq.

(2.68), with those based on Morison's equation, as shown in Equation (2.77). Their findings, presented in Figure 2.13, indicate that for slender structures, both methods yield similar hydrodynamic added masses within the lower 75% of the water height. However, for larger radii and shorter heights, Morison's equation provides larger added mass values throughout the structure's height.

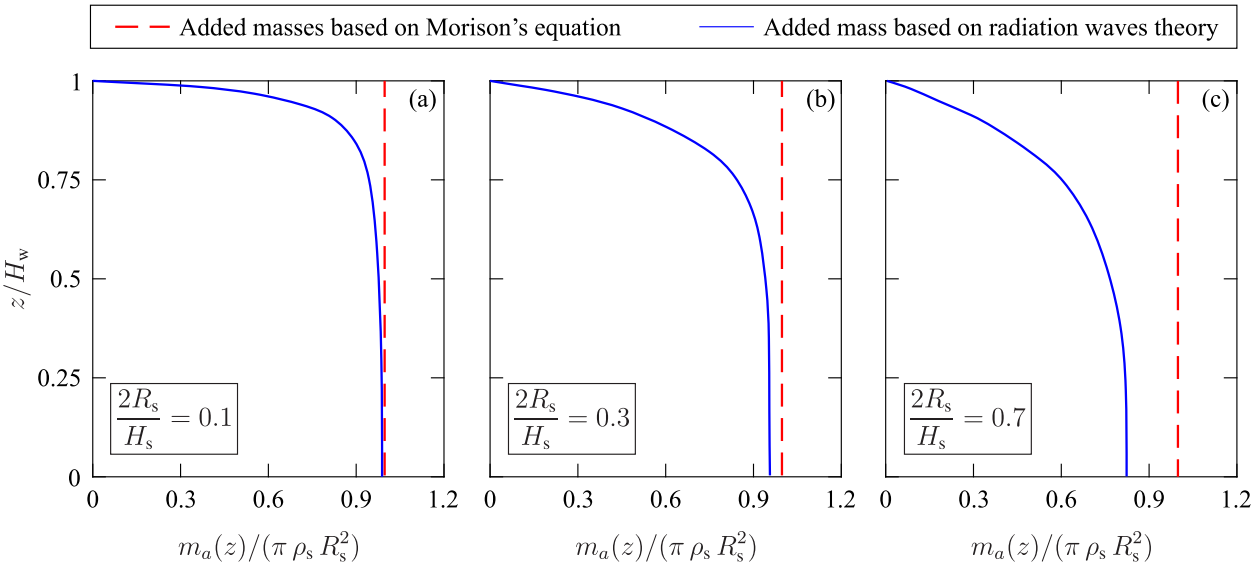

Figure 2.13 Comparison of the distribution of added mass (adapted from [5]).

Wei and his colleagues proposed a simplified method to enhance practical seismic design and safety evaluation of axisymmetric structures in contact with water, eliminating restrictive assumptions [6]. They proposed two formulations: Type I, where the mode shapes of the dry structure are obtained using analytical expressions based on Euler-Bernoulli beam theory, and Type II, where these mode shapes are extracted from finite element analysis. Both formulations account for higher vibration modes, water compressibility, the flexibility of the foundation, and effects of surface gravity waves. Type II formulation further applies to composite axisymmetric structures made of different materials, considering variations in stiffness and mass density along the structure's height, as well as non-uniform hollow cross-sections due to interior wall geometric irregularities. They proposed practical expressions for $\mathcal{D}n(\kappa_n, Rs)$, $\mathcal{E}n(\kappa' n, Rs)$, and $\tau_n Rs$, using curve fitting techniques, as alternatives to Equations (2.62), (2.63), and (2.64). The accuracy of these approximations is illustrated in Figure 2.14, where the results are compared with the exact formulations. These approximation

parameters can be calculated as [6]

$$\mathcal{D}_n(\kappa_n R_\mathrm{s}) = \frac{0.5\,(\kappa_n R_\mathrm{s})^3 - 0.038\,(\kappa_n R_\mathrm{s})^2 + 0.249\,\kappa_n R_\mathrm{s}}{(\kappa_n R_\mathrm{s})^3 - 0.013\,(\kappa_n R_\mathrm{s})^2 + 0.019\,(\kappa_n R_\mathrm{s})^2 + 0.473} \tag{2.78}$$

$$\mathcal{E}_n(\kappa'_n R_\mathrm{s}) = \frac{0.5\,(\kappa'_n R_\mathrm{s})^2 - 0.345\,\kappa'_n R_\mathrm{s}}{(\kappa'_n R_\mathrm{s})^2 - 1.202\,\kappa'_n R_\mathrm{s} + 0.670} \tag{2.79}$$

$$\tau_n R_\mathrm{s} = \tan^{-1}\left[\frac{-3.06\,(\kappa_n R_\mathrm{s})^2 + 0.14\,\kappa_n R_\mathrm{s} - 0.006}{\kappa_n R_\mathrm{s} + 1.46}\right] \tag{2.80}$$

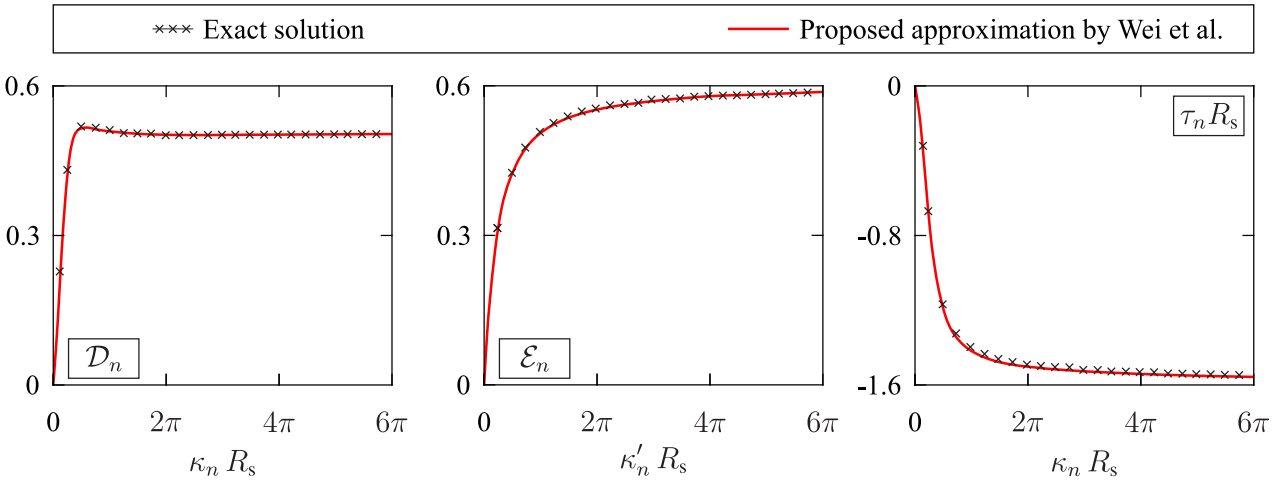

Figure 2.14 Approximation of parameters $\mathcal{D}_n(\kappa_n R_\mathrm{s})$, $\mathcal{E}_n(\kappa'_n R_\mathrm{s})$, and $\tau_n R_\mathrm{s}$ (adapted from [6]).

By providing a literature review covering analytical, simplified, and numerical methods for the seismic analysis of axisymmetric structures surrounded by water, it is evident that each approach has its limitations. Analytical expressions, although precise, remain too complicated for practical engineering use. Numerical methods, while highly accurate, require specialized software and significant expertise to produce valid results. Simplified methods offer ease of use, but their approximations can sometimes fall short in certain scenarios. Therefore, there is still a need for improvement in the seismic analysis of axisymmetric structures surrounded by water to develop methods that are both practical and reliable for day-to-day engineering applications. Specifically, improvements are needed in the response spectrum analysis for this type of structure, ensuring the accurate inclusion of hydrodynamic effects along with the contribution of flexibility higher modes in the analysis.

2.4 Shaking table test of structure-water system and its appurtenant structure

Shaking table tests are a pivotal experimental approach to experimental study dynamic response of structures under applied earthquake signal. However, the complexity of accurately incorporating fluid-structure interaction in experimental shaking table tests poses significant challenges for researchers. It is worth mentioning that for dam-reservoir systems, although there are many numerical studies on the simulation of seismic responses, experimental work is limited due to the large sizes of dams, which restricts the feasibility of laboratory testing. This issue can be addressed by using small-scale models for constructing laboratory specimens or by instrumenting existing dams for in situ tests [11,75]. Additionally, scaling down a large dam for shaking table tests increases its natural frequency, making the dam to be more rigid. To effectively excite these frequencies and capture the flexibility of the scaled-down dam in experimental tests, the shaking table must be capable of operating at high frequencies, potentially up to 100 Hz.

Incorporating hydrodynamic effects during experimental tests presents a significant challenge in conducting shaking table tests for structure-water systems. These challenges arise due to the inherent complexity of fluid-structure interaction and the need for specialized facilities or methods to simulate these effects accurately. This section focuses on how hydrodynamic effects are included in experimental setups for structure-water systems, categorizing the methods into three main groups: (i) underwater shaking table tests, (ii) simplified methods such as added mass concepts or limited length of water flume, and (iii) ignoring hydrodynamic effects due to experimental complexity and safety issues.

2.4.1 Underwater shaking table tests

The underwater shaking table is a specialized facility designed to investigate the response of structure-water systems under seismic loads, wave-current conditions, and combined earthquake and structure-water scenarios. The equipment, including actuators, is protected by waterproof seals to prevent water from entering the equipment room. The five main components of these facilities are the wave-making/attenuation system, the platform and supporting system, the actuation system, the hydraulic power system, and the control system. Japan pioneered the development of underwater shaking tables, with the first facility built in 1977 following the Great Hanshin-Awaji earthquake [7, 46, 62]. However, due to the leakage and component aging of the early devices, their service life was relatively short [7, 62]. At the moment of writing this thesis, six underwater shaking tables are either in service or under construction worldwide. These are located at the Port and Airport Research Institute (PARI) in Japan, Dalian University of Technology in China, Hohai University in China, and Tianjin

University in China. Over the past few decades, China has constructed several large underwater shaking tables. More recently, an underwater shaking table array system with movable platforms is being built at the National Facility for Earthquake Engineering Simulation in China [7, 127]. Figure 2.15 shows the six underwater shaking table facilities. In this section, four of the most recent shaking table tests focusing on the seismic response of structure-water systems using underwater shaking table facilities are reviewed.

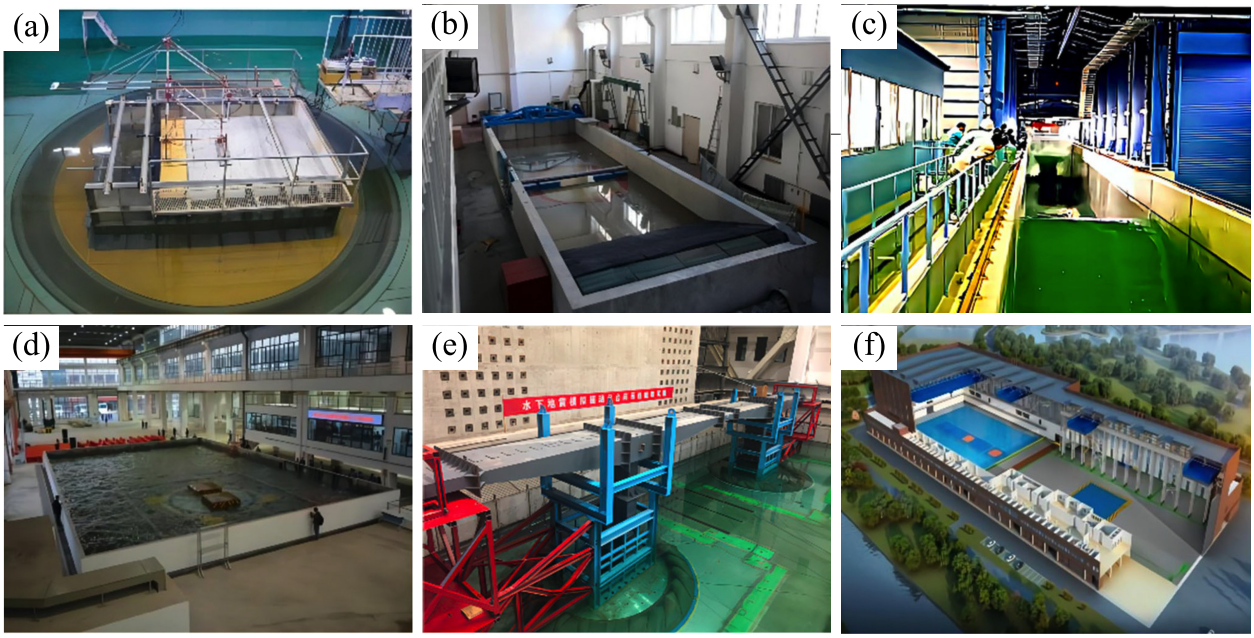

Figure 2.15 Underwater shaking tables in the world [7]: (a) Port and Airport Research Institute (PARI) in Japan; (b) Dalian University of Technology in China; (c) Large Hydro-Geo Flume (LHGF) in PARI, Japan; (d) Hohai University in China; (e) underwater shaking table array system at Tianjin University in China; (f) National Facility for Earthquake Engineering Simulation in China.

Ding and his colleagues conducted a series of underwater shaking table tests at a 50:1 scale on bridge piers, focusing on the combined effects of earthquake, wave, and current actions [8]. These tests, performed at Dalian University of Technology, are notable for their ability to simulate these forces independently and simultaneously within the same flume. To meet the requirements of similitude law, the model design adhered to elasticity and gravity similitude laws, ensuring the fluid density ratio of the prototype and model remained equal. Consequently, the material density of the prototype was matched to that of the model to maintain the similarity of hydrodynamic action on the pier. The experimental program consisted of four main tests: white noise tests, independent earthquake tests, independent wave-current tests, and combined earthquake and wave-current tests. The results showed that when the

system was subjected to independent earthquake action, the peak dynamic responses in water were mostly larger than those without water, with the maximum increase reaching about 15%. These findings highlight the significant impact of hydrodynamic forces on structural responses. Figure 2.16 provides an overview of the test setup, illustrating the complexity and scale of the experimental arrangement.

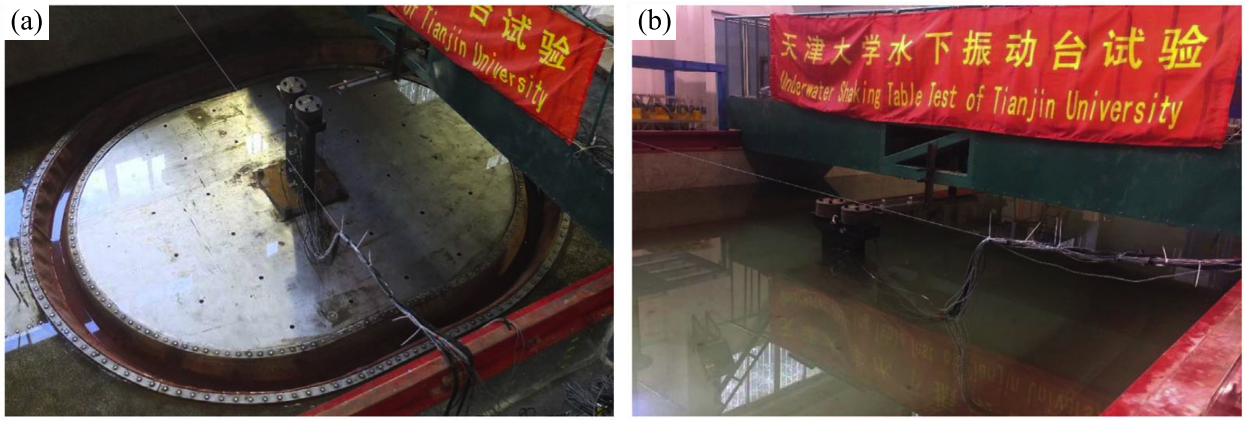

Figure 2.16 Overviews of test setup: (a) dry condition; (b) with water at a depth of 0.65 m [8].

Li and his colleagues conducted dynamic tests on circular steel tubes of various dimensions in a water tank to investigate the hydrodynamic added mass for different tube diameters, water depths, and input frequencies and amplitudes [9]. The study aimed to determine the inertial coefficient used in the Morison equation. These tests were performed at SERVOTEST Testing Systems Ltd in Beijing, China. The water tank had dimensions of $5.2\,\text{m} \times 5.2\,\text{m} \times 1.2\,\text{m}$, and a shaking table with a diameter of 0.9 m was connected to the center of the tank bottom using waterproof cloth. The shaking table was supported by a steel frame and could handle a load capacity of 25 kN with a maximum displacement of ± 75 mm and a frequency range of $0.1 - 100$ Hz. Three water levels of 0.2 m, 0.5 m, and 0.8 m were considered for the experimental tests (As shown in Figure 2.17).

To further validate the proposed method, underwater shaking table tests were conducted at Tianjin University, which is the world's first underwater dual shaking table test system(As shown in Figure 2.18). The shaking tables, each with a diameter of 3.6 m, have load capacities of 20.0 tons without water and 12.0 tons with water. They are installed in a water pool with dimensions of $24.8\,\text{m} \times 12.5\,\text{m} \times 3\,\text{m}$, with a maximum water depth of 2.0 m. Circular steel tubes with diameters of 101 mm and 351 mm and a height of 1.4 m, tested at a water depth of 0.6 m. The ground motions simulated were El-Centro (1940), Taft (1952), and Tianjin (1976) earthquakes, which were used as input signals for the underwater shaking table tests. The

Figure 2.17 Overviews of test setup using water tank on shaking table facility at SERVOTEST Testing Systems Ltd in Beijing [9]: (a) overview of water tank and shaking table; (b) and (c) overview of specimens and instrumentation.

study concluded that the hydrodynamic added mass increased with the structure's diameter and water depth. The added mass could increase by 28 times when the diameter increased from 101 mm to 610 mm and by 14 times when the water depth increased from 0.2 m to 0.8 m. The proposed formula and method matched well with the underwater shaking table test results, demonstrating their applicability in calculating the hydrodynamic added mass of cylindrical structures under earthquake excitation.

In 2024, Chen and his colleagues conducted an experimental study on the dynamic responses and hydrodynamic pressures of deep-water bridge piers under seismic and wave actions using the underwater shaking table facility at Tianjin University [10]. This facility, depicted in

Figure 2.18 Overview of the test setup using the underwater shaking table facility at Tianjin University [9]: (a) shake table in dry condition; (b) shake table in wet condition with the specimen installed; (c) 351 mm diameter specimen mounted on the shaking table in wet condition.

Figure 2.19 (a). The specimen, representing an offshore reinforced concrete high bridge pier with a height of 72 m, was modeled using a special rubber material designed to simulate the elastic behavior of reinforced concrete. This rubber, made from metal powder, allowed for accurate scaling, resulting in a specimen height of 2.4 m according to similitude laws. To replicate the mass of the superstructure, a 64 kg iron block was attached to the top of the specimen. Tests were conducted under three conditions: no water, a water depth of 1.6 m, and a water depth of 2.0 m (Figure 2.19).

The tests included white noise tests to determine the specimen's frequency, seismic tests,

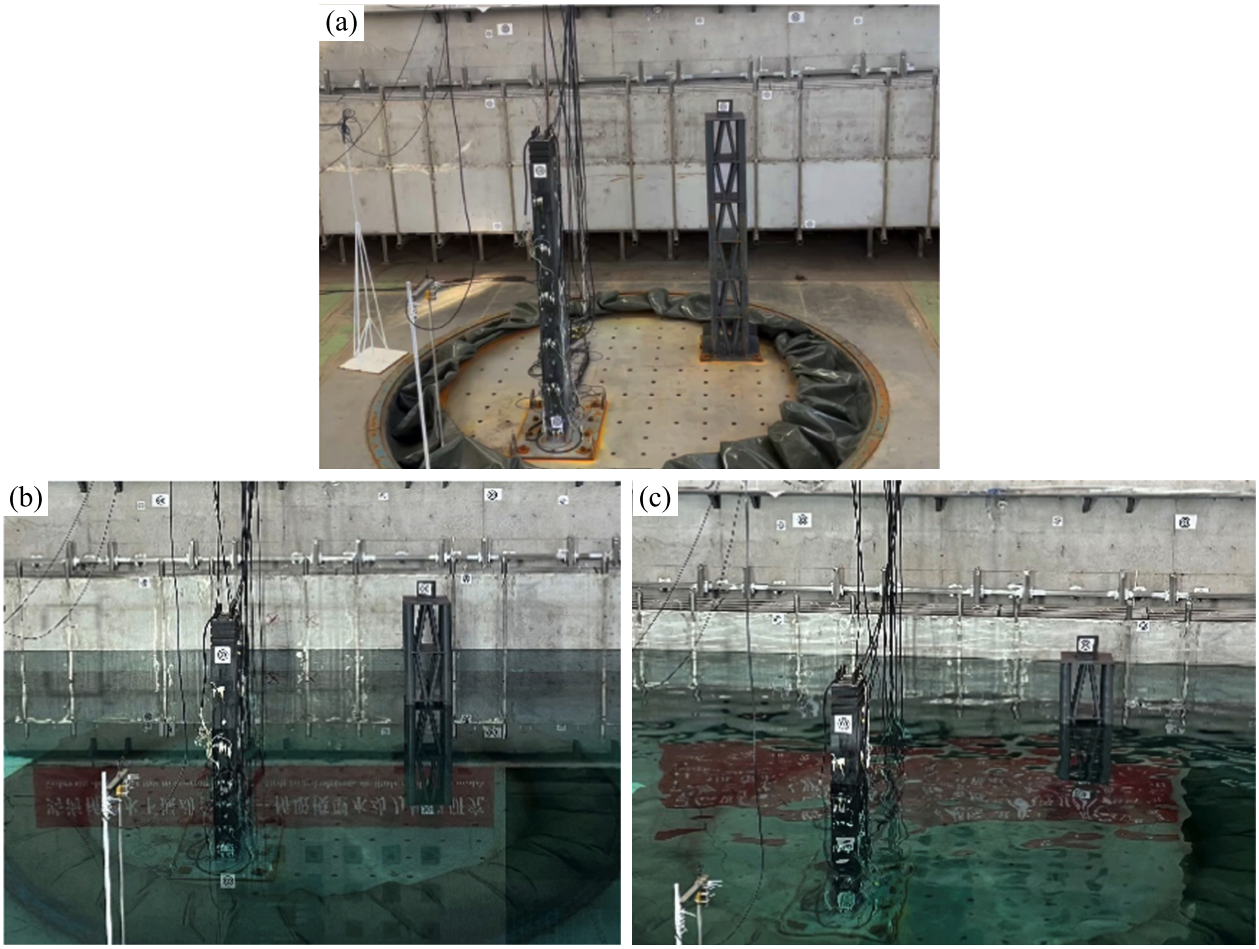

Figure 2.19 View of experimental tests [10]: (a) no water, (b) a water depth of 1.6 m, and (c) a water depth of 2.0 m.

wave maker tests, and combined seismic and wave maker tests. Data on displacements, accelerations, strains, and hydrodynamic pressures were collected, revealing insights into structural model parameters and dynamic response behaviors. Results showed that water reduced the natural frequency of the pier, with a more significant effect at higher water levels. At a 2.0 m water depth, the first-order frequency decreased by 6.31% and the second-order frequency by 21.71%. Additionally, the relative displacement of the pier increased with greater water depth during earthquakes, particularly under pulsed and long-period ground motions. At the 2.0 m water depth, the relative displacement increased by 18.3% for the pulsed Loma Prieta earthquake and by 21.3% for the long-period Chi-Chi earthquake compared to no water conditions.

In most recent underwater shaking table experimental tests in 2024, He and Pan examined the seismic responses and vibration control of offshore wind turbines (OWTs) using an underwater

shaking table, focusing on the complex interaction between seismic and hydrodynamic forces [1]. The study simulated the seismic responses of large-scale offshore wind turbines (OWTs) under "with water" and "without water" conditions. A geometric scale of 1:20 of a typical 5 MW OWT was used. The tests were conducted using underwater shaking table facilities at Hohai University in China. The operating parameters of the table are presented in Table 2.1. The nacelle and blades were simplified to a box based on mass similarity, with an effective

Table 2.1 Operating parameters of the underwater shaking table of Hohai University [1]

Technical indicators	**Technical values**
Operating frequency range	0.1-100 Hz
Overturning moment	60 t.m
Maximum load	40 t
Maximum acceleration	±2.0 g in x and y direction, ±1.33 g in z direction
Water tank size	30 m long, 20 m width, 1.5 m depth

model mass of approximately 153.9 kg and a top box mass of about 38 kg (as shown in Figure 2.20). The water level was set at 1 m, corresponding to 20 m in the prototype, consistent with field conditions. Absorbing boundaries were placed around the tank to reduce water wave reflections. The water tank dimensions were 30 m length, along the seismic input direction, 20 m width and depth of 1.5. Figure 2.20 shows the underwater shake table facility with installed specimen.

The test groups were conducted with water" and "without water" conditions, with each group subjected to different scaled seismic and artificial waves, such as 1:1 and 1:5 scaled El Centro earthquake (NS direction), 1:5 and 1:20 Chichi earthquake (NS direction), and 1:5 and 1:20 scaled Kobe earthquake (00° direction). The study focused on evaluating the natural frequencies and dynamic amplification of the OWT in an elastic state which are primarily dependent on the structural dynamic characteristics, such as bending stiffness, aspect ratio, and damping ratio of the OWT. Acceleration was used as the key indicator to describe the seismic responses since displacement and velocity are challenging to measure accurately. The study concluded that the acceleration amplification factors for monopile-supported OWTs could reach between 3.4 to 7.2 at the nacelle and 2.9 to 6.1 at the upper part of the tower under horizontal earthquake excitation. Hydrodynamic effects were found to significantly influence seismic vibrations, with hydrodynamic damping playing a major role in the first mode and added mass effects dominating for higher modes.

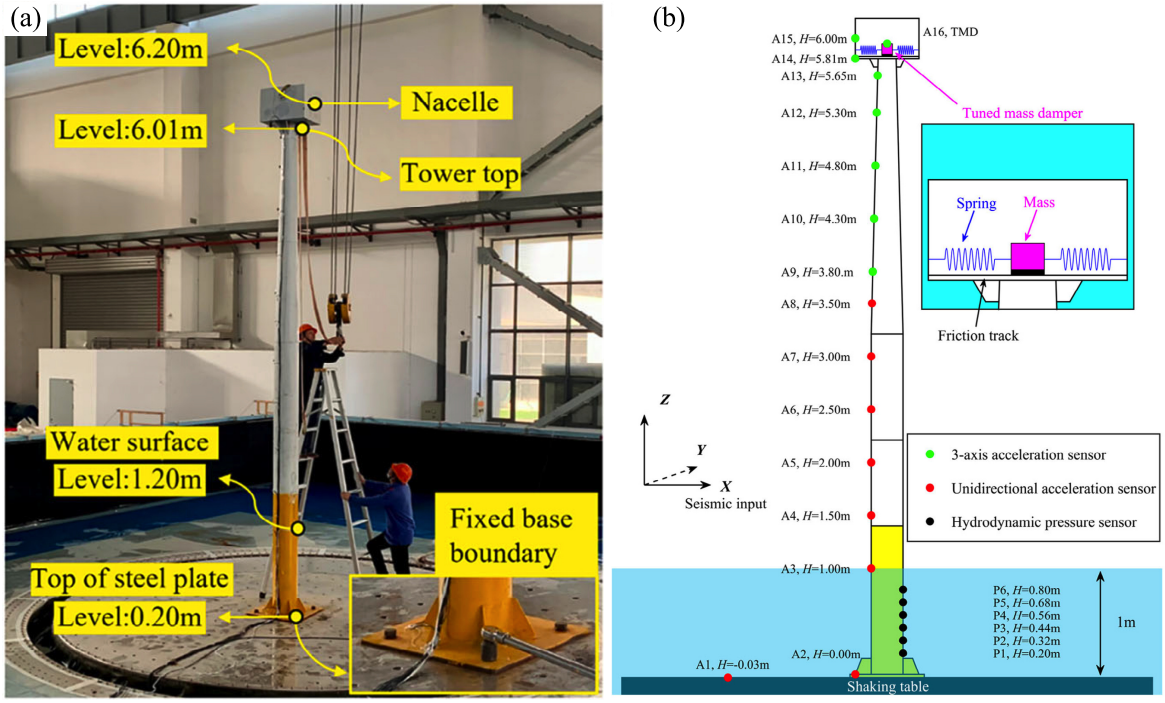

Figure 2.20 View of the specimen and instrumentation [1].

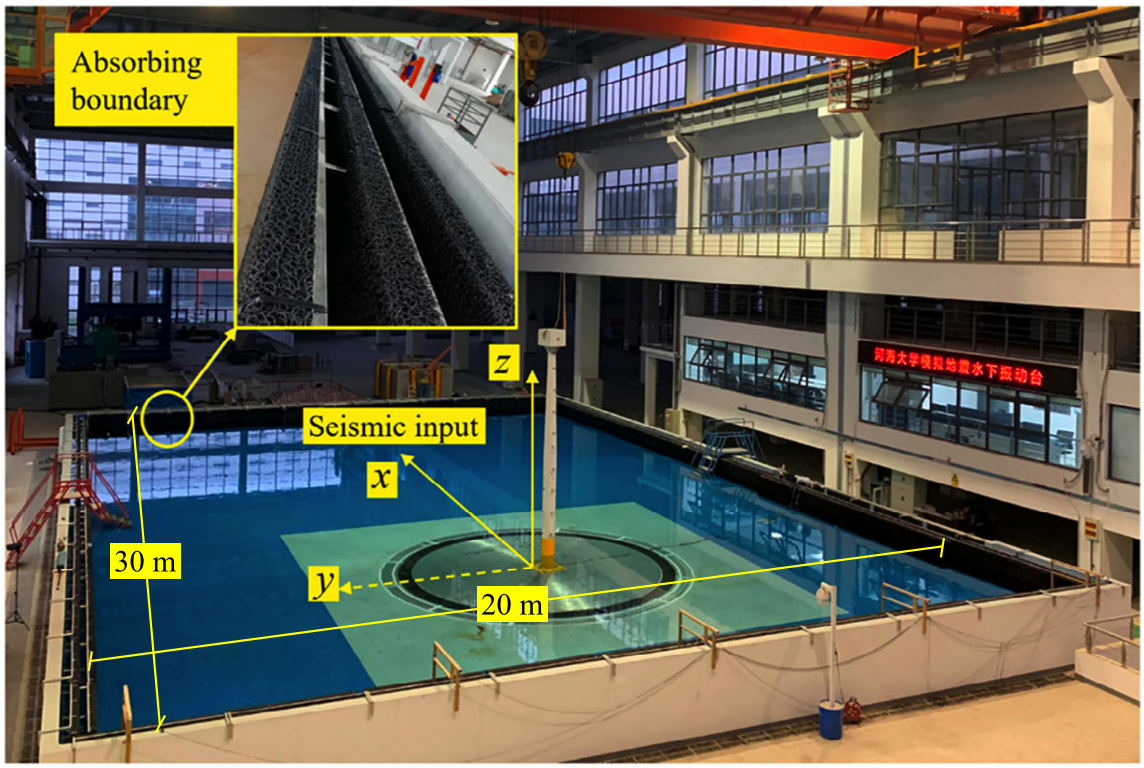

Figure 2.21 View of underwater shaking table test [1].

The researchers also validated the applicability of the theory proposed by Liaw and Chopra [114] by directly measuring the added hydrodynamic mass and hydrodynamic damping effects. While the added hydrodynamic mass did not reduce the first natural frequency of the OWT, it did reduce the higher natural frequencies by 1.6% to 6.6%, aligning with theoretical predictions. Hydrodynamic damping ratios ranged from 0.20% to 0.53%, significantly increased the total damping ratio and reducing seismic vibrations. This study clearly demonstrates the significant impact of hydrodynamic effects on the response of the system, emphasizing the necessity of incorporating dynamic fluid-structure interaction in shaking table tests of structure-water systems.

As discussed, underwater shaking table tests are the most effective methods for investigating the dynamic responses of structure-water systems, and their usage has seen increased interest in the past five years. However, facilities with the necessary operational parameters are limited to a select number of universities and research institutions. Additionally, the size and payload limitations of underwater shaking tables necessitate the use of scaled models, with water typically used as the fluid material. This situation, where the structure is scaled down but the water around it is not scaled down, creates a significant conflict between the similarity laws of seismic and hydrodynamic forces in underwater shaking table tests. Furthermore, leakage problems can damage expensive equipment or necessitate costly maintenance procedures to keep the facilities operational. In addition, specialized underwater measurement equipment is required to capture the structural response, further increasing the complexity and expense associated with underwater shaking table tests.

Due to the aforementioned concerns, these experimental methods are not widely utilized. The risk of water leakage, which can damage equipment or pose significant safety hazards, further complicates their practicality. As a result, there is a need for alternative approaches to effectively study the seismic response of structures while incorporating hydrodynamic effects.

2.4.2 Experimental tests using simplified hydrodynamic representation

While simplifications may impact the accuracy of the results, using simplified methods for experimental tests has long been the most feasible approach for investigating the seismic response of structure-water systems. The term "simplified" in this context refers to methods that, by today's standards, may not fully capture the complexity of the seismic response of structure-water systems. However, these methods were considered advanced at the time they were developed. Simplified methods generally involve using added mass representations of hydrodynamic forces or a limited length of water in contact with the structure at the structure-water interfaces. These approaches offer practical alternatives to more complex and resource-intensive underwater shaking table tests.

In 1976-1977, the Moscow Land Reclamation Institute conducted model investigations on the seismic stability of a dam with a lightweight profile. The aim was to determine the maximum seismic load leading to the loss of bearing capacity of the dam and to understand its failure mode. The experiments were conducted on a 1:200 scale model made of special materials. This model included seven horizontal construction joints and a joint along the concrete-rock contact, as well as four monolithic sections. The reservoir water loads were simulated using a calcium chloride solution with a unit weight of 1.4 tons/m^3, poured into a stationary tank and transmitted to the model through a thin rubber diaphragm. Seismic loads were applied using a seismic platform operating in a seismic shock mode in the forward direction, focusing on the envelope of the calculated seismic spectrum [128].

One of the pioneering studies on the seismic behavior of concrete dams was conducted by Niwa and Clough in 1980 [11]. This study tested two different scaled dam specimens, one an arch and the other a gravity dam. For the arch dam, the added mass concept was employed to simulate hydrodynamic effects, while for the gravity dam, a limited water tank was used to represent hydrodynamic effects. Vibration frequencies of both specimens were measured during each experiment through vibration tests. Similitude laws were strictly enforced to ensure that both the prototype and laboratory specimens experienced the same strain. To achieve this, the density of concrete was kept constant while the compressive strength and modulus of elasticity were scaled. A 1/150-scale model of the Techi Dam in Taiwan was constructed for the tests. The arch rib was assembled on the shaking table in a vertical plane, as shown in Figure 2.22.

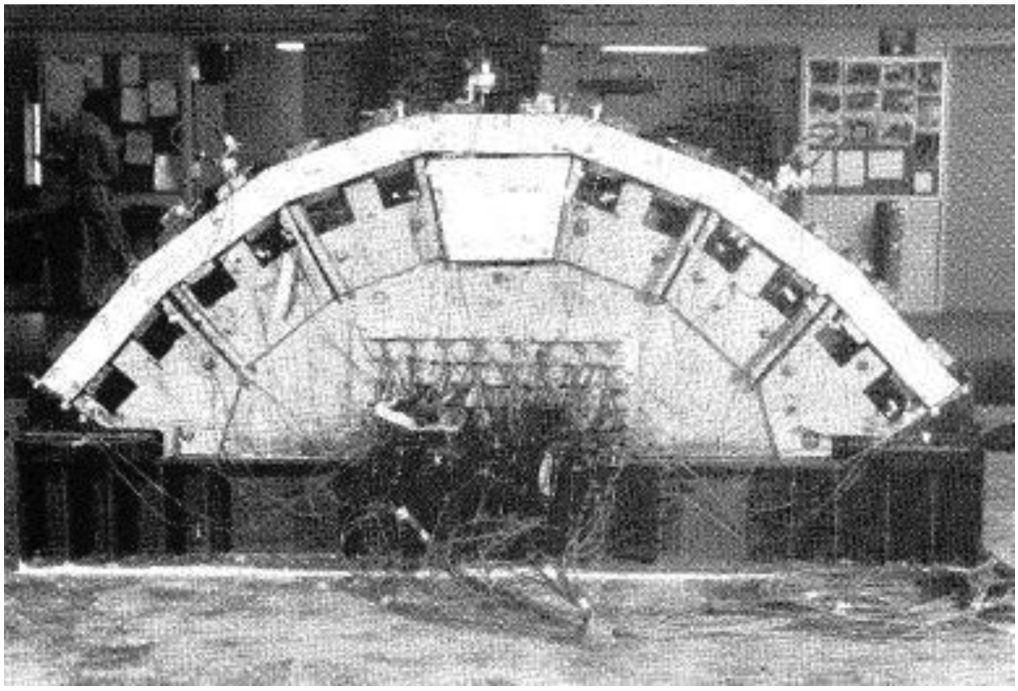

Figure 2.22 Segmented arch model on shaking table [11].

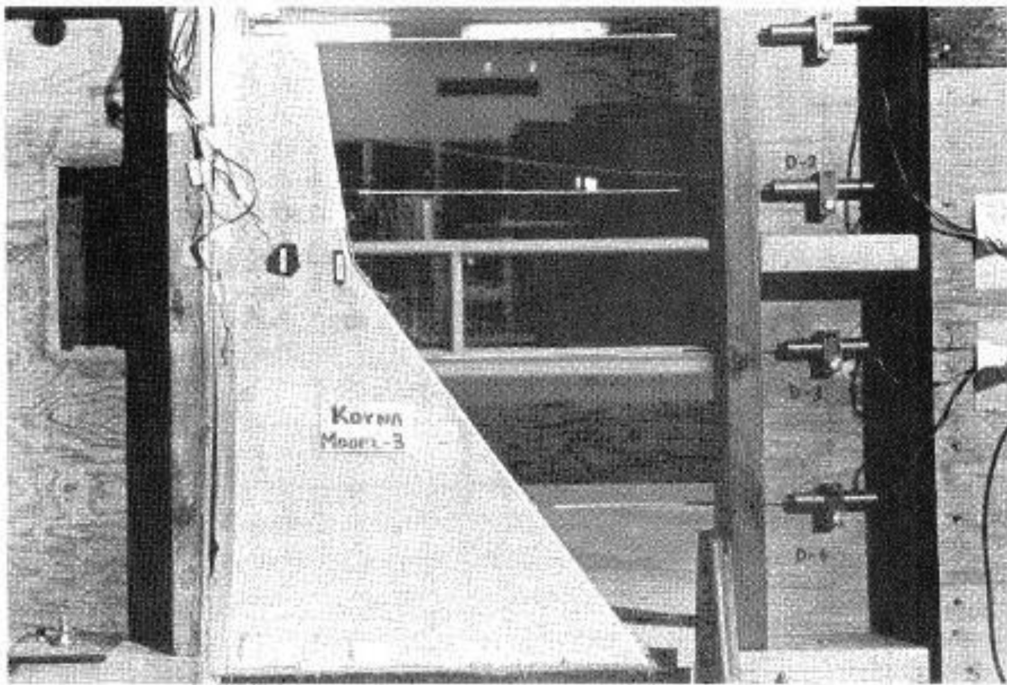

Figure 2.23 Koyna dam model with reservoir tank [11].

In this setup, the dead weight of the blocks simulated the hydrostatic pressure acting hori-

zontally on the prototype arch rings. Different weights were added in various tests to achieve equivalent unit weights of 2419 and 3636 kg/m^3. This incremental weight was intended to approximate the dynamic "added mass" effect of the reservoir. In this test, vertical motions of the shaking table simulated the effect of an upstream-downstream earthquake, while horizontal table motions simulated a cross-canyon earthquake.

For the gravity dam specimen, a 1/150-scale model of the tallest section of the Koyna Dam in India was constructed (Figure 2.23). To include the hydrodynamic effects, a reservoir tank was built and connected to the upstream face of the dam section using a thin plastic layer with negligible resistance. Forced vibration tests were first performed for both the empty and full reservoir conditions. The presence of the reservoir resulted in a 25% change in frequency.

Following this research, there was a surge of interest in the experimental investigation of the seismic response of dams between 1990 and 2000. Donlon and Hall conducted a series of shaking table tests on three small-scale models of Pine Flat dam at the California Institute of Technology [12]. These models had a total height of 1.07 m (42 in) and a thickness of 0.135 mm (0.25 in). A wooden water tank with a length of 1.83 m (72 in), which is 1.7 times the

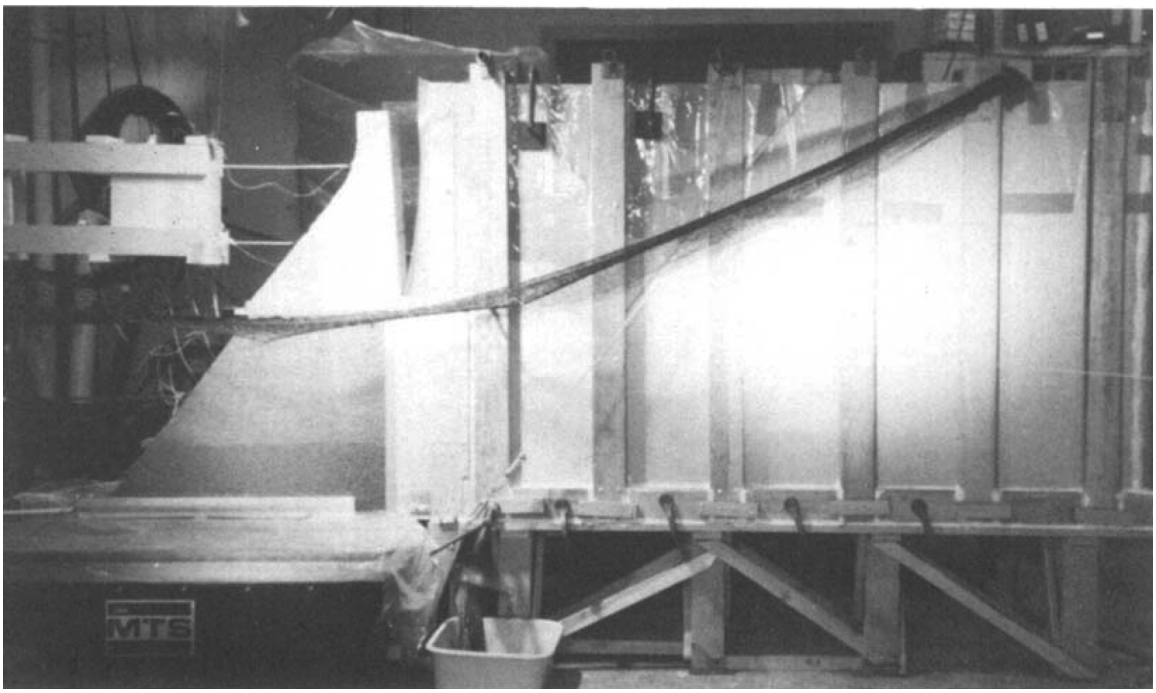

Figure 2.24 Experiment set-up showing a 1/115-scaled Pine Flat dam on the shaking table adjacent to the reservoir [12].

height of the dam, was constructed as a reservoir and filled with water to a level 0.06 m (2 in) below the crest to simulate hydrodynamic effects during the shaking table test. The tank

was positioned off the shaking table adjacent to the upstream face of the dam (Figure2.24). Since water was used as the model fluid, water compressibility did not scale properly, leading to a violation of the similitude law [12].

Other researchers have employed a similar approach of using a limited-length water tank to include hydrodynamic effects in experimental seismic tests of dams. These studies concluded that a water tank at least three times the height of the dam model is generally required to reproduce hydrodynamic pressures accurately, which can lead to very large experimental setup. More importantly, previous fluid-structure experimental investigations determined that any 2D tank arrangement is likely to interact with the contained fluid, producing a complex 3D system due to panel vibrations of the tank, which are difficult to control during seismic excitation. Additionally, using a density scale factor to scale down specimens can cause density scale distortion if water is used in the experiment, as the water density should also be adjusted. This often requires using a lighter fluid, which creates additional challenges for experimental tests. Therefore, as an alternative method, hydrodynamic pressure has been simulated using Westergaard's added mass approach, either by distributing the added mass equally over the height of the dam or by using a very short length tank to represent the block of water interacting with the dam during excitation.

Mir and Taylor incorporated hydrodynamic pressure using Westergaard's added mass approach in a series of shaking table tests conducted at Bristol University [13]. These tests

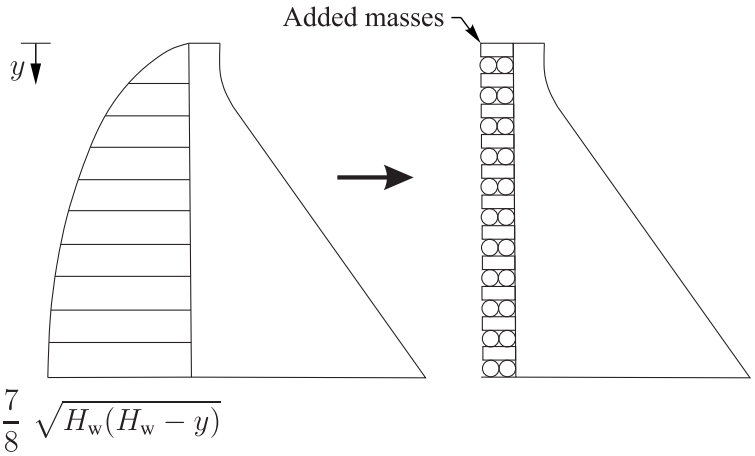

Figure 2.25 Experimental simulation of hydrodynamic pressure [13].

aimed to assess the potential failure mechanisms of medium to low height dams under simple motions and simulated earthquakes. They noted that a long reservoir would require a total experimental setup exceeding 4 m in length, presenting significant challenges. Instead, to

include hydrodynamic effects, they used scaled Westergaard's added masses at 64 equidistant levels along the height of the model (as illustrated in Figure 2.25). The masses were fixed along the upstream face of the dam and separated by plastic sheets containing air bubbles, typically used for packaging. This arrangement minimized friction between the layers, thereby meeting the primary assumption of the Westergaard added mass method. A rigid rectangular steel tank with a 0.230 m × 0.400 m cross-section and 1.1 m height was used to simulate the hydrostatic pressure, as shown in Figure 2.26(a). The inside of the tank was lined with a very low-stiffness rubber foam. The purpose of providing a short tank (0.4 m long) and foam lining was to minimize the formation of hydrodynamic pressures, leaving the water in the tank to produce the required hydrostatic pressure and to hold the loose stack of added masses in position. The complete setup is depicted in Figure 2.26(b).

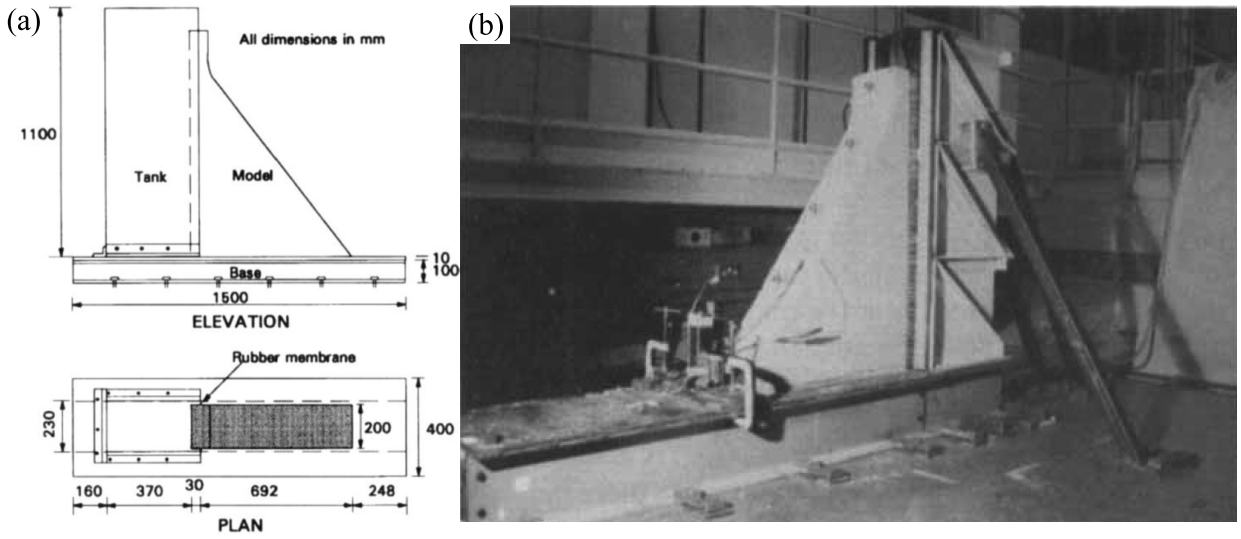

Figure 2.26 Experiment setup [13].

Mridha and Maity examined the dynamic response of reservoir-dam systems using a 1/150 scaled model of the Koyna dam [14]. Hydrodynamic effects were included by attaching a water tank to the dam to simulate Westergaard's added mass effects during experimental tests. Three dam models were prepared by mixing cement, sand, bentonite, and water respecting the similitude law to achieve the target properties of the dam. A reservoir of size 0.78 m ×0.32 m ×0.14 m, was constructed using a 0.01 m thick perspex sheet on a wooden base plate. The top of the reservoir was left open, with the bottom and three sides made of perspex sheets, reinforced with steel angles and sheets. The side facing the dam model had a thin polyethylene sheet to prevent water leakage while transmitting hydrodynamic effects to the dam. Both the dam and reservoir were assembled on a large wooden base plate

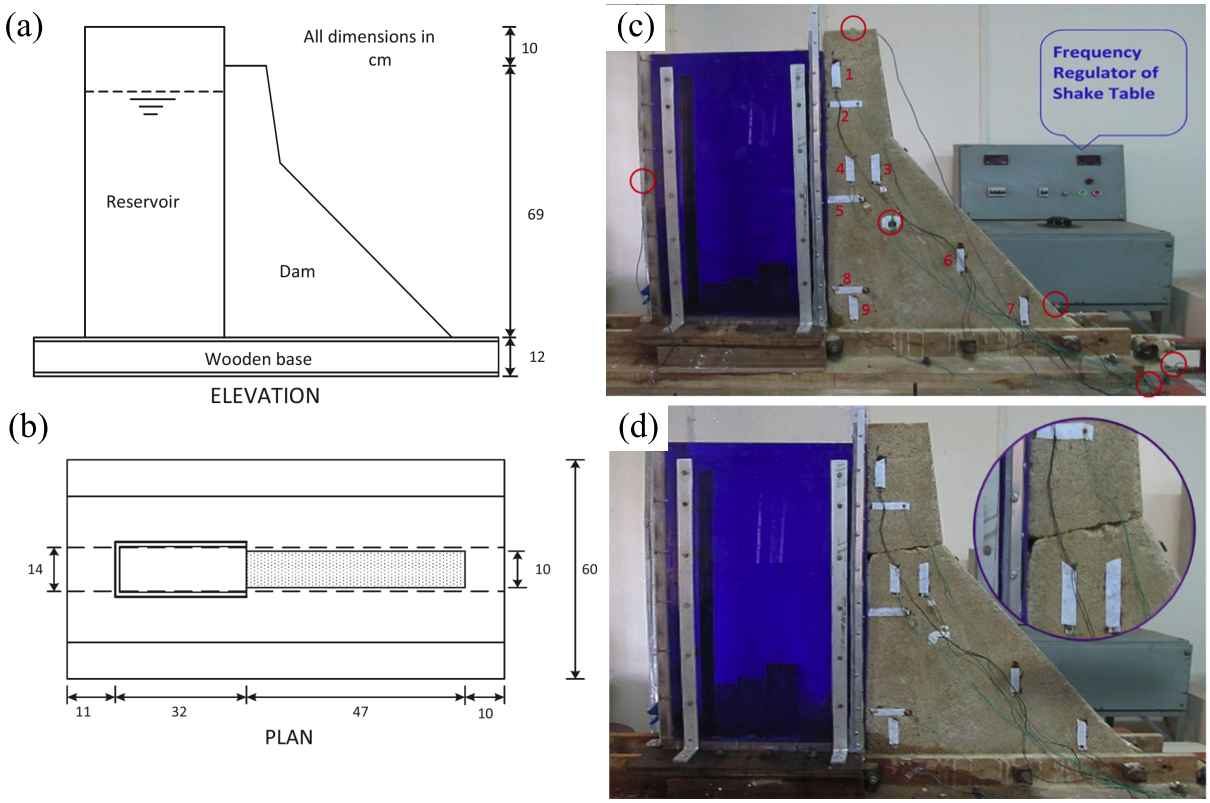

Figure 2.27 Experiment setup [14]: (a) and (b): elevation and plan view of the system; (c) experimental setup with instrumentation; (d) crack pattern in dam model.

and secured with nuts and bolts to prevent sliding. Figures 2.27(a), (b), and (c) illustrate the elevation and plan view of the system with the experimental setup, respectively. The experimental results were compared with a numerical model, showing that the estimated cracks matched well with the observed test results, as depicted in Figures 2.27(d).

Wang and his colleagues conducted a dynamic test a section of 2 m high gravity dam to study the responses of the dam-reservoir coupling system during an earthquake [15]. The research focused on evaluating the hydrodynamic pressure, natural frequency of the dam-reservoir system, and acceleration amplification factors along the dam height. The section of the Huangdeng gravity dam in China was selected as the prototype for the shaking table tests. These tests were conducted at the Research Laboratory of Earthquake Engineering at Dalian University of Technology in China. The main test equipment included a large simulation system for underwater earthquakes, a digital signal acquisition and processing system (DSPS), water pressure sensors, and acceleration sensors. Knowing the prototype dam section's size, the shaking table's loading capabilities, and the properties of the model material, a geometric scale of 1 : 100 was chosen for the model.

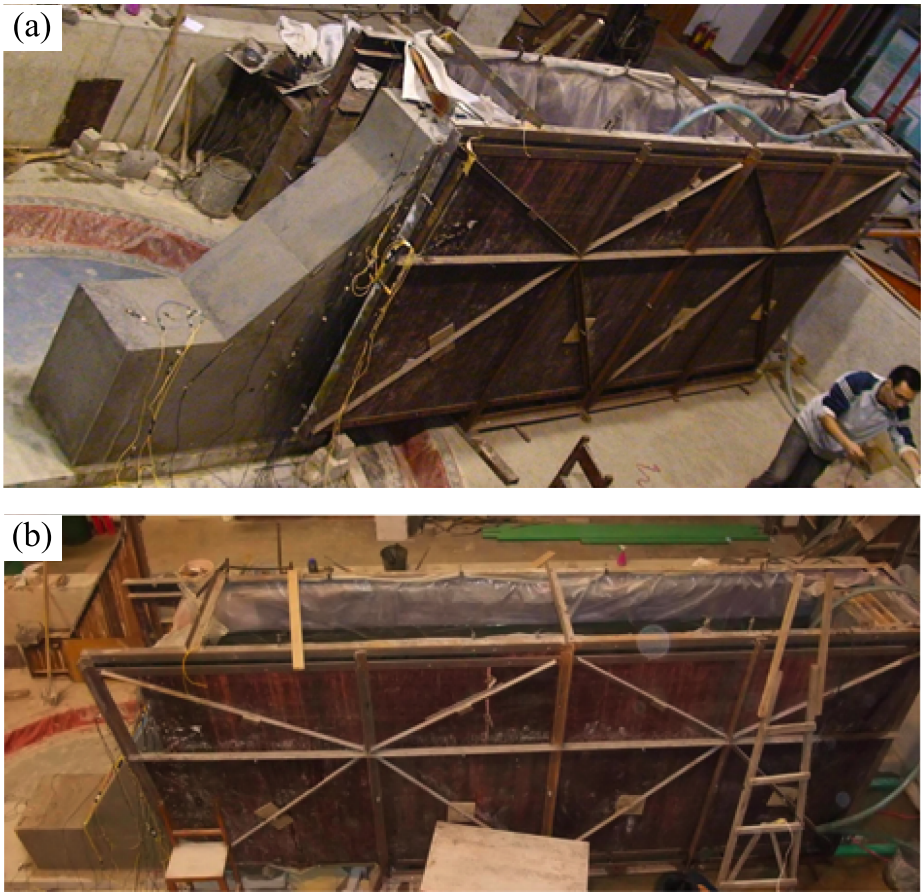

Figure 2.28 The model for the dam-reservoir coupling system [15]: (a) the model cured for 24 h; (b) the model of full reservoir.

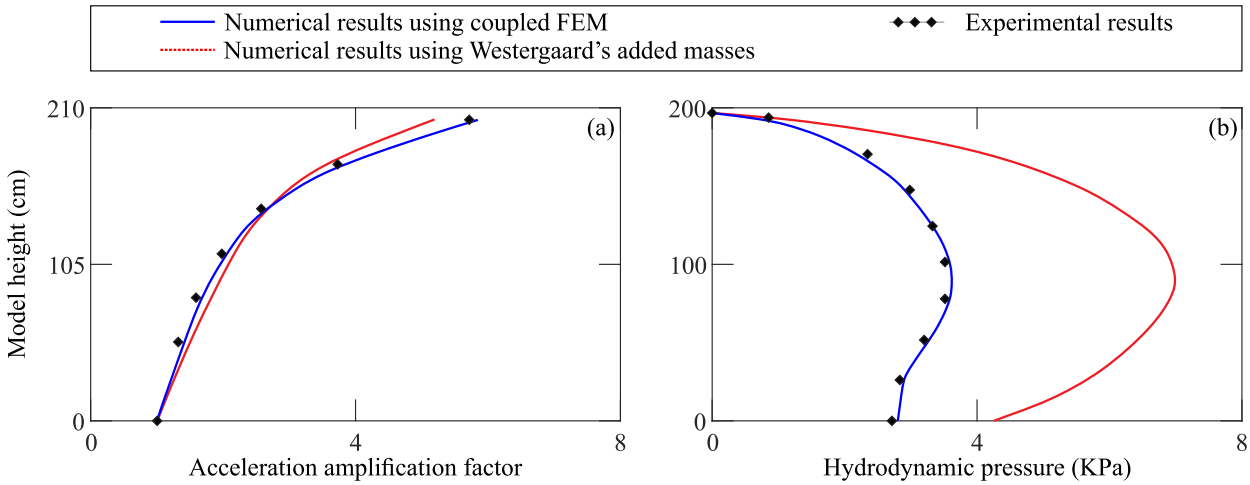

Figure 2.29 Comparison of the the experimenal results with numerical models (adapted from [15]): (a) the distributions of acceleration amplification factors along the model height; (b) the distributions of hydordynamic pressure along the model height.

A concrete-like material was used to construct the dam section model, with water serving as the fluid in the tests. The dynamic model of the dam section was 203 cm high and 25 cm thick, weighing approximately 3.5 tons. A water tank measuring 6.0 × 0.8 × 2.2 m was installed on the water side of the model (Figure 2.28). Ten pressure sensors, spaced 25 cm apart along the dam model to record hydrodynamic pressure. An artificial wave from the Qian'an seismic response spectrum, with a PGA of 0.251 g, was. Two finite element models simulated dam-reservoir interaction: one with Westergaard's added mass and the other using a coupled fluid-structure interaction based on the Lagrangian formulation. Figure 2.29 compares the experimental and numerical results, showing excellent agreement between the coupled finite element model and experimental data [15].

Another example that utilized the added mass representation for hydrodynamic effects is presented by Ansari and Agarwal in their study on rehabilitation techniques for severely damaged concrete gravity dams [16]. They compared the cyclic behavior of small-scale con-

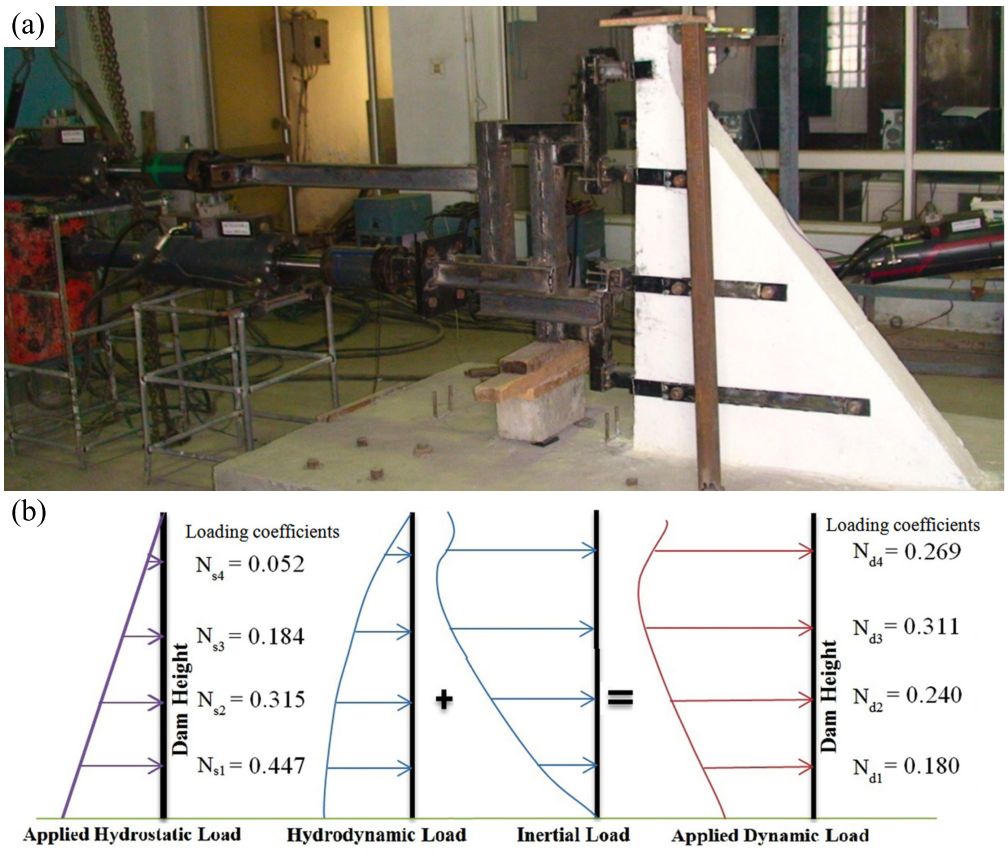

Figure 2.30 Experimental setup [16]: (a) concrete gravity dam model along with loading arrangements; (b) load pattern applied over the model for the hydrostatic and coupled-dynamic loads.

crete gravity dam models before and after retrofitting. The retrofitting involved the use of external buttress walls and anchor bolts with epoxy grouting. Four equivalent concentrated quasi-static loads were applied to the upstream face of the model to simulate hydrostatic and dynamic loads as shown in Figure 2.30 (a). A loading mechanism designed to ensured proper force distribution. Two actuators were used, one for hydrostatic loading and another for coupled-dynamic loading, which combined inertia and hydrodynamic loads. The lateral loads, including inertial and hydrodynamic effects generated during an earthquake, were applied through this mechanism, as shown in Figure 2.30 (b).

Aldemir and his colleagues proposed a pseudo-dynamic (PsD) testing procedure for seismic loading of distributed mass systems [17]. This method was validated through analytical

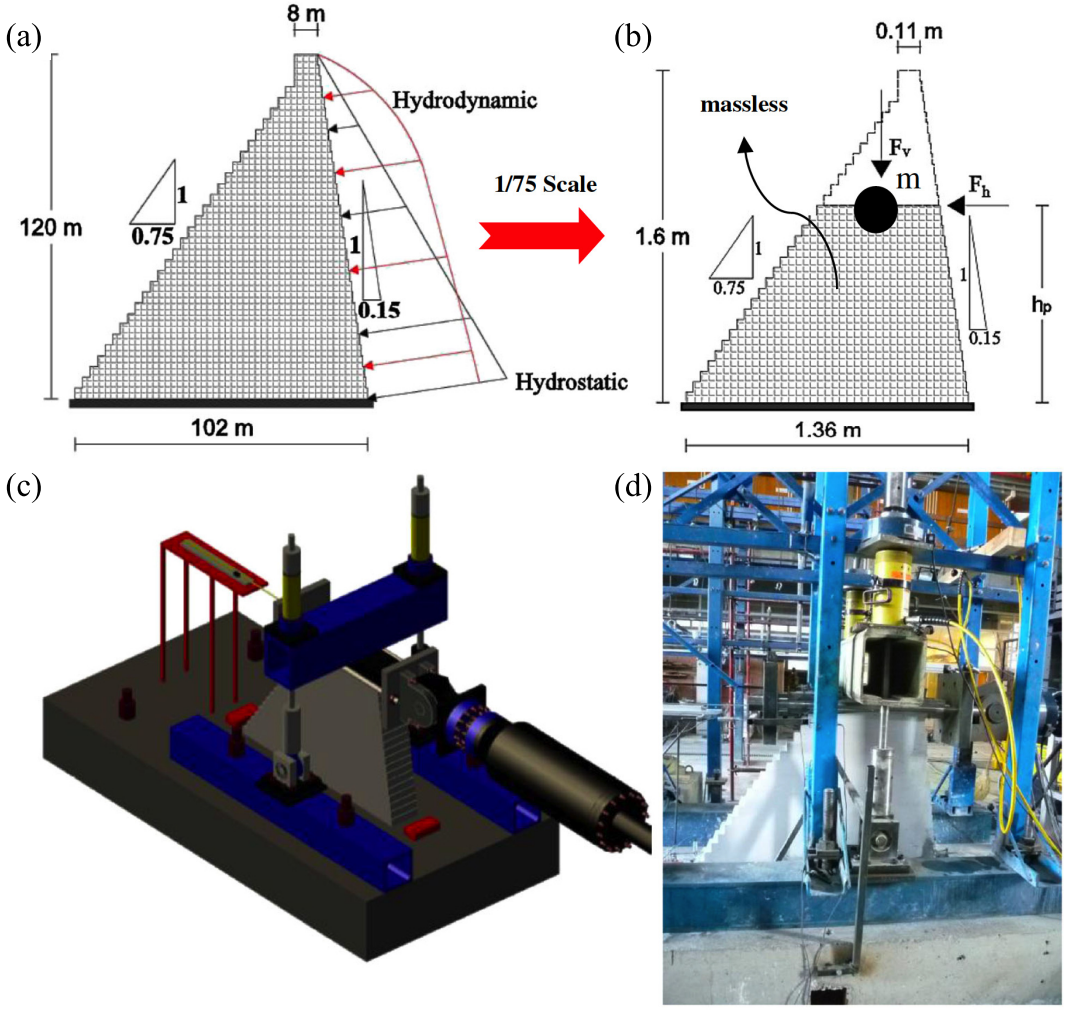

Figure 2.31 Models used in the experimental test and numerical validation of the pseudo-dynamic test [17]: (a) prototype dam; (b) scaled dam model/specimen; (c) and (d) sketch and experimental test setup.

studies, assuming hydrodynamic effects act on the dam specimen under both both static and dynamic loading conditions (Figure 2.31). Inspired by the simplified single degree of freedom (SDOF) modeling approach used in the preliminary design of concrete gravity dams, a pseudo-dynamic testing method was devised for the seismic testing of a concrete gravity dam section [101]. The test specimen was a 1/75 scaled section of the 120-m-high monolith of the Melen dam. After validating the concept with numerical simulations, PsD tests were conducted on the specimen using three ground motions corresponding to different hazard levels. Lateral displacement and base shear demands were measured, along with crack propagation at the base, monitored by crack width and base sliding displacements. Following the PsD loading, a static pushover test determined the reserve capacity of the specimen. They concluded that, despite significant cracking at the monolith's base, no noticeable sliding or stability concerns were identified that could jeopardize the dam's overall stability or integrity.

In the literature, various methods have been employed to simulate hydrodynamic forces on dam structures by applying a force directly to the dam's face. For example, Javanmardi and his colleagues investigated the seismic structural stability of concrete gravity dams, considering transient uplift pressures in cracks [76]. They noted that hydrodynamic dam-reservoir interaction can either increase or decrease water pressure on the upstream face and the crack mouth in contact with the reservoir. In their experimental tests, the crack mouth pressure (P_{crm}) was calculated by summing the hydrostatic pressure and hydrodynamic pressure, with the latter determined using Westergaard's added mass formulation.

For the experimental seismic evaluation of bridge piers surrounded by water, numerous studies have incorporated hydrodynamic effects by constructing water-filled boxes around the specimens for shaking table tests. One notable example is the work of Wei and his colleagues, who assessed the modal dynamic response of bridge foundation piles submerged in water [18]. They built a rigid brick basin to conduct dynamic tests on reduced-scale bridge pile foundations, as shown in Figure 2.32. This experimental test aimed to investigate fluid-structure interaction effects on the modal dynamic response of three bridge pile foundations, varying in the number of piles (nine, five, and four) and their geometrical patterns. The study presented results from ambient and forced vibration tests, analyzing them based on surrounding water levels and pile configurations. Key findings included that the fluid-structure interaction effect on grouped piles increases with water height, consistent with observations for single pile or tower structures in previous research. The study also highlighted that period lengthening due to fluid-structure interaction is more significant when the pile cap is submerged. Hydrodynamic pressures decreased as the number of piles was reduced from nine to four, likely due to decreased structural stiffness and increased spacing between piles. Furthermore, they compared the experimental results with numerical finite

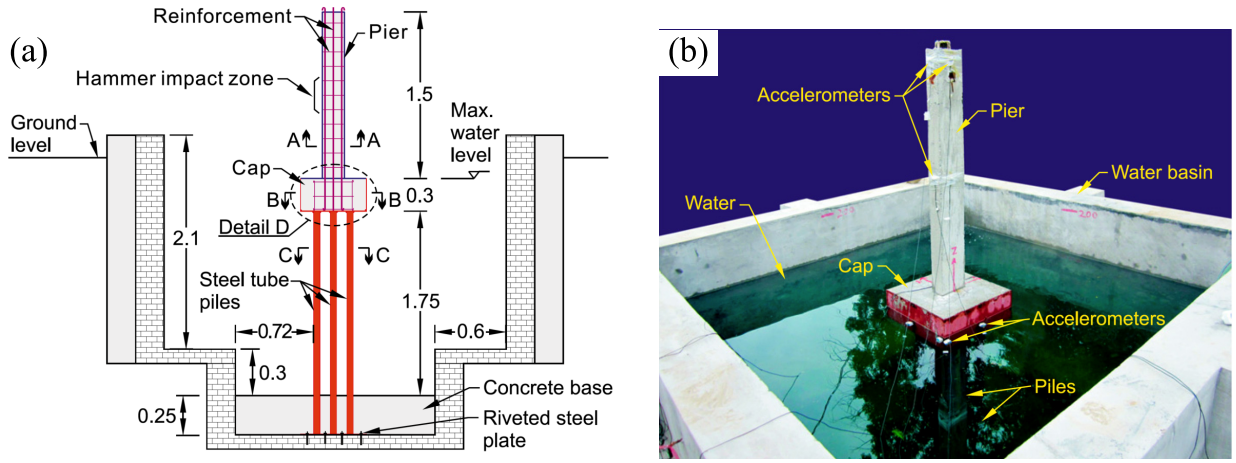

Figure 2.32 Dimensions and details of the experimental setup [18]: (a) dimensions of the rigid brick basin and specimen; (b) global view of the specimen and testing setup.

element models using coupled 3D solid elements for the structural components and 3D solid potential-based elements for the fluid, modeled in the ADINA software [92]. The numerical results showed excellent agreement with the experimental results [18].

2.4.3 Experimental tests neglecting hydrodynamic effects

Due to the challenges highlighted in previous sections, such as the high costs of facilities, maintenance issues, Safety concerns related to water leakage, and similitude violations requiring alternative fluid materials, many researchers have chosen to ignore hydrodynamic effects during shaking table tests of structure-water systems. Although they acknowledge that excluding these effects can impact the results, the complexity and practicality of including hydrodynamic forces often outweigh the benefits. Consequently, many studies focus solely on the seismic response of the structure, neglecting hydrodynamic effects.

For example, Harris and his colleagues conducted shaking table tests on 2D models of concrete gravity dams using a 1:50-scaled Koyna Dam [129]. These tests aimed to simulate seismic effects and provide data for calibrating computer models. Two models were tested. In these experiments, reservoir effects were not modeled.

Tinawi and his colleagues conducted shake table experiments on four 3.4-meter-high concrete gravity dam models to investigate their dynamic cracking and sliding responses [65]. The experimental results were compared with a smeared cracked finite-element simulation using a nonlinear concrete constitutive model based on fracture mechanics. To induce downstream sliding, a 700 kg hanging mass was attached to the upstream face of the specimen with a

cable. Due to the size of the specimen, the hydrodynamic effects were neglected in this study. Zhou and his colleagues conducted a series of dynamic experiments for 20 models of high arch dams were recently performed on a shaking table, with the water ignored [66].

Ghaemmagham and Ghaemian [67] conducted shaking table tests to investigate the seismic response of a geometric 1:30 scaled model of the Sefid-rud concrete buttress dam. The tests focused on the seismic response of the highest monolith with an empty reservoir. The shaking table, equipped with high-frequency capability, was used to study the dynamic cracking of the model and provide data for calibrating nonlinear computer models. Experimental results were compared with smeared crack and damage mechanics finite-element simulations using nonlinear concrete constitutive models based on fracture mechanics. The authors noted that other factors such as hydrodynamic effects, foundation flexibility, and pre-seismic cracking can significantly influence the seismic behavior of the prototype. Due to experimental limitations, these factors were neglected in the study, and such omissions were acknowledged as potential sources of error in simulating the prototype's behavior.

In a recent study, Zhang and his colleagues conducted shaking table tests to investigate the seismic responses of slender intake tower-hoist chamber systems [19]. They performed a series of experiments with incremental earthquake levels on a $1:40$-scaled model representing a 105 m tall intake tower. To account for the dynamic interactions between the intake tower and backfill concrete, a steel frame was designed to connect the shaking table to the model. They observed that acceleration was amplified by about 4 to 5 times from the bottom to the top of the main tower and over 10 times at the hoist chamber under designed earthquake conditions. Despite knowing that hydrodynamic effects could significantly impact the results, the interaction between water and the structure was not considered in the experiment. The primary reasons for neglecting hydrodynamic effects were limitations related to the geometric scale of the hoist chamber, underwater measuring technology, and visual observation conditions [19] The experimental setup and the residual deformation of the model system at the end of the experiment are shown in Figure 2.33.

Figure 2.33 Experimental set up and residual deformation of the model system at the end of the experiment [19].

CHAPTER 3 ARTICLE 1: RESPONSE SPECTRUM AND MODAL DYNAMIC ANALYSES OF GRAVITY DAMS USING GROUND MOTION ACCELERATIONS MODIFIED TO ACCOUNT FOR HYDRODYNAMIC EFFECTS

Ramtin Kouhdasti[a], Najib Bouaanani[a]

[a]Department of Civil, Geological and Mining Engineering, Polytechnique Montréal, Montréal, QC H3C 3A7, Canada.

Paper published in Journal of Earthquake Spectra on June 16, 2024.

3.1 Abstract

This research proposes simplified methods for response spectrum and modal dynamic analyses of gravity dams using time-history and spectral seismic accelerations modified to directly account for hydrodynamic effects. The developed methods waive the need for specialized fluid-structure interaction software. They also lead to more accurate assessment of coupled structural flexibility and hydrodynamic effects due to each vibration mode than the static correction method commonly used in traditional simplified methods. The methodology utilizes analytical formulations of hydrodynamic pressure or simplified added-masses to obtain the contributions of the selected vibration modes to the total seismic response. A hydrodynamic modification factor characterising the amplification/deamplification of acceleration seismic demands due to earthquake-induced hydrodynamic effects is also introduced. The application of the proposed methods is illustrated numerically through examples of two typical gravity dam-reservoir systems subjected to four earthquakes. The obtained results are in excellent agreement with the classical reference solutions. Time-history and spectral seismic acceleration demands modified by hydrodynamic effects as well as selected key response indicators, such as relative displacements and stresses within the studied gravity dams, are discussed.

Nomenclature

Abbreviations

ESDOF	Equivalent single degree of freedom
FEA	Finite element analysis
DFFT	Discrete fast Fourier transform
IDFFT	Inverse discrete Fourier transform
FRF	Frequency response function
HMF	Hydrodynamic modification factor
RSA	Response spectrum analysis
SDOF	Single degree of freedom
SRSS	Square root of the sum of the squares
THMSA	Time-history modal superposition analysis

Roman symbols

$a_{\mathrm{g}}^{(j)}$	Modified horizontal ground motion acceleration corresponding to vibration mode j [Eqs. (3.41)]
$C_{\mathrm{f}}\,;C_{\mathrm{w}}$	Velocity of pressure waves in the foundation and reservoir, respectively
$\mathbf{F}_{\mathrm{h}}$	Earthquake-induced lateral hydrodynamic forces
$\widehat{f}_j(y)$	Equivalent lateral static force on the dam impounding a reservoir subjected to original horizontal ground motion acceleration $\ddot{x}_{\mathrm{g}}$, and considering only the contribution of vibration mode j [Eq. (3.56)]
$\widetilde{f}_j(y)$	Equivalent lateral static force on the dam with empty reservoir subjected to modified horizontal ground motion acceleration $a_{\mathrm{g}}^{(j)}$, including hydrodynamic effects and considering only the contribution of vibration mode j [Eq. (3.56)]
$f_j(y)$	Equivalent lateral static force on the dam with empty reservoir subjected to original horizontal ground motion acceleration $\ddot{x}_{\mathrm{g}}$ considering only the contribution of vibration mode j [Eq. (3.59)]
$H_{\mathrm{s}}\,;H_{\mathrm{w}}$	Dam and reservoir heights, respectively
$I_{0,n}\,;I_{j,n}$	Integral terms given by Eq. (3.73) and Eq. (3.74), respectively
$K_j\,;C_j$	Stiffness and viscous damping of the SDOF systems corresponding to vibration mode j given by Eqs. (3.43) and (3.44), respectively
$\mathbf{M}\,;\mathbf{C}\,;\mathbf{K}$	Mass, damping, and stiffness matrices of the dam with empty reservoir, respectively
$M_j\,;L_j$	Generalized modal mass and force of the dam with empty reservoir corresponding to vibration mode j given by Eq. (3.38) and Eq. (3.39), respectively
$N_{\mathrm{P}}=2^k$	Number of excitation frequencies for DFFT and IDFFT with k integer
$N_{\mathrm{s}}\,;\,N_{\mathrm{w}}$	Number of structural and water (i.e. acoustical) modes, respectively

Roman symbols

p_0	FRF of hydrodynamic pressure at rigid dam-reservoir interface due to horizontal ground motion acceleration $\ddot{x}_{\mathrm{g}}$ [Eq. (62)]
p_j	FRF of hydrodynamic pressure at dam-reservoir interface due to horizontal ground motion acceleration corresponding to the x–component of structural mode shape $\psi_j^{(x)}$ [Eq. (3.63)]
p	FRF of total hydrodynamic pressure
q	Damping coefficient accounting for reservoir bottom wave absorption due to sedimentation [Eq. (3.66)]
$\widehat{\mathbf{Q}}\,;\widehat{Q}_m$	Matrix in Eq. (3.45) and its elements given by Eq. (3.47), respectively
$\left\lvert\,\tilde{r}\,\right\rvert^{(\max)}$	Maximum absolute total seismic response including hydrodynamic effects
$\left\lvert\,\tilde{r}_j\,\right\rvert^{(\max)}$	Maximum absolute modal seismic response including hydrodynamic effects
$\widehat{\mathbf{S}}\,;\widehat{S}_{j,m}(\omega)$	Vector in Eq. (3.45) and its elements given by Eq. (3.46), respectively
$S_{\mathrm{A}}^{[a_{\mathrm{g}}^{(j)}]}\,;\,S_{\mathrm{D}}^{[a_{\mathrm{g}}^{(j)}]}$	Pseudo-acceleration and displacement response spectra of modified ground motion acceleration $a_{\mathrm{g}}^{(j)}$ corresponding to vibration mode j, respectively
$S_{\mathrm{A}}^{[\ddot{x}_{\mathrm{g}}]}$	Pseudo-acceleration response spectrum of the original ground motion acceleration $\ddot{x}_{\mathrm{g}}$
T_j	Vibration period of the dam with empty reservoir corresponding to mode j
t_a	Duration of the applied accelerogram
$\ddot{\mathbf{U}}\,;\dot{\mathbf{U}}\,;\mathbf{U}$	Vectors of nodal relative accelerations, relative velocities, and relative displacements of the dam with empty reservoir subjected to original ground motion acceleration $\ddot{x}_{\mathrm{g}}$, respectively
$\ddot{\widehat{\mathbf{U}}}\,;\dot{\widehat{\mathbf{U}}}\,;\widehat{\mathbf{U}}$	Vectors of nodal relative accelerations, relative velocities, and relative displacements of the dam impounding a reservoir and subjected to original ground motion acceleration $\ddot{x}_{\mathrm{g}}$, respectively
$\widehat{u}\,;\,\ddot{\widehat{u}}\,;\,u\,;\,\ddot{u}$	Total of relative horizontal displacements and accelerations of the dam-reservoir system, and total of relative horizontal displacements and accelerations of the dam with empty reservoir subjected to original ground motion acceleration $\ddot{x}_{\mathrm{g}}$, respectively
$\widetilde{u}\,;\,\ddot{\widetilde{u}}$	Total of relative horizontal displacements and accelerations of the dam with empty reservoir subjected to modified ground motion acceleration, respectively
$u_j\,;\ddot{u}_j$	Relative horizontal displacement and relative horizontal acceleration of the dam with empty reservoir subjected to original ground motion acceleration $\ddot{x}_{\mathrm{g}}$ considering only the contribution of vibration mode j, respectively
$\widehat{u}_j\,;\,\ddot{\widehat{u}}_j$	Relative horizontal displacement and relative horizontal acceleration of the dam-reservoir system subjected to original ground motion acceleration $\ddot{x}_{\mathrm{g}}$ considering only the contribution of vibration mode j, respectively

Roman symbols

$\widetilde{u}_j$; $\ddot{\widetilde{u}}_j$ — Relative horizontal displacement and relative horizontal acceleration of the dam with empty reservoir subjected to modified ground motion acceleration $a_{\mathrm{g}}^{(j)}$ considering only the contribution of vibration mode j, respectively

$\left|u_j(x,y,t)\right|^{(\max)}$ — Maximum (i.e. peak) absolute value of seismic relative horizontal displacement of a point of coordinates (x,y) of the dam with empty reservoir subjected to the original ground motion acceleration $\ddot{x}_{\mathrm{g}}$ considering only the contribution of mode j

$\left|\widehat{u}_j(x,y,t)\right|^{(\max)}$ — Maximum (i.e. peak) absolute value of seismic relative horizontal displacement of a point of coordinates (x,y) of the dam-reservoir system subjected to the original ground motion acceleration $\ddot{x}_{\mathrm{g}}$ considering only the contribution of mode j

$\left|\widetilde{u}_j(x,y,t)\right|^{(\max)}$ — Maximum (i.e. peak) absolute value of seismic relative horizontal displacement of a point of coordinates (x,y) of the dam with empty reservoir subjected to the modified ground motion acceleration $a_{\mathrm{g}}^{(j)}$ considering only the contribution of vibration mode j

$\left|u_j(y,t)\right|^{(\max)}$ — Maximum (i.e. peak) absolute value of seismic relative horizontal displacement of a point of coordinate y at the upstream face of the dam with empty reservoir subjected to the original ground motion acceleration $\ddot{x}_{\mathrm{g}}$ considering only the contribution of mode j

$\left|\widehat{u}_j(y,t)\right|^{(\max)}$ — Maximum (i.e. peak) absolute value of seismic relative horizontal displacement of a point of coordinate y at the upstream face of the dam impounding a reservoir and subjected to the original ground motion acceleration $\ddot{x}_{\mathrm{g}}$ considering only the contribution of mode j

$\left|\widetilde{u}_j(y,t)\right|^{(\max)}$ — Maximum (i.e. peak) absolute value of seismic relative horizontal displacement of a point of coordinate y at the upstream face of the dam with empty reservoir subjected to the modified ground motion acceleration $a_{\mathrm{g}}^{(j)}$ considering only the contribution of vibration mode j

$\ddot{x}_{\mathrm{g}}$ — Original horizontal ground motion acceleration

$\ddot{Z}_j$; $\dot{Z}_j$; Z_j — Relative acceleration, relative velocity, and relative displacement of the SDOF system equivalent to the dam with empty reservoir subjected to original ground motion acceleration $\ddot{x}_{\mathrm{g}}$ considering only the contribution of vibration mode j, respectively

Roman symbols

$\ddot{\widehat{Z}}_j\,;\,\dot{\widehat{Z}}_j\,;\,\widehat{Z}_j$	Relative acceleration, relative velocity, and relative displacement of the SDOF system equivalent to the dam-reservoir system subjected to original ground motion acceleration $\ddot{x}_{\mathrm{g}}$ considering only the contribution of vibration mode j, respectively
$\ddot{\widetilde{Z}}_j\,;\,\dot{\widetilde{Z}}_j\,;\,\widetilde{Z}_j$	Relative acceleration, relative velocity, and relative displacement of the SDOF system equivalent to the dam with empty reservoir subjected to modified ground motion acceleration $a_{\mathrm{g}}^{(j)}$ considering only the contribution of vibration mode j, respectively

Greek symbols

α	Wave reflection coefficient at reservoir bottom
$\beta_n\,;\,\kappa_n$	Parameters given by Eq. (3.71) and Eq. (3.72) , respectively
$\Delta t^{(\mathrm{init})}$	Initial time interval of the original ground motion acceleration
$\Delta t^{(\mathrm{new})}$	New time interval of the original ground motion acceleration
$\psi_j^{(x)}\,;\psi_j^{(y)}$	x- and y-components of structural mode shape j, respectively
ξ_j	Viscous damping ratio corresponding to vibration mode j
ω_j	Vibration frequency of the dam with empty reservoir corresponding to mode j
$\vartheta_{0,m}\,;\,\vartheta_{j,m}$	Integral terms given by Eqs. (3.48) and (3.49) for analytical formulation of hydrodynamic pressure, or Eqs. (3.50) and (3.51) for Westergaard added-mass formulation, respectively
$\rho_{\mathrm{f}}\,;\,\rho_{\mathrm{s}}\,;\,\rho_{\mathrm{w}}$	Mass densities of foundation, dam, and water, respectively
μ_{s}	Mass of the dam per unit height
ω	Exciting frequency
$\lambda_n\,;\,Y_n$	Reservoir eigenvalue and eigenvector corresponding to water (i.e. acoustical) mode n, respectively

3.2 Introduction

Investigating the dynamic behaviour of dam-reservoir systems and evaluating their seismic safety have been major research and engineering concerns for the last several decades. These systems have the particularity of being subjected to hydrodynamic effects induced by the impounded reservoir during earthquakes [25, 41, 81, 130, 131]. Appropriate modeling of such effects can be achieved using a variety of analytical and numerical methods (e.g. [2–4, 21–26, 28–34,36–38,40,132]). Although several sophisticated methods have been successfully applied to the seismic assessment of dam-reservoir systems, practical approaches are still in high demand due to their simplicity, ease of application and rapid implementation, particularly for routine engineering tasks. In this regard, dynamic modal superposition and response spectrum analyses (RSA) are popular among the broad range of available numerical tools, as they allow the dissection of a structure's response into the contributions of multiple vibration modes, thus enabling a comprehensive understanding of each mode's impact on the total seismic response (e.g. [68, 133]). For a dam-reservoir system, such analyses can be conducted using finite element formulations coupling solid and fluid elements to model earthquake-induced responses of the dam and the reservoir, respectively (e.g. [2,82,96,132,134]). However, such solutions still generally require specialized software and a high-level of expertise to obtain valid results. Indeed, appropriate modeling of reservoir domain, fluid-structure interaction, and relevant boundary conditions can be challenging in day-to-day engineering practice (e.g. [87, 97, 130, 135]). Alternative approaches consist of modelling water effects analytically, through the formulation of added-masses attached to the dam upstream face (e.g. [21]) or hydrodynamic pressures acting at the dam-reservoir interface (e.g. [26, 41, 81]). The added-masses concept is still widely used in practice for its simplicity although it has been proven to be potentially inaccurate depending on the type of ground motion and the dam studied (e.g. [136, 137]). A more accurate alternative is the implementation of earthquake-induced hydrodynamic forces acting on the upstream face of a gravity dam modelled using solid finite elements, i.e. sub-structuring dynamic analysis (e.g. [26, 41]).

Although semi-analytical techniques are generally limited by the simple geometry of the reservoir, and water modeling assumptions (e.g. added-masses vs water compressibility), they can provide a wealth of useful information about the seismic behaviour of gravity dams, especially in the preliminary stages of design or safety evaluation of such critical structures. To further enhance the implementation of earthquake analysis of gravity dams on a routine basis in engineering practice, Fenves and Chopra proposed a simplified method that can be used to estimate a gravity dam's peak seismic response directly from an earthquake design spectrum [26]. This technique consists of modeling a gravity dam as an equivalent

single degree of freedom (ESDOF) system used to evaluate the fundamental mode response of the dam through equivalent lateral static forces and response spectrum analysis. The effects of higher vibration modes are accounted for approximately through a static correction method [29,68]. These simplified procedures have been widely used in practice and have been programmed in-house or in commercial software such as CADAM3D (Computer Analysis of DAMs) [103]. They also served as the basis for several investigations of the behaviour of dam-reservoir systems. For example, Hariri-Ardebili and Saouma introduced a random simplified response spectrum method for gravity dams, utilizing equivalent static lateral forces to assess the seismic risk associated with these structures [39]. The authors also employed a numerical technique to assess the effects of uncertainties in input parameters on the results. Kita and his colleagues used Chopra's simplified method to investigate the effects of selecting a seismic hazard model on the assessment of the structural integrity of an existing dam ("Le Grazie") located in the high seismic risk region of Central Italy [113].

In this article, an alternative simplified approach is proposed to conduct time-history modal superposition and response spectrum analyses of a dam-reservoir system while directly accounting for higher mode effects in lieu of static correction. The proposed approach is based on the inclusion of earthquake-induced reservoir effects into modified versions of the original ground motion acceleration and its response spectrum that can be applied directly to the dam with empty reservoir (i.e. without water). Therefore, specialized software accounting for fluid-structure dynamic interaction is not required. A similar approach was developed by [4], but their focus was on direct integration time-history dynamic analysis of dam-reservoir systems rather than response spectrum and modal superposition analyses.

The article is organized as follows. First, the theoretical background of the proposed methods is presented considering fundamental and higher vibration modes. The equations and steps of the proposed dynamic modal superposition and response spectrum analyses are then provided. Numerical case studies of two typical gravity dam-reservoir systems subjected to four earthquakes are used next to illustrate the application of the proposed methods. The obtained results are discussed including time-history and spectral seismic acceleration demands modified by hydrodynamic effects as well as selected key response indicators such as relative displacements and stresses within the studied gravity dams.

3.3 Theoretical background and proposed methods

3.3.1 Basic assumptions

A typical gravity dam-reservoir system, as shown in Fig. 3.1, is considered. The dam monolith and the impounded rectangular reservoir have heights of H_{s} and H_{w}, respectively. A Cartesian coordinate system with axes x and y with origin at the heel of the dam is adopted and the following main assumptions are made: (i) the dam has a vertical upstream face and a linear elastic behaviour (i.e. no concrete cracking, degradation or sliding at the joints are considered); (ii) the dam foundation is massless and rigid; (iii) foundation radiation damping is neglected; (iv) the water in the reservoir, of mass density ρ_{w}, is assumed inviscid, with its motion irrotational and limited to small amplitudes; (v) gravity surface waves and compulsive effects are neglected; (vi) effects of sediments that may be deposited at reservoir bottom can be considered; (vii) the applied ground motion acceleration is horizontal (i.e. no vertical earthquake component is applied).

$$\mathbf{M}\,\ddot{\mathbf{U}}(t) + \mathbf{C}\,\dot{\mathbf{U}}(t) + \mathbf{K}\,\mathbf{U}(t) = -\mathbf{M}\,\mathbf{1}^{(x)}\,\ddot{x}_{\mathrm{g}}(t) \tag{3.1}$$

3.3.2 Equations of motion

The equations of motion of a dam-reservoir system subjected to horizontal ground motion acceleration $\ddot{x}_{\mathrm{g}}(t)$ can be expressed as [2, 26]

$$\mathbf{M}\,\ddot{\widehat{\mathbf{U}}}(t) + \mathbf{C}\,\dot{\widehat{\mathbf{U}}}(t) + \mathbf{K}\,\widehat{\mathbf{U}}(t) = -\mathbf{M}\,\mathbf{1}^{(x)}\,\ddot{x}_{\mathrm{g}}(t) + \mathbf{F}_{\mathrm{h}}(t) \tag{3.2}$$

in which $\ddot{\widehat{\mathbf{U}}}(t)$, $\dot{\widehat{\mathbf{U}}}(t)$ and $\widehat{\mathbf{U}}(t)$ are column-vectors containing the time-history nodal accelerations, velocities and displacements of the finite element nodes of the structure relative to the ground, respectively, $\mathbf{M}$, $\mathbf{C}$ and $\mathbf{K}$ are the structure's mass, damping and stiffness matrices, respectively, $\mathbf{1}^{(x)}$ is a column-vector containing zeros except along horizontal degrees of freedom corresponding to earthquake direction, and $\mathbf{F}_{\mathrm{h}}(t)$ is a column-vector representing earthquake-induced hydrodynamic forces on the structure. When the dam reservoir is empty, Eq. (3.2) simplifies to

3.3.3 Fundamental mode analysis

Modeling the dam as an ESDOF system and considering only fundamental mode response, the horizontal relative displacement at a point of coordinate (x, y) of the structure can be approximated as

$$\widehat{u}(x, y, t) \approx \widehat{u}_1(x, y, t) = \psi_1^{(x)}(x, y)\,\widehat{Z}_1(t) \tag{3.3}$$

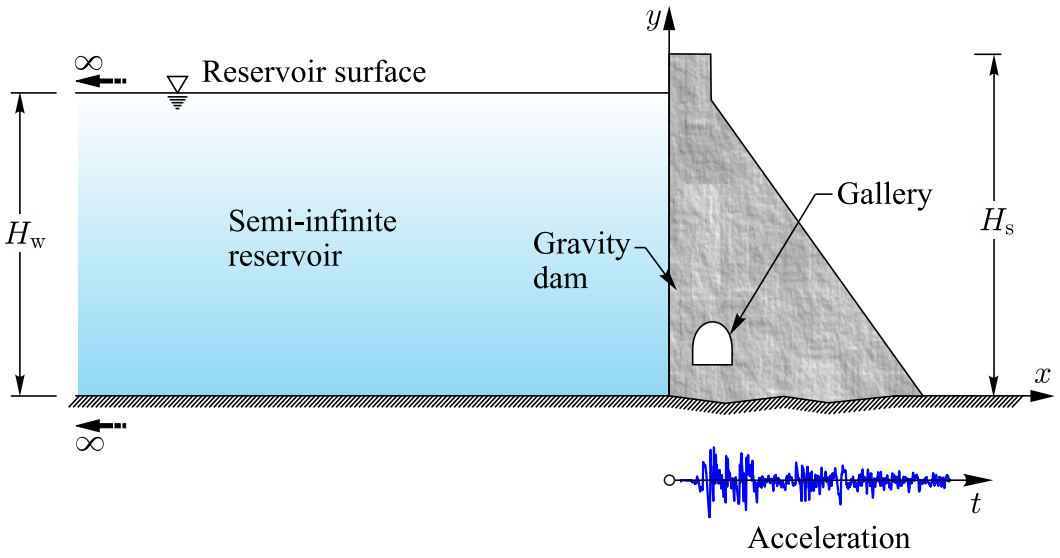

Figure 3.1 Geometry of typical dam-reservoir system studied.

in which $\psi_1^{(x)}(x,y)$ denotes the x–component of the fundamental structural mode shape and $\widehat{Z}_1$ the associated generalized modal coordinate. Eq. (3.2) then simplifies to [26, 87]

$$M_1 \left[\ddot{\widehat{Z}}_1(t) + 2\,\xi_1\,\omega_1\,\dot{\widehat{Z}}_1(t) + \omega_1^2\,\widehat{Z}_1(t) \right] = -L_1\,\ddot{x}_g(t) + \int_0^{H_w} p(y,t)\,\psi_1^{(x)}(y)\,\mathrm{d}y \tag{3.4}$$

where ξ_1 denotes the fraction of critical damping at the fundamental vibration mode of the dam with empty reservoir, ω_1 the fundamental natural vibration frequency, $p(y,t)$ the time-history of hydrodynamic pressure acting at a point of coordinate y on the dam-reservoir interface, and $\psi_1^{(x)}(y)$ the x–component of the fundamental structural mode shape at the same point. The generalized modal mass M_1 and modal participation factor L_1 of the dam with empty reservoir are given by [26, 87]

$$M_1 = \iint \rho_s(x,y) \left\{ \left[\psi_1^{(x)}(x,y)\right]^2 + \left[\psi_1^{(y)}(x,y)\right]^2 \right\} \mathrm{d}x\,\mathrm{d}y \approx \int_0^{H_s} \mu_s(y) \left[\psi_1^{(x)}(y)\right]^2 \mathrm{d}y \tag{3.5}$$

$$L_1 = \iint \rho_s(x,y)\,\psi_1^{(x)}(x,y)\,\mathrm{d}x\,\mathrm{d}y \approx \int_0^{H_s} \mu_s(y)\,\psi_1^{(x)}(y)\,\mathrm{d}y \tag{3.6}$$

with ρ_s and μ_s denoting the density and mass per unit height of the structure, respectively. Considering a unit harmonic horizontal ground motion $\ddot{x}_g(t) = \mathrm{e}^{\mathrm{i}\omega t}$, Eq. (3.4) can be written in the frequency domain as

$$M_1 \left(-\omega^2 + 2\,\mathrm{i}\,\xi_1\,\omega\,\omega_1 + \omega_1^2 \right) \widehat{Z}_1(\omega) = -L_1 + \int_0^{H_w} p(y,\omega)\,\psi_1^{(x)}(y)\,\mathrm{d}y \tag{3.7}$$

or

$$\left[M_1\left(-\omega^2+2\,\mathrm{i}\,\xi_1\,\omega\,\omega_1+\omega_1^2\right)+\omega^2\int_0^{H_\mathrm{w}} p_1(y,\omega)\,\psi_1^{(x)}(y)\,\mathrm{d}y\right]\widehat{Z}_1(\omega)= \\ -L_1+\int_0^{H_\mathrm{w}} p_0(y,\omega)\,\psi_1^{(x)}(y)\,\mathrm{d}y \tag{3.8}$$

where the frequency response function (FRF) of hydrodynamic pressure was separated in the frequency domain as [26, 41]

$$p(y,\omega)=p_0(y,\omega)-\omega^2\,\widehat{Z}_1(\omega)\,p_1(y,\omega) \tag{3.9}$$

with p_0 denoting the hydrodynamic pressure FRF at *rigid* dam-reservoir interface due to horizontal ground motion $\ddot{x}_\mathrm{g}$ and p_1 the hydrodynamic pressure FRF at *flexible* dam-reservoir interface due to horizontal acceleration $\psi_1^{(x)}(0,y)$ of the structure [26, 41]. The FRFs p_0 and p_1 can be evaluated using the expressions given in Appendix A for convenient reference or the simplified formulations proposed by Bouaanani and Perrault [41]. The generalized modal coordinate corresponding to the fundamental structural mode of the dam can then be obtained from Eq. (3.8) as

$$\widehat{Z}_1(\omega)=\frac{L_1}{M_1}\times\frac{1-\vartheta_{0,1}(\omega)/L_1}{\left[1-\vartheta_{1,1}(\omega)/M_1\right]\omega^2-2\,\mathrm{i}\,\xi_1\,\omega\,\omega_1-\omega_1^2} \tag{3.10}$$

in which the frequency-dependent parameters $\vartheta_{0,1}$ and $\vartheta_{1,1}$ are given by

$$\vartheta_{0,1}(\omega)=\int_0^{H_\mathrm{w}} p_0(y,\omega)\,\psi_1^{(x)}(y)\,\mathrm{d}y \tag{3.11}$$

$$\vartheta_{1,1}(\omega)=\int_0^{H_\mathrm{w}} p_1(y,\omega)\,\psi_1^{(x)}(y)\,\mathrm{d}y \tag{3.12}$$

These two parameters can also be evaluated using the simplified procedure proposed by [87]. The previous equations are based on the modeling of earthquake-induced water effects through hydrodynamic pressures interacting with the vibrations of the dam monolith. If the simplified Westergaard added-mass formulation [21] is considered instead, Eqs. (3.11) and (3.12) can be replaced by

$$\vartheta_{0,1}(\omega)=\frac{7}{8}\rho_\mathrm{w}\int_0^{H_\mathrm{w}}\sqrt{H_\mathrm{w}(H_\mathrm{w}-y)}\,\psi_1^{(x)}(y)\,\mathrm{d}y \tag{3.13}$$

$$\vartheta_{1,1}(\omega)=\frac{7}{8}\rho_\mathrm{w}\int_0^{H_\mathrm{w}}\sqrt{H_\mathrm{w}(H_\mathrm{w}-y)}\left[\psi_1^{(x)}(y)\right]^2\mathrm{d}y \tag{3.14}$$

The modal relative horizontal displacement $\widehat{u}_1$ and acceleration $\ddot{\widehat{u}}_1$ of the dam-reservoir system

subjected to a ground motion acceleration $\ddot{x}_{\mathrm{g}}(t)$ can be expressed as follows

$$\widehat{u}_1(x,y,\omega) = \ddot{x}_{\mathrm{g}}(\omega)\,\widehat{Z}_1(\omega)\,\psi_1^{(x)}(x,y)\,; \qquad \ddot{\widehat{u}}_1(x,y,\omega) = -\ddot{x}_{\mathrm{g}}(\omega)\,\omega^2\,\widehat{Z}_1(\omega)\,\psi_1^{(x)}(x,y) \tag{3.15}$$

where the Fourier transform $\ddot{x}_{\mathrm{g}}(\omega)$ of ground motion acceleration $\ddot{x}_{\mathrm{g}}(t)$ is given by

$$\ddot{x}_{\mathrm{g}}(\omega) = \int_0^{t_a} \ddot{x}_{\mathrm{g}}(t)\,\mathrm{e}^{-\mathrm{i}\omega t}\,\mathrm{d}t \tag{3.16}$$

in which t_a is the time duration of the applied accelerogram.

For a dam with empty reservoir, Eqs. (3.3), (3.4), (3.7), (3.10) and (3.15) are, respectively, substituted by

$$u(x,y,t) \approx u_1(x,y,t) = \psi_1^{(x)}(x,y)\,Z_1(t) \tag{3.17}$$

$$M_1\left[\ddot{Z}_1(t) + 2\,\xi_1\,\omega_1\,\dot{Z}_1(t) + \omega_1^2\,Z_1(t)\right] = -L_1\,\ddot{x}_{\mathrm{g}}(t) \tag{3.18}$$

$$M_1\left(-\omega^2 + 2\,\mathrm{i}\,\xi_1\,\omega\,\omega_1 + \omega_1^2\right) Z_1(\omega) = -L_1 \tag{3.19}$$

$$Z_1(\omega) = \frac{L_1}{M_1} \times \frac{1}{\left(\omega^2 - 2\,\mathrm{i}\,\xi_1\,\omega\,\omega_1 - \omega_1^2\right)} \tag{3.20}$$

Next, the objective is to define a ground motion acceleration, denoted hereafter as $a_{\mathrm{g}}^{(1)}$, that when applied to a dam without reservoir, produces the same effects than the original ground motion acceleration applied to the same dam impounding a reservoir. The modal relative horizontal displacement $\widetilde{u}_1$ and acceleration $\ddot{\widetilde{u}}_1$ at a point (x,y) of the dam with empty reservoir subjected to this modified ground motion acceleration can be expressed as

$$\widetilde{u}_1(x,y,\omega) = a_{\mathrm{g}}^{(1)}(\omega)\,Z_1(\omega)\,\psi_1^{(x)}(x,y) \tag{3.21}$$

and

$$\ddot{\widetilde{u}}_1(x,y,\omega) = -\omega^2\,a_{\mathrm{g}}^{(1)}(\omega)\,Z_1(\omega)\,\psi_1^{(x)}(x,y) \tag{3.22}$$

For these quantities to be equal to those produced by the original ground motion acceleration provided by Eq. (3.15), i.e. $\widetilde{u}_1 = \widehat{u}_1$ and $\ddot{\widetilde{u}}_1 = \ddot{\widehat{u}}_1$, the following equality has to be satisfied

$$a_{\mathrm{g}}^{(1)}(\omega)\,Z_1(\omega)\,\psi_1^{(x)}(x,y) = \ddot{x}_{\mathrm{g}}(\omega)\,\widehat{Z}_1(\omega)\,\psi_1^{(x)}(x,y) \tag{3.23}$$

yielding the expression of a mode- and frequency-dependent ground motion acceleration $a_{\mathrm{g}}^{(1)}$ defined by modifying the original input ground motion acceleration $\ddot{x}_{\mathrm{g}}$ as follows

$$a_{\mathrm{g}}^{(1)}(\omega) = \ddot{x}_{\mathrm{g}}(\omega)\,\frac{\widehat{Z}_1(\omega)}{Z_1(\omega)} \tag{3.24}$$

Substituting $\widehat{Z}_1(\omega)$ and $Z_1(\omega)$ by their expressions from Eqs. (3.10) and (3.20), respectively, into Eq. (3.24), yields the following expression of the modified ground motion acceleration $a_{\rm g}^{(1)}(\omega)$

$$a_{\rm g}^{(1)}(\omega) = \ddot{x}_{\rm g}(\omega) \times \left[1 - \frac{\vartheta_{0,1}(\omega)}{L_1}\right] \frac{\left(\omega^2 - 2\,{\rm i}\,\xi_1\,\omega\,\omega_1 - \omega_1^2\right)}{\left[1 - \vartheta_{1,1}(\omega)/M_1\right]\omega^2 - 2\,{\rm i}\,\xi_1\,\omega\,\omega_1 - \omega_1^2}$$

$$= \ddot{x}_{\rm g}(\omega) \times \left[1 - \frac{\vartheta_{0,1}(\omega)}{L_1}\right] \frac{M_1\left(1 - 2\,{\rm i}\,\xi_1\,\omega_1/\omega - \omega_1^2/\omega^2\right)}{M_1\left(1 - 2\,{\rm i}\,\xi_1\,\omega_1/\omega - \omega_1^2/\omega^2\right) - \vartheta_{1,1}(\omega)} \tag{3.25}$$

or

$$a_{\rm g}^{(1)}(\omega) = \ddot{x}_{\rm g}(\omega) \left[1 - \frac{\vartheta_{0,1}(\omega)}{L_1}\right] \left[1 - \frac{\vartheta_{1,1}(\omega)}{M_1\left(1 - 2\,{\rm i}\,\xi_1\,\omega_1/\omega - \omega_1^2/\omega^2\right)}\right]^{-1} \tag{3.26}$$

Applying Fourier inverse transform to $a_{\rm g}^{(1)}(\omega)$ yields the following modified time-history ground motion acceleration corresponding to the fundamental structural mode

$$a_{\rm g}^{(1)}(t) = \frac{1}{2\pi}\int_{-\infty}^{\infty} a_{\rm g}^{(1)}(\omega)\,{\rm e}^{{\rm i}\omega t}\,{\rm d}\omega \tag{3.27}$$

This accelerogram can be directly applied to the dam with *empty* reservoir to obtain the contribution of the fundamental mode to the time-history response of the dam-reservoir system through the solution of the equation

$$\ddot{\widetilde{Z}}_1(t) + 2\,\xi_1\,\omega_1\,\dot{\widetilde{Z}}_1(t) + \omega_1^2\,\widetilde{Z}_1(t) = -\frac{L_1}{M_1}\,a_{\rm g}^{(1)}(t) \tag{3.28}$$

for the generalized coordinate $\widetilde{Z}_1$. In other terms, the solution of Eq. (3.28) is the same as that of Eq. (3.4), i.e. $\widetilde{Z}_1 = \widehat{Z}_1$. In a finite element analysis (FEA), the dynamic response of the dam-reservoir system can be obtained through fundamental modal dynamic (time-history) analysis of the dam with empty reservoir subjected to the modified ground motion accelerations $a_{\rm g}^{(1)}(t)$.

The solution $\widetilde{Z}_1(t)$ of Eq. (3.28) can be obtained as the time-history displacement of an SDOF system with mass M_1 given by Eq. (3.5), stiffness

$$K_1 = \frac{4\pi^2}{T_1^2}\,M_1 \tag{3.29}$$

and viscous damping

$$C_1 = \frac{4\pi}{T_1}\,\xi_1\,M_1 \tag{3.30}$$

subjected to ground motion acceleration $L_1\,a_{\rm g}^{(1)}(t)$.

The maximum (i.e. peak) absolute value of the seismic relative horizontal displacement of the dam-reservoir system considering only fundamental mode contribution can then be obtained as

$$\begin{aligned}\left|\widehat{u}_1(x,y,t)\right|^{(\max)} &= \left|\widetilde{u}_1(x,y,t)\right|^{(\max)} \\ &= \frac{L_1}{M_1}\, S_{\mathrm{D}}^{[a_{\mathrm{g}}^{(1)}]}(T_1,\xi_1)\, \psi_1^{(x)}(x,y) \\ &= \frac{L_1}{M_1}\, \frac{T_1^2}{4\pi^2}\, S_{\mathrm{A}}^{[a_{\mathrm{g}}^{(1)}]}(T_1,\xi_1)\, \psi_1^{(x)}(x,y)\end{aligned} \tag{3.31}$$

in which $S_{\mathrm{D}}^{[a_{\mathrm{g}}^{(1)}]}(T_1,\xi_1)$ and $S_{\mathrm{A}}^{[a_{\mathrm{g}}^{(1)}]}(T_1,\xi_1)$ denote, respectively, the spectral displacement and pseudo-acceleration of modified ground motion acceleration $a_{\mathrm{g}}^{(1)}(t)$ at the fundamental period T_1 of the dam with empty reservoir, considering a modal viscous damping ξ_1. Assuming that the dam fundamental vibration mode shape and displacements are practically constant over the breadth of the dam monolith [29], i.e. $\psi_1^{(x)}(x,y) \approx \psi_1^{(x)}(0,y)$ and $\widehat{u}_1(x,y,t) \approx \widehat{u}_1(0,y,t)$, Eq. (3.31) could be rewritten as

$$\left|\widehat{u}_1(y,t)\right|^{(\max)} = \left|\widetilde{u}_1(y,t)\right|^{(\max)} = \frac{L_1}{M_1}\, \frac{T_1^2}{4\pi^2}\, S_{\mathrm{A}}^{[a_{\mathrm{g}}^{(1)}]}(T_1,\xi_1)\, \psi_1^{(x)}(y) \tag{3.32}$$

in which $\psi_1^{(x)}(y)$, $\widehat{u}_1(y,t)$ and $\widetilde{u}_1(y,t)$ replace $\psi_1^{(x)}(0,y)$, $\widehat{u}_1(0,y,t)$ and $\widetilde{u}_1(0,y,t)$, respectively, for simplicity of notation.

It is worth mentioning that the maximum absolute value of the seismic relative horizontal displacement of the dam with empty reservoir subjected to original ground motion acceleration can be obtained as

$$\left|u_1(y,t)\right|^{(\max)} = \frac{L_1}{M_1}\, \frac{T_1^2}{4\pi^2}\, S_{\mathrm{A}}^{[\ddot{x}_{\mathrm{g}}]}(T_1,\xi_1)\, \psi_1^{(x)}(y) \tag{3.33}$$

in which $S_{\mathrm{A}}^{[\ddot{x}_{\mathrm{g}}]}(T_1,\xi_1)$ denotes the pseudo-acceleration of the original ground motion acceleration $\ddot{x}_{\mathrm{g}}(t)$ at the fundamental period T_1 of the dam with empty reservoir, considering a modal viscous damping ξ_1. Hydrodynamic-induced modifications to seismic demands (i.e. amplification or de-amplification) corresponding to the dam's fundamental mode can then be evaluated through the ratio of maximum absolute value of the seismic relative horizontal displacements with and without reservoir. This ratio is also equal to that of pseudo-accelerations of the modified and original ground motion accelerations according to Eqs. (3.32) and (3.33), i.e. $\left|\widehat{u}_1(y,t)\right|^{(\max)} / \left|u_1(y,t)\right|^{(\max)} = S_{\mathrm{A}}^{[a_{\mathrm{g}}^{(1)}]}(T_1,\xi_1) / S_{\mathrm{A}}^{[\ddot{x}_{\mathrm{g}}]}(T_1,\xi_1)$. It is important to note that another advantage of the proposed approach is that it does not require the evaluation of the vibration period and damping corresponding to the fundamental mode of the dam-reservoir system, which are different from those of the dam with empty reservoir, i.e. T_1 and ξ_1.

The heightwise distribution of the equivalent lateral static force including hydrodynamic effects at the fundamental vibration mode of the dam can then be obtained as

$$\widehat{f}_1(y) = \widetilde{f}_1(y) = \frac{4\pi^2}{T_1^2}\,\mu_s(y)\left|\widehat{u}_1(y,t)\right|^{(\max)} \tag{3.34}$$

or using Eq. (3.32)

$$\widehat{f}_1(y) = \widetilde{f}_1(y) = \frac{L_1}{M_1}\,\mu_{\rm s}(y)\,S_{\rm A}^{[a_{\rm g}^{(1)}]}(T_1,\xi_1)\,\psi_1^{(x)}(y) \tag{3.35}$$

This equivalent lateral static force can be applied to the dam with *empty* reservoir to approximate the maximum seismic response of the dam-reservoir system including only the contribution of the fundamental vibration mode.

The heightwise distribution of the equivalent lateral static force corresponding to the dam with empty reservoir subjected to original ground motion acceleration at the fundamental vibration mode is given by

$$f_1(y) = \frac{L_1}{M_1}\,\mu_{\rm s}(y)\,S_{\rm A}^{[\ddot{x}_{\rm g}]}(T_1,\xi_1)\,\psi_1^{(x)}(y) \tag{3.36}$$

Similarly to the maximum absolute value of relative horizontal displacements above, comparing Eqs. (3.35) and (3.36) shows that the ratio of the equivalent lateral static forces at a given coordinate $y > 0$ including and excluding hydrodynamic effects, i.e. $\widehat{f}_1(y)/f_1(y)$, is also equal to the ratio of the pseudo-accelerations of the modified and original ground motion accelerations, i.e. $S_{\rm A}^{[a_{\rm g}^{(1)}]}(T_1,\xi_1)/S_{\rm A}^{[\ddot{x}_{\rm g}]}(T_1,\xi_1)$. It is worth mentioning that this ratio is independent of the coordinate y.

3.3.4 Effects of higher modes

When $N_{\rm s}$ structural modes are to be included in the analysis, Eq. (3.28) can be extended to generalized modal coordinates $\widetilde{Z}_j$ corresponding to each mode $j = 1 \ldots N_{\rm s}$ of the dam with *empty* reservoir subjected to a modified ground motion acceleration $a_{\rm g}^{(j)}(t)$, i.e.

$$\ddot{\widetilde{Z}}_j(t) + 2\,\xi_j\,\omega_j\,\dot{\widetilde{Z}}_j(t) + \omega_j^2\,\widetilde{Z}_j(t) = -\frac{L_j}{M_j}\,a_{\rm g}^{(j)}(t)\,, \qquad j = 1 \ldots N_{\rm s} \tag{3.37}$$

where ω_j denotes the natural vibration frequency of structural mode j, ξ_j the corresponding viscous damping ratio, M_j and L_j the generalized modal mass and participation factor that

can be obtained as

$$M_j = \iint \rho_{\mathrm{s}}(x,y) \left\{ \left[\psi_j^{(x)}(x,y)\right]^2 + \left[\psi_j^{(y)}(x,y)\right]^2 \right\} \mathrm{d}x\, \mathrm{d}y \approx \int_0^{H_{\mathrm{s}}} \mu_{\mathrm{s}}(y) \, \left[\psi_j^{(x)}(y)\right]^2 \mathrm{d}y \tag{3.38}$$

$$L_j = \iint \rho_{\mathrm{s}}(x,y)\, \psi_j^{(x)}(x,y)\, \mathrm{d}x\, \mathrm{d}y \approx \int_0^{H_{\mathrm{s}}} \mu_{\mathrm{s}}(y)\, \psi_j^{(x)}(y)\, \mathrm{d}y \tag{3.39}$$

and $a_{\mathrm{g}}^{(j)}(t)$ the modified ground motion acceleration given by

$$a_{\mathrm{g}}^{(j)}(t) = \frac{1}{2\pi} \int_{-\infty}^{\infty} a_{\mathrm{g}}^{(j)}(\omega)\, \mathrm{e}^{\mathrm{i}\omega t}\, \mathrm{d}\omega\,, \qquad j = 1 \ldots N_{\mathrm{s}} \tag{3.40}$$

with

$$a_{\mathrm{g}}^{(j)}(\omega) = \ddot{x}_{\mathrm{g}}(\omega)\, \frac{\widehat{Z}_j(\omega)}{Z_j(\omega)}\,, \qquad j = 1 \ldots N_{\mathrm{s}} \tag{3.41}$$

In other terms, the modified ground motion acceleration $a_{\mathrm{g}}^{(j)}(t)$ can be directly applied to the dam with *empty* reservoir to obtain the contribution of any given mode j to the time-history response of the *dam-reservoir* system through the solution of Eq. (3.37) for generalized coordinates $\widetilde{Z}_j$. Using a finite element software, such procedure consists of conducting a time-history modal dynamic analysis of the dam with empty reservoir including only the contribution of vibration mode j of concern. As for the fundamental vibration mode, the solutions $\widetilde{Z}_j(t)$ of Eq. (3.37) can be obtained for each mode $j = 1 \ldots N_{\mathrm{s}}$ as the time-history relative displacements of SDOF systems with mass M_j given by Eq. (3.38), stiffness

$$K_j = \frac{4\pi^2}{T_j^2}\, M_j \tag{3.42}$$

and viscous damping

$$C_j = \frac{4\pi}{T_j}\, \xi_j\, M_j \tag{3.43}$$

to ground motion $L_j\, a_{\mathrm{g}}^{(j)}(t)$.

In Eq. (3.41), the generalized modal coordinates Z_j, $j = 1 \ldots N_{\mathrm{s}}$, corresponding to the dam with empty reservoir are given by, i.e. extension of Eq. (3.20) to higher modes

$$Z_j(\omega) = \frac{-L_j}{M_j} \times \frac{1}{\left(-\omega^2 + 2\,\mathrm{i}\,\xi_j\,\omega\,\omega_j + \omega_j^2 \right)} \tag{3.44}$$

while the vector $\widehat{\mathbf{Z}}$ of generalized modal coordinates $\widehat{Z}_j$ corresponding to the dam-reservoir system is obtained by solving the system of equations [26, 41]

$$\widehat{\mathbf{S}}\, \widehat{\mathbf{Z}} = \widehat{\mathbf{Q}} \tag{3.45}$$

in which the elements of the matrix $\widehat{\mathbf{S}}$ and vector $\widehat{\mathbf{Q}}$ are given for $m = 1 \ldots N_\mathrm{s}$ and $j = 1 \ldots N_\mathrm{s}$ as

$$\widehat{S}_{j,m}(\omega) = \Big(-\omega^2 + 2\,\mathrm{i}\,\xi_j\,\omega\,\omega_j + \omega_j^2 \Big)\, M_j\,\delta_{j,m} + \omega^2\,\vartheta_{j,m}(\omega) \tag{3.46}$$

$$\widehat{Q}_m(\omega) = -L_m + \vartheta_{0,m}(\omega) \tag{3.47}$$

where $\delta_{j,m}$ is the Kronecker symbol and where

$$\vartheta_{0,m}(\omega) = \int_0^{H_\mathrm{w}} p_0(y,\omega)\,\psi_m^{(x)}(y)\,\mathrm{d}y \tag{3.48}$$

$$\vartheta_{j,m}(\omega) = \int_0^{H_\mathrm{w}} p_j(y,\omega)\,\psi_m^{(x)}(y)\,\mathrm{d}y \tag{3.49}$$

with p_j denoting the hydrodynamic pressure FRF due to horizontal acceleration corresponding to the x–component of structural mode shape $\psi_j^{(x)}$. The FRF p_j can be evaluated using the expression given in Appendix A for convenient reference or the practical formulation proposed by [41]. The solutions of Eq. (3.45) can also be evaluated using the simplified expressions proposed by [4] and provided in Appendix A for convenient reference.

The previous equations are based on the modeling of earthquake-induced water effects through hydrodynamic pressures interacting with the vibrations of the dam monolith. If the simplified Westergaard added-mass formulation [21] is considered instead, Eqs. (3.48) and (3.49) can be replaced by

$$\vartheta_{0,j}(\omega) = \frac{7}{8}\,\rho_\mathrm{w} \int_0^{H_\mathrm{w}} \sqrt{H_\mathrm{w}(H_\mathrm{w}-y)}\;\psi_j^{(x)}(y)\,\mathrm{d}y \tag{3.50}$$

$$\vartheta_{j,m}(\omega) = \frac{7}{8}\,\rho_\mathrm{w} \int_0^{H_\mathrm{w}} \sqrt{H_\mathrm{w}(H_\mathrm{w}-y)}\;\psi_j^{(x)}(y)\,\psi_m^{(x)}(y)\,\mathrm{d}y \tag{3.51}$$

The total of relative horizontal displacements at a point (x, y) of the dam-reservoir can be computed as the summation of modal contributions

$$\widehat{u}(x,y,t) = \widetilde{u}(x,y,t) = \sum_{j=1}^{N_\mathrm{s}} \widetilde{u}_j(x,y,t) = \sum_{j=1}^{N_\mathrm{s}} \widetilde{Z}_j(t)\,\psi_j^{(x)}(x,y) \tag{3.52}$$

$$\ddot{\widehat{u}}(x,y,t) = \ddot{\widetilde{u}}(x,y,t) = \sum_{j=1}^{N_\mathrm{s}} \ddot{\widetilde{u}}_j(x,y,t) = \sum_{j=1}^{N_\mathrm{s}} \ddot{\widetilde{Z}}_j(t)\,\psi_j^{(x)}(x,y) \tag{3.53}$$

The maximum absolute value of the seismic relative horizontal displacement of the dam-

reservoir corresponding to a given vibration mode $j = 1 \dots N_\mathrm{s}$ can then be evaluated as

$$\begin{aligned} \left|\widehat{u}_j(x,y,t)\right|^{(\max)} &= \left|\widetilde{u}_j(x,y,t)\right|^{(\max)} \\ &= \frac{L_j}{M_j}\, S_\mathrm{D}^{[a_\mathrm{g}^{(j)}]}(T_j,\xi_j)\, \psi_j^{(x)}(x,y) \\ &= \frac{L_j}{M_j}\, \frac{T_j^2}{4\pi^2}\, S_\mathrm{A}^{[a_\mathrm{g}^{(j)}]}(T_j,\xi_j)\, \psi_j^{(x)}(x,y) \end{aligned} \tag{3.54}$$

in which $S_\mathrm{D}^{[a_\mathrm{g}^{(j)}]}(T_j,\xi_j)$ and $S_\mathrm{A}^{[a_\mathrm{g}^{(j)}]}(T_j,\xi_j)$ denote, respectively, the spectral displacement and pseudo-acceleration of ground motion $a_\mathrm{g}^{(j)}(t)$ at period T_j of the dam with empty reservoir, considering a modal viscous damping ξ_j. Assuming, as previously, that the dam vibration mode shapes and displacements are practically constant over the breadth of the dam monolith, Eq. (3.54) could be rewritten as

$$\left|\widehat{u}_j(y,t)\right|^{(\max)} = \left|\widetilde{u}_j(y,t)\right|^{(\max)} = \frac{L_j}{M_j}\, \frac{T_j^2}{4\pi^2}\, S_\mathrm{A}^{[a_\mathrm{g}^{(j)}]}(T_j,\xi_j)\, \psi_j^{(x)}(y) \tag{3.55}$$

in which $\psi_j^{(x)}(y)$, $\widehat{u}_j(y,t)$ and $\widetilde{u}_j(y,t)$ denote $\psi_j^{(x)}(0,y)$, $\widehat{u}_j(0,y,t)$ and $\widetilde{u}_j(0,y,t)$, respectively, for simplicity of notation.

The heightwise distribution of the equivalent lateral static forces including hydrodynamic effects corresponding to each higher mode j of the dam can then be obtained as

$$\widehat{f}_j(y) = \widetilde{f}_j(y) = \frac{L_j}{M_j}\, \mu_\mathrm{s}(y)\, S_\mathrm{A}^{[a_\mathrm{g}^{(j)}]}(T_j,\xi_j)\, \psi_j^{(x)}(y) \tag{3.56}$$

These equivalent static forces can be applied to the finite element model of a dry dam to approximate the maximum contribution $\tilde{r}_j^{(\max)}$ of each mode j to a given key response indicator $\tilde{r}$. When applicable, the absolute maximum total seismic response can then be obtained using a combination rule such as the Square Root of the Sum of the Squares (SRSS)

$$\left|\,\tilde{r}\,\right|^{(\max)} = \sqrt{\sum_{j=1}^{N_\mathrm{s}} \left[\left|\,\tilde{r}_j\,\right|^{(\max)}\right]^2} \tag{3.57}$$

The maximum absolute value of the seismic relative horizontal displacement and heightwise distribution of the equivalent lateral static forces corresponding to the dam with empty reservoir subjected to original ground motion acceleration can be expressed for each higher

mode j of the dam as

$$\left|u_j(y,t)\right|^{(\max)} = \frac{L_j}{M_j}\,\frac{T_j^2}{4\pi^2}\,S_{\mathrm{A}}^{[\ddot{x}_{\mathrm{g}}]}(T_j,\xi_j)\,\psi_j^{(x)}(y) \tag{3.58}$$

$$f_j(y) = \frac{L_j}{M_j}\,\mu_{\mathrm{s}}(y)\,S_{\mathrm{A}}^{[\ddot{x}_{\mathrm{g}}]}(T_j,\xi_j)\,\psi_j^{(x)}(y) \tag{3.59}$$

From Eqs. (3.55), (3.56), (3.58) and (3.59), it can be seen that, as observed for the fundamental mode, the following ratios are equal: (i) the ratio of maximum absolute value of the seismic relative horizontal displacements with and without reservoir at a given mode j, (ii) the ratio of the equivalent lateral static forces at a given coordinate $y > 0$ including and excluding hydrodynamic effects at a given mode j, and (iii) the ratio of the pseudo-acceleration of the modified record corresponding to mode j to that of the original ground motion acceleration, i.e.

$$\frac{\left|\widehat{u}_j(y,t)\right|^{(\max)}}{\left|u_j(y,t)\right|^{(\max)}} = \frac{\widehat{f}_j(y)}{f_j(y)} = \frac{S_{\mathrm{A}}^{[a_{\mathrm{g}}^{(j)}]}(T_j,\xi_j)}{S_{\mathrm{A}}^{[\ddot{x}_{\mathrm{g}}]}(T_j,\xi_j)} \qquad \text{for} \quad j = 1\ldots N_{\mathrm{s}} \quad \text{and} \quad y > 0 \tag{3.60}$$

In what follows, the ratio defined by Eq. (3.60) will be referred to as the *hydrodynamic modification factor* for a given vibration mode, and abbreviated as HMF. As emphasized for the fundamental mode, the proposed formulations and resulting HMF only require the evaluation of the period and damping corresponding to a specific vibration mode of the dam with empty reservoir, rather than those of the dam-reservoir system which are generally different.

3.3.5 Summary of proposed procedures

Figure 3.2 illustrates the classical technique, denoted hereafter as the reference method, to determine the seismic response of a dam-reservoir system, as well as the new procedures proposed above, classified into three techniques denoted hereafter as methods A, B and C. The reference technique in Fig. 3.2 (a) consists of the seismic analysis of a dam-reservoir system with water effects modelled based on hydrodynamic pressure or added-masses. The results of this approach were previously verified against coupled dam-reservoir system solutions, consisting of water and dam domains modelled using potential-based fluid finite elements and solid plain strain finite elements, respectively, while interacting through a fluid-structure interaction interface [2]. In method A (Fig. 3.2 (b)), the seismic response of the dam-reservoir system is obtained through the superposition of the time-history modal dynamic responses (i.e. Time-history modal superposition analysis abbreviated as THMSA hereafter) of the

dam monolith with empty reservoir subjected to modified ground motion accelerations $a_g^{(j)}(t)$, $j = 1 \dots N_s$ (Note: $N_s = 5$ modes are considered in Fig. 3.2 (b) for illustration purposes). It is important to note that the time-history modal superposition analysis of the dam under the effects of modified time-history ground motion accelerations $a_g^{(j)}(t)$ must include only the contribution of vibration mode $j = 1 \dots N_s$. This can be achieved in a finite element software by selecting and including only each mode j of concern in the modal dynamic analysis.

In method B (Fig. 3.2 (c)), the time-dependent generalized modal coordinates $\widetilde{Z}_j(t)$ corresponding to vibration modes $j = 1 \dots N_s$ are first determined as the relative horizontal displacements of SDOFs with mass M_j, stiffness $K_j = 4\pi^2 M_j / T_j^2$ and viscous damping $C_j = 4\pi\xi_j M_j / T_j$, subjected each to ground motion acceleration $L_j\, a_g^{(j)}(t)$, $j = 1 \dots N_s$. The relative horizontal displacement $\widetilde{u}(x, y, t)$ of any point of coordinates (x, y) of the dam monolith can then be obtained according to Eqs. (3.52) as the sum of the N_s modal relative horizontal displacements $\widetilde{u}_j(x, y, t) = \widetilde{Z}_j(t)\, \psi_j^{(x)}(x, y)$, i.e. through THMSA.

In method C (Fig. 3.2 (d)), the pseudo-spectral accelerations $S_A^{[a_g^{(j)}]}(T_j, \xi_j)$ of the modified ground motion accelerations $a_g^{(j)}(t)$ are first determined at periods T_j and for damping factors ξ_j, $j = 1 \dots N_s$. The maximum absolute value of relative horizontal displacements $\left|\widetilde{u}_j(y, t)\right|^{(\max)}$ corresponding to each mode $j = 1 \dots N_s$ at a given point of the dam at coordinate y can then be obtained using Eqs. (3.32) and (3.55), i.e. Response spectrum analyses (RSA). The heightwise distribution of the equivalent lateral static forces $\widetilde{f}_j(y)$ corresponding to each mode j can also be obtained from Eqs. (3.35) and (3.56). These static forces can be used to estimate the peak seismic response of the dam in each mode and then use a combination rule to assess its global seismic behaviour. Figure 3.3 presents a flowchart to further illustrate the steps of proposed procedures and facilitate their application.

3.4 Numerical examples, results and discussion

3.4.1 Case studies

The methods described above are applied next to evaluate the seismic response of two gravity dam monoliths, referred to hereafter as D35 and D90, with heights H_s of 35 m, and 90 m, respectively, to illustrate flexibility effects. The dams impound reservoirs with heights H_w of 32 m and 86 m, respectively. The geometries of both dam-reservoir systems are illustrated in Fig. 3.4. A mass density $\rho_s = 2400$ kg/m^3, a Poisson's ratio $\nu = 0.2$ and a modulus of elasticity $E_s = 25$ GPa are assumed as concrete material properties for each dam. A water mass density of $\rho_w = 1000$ kg/m^3 is considered with a pressure wave velocity of $C_w = 1440$ m/s when water compressibility effects are included in the analysis. Full wave reflection is assumed at reservoir

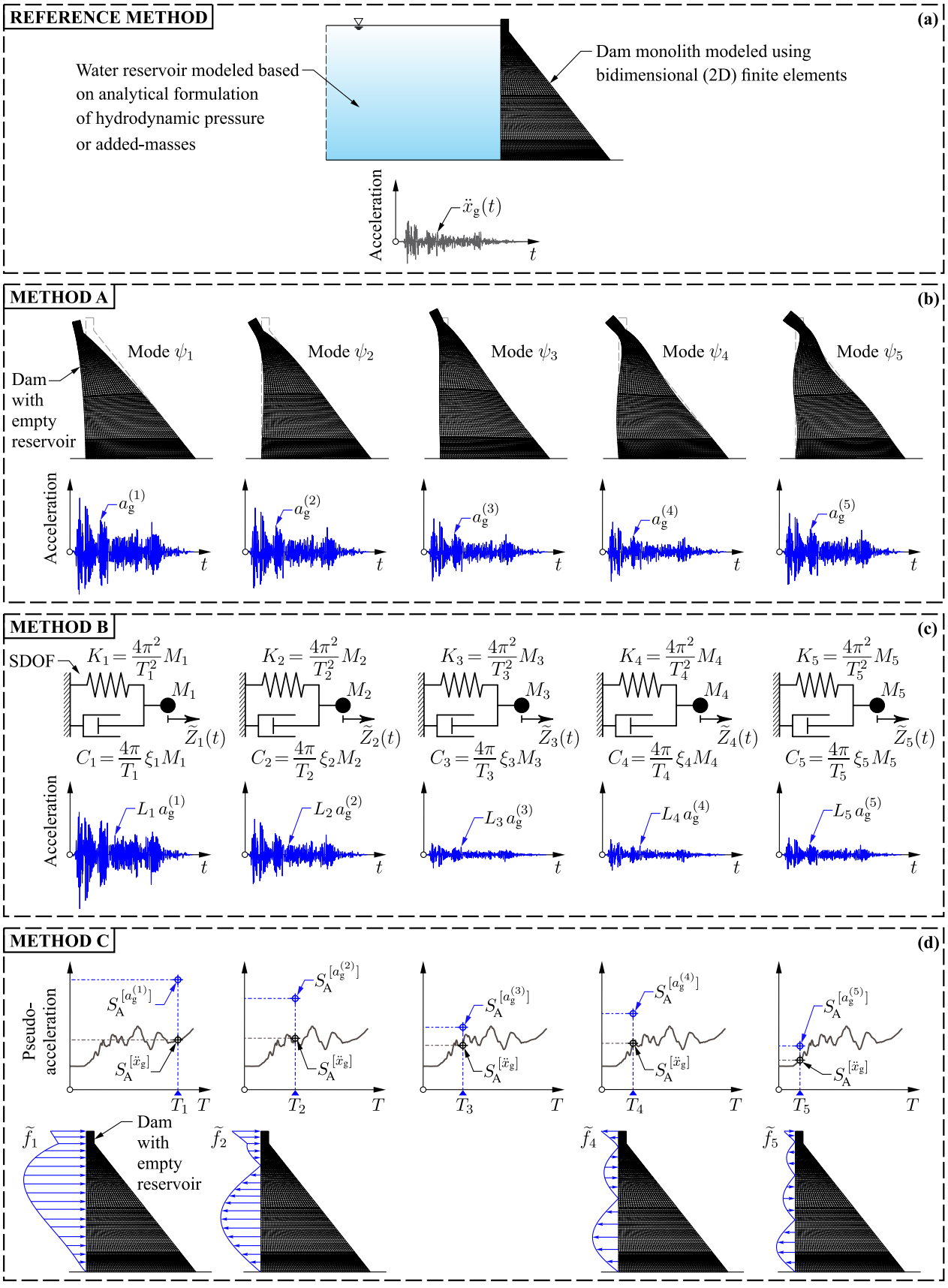

Figure 3.2 Proposed procedures: (a) Reference method; (b) THMSA of the dam-reservoir system including only the contribution of the vibration mode j; (c) THMSA of SDOF systems; (d) RSA of the dam-reservoir system including higher modes effects.

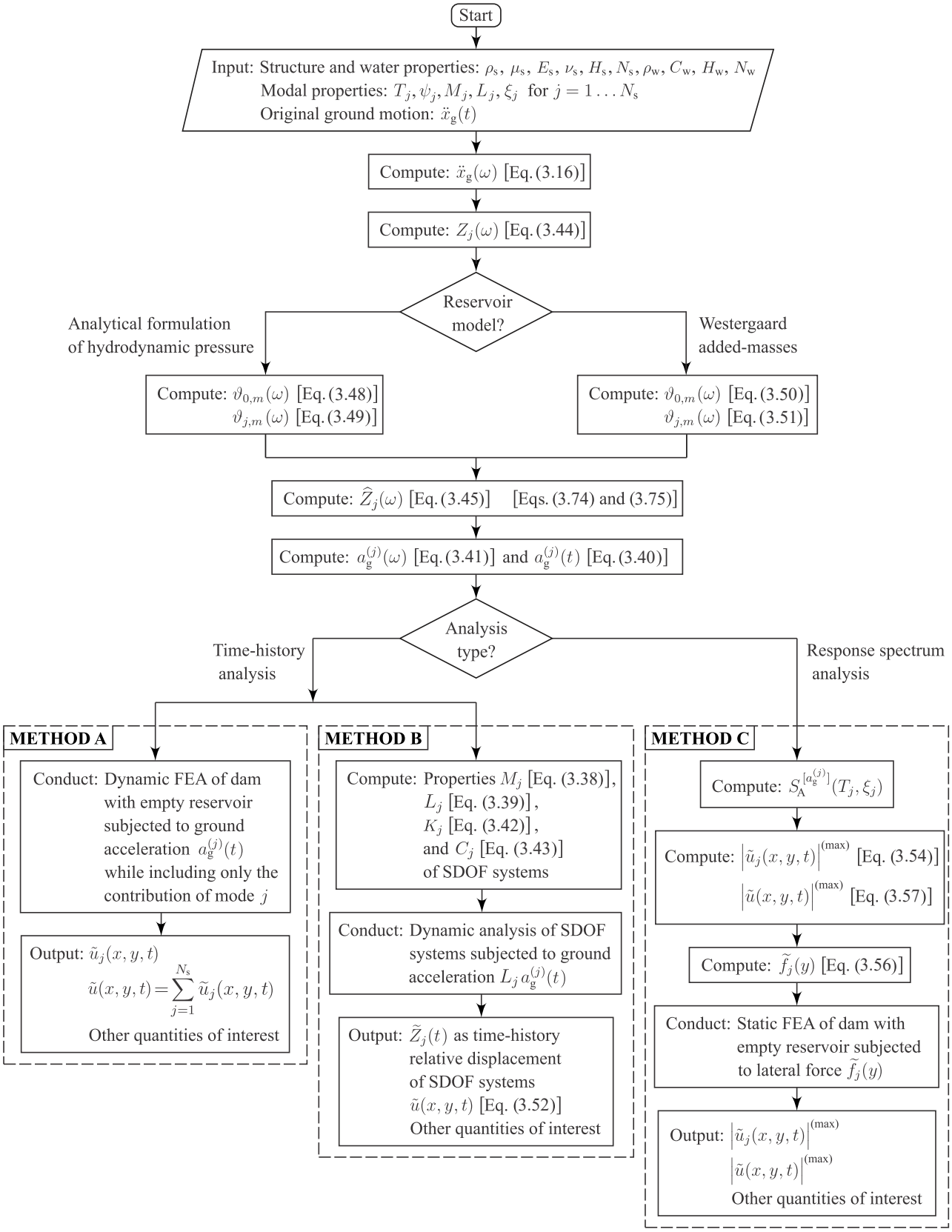

Figure 3.3 Flowchart of the proposed procedures.

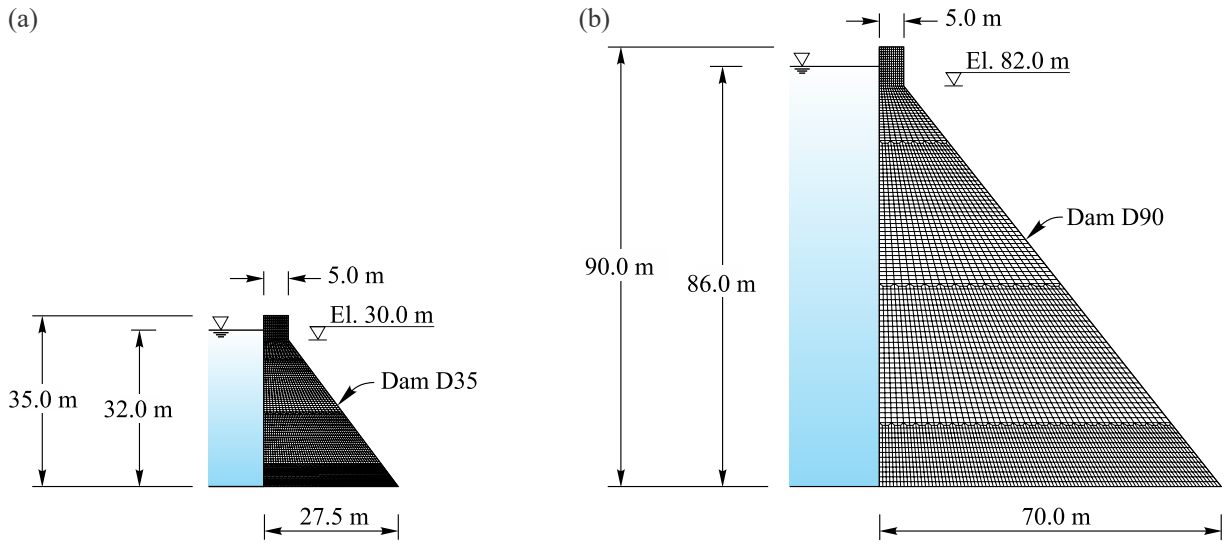

Figure 3.4 Dimensions and solid finite element meshes of the studied dam-reservoir systems: (a) 35-m height gravity monolith dam (D35), (b) 90-m height gravity dam monolith (D90).

bottom. A constant 5 % modal viscous damping ratio is considered for all the vibration modes of the dam with empty reservoir, i.e. $\xi_j = 0.05$ for $j = 1$ to 5. The dam monoliths are discretized into 4-node plane strain finite elements using the software ADINA [92] as shown in Fig. 3.4. We note that any other standard finite element structural engineering software or code available to the analyst could be used for this purpose. Figures 3.5 and 3.6 illustrate the first five modes as well as the corresponding vibration periods, i.e. T_1 to T_5 of the two dams with empty reservoirs, respectively. The relative importance of the contribution of each mode $j = 1 \ldots 5$ to the global seismic response of the dam monoliths is highlighted by the horizontal and vertical modal mass participation factors $\Lambda_j^{(x)}$ and $\Lambda_j^{(y)}$, respectively, also shown in Figs. 3.5 and 3.6. For both dams, it is observed that the fundamental and second modes predominate the seismic response and that the third mode is essentially vertical.

The seismic response of each dam monolith is studied under the effects of four ground motion accelerations differing by their frequency content and time signature: (i) a horizontal component of Imperial Valley earthquake (1940) at station El Centro, (ii) a horizontal component of Loma Prieta earthquake (1989) at station Gilroy Array no. 2, (iii) a horizontal component of Parkfield earthquake (1966) at station Cholame no. 5, and (iv) a horizontal component of Nahanni earthquake (1985) at station Iverson. The acceleration time-histories, acceleration pseudo-spectra and Fourier amplitudes of these ground motions are illustrated in Fig. 3.7.

3.4.2 Modified ground motion accelerations, response spectra and seismic demands

The modified accelerograms corresponding to each of the four earthquake components described above are shown in Figs. 3.8 and 3.9 for dams D35 and D90, respectively. The original ground motion accelerations are also shown in the same figure for comparison purposes. For convenient reference, a step-by-step procedure to obtain the modified accelerogram $a_{\mathrm{g}}^{(1)}$ corresponding to dam D90 and Imperial Valley (1940) ground motion is provided in Appendix B. It is first seen that the amplitudes of the modified accelerations are different from those of the original accelerograms for both dams and all the ground motions studied herein. By comparing the results in Fig. 3.8 to those in Fig. 3.9, it is apparent that the amplification of modified ground motions is more important as the dam is more flexible.

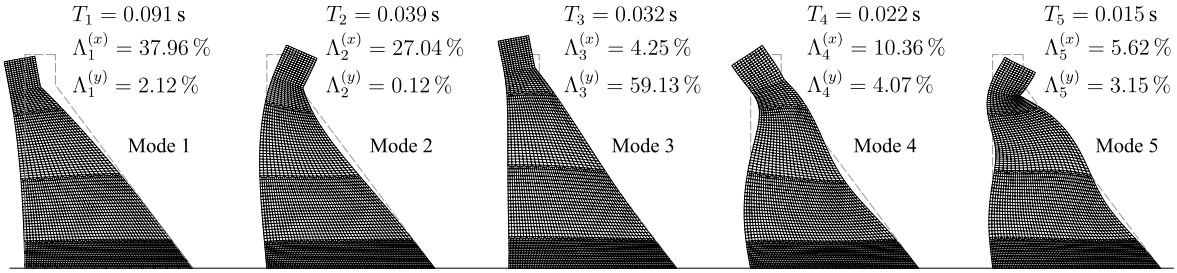

Figure 3.5 Five first mode shapes and corresponding vibration periods of the 35 m high gravity dam monolith (D35).

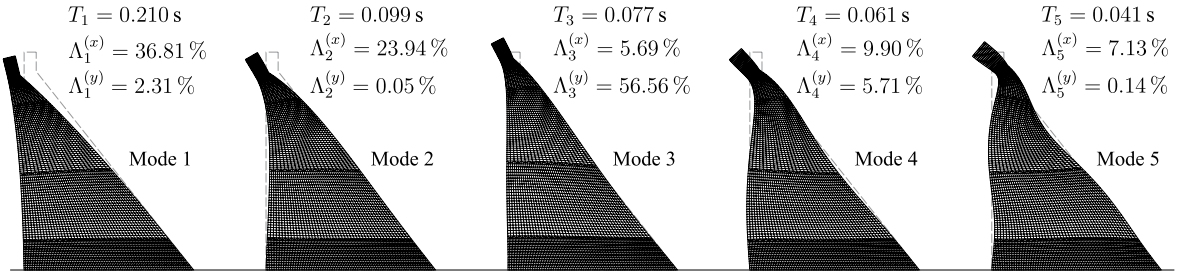

Figure 3.6 Five first mode shapes and corresponding vibration periods of the 90 m high gravity dam monolith (D90).

It is also deduced that, as expected, the frequency content of the modified accelerations is altered from that of the original accelerograms and that such alterations depend on the specific dam being studied as well as the characteristics of the original ground motion. It is important to note that although an assumption of full wave reflection at reservoir bottom was adopted herein for the sake of brevity, the formulation proposed can also account for wave

absorption at reservoir bottom due to sedimentation. Such effects are included through the wave reflection parameters q and α [Eq. (66) in Appendix A] intervening in the determination of hydrodynamic pressures as reviewed in Appendix A. For illustration purposes, Fig. 3.10 shows the effects of wave absorption at reservoir bottom on the modified accelerations $a_g^{(1)}$ to $a_g^{(5)}$ for dam D90 subjected to Imperial Valley (1940) and Nahanni (1985) earthquakes.

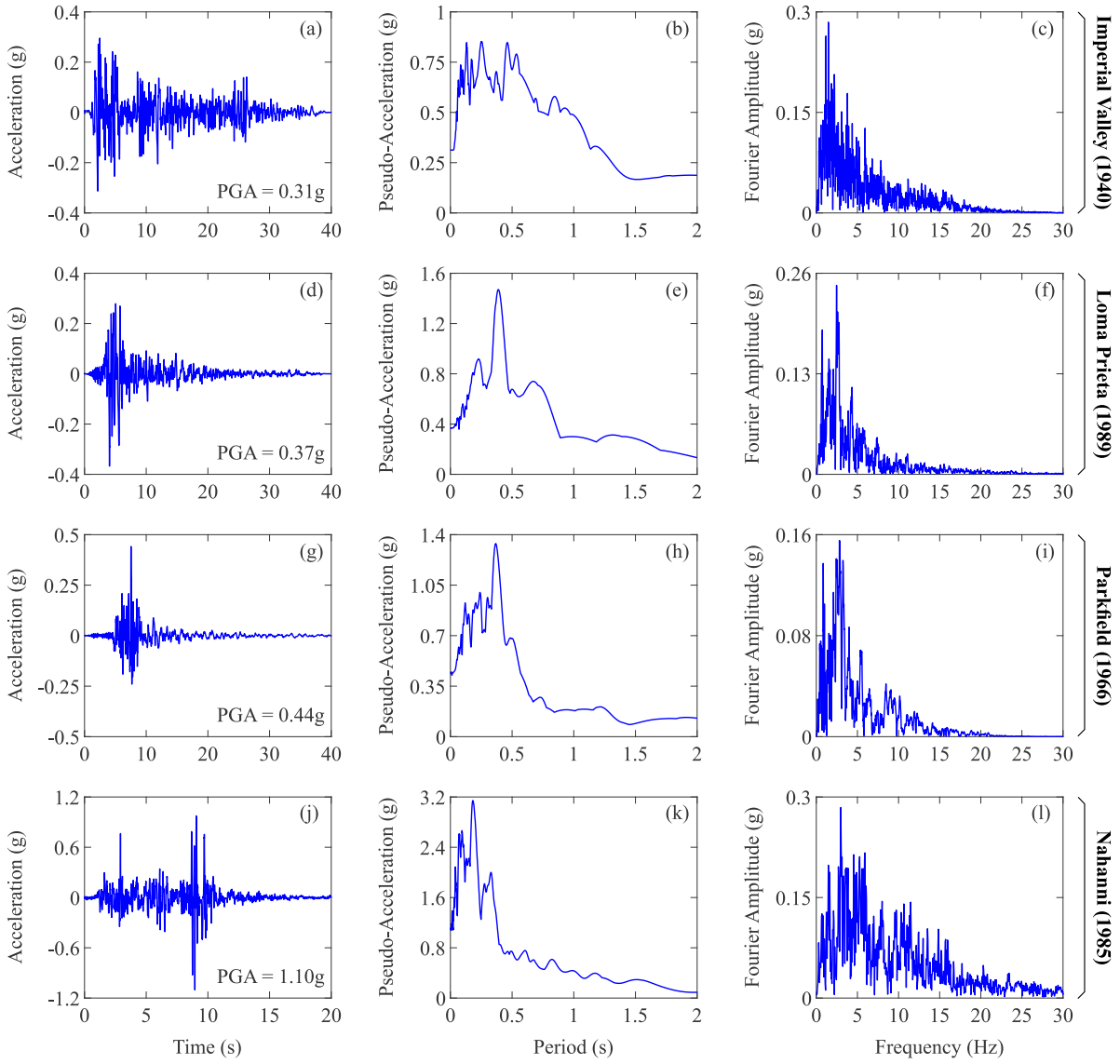

Figure 3.7 Time-history accelerations, pseudo-acceleration response spectra and Fourier amplitudes of the ground motions selected for this study: (a) to (c) Imperial Valley (1940) earthquake; (d) to (f) Loma Prieta (1989) earthquake; Parkfield (1966) earthquake; and Nahanni (1985) earthquake.

The 5%-damped pseudo-acceleration response spectra of the modified ground motion accelerations are obtained next for the first five vibration periods T_1 to T_5, i.e. $S_A^{[a_g^{(j)}]}(T_j, 5\%)$, $j =$

1 . . . 5. These results are provided (with values indicated in blue) in Fig. 3.11 along with the pseudo-spectral accelerations of the original ground motions corresponding to the same vibration periods (values indicated in black).

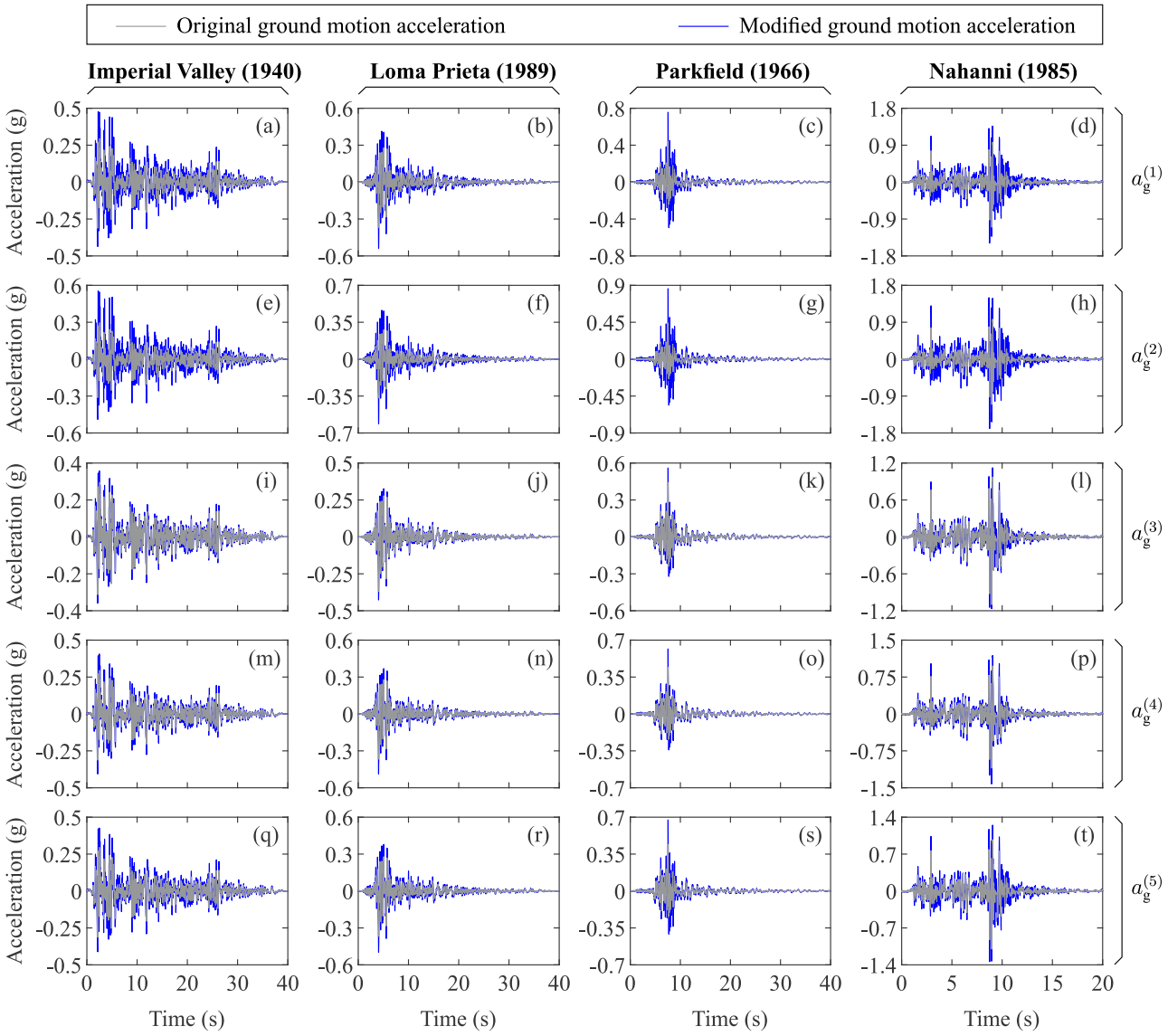

Figure 3.8 Original and modified ground motion accelerations $a_g^{(1)}$ to $a_g^{(5)}$ corresponding to the first five mode shapes of the 35 m high dam (D35) and the ground motions considered: (a) to (d) $a_g^{(1)}$; (e) to (h) $a_g^{(2)}$; (i) to (l) $a_g^{(3)}$; (m) to (p) $a_g^{(4)}$; (q) to (t) $a_g^{(5)}$.

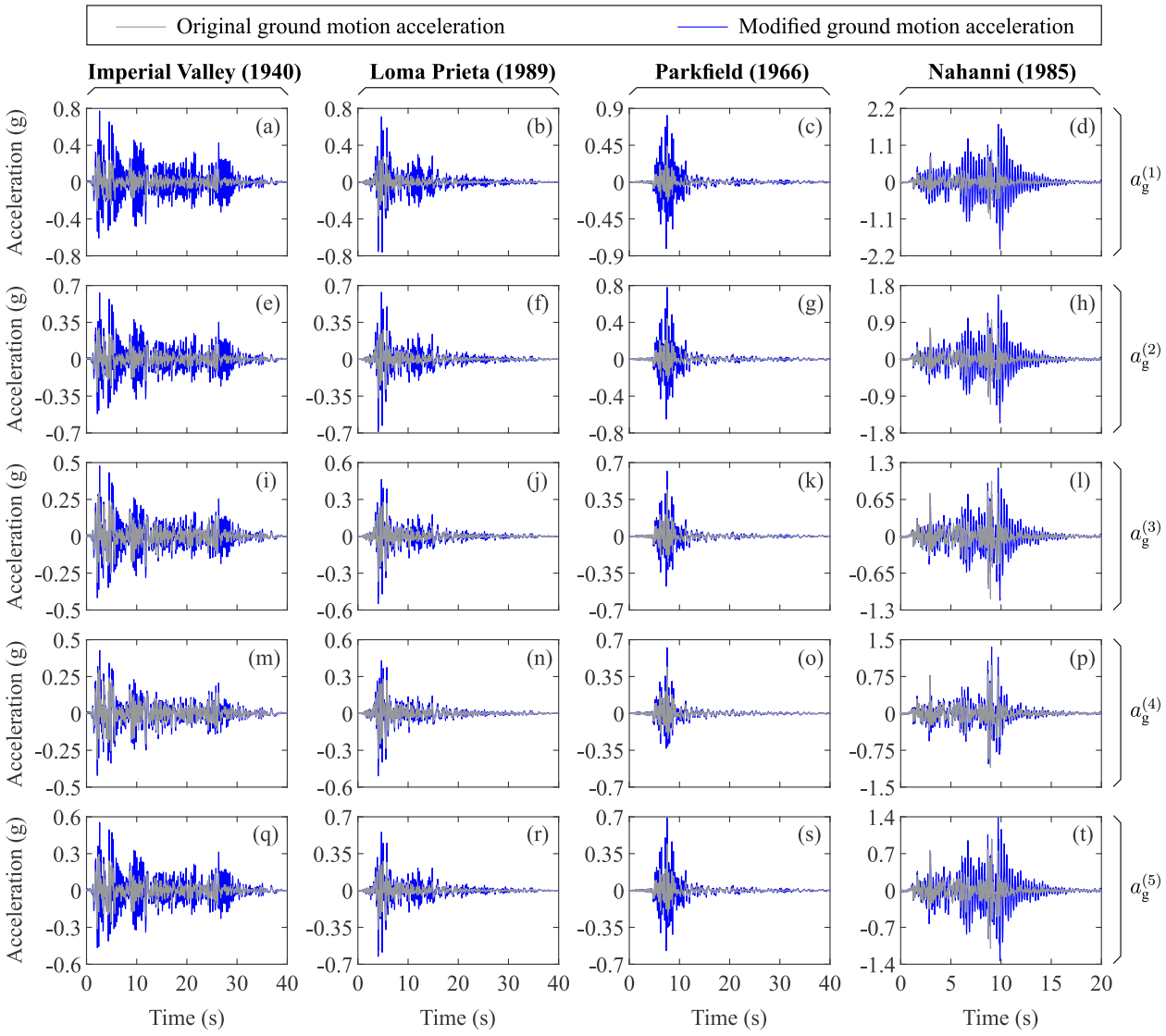

Figure 3.9 Original and modified ground motion accelerations $a_g^{(1)}$ to $a_g^{(5)}$ corresponding to the first five mode shapes of the 90 m high dam (D90) and the ground motions considered: (a) to (d) $a_g^{(1)}$; (e) to (h) $a_g^{(2)}$; (i) to (l) $a_g^{(3)}$; (m) to (p) $a_g^{(4)}$; (q) to (t) $a_g^{(5)}$.

Again, as expected, it is clear that the hydrodynamic-induced modifications to acceleration seismic demands depend on both the dam studied and the input ground motion. For example, from Figs. 3.11 (a) and (b), it is seen that the acceleration demands corresponding to the fundamental modes of dams D35 and D90 with empty reservoirs are roughly the same when subjected to Imperial Valley ground motion (i.e. 0.67 and 0.66 respectively). These acceleration demands increase by 46 %, i.e. $(0.98-0.67)/0.67\times 100$ for dam D35 and 115 %, i.e. $(1.42-0.66)/0.66\times 100$ for dam D90 when hydrodynamic effects are included. The larger amplification associated with Dam D90 is mainly due to its higher flexibility com-

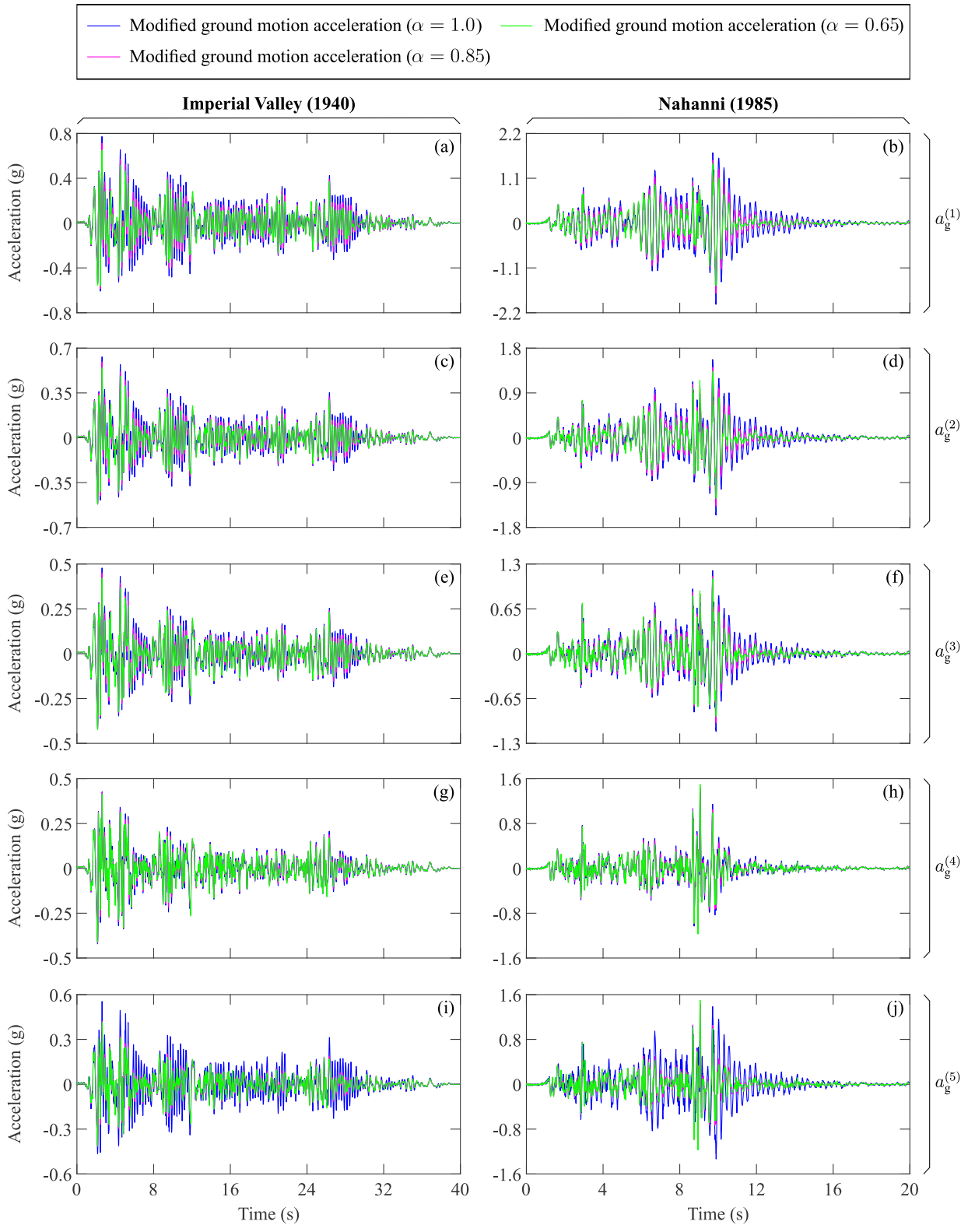

Figure 3.10 Modified ground motion accelerations $a_g^{(1)}$ to $a_g^{(5)}$ corresponding to the first five mode shapes of the 90 m high dam (D90) subjected to two ground motion accelerations, and obtained for fully reflective reservoir bottom(i.e. $\alpha = 1.00$) and absorptive reservoir bottoms with $\alpha = 0.85$ and $\alpha = 0.65$: (a), (c), (e), (g), and (i) Imperial Valley (1940) earthquake; and (b), (d), (f), (h), and (j) Nahanni (1985) earthquake.

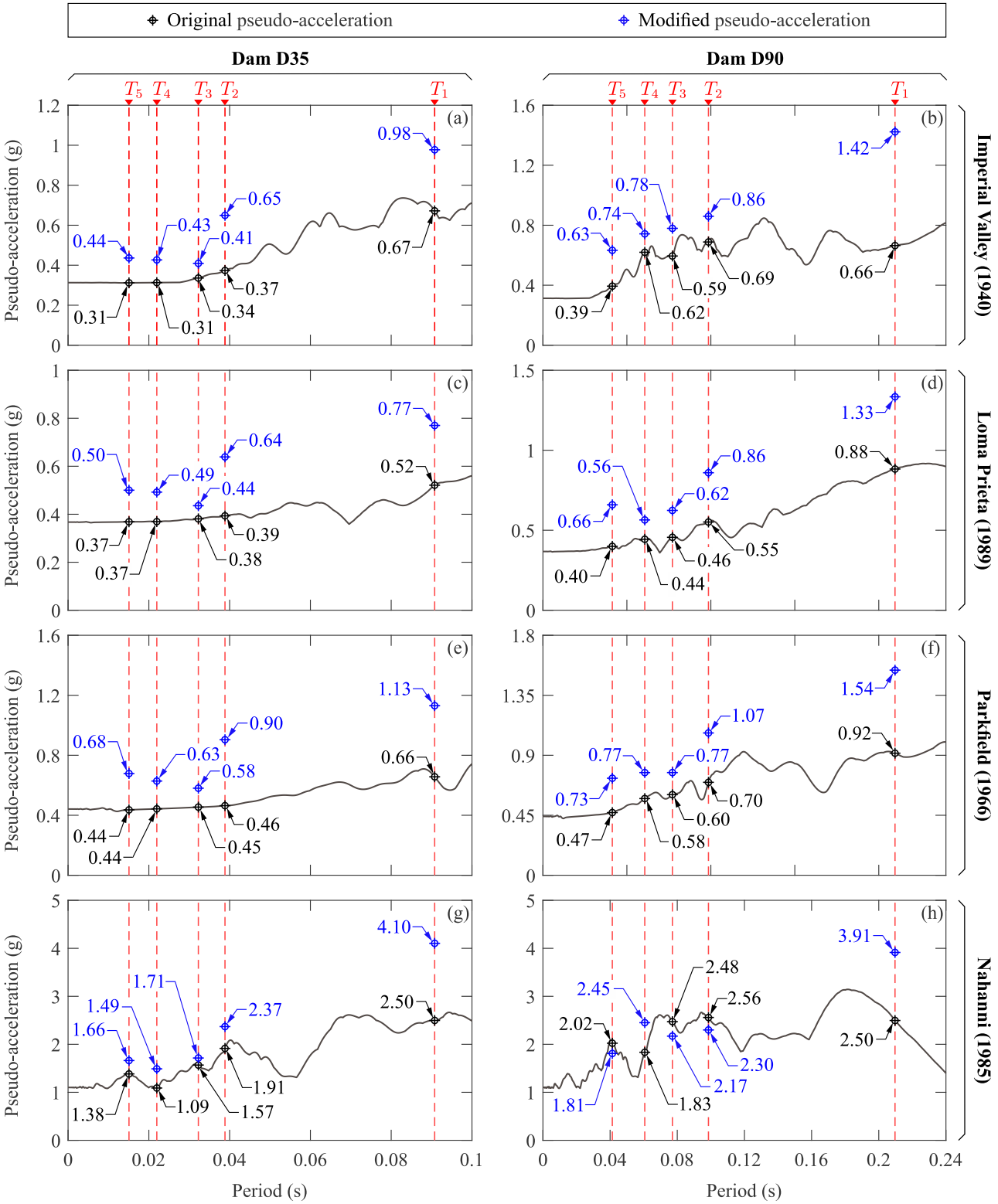

Figure 3.11 5%-damped pseudo-acceleration response spectra of the original ground motions and those of the modified ground motions corresponding to each of the first five vibration modes obtained assuming compressible water in the reservoir: (a), (c), (e), (g) dam D35; (b), (d), (f), (h) dam D90.

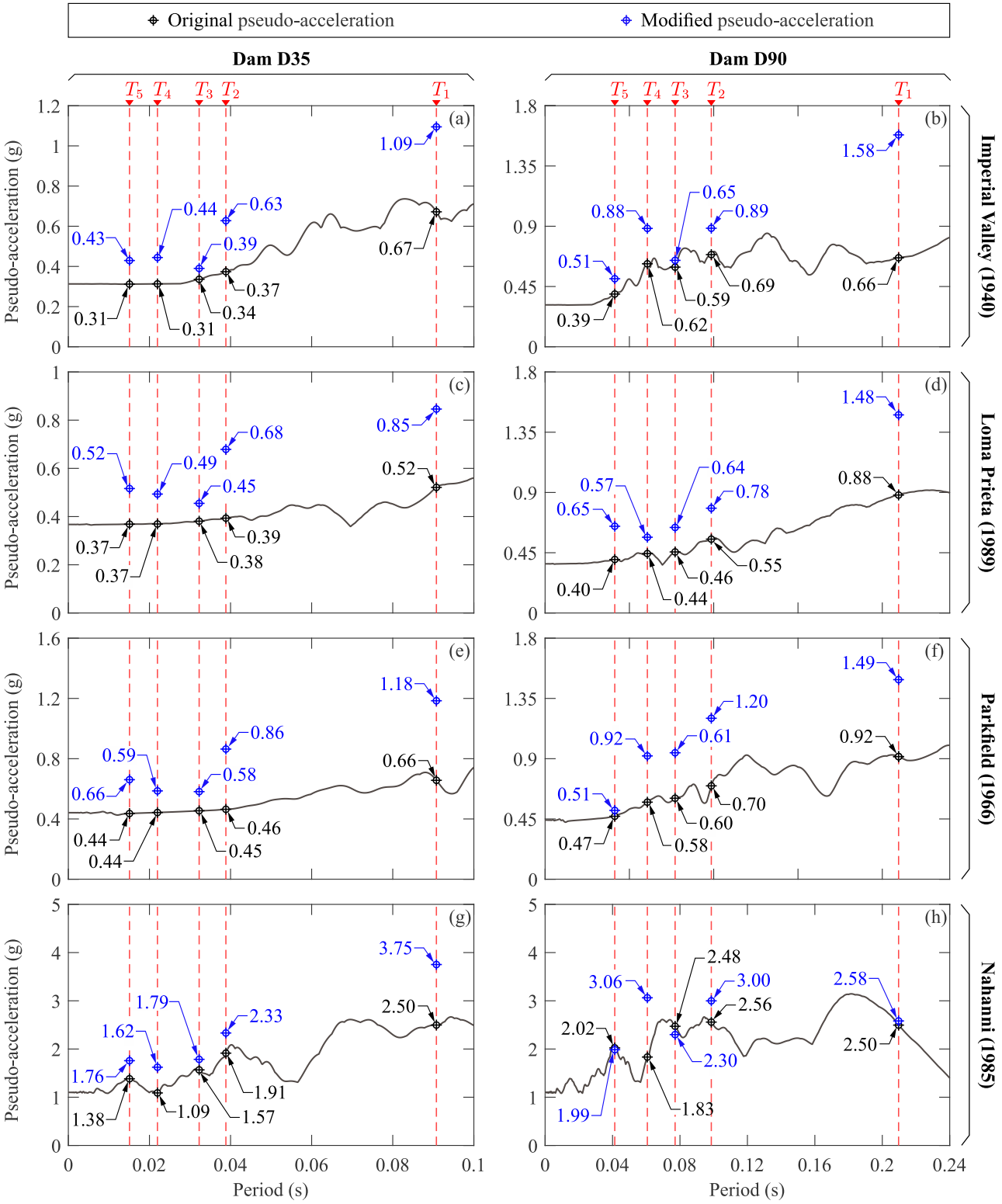

Figure 3.12 5%-damped pseudo-acceleration response spectra of the original ground motions and those of the modified ground motions corresponding to each of the first five vibration modes obtained assuming incompressible water in the reservoir: (a), (c), (e), (g) dam D35; (b), (d), (f), (h) dam D90.

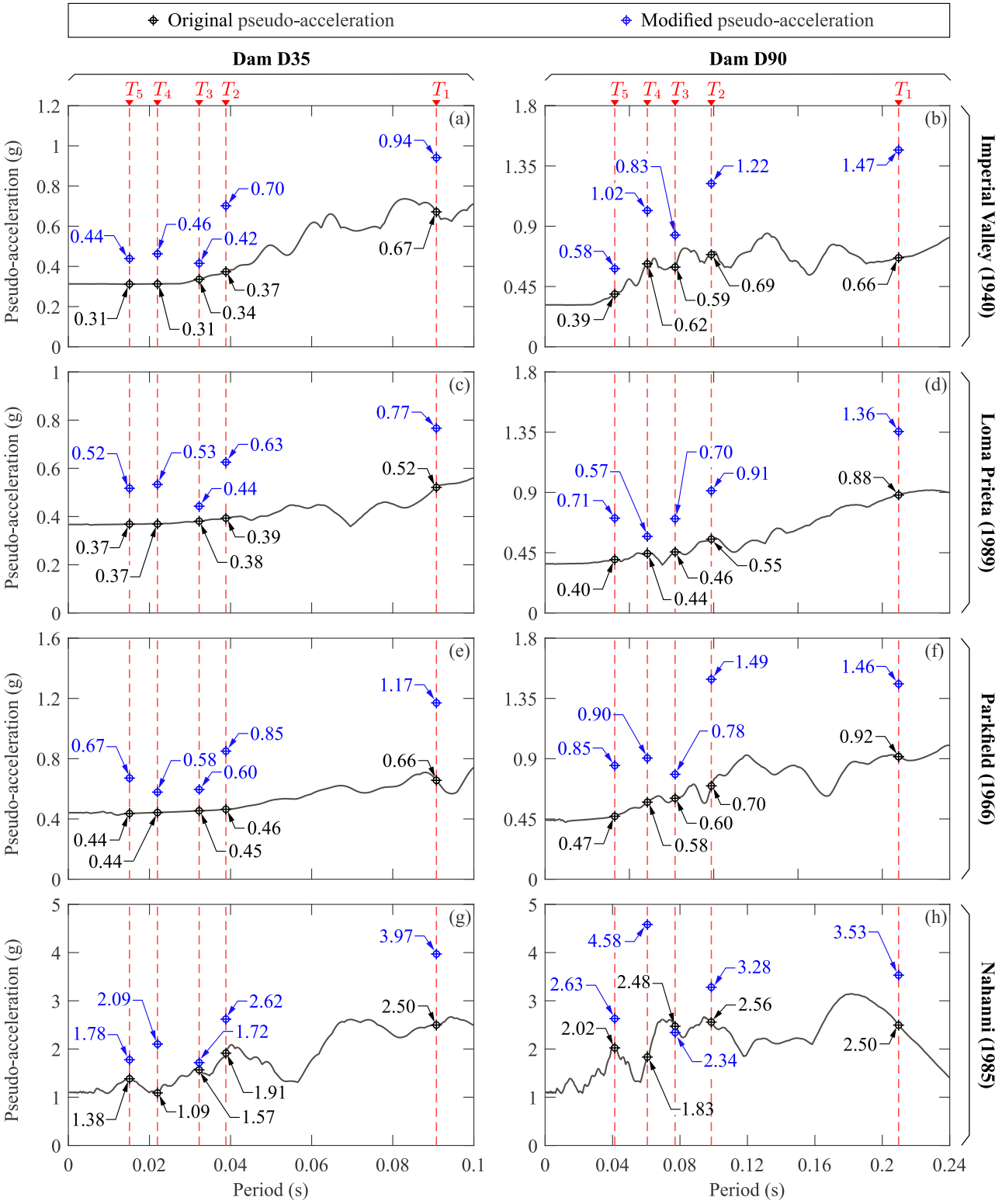

Figure 3.13 5%-damped pseudo-acceleration response spectra of the original ground motions and those of the modified ground motions corresponding to each of the first five vibration modes obtained using Westergaard added-masses: (a), (c), (e), (g) dam D35; (b), (d), (f), (h) dam D90.

pared to dam D35. Comparing Figs. 3.11 (a) and (e), it is observed that Parkfield ground motion induces practically the same acceleration demand on dam D35 with empty reservoir than Imperial Valley record when only fundamental mode contribution is included (i.e. 0.66 and 0.67). Nonetheless, the acceleration demand increase induced by hydrodynamic effects is 71 %, i.e. $(1.13 - 0.66)/0.66 \times 100$ under this ground motion compared to 46 % under Imperial Valley accelerogram. Figure 3.11 also shows the relative importance of hydrodynamic effects along the various vibration modes of a given structure. For instance, it can be deduced from Fig. 3.11 (d) that the acceleration demands corresponding to modes 1 to 5 of dam D90 increase by 51 %, 56 %, 35 %, 27 %, and 65 %, respectively, due to hydrodynamic effects when subjected to Loma Prieta ground motion. Figures 3.11 (g) and (h) highlight the seismic acceleration demands including hydrodynamic effects induced by Nahanni ground motion acceleration on dams D35 and D90, respectively. Both dams are subjected to the same acceleration demand at their fundamental vibration modes, i.e. 2.5 g. This demand increases roughly by the same amount when hydrodynamic effects are considered, i.e. 64 % for dam D35 vs 56 % for dam D90. In the second vibration mode though, the acceleration demand increases by 24 % for dam D35 due to hydrodynamic effects, while it *decreases* by 10 % for dam D90. This example clearly illustrates that the efficiency of the proposed modified spectral accelerations in assessing hydrodynamic effects on dam seismic demands. To illustrate the effects of water modelling assumptions, the pseudo-acceleration response spectra assuming incompressible water in the reservoir or Westergaard added-masses formulation are also given in Figs. 3.12 and 3.13, respectively. The assessment of the effects of water modeling assumptions can also be seen from Table 3.1 containing the HMFs obtained using Eq. (3.60) for the first five vibration modes of dams D35 and D90 and the ground motion accelerations considered. For example, it is seen that the HMFs at the fundamental vibration mode of dam D35 are highest considering incompressible water assumption under Imperial Valley (1940), Loma Prieta (1989) and Parkfield (1966), while compressible water assumption yields the highest HMFs under Nahanni (1985) record. In this case, the hydrodynamic-induced amplifications of seismic demands range between 1.40 to 1.79. The same exercise considering the fundamental vibration mode of dam D90 shows that the largest HMFs correspond to: (i) incompressible water assumption under Imperial Valley (1940) and Loma Prieta (1989) ground motions, and to (ii) compressible water assumption under Parkfield (1966) and Nahanni (1985) earthquakes. The HMFs range in this case from 1.03 to 2.39, thus illustrating that the variations in hydrodynamic-induced amplifications of seismic demands depending on water modeling assumptions are more important for the fundamental vibration mode of dam D90 than D35. Similar observations can be deduced from the HMFs given in Table 3.1 for higher vibration modes. For instance, it is found that some HMFs are lower than one

for dam D90 when subjected to Nahanni (1985) ground motion, which illustrates that the seismic demands in these cases are de-amplified due to hydrodynamic effects.

3.4.3 Seismic response of the dams

Figures 3.14 and 3.15 present results of the maximum absolute horizontal displacements obtained along the height of the upstream faces of dam monoliths D35 and D90 under the effects of the considered ground motions. The results corresponding to each mode are obtained using the proposed response spectrum analysis (RSA), i.e. Method C in Fig. 3.2 and the flowchart in Fig. 3.3. Appendix C illustrates the steps and calculations of this procedure applied to evaluate the maximum absolute value of relative horizontal displacement at the crest of the 90 m high dam D90 when subjected to Imperial Valley (1940) ground motion. Figures 3.14 and 3.15 also present the results of time-history analyses (THMSA), i.e. Methods A and B in Fig. 3.2 and the flowchart in Fig. 3.3. It is clearly seen that the results obtained for each vibration mode of dams D35 and D90 using methods A and B are identical. These results are also in excellent agreement with those from the reference method. The *total* of maximum absolute values of relative horizontal displacements shown in Figs. 3.14 and 3.15 (i.e. last columns titled total) are obtained using two approaches: (i) a direct method consisting of the summation of the modal responses of horizontal relative displacements (i.e. algebraic values with signs) and then the computation of the maximum absolute value of the resulting summed response, and (ii) the SRSS method consisting of summing the absolute values of the maximum horizontal relative displacements obtained for each mode. As excepted, the results provided by the direct method are found to be identical to those of the reference solution. For all the earthquakes considered and the two dams studied, it is seen that the SRSS method yields larger values than the direct method at the dam crest and slightly below (i.e. $y/H_{\mathrm{s}} > \approx 0.75$). At lower heights, the total maximum responses obtained using the SRSS method are practically the same as the direct method or slightly smaller. The absolute values of maximum relative horizontal displacements of the dams with empty reservoir subjected to original ground motion acceleration, also shown in Fig. 3.14 and 3.15 for comparison purposes, are found to be lower than those with the reservoir except for the second and third modes of dam D35 subjected to Nahanni ground motion acceleration. This observation is consistent with the discussion above about the seismic acceleration demands induced by this record.

Figures 3.16 and 3.17 show the heightwise distribution of the equivalent lateral static forces, including hydrodynamic effects, computed for each vibration mode $j = 1 \ldots N_{\mathrm{s}}$ of dams D35 and D90 according to Eq. (3.56). The results corresponding to empty reservoir and to reser-

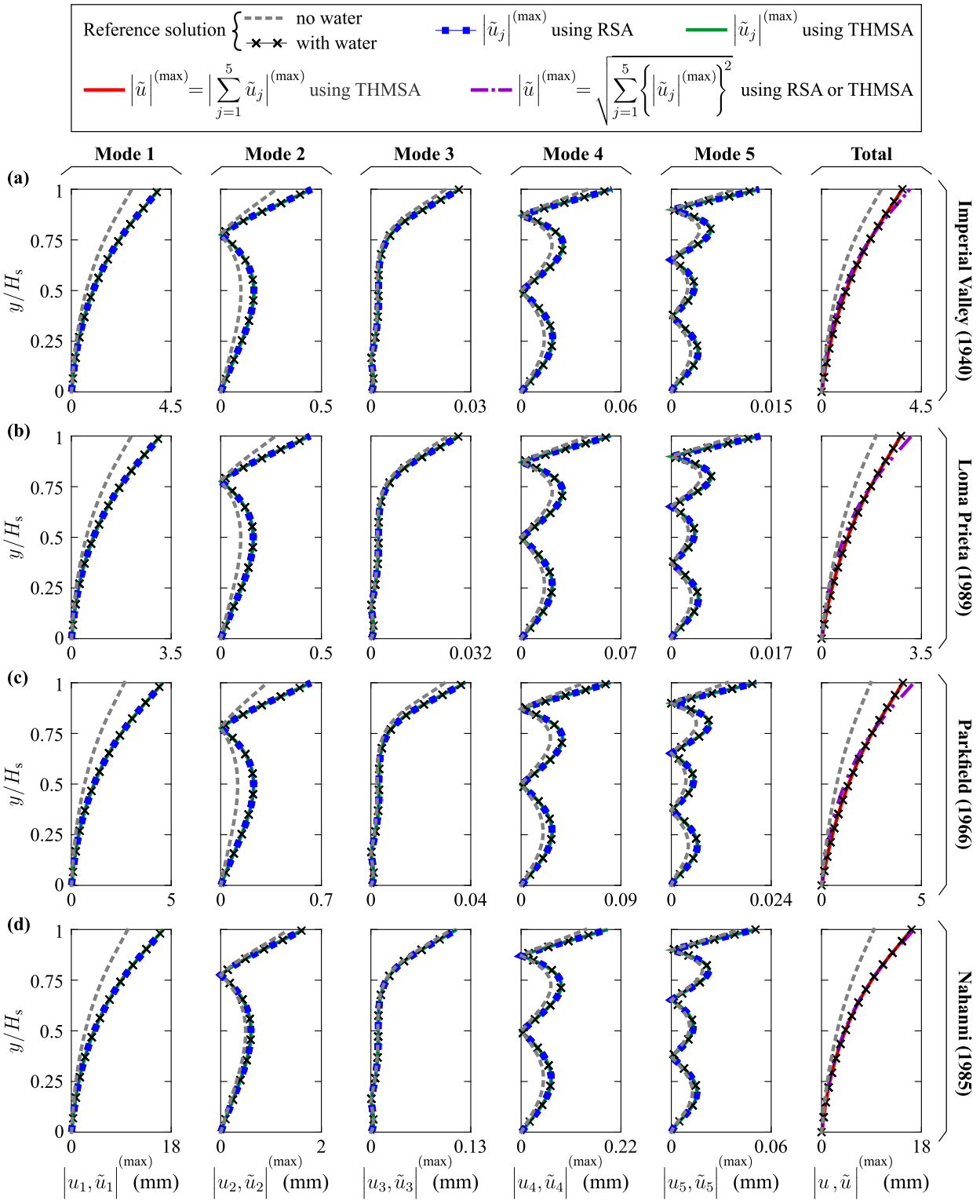

Figure 3.14 Absolute values of maximum relative horizontal displacements along the height of the upstream face of the 35 m high dam (D35) determined for each vibration mode using modified ground motion accelerations $a_g^{(1)}$ to $a_g^{(5)}$ and then combined to obtain total dam response: (a) Imperial Valley (1940) earthquake; (b) Loma Prieta (1989) earthquake; (c) Parkfield (1966) earthquake; and (d) Nahanni (1985) earthquake.

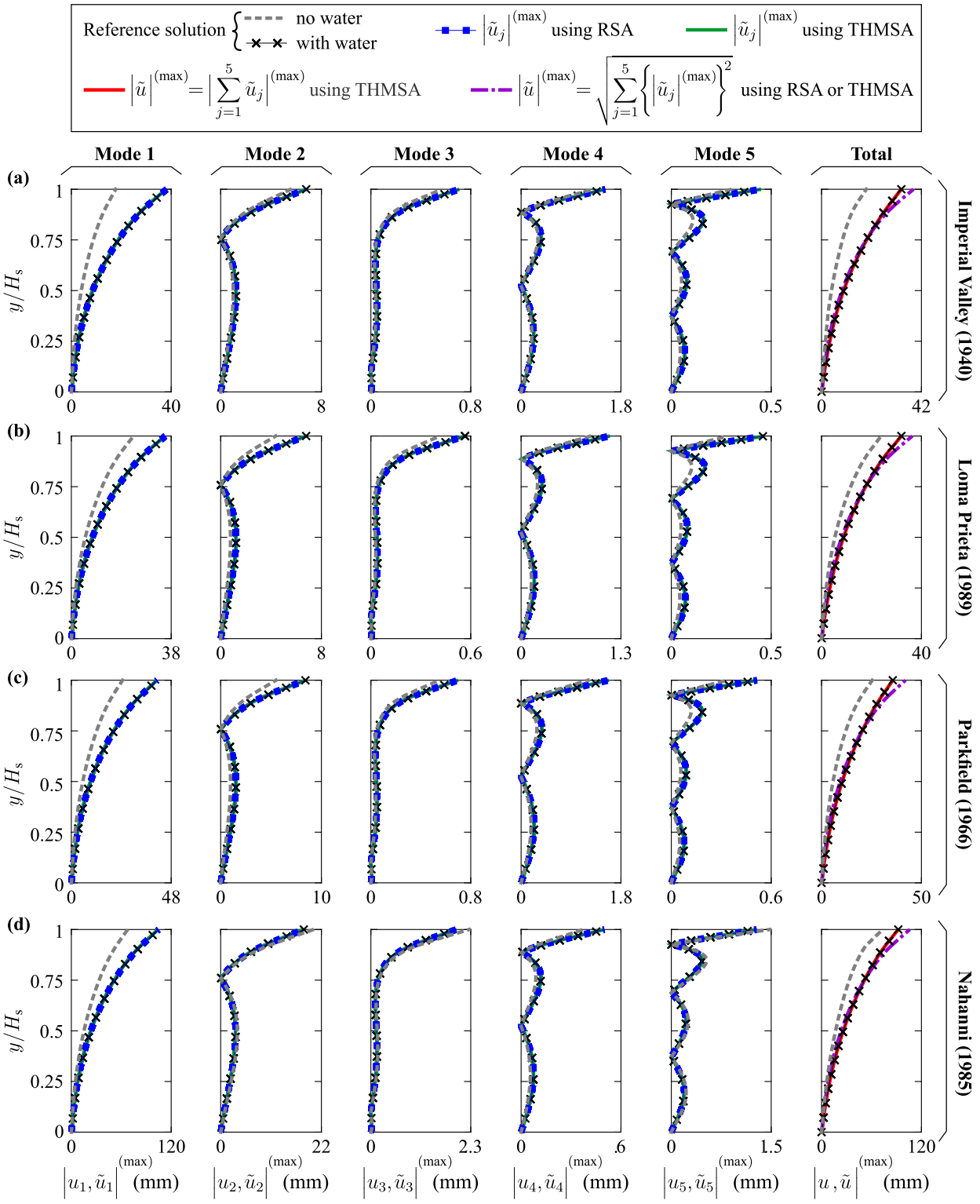

Figure 3.15 Absolute values of maximum relative horizontal displacements along the height of the upstream face of the 90 m high dam (D90) impounding a reservoir determined for each vibration mode using modified ground motion accelerations $a_g^{(1)}$ to $a_g^{(5)}$ and then combined to obtain total dam response: (a) Imperial Valley (1940) earthquake; (b) Loma Prieta (1989) earthquake; (c) Parkfield (1966) earthquake; and (d) Nahanni (1985) earthquake.

voir modeling assumptions of compressible water, incompressible water and Westergaard added-masses are presented. This depiction provides another means to understand and visually compare the effects of reservoir modeling assumptions on dam seismic response along each mode depending on the applied ground motion acceleration. For example, at fundamental vibration mode, the incompressible water assumption yields the largest equivalent lateral static forces on dam D35 when subjected to Imperial Valley (1940), Loma Prieta (1989) and Parkfield (1966) earthquake, while the compressible water assumption corresponds to the largest equivalent lateral static force on dam D35 subjected to Nahanni (1985) record. For dam D90, the largest equivalent lateral static forces at the fundamental vibration mode correspond to: (i) an incompressible water assumption when subjected to Imperial Valley (1940) and Loma Prieta (1989) earthquakes, but to (ii) a compressible water assumption when subjected to Parkfield (1966) and Nahanni (1985) earthquakes. At the second vibration mode, Westergaard added-masses yield the largest equivalent lateral static forces on dam D90 for all the ground motions considered. These results corroborate the findings previously discussed in relation with the seismic acceleration demands and the introduced hydrodynamic modification factors. Similar observations can of course be deduced from Figs. 3.16 and 3.17 for higher vibration modes.

The time-history relative horizontal displacements at any location of the dams can be obtained using methods A and B as described previously. An example is given in Fig. 3.18 depicting the time-history relative displacements at the crest of dam D90 subjected to the four ground motions considered. For comparison purposes, the results are shown for the dams without reservoirs and including compressible water effects. These results are identical to those obtained using the reference solution as shown in Fig. 3.19 depicting the totals of relative horizontal displacements obtained using proposed methods A or B at the crests of dams D35 and D90 subjected to the fours considered grounds motions. For clarity, the results are depicted on a time interval between 5 s and 15 s of each ground motion. The proposed approach can also be used to evaluate the stresses developing in a dam under the effects of an earthquake. This can be achieved based on the time-histories of the displacements obtained at the nodes of the finite element mesh of the dam as illustrated previously, or through application of the equivalent lateral static force to the dam. Figure 3.20 shows an example of the maximum dynamic shear stresses τ_{xy} obtained using proposed methods A or B for each of the five vibration modes of dam D90 subjected to the four earthquakes considered. The total shear stresses evaluated as the summation of the modal stresses are also provided. It is obvious from Fig. 3.20 that the shear stresses under the four ground motions are predominantly controlled by the fundamental vibration mode, although it is worth noting that the second mode's contribution is not negligible. This example demonstrates the effectiveness of

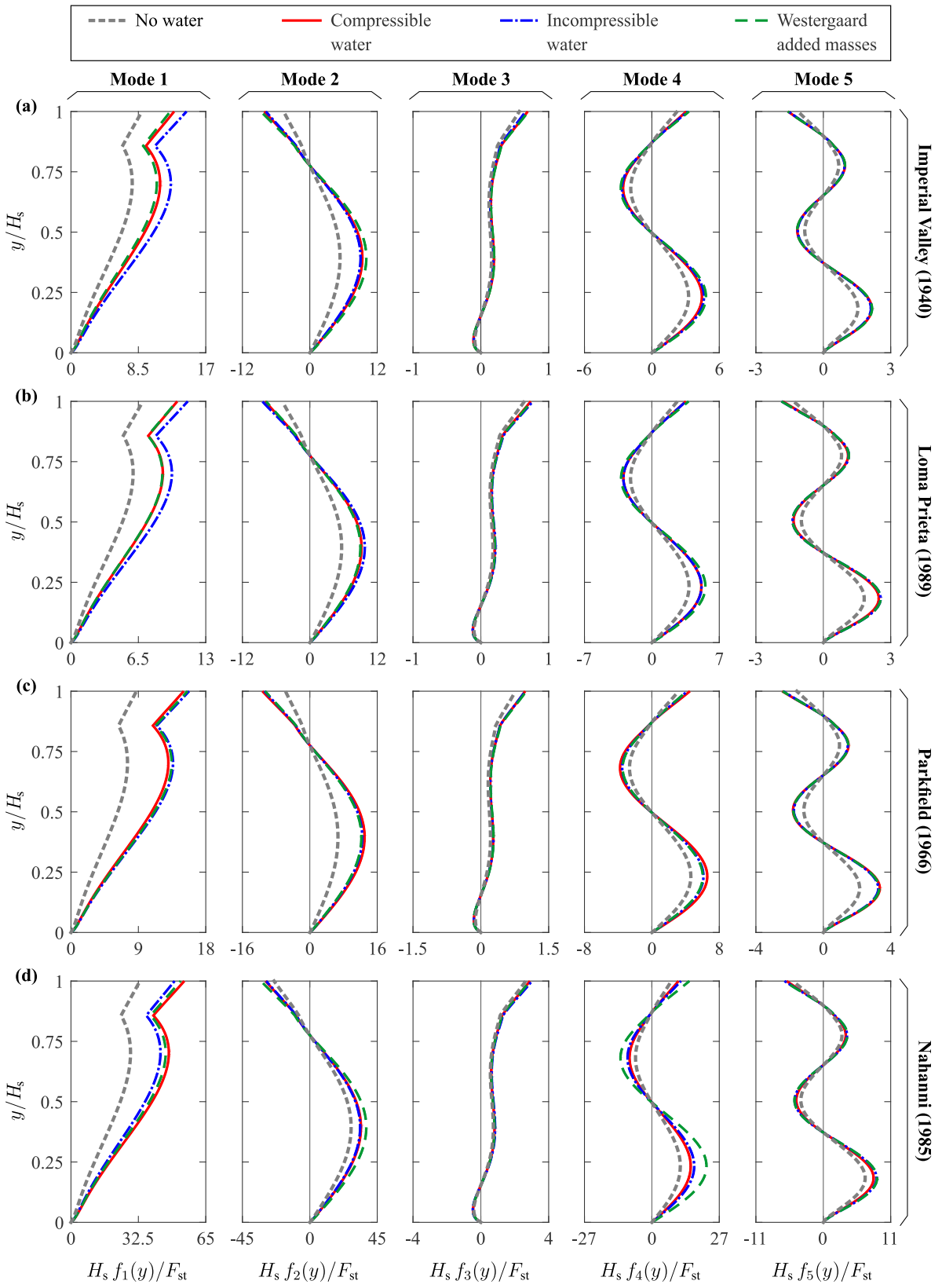

Figure 3.16 Heightwise distribution of the equivalent lateral static forces, including hydrodynamic effects, computed for each of the first vibration modes of dam D35 considering empty reservoir and reservoir modeling assumptions of compressible water, incompressible water and Westergaard added-masses: (a) Imperial Valley (1940) earthquake; (b) Loma Prieta (1989) earthquake; (c) Parkfield (1966) earthquake; and (d) Nahanni (1985) earthquake.

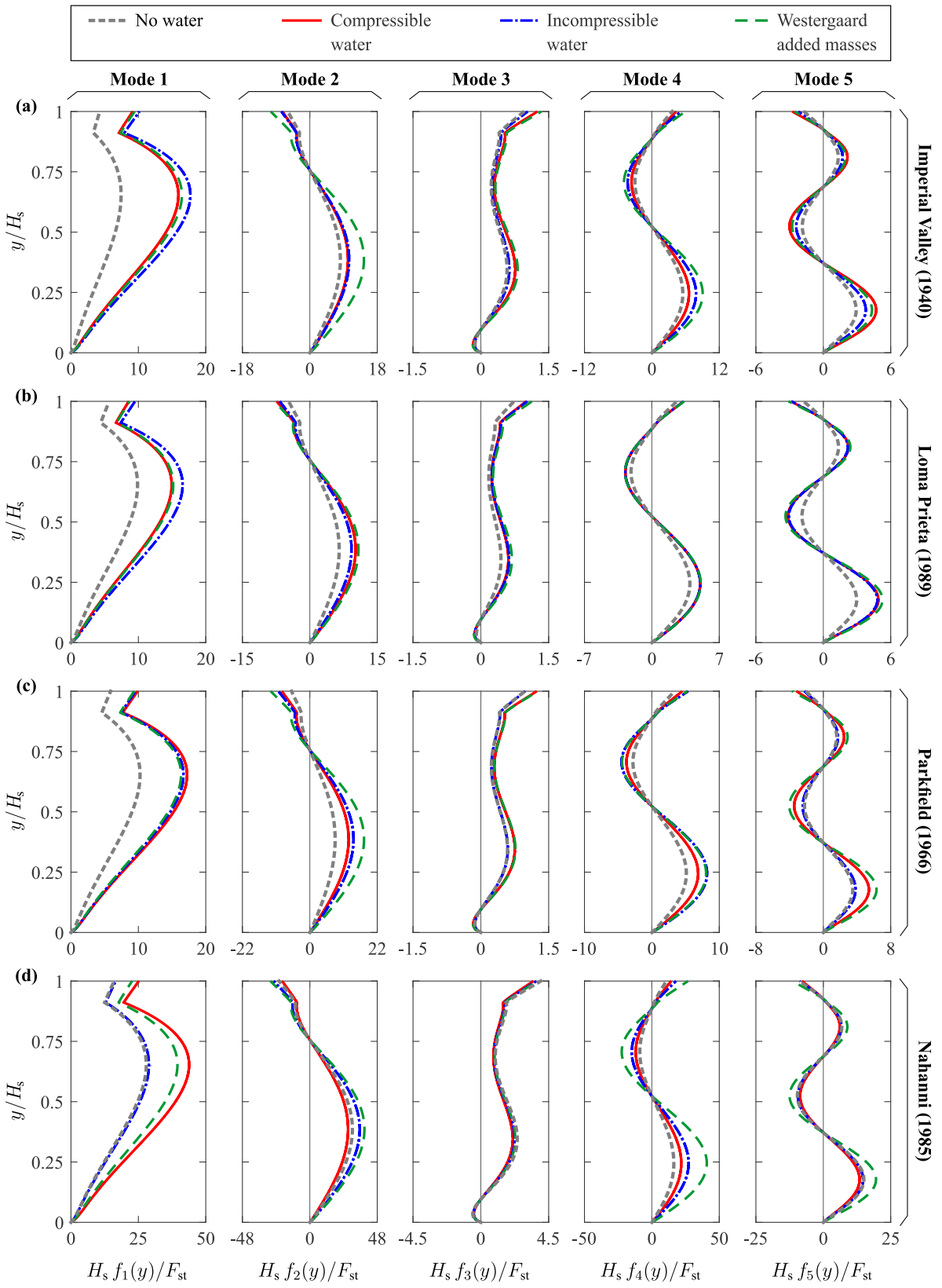

Figure 3.17 Heightwise distribution of the equivalent lateral static forces, including hydrodynamic effects, computed for each of the first vibration modes of dam D90 considering empty reservoir and reservoir modeling assumptions of compressible water, incompressible water and Westergaard added-masses: (a) Imperial Valley (1940) earthquake; (b) Loma Prieta (1989) earthquake; (c) Parkfield (1966) earthquake; and (d) Nahanni (1985) earthquake.

the proposed techniques in comparing the contributions of vibration modes to diverse types of stresses, as well as assessing the significance of these modal contributions.

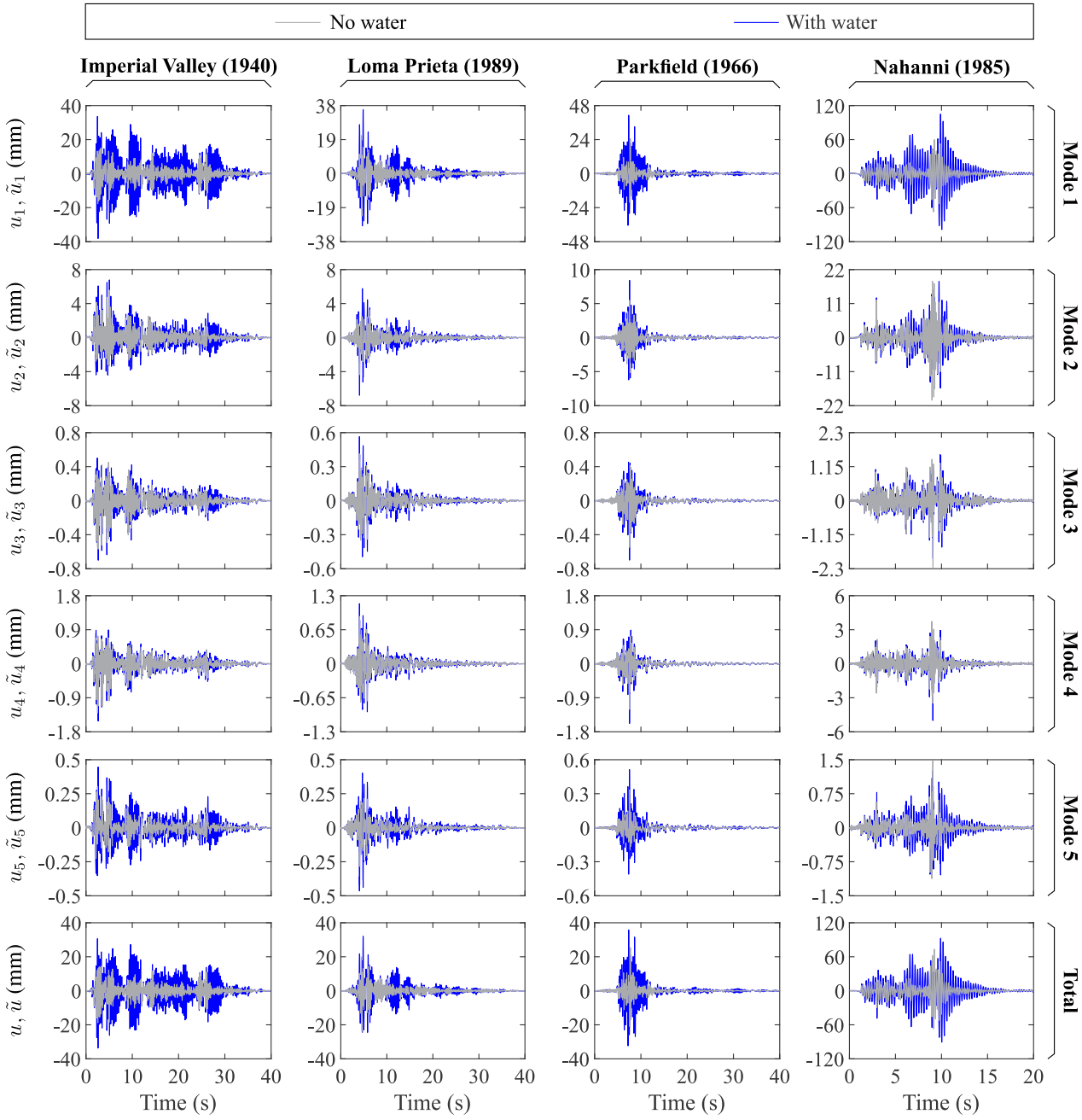

Figure 3.18 Time-histories of relative horizontal displacements at the crest of the 90 m high dam (D90) with impounded reservoir obtained for each vibration mode using modified ground motion accelerations $a_g^{(1)}$ to $a_g^{(5)}$ and then combined to obtain total dam response.

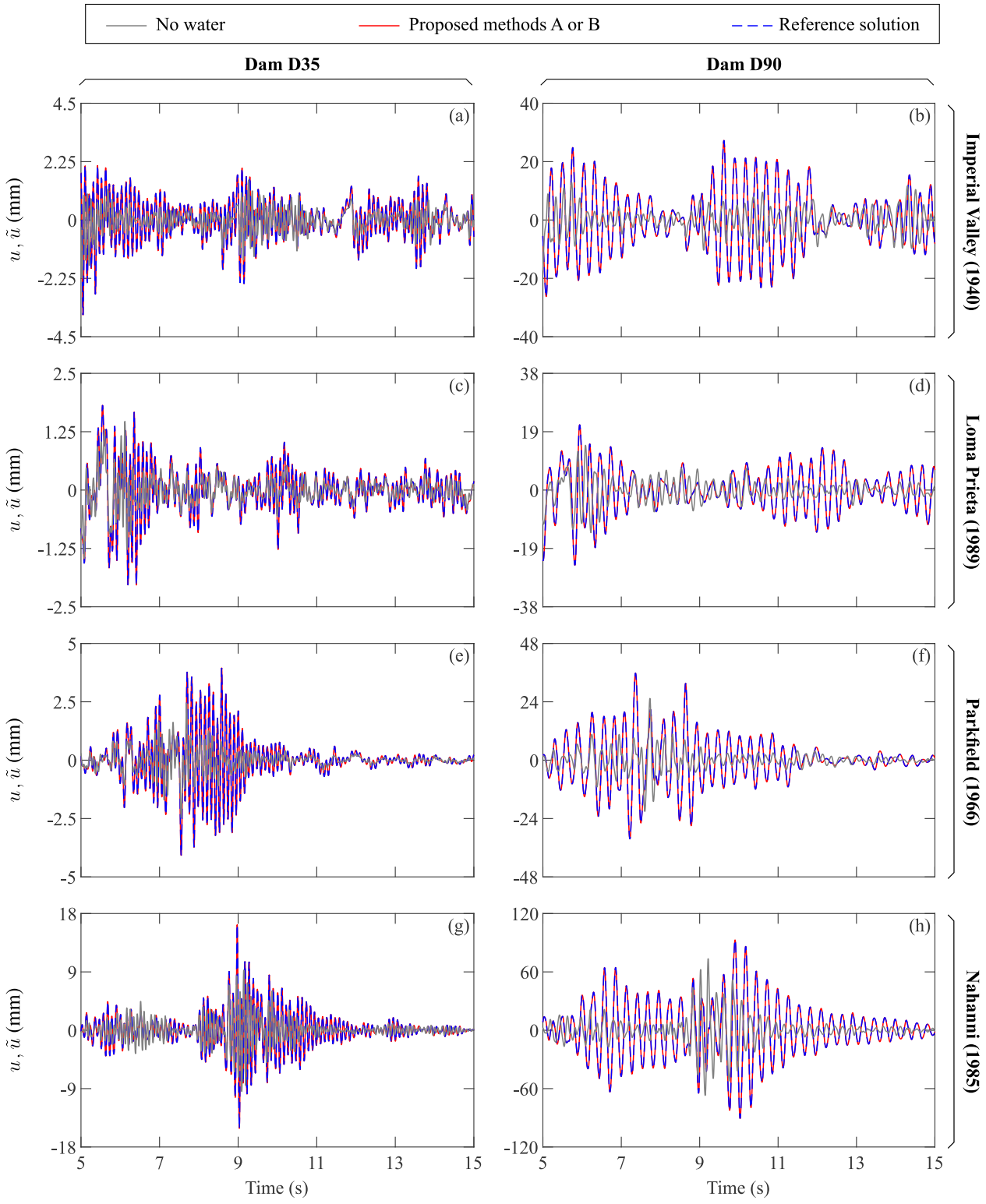

Figure 3.19 Time-histories of the totals of relative horizontal displacements at the crest of the 35 m and 90 m high dams (D35 and D90) with empty reservoir and including compressible water effects: (a) and (b) Imperial Valley (1940) earthquake; (c) and (d) Loma Prieta (1989) earthquake; (e) and (f) Parkfield (1966) earthquake; (g) and (h) Nahanni (1985) earthquake.

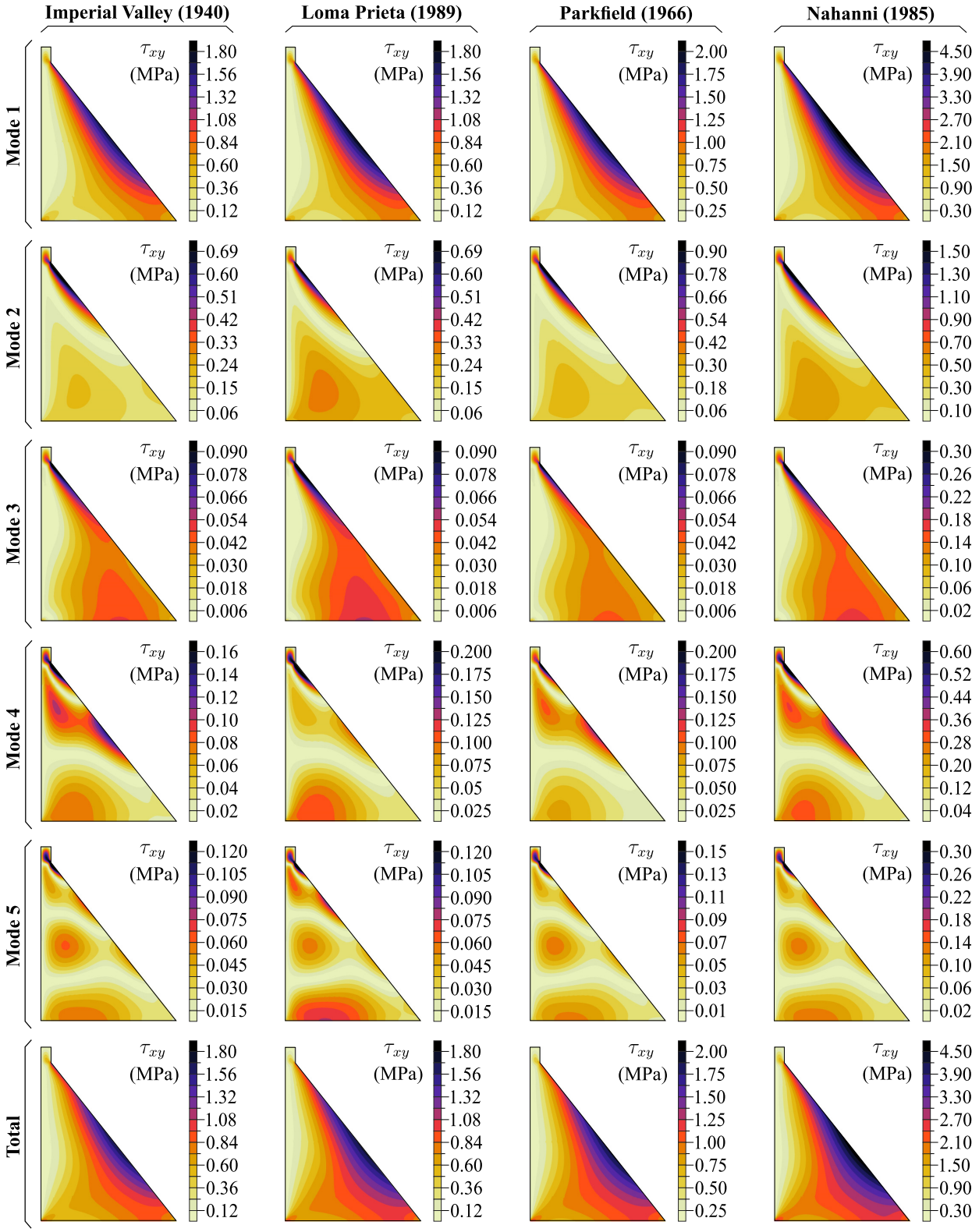

Figure 3.20 Maximum shear stresses τ_{xy} developing within dam D90 subjected to the four earthquakes considered as obtained using proposed methods A or B for each of the first five vibration modes as well as the total dam response.

3.5 Conclusions

This paper proposed new methods to evaluate the seismic response of gravity dam-reservoir systems through dynamic modal superposition and response spectrum analyses. The main originality of the developed techniques is the inclusion of earthquake-induced reservoir effects into modified versions of the original ground motion acceleration and its response spectrum. The modified ground motion time-history and spectral accelerations can then be applied directly to the dam with empty reservoir (i.e. without water), thus eliminating the need for specialized software accounting for fluid-structure interaction dynamic effects. In addition to this practical aspect, the proposed approach allows the evaluation and analysis of the impact of any specific vibration mode on the total seismic response of the gravity dam studied. For example, coupled structural flexibility and hydrodynamic effects due to each vibration mode can be accurately assessed in lieu of the approximate results generally given by the static correction method commonly used in traditional simplified methods. The methodology utilizes analytical formulations of earthquake-induced hydrodynamic pressure in the reservoir or simplified Westergaard added-masses to obtain the contributions of the selected vibration modes to the total seismic response. The developed methods also provide an alternative to the implementation of added masses on each node of the water-structure interface by including the effects of these added masses directly in the modified ground motion time-history or spectral accelerations. Based on the formulations proposed, a hydrodynamic modification factor which can be used to evaluate the amplification or de-amplification of acceleration seismic demands due to earthquake-induced hydrodynamic effects was introduced. The application of the proposed methods was illustrated numerically through examples of two typical gravity dam-reservoir systems subjected to four earthquakes. The obtained results were shown to be in excellent agreement with the classical reference solutions. The findings were discussed to highlight the coupled effects of hydrodynamic-pressure and structural flexibility on the seismic behaviour of the studied dams.

Acknowledgements

The author(s) disclosed receipt of the following financial support for the research, authorship, and/or publication of this article: The authors would like to acknowledge the financial support of the Canada Research Chairs Program and the Natural Sciences and Engineering Research Council of Canada (NSERC).

Appendix A

Using boundary conditions corresponding to free reservoir surface, compatibility at dam-reservoir interface, undisturbed hydrodynamic pressure at reservoir far upstream and wave reflection at reservoir bottom, it can be shown that FRFs p_0 and p_j in Eq. (3.9) can be expressed as [26, 41]

$$p_0(y,\omega) = -2\rho_{\mathrm{w}} H_{\mathrm{w}} \sum_{n=1}^{N_{\mathrm{w}}} \frac{\lambda_n(\omega)^2\, I_{0,n}(\omega)}{\beta_n(\omega)\,\kappa_n(\omega)}\, Y_n(y,\omega) \tag{3.61}$$

$$p_j(y,\omega) = -2\rho_{\mathrm{w}} H_{\mathrm{w}} \sum_{n=1}^{N_{\mathrm{w}}} \frac{\lambda_n(\omega)^2\, I_{j,n}(\omega)}{\beta_n(\omega)\,\kappa_n(\omega)}\, Y_n(y,\omega) \tag{3.62}$$

where N_{w} is the number of water (i.e. acoustical) modes included in the analysis, and λ_n and Y_n are complex-valued frequency-dependent eigenvalues and orthogonal eigenfunctions satisfying for each reservoir acoustical mode n

$$\mathrm{e}^{2\mathrm{i}\lambda_n(\omega)H_{\mathrm{w}}} = -\frac{\lambda_n(\omega) - \omega q}{\lambda_n(\omega) + \omega q} \tag{3.63}$$

$$Y_n(y,\omega) = \frac{\Big[\lambda_n(\omega) - \omega q\Big]\mathrm{e}^{-\mathrm{i}\lambda_n(\omega)\,y} + \Big[\lambda_n(\omega) + \omega q\Big]\mathrm{e}^{\mathrm{i}\lambda_n(\omega)\,y}}{2\lambda_n(\omega)} \tag{3.64}$$

in which q is a damping coefficient defined at reservoir bottom as

$$q = \frac{\rho_{\mathrm{w}}}{\rho_{\mathrm{f}}\, C_{\mathrm{f}}} = \frac{1}{C_{\mathrm{w}}}\frac{1-\alpha}{1+\alpha} \tag{3.65}$$

where ρ_{f} and C_{f} denote the mass density and the compression wave velocity within the reservoir bottom foundation, respectively, C_{w} is compression wave velocity within the reservoir, and α is the wave reflection coefficient representing the portion of the wave amplitude reflected back to the reservoir. Instead of solving the transcendental equation (3.63), the eigenvalues λ_n can be approximated using the closed-form expression developed by Bouaanani and Perrault [41]for moderately to highly reflective reservoir bottoms, i.e. $\alpha \geqslant 0.65$

$$\lambda_n(\omega) = \frac{(2n-1)\pi}{4H_{\mathrm{w}}} + \sqrt{\frac{(2n-1)^2\pi^2}{(4H_{\mathrm{w}})^2} + \mathrm{i}\,\frac{\omega q}{H_{\mathrm{w}}}} \tag{3.66}$$

If full wave reflection at reservoir bottom is assumed (i.e. $\alpha = 1$), the reservoir eigenvalues λ_n are frequency-independent, simplifying to

$$\lambda_n = \frac{(2n-1)\,\pi}{2H_{\mathrm{w}}} \tag{3.67}$$

In this case, hydrodynamic pressure FRFs p_0 and p_j are expressed as

$$p_0(y,\omega) = \frac{-4\rho_{\mathrm{w}}}{\pi} \sum_{n=1}^{N_{\mathrm{w}}} \frac{(-1)^n}{(2n-1)} \frac{\cos(\lambda_n\, y)}{\sqrt{\lambda_n^2 - \dfrac{\omega^2}{C_{\mathrm{w}}^2}}} \tag{3.68}$$

$$p_j(y,\omega) = 2\rho_{\mathrm{w}} \sum_{n=1}^{N_{\mathrm{w}}} \frac{I_{j,n}(\omega)}{\sqrt{\lambda_n^2 - \dfrac{\omega^2}{C_{\mathrm{w}}^2}}} \cos\left(\lambda_n\, y\right) \tag{3.69}$$

The parameters β_n, κ_n, $I_{0,n}$, and $I_{j,n}$ in Eqs. (3.61) and (3.62) are given by

$$\beta_n(\omega) = H_{\mathrm{w}} \left[\lambda_n(\omega)^2 - \omega^2\, q^2\right] + \mathrm{i}\,\omega q \tag{3.70}$$

$$\kappa_n(\omega) = \sqrt{\lambda_n(\omega)^2 - \frac{\omega^2}{C_{\mathrm{w}}^2}} \tag{3.71}$$

$$I_{0,n}(\omega) = \frac{\mathrm{i}\,\mathrm{e}^{-\mathrm{i}\,\lambda_n(\omega) H_{\mathrm{w}}}}{\lambda_n(\omega)^2 H_{\mathrm{w}}} \left[\lambda_n(\omega) - \omega q + \omega q \mathrm{e}^{\mathrm{i}\lambda_n(\omega) H_{\mathrm{w}}}\right] \tag{3.72}$$

$$I_{j,n}(\omega) = \frac{1}{H_{\mathrm{w}}} \int_0^{H_{\mathrm{w}}} \psi_j^{(x)}(y)\, Y_n(y,\omega)\, \mathrm{y} \tag{3.73}$$

For practical computations, the x–component of mode shape $\boldsymbol{\psi}_j$, $j = 1 \ldots N_{\mathrm{s}}$, of the dry structure can be approximated by a polynomial function of order $N_{\boldsymbol{\psi}_j}$ and coefficients $a_{j,k}$ as proposed by [41]. The generalized coordinates, solutions of the system of equations in Eq. (3.45), can also be obtained as proposed by Miquel and Bouaanani [3]

$$\widehat{Z}_1(\omega) = \frac{\widetilde{S}_{2,2}(\omega)\, \widetilde{Q}_1(\omega) - \widetilde{S}_{1,2}(\omega)\, \widetilde{Q}_2(\omega)}{\widetilde{S}_{1,1}(\omega)\, \widetilde{S}_{2,2}(\omega) - \widetilde{S}_{1,2}^2(\omega)} \tag{3.74}$$

$$\widehat{Z}_j(\omega) = \frac{\widetilde{S}_{j-1,j-1}(\omega)\, \widetilde{Q}_j(\omega) - \widetilde{S}_{j-1,j}(\omega)\, \widetilde{Q}_{j-1}(\omega)}{\widetilde{S}_{j-1,j-1}(\omega)\, \widetilde{S}_{j,j}(\omega) - \widetilde{S}_{j-1,j}^2(\omega)} \qquad \text{for } j = 2 \ldots N_{\mathrm{s}} \tag{3.75}$$

Equations (3.74) and (3.75) are exact when only two modes are included in the analysis and approximations otherwise.

Appendix B

This appendix illustrates a step-by-step procedure to generate the modified accelerogram $a_{\mathrm{g}}^{(1)}(t)$ corresponding to the fundamental vibration mode of dam D90 subjected to Imperial Valley (1940) ground motion and assuming compressible water in the reservoir (i.e. Methods A or B in Fig. 3.2 and the flowchart in Fig. 3.3). The procedure is based on discrete fast Fourier transform (DFFT) and inverse discrete fast Fourier transform (IDFFT) for which detailed information is abundant in the literature, e.g. [138–141].

Step 1: The dynamic properties of the structure with an empty reservoir are obtained using a finite element model. The fundamental natural frequency is $\omega_1 = 29.97\,\mathrm{rad/s}$ (corresponding to period $T_1 = 0.210\,\mathrm{s}$), with a generalized modal mass of $M_1 = 1\,\mathrm{kg}$ and modal participation factor $L_1 = -1658.79$. The horizontal component of the fundamental mode shape at the upstream face of the dam with an empty reservoir is also obtained as shown in Fig. 3.21 (a).

Step 2: The duration and initial time step of the used original ground motion acceleration of Imperial Valley earthquake (1940), i.e. $\ddot{x}_{\mathrm{g}}(t)$, are $t_a = 39.99\,\mathrm{s}$ and $\Delta t^{(\mathrm{init})} = 0.01\,\mathrm{s}$, respectively. The initial number of time intervals is 4000. The initial accelerogram is shown in Fig. 3.21 (b).

Step 3: A number of excitation frequencies $N_{\mathrm{P}} = 2^k$, with k integer, is fixed for the representation of the acceleration in the frequency domain. An adequate k value is to be selected as a compromise between accuracy (higher k value) and time of analysis (lower k value). In this work, $k = 14$ was selected, i.e. $N_{\mathrm{P}} = 2^{14}$.

Step 4: The number of excitation frequencies is also equal to the number of new time intervals for the representation of the original ground motion in the time-domain. The new time interval is $\Delta t^{(\mathrm{new})} = t_a / N_{\mathrm{P}} = 0.00244\,\mathrm{s}$. A smaller $\Delta t^{(\mathrm{new})}$ value (i.e. higher N_{P}) corresponds to a finer time-domain representation, thus accounting for rapid and transient signal changes more accurately. A larger $\Delta t^{(\mathrm{new})}$ reduces computational cost but may lead to loss of accuracy.

Step 5: The original ground motion acceleration is interpolated into the new time intervals $\Delta t^{(\mathrm{new})}$, yielding a series of N_{P} acceleration points, and then padded with N_{P} zero accelerations at the end of the interpolated signal to reduce aliasing errors. This operation is illustrated in Fig. 3.21 (c).

Step 6: DFFT is applied to the interpolated and zero-padded original ground motion acceleration time series (i.e. now comprising $2\,N_{\mathrm{P}}$ accelerations) to obtain the frequency-domain representation of the signal, i.e. $\ddot{x}_{\mathrm{g}}(\omega)$, as illustrated in Fig. 3.21 (d).

Step 7: The parameters $\vartheta_{0,1}(\omega)$ and $\vartheta_{1,1}(\omega)$ are evaluated using Eqs. (3.11) and (3.12), respectively. The absolute values of these frequency-dependent parameters are shown in Figs. 3.21 (e) and (f).

Step 8: The frequency-domain representation of the modified ground motion acceleration for the fundamental mode of the structure, i.e. $a_{\mathrm{g}}^{(1)}(\omega)$, is obtained using Eq. (3.26), as illustrated in Fig. 3.21 (g).

Step 9: IDFFT is employed to transform the modified ground motion acceleration from the frequency to the time domain, i.e. $a_{\mathrm{g}}^{(1)}(t)$, as illustrated Fig. 3.21 (h).

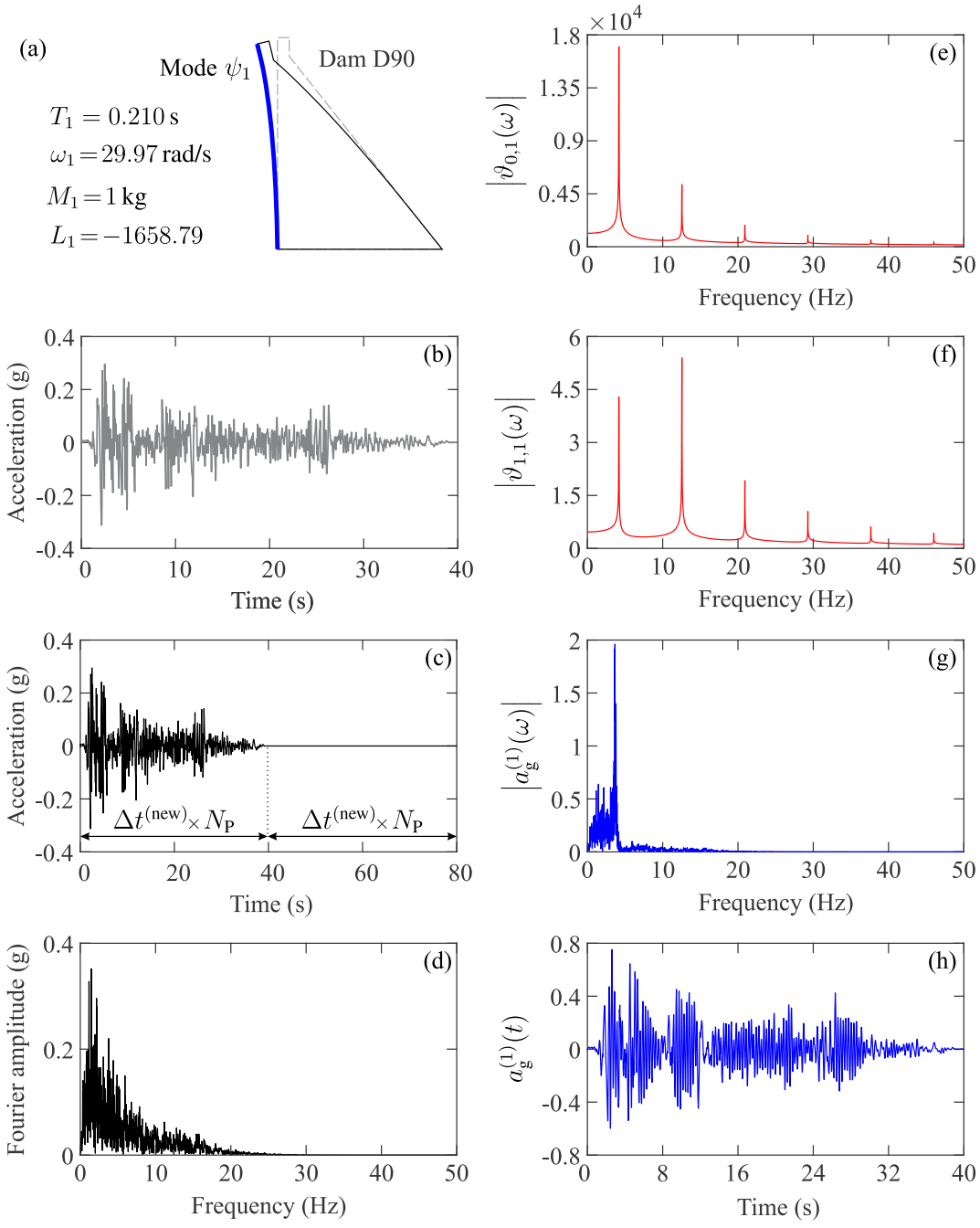

Figure 3.21 Generation of modified ground motion acceleration $a_\text{g}^{(1)}$ for the 90 m high dam (D90) subjected to Imperial Valley (1940) earthquake: (a) Dynamic properties of the dam with an empty reservoir; (b) Initial ground motion acceleration; (c) Interpolated and zero-padded ground motion acceleration; (d) DFFT of the interpolated original ground motion acceleration; (e) Evaluation of $\vartheta_{0,1}(\omega)$; (f) Evaluation of $\vartheta_{1,1}(\omega)$; (g) Evaluation of modified ground motion acceleration $a_\text{g}^{(1)}(\omega)$ in the frequency domain; (h) IDFFT of the modified ground motion acceleration $a_\text{g}^{(1)}(\omega)$ to obtain its time-domain representation $a_\text{g}^{(1)}(t)$.

Appendix C

The following example illustrates the steps and calculations of the proposed response spectrum analysis (i.e. Method C in Fig.3.2 and the flowchart in Fig. 3.3) to evaluate the maximum absolute horizontal displacement at the crest of dam D90 when subjected to Imperial Valley (1940) ground motion. It is to be noted that hand calculations of the following operations may lead to slightly different numerical results than those provided below due to the number of significant digits included in the numerical computations used.

Step 1: The fundamental vibration period of the dam with empty reservoir obtained using a finite element model is $T_1 = 0.210\,\text{s}$.

Step 2: The modified ground motion acceleration $a_{\text{g}}^{(1)}$ is obtained from Eq. (28) as shown in Fig. 3.9(a) and illustrated in Appendix B.

Step 3: The pseudo-spectral acceleration of the modified ground motion acceleration $a_{\text{g}}^{(1)}$ is computed as shown in Fig. 3.11 (b), i.e. $S_{\text{A}}^{[a_{\text{g}}^{(1)}]}\Big(T_1 = 0.210, \xi_1 = 0.05\Big) = 1.42\,\text{g}$.

Step 4: The value of the horizontal component of the fundamental mode shape at the crest of dam with empty reservoir is obtained using a finite element model, i.e. $\psi_1^{(x)}(y_{\text{crest}}) = -1.481 \times 10^{-3}$, as well as the generalized modal mass $M_1 = 1\,\text{kg}$ (i.e. the mode shapes are mass-orthonormalized in this example) and modal participation factor $L_1 = -1658.79$.

Step 5: The maximum absolute value of seismic relative displacement at the crest of the dam-reservoir system corresponding to the fundamental mode is evaluated by Eq. (3.32)

$$\begin{aligned}\Big|\widehat{u}_1(y_{\text{crest}}, t)\Big|^{(\text{max})} &= \frac{L_1}{M_1}\,\frac{T_1^2}{4\pi^2}\,S_{\text{A}}^{[a_{\text{g}}^{(1)}]}(T_1, \xi_1)\,\psi_1^{(x)}(y_{\text{crest}}) \\ &= \left|\frac{(-1658.79)}{1} \times \frac{(0.210)^2}{4\pi^2} \times 1.42 \times 9.81 \times (-1.481) \times 10^{-3}\right| = 38.10\ \text{mm}\end{aligned} \tag{3.76}$$

Step 6: Steps 1 to 5 can be repeated to obtain the maximum absolute value of seismic relative displacements at the crest of the dam-reservoir system corresponding to higher vibration modes of the dam with empty reservoir (i.e. corresponding to natural

periods $T_2 = 0.099\,\text{s}$, $T_3 = 0.077\,\text{s}$, $T_4 = 0.061\,\text{s}$, and $T_5 = 0.041\,\text{s}$), yielding

$$\left|\widehat{u}_2(y_{\text{crest}},t)\right|^{(\max)} = \frac{L_2}{M_2}\,\frac{T_2^2}{4\pi^2}\,S_{\text{A}}^{[a_{\text{g}}^{(2)}]}(T_2,\xi_2)\,\psi_2^{(x)}(y_{\text{crest}})$$
$$= \left|\frac{(-1337.76)}{1} \times \frac{(0.099)^2}{4\pi^2} \times 0.86 \times 9.81 \times (2.445) \times 10^{-3}\right| = 6.79\ \text{mm} \tag{3.77}$$

$$\left|\widehat{u}_3(y_{\text{crest}},t)\right|^{(\max)} = \frac{L_3}{M_3}\,\frac{T_3^3}{4\pi^2}\,S_{\text{A}}^{[a_{\text{g}}^{(3)}]}(T_3,\xi_3)\,\psi_3^{(x)}(y_{\text{crest}})$$
$$= \left|\frac{(-652.03)}{1} \times \frac{(0.077)^2}{4\pi^2} \times 0.78 \times 9.81 \times (-9.412) \times 10^{-4}\right| = 0.71\ \text{mm} \tag{3.78}$$

$$\left|\widehat{u}_4(y_{\text{crest}},t)\right|^{(\max)} = \frac{L_4}{M_4}\,\frac{T_4^2}{4\pi^2}\,S_{\text{A}}^{[a_{\text{g}}^{(4)}]}(T_4,\xi_4)\,\psi_4^{(x)}(y_{\text{crest}})$$
$$= \left|\frac{(-860.15)}{1} \times \frac{(0.061)^2}{4\pi^2} \times 0.74 \times 9.81 \times (-2.598) \times 10^{-3}\right| = 1.51\ \text{mm} \tag{3.79}$$

$$\left|\widehat{u}_5(y_{\text{crest}},t)\right|^{(\max)} = \frac{L_5}{M_5}\,\frac{T_5^2}{4\pi^2}\,S_{\text{A}}^{[a_{\text{g}}^{(5)}]}(T_5,\xi_5)\,\psi_5^{(x)}(y_{\text{crest}})$$
$$= \left|\frac{(730.25)}{1} \times \frac{(0.041)^2}{4\pi^2} \times 0.63 \times 9.81 \times (-2.281) \times 10^{-3}\right| = 0.45\ \text{mm} \tag{3.80}$$

Step 7: The total of maximum absolute values of seismic relative horizontal displacements at the crest of the dam-reservoir system can then be approximated using a combination rule such as the Square Root of the Sum of the Squares (SRSS)

$$\left|\widehat{u}(y_{\text{crest}},t)\right|^{(\max)} = \sqrt{\sum_{j=1}^{N_{\text{s}}=5}\left[\left|\,\widehat{u}_j(y_{\text{crest}},t)\,\right|^{(\max)}\right]^2}$$
$$= \sqrt{(38.10)^2 + (6.79)^2 + (0.71)^2 + (1.51)^2 + (0.45)^2} = 38.74\,\text{mm} \tag{3.81}$$

Tables

Table 3.1 Hydrodynamic modification factors obtained for the first five vibration modes of dams D35 and D90 subjected to the ground motion accelerations considered.

		Dam D35					Dam D90				
		Modes					Modes				
Earthquake	Water assumption	1	2	3	4	5	1	2	3	4	5
Imperial	Compressible	1.46	1.76	1.21	1.39	1.42	2.15	1.25	1.32	1.19	1.62
Valley	Incompressible	1.63	1.70	1.15	1.42	1.39	2.39	1.29	1.10	1.42	1.31
(1940)	Added-masses	1.40	1.89	1.24	1.48	1.42	2.23	1.77	1.41	1.65	1.49
Loma	Compressible	1.48	1.64	1.16	1.32	1.35	1.51	1.56	1.35	1.27	1.65
Prieta	Incompressible	1.63	1.74	1.18	1.32	1.41	1.68	1.42	1.39	1.30	1.63
(1989)	Added-masses	1.48	1.62	1.16	1.43	1.41	1.55	1.65	1.52	1.30	1.78
Parkfield	Compressible	1.71	1.96	1.29	1.43	1.55	1.67	1.53	1.28	1.33	1.55
(1966)	Incompressible	1.79	1.87	1.29	1.34	1.50	1.62	1.71	1.02	1.59	1.09
	Added-masses	1.77	1.85	1.33	1.32	1.52	1.59	2.13	1.30	1.55	1.81
Nahanni	Compressible	1.64	1.24	1.09	1.37	1.20	1.56	0.90	0.88	1.34	0.90
(1985)	Incompressible	1.50	1.22	1.14	1.49	1.28	1.03	1.17	0.93	1.67	0.99
	Added-masses	1.59	1.37	1.10	1.92	1.29	1.41	1.28	0.94	2.50	1.30

CHAPTER 4 ARTICLE 2: AN EFFICIENT PROCEDURE FOR MODAL SEISMIC RESPONSE ANALYSIS OF AXISYMMETRIC STRUCTURES SURROUNDED BY WATER

Ramtin Kouhdasti[a], Najib Bouaanani[a]
[a]Department of Civil, Geological and Mining Engineering, Polytechnique Montréal, Montréal, QC H3C 3A7, Canada.

Paper published in Journal of Ocean Engineering on July 15, 2024.

4.1 Abstract

This paper presents a new procedure for the seismic response assessment of water-surrounded axisymmetric structures through the inclusion of earthquake-induced hydrodynamic effects into input ground motion accelerations. The resulting modified time-history and spectral ground motion accelerations can then be applied directly to the dry axisymmetric structure (i.e. without water) through dynamic modal superposition or response spectrum analyses. Therefore, recourse to specialized software accounting for fluid-structure interaction dynamic effects can be avoided. The proposed approach evaluates the individual impact of hydrodynamic effects associated with any specific structural vibration mode on the global structural seismic response. The procedure implements hydrodynamic pressure formulation or simplified added masses as an alternative to classical nodal lumping. A hydrodynamic modification factor to efficiently estimate amplification or de-amplification of acceleration seismic demands due to earthquake-induced hydrodynamic effects is proposed. The application of the proposed methods is illustrated numerically through examples of three water-surrounded axisymmetric structures subjected to two earthquakes. The results of key response indicators, including relative displacements, base shear, and stresses are shown to be in excellent agreement with the coupled finite element solutions. The coupled effects of hydrodynamic-pressure and structural flexibility on the seismic behaviour of the studied systems are discussed.

Keywords: Axisymmetric water-structure systems, Hydrodynamic pressure, Seismic response, Dynamic modal superposition, Modal time-history analysis, Fluid-structure interaction, Simplified methods.

4.2 Introduction

The seismic response of axisymmetric water-surrounded structures can be affected by earthquake induced hydrodynamic pressure and fluid-structure interaction. This topic has been ex-

tensively covered by many researchers (eg. [6,45,46,114,142–151]). Analytical solutions for hydrodynamic pressures on an elastic cylindrical tower based on radiation wave theory have been developed including water compressibility [144,152,152–155]. Simplified added mass formulations simulating hydrodynamic effects have also been proposed [21, 42, 114, 117, 147, 153, 156]. Morison's equation has gained widespread acceptance to evaluate hydrodynamic effects on slender cylinders due to its simplicity [43, 44, 121, 122, 157]. Originally proposed by Morison [47] for calculating wave loads, this semi-empirical formula was later modified by y Penzien and Kaul [48] to account for hydrodynamic forces on cylindrical structures during earthquakes. Numerical techniques such as finite element, boundary element, and scaled boundary element methods are other common alternatives widely used to investigate earthquake-induced hydrodynamic effects on axisymmetric water-surrounded structures (eg. [49–61]). These techniques generally allow for the coupling of structural and hydrodynamic responses through fluid-structure interface elements. However, implementing such coupled solutions often requires specialized software, extensive time necessary to build and execute the models, and a considerable level of expertise to ensure reliable and accurate results ([2, 6, 114, 158]).

Despite the multitude of available methods for the seismic analysis of water-surrounded axisymmetric structures, engineering practice still needs new alternative techniques with a fair balance between complexity, efficiency, and simplicity of application and interpretation of the obtained results. The semi-analytical approach proposed in this paper breaks down earthquake-induced hydrodynamic effects on the seismic response of the studied water-structure system along multiple vibration modes of the dry structure (i.e. without water). This process enables a better understanding of the impact of each mode and associated hydrodynamic effects of the global seismic response. For this purpose, a methodology is developed to include earthquake-induced hydrodynamic effects into input ground motion accelerations. The resulting modified time-history and spectral ground motion accelerations can then be applied directly to the dry axisymmetric structure through dynamic modal superposition or response spectrum analyses. Therefore, recourse to specialized software accounting for fluid-structure interaction dynamic effects can be avoided. The procedure implements hydrodynamic pressure formulation or simplified added masses as an alternative to classical nodal lumping.

The article is structured as follows. First, the theoretical background of the proposed method is presented, as well as detailed procedures illustrating the application of the proposed dynamic modal superposition and response spectrum analyses. Numerical case studies of three axisymmetric structures with different heights are presented and the results of key response indicators, including relative displacements, base shear, and stresses are discussed and compared to classical coupled finite element solutions accounting for dynamic fluid-structure

interaction.

4.3 Theoretical background and proposed methods

4.3.1 Basic assumption and governing equations

An axisymmetric structure, as the one depicted in Fig. 4.2 (a), is considered to illustrate the procedure proposed. The structure has a total height H_s and is surrounded by an infinite water domain with a constant depth H_w. The submerged section of the structure has a uniform outer radius R_s. Two coordinate systems are employed to define the geometry: (i) a Cartesian system (x, y, z), originating at the center of the bottom cross-section of the structure, with the z-axis aligning with the axis of symmetry; and (ii) a cylindrical system (r, θ, z), where r represents the radial distance and θ the azimuth between the reference x-axis and the line from the origin to the projection of the point of interest on the (x, y) plane. The structure's dynamic response is analyzed under the effect of a horizontal ground motion acceleration $\ddot{x}_\mathrm{g}(t)$ applied along the x-direction. The axisymmetric structure can be composed of one or more materials and its cross-section can be solid or hollow, with uniform or varying internal radius. The following main assumptions are made: (i) all constitutive materials exhibit linear elastic behaviour during seismic excitation, (ii) water is assumed to be inviscid, but can be compressible or incompressible, with its motion irrotational and of small amplitudes, (iii) convective effects and surface gravity waves in water are neglected, and (iv) the foundation is massless and rigid.

It can be shown that dynamic behaviour of the axisymmetric water-structure tower subjected to a unit horizontal harmonic ground acceleration $\ddot{x}_\mathrm{g}(t) = \mathrm{e}^{\mathrm{i}\omega t}$, with ω denoting the forcing frequency, can be determined through the solution of a system of equations [6, 114]

$$\widehat{\mathbf{S}}\,\widehat{\mathbf{Z}} = \widehat{\mathbf{Q}} \tag{4.1}$$

in which $\widehat{\mathbf{Z}}$ denotes the vector of generalized coordinates $\widehat{Z}_j$, and the elements of the matrix $\widehat{\mathbf{S}}$ and vector $\widehat{\mathbf{Q}}$ are given for $m = 1 \ldots N_\mathrm{s}$ and $j = 1 \ldots N_\mathrm{s}$ as

$$\widehat{S}_{j,m}(\omega) = \left(-\omega^2 + 2\,\mathrm{i}\,\xi_j\,\omega\,\omega_j + \omega_j^2 \right) M_j\,\delta_{j,m} - \omega^2\,\vartheta_{j,m}(\omega) \tag{4.2}$$

$$\widehat{Q}_m(\omega) = -L_m^{(x)} - \vartheta_{0,m}(\omega) \tag{4.3}$$

where $\delta_{j,m}$ denote the Kronecker symbol, ω_j the natural vibration frequency corresponding to structural mode $\boldsymbol{\psi}_j$ of the dry structure, i.e. without water, ξ_j the fraction of critical damping, $M_j = \boldsymbol{\psi}_j^\mathrm{T}\,\mathbf{M}\,\boldsymbol{\psi}_j$ the generalized modal mass, $L_m^{(x)} = \boldsymbol{\psi}_m^\mathrm{T}\,\mathbf{M}\,\mathbf{1}^{(x)}$ the horizontal modal participation factor, with $\mathbf{1}^{(x)}$ a column-vector containing zeros except along horizontal de-

grees of freedom corresponding to earthquake direction, and where the parameters $\vartheta_{0,m}(\omega)$ and $\vartheta_{j,m}(\omega)$ are given by

$$\vartheta_{0,m}(\omega) = R_{\mathrm{s}} \int_0^{H_{\mathrm{w}}} \int_0^{2\pi} p_0(R_{\mathrm{s}}, \theta, z, \omega)\, \cos(\theta)\, \psi_m^{(x)}(R_{\mathrm{s}}, 0, z)\, \mathrm{d}\theta\, \mathrm{d}z \tag{4.4}$$

$$\vartheta_{j,m}(\omega) = R_{\mathrm{s}} \int_0^{H_{\mathrm{w}}} \int_0^{2\pi} p_j(R_{\mathrm{s}}, \theta, z, \omega)\, \cos(\theta)\, \psi_j^{(x)}(R_{\mathrm{s}}, 0, z)\, \psi_m^{(x)}(R_{\mathrm{s}}, 0, z)\, \mathrm{d}\theta\, \mathrm{d}z \tag{4.5}$$

for $j, m = 1 \ldots N_{\mathrm{s}}$, with p_0 denoting the hydrodynamic pressure FRF at *rigid* structure-water interface due to horizontal ground motion $\ddot{x}_{\mathrm{g}}$ and p_j the hydrodynamic pressure FRF at *flexible* structure-water interface due to horizontal acceleration $\psi_j^{(x)}(R_{\mathrm{s}}, 0, z)$, $j = 1 \ldots N_{\mathrm{s}}$. The FRFs p_0 and p_j can be evaluated using the expressions given in Appendix A.

The previous equations are based on the modeling of earthquake-induced water effects through hydrodynamic pressures interacting with the vibrating structure. When hydrodynamic effects are modelled using the simplified formulation of added masses [114], Eqs. (4.4) and (4.5) can be substituted as follows

$$\vartheta_{0,m} = R_{\mathrm{s}} \int_0^{H_{\mathrm{w}}} \int_0^{2\pi} p_0(R_{\mathrm{s}}, \theta, z)\, \cos(\theta)\, \psi_m^{(x)}(R_{\mathrm{s}}, 0, z)\, \mathrm{d}\theta\, \mathrm{d}z \tag{4.6}$$

$$\vartheta_{j,m} = R_{\mathrm{s}} \int_0^{H_{\mathrm{w}}} \int_0^{2\pi} p_0(R_{\mathrm{s}}, \theta, z)\, \cos(\theta)\, \psi_j^{(x)}(R_{\mathrm{s}}, 0, z)\, \psi_m^{(x)}(R_{\mathrm{s}}, 0, z)\, \mathrm{d}\theta\, \mathrm{d}z \tag{4.7}$$

where $p_0(R_{\mathrm{s}}, \theta, z)$ can be interpreted as the water added mass per unit height of the structure [114]. Alternatively to this formulation based on the radiation wave theory, water added masses can also be expressed using Morison's equation [47, 48]. Assuming that the terms associated with drag force and hydrodynamic damping can be neglected [5], Eqs. (4.4) and (4.5) can be shown to simplify to

$$\vartheta_{0,m} = \pi\, \rho_{\mathrm{w}}\, R_{\mathrm{s}}^2 \int_0^{H_{\mathrm{w}}} \psi_m^{(x)}(R_{\mathrm{s}}, 0, z)\, \mathrm{d}z \tag{4.8}$$

$$\vartheta_{j,m} = \pi\, \rho_{\mathrm{w}}\, R_{\mathrm{s}}^2 \int_0^{H_{\mathrm{w}}} \psi_j^{(x)}(R_{\mathrm{s}}, 0, z)\, \psi_m^{(x)}(R_{\mathrm{s}}, 0, z)\, \mathrm{d}z \quad \text{for} \quad j, m = 1 \ldots N_{\mathrm{s}} \tag{4.9}$$

The total horizontal relative displacement $\widehat{u}$ and acceleration $\ddot{\widehat{u}}$ at a point (x, y, z) of the water-surrounded axisymmetric structure can be computed as the summation of modal contributions

$$\widehat{u}(x, y, z, t) = \sum_{j=1}^{N_{\mathrm{s}}} \widehat{u}_j(x, y, z, t) = \sum_{j=1}^{N_{\mathrm{s}}} \widehat{Z}_j(t)\, \psi_j^{(x)}(x, y, z) \tag{4.10}$$

$$\ddot{\widehat{u}}(x, y, z, t) = \sum_{j=1}^{N_{\mathrm{s}}} \ddot{\widehat{u}}_j(x, y, z, t) = \sum_{j=1}^{N_{\mathrm{s}}} \ddot{\widehat{Z}}_j(t)\, \psi_j^{(x)}(x, y, z) \tag{4.11}$$

where $\widehat{u}_j$ and $\ddot{\widehat{u}}_j$ denote the modal relative horizontal displacement and acceleration at a point (x, y, z) of water-surrounded axisymmetric structure subjected to original ground acceleration $\ddot{x}_{\mathrm{g}}$.

The dynamic response of the structure without water can be obtained as the superposition of N_{s} responses of equivalent single degree-of-freedom (ESDOF) systems with generalized coordinates along the x-direction Z_j satisfying [6, 26, 41, 114]

$$Z_j(\omega) = \frac{L_j^{(x)}}{M_j} \times \frac{1}{\left(-\omega^2 + 2\,\mathrm{i}\,\xi_j\,\omega\,\omega_j + \omega_j^2 \right)} \tag{4.12}$$

The total horizontal relative displacement u and acceleration $\ddot{u}$ at a point (x, y, z) of the structure without surrounding water can be computed as the summation of modal contributions

$$u(x, y, z, t) = \sum_{j=1}^{N_{\mathrm{s}}} u_j(x, y, z, t) = \sum_{j=1}^{N_{\mathrm{s}}} Z_j(t)\,\psi_j^{(x)}(x, y, z) \tag{4.13}$$

$$\ddot{u}(x, y, z, t) = \sum_{j=1}^{N_{\mathrm{s}}} \ddot{u}_j(x, y, z, t) = \sum_{j=1}^{N_{\mathrm{s}}} \ddot{Z}_j(t)\,\psi_j^{(x)}(x, y, z) \tag{4.14}$$

with u_j and $\ddot{u}_j$ denote the modal relative horizontal displacement and acceleration at a point (x, y, z) of the structure with empty reservoir (without water) considering a unit harmonic horizontal ground motion $\ddot{x}_{\mathrm{g}}(t) = \mathrm{e}^{\mathrm{i}\omega t}$.

The previous equations were developed under the assumption of a unit horizontal harmonic ground acceleration $\ddot{x}_{\mathrm{g}}(t)$. In the general case, the Fourier transform of a given ground motion acceleration $\ddot{x}_{\mathrm{g}}(t)$ can be determined as

$$\ddot{x}_{\mathrm{g}}(\omega) = \int_0^{t_a} \ddot{x}_{\mathrm{g}}(t)\,\mathrm{e}^{-\mathrm{i}\omega t}\,\mathrm{d}t \tag{4.15}$$

in which t_a is the time duration of the applied accelerogram. The total horizontal relative displacements $\widehat{u}$ and u of the system with and without surrounding water, respectively, subjected to ground motion acceleration $\ddot{x}_{\mathrm{g}}(t)$ can be expressed in the frequency domain as

$$\widehat{u}(x, y, z, \omega) = \ddot{x}_{\mathrm{g}}(\omega) \sum_{j=1}^{N_{\mathrm{s}}} \widehat{u}_j(x, y, z, \omega) = \ddot{x}_{\mathrm{g}}(\omega) \sum_{j=1}^{N_{\mathrm{s}}} \widehat{Z}_j(\omega)\,\psi_j^{(x)}(x, y, z) \tag{4.16}$$

$$u(x, y, z, \omega) = \ddot{x}_{\mathrm{g}}(\omega) \sum_{j=1}^{N_{\mathrm{s}}} u_j(x, y, z, \omega) = \ddot{x}_{\mathrm{g}}(\omega) \sum_{j=1}^{N_{\mathrm{s}}} Z_j(\omega)\,\psi_j^{(x)}(x, y, z) \tag{4.17}$$

4.3.2 Proposed formulations

A mode- and frequency-dependent ground acceleration $a_{\mathrm{g}}^{(j)}$ is defined by modifying the original input ground acceleration $\ddot{x}_{\mathrm{g}}(\omega)$ as follows

$$a_{\mathrm{g}}^{(j)}(\omega) = \ddot{x}_{\mathrm{g}}(\omega)\,\frac{\widehat{Z}_j(\omega)}{Z_j(\omega)} \quad \text{for} \quad j = 1 \ldots N_{\mathrm{s}} \tag{4.18}$$

The modal horizontal relative displacements $\widetilde{u}_j$ at a point (x, y, z) of the dry structure subjected to modified ground acceleration $a_{\mathrm{g}}^{(j)}$ can be expressed as

$$\widetilde{u}_j(x, y, z, \omega) = a_{\mathrm{g}}^{(j)}(\omega)\, Z_j(\omega)\, \psi_j^{(x)}(x, y, z) = \ddot{x}_{\mathrm{g}}(\omega)\, \widehat{Z}_j(\omega)\, \psi_j^{(x)}(x, y, z) \tag{4.19}$$

Comparing with Eq. (4.10), it is seen that these modal relative displacement and acceleration are the same as those of the water-structure system subjected to the original ground acceleration $\ddot{x}_{\mathrm{g}}$, i.e. $\widetilde{u}_j = \widehat{u}_j$ and $\ddot{\widetilde{u}}_j = \ddot{\widehat{u}}_j$. Applying Fourier inverse transform to $a_{\mathrm{g}}^{(j)}(\omega)$ yields the following modified time-history ground acceleration for each structural mode $j = 1 \ldots N_{\mathrm{s}}$

$$a_{\mathrm{g}}^{(j)}(t) = \frac{1}{2\pi} \int_{-\infty}^{\infty} a_{\mathrm{g}}^{(j)}(\omega)\, \mathrm{e}^{\mathrm{i}\omega t}\, \mathrm{d}\omega \tag{4.20}$$

This accelerogram can be directly applied to the dry structure to obtain the contribution of any given mode j to the time-history response of the wet structure (i.e. with water) through the solution of the equation

$$\ddot{\widetilde{Z}}_j(t) + 2\,\xi_j\,\omega_j\,\dot{\widetilde{Z}}_j(t) + \omega_j^2\,\widetilde{Z}_j(t) = -\frac{L_j^{(x)}}{M_j}\, a_{\mathrm{g}}^{(j)}(t) \quad \text{for} \quad j = 1 \ldots N_{\mathrm{s}} \tag{4.21}$$

for the generalized coordinate $\widetilde{Z}_j(t)$. In other terms, the solution of Eq. (4.21) is the same as the solution of the system with water subjected to original ground acceleration, i.e $\widetilde{Z}_j(t) = \widehat{Z}_j(t)$. This method is shown in Fig. 4.1 (a), where the seismic response of an axisymmetric water-surrounded structure is obtained through the superposition of the time-history modal dynamic responses (i.e. Time-history modal superposition analysis abbreviated as THMSA hereafter) of the tower without water (dry system) subjected to modified ground accelerations $a_{\mathrm{g}}^{(j)}(t)$, $j = 1 \ldots N_{\mathrm{s}}$ (Note: $N_{\mathrm{s}} = 4$ modes are considered in Fig. 4.1 for illustration purposes). In a finite element analysis (FEA), such procedure consists of conducting a time-history modal dynamic analysis of the dry structure (i.e without water) including only the contribution of vibration mode j of concern. The solutions $\widetilde{Z}_j(t)$ of Eq. (4.21) can be obtained for each mode $j = 1 \ldots N_{\mathrm{s}}$ as the time-history relative displacements of single

degree-of-freedom (SDOF) systems with mass M_j, stiffness

$$K_j = \frac{4\pi^2}{T_j^2}\, M_j \tag{4.22}$$

and viscous damping

$$C_j = \frac{4\pi}{T_j}\, \xi_j\, M_j \tag{4.23}$$

while subjected to ground motion $L_j^{(x)}\, a_{\mathrm{g}}^{(j)}(t)$. This procedure is illustrated in Fig. 4.1 (b). The maximum (i.e. peak) absolute seismic horizontal relative displacement of the water-surrounded axisymmetric structure corresponding to a given vibration mode $j = 1 \ldots N_{\mathrm{s}}$ can then be evaluated as

$$\begin{aligned} \left|\widehat{u}_j(x,y,z,t)\right|^{(\max)} &= \left|\widetilde{u}_j(x,y,z,t)\right|^{(\max)} \\ &= \frac{L_j^{(x)}}{M_j}\, S_{\mathrm{D}}^{[a_{\mathrm{g}}^{(j)}]}(T_j,\xi_j)\, \psi_j^{(x)}(x,y,z) \\ &= \frac{L_j^{(x)}}{M_j}\, \frac{T_j^2}{4\pi^2}\, S_{\mathrm{A}}^{[a_{\mathrm{g}}^{(j)}]}(T_j,\xi_j)\, \psi_j^{(x)}(x,y,z) \end{aligned} \tag{4.24}$$

in which $S_{\mathrm{D}}^{[a_{\mathrm{g}}^{(j)}]}(T_j,\xi_j)$ and $S_{\mathrm{A}}^{[a_{\mathrm{g}}^{(j)}]}(T_j,\xi_j)$ denote, respectively, the spectral displacement and pseudo-acceleration of ground motion $a_{\mathrm{g}}^{(j)}(t)$ at the period T_j of the structure without water, considering a modal viscous damping ξ_j. This approach is illustrated in Fig. 4.1 (c). The maximum absolute total horizontal relative displacement at a point of coordinates (x,y,z) of the structure can then be obtained using a combination rule such as the Square Root of the Sum of the Squares (SRSS)

$$\left|\widehat{u}(x,y,t)\right|^{(\max)} = \sqrt{\sum_{j=1}^{N_{\mathrm{s}}} \left[\left|\widehat{u}_j(x,y,z,t)\right|^{(\max)}\right]^2} \tag{4.25}$$

or the complete quadratic combination (CQC)

$$\left|\widehat{u}(x,y,t)\right|^{(\max)} = \sqrt{\sum_{j=1}^{N_{\mathrm{s}}} \sum_{m=1}^{N_{\mathrm{s}}} A_{j,m} \left|\widehat{u}_j(x,y,z,t)\right|^{(\max)} \left|\widehat{u}_m(x,y,z,t)\right|^{(\max)}} \tag{4.26}$$

where $A_{j,m}$ is the correlation coefficient

$$A_{j,m} = \frac{1}{1+\epsilon_{j,m}^2} \tag{4.27}$$

with

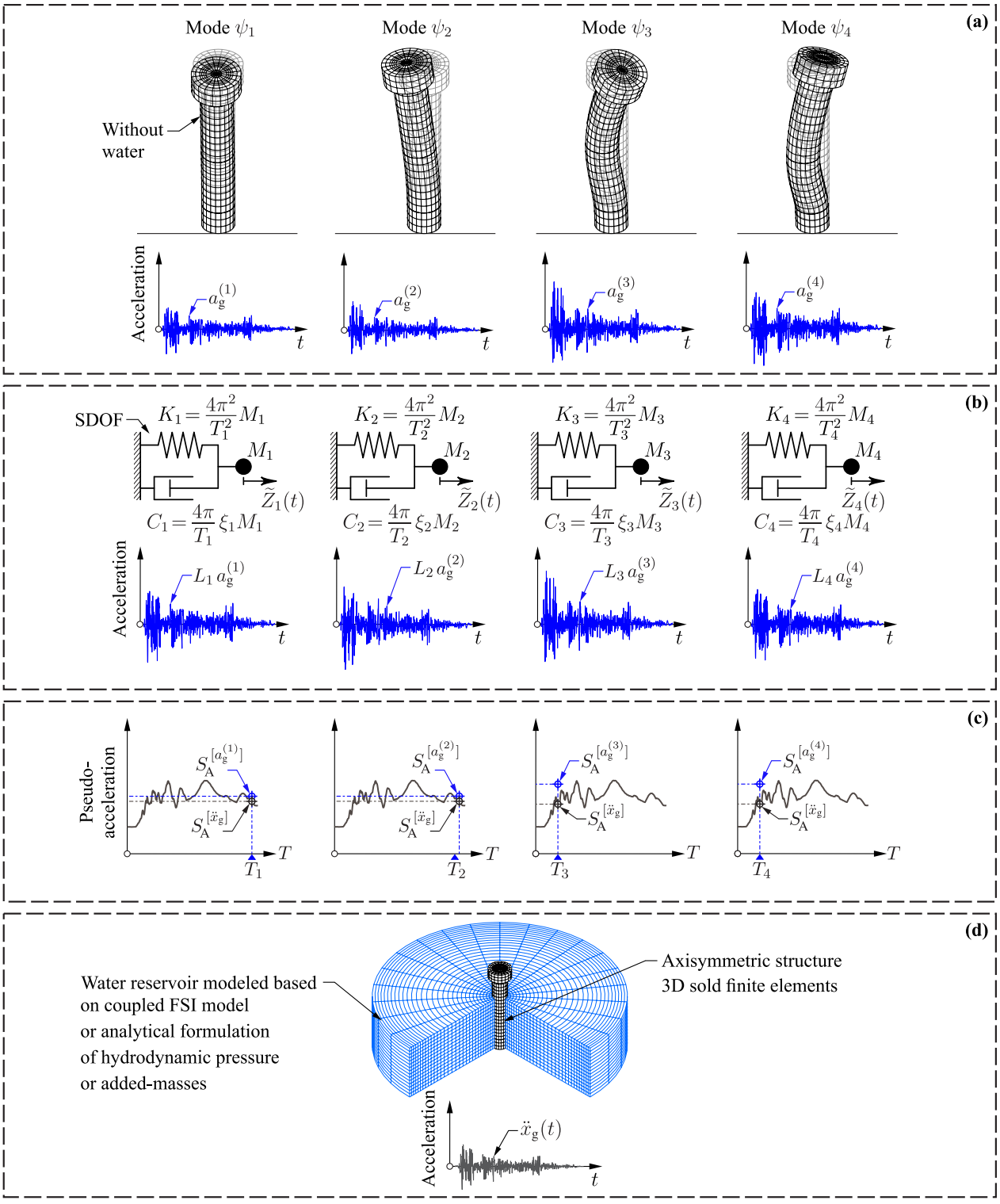

Figure 4.1 Proposed procedures.

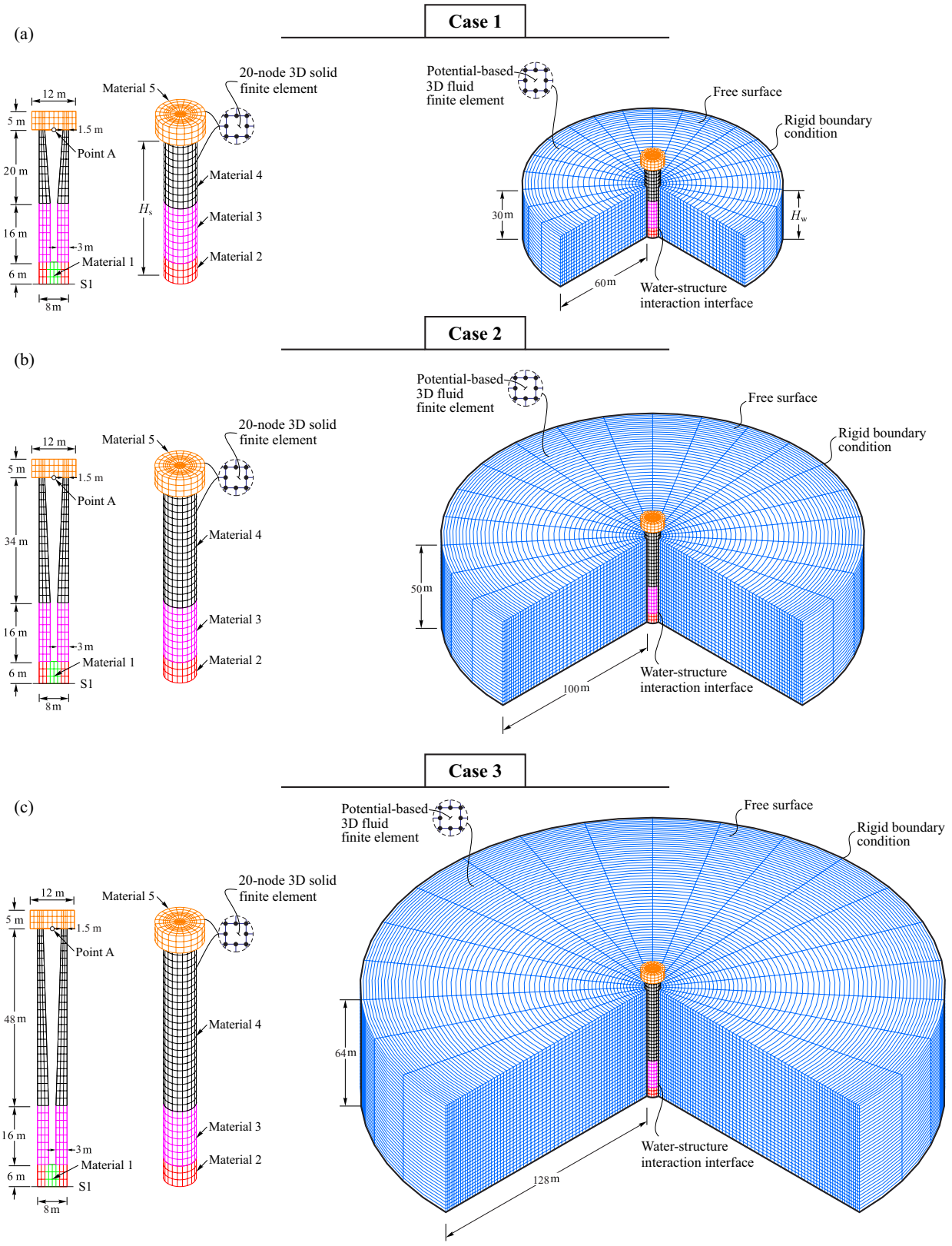

Figure 4.2 Dimensions, materials and finite element meshes of the studied water-surrounded axisymmetric structures: (a) Case no. 1 - 42-m height tower; (b) Case no. 2 - 56-m height tower; (c) Case no. 3 - 70-m height tower.

$$\epsilon_{j,m} = \frac{\omega_j\sqrt{(1-\xi_j^2)} - \omega_m\sqrt{(1-\xi_m^2)}}{\xi'_j\,\omega_j + \xi'_m\,\omega_m}\,, \qquad \xi'_j = \xi_j + \frac{2}{\omega_j\,s} \tag{4.28}$$

with s representing the duration of the strong phase of the earthquake excitation. For systems with the same damping ratio in all modes subjected to earthquake excitation with duration s long enough (i.e. $\xi'_j = \xi_j$), Eq. (4.27) can be simplified to

$$A_{j,m} = \frac{\xi^2(1+\omega_j/\omega_m)^2}{(1-\omega_j/\omega_m)^2 + 4\,\xi^2\,\omega_j/\omega_m} \tag{4.29}$$

When applicable, the above combination rules or similar can be used to obtain other response quantities of interest. It is worth mentioning that the maximum absolute seismic horizontal relative displacement of the structure without surrounding water subjected to original ground motion acceleration can be expressed for each structural mode j as

$$\Big|u_j(x,y,z,t)\Big|^{(\max)} = \frac{L_j^{(x)}}{M_j}\,\frac{T_j^2}{4\pi^2}\,S_{\mathrm{A}}^{[\ddot{x}_{\mathrm{g}}]}(T_j,\xi_j)\,\psi_j^{(x)}(x,y,z) \tag{4.30}$$

From Eqs. (4.24) and (4.30), it can be seen that, the ratio of maximum absolute seismic horizontal relative displacements with and without water at a given mode j is equal to the ratio of the pseudo-acceleration of the modified record corresponding to mode j to that of the original ground motion acceleration, i.e.

$$\frac{\Big|\widetilde{u}_j(x,y,z,t)\Big|^{(\max)}}{\Big|u_j(x,y,z,t)\Big|^{(\max)}} = \frac{S_{\mathrm{A}}^{[a_{\mathrm{g}}^{(j)}]}(T_j,\xi_j)}{S_{\mathrm{A}}^{[\ddot{x}_{\mathrm{g}}]}(T_j,\xi_j)} \qquad \text{for} \quad j=1\ldots N_{\mathrm{s}} \quad \text{and} \quad z>0 \tag{4.31}$$

In what follows, the ratio defined by Eq. (4.31) will be referred to as the *hydrodynamic modification factor* for a given vibration mode, and abbreviated as HMF. The proposed formulations and resulting HMF only require the evaluation of the period and damping corresponding to a specific vibration mode of the structure without surrounding water, rather than those of the water-structure system which are generally different.

4.4 Numerical examples, results and discussion

4.4.1 Case studies

Three composite axisymmetric cylindrical towers with different heights are considered in this section to illustrate the application of the proposed methods.

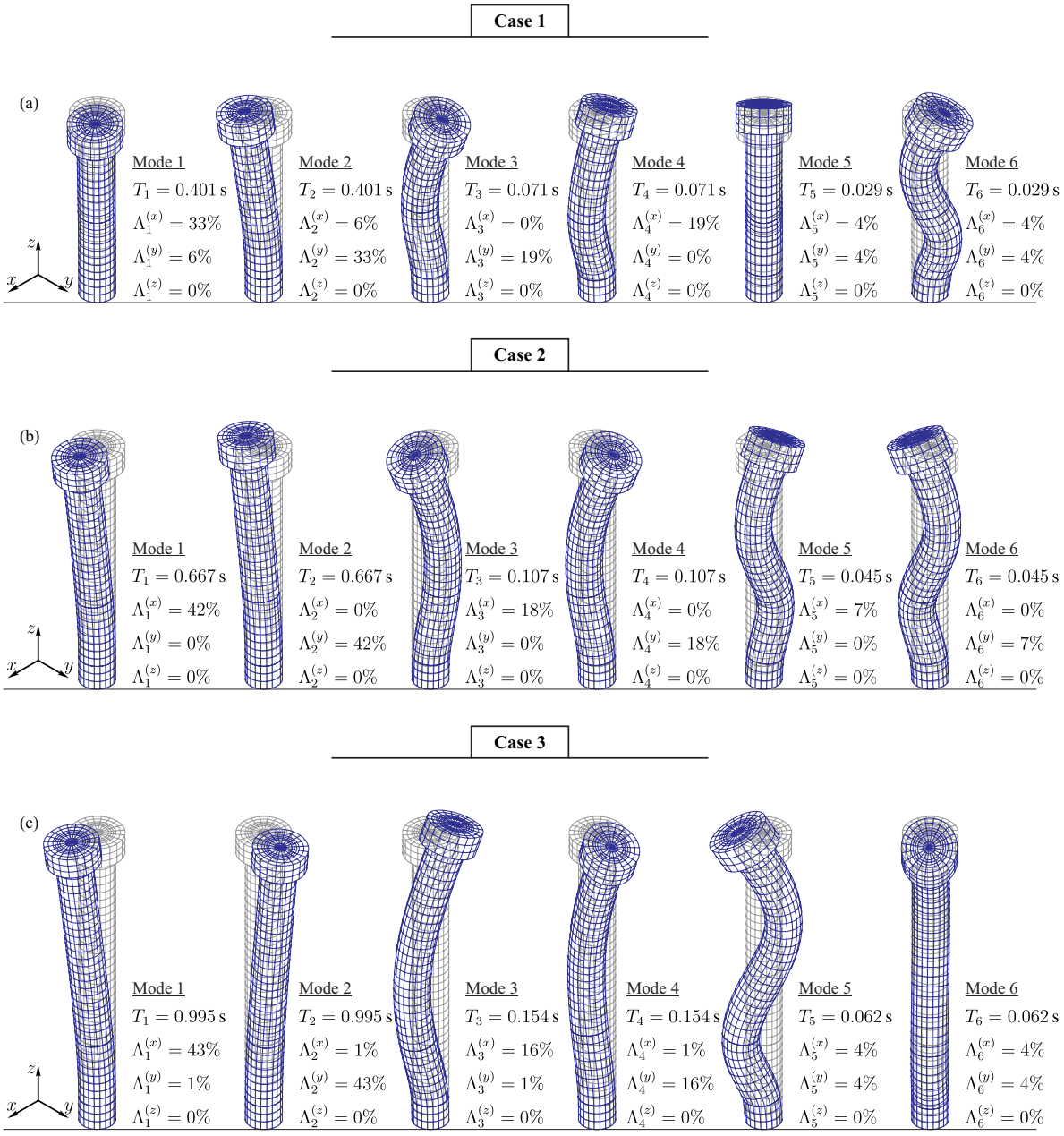

Figure 4.3 Finite element mode shapes and corresponding vibration periods of the towers, as well as the modal mass participation factors: (a) Case no. 1; (b) Case no. 2; (c) Case no. 3.

The three towers, illustrated in Fig. 4.2, are referred to as Cases no. 1 to 3, have the same external radius $R_s = 4\,\text{m}$, and heights H_s of 42 m, 56 m, and 70 m, respectively. The top of the towers are made of a solid cylindrical part with a hight of 5 m and a diameter of 12 m. Table 4.1 contains the mechanical properties of the towers. The towers in Cases no. 1

Table 4.1 Constitutive materials of the axisymmetric structures (Fig. 4.2)

Materials	Mass density (kg/m^3)	Elastic modulus(GPa)	Poisson'sratio
Material 1	7850	210	0.3
Material 2	2400	35	0.2
Material 3	2500	25	0.2
Material 4	1900	50	0.2
Material 5	2400	30	0.2

to 3 are surrounded by an infinite water domain with heights H_w of 30 m, 50 m and 64 m, respectively. A water mass density $\rho_w = 1000$ kg/m^3, a pressure wave velocity $C_w = 1440$ m/s are considered. Figure 4.3 presents the six lateral mode shapes and corresponding vibration periods (T_1 to T_6) for the three dry structures, as well as the modal mass participation factors along x, y and z, i.e. $\Lambda_j^{(x)}$, $\Lambda_j^{(y)}$ and $\Lambda_j^{(z)}$, respectively, indicating the relative importance of each mode in the global seismic response of the structures. A constant 5 % modal viscous damping ratio is considered, i.e. $\xi_j = 0.05$ for $j = 1$ to 6. To verify the results, coupled 3D finite element analyses of the tower-water systems are also conducted. The towers and surrounding water are modeled in [92] using 3D 20-node solid and potential-based finite elements, respectively, as shown in Fig. 4.2. A fixed rigid wall boundary condition is applied at a far end located at a radius of $2H_w$ around the structures. Fluid-structure interaction is accounted for through special interface elements included in ADINA [2, 92]. In the following discussion, the results of the coupled finite element models are referred to as the reference solution, also illustrated in Fig. 4.1 (d). Figure 4.4, shows the frequency response functions (FRFs) for horizontal acceleration $\ddot{\tilde{u}}$ and $\ddot{u}$ at point A of studied structures. Two water levels H_w and $0.5H_w$ are considered as well as the dry case for comparison purposes. The blue curves represent the FRFs of the towers surrounded by water, while the gray curves depict those of the towers without water. Comparing these results shows that the FRFs generally shift toward lower frequencies from the dry case to the case with a water level of $0.5H_w$, and then H_w. This expected behaviour confirms that the system becomes generally more flexible with higher water levels. The influence of water level must however be considered in light of the frequency content of the seismic excitation. For example, according to the FRFs in Fig. 4.4 a ground motion with a predominant exciting frequency of 3 Hz results in the same horizontal acceleration response for Case no. 1 irrespective of the water level. The same

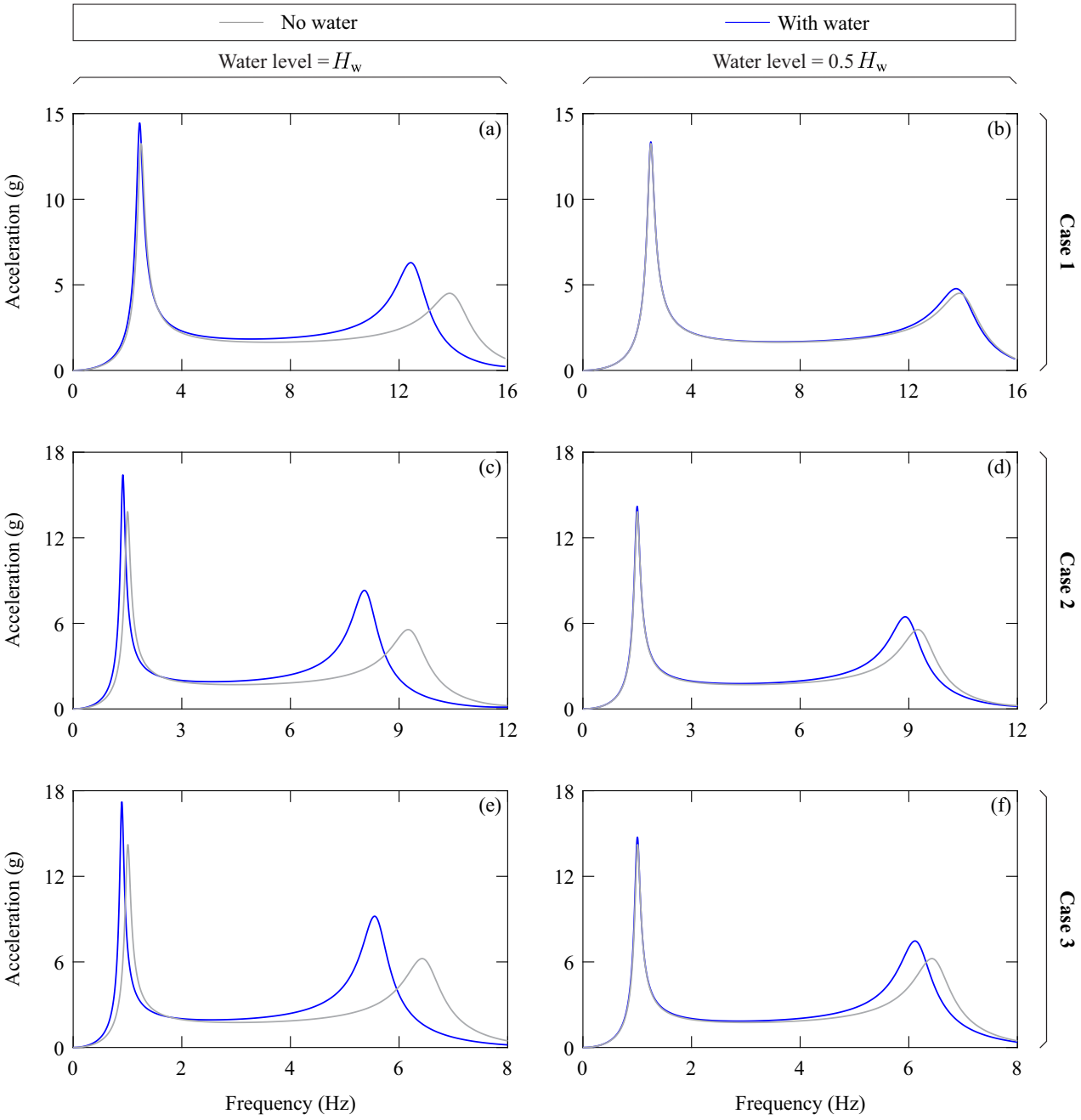

Figure 4.4 Frequency response functions for horizontal acceleration $\ddot{\hat{u}}$ and $\ddot{u}$ at point A of the tower-water systems studied: (a) and (b): Tower Case no. 1 assuming water level to be H_w and $0.5H_w$, respectively; (c) and (d): Tower Case no. 2 assuming water level to be H_w and $0.5H_w$, respectively; (e) and (f): Tower Case no. 3 assuming water level to be H_w and $0.5H_w$, respectively;

applies to Cases nos. 2 and 3. However, at a predominant excitation frequency of 6 Hz, the effect of water level is obvious from Fig. 4.4 (e) for Case no. 3, while this effect vanishes for Case no. 1 as shown in Fig. 4.4 (a).

4.4.2 Original and modified ground motions used

The seismic response of each tower is studied under the effects of two ground motion accelerations differing by their frequency content and time signature: (i) a horizontal component of Imperial Valley earthquake (1940) at station El Centro, (ii) a horizontal component of Loma Prieta earthquake (1989) at station Gilroy Array no. 2. The acceleration time-histories, acceleration pseudo-spectra and Fourier amplitudes of these ground motions are illustrated in Fig. 4.5. The modified accelerograms corresponding to both records are compared to the original ground motions in Figs. 4.6 and 4.7 for the three cases assuming compressible water. Figure 4.8 illustrates the impact of different water assumptions on the generated modified

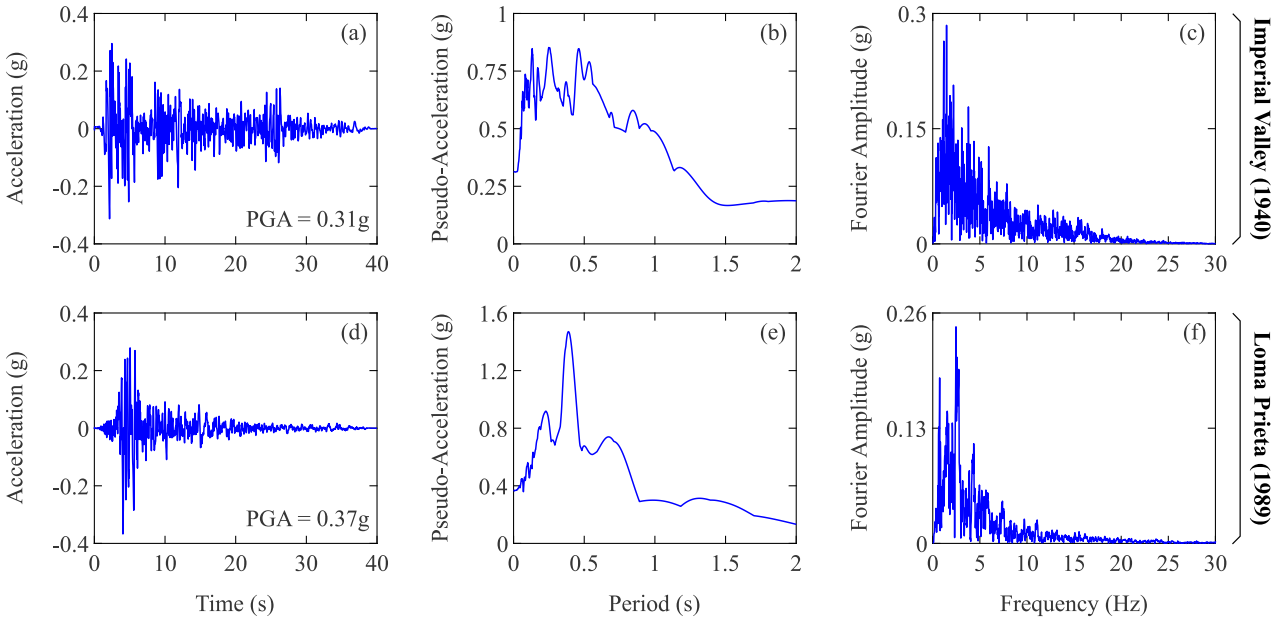

Figure 4.5 Time-history accelerations, pseudo-acceleration response spectra and Fourier amplitudes of the ground motions selected for this study: (a) to (c) Imperial Valley (1940) earthquake; (d) to (f) Loma Prieta (1989) earthquake.

accelerograms of Imperial Valley (1940) earthquake for the three cases. It is observed that the different water assumptions yield closely similar results for the shortest tower (Case no. 1). As structural flexibility increases (Cases nos. 1 and 2), the simplified added mass using Morison equations exhibit higher discrepancies compared to the ones with compressible water assumption. The added masses based on radiation wave theory yield modified accelerations

closer to those using compressible water assumption than the Morison's added mass formulation. In this figure, the effects of Morison's added mass on the modified ground acceleration for each mode can be observed. Notably, a larger peak ground acceleration (PGA) for higher modes is achieved through Morison's added masses formulation.

The pseudo-acceleration response spectra $S_{\mathrm{A}}^{[a_{\mathrm{g}}^{(j)}]}(T_j, 5\%),\ j=1\ldots6$, of the modified ground accelerations are computed for the six vibration periods T_1 to T_6 considering a 5 % viscous damping. These results are shown (values in blue) in Figs. 4.9, 4.10 and 4.11 for the different water assumptions. The pseudo-acceleration spectra $S_{\mathrm{A}}^{[\ddot{x}_{\mathrm{g}}]}(T_j, 5\%),\ j=1\ldots6$, corresponding to the original ground motions are also depicted (values in black) in the same figures. As expected, the hydrodynamic-induced modifications to acceleration seismic demands depend on the structural dynamic properties for each tower and the input ground motion. Table 4.2 contains the Hydrodynamic Modification Factor (HMF) obtained from Figs. 4.9, 4.10 and 4.11 by dividing the values in blue by those in black for each vibration period.

Table 4.2 Hydrodynamic modification factors obtained for the six vibration modes of towers Cases nos. 1, 2, and 3 subjected to the ground motion accelerations considered.

		Imperial Valley (1940)						Loma Prieta (1989)					
		Modes						Modes					
Case	Water assumption	1	2	3	4	5	6	1	2	3	4	5	6
No. 1	Compressible water	1.04	1.04	1.09	1.09	1.58	1.58	1.08	1.08	1.36	1.36	1.40	1.40
	Added masses - Eqs. (4.6)-(4.7)	1.03	1.03	1.15	1.15	1.60	1.60	1.08	1.08	1.27	1.27	1.40	1.40
	Added masses - Eqs. (4.8)-(4.9)	1.09	1.09	1.66	1.66	1.66	1.66	1.09	1.09	1.74	1.74	1.48	1.48
No. 2	Compressible water	1.19	1.19	0.96	0.96	1.23	1.23	1.27	1.27	1.33	1.33	1.52	1.52
	Added masses - Eqs. (4.6)-(4.7)	1.18	1.18	1.10	1.10	1.22	1.22	1.27	1.27	1.39	1.39	1.63	1.63
	Added masses - Eqs. (4.8)-(4.9)	1.26	1.26	2.17	2.17	1.96	1.96	1.29	1.29	1.61	1.61	1.92	1.92
No. 3	Compressible water	1.04	1.04	1.39	1.39	1.14	1.14	1.32	1.32	1.58	1.58	1.38	1.38
	Added masses - Eqs. (4.6)-(4.7)	1.03	1.03	1.55	1.55	0.98	0.98	1.32	1.32	1.48	1.48	1.57	1.57
	Added masses - Eqs. (4.8)-(4.9)	1.05	1.05	1.92	1.92	1.61	1.61	1.34	1.34	1.75	1.75	1.50	1.50

From Figs. 4.9 (a) and (c), it is seen that the acceleration demands corresponding to the fundamental modes of Cases nos. 1 and 2 without water are close when subjected to Imperial Valley ground motion (i.e. 0.61 and 0.57, respectively). These acceleration demands increase by 4 % for Case no. 1 and 19 % for Case no. 2 when hydrodynamic effects are included assuming compressible water. The larger amplification associated with Case no. 2 is mainly due to its higher flexibility compared to Case no. 1. Comparing Figs. 4.9 (a) and (e), it is observed that the acceleration demand increase induced by hydrodynamic effects is 4% for both Cases nos. 1 and 3 when only the fundamental mode contribution is considered under the effect of Imperial Valley ground motion acceleration. Despite Case no. 3 being more flexible than Case no. 1, the frequency shift caused by hydrodynamic effects has led to the same increase in acceleration demands for both structures.

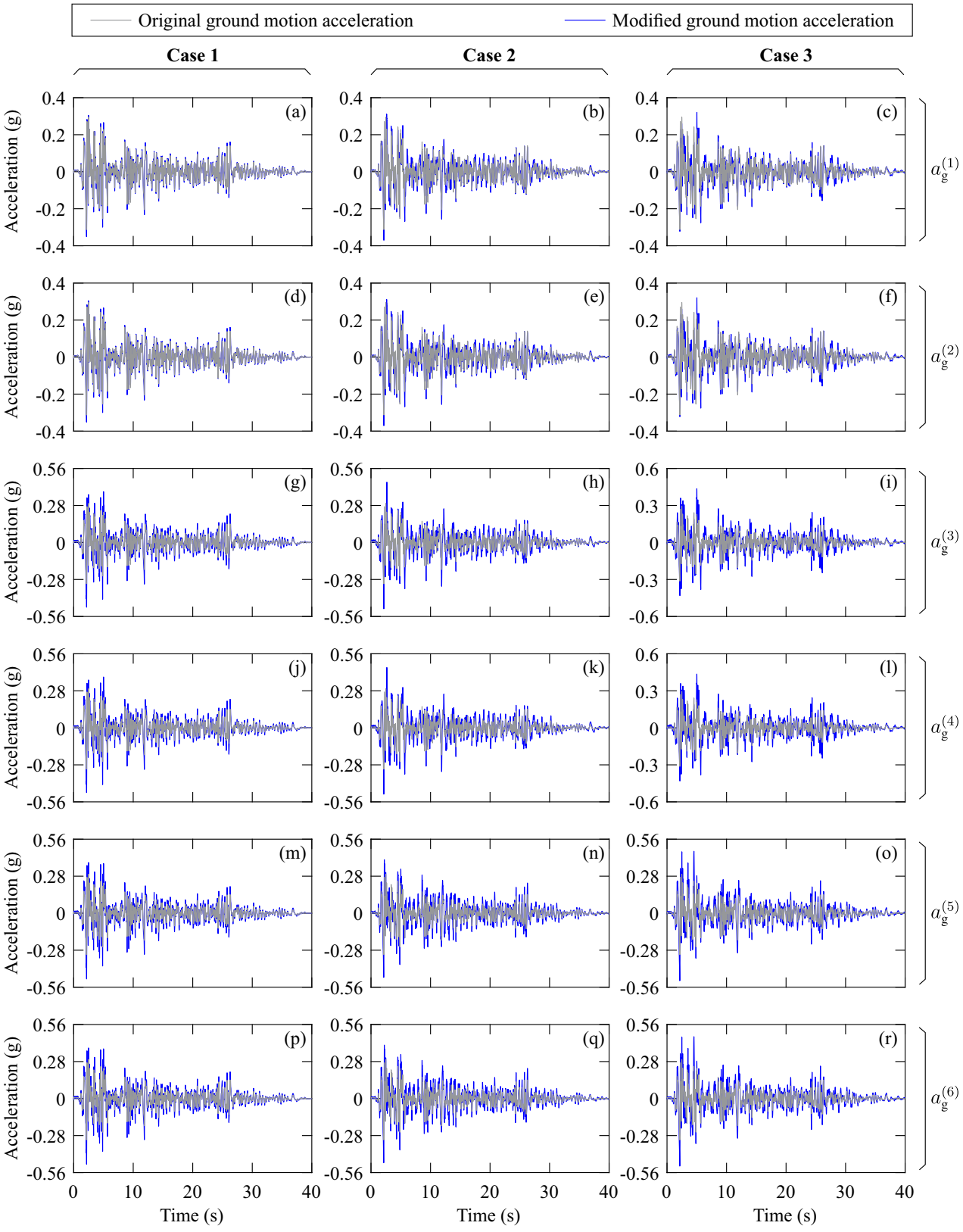

Figure 4.6 Original and modified ground accelerations $a_g^{(1)}$ to $a_g^{(6)}$ corresponding to the six mode shapes of the 42 m (Case no. 1), 56 m (Case no. 2) and 70 m (Case no. 3) high towers, subjected to Imperial Valley (1940) earthquake with compressible water assumption.

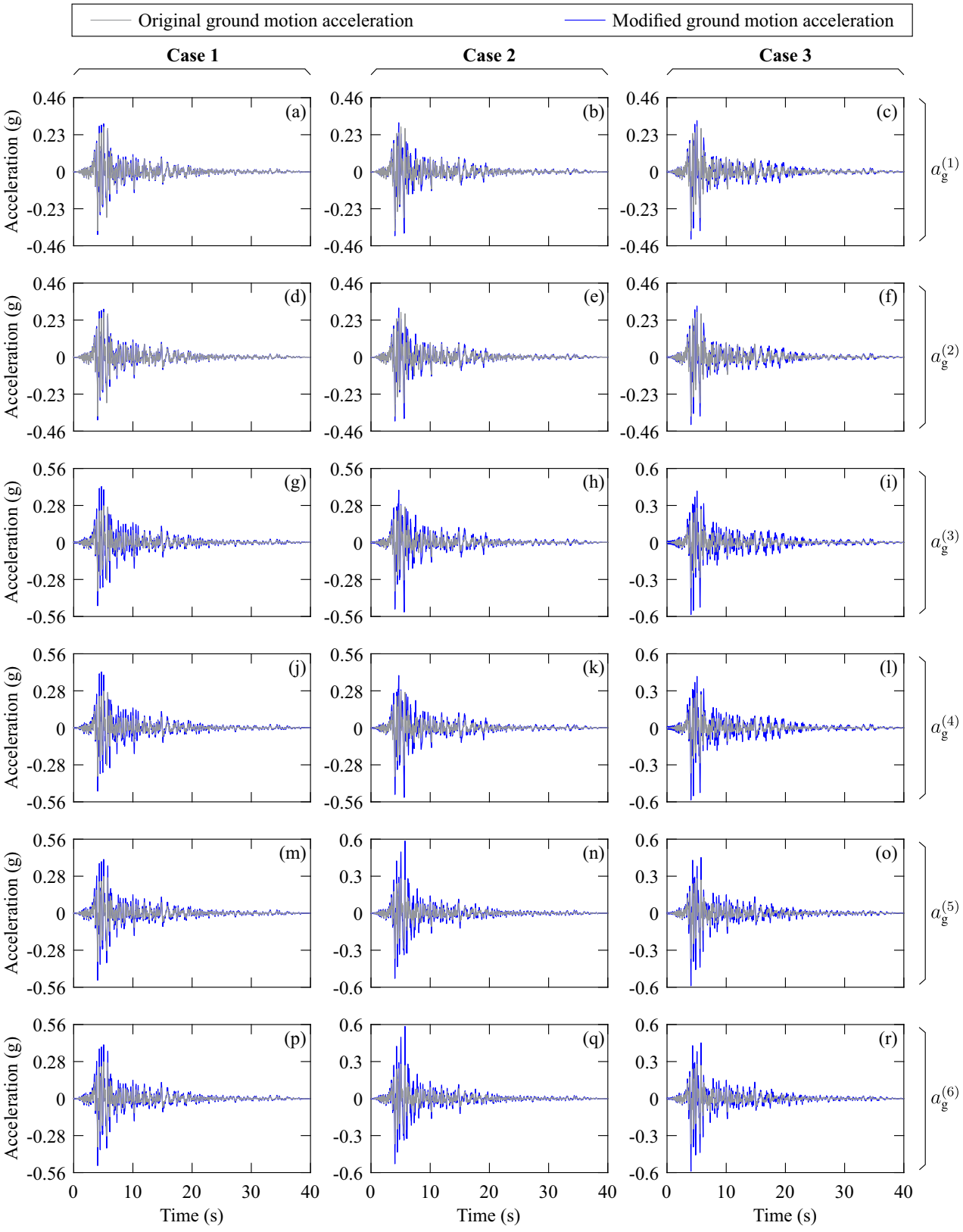

Figure 4.7 Original and modified ground accelerations $a_g^{(1)}$ to $a_g^{(6)}$ corresponding to the six mode shapes of the 42 m (Case no. 1), 56 m (Case no. 2) and 70 m (Case no. 3) high towers, subjected to Loma Prieta (1989) earthquake with compressible water assumption.

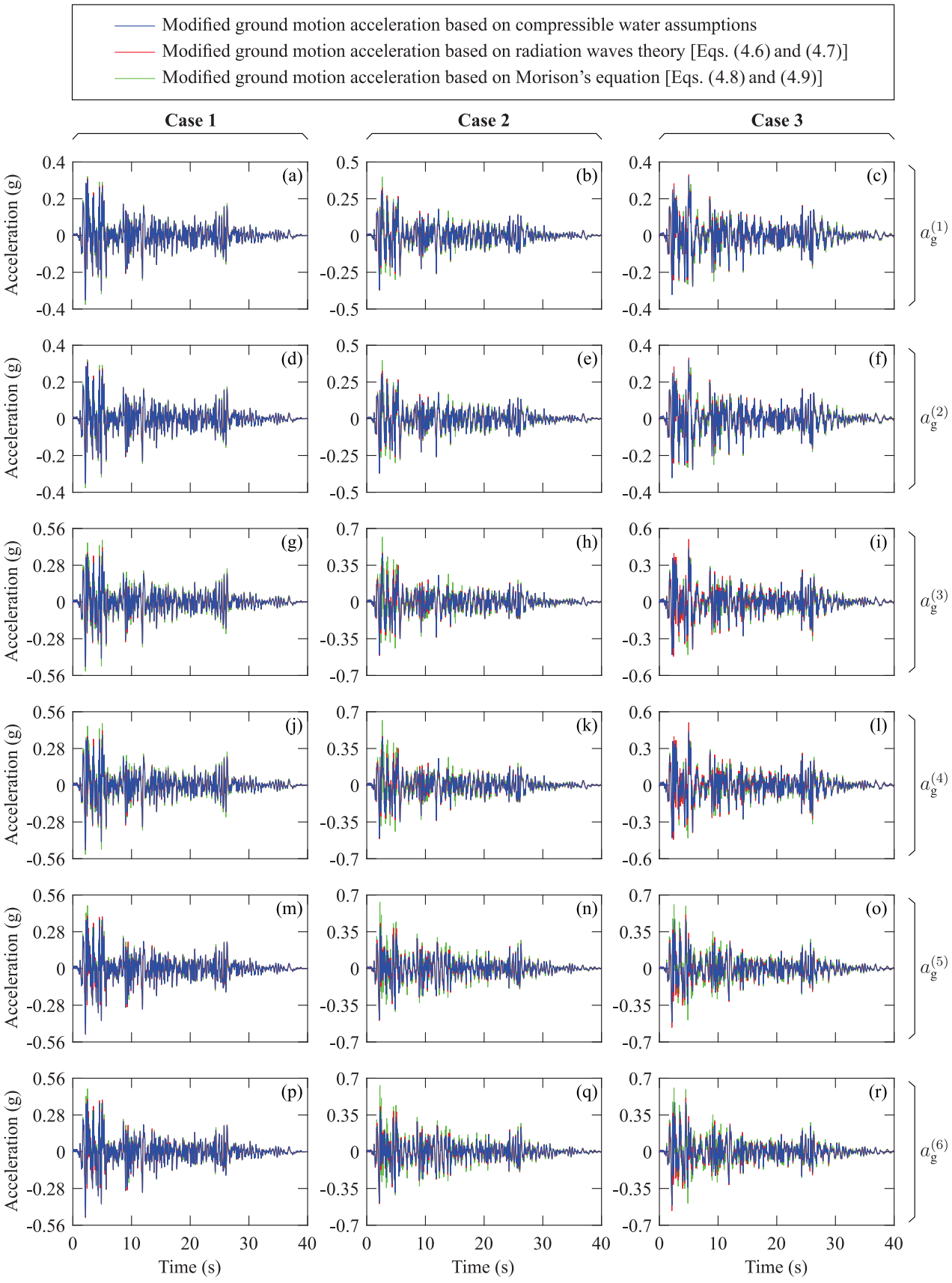

Figure 4.8 Modified ground accelerations $a_g^{(1)}$ to $a_g^{(6)}$ corresponding to the selected six vibration modes of the studied towers subjected to Imperial Valley (1940) earthquake considering different water assumptions.

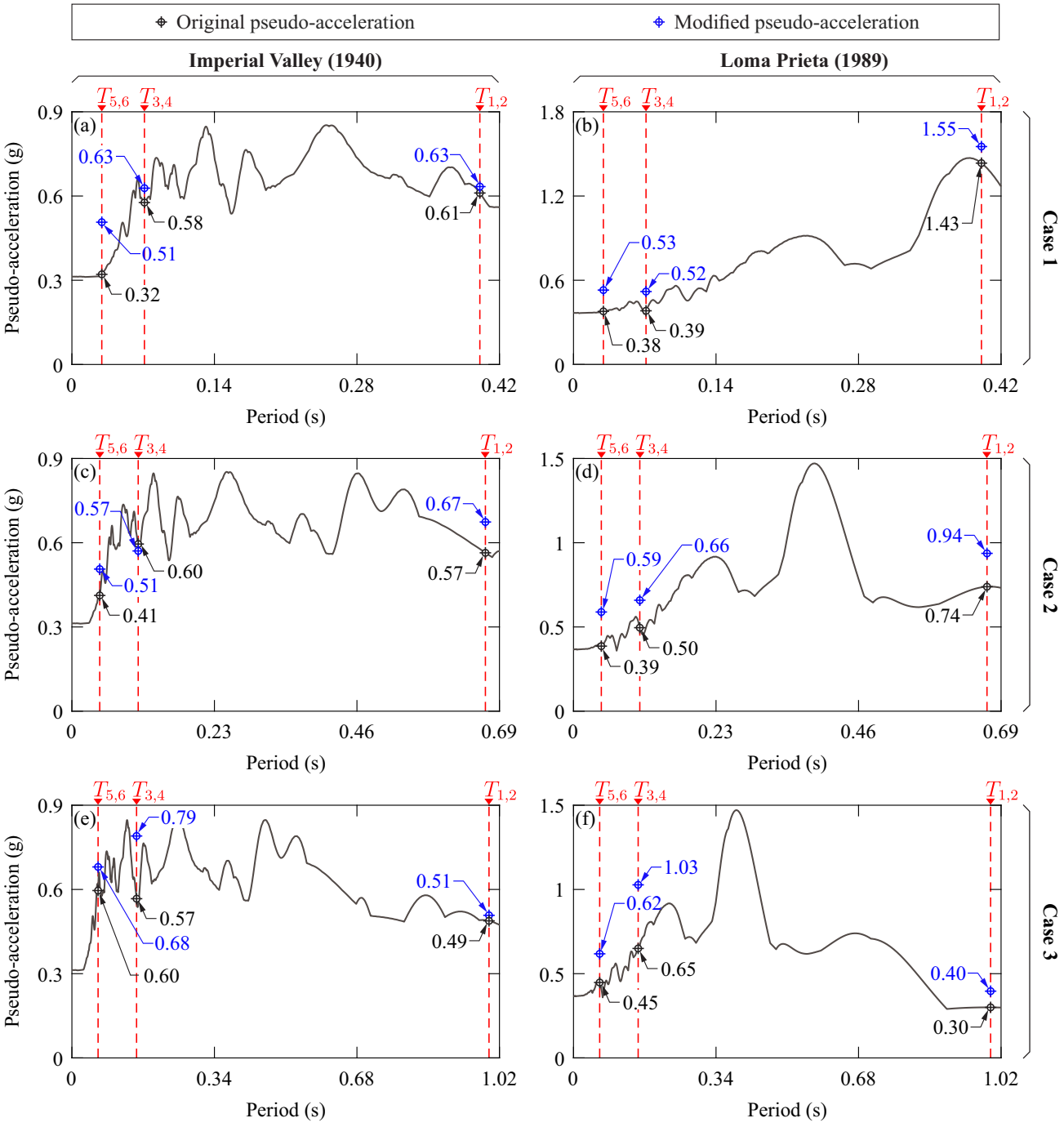

Figure 4.9 5%-damped pseudo-acceleration response spectra of the original ground motions and those of the modified ground motions corresponding to each of the selected six vibration modes assuming compressible water.

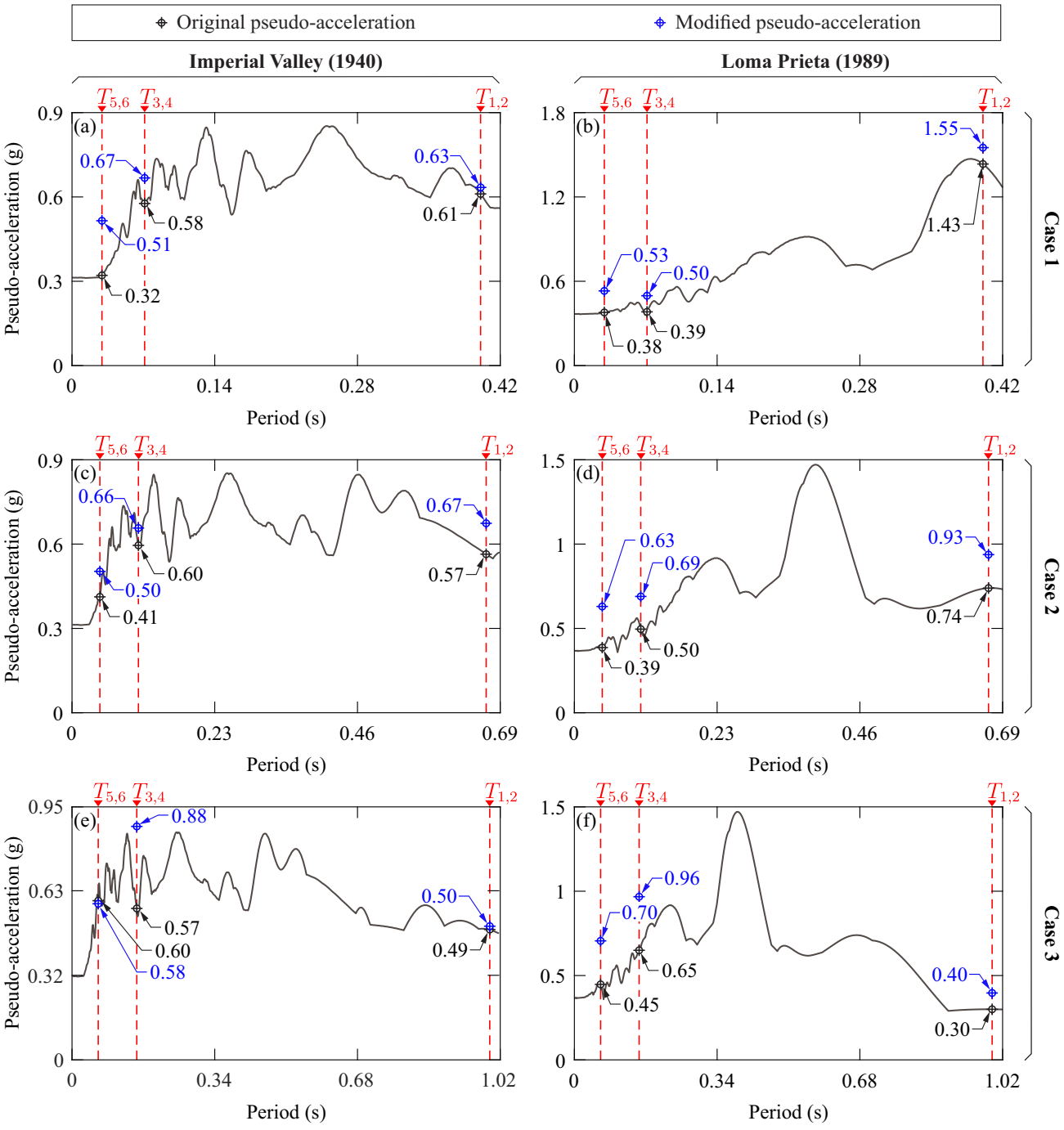

Figure 4.10 5%-damped pseudo-acceleration response spectra of the original ground motions and those of the modified ground motions corresponding to each of the six selected vibration modes obtained assuming simplified added mass formulation for the water surrounding the towers.

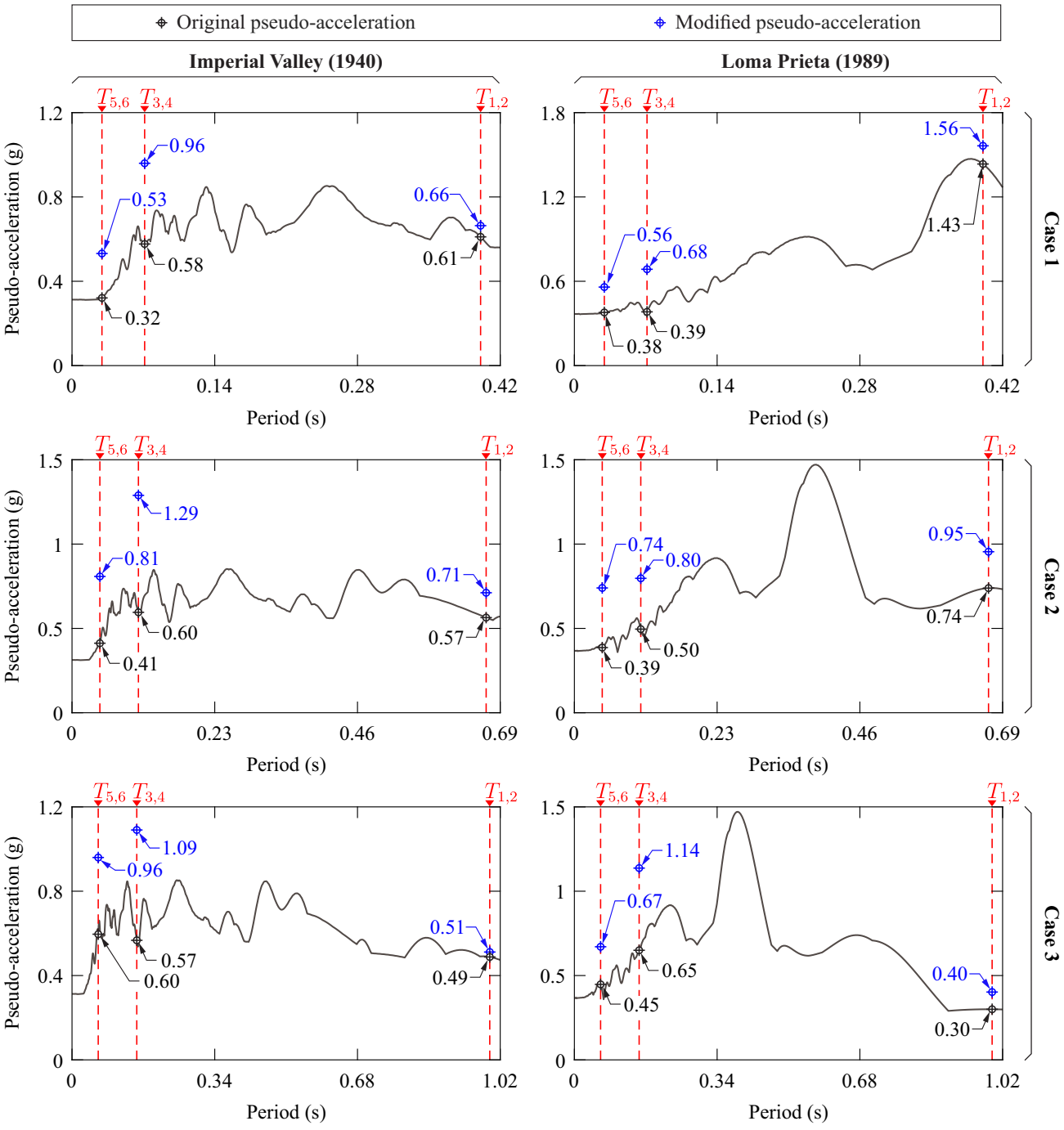

Figure 4.11 5%-damped pseudo-acceleration response spectra of the original ground motions and those of the modified ground motions corresponding to each of the six selected vibration modes obtained assuming Morison's added mass formulation for the water surrounding the towers.

Figures 4.9 (c) shows a 4% *decrease* in acceleration demand for Case no. 2 due to hydrodynamic effects in the third and fourth vibration modes when subjected to Imperial Valley ground motion acceleration. Conversely, the same structure undergoes a 33% *increase* in acceleration demand when subjected to Loma Prieta ground motion acceleration along the same modes (Figs. 4.9 (d)). This effect is attributed to differences in the frequency content of input ground motion acceleration. The pseudo-acceleration response spectra assuming two added-masses formulation approaches are also given in Figs. 4.10 and 4.11 to illustrate the influence of water modelling assumptions. The assessment of the effects of water modeling assumptions can also be seen from table 4.2 containing the HMFs obtained using Eq. (4.31) for six vibration modes of the towers and the ground motion accelerations considered. For example, it is seen that the increase in acceleration demands due to hydrodynamic effects are more pronounced when water is modeled using Morison added masses. Acceleration demands for Case no. 3 *decrease* along modes 5 and 6 due to hydrodynamic effects for Imperial Valley (1940) earthquake. In contrast, they *decrease* along the same modes when the tower is subjected to the Loma Prieta (1989) earthquake. The results in Table 4.2 can be used to assess the effectiveness of Morison's added masses across various vibration modes.

4.4.3 Seismic response of the water-surrounded axisymmetric structures

Figure 4.12 presents the maximum absolute horizontal relative displacements obtained along the height of the towers subjected to the considered ground motions and assuming compressible water. The results corresponding to each mode are obtained using the proposed response spectrum analysis (RSA). Figures 4.13 and 4.14 show the results obtained using the proposed time-history analyses (THMSA). The results are in excellent agreement with those from the classical coupled finite element solutions. The total horizontal relative displacements at point A of the studied towers including hydrodynamic effects (compressible water assumption and added masses) are shown in Fig. 4.15 for the first twelve seconds of Imperial Valley (1940) and Loma Prieta (1989) earthquakes. A close match between the results for the compressible water assumption and the reference solution is found. The same observation applies to the results corresponding to the added mass formulation based on radiation waves theory. This observation is expected as the effects of water compressibility are known to be negligible for this type of structures (eg. Liaw and Chopra 1974). Figure 4.15 shows that the results corresponding to the added masses based on Morison's equation are slightly different from the others. The shear forces at the base of the towers (location S1 in Fig. 4.2) are also compared in Fig. 4.16 under the effect of Imperial Valley (1940) ground motion acceleration.

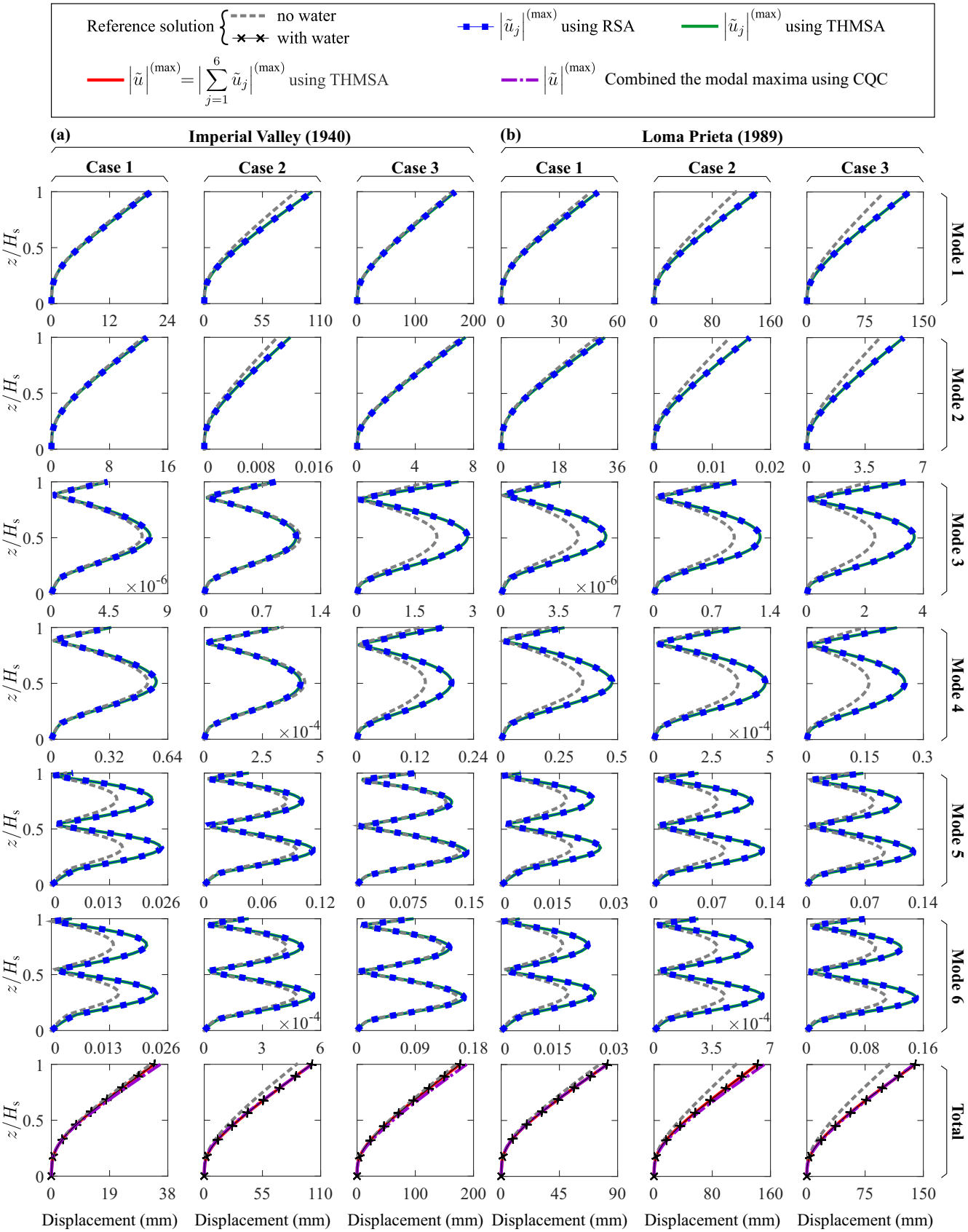

Figure 4.12 Absolute maximum relative displacements along the height of the face of towers determined for each vibration mode using modified ground accelerations $a_g^{(1)}$ to $a_g^{(6)}$ and then combined to obtain total response: (a) Imperial Valley (1940) earthquake; (b) Loma Prieta (1989) earthquake obtained assuming compressible water in the reservoir.

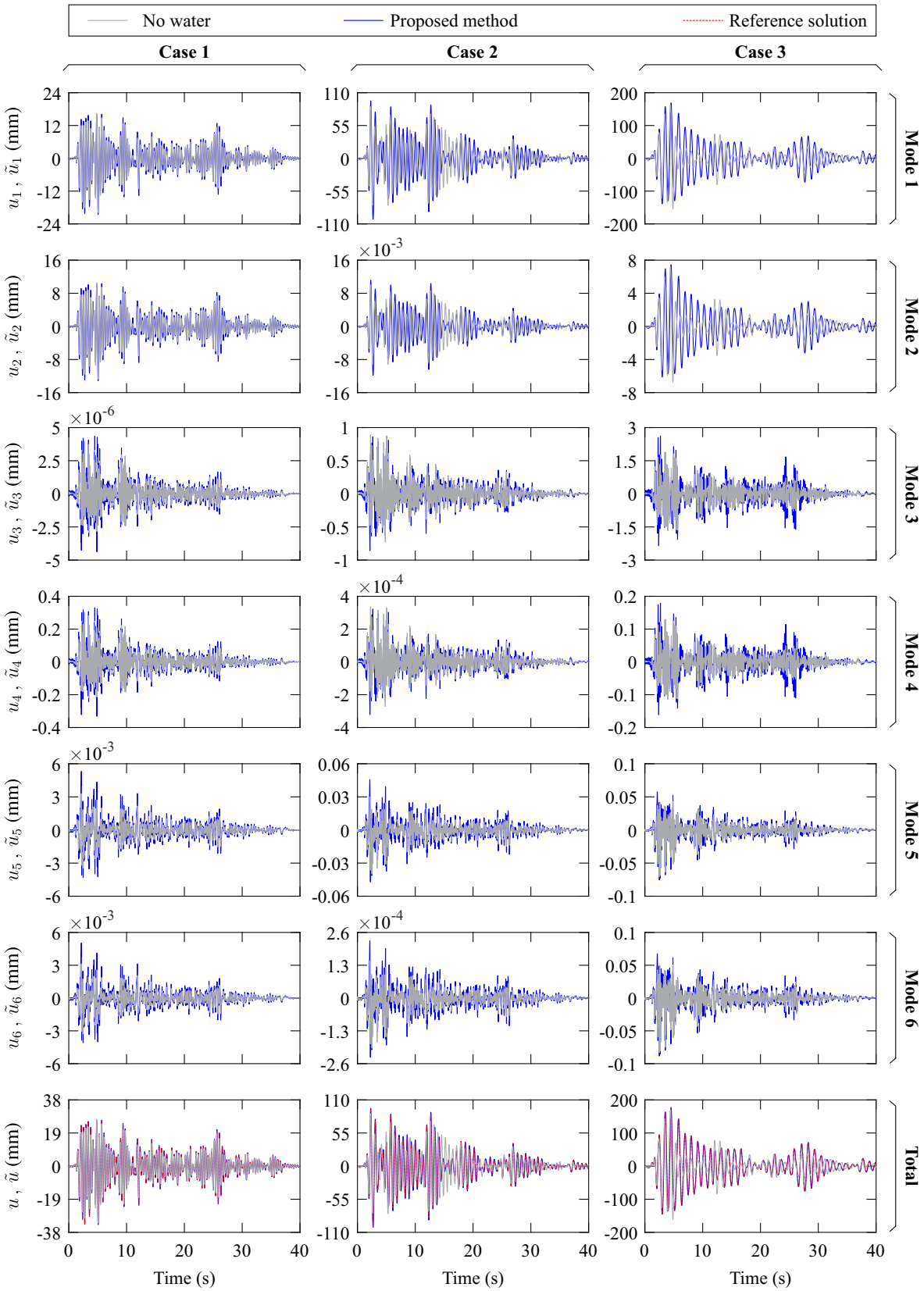

Figure 4.13 Time-history horizontal relative displacements at point A of studied towers with hydrodynamic effects obtained for each vibration mode using modified ground accelerations $a_g^{(1)}$ to $a_g^{(6)}$ subjected to Imperial Valley (1940) earthquake assuming compressible water, and then combined to obtain total seismic response.

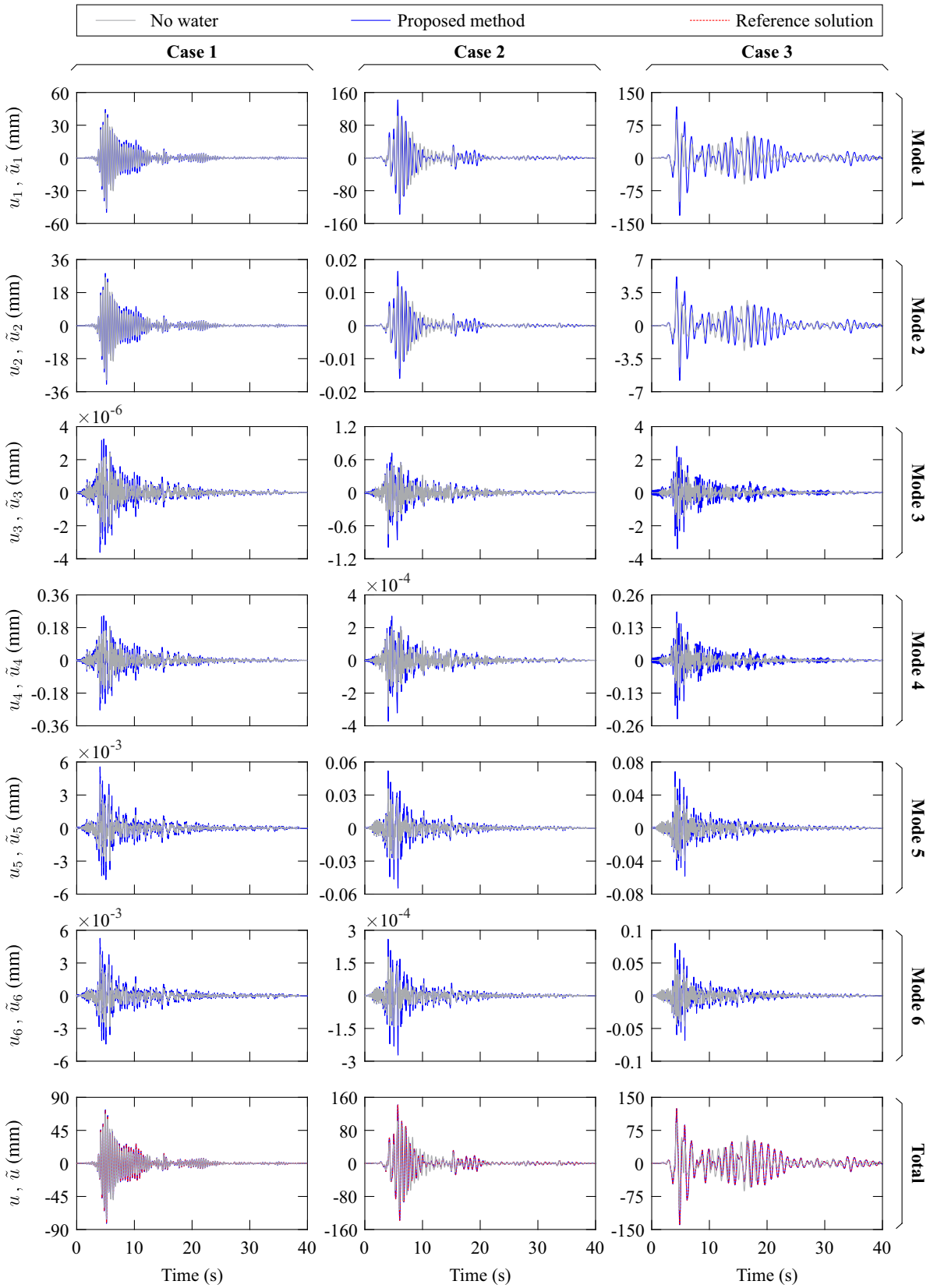

Figure 4.14 Time-history horizontal relative displacements at point A of studied towers with hydrodynamic effects obtained for each vibration mode using modified ground accelerations $a_g^{(1)}$ to $a_g^{(6)}$ subjected to Loma Prieta (1989) earthquake assuming compressible water, and then combined to obtain total seismic response.

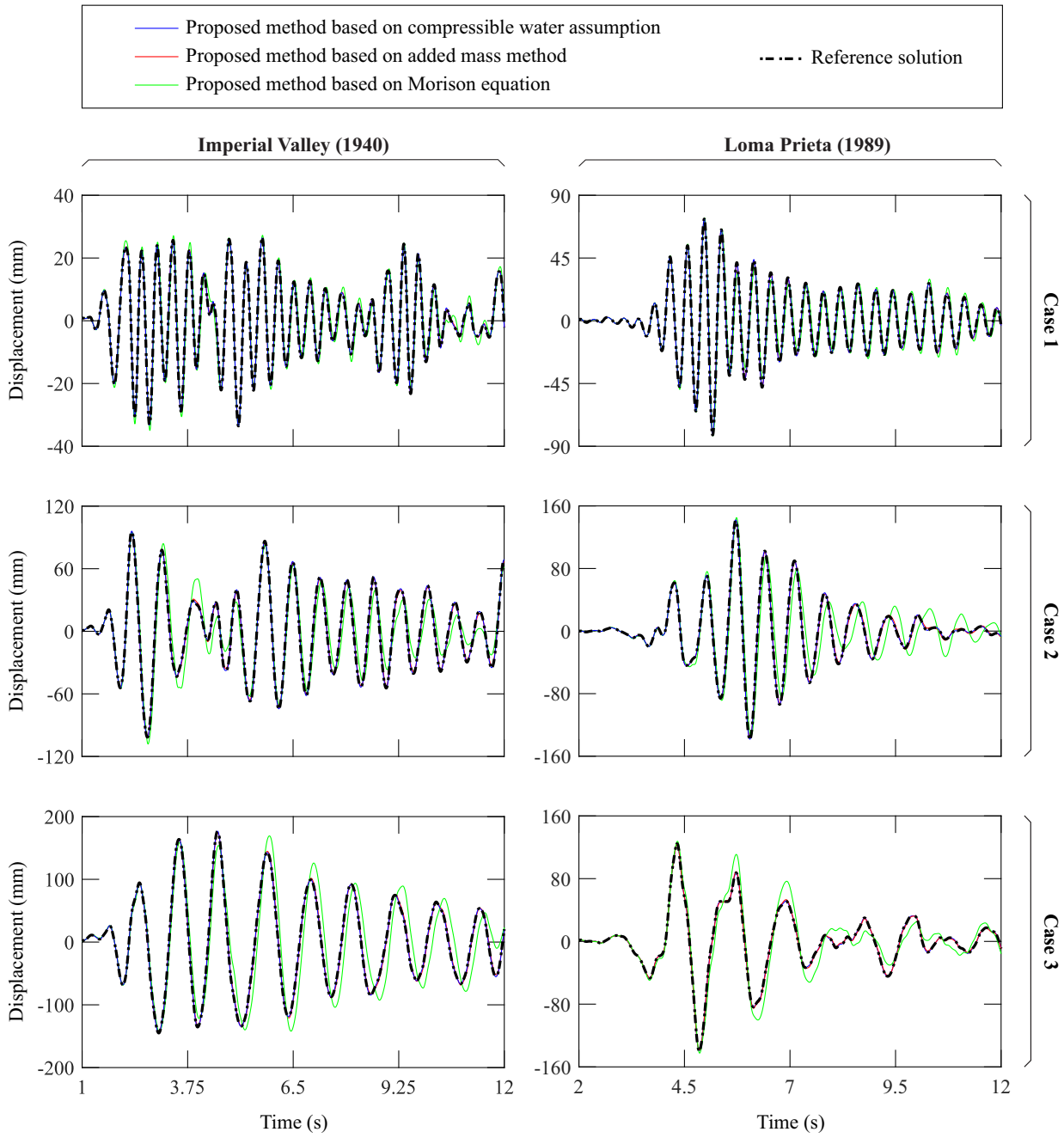

Figure 4.15 Time-history of total horizontal relative displacements at point A of the studied towers including hydrodynamic effect considering Imperial Valley (1940) and Loma Prieta (1989) earthquakes obtained for different water assumptions.

The maximum absolute total horizontal relative displacements shown in Figs. 4.12 (i.e. last row titled total) are obtained using two approaches: (i) a direct method consisting of the summation of the modal responses of horizontal relative displacements (i.e. algebraic values with signs) and then the computation of the maximum value of the resulting summed response, and (ii) the CQC method consisting of combining the absolute values of the maximum horizontal relative displacements obtained for each mode. As excepted, the results provided by the direct method are found to be identical to those of the reference solution. For both analyzed earthquakes and the three studied towers, the CQC method exhibits slightly higher values than the direct method at the upper sections of the towers (i.e. $z/H_{\mathrm{s}} > \approx 0.75$). However, at lower heights, the total maximum responses obtained through the CQC method are nearly identical to those from the direct method. Notably, for tower Case no. 1 subjected to Imperial Valley (1940) ground motion acceleration and towers Case no. 2 and Case no. 3 subjected to the Loma Prieta (1989) earthquake, the CQC method demonstrates excellent agreement with the reference solution.

Figs. 4.13 and 4.14 present the time-history horizontal relative displacements at point A of the towers under the effect of Imperial Valley (1940) and Loma Prieta (1989) ground motions, respectively. These results confirm the excellent agreement between the results obtained using the proposed methods and the classical coupled finite element solutions. Finally, the earthquake-induced stresses in the water-surrounded structure can be determined based on the time-histories of the nodal displacements computed using the proposed approach. For instance, the obtained maximum dynamic shear stress τ_{xz} and normal stress σ_{zz} within tower Cases no. 1 and no. 2 subjected to Imperial Valley (1940) earthquake and assuming compressible water are presented in Fig. 4.17. An excellent agreement with the stresses from the classical coupled finite element solutions is found.

4.5 Conclusions

This paper proposed novel methods to evaluate the seismic response of water-surrounded axisymmetric structures through dynamic modal superposition and response spectrum analyses. The developed techniques include earthquake-induced hydrodynamic effects into modified versions of the original ground motion acceleration and its response spectrum. The modified ground motion time-history and spectral accelerations can then be applied directly to the dry structure (i.e. without water), thus eliminating the need for specialized software accounting for fluid-structure interaction dynamic effects.

The proposed approach also allows the evaluation of the impact of any specific vibration mode and associated hydrodynamic effect on the structural seismic response. Coupled structural

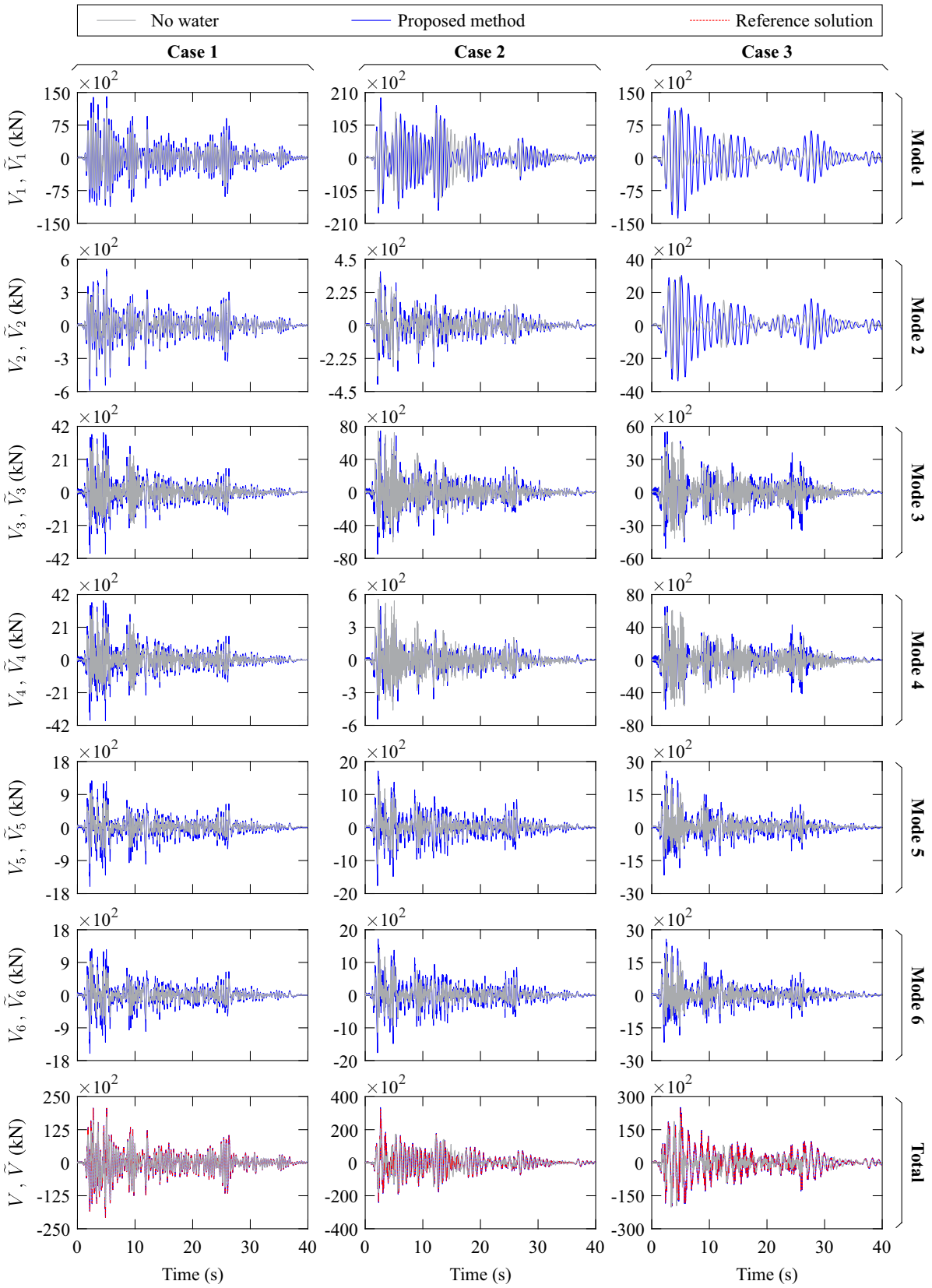

Figure 4.16 Time-history shear force at the base of studied towers with surrounding water obtained for each vibration mode using modified ground accelerations $a_g^{(1)}$ to $a_g^{(6)}$ under the effect of Imperial Valley (1940) earthquake assuming compressible water, and then combined to obtain total seismic response.

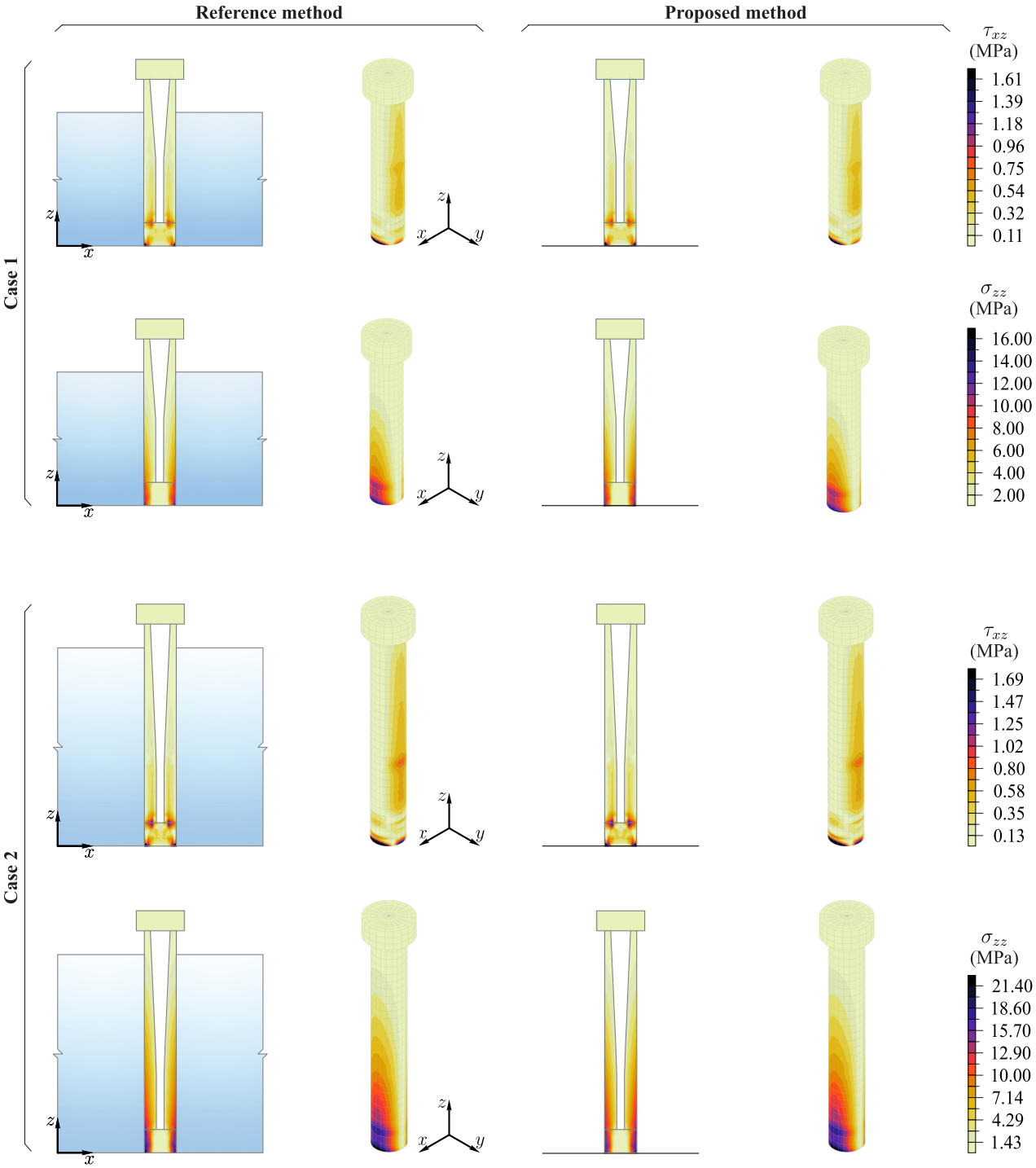

Figure 4.17 Maximum shear stresses τ_{xz} and σ_{zz} developing within towers Case no. 1 and Case no. 2 subjected to Imperial Valley (1940) earthquake assuming compressible water.

flexibility and hydrodynamic effects due to each vibration mode can be accurately assessed in lieu of the approximate results generally given by the static correction method commonly used in traditional simplified methods.

The methodology utilizes analytical formulations of earthquake-induced hydrodynamic pressure in the reservoir or simplified added-masses to obtain the contributions of the selected vibration modes to the total seismic response. It is shown that the developed methods also provide an alternative to the implementation of added masses by including their effects directly in the modified ground motion time-history or spectral accelerations.

Based on the formulations proposed, a hydrodynamic modification factor which can be used to evaluate the amplification or de-amplification of acceleration seismic demands due to earthquake-induced hydrodynamic effects was introduced. The proposed method can be applied to a broad range of axisymmetric structures surrounded by water, such as axisymmetric towers supporting wind turbines, intake towers, or bridge circular piers. For purpose of illustration, application examples of three water-surrounded axisymmetric structures subjected to two earthquakes were presented.

The obtained results were shown to be in excellent agreement with the coupled finite element solutions. The findings were discussed to highlight the coupled effects of hydrodynamic-pressure and structural flexibility on the seismic behaviour of the studied systems. Two main limitations of the proposed formulation are that the structures must be of cylindrical shape, and that the foundation is rigid. The rigid foundation assumption was adopted to focus on the modelling of the effects of water-structure interaction. The formulation presented can however be extended by including soil-structure interaction effects in the modal properties constituting the input of the proposed technique.

Data Availability

Data will be made available from the corresponding author upon reasonable request.

Acknowledgements

The authors would like to acknowledge the financial support of the Canada Research Chairs and the Natural Sciences and Engineering Research Council of Canada (NSERC).

Appendix A

The FRFs p_0 and p_j, $j=1\ldots N_\mathrm{s}$ can be evaluated as [114]; [6]

$$p_0(R_\mathrm{s},\theta,z,\omega) = \frac{4\rho_\mathrm{w}}{H_\mathrm{w}}\left[-\sum_{n=1}^{\bar{n}-1}\frac{I_{0n}}{\kappa_n}\,\mathcal{D}_n(\kappa_n R_\mathrm{s})\cos(\lambda_n z)\,\mathrm{e}^{\mathrm{i}\,\tau_n R_\mathrm{s}} + \sum_{n=\bar{n}}^{N_\mathrm{w}}\frac{I_{0n}}{\kappa'_n}\,\mathcal{E}_n(\kappa'_n R_\mathrm{s})\cos(\lambda_n z)\right]\cos(\theta) \tag{4.32}$$

$$p_j(R_\mathrm{s},\theta,z,\omega) = \frac{4\rho_\mathrm{w}}{H_\mathrm{w}}\left[-\sum_{n=1}^{\bar{n}-1}\frac{I_{jn}}{\kappa_n}\mathcal{D}_n(\kappa_n R_\mathrm{s})\cos(\lambda_n z)\,\mathrm{e}^{\mathrm{i}\,\tau_n R_\mathrm{s}} + \sum_{n=\bar{n}}^{N_\mathrm{w}}\frac{I_{jn}}{\kappa'_n}\,\mathcal{E}_n(\kappa'_n R_\mathrm{s})\cos(\lambda_n z)\right]\cos(\theta) \tag{4.33}$$

where N_w is the number of considered acoustical water modes, and the parameters λ_n, κ_n, κ'_n, I_{0n}, I_{jn}, $\mathcal{D}_n$, $\mathcal{E}_n$ and τ_n are given by

$$\lambda_n = \frac{(2n-1)\,\pi}{2H_\mathrm{w}}\,; \qquad \kappa_n = \sqrt{\frac{\omega^2}{C_\mathrm{w}^2}-\lambda_n^2}\,; \qquad \kappa'_n = -\mathrm{i}\,\kappa_n \tag{4.34}$$

$$I_{0n} = -\frac{2H_\mathrm{w}(-1)^n}{\pi(2n-1)}\,; \qquad I_{jn} = \int_0^{H_\mathrm{w}}\psi_j^{(x)}(z)\,\cos(\lambda_n z)\,\mathrm{d}z \tag{4.35}$$

$$\mathcal{D}_n(\kappa_n R_\mathrm{s}) = \sqrt{\frac{\left[\mathrm{J}_1(\kappa_n R_\mathrm{s})\right]^2+\left[\mathrm{Y}_1(\kappa_n R_\mathrm{s})\right]^2}{\left[\mathrm{J}_0(\kappa_n R_\mathrm{s})-\mathrm{J}_2(\kappa_n R_\mathrm{s})\right]^2+\left[\mathrm{Y}_0(\kappa_n R_\mathrm{s})-\mathrm{Y}_2(\kappa_n R_\mathrm{s})\right]^2}} \tag{4.36}$$

$$\mathcal{E}_n(\kappa'_n R_\mathrm{s}) = \frac{\mathrm{K}_1(\kappa'_n R_\mathrm{s})}{\mathrm{K}_0(\kappa'_n R_\mathrm{s})+\mathrm{K}_2(\kappa'_n R_\mathrm{s})} \tag{4.37}$$

$$\tau_n R_\mathrm{s} = \tan^{-1}\left\{\frac{\left[\mathrm{Y}_0(\kappa_n R_\mathrm{s})-\mathrm{Y}_2(\kappa_n R_\mathrm{s})\right]\mathrm{J}_1(\kappa_n R_\mathrm{s})-\left[\mathrm{J}_0(\kappa_n R_\mathrm{s})-\mathrm{J}_2(\kappa_n R_\mathrm{s})\right]\mathrm{Y}_1(\kappa_n R_\mathrm{s})}{\left[\mathrm{J}_0(\kappa_n R_\mathrm{s})-\mathrm{J}_2(\kappa_n R_\mathrm{s})\right]\mathrm{J}_1(\kappa_n R_\mathrm{s})+\left[\mathrm{Y}_0(\kappa_n R_\mathrm{s})-\mathrm{Y}_2(\kappa_n R_\mathrm{s})\right]\mathrm{Y}_1(\kappa_n R_\mathrm{s})}\right\} \tag{4.38}$$

in which K_ℓ is the modified Bessel function of order ℓ of the second kind and J_ℓ and Y_ℓ are the Bessel functions of order ℓ of the first and second kind, respectively. The integer $\bar{n}$ in the first sums of Eqs. (4.32) and (4.33) is the smallest value of integer n such that $\lambda_n > \dfrac{\omega}{C_\mathrm{w}}$. We note that the first series in Eqs. (4.32) and (4.33) vanishes if $\bar{n}=1$. If water compressibility is neglected, the frequency-independent hydrodynamic pressure solutions p_0 and p_j given by

Eq. (4.32) and (4.33) can be simplified to

$$p_0(R_\mathrm{s}, z, \theta) = \sum_{n=1}^{N_\mathrm{w}} \frac{4\rho_\mathrm{w}}{H_\mathrm{w}} \frac{I_{0n}}{\kappa'_n} \mathcal{E}_n(\kappa'_n R_\mathrm{s}) \cos(\lambda_n z) \cos(\theta) \tag{4.39}$$

$$p_j(R_\mathrm{s}, z, \theta) = \sum_{n=1}^{N_\mathrm{w}} \frac{4\rho_\mathrm{w}}{H_\mathrm{w}} \frac{I_{jn}}{\kappa'_n} \mathcal{E}_n(\kappa'_n R_\mathrm{s}) \cos(\lambda_n z) \cos(\theta) \tag{4.40}$$

in which λ_n, I_{0n}, I_{jn} and $\mathcal{E}_n(\kappa'_n R_\mathrm{s})$ are given by Eqs. (4.34), (4.35) and (4.37), respectively, and

$$\kappa'_n = \frac{(2n-1)\,\pi}{2H_\mathrm{w}} \tag{4.41}$$

CHAPTER 5 INNOVATIVE SHAKING TABLE TEST FOR EVALUATING THE SEISMIC RESPONSE OF STRUCTURE-WATER SYSTEMS AND THEIR APPURTENANT STRUCTURES USING MODIFIED GROUND MOTION ACCELERATION

5.1 Introduction

The seismic response of structure-water systems, influenced by the combined effects of hydrodynamic forces and structural flexibility, has remained a significant challenge for researchers over the years. The response of the primary structure and its secondary appurtenant structures is influenced by water levels in two primary ways: hydrodynamic pressure effects and hydrodynamic damping effects. Together, these factors can alter the dynamic behavior of the system by lowering natural frequencies and modifying the damping ratios of the primary structure's lateral vibrations [1, 114, 158]. However, the amplification resulting from the coupled interaction of hydrodynamic effects and the flexibility of the primary supporting structure is often overlooked, which can lead to significant damage to appurtenant structures during seismic events. This underscores the vital importance of experimental studies on structure-water systems in dynamic testing, a field that has attracted significant attention and remained a central focus of research for decades.

Shaking table testing is one of the most widely utilized methods for experimentally investigating the seismic response of structures. This method enables the study of dynamic structural responses under real or artificial earthquake signals. For structure-water systems, where hydrodynamic effects significantly impact the response, incorporating these effects into shaking table tests is essential. The available approaches for conducting shaking table tests on structure-water systems can generally be categorized into the following groups: (i) The most advanced method for studying the seismic response of structure-water systems, which has gained significant popularity in recent years, is the underwater shaking table test. The underwater shaking table is a specialized facility designed to investigate the response of structure-water systems under seismic loads, wave-current conditions, and combined earth- quake and structure-water scenarios. By including hydrodynamic effects directly into shaking table test setup, underwater shaking table tests provide precise and detailed insights into the seismic behaviour of structure-water systems and their appurtenant structures, making them a valuable tool for research and practical applications [1,8–10,46,63,64,159–166]. (ii) The other approach involves using simplified methods, either by applying added mass concepts to represent hydrodynamic effects or by constructing a limited-length water reservoir around the structure or at the fluid-structure interface. Westergaard's added mass and Morison's formulation are

among the most widely used techniques in this category [11, 13, 14, 18, 21, 47, 48, 76, 167, 168]. (iii) The third group is simply the shaking table tests that neglect hydrodynamic effects. Due to the challenges of incorporating hydrodynamic effects in dynamic experimental tests, such as high facility costs, maintenance difficulties, and safety concerns related to potential water leakage, some researchers have opted to exclude hydrodynamic effects in shaking table tests of structure-water systems [19, 65–67, 129].

While each of these methods is developed with specific objectives and based on particular assumptions for performing shaking table tests, they all face significant challenges due to the inherent complexity of the topic. Underwater shaking table tests, while offering high accuracy, require expensive facilities and pose safety risks, particularly from potential water leakage. Moreover, adjusting the water's density to meet similitude laws often leads to violations of those similitude laws [64]. Simplified approaches, on the other hand, may compromise result accuracy due to their underlying assumptions, making them insufficient for detailed seismic studies. Distributing added mass evenly along the specimen's height also proves difficult, especially during dynamic loading, where maintaining the masses in fixed positions can be problematic. Another challenge with the presence of water is the difficulty in achieving the correct boundary conditions, which are important for accurately representing wave propagation effects. Due to these complexities, many studies in this field choose to neglect fluid-structure interaction effects during experimental tests. While it is acknowledged that excluding these effects can significantly influence the results, the challenges and practicality of incorporating hydrodynamic forces often outweigh the potential benefits. As a result, there is a need for an alternative approach that can accurately incorporate dynamic fluid-structure interaction in shaking table tests without the need for specialized and costly experimental equipment or complex instrumentation. This would provide a practical solution for researchers to study the seismic response of structure-water systems and their appurtenant structures while overcoming the limitations associated with available methods.

In this chapter, an innovative method is proposed for conducting shaking table tests to assess the seismic response of appurtenant structures on supporting structure-water systems. The proposed method employs analytical formulations of earthquake-induced hydrodynamic pressure within the fluid domain or uses simplified added masses to generate modified ground motion accelerograms. These modified ground accelerations can then be used as input signals for shaking table tests. This approach addresses the challenges previously mentioned and enables innovative shaking table tests on a standard shaking table in a safe environment.

This chapter is structured as follows: first, the shaking table test is discussed, including information about the facilities, the selection of the specimen as the structure-water system,

instrumentation, and the data acquisition system. This section also covers the dynamic property identification of the specimen. In the next section, the numerical finite element model used to generate modified ground acceleration, based on calibration with experimental measurement data, is presented. In this study, two ground accelerations used, and modified ground accelerograms were generated for these two earthquakes, assuming different water levels and considering a compressible water assumption. To demonstrate the effectiveness of the method, a simplified Morison's added mass formulation is also used to generate modified ground motion accelerations at full water level. The subsequent section provides details about the modified ground acceleration method and includes a brief review of the theoretical background. Finally, the experimental and numerical results are presented and discussed.

The study relies on the following main assumptions: (i) the primary structure possesses a vertical upstream face and exhibits linear elastic behaviour, with no consideration of cracking, degradation, or sliding at the joints; (ii) the water in the reservoir is assumed inviscid, with its motion irrotational and limited to small amplitudes; (v) gravity surface waves and convective effects are neglected; (vi) effects of sediments that may be deposited at reservoir bottom can be considered; (vii) the applied ground motion acceleration is horizontal (i.e. no vertical earthquake component is applied); (viii) the appurtenant structure may exhibit linear or nonlinear behaviour, but its mass is negligible compared to that of the primary structure.

5.2 Shaking table test

In this section, the shaking table test of a structure-water system subjected to two earthquakes is conducted using modified ground acceleration method. By comparing the seismic response of the system in the experimental setup with coupled fluid-structure interaction finite element solutions, it is verified that the responses of the structure-water system can be accurately obtained using the proposed method.

5.2.1 Single-axis shaking table facility at Polytechnique Montréal

The high-performance single-axis (unidirectional) earthquake simulator at Polytechnique Montréal is a facility designed to conduct rigorous seismic testing on various structural systems. This simulator is capable of replicating ground motions, enabling the study of structural responses to seismic events. The simulator platform measures 3353 mm × 3353 mm (approximately 3.4 m × 3.4 m), offering a substantial testing area suitable for diverse structural experiments. It has a maximum payload capacity of 13600 kg (133 kN) and operates within a frequency range of $0-60$ Hz. The table allows for a maximum displacement of ± 125 mm and can achieve velocities up to 1.0 m/s when fully loaded and 1.3 m/s when

bare. The table can generate accelerations up to ±1 g with a full payload and up to ±3 g when unloaded. Additionally, it has an overturning moment capacity of 620 kN.m under full load and 780 kN.m when bare. The shaking table is mounted on an all-welded steel caisson, supported by four linear hydrostatic bearings that allow smooth horizontal movement driven by a dynamic hydraulic actuator. This setup, provided and managed by MTS Systems Corp., ensures precision and reliability during tests. Access to the testing area is facilitated by a 15 ton capacity overhead crane, which simplifies the handling and positioning of specimens. The laboratory offers a clear height of 12.2 m under the roof structure and 10.7 m under the crane hook, providing ample vertical space for various experimental setups. The platform itself includes threaded holes with a net uplift capacity of 160 kN per anchor point, ensuring the secure anchoring of test specimens during dynamic simulations. The simulator is powered by a 1440 lpm hydraulic supply that drives the high-performance actuator, capable of a total stroke of 300 mm and a dynamic capacity of 220 kN. The control system, managed by an MTS-469 System controller, allows for precise control over the testing process. This includes three-variable control, which manages acceleration, velocity, and displacement to accurately replicate seismic testing. The amplitude phase control ensures that the desired input motions are precisely reproduced by the table, while adaptive inverse control and online iteration schemes enable real-time adjustments during testing, ensuring that the test conditions remain aligned with the intended simulation parameters. Figure 5.1 presents the shaking table facility located in the structural laboratory of Polytechnique Montréal.

While the shaking table at Polytechnique Montréal offers robust physical capabilities and advanced control features, making it a powerful tool for seismic testing of various structural systems, there are certain limitations that need to be considered when planning and scheduling tests. One key limitation is that the simulator is unidirectional, meaning it can only apply earthquake motions in a single direction. Additionally, the platform, measuring 3.4 m × 3.4 m, restrict the base size of the test specimens to less than 3.2 m. The total weight of the specimen is also restricted to 13600 kg (13.6 tons), which imposes limitations on the size and mass of the structures that can be tested.

Two key limitations to consider are the operational frequency range and the maximum acceleration capacity of the shaking table. The operational frequency range of 0 to 60 Hz means that if a small-scaled specimen has a natural frequency above 60 Hz, it is practically impossible to excite the flexible response of the specimen and the structure moves as a rigid body. Furthermore, the shake table's maximum operational acceleration ranges from 1 g to 3 g. This limitation requires careful consideration when using the modified ground acceleration method, as it may necessitate scaling the input ground motion to stay within the shake table's maximum operational capacity.

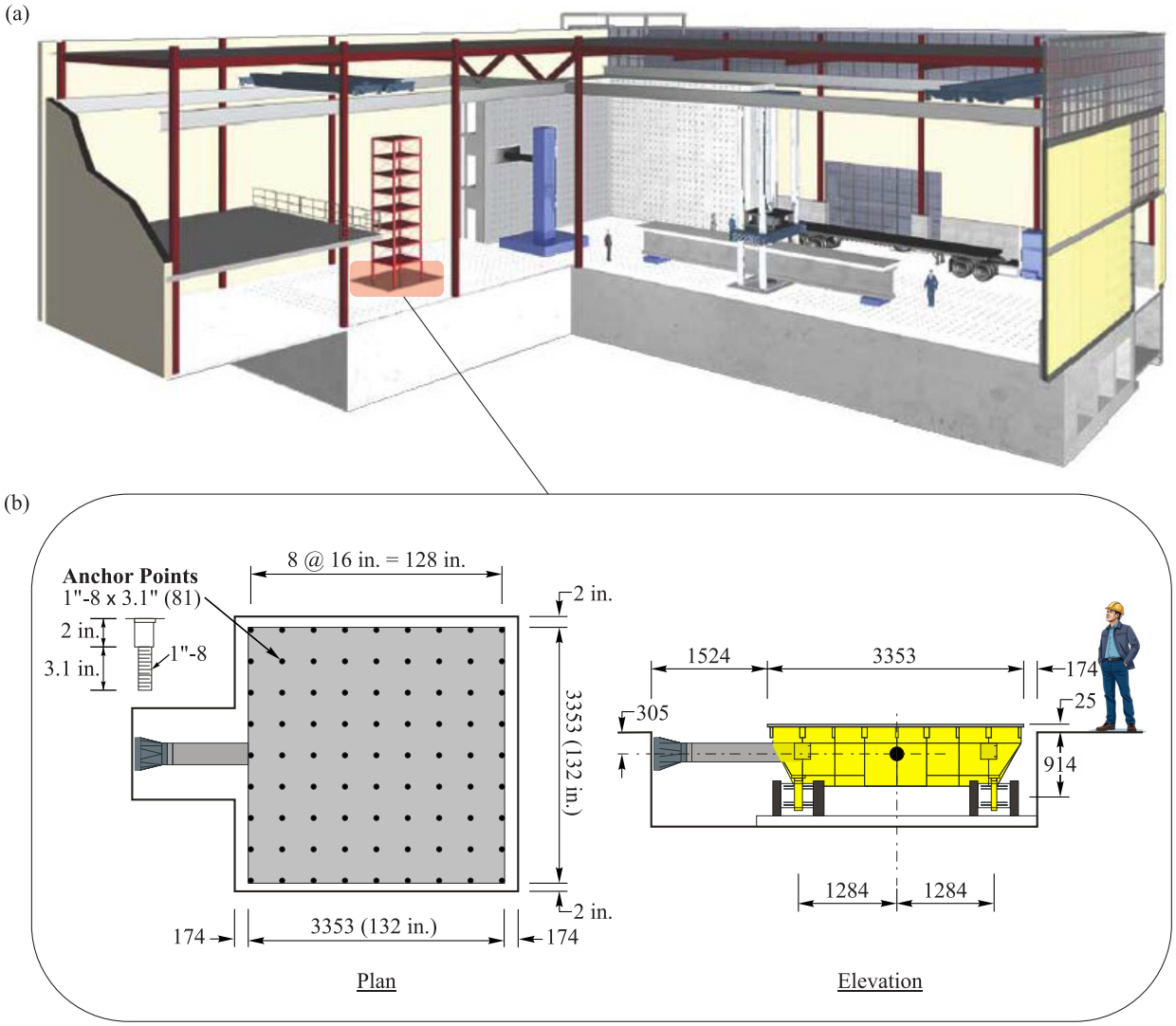

Figure 5.1 Experimental facilities at Polytechnique Montréal (adopted from [20]): (a) structural laboratory; (b) detail of the shaking table.

5.2.2 Primary structure and appurtenant secondary structure

The selection process for the structure-water system considered the experimental limitations outlined earlier. Given the operational limitation and the need to effectively incorporate hydrodynamic effects, an axisymmetric structure surrounded by water was chosen as the structure-water system. Several scenarios for selecting a suitable axisymmetric structure were carefully considered and evaluated, including variations in height, material properties, and cross-sectional geometry. A detailed discussion of the evaluation process for selecting the axisymmetric structure is provided in Chapter 6.

The first criteria was to choose a system that is flexible enough to have a natural frequency

below 30 Hz. The second criteria was to select a system that clearly exhibits the effects of hydrodynamic forces. In other words, a light structure was chosen so that its mass would not be too large to ignore the added masses due to hydrodynamic effects. The other criteria was to avoid any effects of similitude laws in this study to keep the time and frequency content of the signal unchanged in this experimental study. Therefore, an aluminum hollow circular cross-section axisymmetric tower surrounded by water was selected as the structure-water system. Figure 5.2 shows the primary structure with an outer diameter of 3 inches (76.2 mm) and a thickness of 0.25 inches (6.33 mm). The height of the specimen is 118-1/4 inches (3003.55 mm). The material used for the specimen is AL 6061-T6, which is a common aluminum alloy known for its excellent strength-to-weight ratio and good fatigue resistance. The mechanical properties of the material include a tensile yield strength of 276 MPa, an ultimate tensile strength of 310 MPa, a modulus of elasticity of 68.9 GPa, a Poisson's ratio of 0.33, and a density of 2700 kg/m^3. The specimen is welded onto an aluminum plate and bolted at the shaking table interface. The appurtenant structure can be represented by a Single Degree of Freedom (SDF) system with a concentrated mass (m_s) at the top of the appurtenant structure. It is assumed that the mass of the appurtenant SDF system is light enough that its dynamic response does not affect the dynamic response of structure-water system. Conversely, the amplification due to the coupled influence of hydrodynamic effects and the flexibility of the primary structure can significantly affect the seismic response of the appurtenant structure. After a series of tests, an appurtenant structure with a total height, width, and thickness of 200 mm, 10 mm, and 0.635 mm, respectively, was selected. Figure 5.3 illustrates the appurtenant structure having a 25 gram mass and fixed at the top of the tower. A unidirectional accelerometer is attached to the top of the specimen, serving both to capture the tower's acceleration response and to act as a concentrated mass at the top of the appurtenant structure (accelerometer No.2 in Fig. 5.3). To control the non-linear behaviour of the appurtenant structure, a 4 mm notch, both in length and depth, was introduced 2 mm above the top of the ⌞ -shaped sections where the appurtenant structure is fixed to the primary tower structure. The material properties are detailed in Table 5.1.

5.2.3 Instrumentation and data acquisition

The dynamic behavior of the structure during testing was measured using six accelerometers and two strain gauges. Figure 5.4 illustrates the layout of the instrumentation utilized in the experimental setup. The accelerometers were PCB Piezotronics model, which have a sensitivity of 10 mV/g and a frequency range of 0.5 to 4000 Hz. Two 20g accelerometers were placed at Point A and B as shown in Fig 5.3. Three 10g accelerometers were used to measure horizontal accelerations at 0.75, 0.5, and 0.25 of the height of the primary structure, and

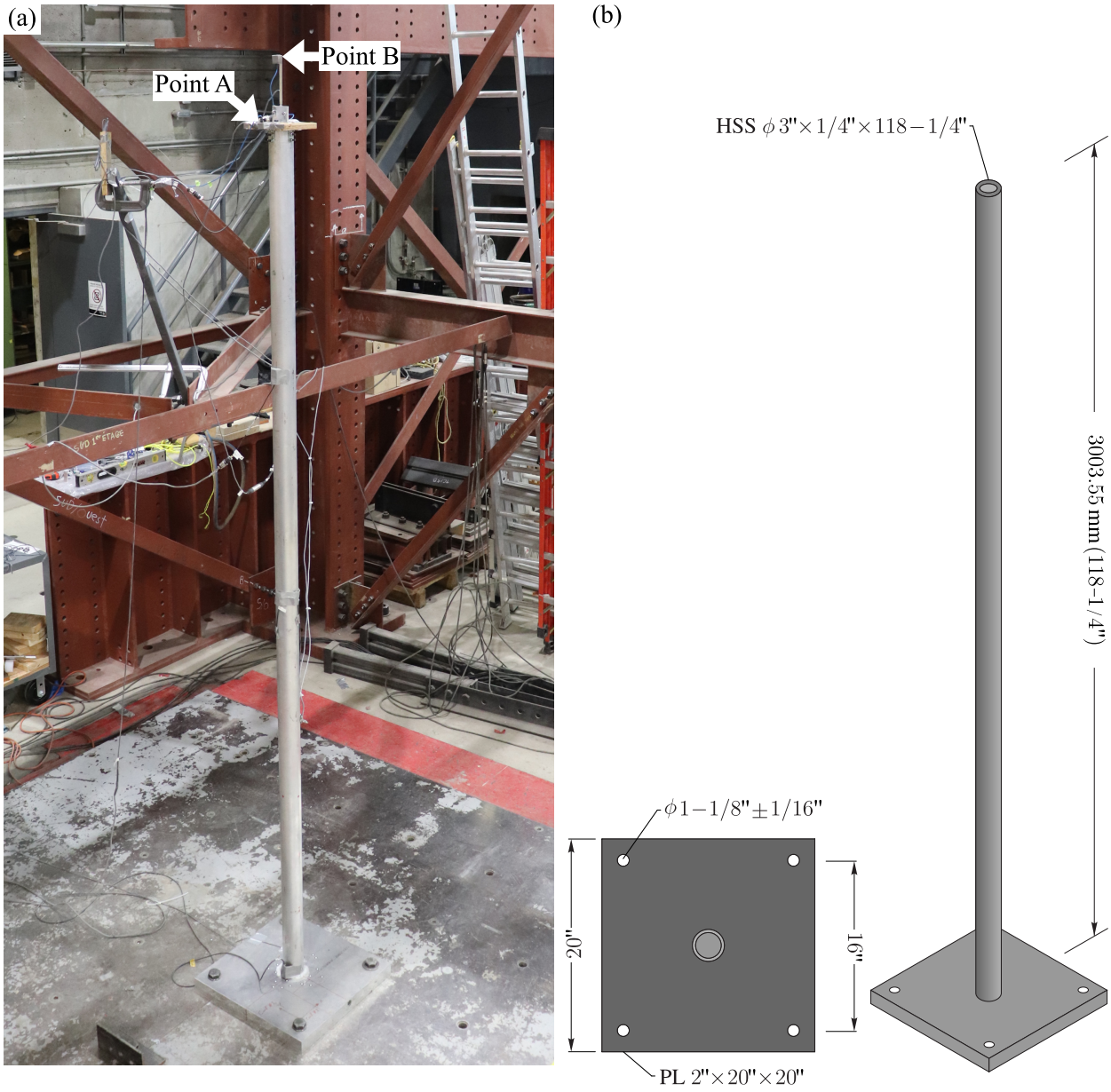

Figure 5.2 Test setup: (a) specimen fixed on the shaking table; (b) dimensions and details of the primary structure.

one 3D 2g accelerometers were placed at base of the primary structure (as shown in Fig 5.4). The strain gauges, Vishay Precision Group model CEA-06-125UW-120 with a sensitivity of 2.0 mV/V, were attached using a high-temperature adhesive. One was positioned at the base of the primary structure (Fig. 5.4), and another was placed at the notch on the appurtenant structure, as shown in Fig. 5.3. All data were recorded using an HBM synchronized data acquisition system and processed with Catman DAQ software [169], with a sampling frequency of 600 Hz for all tests.

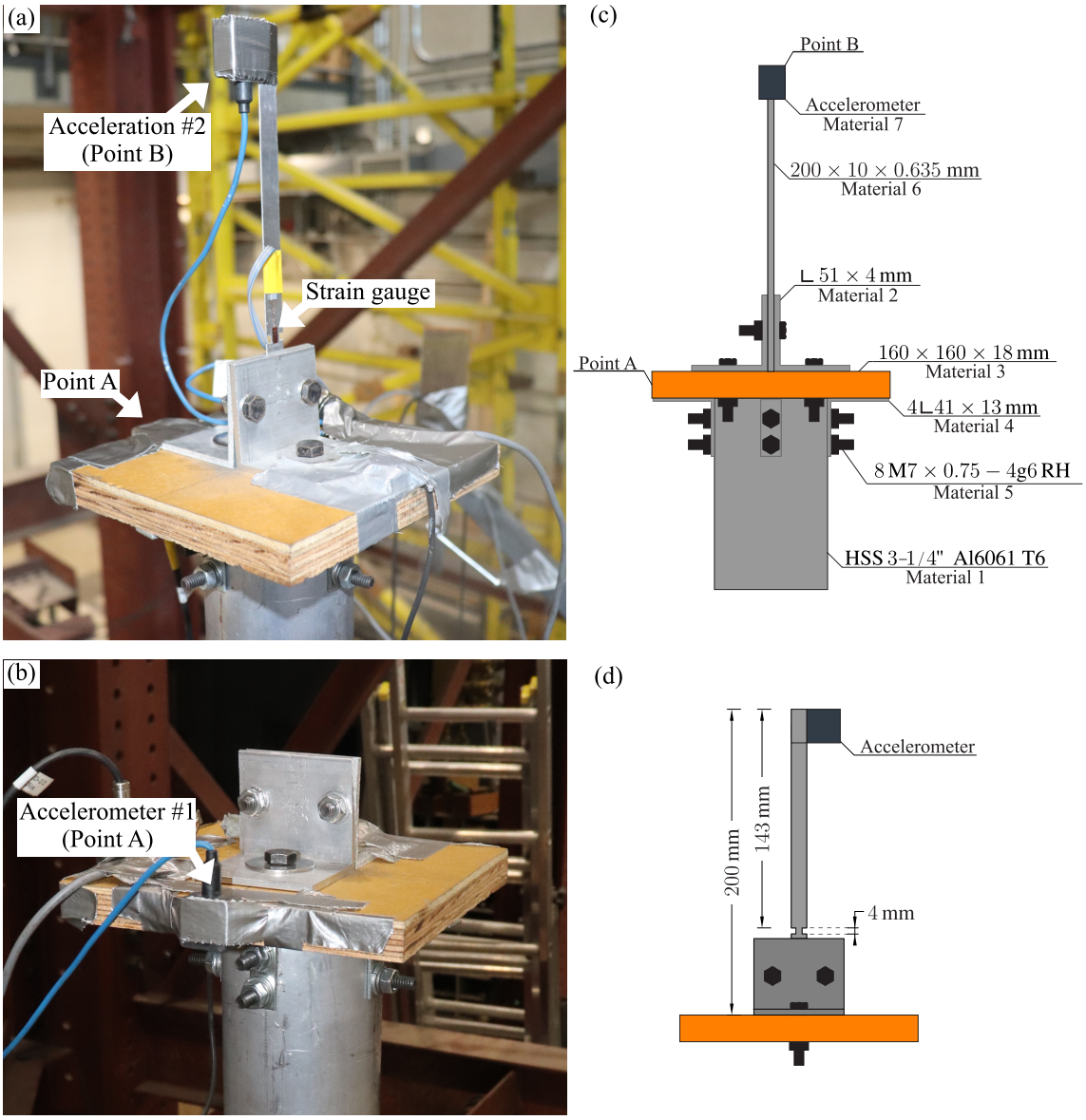

Figure 5.3 Details of the apartment structure fixed at the top of the tower.

5.2.4 Determination of the dynamic properties of the tested structure

After fixing the tower on the shaking table and installing the instrumentation, a series of preliminary tests were conducted to evaluate the dynamic properties of the structures. First, harmonic excitation was applied as an input ground motion at a selected frequencies. The structural response was observed until the transient part damped out, and the amplitude of the steady-state acceleration was measured. The frequency of the input signal was then adjusted to a new value, and the measurements were repeated. The forcing frequency varied from 2 Hz to 45 Hz, a range that includes the natural frequency of the tested structure.

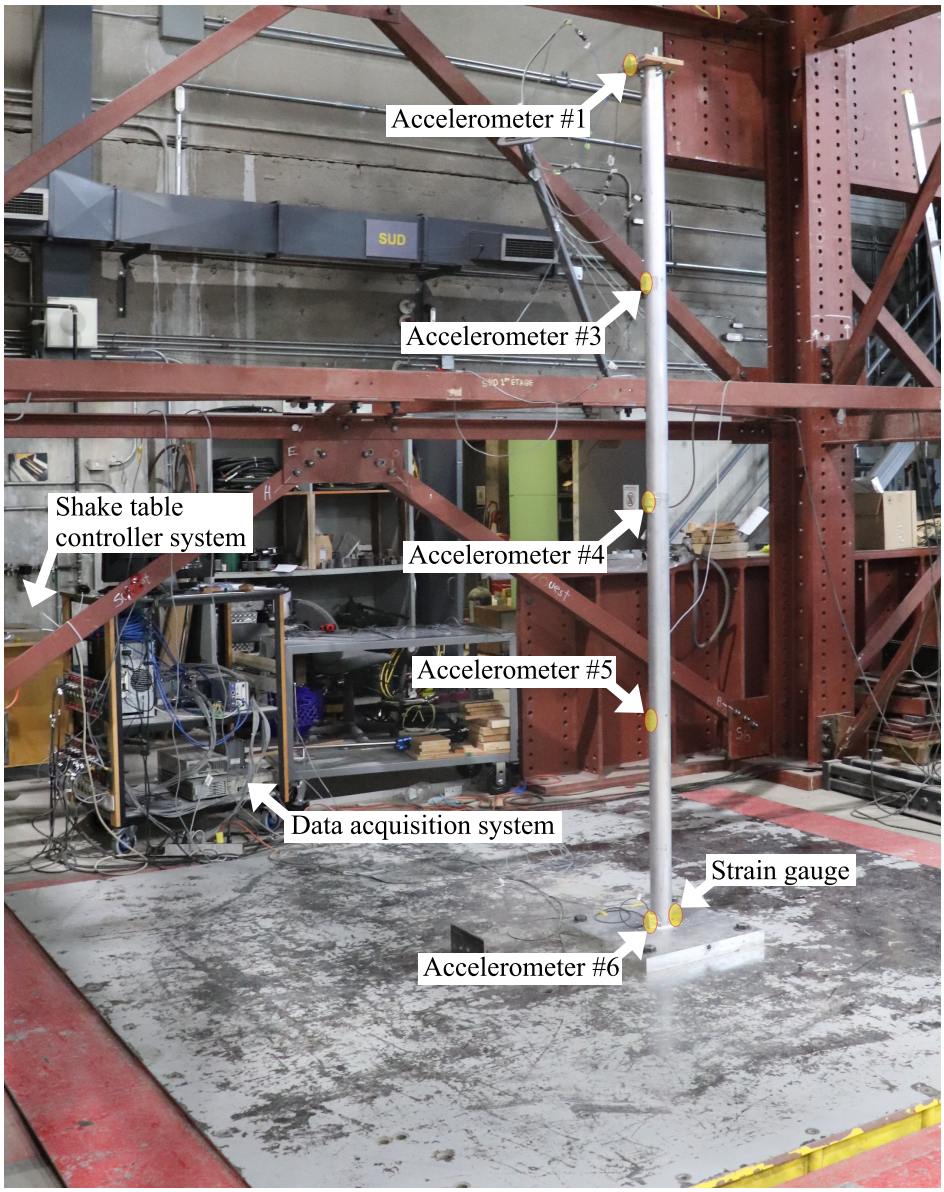

Figure 5.4 Instrumentation layout for the experimental test.

Figure 5.5 illustrates the harmonic excitation with forcing frequencies of 5, 7, 15, and 40 Hz, and the time history acceleration response of the tower at point A. The frequency response curve was then plotted from the measured data, as shown in Fig. 5.6. The black dots represent the experimental data measured using the aforementioned procedure over the forcing frequency range of 2 Hz to 45 Hz, while the red curve represents an analytical solution fitted to the experimental data. As shown in the figure, the response values were normalized relative to the maximum amplitude. Secondly, Pull-release tests were performed to determine the dynamic properties of the specimen. This process involved installing two String Pot Dis-

Table 5.1 Material properties of the tower and the apartment structure

Materials	**Mass density (kg/m^3)**	**Elastic modulus (GPa)**	**Poisson'sratio (-)**	**Yeilding stress (MPa)**
Material 1	2700	68.9	0.33	276
Material 2	7400	70	0.33	-
Material 3	1500	10	0.3	-
Material 4	4000	70	0.33	-
Material 5	8000	200	0.3	-
Material 6	2700	68.9	0.33	276
Material 7	15000	200	0.3	-

placement Sensors to measure the initial displacement, one aligned with the stream direction of the initial displacement and the other positioned at a 45° diagonal angle. The pulling tests were performed by applying a small horizontal force at 0.70 of the total height of the tower (Figure 5.7). Figure 5.8 (a) and (b) illustrate the normalized displacement of the tower at point A in the time and frequency domains, respectively. The blue curves in Fig. 5.8 (c) and (d) represent the normalized acceleration at point A. The pull-release tests were performed without the appurtenant structure installed on top of the tower, focusing on determining the dynamic properties of the primary structure. To evaluate the effect of the appurtenant structure on the dynamic properties of the primary structure and to determine the dynamic properties of the appurtenant structure itself, pull-release tests were repeated with the appurtenant structure mounted on the top of the primary structure. The red curves in Fig. 5.8 (c) and (d) show the normalized acceleration of the tower with appurtenant structure.

It is evident that the presence of the appurtenant structure does not significantly affect the dynamic response of the tower. This validates the assumption that the appurtenant structure is light enough not to impact the tower's dynamic responses. Therefore, the tower without the appurtenant structure can be used to generate the modified ground acceleration, considering that the appurtenant structure does not affect the hydrodynamic pressure within the reservoir. Figure 5.8 (e) and (f) show the relative horizontal acceleration response of the appurtenant structure at point B in the time and frequency domains, respectively. Based on the experimentally measured data, the natural frequency of the primary structure without surrounding water was calculated to be 6.33 Hz for the first two symmetric modes (i.e. $f_{1,2} = 6.33$ Hz) and 41.7 Hz for the third and fourth modes (i.e. $f_{3,4} = 41.7$ Hz). A constant viscous damping ratio of 0.25% was determined from the harmonic excitation and pull-release tests. Also, the results indicated that the fundamental frequency and viscous damping ratio of the appurtenant structure are 4.1 Hz (i.e. $f_1^* = 4.1$ Hz) and 1%, respectively.

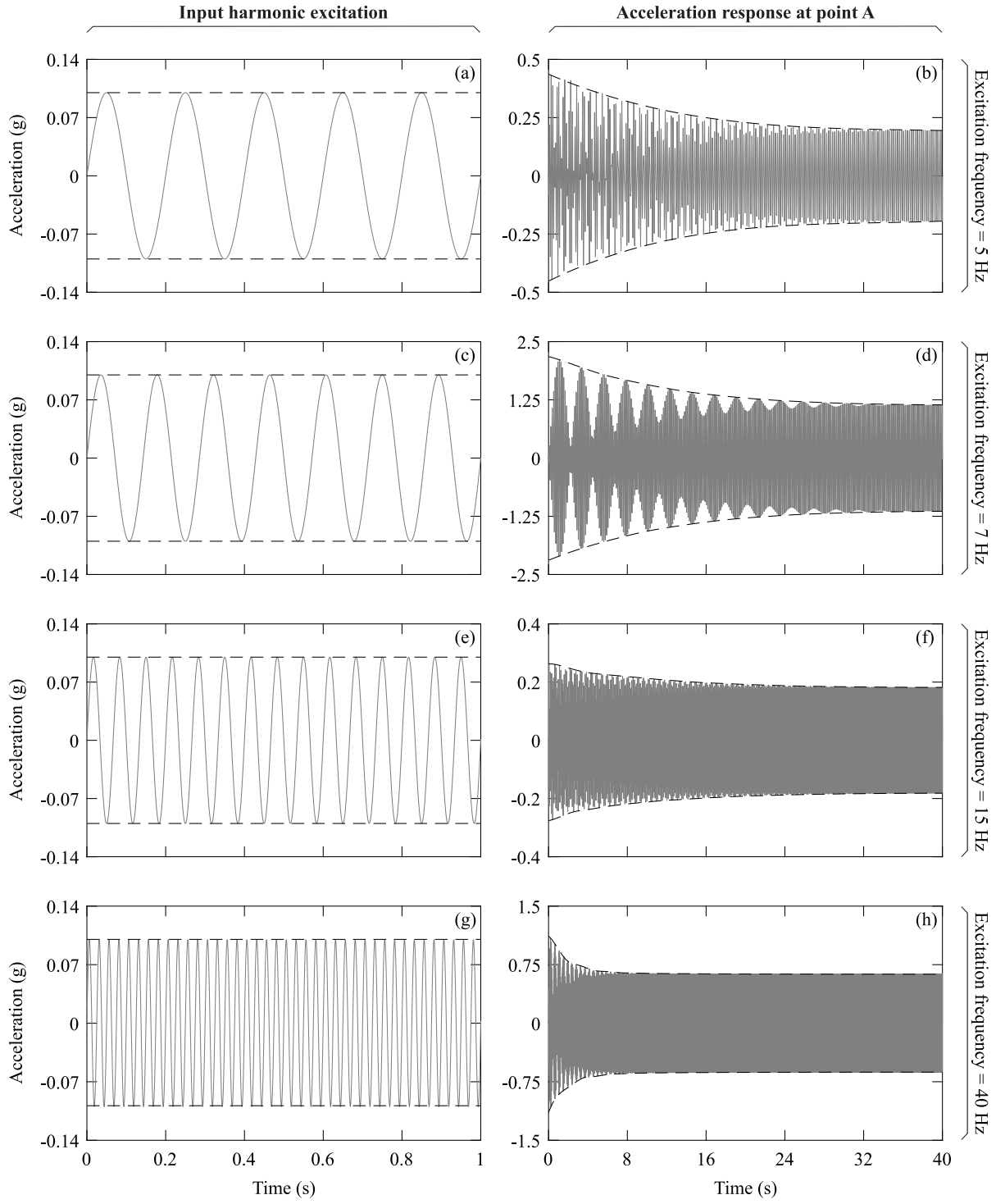

Figure 5.5 Input harmonic excitation and acceleration response of the studied tower at point A: (a) and (b) 5 Hz excitation frequency; (c) and (d) 7 Hz excitation frequency; (e) and (f) 15 Hz excitation frequency; (g) and (h) 40 Hz excitation frequency.

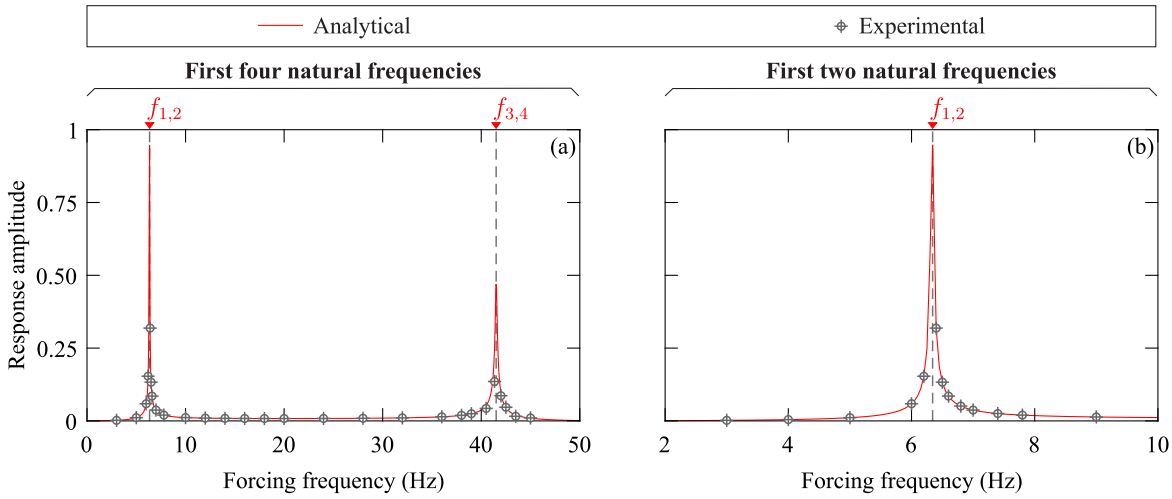

Figure 5.6 Normalized frequency response function of the tower at point A without surrounded-water due to harmonic horizontal excitation: (a) first four natural frequencies; (b) first two natural frequencies.

5.3 Finite Element Models

Three-dimensional (3D) finite element models of the tower and its appurtenant structure are developed and used as the calibrated numerical model of the dry system to generate the modified ground accelerograms. Subsequently, a fluid domain is added to the system to create a coupled structure-water finite element model referred to hereafter as reference solution. The primary tower structure, with the fixture at the top discretized into 20-node 3D-solid finite elements using the software ADINA [92]. Figure 5.9 shows the finite element model developed for two purposes: (i) to serve as the numerical model for generating modified ground motion accelerations, and (ii) to provide reference solutions for comparison with the experimental results. The detailed modeling aims to replicate the experimental setup as closely as possible for an accurate comparison and validation of the results. It is worth mentioning that while a simplified finite element model using beam elements could have been used, a more detailed model was selected to provide better illustration and ensure more accurate comparisons. The tower has a height of 3.00 m and is fixed at its base. The material used for the primary structure is linear elastic, as it remained within the elastic range during all tests. The appurtenant structure is modeled using 20-node 3D solid finite elements with a bilinear elastic-plastic material. The accelerometer is modeled with its dimensions of $20 \times 20 \times 10\,\text{mm}^3$ and a density of $15000\,\text{kg/m}^3$, resulting in a mass of 25 grams. Using rigid links, the accelerometer is constrained to the top of the appurtenant structure. The notch location was accurately modeled following the same dimensions as the

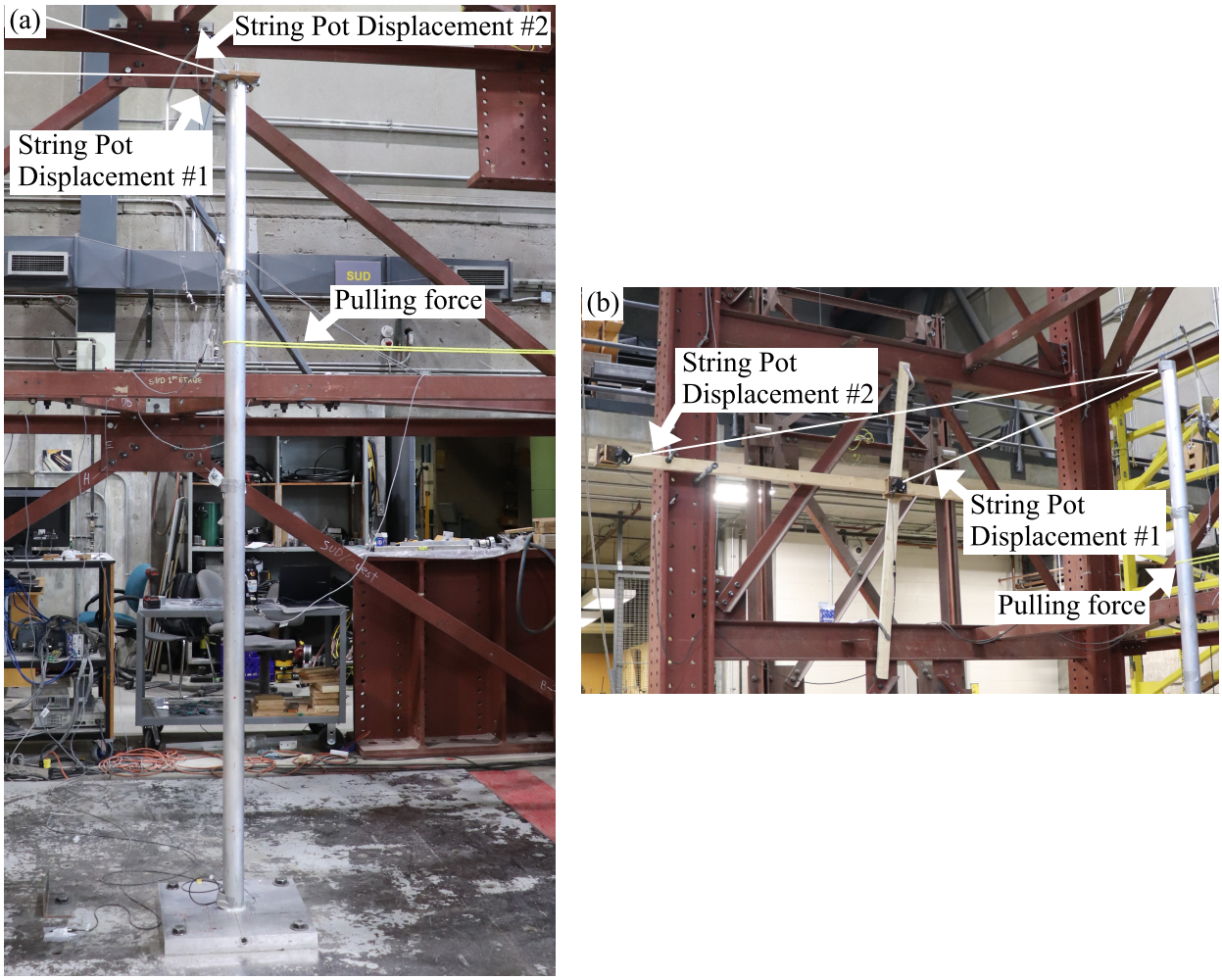

Figure 5.7 Free vibration test with instrumentation: (a) the studied tower subjected to an initial displacement at 0.70% of its total height; (b) two string pot displacements used to capture the initial displacement.

specimen in experimental test. Figure 5.10 shows the details of the finite element models of the appurtenant structure. The material properties of the tower, fixture and the appurtenant structure are presented in Table 5.1.

Figure. 5.11 illustrates the tower surrounded by an infinite water domain with heights of $0.5H_{\mathrm{w}}$, $0.75H_{\mathrm{w}}$, and H_{w}, which correspond to 1.48 m, 2.22 m, and 2.96 m, respectively. The water is modeled using 3D 20-node potential-based finite elements, as depicted in Fig. 5.12. An infinite boundary condition is applied at a far end located at a radius of two times of the water level around the structures (Fig 5.12). The finite element software ADINA [92] utilizes the $\phi - U$ formulation to incorporate fluid effects and has been validated in previous studies against analytical and experimental results from dynamic fluid-structure interaction

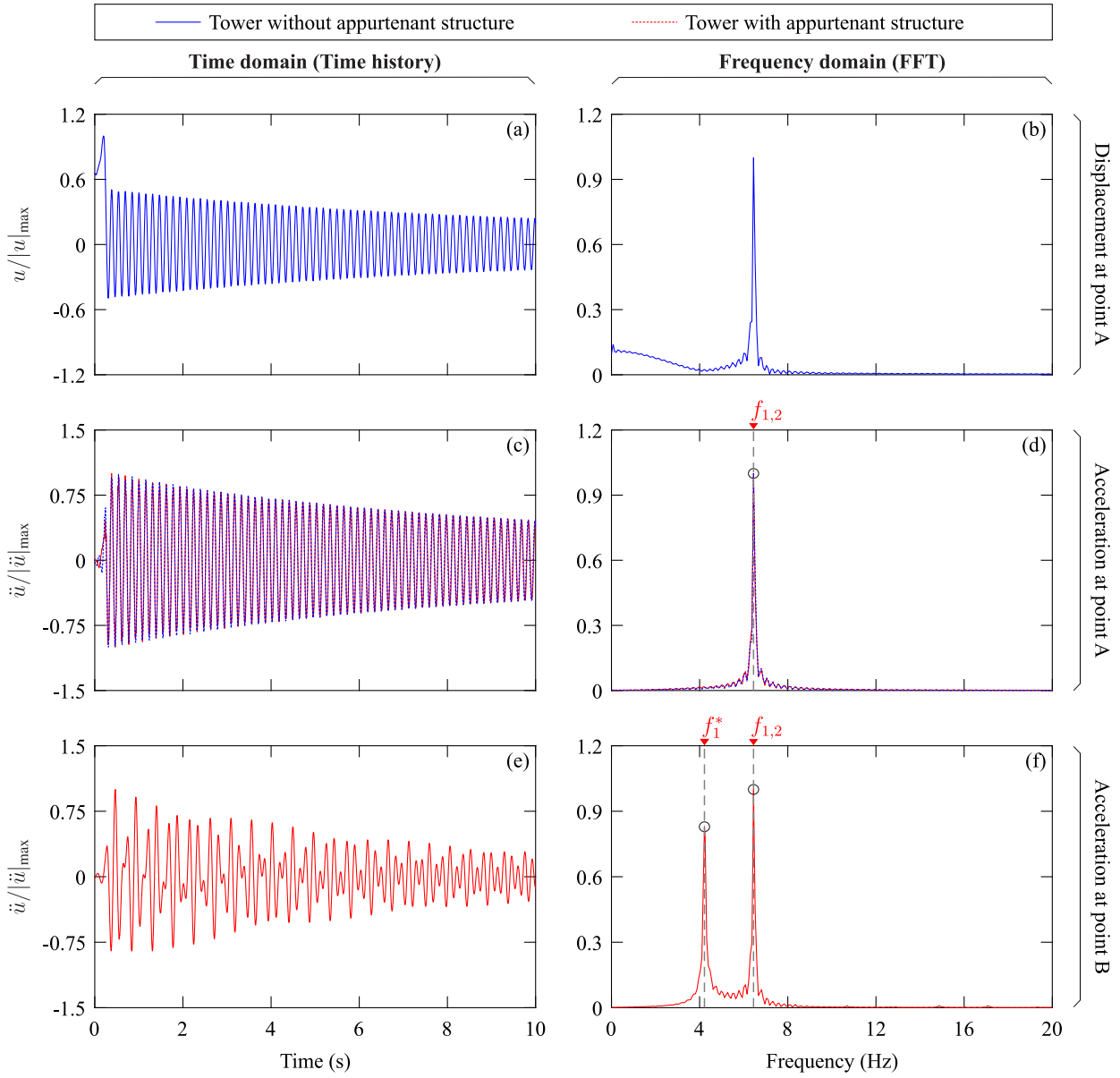

Figure 5.8 Free vibration response of the studied tower with and without appurtenant structure subjected to an initial displacement: (a) and (b) time history and FFT of the normalized displacement applied at 0.70 height of the tower, respectively; (c) and (d) time history and FFT of the normalized acceleration of the tower at point A, respectively; (e) and (f) time history and FFT of the normalized acceleration of the tower at point B, respectively.

problems in civil engineering [2, 18, 170–172]. In this method, the hydrodynamic pressures developed within the potential-based fluid elements are two-way coupled to the vibrations of the solid elements modeling the structure [18]. MATLAB [173] scripts were developed to create refined meshes for the structure and the surrounding water, ensuring proper accounting for fluid-structure interaction. The mesh densities of the finite-element models were adjusted

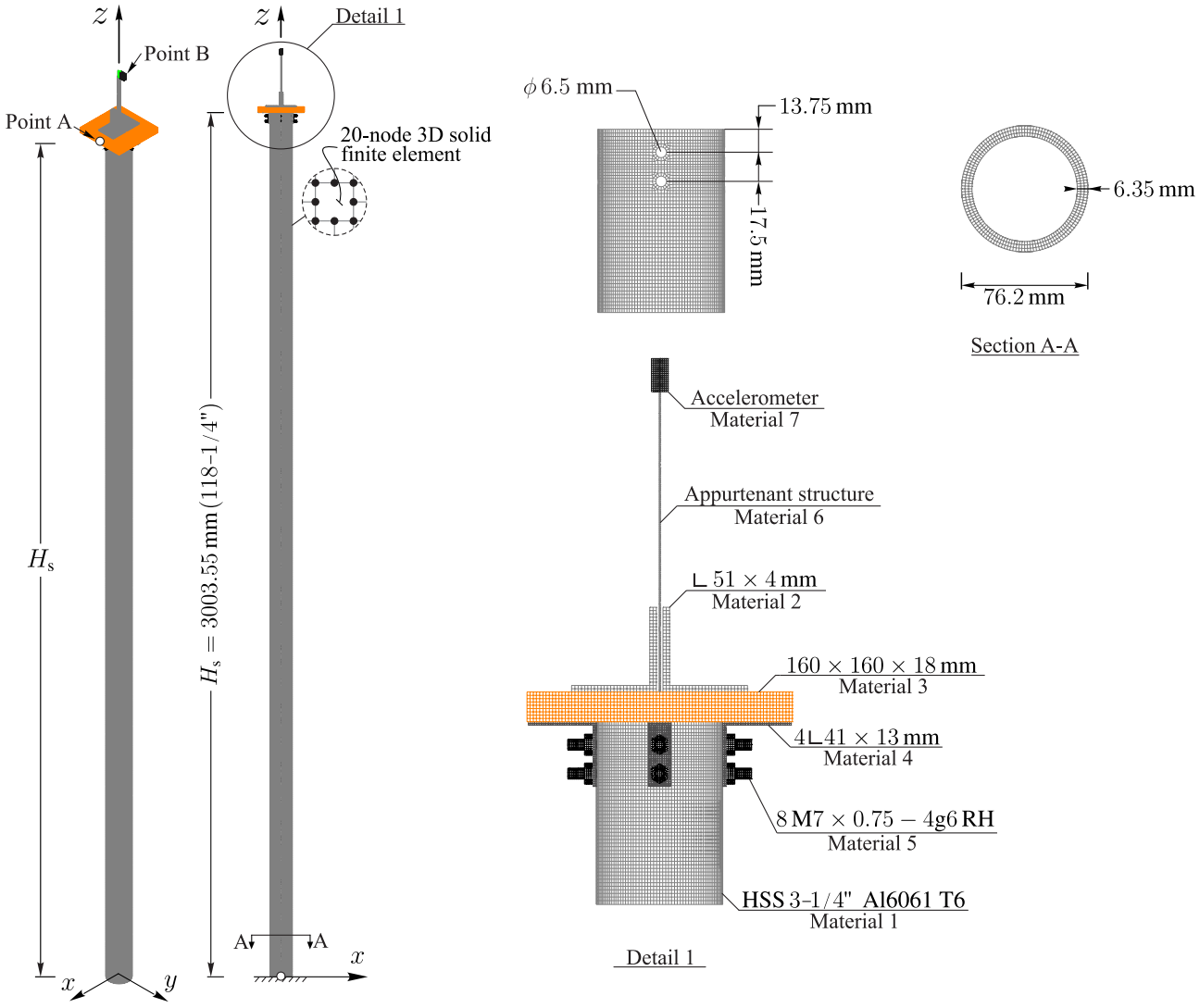

Figure 5.9 Finite-element model of the tower and the appurtenant structure.

and refined until the results converged. The outcomes of the 3D coupled structure-water finite element models are referred to as the reference solution.

Figure 5.13 presents the six lateral mode shapes and corresponding vibration periods (T_1 to T_6) of the dry structures, as well as the modal mass participation factors along x, y and z, i.e. $\Lambda_j^{(x)}$, $\Lambda_j^{(y)}$ and $\Lambda_j^{(z)}$, respectively, indicating the relative importance of each mode in the global seismic response of the structures. To obtain the time history response of the tower, a direct integration time history dynamic analysis and Rayleigh damping were used.

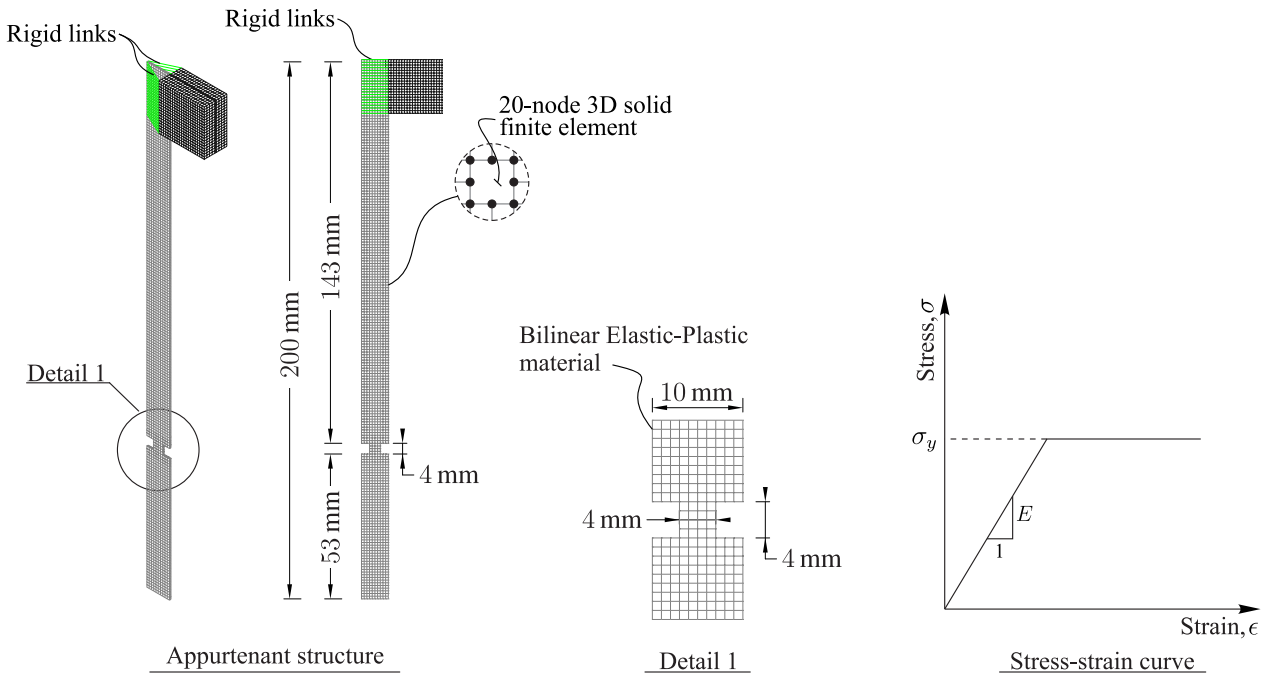

Figure 5.10 Details of finite-element model of the appurtenant structure.

5.4 Shaking table test of structure-water system

To incorporate hydrodynamic pressure in the shaking table test of an appurtenant structure mounted on a tower, a modified ground acceleration signal that accounts for hydrodynamic effects was used. As discussed in Chapter 1, this approach transfers earthquake-induced reservoir effects into modified version of the ground motion accelerations. These modified accelerations can then be applied directly to the structure without water (i.e. a dry structure). In this study, a modified ground motion acceleration is generated, incorporating the effects of all considered modes into a single ground motion. The technique, originally developed by Miquel and Bouaanani [4], has been extended in this study to apply to axisymmetric structures. It can be shown that a mode- and coordinate-independent accelerogram $\widetilde{a}_{\mathrm{g}}(\omega)$ can be define by modifying the original input ground acceleration $\ddot{x}_{\mathrm{g}}(\omega)$ as follows [4]

$$\widetilde{a}_{\mathrm{g}}(\omega) = \ddot{x}_{\mathrm{g}}(\omega) \frac{\sum_{j=1}^{N_{\mathrm{s}}} \widehat{Z}_j(\omega)}{\sum_{j=1}^{N_{\mathrm{s}}} Z_j(\omega)} \tag{5.1}$$

where $\ddot{x}_{\mathrm{g}}(\omega)$ is Fourier transform of ground motion acceleration $\ddot{x}_{\mathrm{g}}(t)$ and given by Eq. (3.27). $\widehat{Z}_j$ and Z_j denote the generalized coordinates of structure-water system and system without

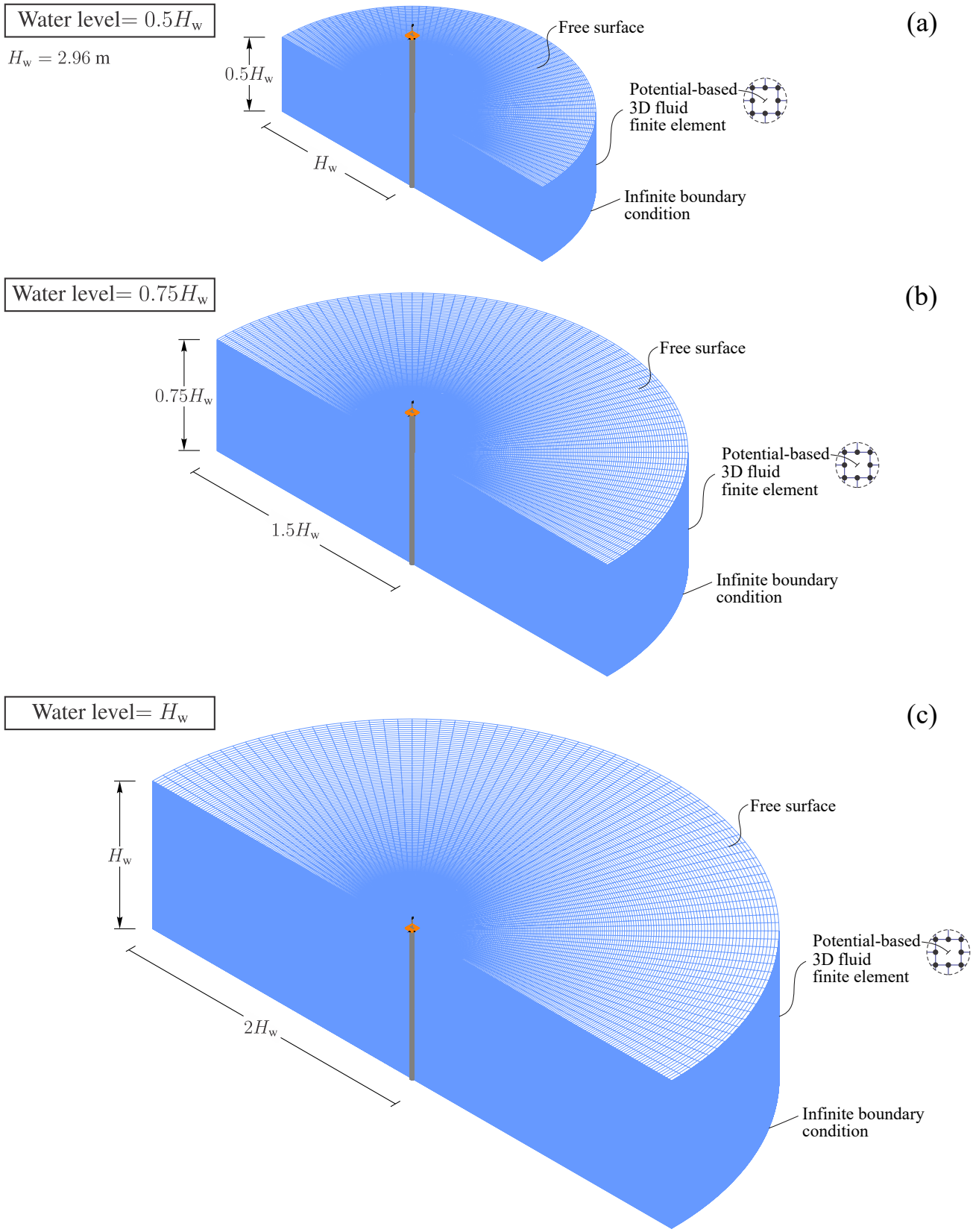

Figure 5.11 Different water levels surrounding the structure: (a) assuming water level to be $0.5H_w$; (b) assuming water level to be $0.75H_w$; (c) assuming water level to be H_w.

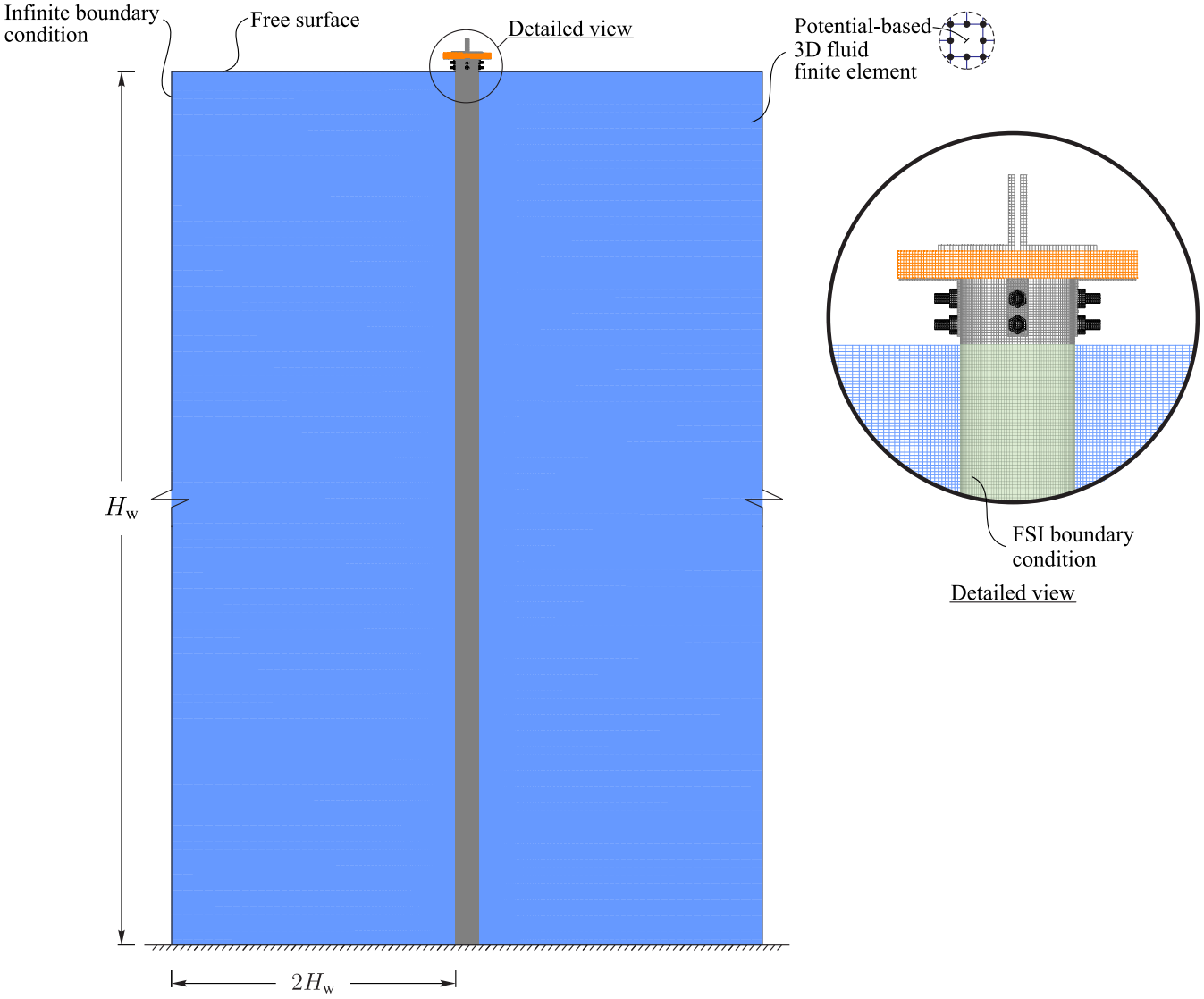

Figure 5.12 Finite-element model of coupled structure-water system.

water, respectively, and N_s is the number of structural modes. The modified ground acceleration was derived from the calibrated numerical model described above, and then applied as an input acceleration to the shaking table. Since the generation of the modified ground acceleration is based on analytical expressions, various water assumptions and levels can be used to incorporate hydrodynamic effects into the ground motion acceleration.

To perform a shaking table test of structure-water system using the proposed method, several steps are required as outlined in the flowchart (Fig. 5.14). The first step is to identify the properties of the specimen that will be used as the structure in contact with water. As mentioned before, this can be achieved through various methods such as pull-release, applying

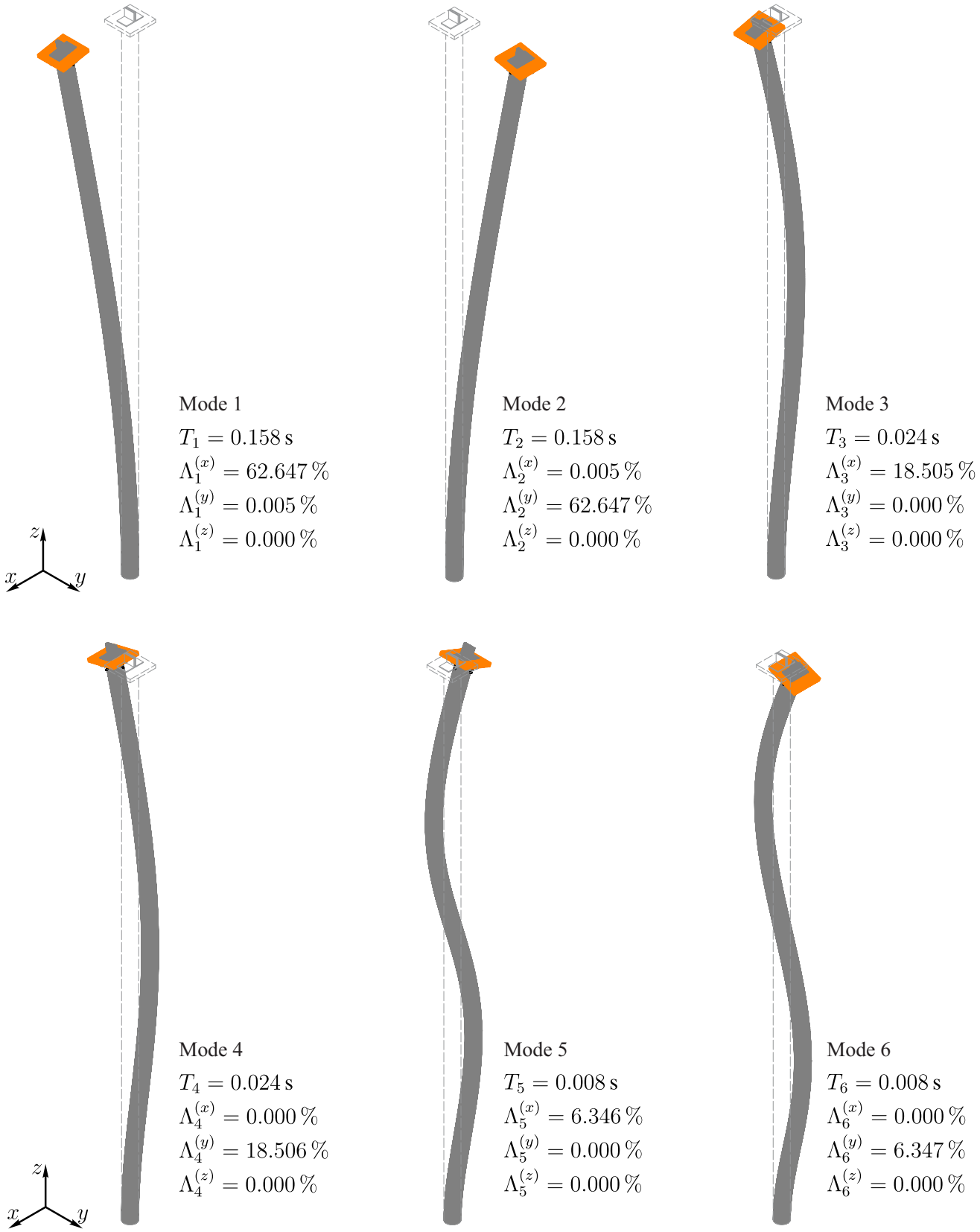

Figure 5.13 First six lateral mode shapes and corresponding vibration periods of the tower.

white noise, or harmonic excitation. The next important step is to build an accurate finite element model of the primary structure, which is intended to be in contact with water. This model is essential for preparing the modified ground accelerograms. For this purpose, only the primary structure in contact with water needs to be modeled, assuming that the appurtenant structure will not affect the dynamic response of the structure-water system. If the appurtenant structure does have an impact, it should also be included in the model to generate the modified ground accelerograms. By performing several modal analysis, a calibrated numerical model of the specimen can be developed. This model can then be used to determine the structure's dynamic modal properties, including natural periods (T_j), structural mode shapes at the structure-water interface along the excitation direction ($\psi^{(x)}$), modal mass and forces (M_j and L_j, respectively), and modal damping (ξ_j). The number of modes (N_s) to be included should be selected based on the type of structure-water system, the flexibility of the structure, and the frequency content of the excitation. Software ADINA [92] is used for these analyses and six lateral mode shapes are considered (Fig. 5.13). However, any other standard finite element structural engineering software or code available for performing modal analysis could also be used. Then, the generalized modal coordinate $Z_j(\omega)$ of the dry structure is calculated using any standard programming software. In this study, MATLAB [173] was used to calculate all required parameters. The next step involves calculating the hydrodynamic pressure. Parameters such as water density (ρ_w), water level (H_w), pressure wave velocity (C_w), and the number of acoustical modes (N_w) are selected. Analytical formulations of earthquake-induced hydrodynamic pressure in the reservoir are used to transfer the hydrodynamic effects into a modified version of the ground motion acceleration. As detailed in Chapter 4, these analytical formulations can be based on different water assumptions, including compressible, incompressible, or simplified added mass approaches. he generalized coordinates of the structure-water system ($\widehat{Z}_j$) are determined, enabling the calculation of the modified ground accelerograms in the frequency domain. Finally, applying the Fourier inverse transform yields the modified ground accelerograms that incorporate hydrodynamic effects. These steps are elaborated in Chapters 3 and 4.

The modified ground motion acceleration is prepared based on the calibrated numerical model. These new accelerograms can then be applied as the input signal for the shaking table tests, converting a structure-water system subjected to original ground acceleration into the shaking table test of a dry system subjected to a modified version of the ground motion acceleration that includes dynamic structure-water interaction effects. Since analytical formulations were used to transfer the hydrodynamic effects into the ground motion acceleration, different water levels and assumptions can be utilized to prepare the modified ground accelerograms. Utilizing these ground accelerograms eliminates the need for presenting water

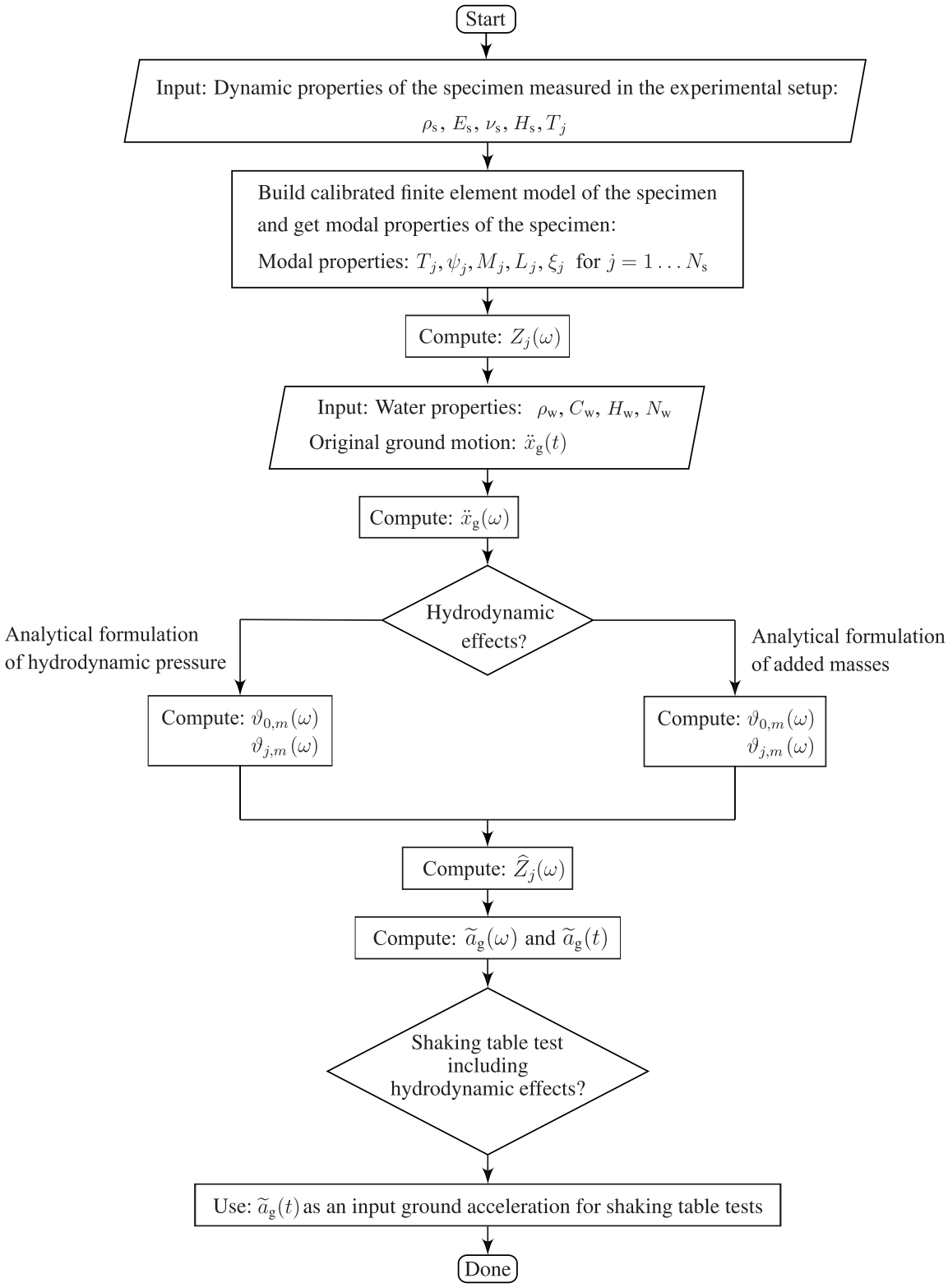

Figure 5.14 Flowchart of the proposed procedures.

in the experimental setup or using specialized facilities like underwater shaking tables with underwater measurement systems. Even for simplified methods that employ added mass representation in shaking table tests, this approach can generate a modified version of the ground motion acceleration that incorporates hydrodynamic added mass effects.

5.4.1 Original and modified ground motions

The seismic response of the selected structure-water system is studied under the effects of two ground motion accelerations differing by their frequency content and time signature: (i) a horizontal component of Nahanni earthquake (1985) at station Iverson, (ii) a horizontal component of El Salvador earthquake (2001). The acceleration time histories, acceleration pseudo-spectra, and Fourier amplitudes of these ground motions are illustrated in Fig. 5.15. The modified accelerograms corresponding to each of the two earthquake components, prepared for different water levels assuming compressible water, are shown in Fig. 5.16. To obtain the modified ground accelerograms, a constant 0.25 % modal viscous damping ratio is considered for all the vibration modes of the tower without water, i.e. $\xi_j = 0.0025$ for $j = 1$ to 6, and the dynamic modal properties of the calibrated numerical model of the primary structure were used as shown in Fig. 5.13. For comparison purposes, the original ground motion accelerations are also shown in Fig. 5.16.

It is observed that the amplitudes of the modified accelerations differ from those of the original accelerograms for both earthquakes across all water level conditions. Increasing water levels result in higher peak ground acceleration (PGA) for both earthquakes. For example, in Fig. 5.16 (a) and (e), the PGA of the modified ground accelerogram corresponding to the half water level condition ($0.5H_{\mathrm{w}}$) increased by 57%, i.e. $(1.73 - 1.10)/1.10 \times 100$, while the modified ground accelerogram corresponding to the full water level condition (H_{w}) increased by 421%, i.e. $(5.74 - 1.10)/1.10 \times 100$. The increase in the PGA is due to the frequency content of the earthquake, the water level, and the damping which is very low in this structure. Fig. 5.16 (e) and (f) show the modified ground accelerograms generated for the Nahanni earthquake (1985) and the El Salvador earthquake (2001), respectively, for the full water condition. It is observed that the hydrodynamic effects cause a higher increase in PGA for the Nahanni earthquake (1985), with an increase of 421%, while for the EL Salvador earthquake (2001), the increase is 191%, i.e., $(1.17 - 0.40)/0.40 \times 100$. This is due to the differences in the frequency content of these two original ground accelerations. It is important to note that although an assumption of full wave reflection at reservoir bottom was used, the formulation proposed can also account for wave absorption at reservoir bottom due to sedimentation.

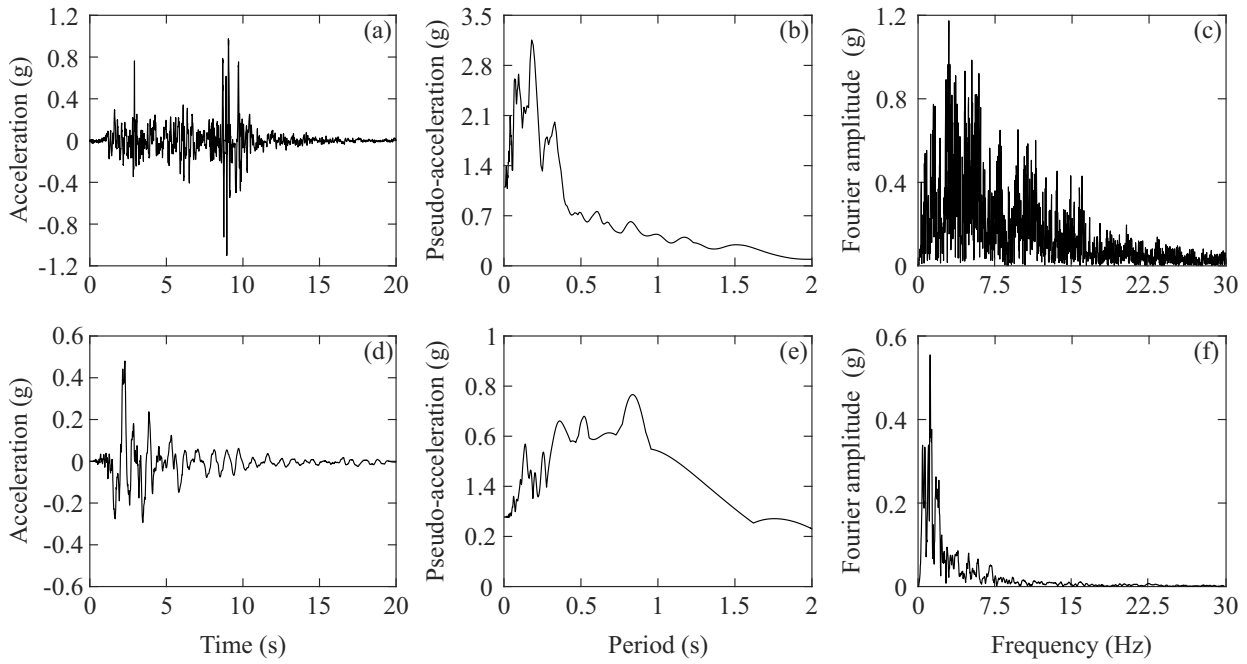

Figure 5.15 Time-history accelerations, pseudo-acceleration response spectra and Fourier amplitudes of the ground motions selected for this study: (a) to (c) Nahanni (1985) earthquake; (d) to (f) El Salvador (2001) earthquake.

Figure 5.17 depicts the modified ground accelerograms generated using the Morison's added mass formulation, assuming full water level condition (i.e. $H_{\mathrm{w}} = 2.96$) for both earthquakes. As observed, the amplification due to added mass effects is significantly higher for the Nahanni earthquake (1985) compared to the El Salvador earthquake (2001).

Figure 5.18 compares the impact of different water assumptions on the modified ground accelerograms. As clearly seen for the Nahanni earthquake in Fig. 5.18(a), using the simplified Morison's added mass formulation changes both the PGA and the frequency content of the original ground motion acceleration. The PGA slightly increases with the simplified water assumption, and there is also a noticeable time shift. For the El Salvador earthquake as shown in Fig. 5.18(b), during the strong phase of the ground motion acceleration (first 5 seconds), both water assumptions yield the same effects on the ground motion acceleration due to the hydrodynamic pressure.

5.5 Experimental and numerical results

The tests were conducted in different series. The first series focused on the response of the tower and its appurtenant structure without surrounding water (i.e. dry system). In these tests, the seismic response of the tower was assessed by applying the original ground

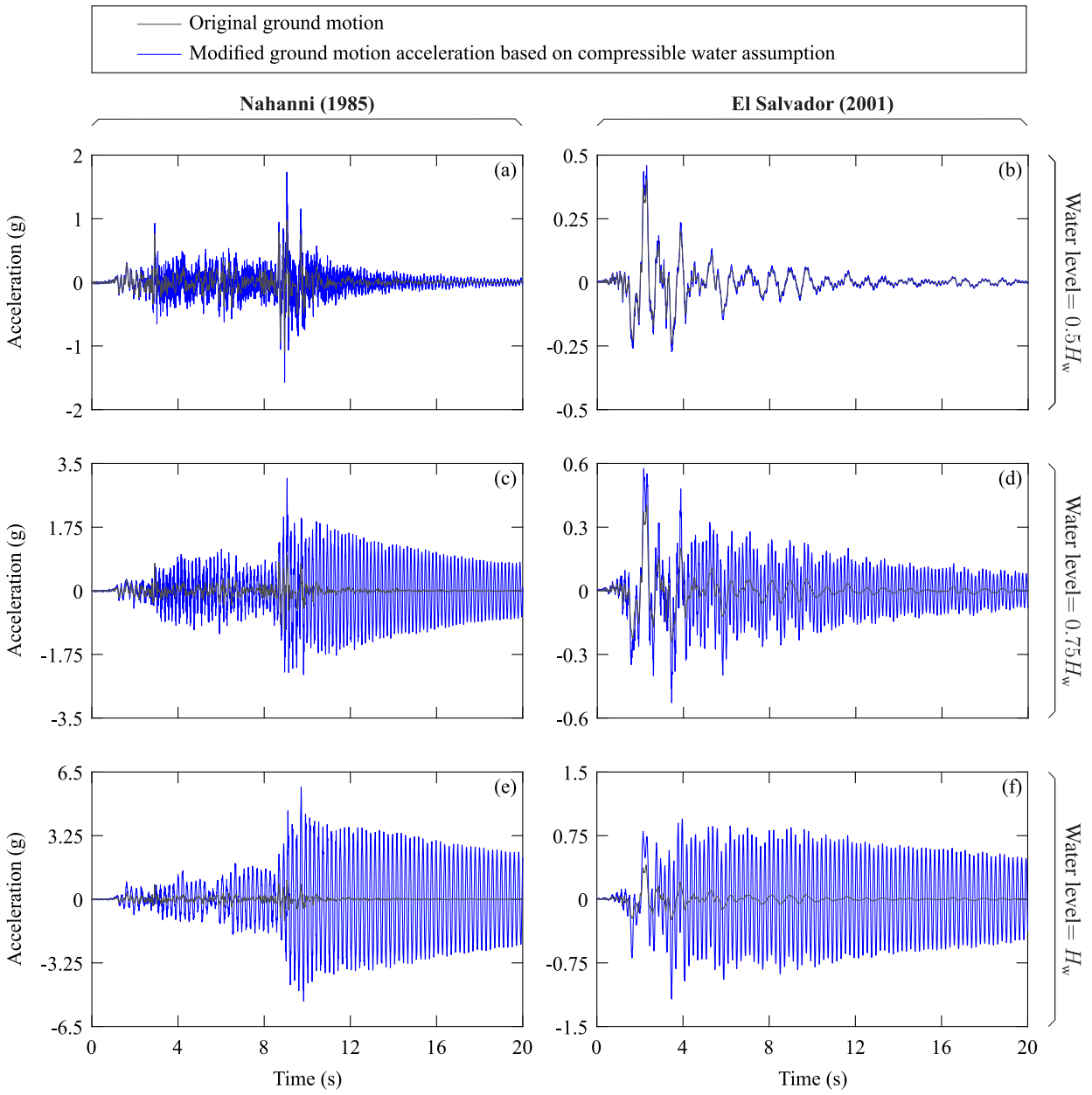

Figure 5.16 Original and modified ground accelerations generated for the tower with different water levels subjected to Nahanni (1985) and El Salvador (2001) earthquakes with compressible water assumption: (a) and (b) assuming water level to be $0.5H_w$; (c) and (d) assuming water level to be $0.75H_w$; (e) and (f) assuming water level to be H_w.

acceleration as the input signal for the shaking table, using scale factors of 25% and 50% to ensure that the structure remained within the elastic range throughout the testing.

Figures 5.19 and 5.20 illustrate the time histories of relative horizontal accelerations at points A and B of the studied structure, respectively, when subjected to 25% and 50% scaled

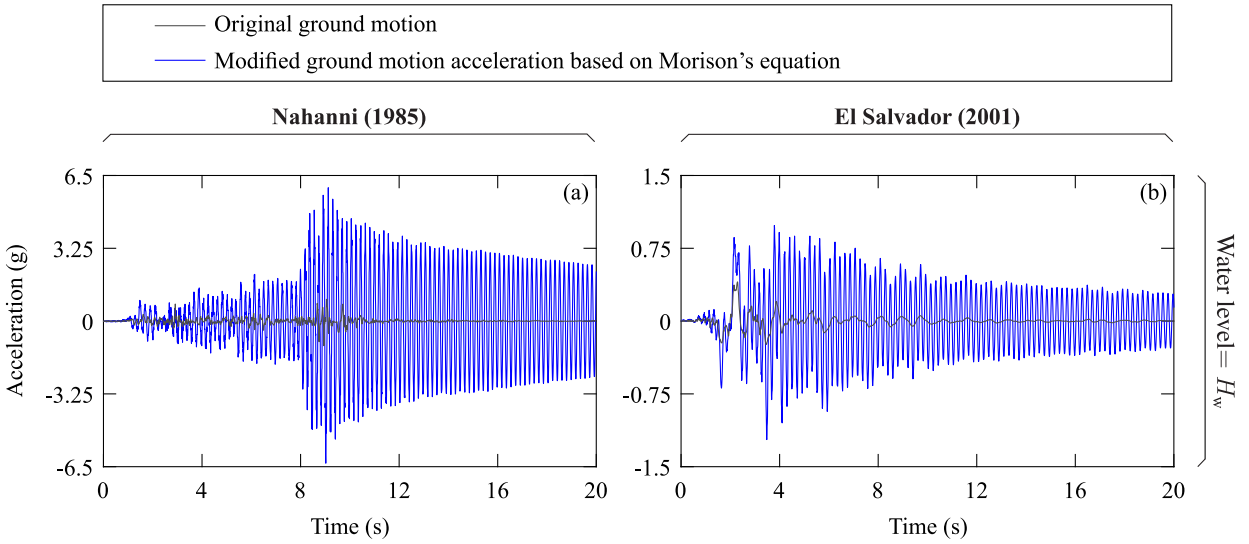

Figure 5.17 Original and modified ground accelerations generated for the tower subjected to Nahanni (1985) and El Salvador (2001) earthquakes with Morison's added mass formulation assuming water level to be H_w: (a) Nahanni (1985) earthquake; (b) El Salvador (2001) earthquakes.

Nahanni (1985) and El Salvador (2001) earthquakes. The blue curves represent the response data measured during the experimental tests, while the red curves depict the numerical results obtained from the finite element calibrated model, as detailed in the previous section.

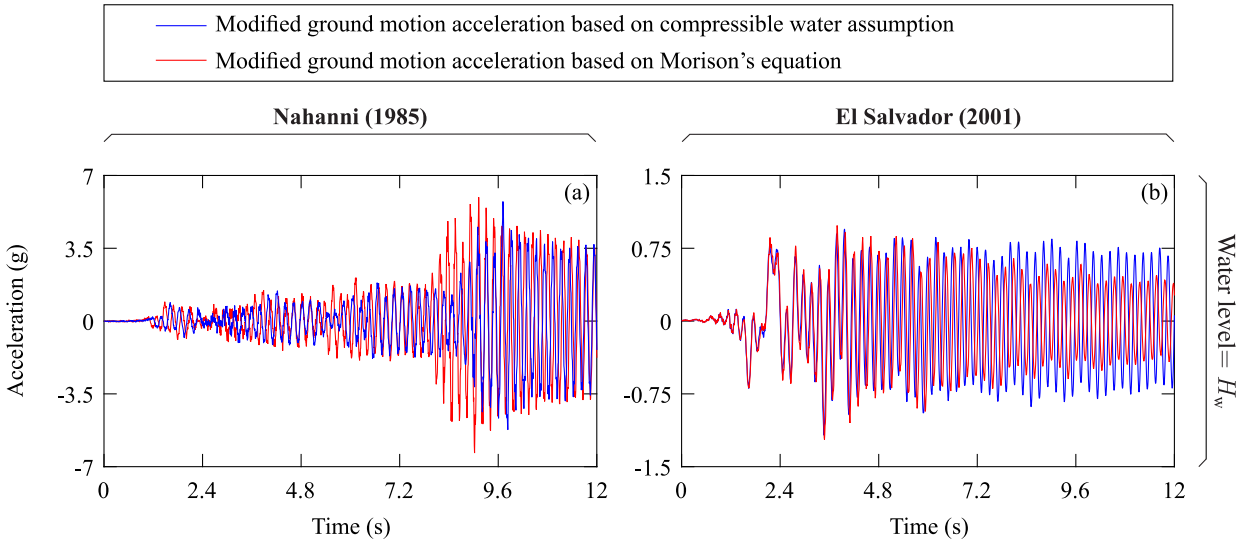

Figure 5.18 Comparison of modified ground accelerograms generated for the tower under two different water assumptions for the surrounding water, subjected to: (a) Nahanni (1985) earthquake; (b) El Salvador (2001) earthquake.

The results demonstrate excellent agreement between the numerical model and experimental data, indicating that the numerical model is well calibrated.

The second series of tests assumed the tower was surrounded by different water level heights ($0.5H_{\mathrm{w}}$, $0.75H_{\mathrm{w}}$, and H_{w}) and subjected to the Nahanni (1985) and El Salvador (2001) earthquakes. The shaking table tests were conducted by subjecting the structure to modified versions of the ground motion accelerations, which incorporate hydrodynamic effects. These modified ground motion accelerations were defined as new input signals for the shaking table control system. The tower's response in this set of tests resembled a system surrounded by *virtual water* with different water levels. The term "*virtual water*" is used because, although water is not physically present in the experimental tests, the use of modified ground acceleration effectively incorporates hydrodynamic fluid-structure interaction effects into the tower's response. Scaling factors starting at 10% were applied to the modified ground accelerograms and progressively increased until the response of the appurtenant structure exceeded the elastic range. To measure the structure's nonlinearity, one strain gauge was installed at the notch location, as previously described and shown in Fig.5.4 (a).

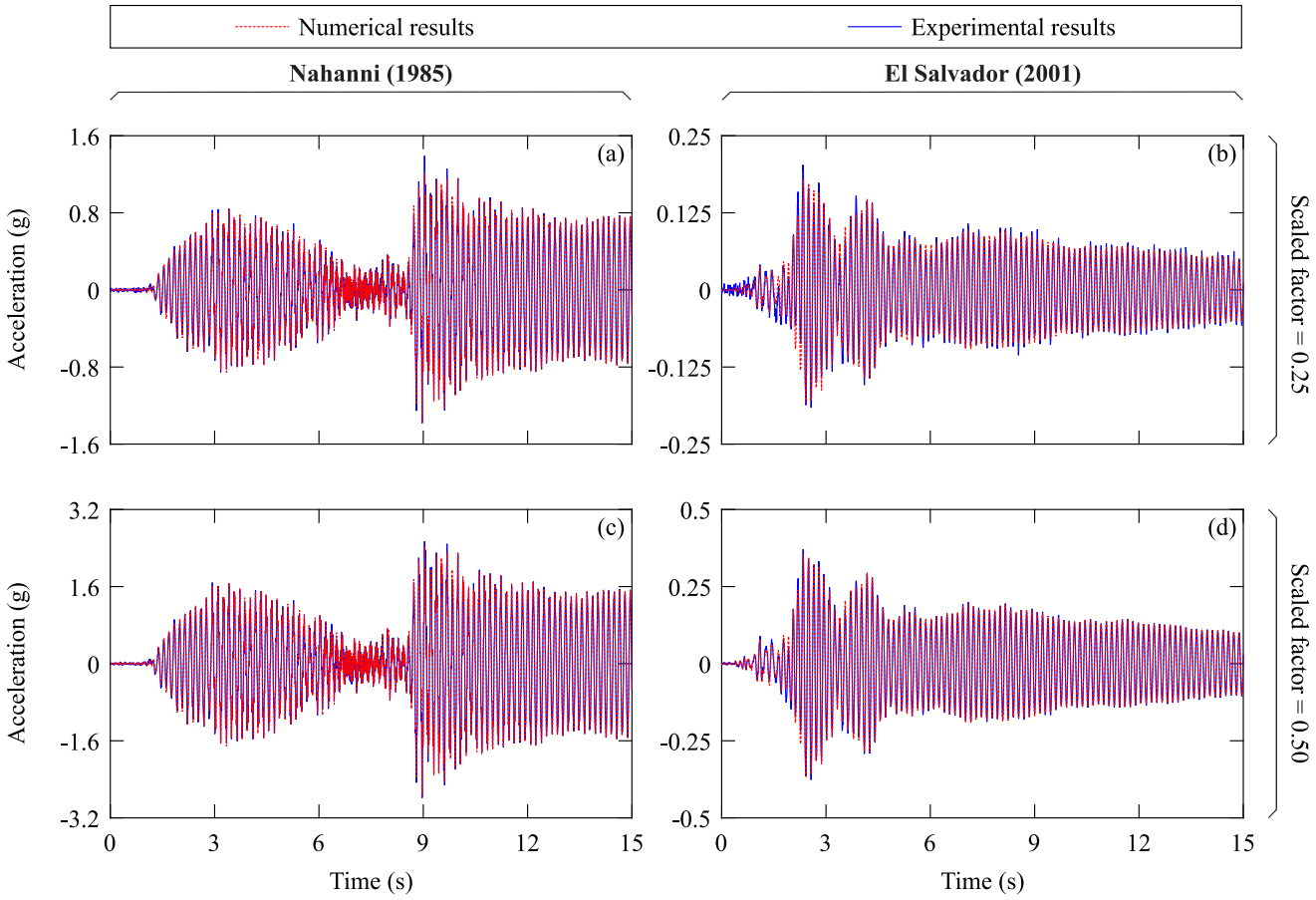

Figure 5.19 Time-histories of relative horizontal accelerations at point A of studied tower without water subjected to Nahanni (1985) and El Salvador (2001) earthquakes: (a) and (b) using 25% scaled factor; (c) and (d) using 50% scaled factor.

Figure 5.21 illustrates the time histories of relative horizontal accelerations at point A of the tower, surrounded by different water levels, assuming the water to be compressible and subjected to the Nahanni (1985) earthquake. The blue curves represent the experimental data measured during the shaking table test using the proposed method, while the red curves show the numerical results at point A obtained from the finite element model. There is an excellent agreement between the experimental test results and the reference solution.

As expected, increasing the water level from $0.5H_{\mathrm{w}}$ led to an increase in acceleration at point A. Surprisingly, despite the PGA of the modified ground acceleration for the case with full water level (H_{w}) was higher, as shown in Fig. 5.16, the maximum acceleration at point A was lower when the water level was increased to H_{w} compared to the maximum acceleration for the case with a $0.75H_{\mathrm{w}}$ water level. This is due to the difference in frequency content of the modified ground accelerograms. A similar observation can be made from Figure 5.22,

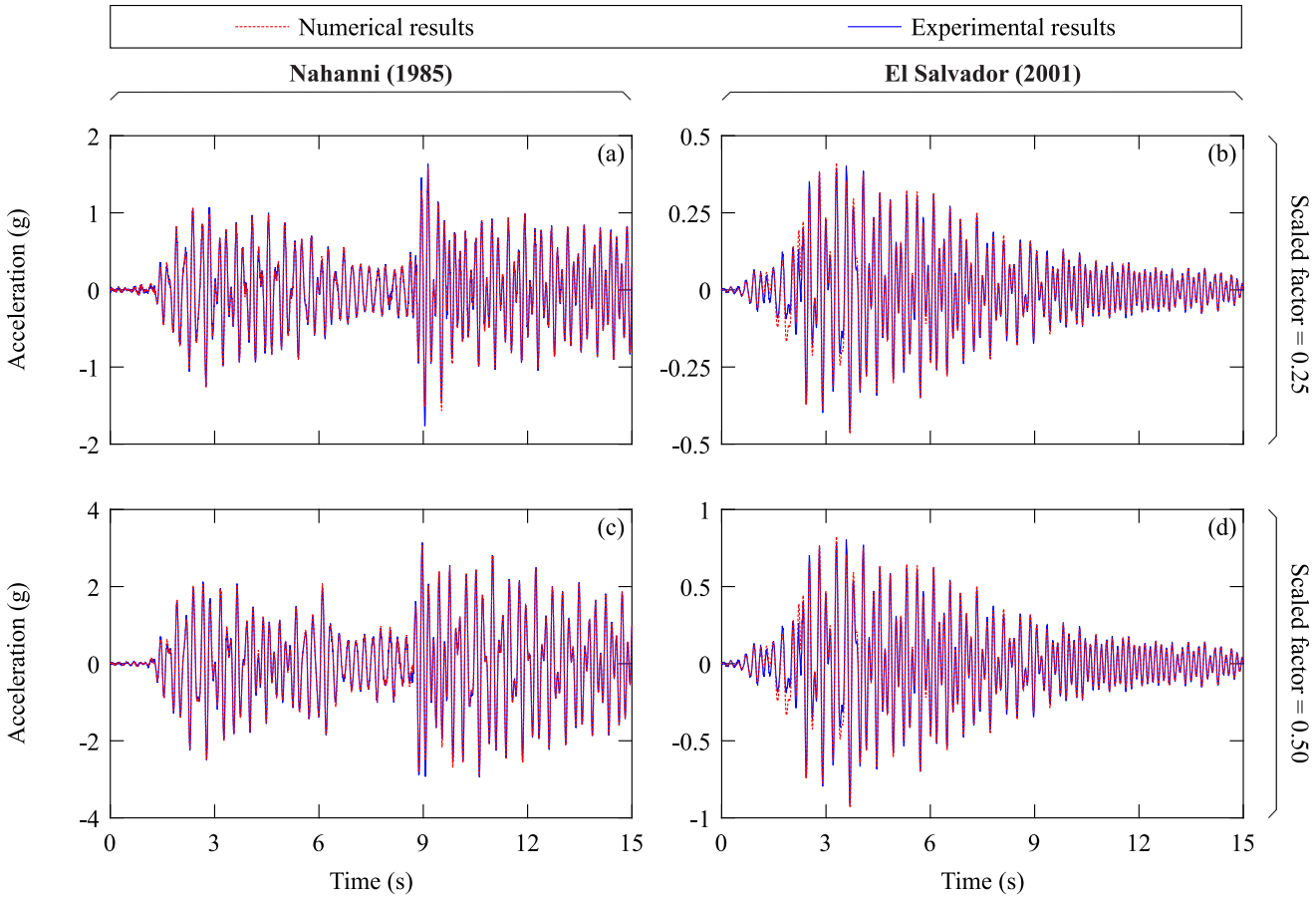

Figure 5.20 Time-histories of relative horizontal accelerations at point B of the appurtenant structure without water subjected to Nahanni (1985) and El Salvador (2001) earthquakes: (a) and (b) using 25% scaled factor; (c) and (d) using 50% scaled factor.

which illustrates the time histories of relative horizontal accelerations at point A of the tower, surrounded by different water levels, assuming the water to be compressible and subjected to the El Salvador (2001) earthquake. As seen, increasing the water level leads to an increase in the response of the structure. However, increasing the water level from $0.75H_{\mathrm{w}}$ to H_{w} has a similar effect on the maximum response values, while the time signature of the response shows distinct differences.

Figure 5.23 illustrates the time histories of relative horizontal accelerations of the appurtenant structure at point B for the Nahanni (1985) earthquake assuming compressible water surrounding the structure. As seen, increasing the water level led to an increase in the response of the appurtenant structure. For the system with a water level of $0.5H_{\mathrm{w}}$, nonlinearity occurred when the scaling factor reached to 30%, while for the other two cases ($0.75H_{\mathrm{w}}$ and H_{w}), the appurtenant structure experienced nonlinear responses at a 20% scaling factor. This

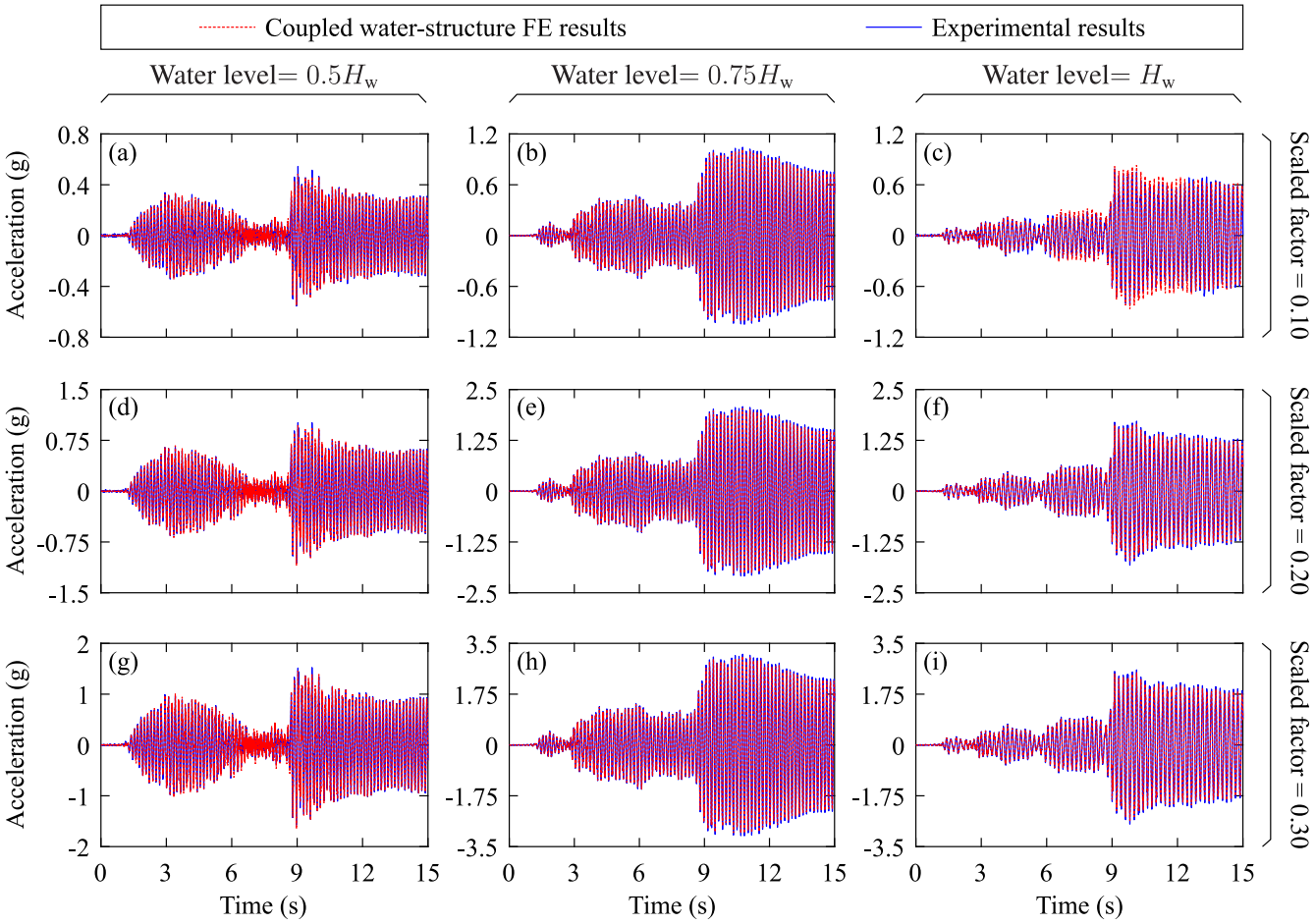

Figure 5.21 Time-histories of relative horizontal accelerations at point A of studied tower including hydrodynamic effects subjected to Nahanni (1985) earthquake considering compressible water assumption with different water levels: (a), (d) and (g) water level selected to be $0.5H_w$; (b), (e) and (h) water level selected to be $0.75H_w$; (c), (f) and (i) water level selected to be H_w.

is clearly shown in Fig. 5.25, which displays the strain gauge measured data at the notch location for the water level assumed to be H_w and subjected to the Nahanni (1985) earthquake considering compressible water assumption.

Similarly, Figure 5.24 illustrates the time histories of relative horizontal accelerations at point B of the appurtenant structure for the El Salvador (2001) earthquake assuming compressible water surrounding the structure. Once again, increasing the water level led to a corresponding increase in the response of the appurtenant structure. Due to the lower PGA of this earthquake, the appurtenant structure became nonlinear at a 50% scaling factor for the system with a water level of H_w. For water levels of $0.5H_w$ and $0.75H_w$, the appurtenant structure remained within the elastic range even at a 50% scaling factor. This behavior is

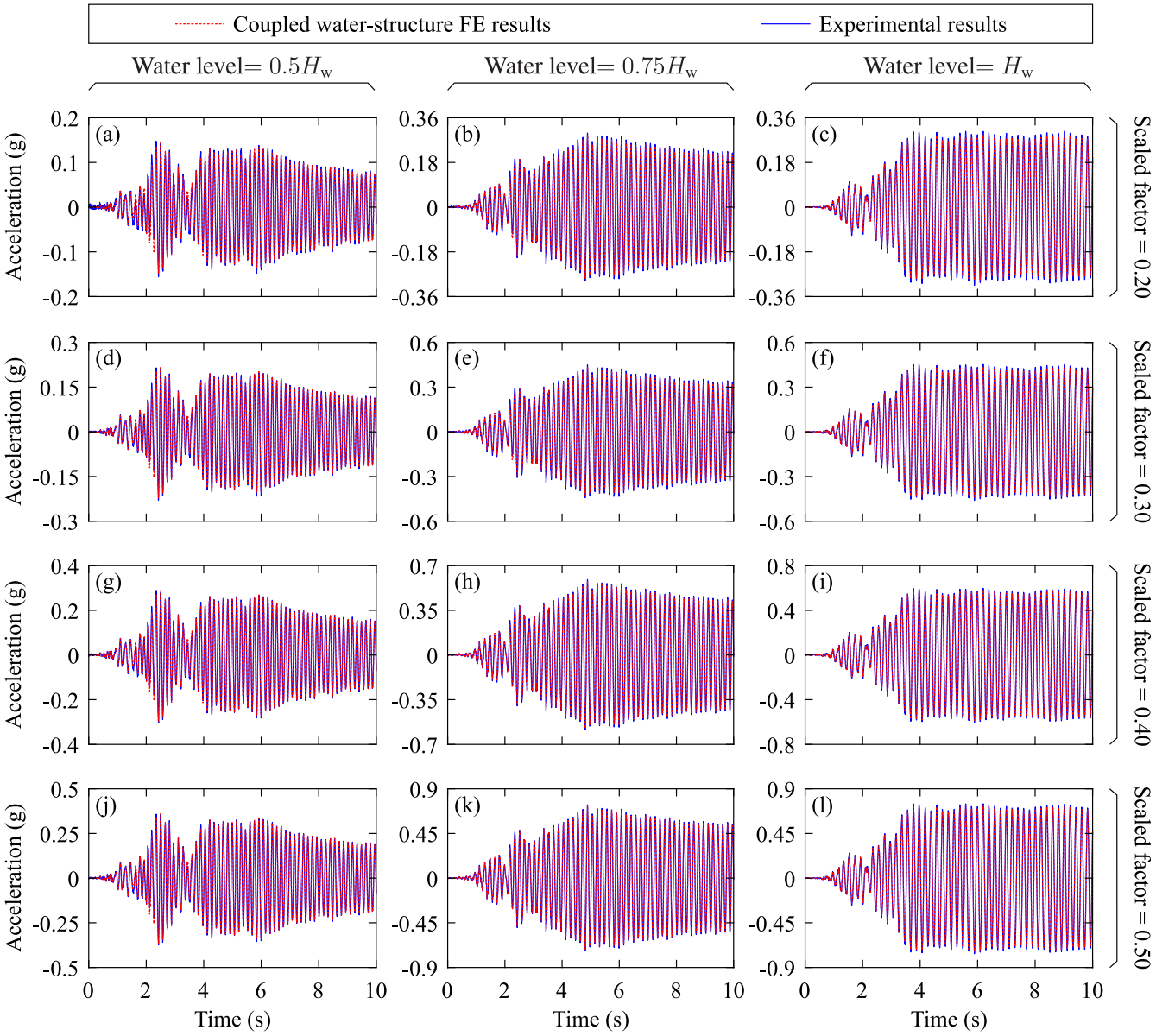

Figure 5.22 Time-histories of relative horizontal accelerations at point A of studied tower including hydrodynamic effects subjected to El Salvador (2001) earthquake considering compressible water assumption with different water levels: (a), (d), (g) and (j) water level selected to be $0.5H_w$; (b), (e), (h) and (k) water level selected to be $0.75H_w$; (c), (f), (i) and (l) water level selected to be H_w.

illustrated in Fig. 5.26, which shows the strain gauge data at the notch location for the water level H_w during the El Salvador (2001) earthquake. The displacement limitations of the shaking table prevented higher scaling factors to be tested.

Figures 5.23 and 5.24 also compared the reference solutions with experimental data. The

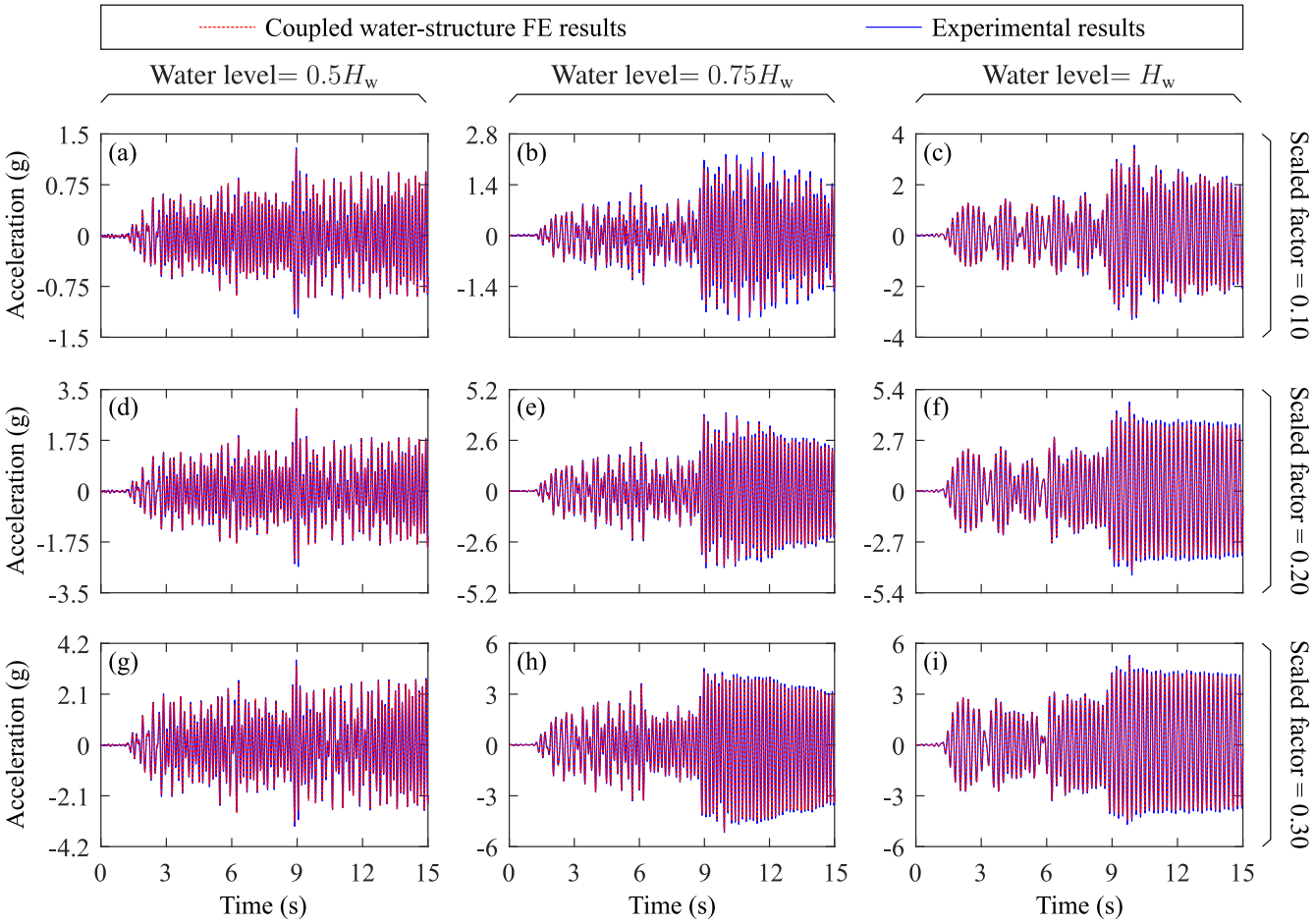

Figure 5.23 Time-histories of relative horizontal accelerations at point B of studied tower including hydrodynamic effects subjected to Nahanni (1985) earthquake considering compressible water assumption with different water levels: (a), (d) and (g) water level selected to be $0.5H_w$; (b), (e) and (h) water level selected to be $0.75H_w$; (c), (f) and (i) water level selected to be H_w.

blue curves represent the experimental data measured during the shaking table test using the proposed method, while the red curves show the numerical results at point A obtained from the finite element model. The agreement between these results is excellent, as clearly demonstrated in these figures. The slight discrepancies between the experimental results and the finite element results primarily stem from: (i) noise levels during the experimental tests, particularly noticeable in tests with lower scaling factors. It is observed that the agreement between numerical and experimental results improves as the scaling factor increases. (ii) since the modified ground accelerograms are generated based on analytical formulations, the finite element discretization and the far end location of the infinite boundary condition in the coupled structure-water finite element model can also cause slight differences. (iii) Damping

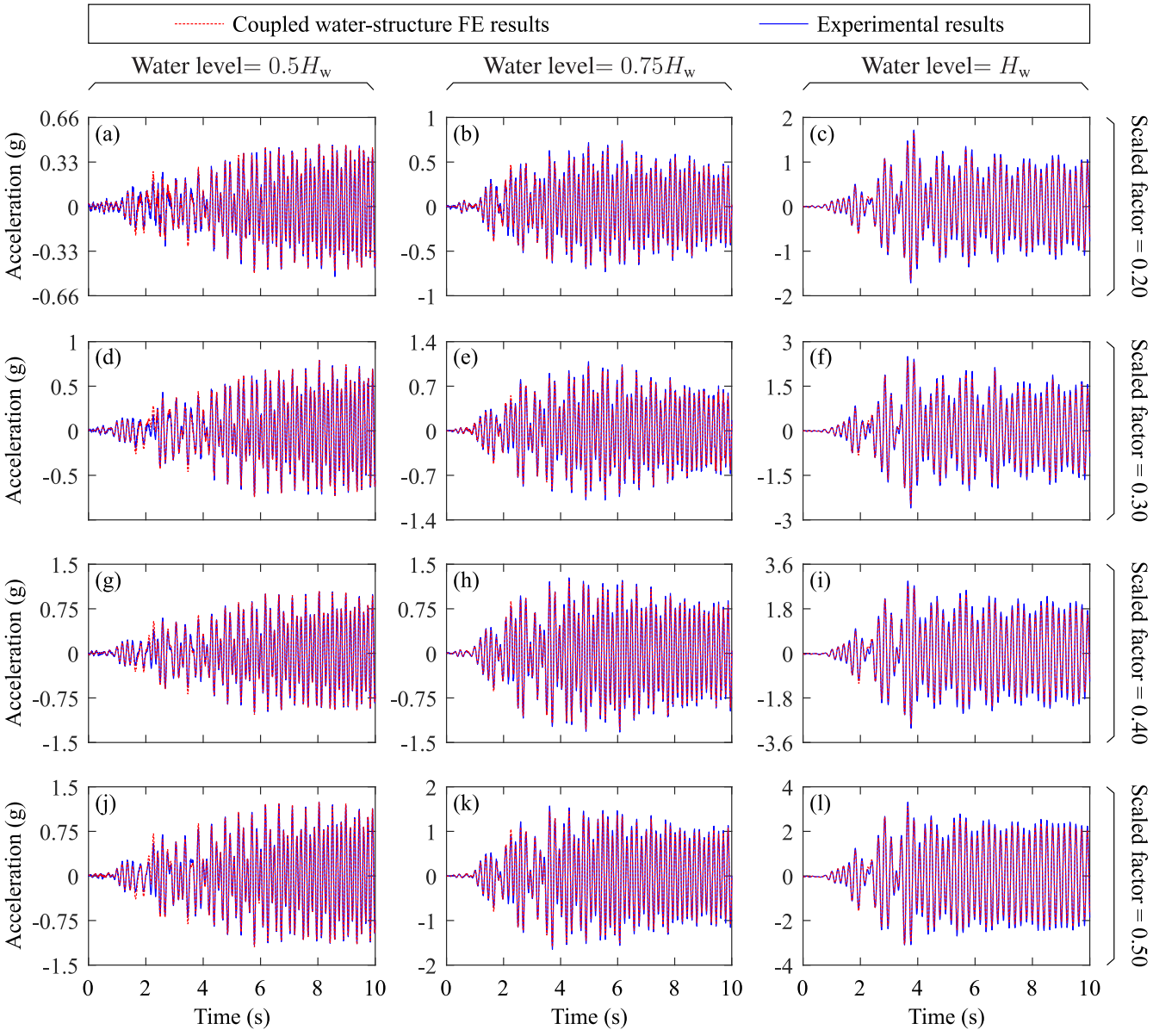

Figure 5.24 Time-histories of relative horizontal accelerations at point B of studied tower including hydrodynamic effects subjected to El Salvador (2001) earthquake considering compressible water assumption with different water levels: (a), (d), (g) and (j) water level selected to be $0.5H_w$; (b), (e), (h) and (k) water level selected to be $0.75H_w$; (c), (f), (i) and (l) water level selected to be H_w.

is another factor that can contribute to discrepancies; the use of modal damping versus Rayleigh damping, along with the inherent damping of the specimen, adds complexity to the system.

Figures 5.25 and 5.26 show the the time history of measured strain gauge values at the notch

location of the appurtenant structure for Nahanni (1985) and El Salvador (2001) earthquakes, respectively.In these figures, the 25% and 50% scaling factors represent the measured data from the tests where the tower was subjected to the original acceleration. In Fig. 5.25, the 10% and 20% scaling factors correspond to the tests where the structure was subjected to modified ground acceleration, assuming a water level of H_{w} and considering the compressible water assumption. Similarly, in Fig. 5.26, the 20% and 50% scaling factors correspond to tests where the structure was subjected to modified ground acceleration.

In Figs 5.25 and 5.26, (a) illustrates the time history of strain measured with the strain gauge glued at the notch location of the appurtenant structure, (b) shows the strain-acceleration curve, where the acceleration is the response at point B measured using accelerometer No. 2 (Fig. 5.3). The maximum shear stress ($|\tau_{xz}|^{(\max)}$) at the notch, obtained from the finite element model, is shown in Fig. 5.25(c).

Additional series of tests were conducted using modified accelerograms of the considered earthquakes, generated with Morison's added mass formulation to account for hydrodynamic added mass effects assuming full water level of H_{w}. Figure 5.27 presents the time histories of relative horizontal accelerations at points A and B of studied structure subjected to modified ground motion acceleration of Nahanni (1985) earthquake. Two scaling factor considered in this tests as shown in Fig. 5.27. Figures 5.28 also shows the acceleration response at points A and B of studied structure subjected to modified ground motion acceleration of El Salvador (2001) earthquake. Three scaling factor considered in this tests as shown in Fig. 5.28. In Both figures, red curves are the numerical results, while he blue curves show the experimental measure data. This approach models the hydrodynamic effects through added masses without the need to lump masses at the nodes or alter the material density to account for the added mass effects [171, 172].

5.6 Summary and Conclusions

The primary novelty of the proposed experimental program lies in the incorporation of earthquake-induced water effects into modified versions of the original ground motion accelerations, effectively eliminating the need for actual water presence in the experimental setup. Previous studies have shown that seismic response investigations of structure-water systems typically require specialized facilities, such as underwater shaking tables, and specialized instrumentation to capture responses underwater, which also pose safety concerns like water leakage. Furthermore, when similitude laws are applied to scale down specimens for experimental testing, the properties of the water in the underwater shaking table must also be modified in accordance with these laws, which can be challenging. Another approach

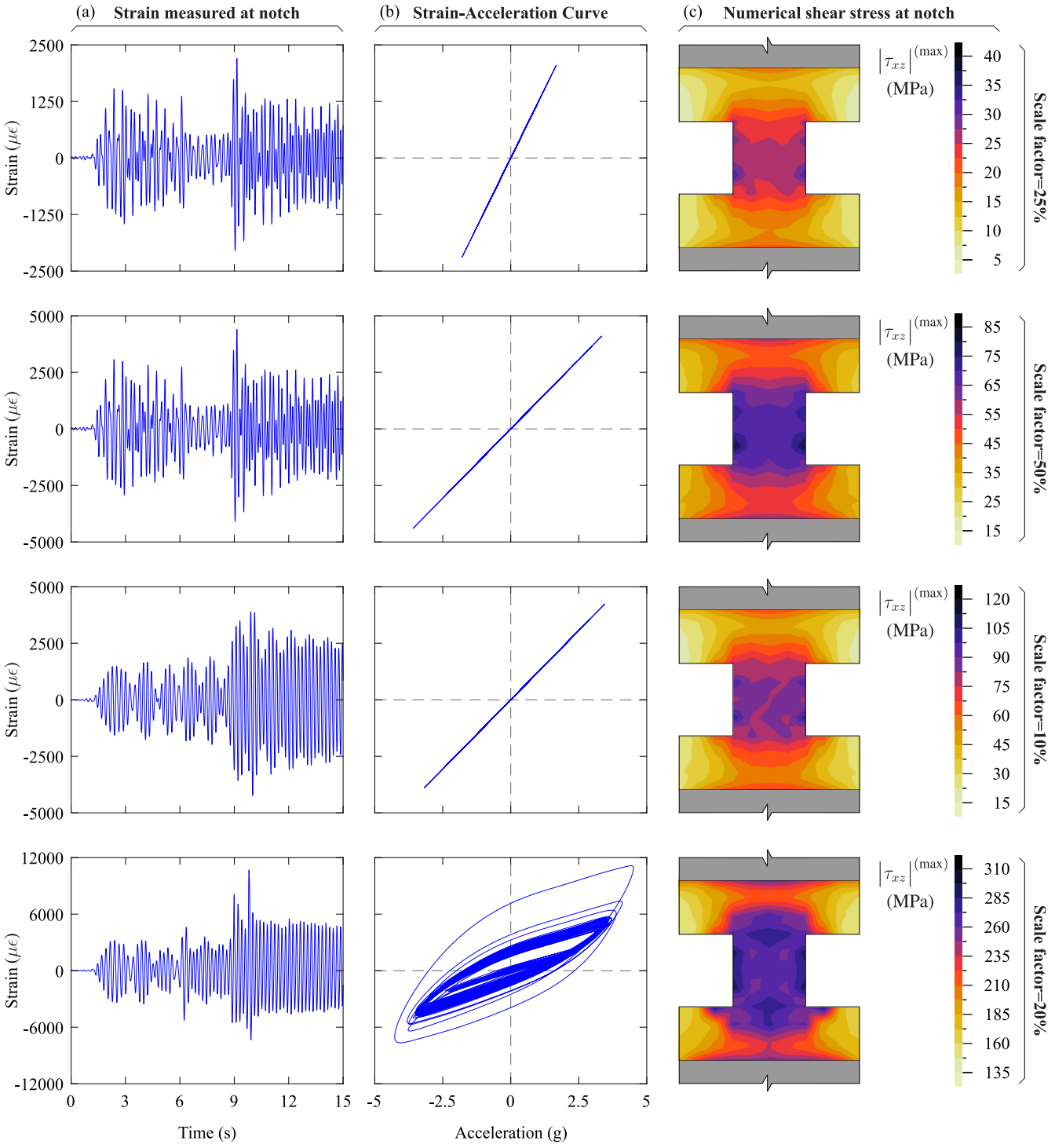

Figure 5.25 Strain-acceleration curve and maximum shear stress developed at notch location subjected to Nahanni (1985) earthquake: (a) strain measured using the strain gauged installed at the notch location; (b) strain-acceleration curve; (c) maximum shear stresses τ_{xy} developing within the notch of the appurtenant structure.

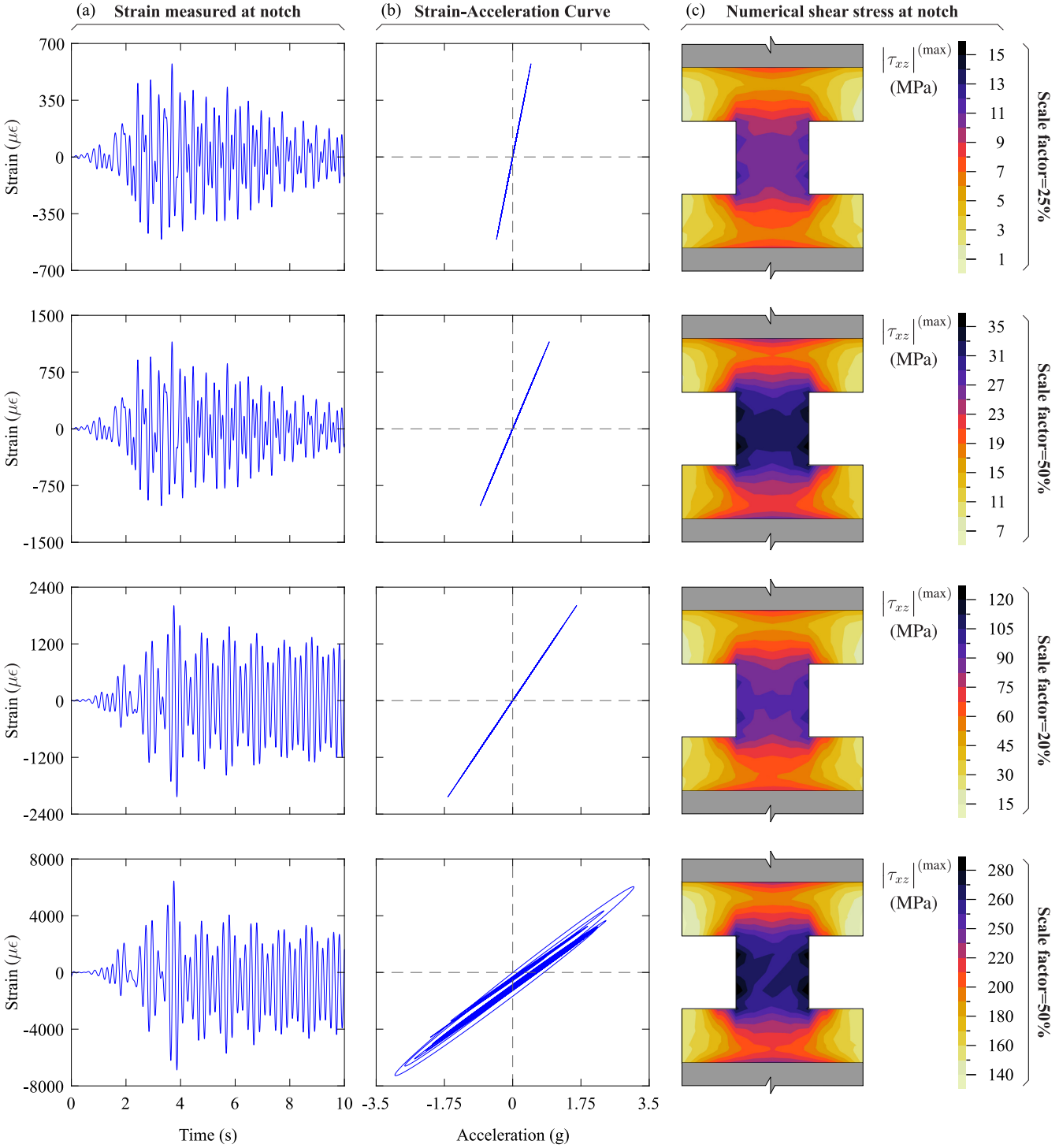

Figure 5.26 Strain-acceleration curve and maximum shear stress developed at notch location subjected to El Salvador (2001) earthquake: (a) strain measured using the strain gauged installed at the notch location; (b) strain-acceleration curve; (c) maximum shear stresses τ_{xy} developing within the notch of the appurtenant structure.

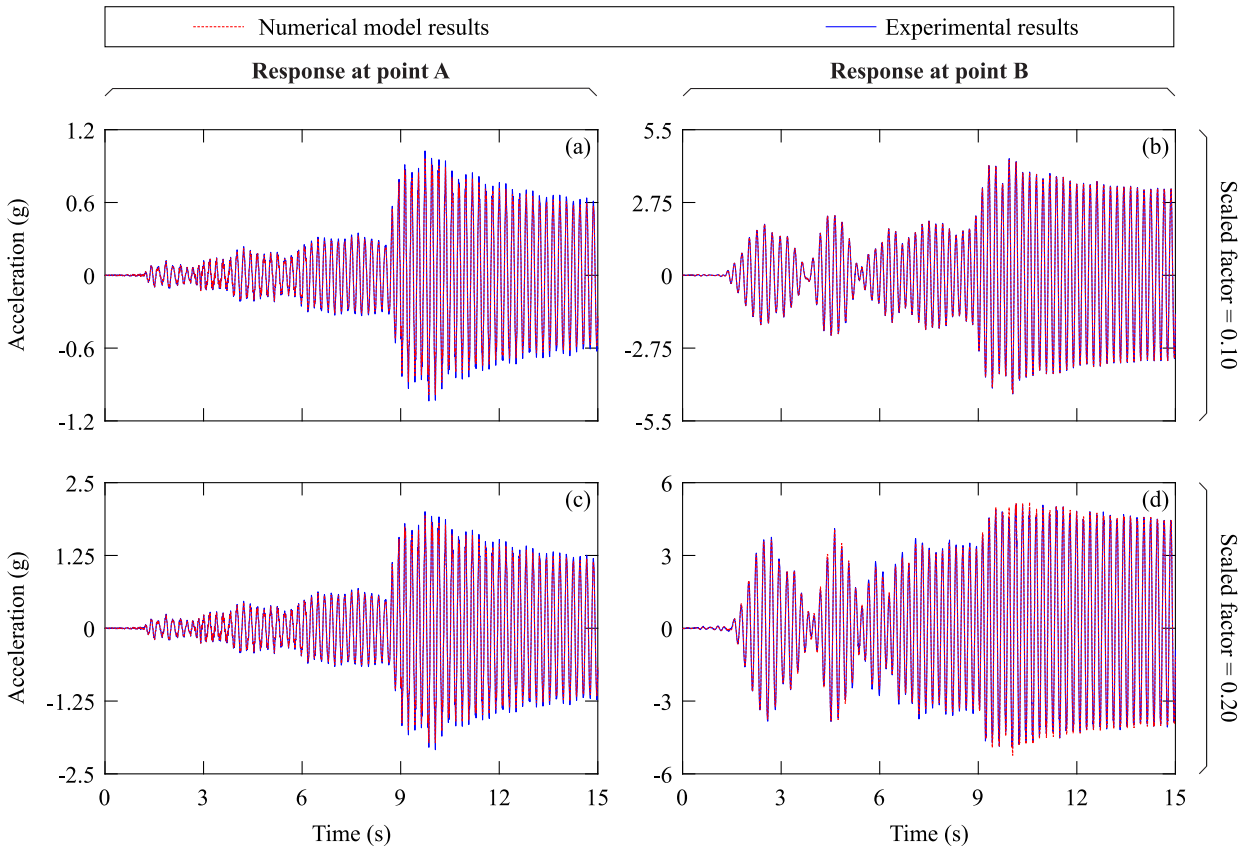

Figure 5.27 Time-histories of relative horizontal accelerations at points A and B of studied structure including hydrodynamic effects subjected to Nahanni (1985) earthquake considering added mass formulation and assuming full water level of H_w: (a) and (c) acceleration response at point A; (b) and (d) acceleration response at point B.

used for shaking table tests of structure-water systems involves the simplified added mass concept, which presents two significant challenges. Firstly, distributing the added mass over the height of the specimen is challenging. Secondly, this simplified method relies on several assumptions that may not be valid in all situations. This underscores the need for alternative methods that can more reliably simulate the dynamic effects of water on structures.

The methodology utilizes analytical formulations of earthquake-induced hydrodynamic pressure within the fluid domain or employs simplified added masses to generate modified ground motion accelerograms. These modified versions of the original ground acceleration can then be used as input signals for shaking table tests. This approach overcomes the challenges previously mentioned and enables innovative shaking table tests on a standard shaking table in a safe environment, thereby significantly enhancing both feasibility and safety. The proposed experimental program was then used to investigate the seismic response of an axisymmetric structure surrounded by water and its appurtenant structure. The experimental tests were

conducted in the following steps: (i) evaluating the dynamic properties of the specimen, including natural frequencies and damping ratio; (ii) building and calibrating a numerical model of the dry specimen using any standard finite element structural engineering software; (iii) generating modified ground accelerograms for the Nahanni (1985) and El Salvador (2001) earthquakes at different water levels ($0.5H_{\mathrm{w}}$, $0.75H_{\mathrm{w}}$, and H_{w}) using a compressible

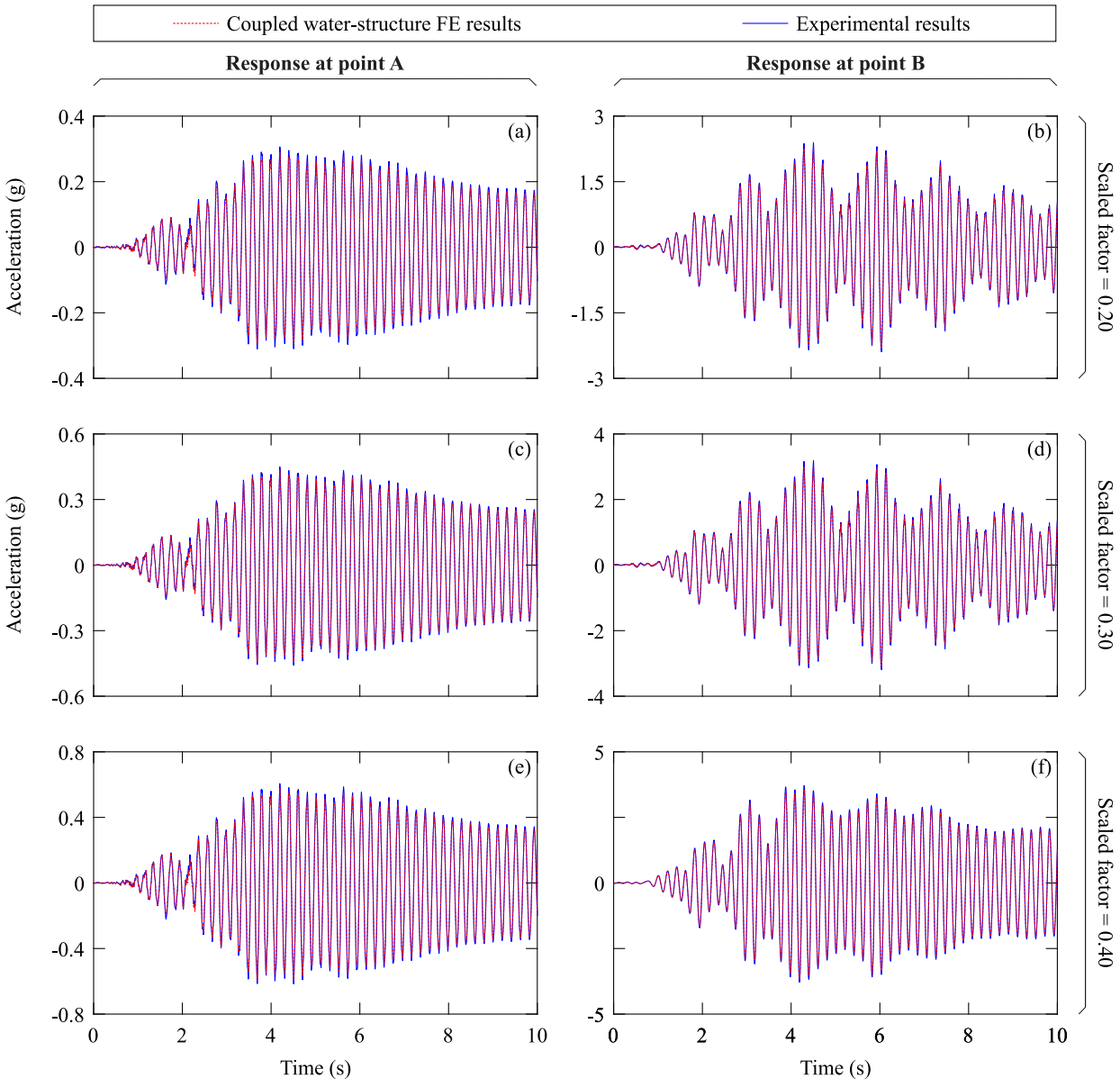

Figure 5.28 Time-histories of relative horizontal accelerations at points A and B of studied structure including hydrodynamic effects subjected to El Salvador (2001) earthquake considering added mass formulation and assuming full water level of H_{w}: (a), (c) and (e) acceleration response at point A; (b), (d) and (f) acceleration response at point B.

water assumption and simplified Morison's added mass formulation to include hydrodynamic effects; (iv) applying the modified ground accelerograms as input ground motion signals for shaking table tests.

An appurtenant structure with a notch was utilized to examine the seismic linear and nonlinear responses. The study showed the amplification effects due to the flexibility of the primary structure and hydrodynamic effects. For the Nahanni (1985) earthquake, amplification due to the primary structure's flexibility alone exceeded six times, whereas for the El Salvador (2001) earthquake, it was more than twice. The experiments demonstrated that including hydrodynamic effects further increased amplification: more than 6.5 times, 12 times, and 10 times for water levels of $0.5H_{\mathrm{w}}$, $0.75H_{\mathrm{w}}$, and H_{w}, respectively, under the Nahanni (1985) earthquake. For the El Salvador (2001) earthquake, these amplification factors changed to 2.5 times, 4 times, and 5 times for water levels of $0.5H_{\mathrm{w}}$, $0.75H_{\mathrm{w}}$, and H_{w}, respectively.

The measured response of the structure was also compared with numerical results obtained from finite element models, showing excellent agreement. The findings were analyzed to emphasize the combined influence of hydrodynamic effects and structural flexibility on the seismic behavior of the studied specimen and its appurtenant structure. Despite the good correlation between the experimental and numerical results for the dynamic responses, caution and engineering judgment must be applied when generalizing these experimental results.

In this research, an axisymmetric structure surrounded by water was chosen as the focus of the study. The method developed for modified ground acceleration is versatile and can be applied to various other types of structure-water systems.

CHAPTER 6 DISCUSSION

6.1 Objectives of the discussion

This discussion section provides a thorough analysis of the proposed seismic analysis method for structure-water systems using modified ground motion acceleration methods, emphasizing its numerical validation, practical application using general-purpose software, and experimental considerations for shaking table test of structure-water system. The method is validated by analyzing how structural flexibility and water levels influence and amplify the modified ground acceleration, altering its frequency content. A mathematical derivation of the closed-form equation for modified ground acceleration, considering fundamental mode, is provided. The discussion also explores the practical application of the method using general-purpose software like SAP2000, applying it to the seismic analysis of dam-reservoir systems and axisymmetric structures surrounded by water, effectively incorporating hydrodynamic effects without the need for a fluid domain. Additionally, this section discusses the experimental approach for shaking table tests on structure-water systems, focusing on the selection of an axisymmetric structure surrounded by water due to laboratory constraints. It provides a detailed analysis of the rationale behind this choice and examines the effects of low damping on modified ground acceleration.

6.2 Numerical validation of proposed method

In this section, the proposed method is further validated by evaluating the effects of structural flexibility and water levels on modified ground acceleration. These factors contribute to both amplifying the original ground acceleration and altering its frequency content. A detailed mathematical derivation is provided to obtain the closed-form equation for modified ground acceleration considering fundamental mode. To illustrate the method's versatility across different frequency ranges, various harmonic excitations are examined. Furthermore, the method is validated through two case studies: Pine Flat Dam, which represents a dam-reservoir system, and San Bernardino Intake Tower, which represents an axisymmetric structure surrounded by water.

6.2.1 Frequency effects on the modified ground acceleration

The formulation of the *modified* ground acceleration was developed based on a unit horizontal harmonic *original* ground acceleration $\ddot{x}_{\mathrm{g}}(t) = \mathrm{e}^{\mathrm{i}\omega t}$, with ω as the forcing frequency. This

formulation can be extended to any arbitrary ground acceleration through Fourier transform. In this section, the mathematical representation of the modified ground acceleration is presented in more detail. Considering only fundamental mode, modal equation of motion for fundamental mode for the dam-reservoir system subjected to original ground motion harmonic excitation acceleration $\ddot{x}_{\mathrm{g}}(t) = \mathrm{e}^{\mathrm{i}\omega t}$ having can be written as [26, 41]

$$M_1 \left(-\omega^2 + 2\,\mathrm{i}\,\xi_1\,\omega\,\omega_1 + \omega_1^2 \right) \widehat{Z}_1(\omega) = -L_1 + \int_0^{H_{\mathrm{w}}} p(y,\omega)\,\psi_1^{(x)}(y)\,\mathrm{d}y \tag{6.1}$$

with $\widehat{Z}_1$ denotes generalized coordinates of dam-reservoir system. By separating FRF of hydrodynamic pressure $p(y,\omega) = p_0(y,\omega) - \omega^2\,\widehat{Z}_1(\omega)\,p_1(y,\omega)$, the modal equation of motion can be written as [26, 41]

$$\left[M_1 \left(-\omega^2 + 2\,\mathrm{i}\,\xi_1\,\omega\,\omega_1 + \omega_1^2 \right) + \omega^2 \vartheta_{1,1}(\omega) \right] \widehat{Z}_1(\omega) = -L_1 + \vartheta_{0,1}(\omega) \tag{6.2}$$

with

$$\vartheta_{0,1}(\omega) = \int_0^{H_{\mathrm{w}}} p_0(y,\omega)\,\psi_1^{(x)}(y)\,\mathrm{d}y\,; \qquad \vartheta_{1,1}(\omega) = \int_0^{H_{\mathrm{w}}} p_1(y,\omega)\,\psi_1^{(x)}(y)\,\mathrm{d}y \tag{6.3}$$

The modal equation of motion for fundamental mode for the dry dam (i.e. without water) subjected to modified ground acceleration including fundamental mode $a_{\mathrm{g}}^{(1)}(\omega) \times \mathrm{e}^{\mathrm{i}\omega t}$ can be written as

$$M_1 \left(-\omega^2 + 2\,\mathrm{i}\,\xi_1\,\omega\,\omega_1 + \omega_1^2 \right) \widetilde{Z}_1(\omega) = -L_1 a_{\mathrm{g}}^{(1)}(\omega) \tag{6.4}$$

with $\widetilde{Z}_1$ denotes generalized coordinates of dry dam subjected to modified ground motion acceleration. For a dam with empty reservoir subjected to original ground motion harmonic excitation acceleration $\ddot{x}_{\mathrm{g}}(t) = \mathrm{e}^{\mathrm{i}\omega t}$, the modal equation of motion for fundamental mode can be rewrite as

$$M_1 \left(-\omega^2 + 2\,\mathrm{i}\,\xi_1\,\omega\,\omega_1 + \omega_1^2 \right) Z_1(\omega) = -L_1 \tag{6.5}$$

with Z_1 denotes generalized coordinates of dry dam subjected to original ground motion. From Equations (6.2), (6.4), and (6.5), $\widehat{Z}_1(\omega)$, $\widetilde{Z}_1(\omega)$, and $Z_1(\omega)$ can be rewritten as

$$\widehat{Z}_1(\omega) = \frac{L_1}{M_1} \times \frac{1 - \vartheta_{0,1}(\omega)/L_1}{\left[1 - \vartheta_{1,1}(\omega)/M_1 \right] \omega^2 - 2\,\mathrm{i}\,\xi_1\,\omega\,\omega_1 - \omega_1^2} \tag{6.6}$$

$$\widetilde{Z}_1(\omega) = \frac{L_1}{M_1} \times \frac{1}{\left(\omega^2 - 2\,\mathrm{i}\,\xi_1\,\omega\,\omega_1 - \omega_1^2 \right)}\, a_{\mathrm{g}}^{(1)}(\omega) \tag{6.7}$$

$$Z_1(\omega) = \frac{L_1}{M_1} \times \frac{1}{\left(\omega^2 - 2\,\mathrm{i}\,\xi_1\,\omega\,\omega_1 - \omega_1^2 \right)} \tag{6.8}$$

Assuming both system give the same response, the modal displacement at a point (x, y) of the dam can be written as

$$\widehat{u}_1(x, y, \omega) = \widetilde{u}_1(x, y, \omega) \tag{6.9}$$

$$\widehat{Z}_1(\omega)\, \psi_1(x, y) = \widetilde{Z}_1(\omega)\, \psi_1(x, y) \tag{6.10}$$

$$\widehat{Z}_1(\omega) = \widetilde{Z}_1(\omega) = Z_1(\omega) \times a_{\mathrm{g}}^{(1)}(\omega) \tag{6.11}$$

Therefore, the modified ground acceleration $a_{\mathrm{g}}^{(1)}(\omega)$ can be expressed as

$$a_{\mathrm{g}}^{(1)}(\omega) = \frac{\widehat{Z}_1(\omega)}{Z_1(\omega)} \tag{6.12}$$

$$\begin{aligned}
a_{\mathrm{g}}^{(1)}(\omega) &= \frac{\dfrac{L_1}{M_1} \times \dfrac{1 - \vartheta_{0,1}(\omega)/L_1}{\left[1 - \vartheta_{1,1}(\omega)/M_1\right] \omega^2 - 2\,\mathrm{i}\,\xi_1\,\omega\,\omega_1 - \omega_1^2}}{\dfrac{L_1}{M_1} \times \dfrac{1}{\left(\omega^2 - 2\,\mathrm{i}\,\xi_1\,\omega\,\omega_1 - \omega_1^2\right)}} \\
&= \left[1 - \frac{\vartheta_{0,1}(\omega)}{L_1}\right] \left[\frac{\left[1 - \vartheta_{1,1}(\omega)/M_1\right] \omega^2 - 2\,\mathrm{i}\,\xi_1\,\omega\,\omega_1 - \omega_1^2}{\omega^2 - 2\,\mathrm{i}\,\xi_1\,\omega\,\omega_1 - \omega_1^2}\right]^{-1} \\
&= \left[1 - \frac{\vartheta_{0,1}(\omega)}{L_1}\right] \left[1 - \frac{\left[\vartheta_{1,1}(\omega)/M_1\right] \omega^2}{\omega^2 - 2\,\mathrm{i}\,\xi_1\,\omega\,\omega_1 - \omega_1^2}\right]^{-1} \\
&= \left[1 - \frac{\vartheta_{0,1}(\omega)}{L_1}\right] \left[1 - \frac{\vartheta_{1,1}(\omega)}{M_1\left(1 - 2\,\mathrm{i}\,\xi_1\,\omega_1/\omega - \omega_1^2/\omega^2\right)}\right]^{-1}
\end{aligned} \tag{6.13}$$

To illustrate the effects of $a_{\mathrm{g}}^{(1)}(\omega)$ on the frequency content of original ground motion acceleration, Equation (6.13) is plotted for two gravity dam monoliths, D35 and D90, with heights H_{s} of 35 m and 90 m, respectively. Three water levels H_{w}, $0.75H_{\mathrm{w}}$, and $0.5H_{\mathrm{w}}$ are considered, with maximum heights H_{w} of 32 m for D35 and 86 m for D90. The geometries of both dam-reservoir systems are illustrated in Figure 6.1. It is worth mentioning that the changes in the frequency content of the original ground motion acceleration result from hydrodynamic effects, which are caused by both the added mass of water and variations in damping due to fluid-structure interaction.

Figure 6.2 illustrates the variation of absolute value of this complex-valued $a_{\mathrm{g}}^{(1)}(\omega)$ for both dams with three different water levels, covering forcing frequencies from 0 to 30 Hz for dam D35 and 0 to 10 Hz for dam D90. The fundamental natural frequencies of Dams D35 and

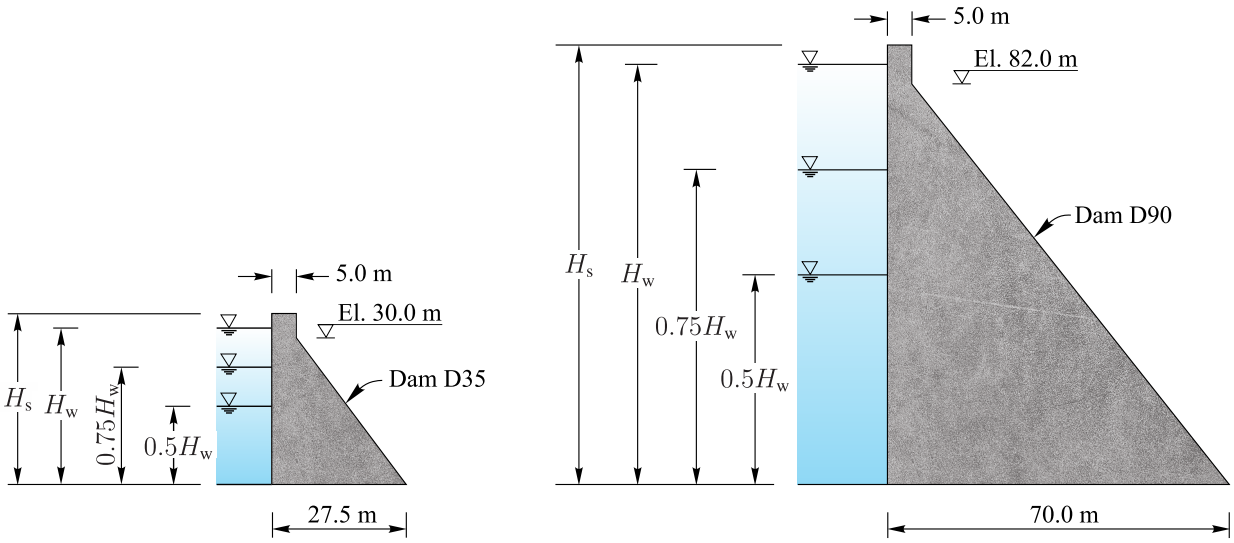

Figure 6.1 Dimensions of the studied dam-reservoir systems having three water levels H_w, $0.75H_w$, and $0.5H_w$.

D90, are 10.99 Hz and 4.76 Hz respectively, and indicated in the figure. It is evident that for both dams, when the reservoir water levels are at H_w or $0.75H_w$, $\left|a_g^{(1)}(\omega)\right|$ has a value lower than 1 at the forcing frequency equal to the fundamental natural frequency of the dams, as shown in Figures 6.2 (a), (b), (c), and (d). This indicates that the magnitude of the original ground acceleration in the frequency domain at these forcing frequencies will be reduced due to the dam-reservoir interaction at these specific frequencies. When the water level is at $0.5H_w$ for both dams, $\left|a_g^{(1)}(\omega)\right|$ is greater than one, as shown in Figures 6.2 (e) and (f). This indicates that the magnitude of the original ground acceleration in the frequency domain at these forcing frequencies will be increased.

For both dams, with reservoirs at a height of H_w, the maximum increase of $\left|a_g^{(1)}(\omega)\right|$ occurred at a forcing frequency lower than the fundamental natural frequency of the dry dams (i.e., without water). These peaks represent the fundamental natural vibration frequency of the dam-reservoir system, indicating that the presence of water makes the system more flexible due to hydrodynamic added masses. This shows that the amplitude of the original ground motion acceleration at these forcing frequencies can increase up to 6 times for dam D35 and 12 times for dam D90, as shown in Figures 6.2 (a) and (b). In Figures 6.2 (c), (d), (e), and (f), which correspond to the dams with different water levels, the increased flexibility of the system due to hydrodynamic effects is evident as peaks in the curves at forcing frequencies lower than the natural frequencies of the dry dams. These peaks represent the natural frequencies of the dam-reservoir systems. However, the maximum increase in the amplitude of $\left|a_g^{(1)}(\omega)\right|$ can occur at different forcing frequencies than these peak locations. For example,

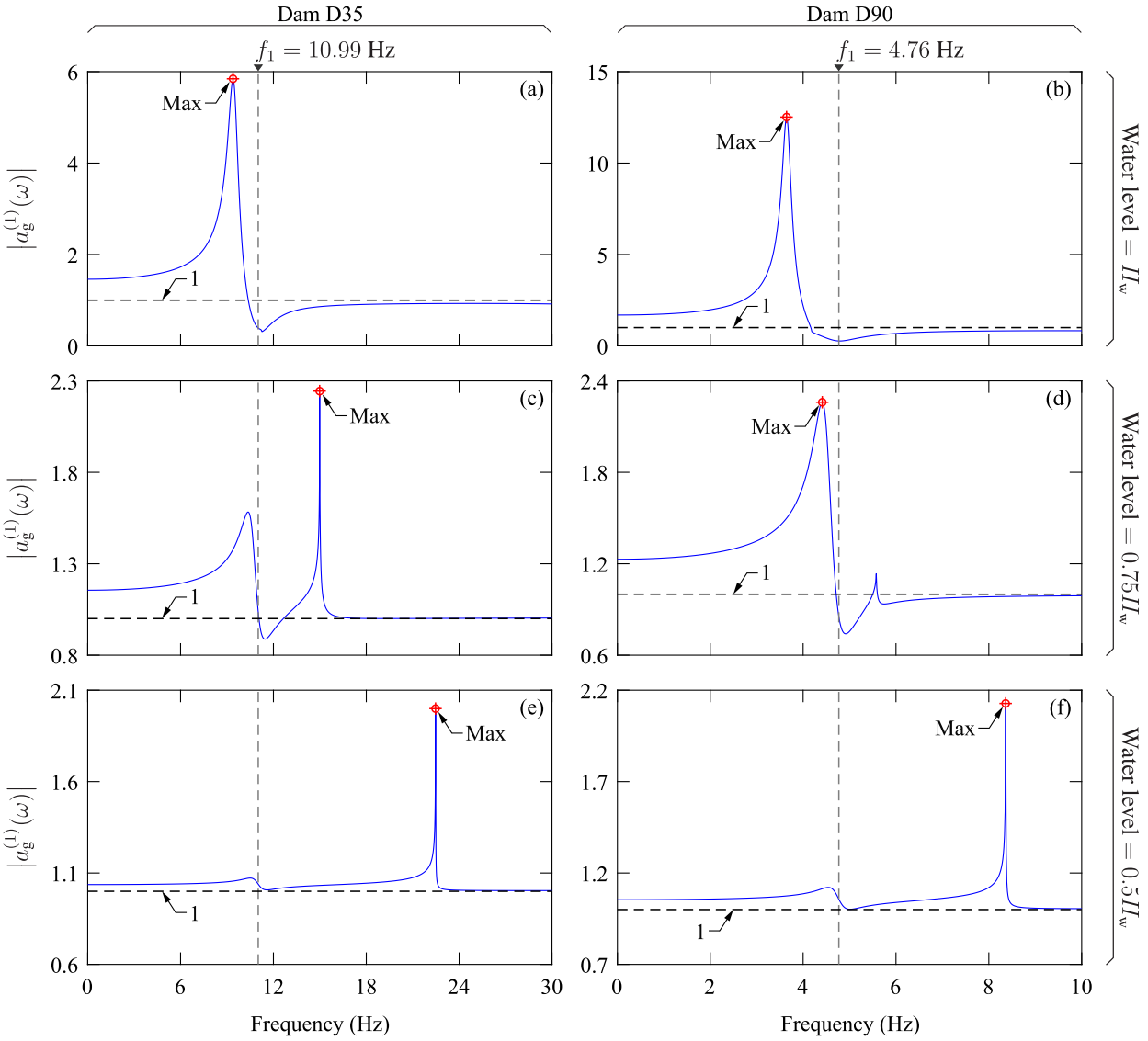

Figure 6.2 Variation of absolute value of $a_g^{(1)}(\omega)$ for studied dams D35 and D90 considering compressible water assumption with water level assumed to be: (a) and (b) H_w; (c) and (d) $0.75H_w$; and (e) and (f) $0.5H_w$.

for dam D35 with the reservoir at a level of $0.75H_w$, the maximum value of $\left|a_g^{(1)}(\omega)\right|$ occurs at a forcing frequency higher than the natural frequency of the dry dam D35 (i.e., $f > f_1 = 10.99$ Hz), as shown in Figure 6.2 (c). This maximum peak corresponds to the first natural vibration frequency of the impounded water with a non-absorptive reservoir bottom (i.e., $\omega_0 = \pi, C_w/2H_w \approx 94.25$ rad/s, equivalent to 15 Hz). Similar observations can be made for dam D90 with a water level of $0.5H_w$ as shows in Figure 6.2 (f). In this case, the maximum increase in the magnitude of the original ground acceleration occurs at the forcing frequency equal to the first natural vibration frequency of the impounded water, which is $f_0 = 8.4$ Hz.

In the general case, when the original ground acceleration is an arbitrary time history signal, the Fourier transform of the given ground acceleration $\ddot{x}_{\mathrm{g}}(t)$ can be determined as

$$\ddot{x}_{\mathrm{g}}(\omega) = \int_0^{t_a} \ddot{x}_{\mathrm{g}}(t)\, \mathrm{e}^{-\mathrm{i}\omega t}\, \mathrm{d}t \tag{6.14}$$

Thus, the modified ground acceleration considering only fundamental mode can be expressed as

$$a_{\mathrm{g}}^{(1)}(\omega) = \ddot{x}_{\mathrm{g}}(\omega)\, \frac{\widehat{Z}_1(\omega)}{Z_1(\omega)} \tag{6.15}$$

$$a_{\mathrm{g}}^{(1)}(\omega) = \ddot{x}_{\mathrm{g}}(\omega) \left[1 - \frac{\vartheta_{0,1}(\omega)}{L_1}\right] \left[1 - \frac{\vartheta_{1,1}(\omega)}{M_1 \left(1 - 2\,\mathrm{i}\,\xi_1\,\omega_1/\omega - \omega_1^2/\omega^2\right)}\right]^{-1} \tag{6.16}$$

Applying Fourier inverse transform to $a_{\mathrm{g}}^{(1)}(\omega)$ yields the following modified time-history ground motion acceleration corresponding to the fundamental structural mode

$$a_{\mathrm{g}}^{(1)}(t) = \frac{1}{2\pi} \int_{-\infty}^{\infty} a_{\mathrm{g}}^{(1)}(\omega)\, \mathrm{e}^{\mathrm{i}\omega t}\, \mathrm{d}\omega \tag{6.17}$$

Figures 6.3, 6.4, and 6.5 illustrate the modified and original ground motion acceleration for the horizontal components of the Imperial Valley earthquake (1940) at El Centro station and the Nahanni earthquake (1985) at Iverson station for dams D35 and D90. In these figures, the modified ground accelerations are generated using the assumption of compressible water, with three different water levels considered: H_{w}, $0.75H_{\mathrm{w}}$, and $0.5H_{\mathrm{w}}$. In these figures, (a) and (b) represent the original ground motion acceleration in the frequency domain, calculated using Equation (6.14) and labeled as the FFT of the original ground acceleration (i.e., $\left|\ddot{x}_{\mathrm{g}}(\omega)\right|$). The amplitudes are normalized using the maximum absolute value of the FFT of the original ground acceleration (i.e., $\left|\ddot{x}_{\mathrm{g}}(\omega)\right|^{(\max)}$). (c) and (d) depict the modified ground acceleration generated for a single harmonic ground motion, calculated using Equation (6.2). In these figures, the blue curves represent dam D35 and, while the red curves represent dam D90. To avoid confusion with the modified ground acceleration generated for general arbitrary ground acceleration, the vertical axes in these figures are labeled as $\left|\widehat{Z}_1(\omega)/Z_1(\omega)\right|$. (e) and (f) in Figs. 6.3, 6.4, and 6.5, are the modified ground motion acceleration for Imperial Valley and Nahanni ground motions. These modifications are calculated using Equation (6.16). The amplitude of the modified ground acceleration is normalized with the maximum absolute value of the FFT of the original ground acceleration and is labeled on the vertical axes as $\left|a_{\mathrm{g}}^{(1)}(\omega)\right| / \left|\ddot{x}_{\mathrm{g}}(\omega)\right|^{(\max)}$. The modified ground acceleration for dam D35 is shown in blue, while that for dam D90 is depicted in red. These figures clearly illustrate the changes in the frequency content and

amplitude of the original signal, resulting in a modified ground motion acceleration that incorporates hydrodynamic effects. These effects include the dynamic flexibility interaction of the dam-reservoir system, damping effects, and wave propagation effects due to the reservoir's natural frequency. It is important to note that while a full wave reflection assumption at the reservoir bottom (i.e., $\alpha = 1.00$) was used, the proposed formulation can also account for wave absorption at the reservoir bottom due to sedimentation, which further influences the frequency content of the original ground motion acceleration.

In the last row, (g) and (h) presents the time histories of the original and modified ground accelerations for the Imperial Valley (1940) and Nahanni (1985) earthquakes. The hydrodynamic effects are clearly visible in these figures, highlighting the significant influence of the system's flexibility on the modified ground acceleration. Additionally, when focusing on a single dam and comparing the effects of different water levels on the modified ground acceleration, it is evident that higher water levels lead to a larger peak ground acceleration (PGA) in the modified ground accelerations. For instance, comparing Figs. 6.5 (g) and (h) with 6.3 (g) and (h) clearly demonstrates that increasing the water level from $0.5H_{\mathrm{w}}$ to H_{w} results in a noticeable amplification of the modified ground motion due to hydrodynamic effects for both dams under the influence of the considered earthquakes.

Additionally, when the water level is at $0.5H_{\mathrm{w}}$, as shown in Figure 6.5, the maximum amplification occurs at higher frequencies corresponding to the fundamental natural frequency of the reservoirs for both dams. Although dam D90 exhibits higher flexibility compared to dam D35, the increase in the frequency content of ground motion acceleration is similar for both dams. This indicates that the acceleration demand does not significantly increase for either dam when the water level is at $0.5H_{\mathrm{w}}$.

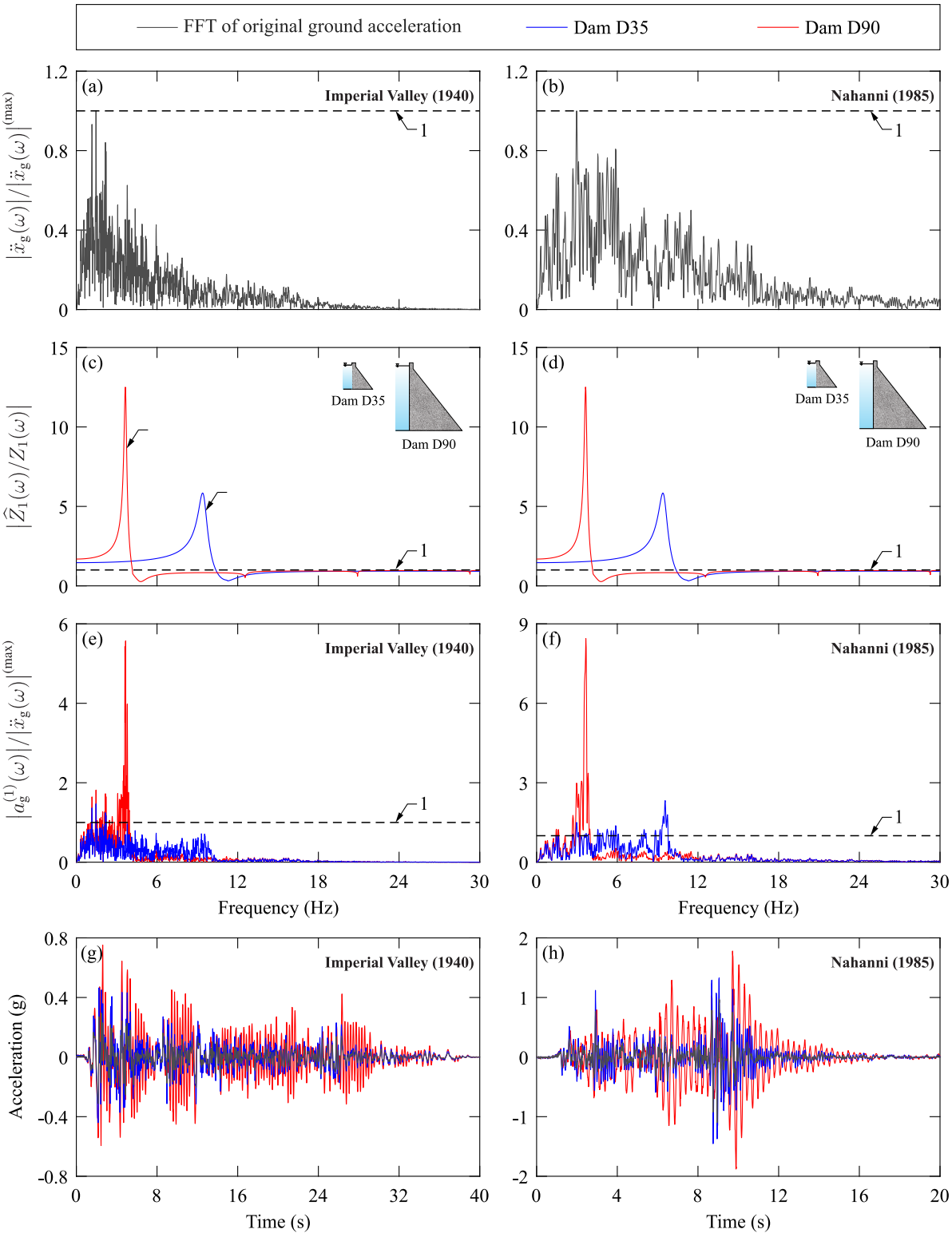

Figure 6.3 Modifying original ground motion acceleration in the frequency domain for studied dams D35 and D90 assuming water level to be H_w considering compressible water assumption: (a) and (b) normalized FFT of Imperial Valley (1940) and Nahanni (1985) earthquakes, respectively; (c) and (d) variation of absolute value of $a_g^{(1)}(\omega)$ calculated using Equation (6.13); (e) and (f) normalized $a_g^{(1)}(\omega)$ calculated using Equation (6.16); (g) and (h) time histories of original and modified ground accelerograms.

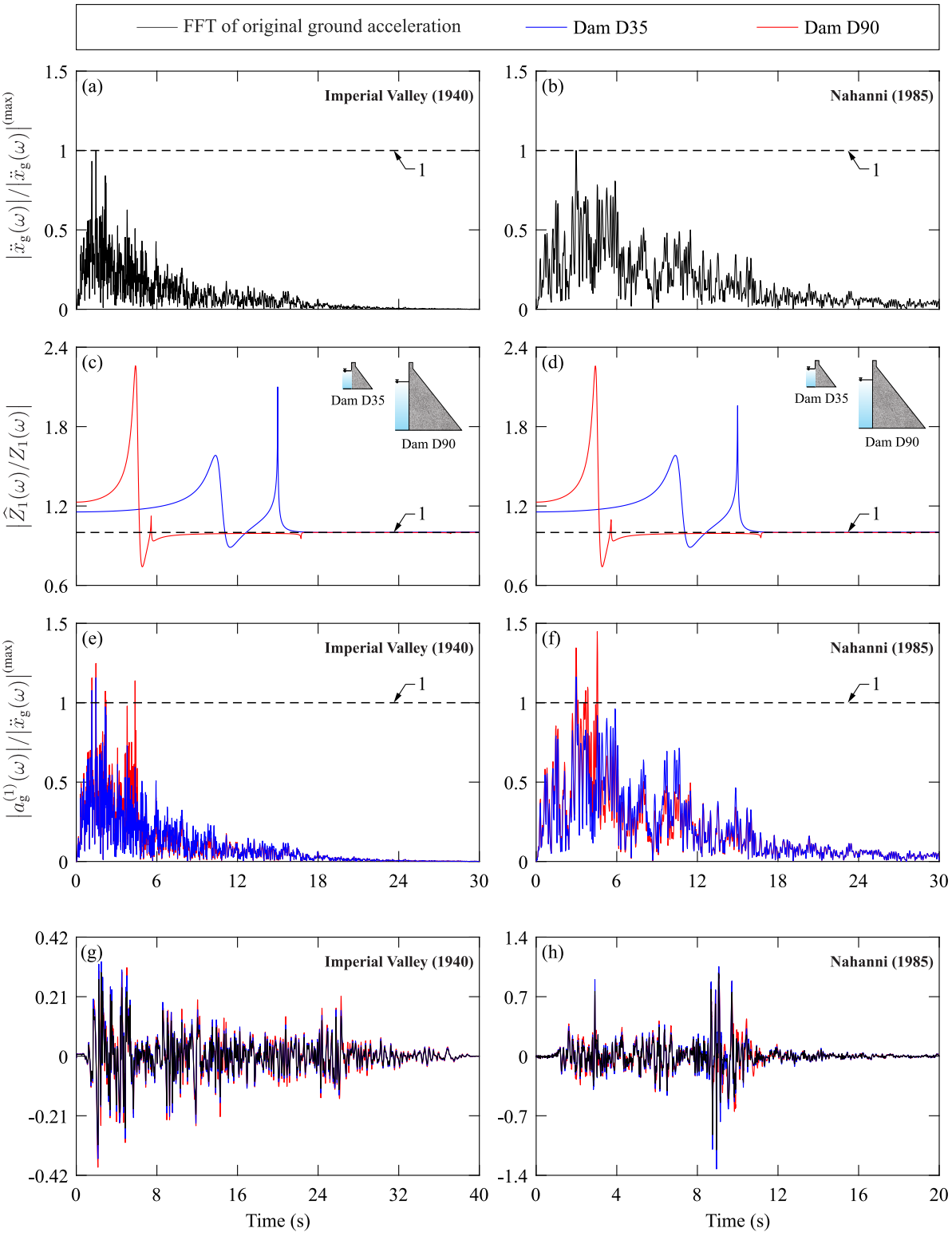

Figure 6.4 Modifying original ground motion acceleration in the frequency domain for studied dams D35 and D90 assuming water level to be $0.75H_{\mathrm{w}}$ considering compressible water assumption: (a) and (b) normalized FFT of Imperial Valley (1940) and Nahanni (1985) earthquakes, respectively; (c) and (d) variation of absolute value of $a_{\mathrm{g}}^{(1)}(\omega)$ calculated using Equation (6.13); (e) and (f) normalized $a_{\mathrm{g}}^{(1)}(\omega)$ calculated using Equation (6.16); (g) and (h) time histories of original and modified ground accelerograms.

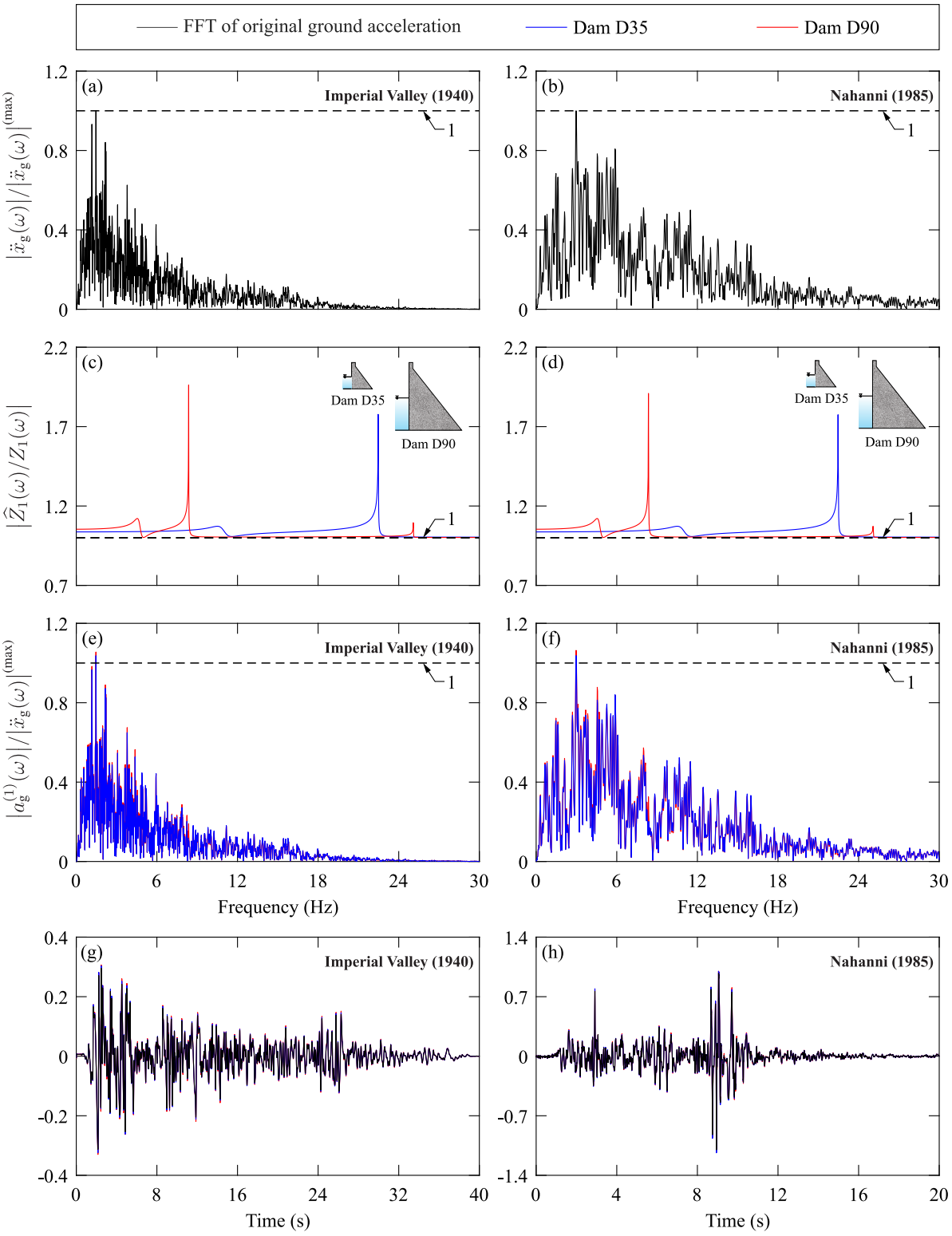

Figure 6.5 Modifying original ground motion acceleration in the frequency domain for studied dams D35 and D90 assuming water level to be $0.5H_{\mathrm{w}}$ considering compressible water assumption: (a) and (b) normalized FFT of Imperial Valley (1940) and Nahanni (1985) earthquakes, respectively; (c) and (d) variation of absolute value of $a_{\mathrm{g}}^{(1)}(\omega)$ calculated using Equation (6.13); (e) and (f) normalized $a_{\mathrm{g}}^{(1)}(\omega)$ calculated using Equation (6.16); (g) and (h) time histories of original and modified ground accelerograms.

To further illustrate the performance of the proposed method regardless of the forcing frequencies, harmonic ground motion accelerations denoted as Cases 1 to 5 in Table 6.1 are considered, with forcing frequencies of $0.25\,\omega_1$, $0.5\,\omega_1$, ω_1, $2\,\omega_1$, and $4\,\omega_1$, where ω_1 is the fundamental natural frequency of dams D35 or D90. The term $(t - \pi/\omega_1)$ in the table is defined to ensure that the signal starts at zero at the initial time step (i.e. $t = 0\,\text{s}$).

Table 6.1 Harmonic ground motion excitation with forcing frequencies as a function of the fundamental natural frequency of dams D35 or D90

Cases	**Dam D35** ($\omega_1 = 69.05$ rad/s)	**Dam D90** ($\omega_1 = 29.92$ rad/s)
Case 1	$\ddot{x}_{\text{g}}(t) = \sin\Big(0.25\,\omega_1(t - \pi/\omega_1)\Big)$	
Case 2	$\ddot{x}_{\text{g}}(t) = \sin\Big(0.50\,\omega_1(t - \pi/\omega_1)\Big)$	
Case 3	$\ddot{x}_{\text{g}}(t) = \sin\Big(1.00\,\omega_1(t - \pi/\omega_1)\Big)$	
Case 4	$\ddot{x}_{\text{g}}(t) = \sin\Big(2.00\,\omega_1(t - \pi/\omega_1)\Big)$	
Case 5	$\ddot{x}_{\text{g}}(t) = \sin\Big(4.00\,\omega_1(t - \pi/\omega_1)\Big)$	

Figure 6.7 presents the time-history horizontal relative displacements at the crest of dams D35 and D90 subjected to harmonic excitation Cases 1 to 5, obtained using proposed methods and the classical solution (dam modelled using finite elements and the hydrodynamic pressures modelled analytically, e.g. [2, 26]). It is clearly seen that the results from both approaches are superposed for a wide frequency range, thus confirming the excellent performance of the proposed methods.

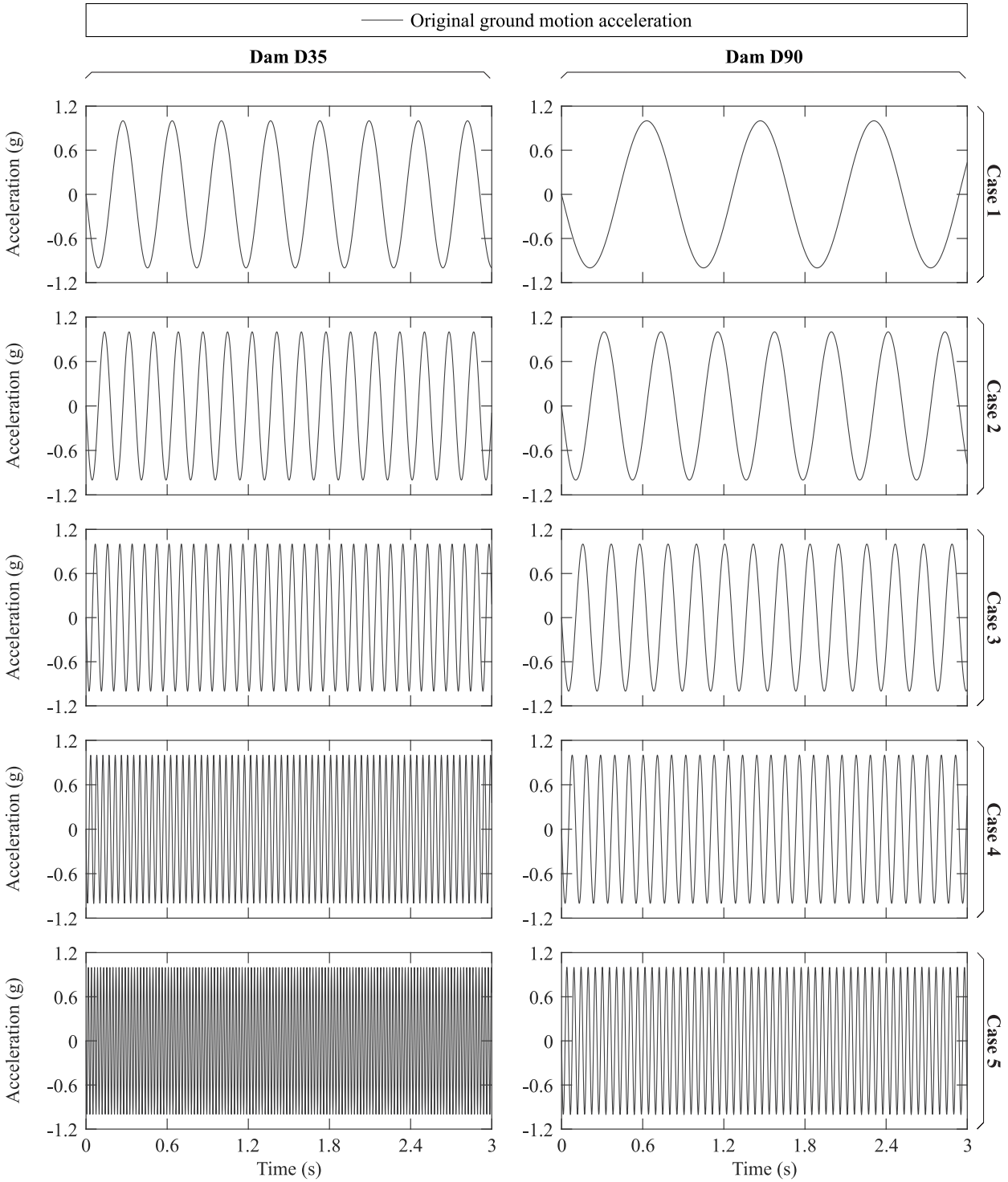

Figure 6.6 Original harmonic ground motion accelerations.

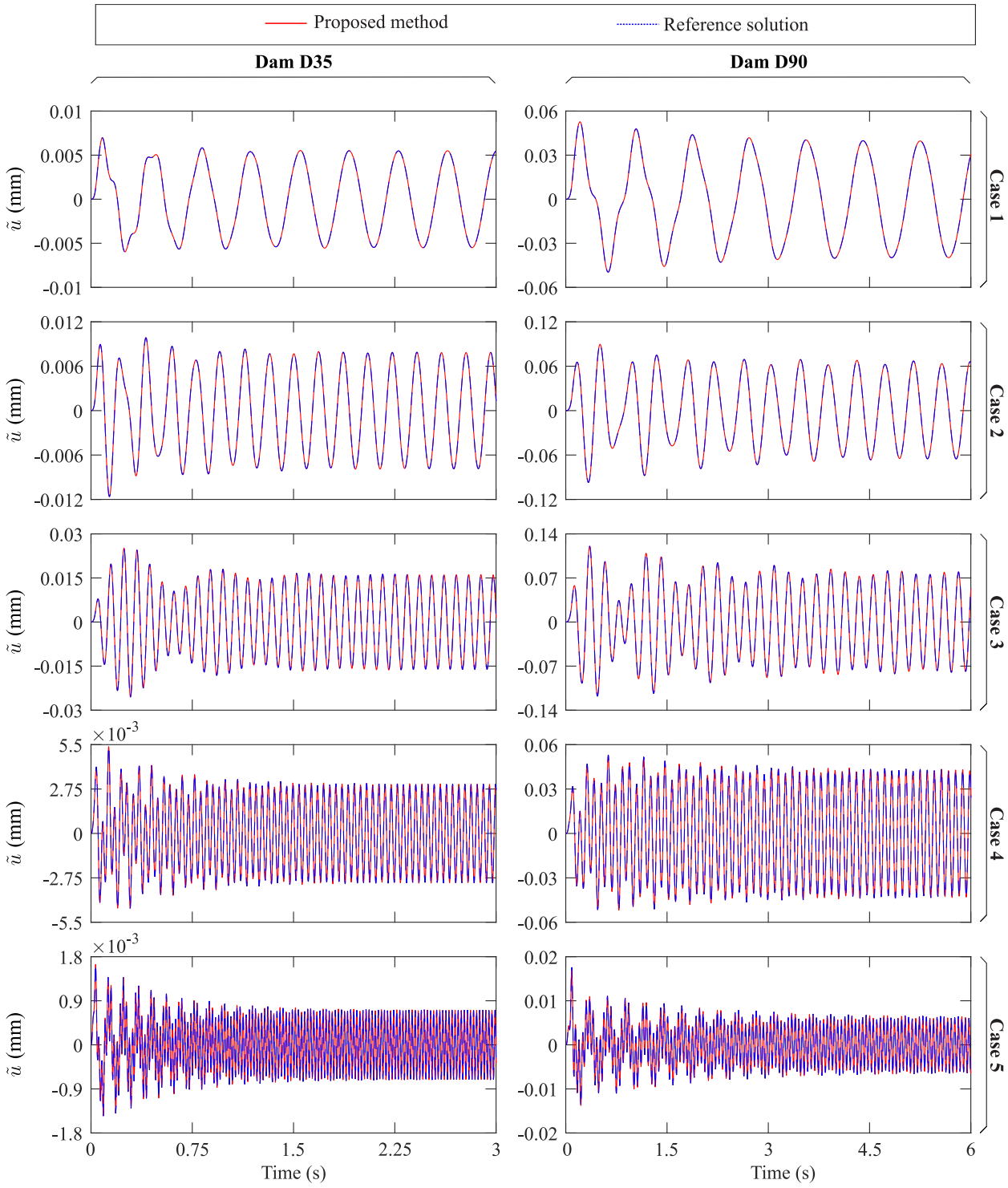

Figure 6.7 Time-history relative horizontal displacements at the crest of dams D35 and D90 subjected to harmonic excitation case 1 to case 5 according to two different approaches: Red curves, proposed method for each vibration mode using modified ground accelerations $a_g^{(1)}$ to $a_g^{(5)}$ and then combined to obtain total dam response; Blue curves, dam-reservoir system based on analytical formulation.

6.2.2 Dam-reservoir case study: Pine Flat dam

The non-overflow monolith (No. 16) of Pine Flat dam, located in Fresno County, California, is considered to further validate the application of the proposed method. The dam impounds a reservoir with a height H_w of 116.3 m. The dimension of the Pine Flat dam monolith along with the ground motion considered in this section, are shown in Fig. 6.8. The concrete material properties used in this analysis is summarized in Table 6.2. The dam monolith is modeled using 4-node plane strain finite elements in ADINA [92]. For the fluid domain, the water is assumed to be non-viscous, irrotational, and compressible, with a density of $\rho_w = 1000$ kg/m^3 and a bulk modulus of 2.069 GPa, corresponding to a wave propagation velocity of $C_w = 1440$ m/s.

Table 6.2 Material properties used for the Pine Flat dam model

Materials	**parameters**	**Values**
Concrete	Modulus of elasticity	22.4 GPa
	Density	2482.8 kg/m^3
	Poisson's ratio	0.20

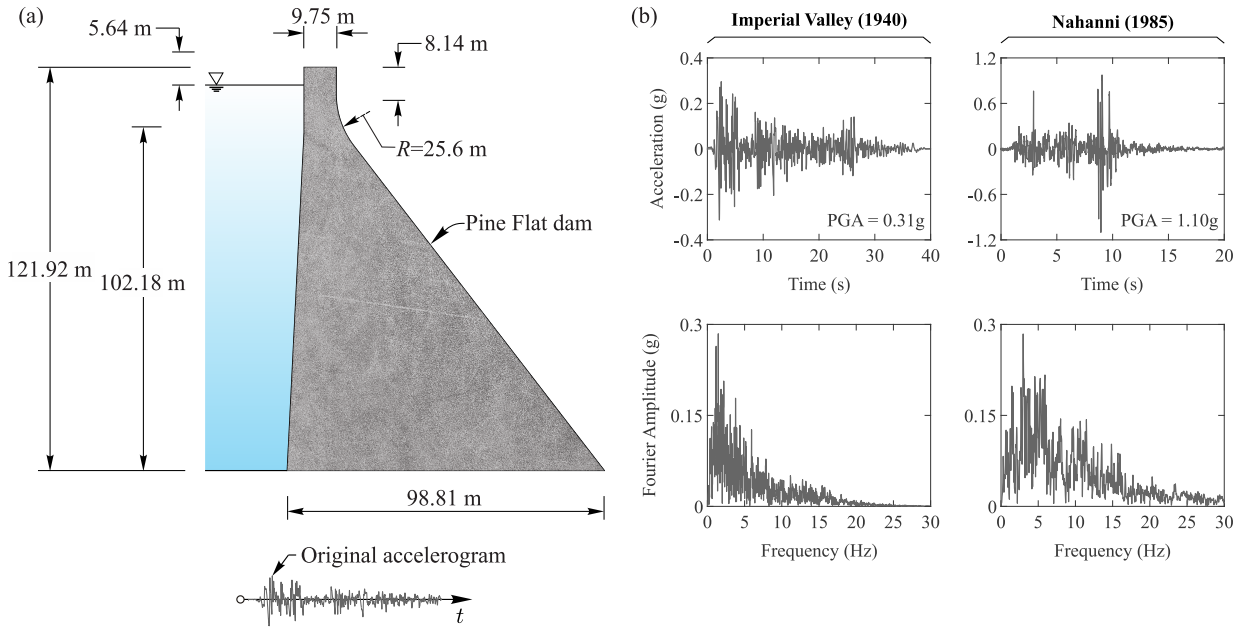

Figure 6.8 Studied dam-reservoir system and original ground acceleration: (a) dimensions of Pine Flat dam; (b) time-history accelerations and Fourier amplitudes of Imperial Valley (1940) and Nahanni (1985) earthquakes.

The dam monolith is subjected to the horizontal components of ground motions recorded during the Imperial Valley earthquake (1940) at station El Centro and Nahanni earthquake (1985) at station Iverson, as shown in Figure 6.8 (b). A constant 5% modal viscous damping ratio is considered for all the vibration modes of the dam with empty reservoir, i.e. $\xi_j = 0.05$ for $j = 1$ to 5.

Figure 6.9 illustrates the first five modes as well as the corresponding vibration periods, i.e. T_1 to T_5 of the dam with empty reservoirs. This figure also shows the horizontal and vertical effective modal masses, i.e. $\Lambda_j^{(x)}$ and $\Lambda_j^{(z)}$, respectively, reflecting the relative importance of the contribution of each mode $j = 1 \ldots 5$ to the global seismic response of the dam. It is observed that the fundamental and second modes predominate the seismic response and that the third mode is essentially vertical.

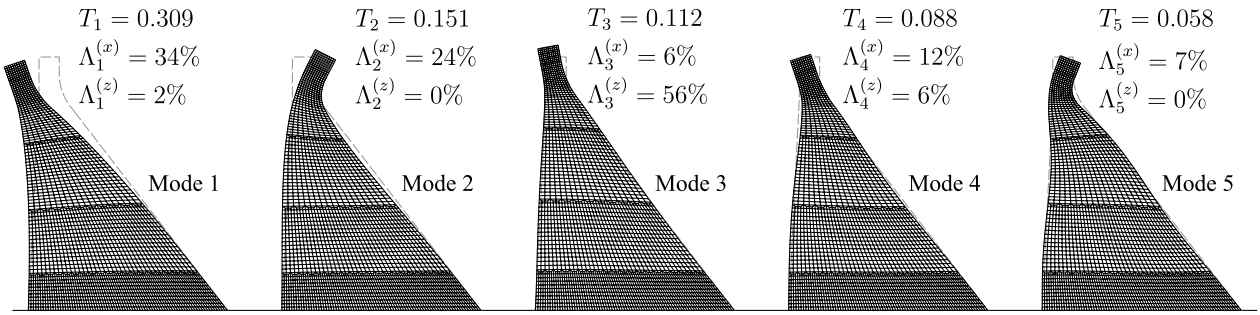

Figure 6.9 Five first mode shapes, corresponding vibration periods and effective modal masses of the studied Pine Flat dam monolith.

The modified accelerograms corresponding are displayed in Figure 6.10 for Pine Flat dam assuming compressible water in the reservoir. In the same figure, the original ground accelerations are also presented for comparison purposes. It is seen that the amplitudes of the modified accelerations are generally greater than those of the original accelerograms for both ground motions. The results also confirm, as anticipated, that the frequency content of the modified accelerations differs from that of the original accelerograms and that such alterations depend on the specific dam being studied as well as the characteristics of the original ground motion.

The 5%-damped pseudo-acceleration response for the modified ground accelerations are then obtained for the first five vibration periods T_1 to T_5. In Figure 6.11, these results are presented with values highlighted in blue. The pseudo-spectral accelerations of the original ground motions for the corresponding vibration periods are also shown, with values marked in black. It is seen that the acceleration demands for the fundamental mode of the Pine Flat dam increase significantly by 110%, i.e. $(1.39 - 0.67)/0.67 \times 100$ when hydrodynamic effects

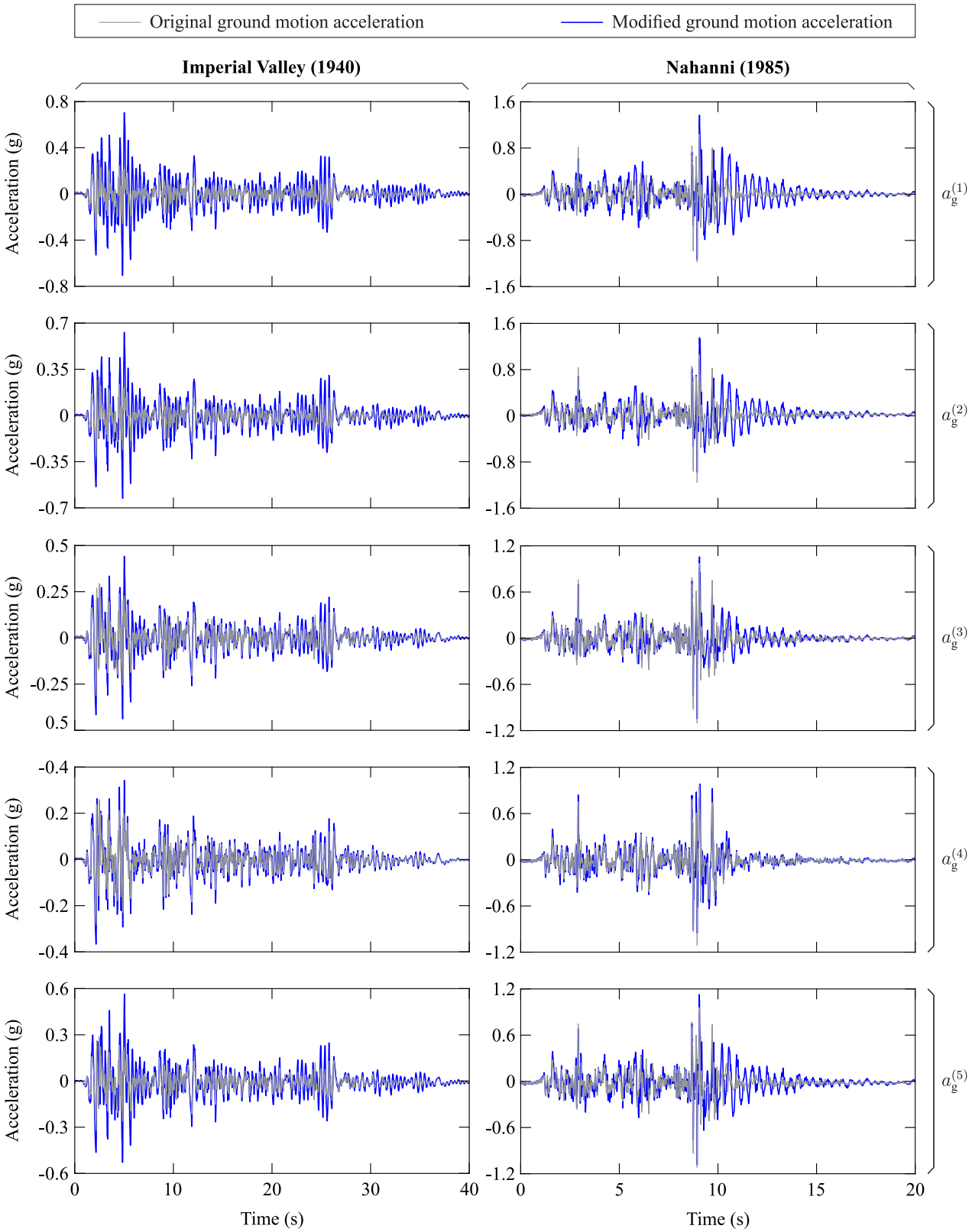

Figure 6.10 Original and modified Imperial Valley (1940) and Nahanni (1985) ground motion accelerations corresponding to Pine Flat dam assuming compressible water in the reservoir.

are included for the Imperial Valley (1940) earthquake. However, for the Nahanni (1985) earthquake, although the acceleration demands for the fundamental mode of the Pine Flat dam with an empty reservoir are 2.7 times higher than those for the same mode under the Imperial Valley (1940) earthquake (i.e., 1.80/0.67), the increase in acceleration demand is only 3%, i.e. $(1.85 - 1.80)/1.80 \times 100$ when hydrodynamic effects are included. Additionally, it can be observed that for the Nahanni (1985) earthquake, the acceleration demand for the second mode decreased by 6%, i.e. $(2.22 - 2.09)/2.22 \times 100$ due to hydrodynamic effects. Similar analyses can be performed to elucidate the hydrodynamic effects corresponding to different vibration modes of any dam studied. Figure 6.12 presents results of the maximum

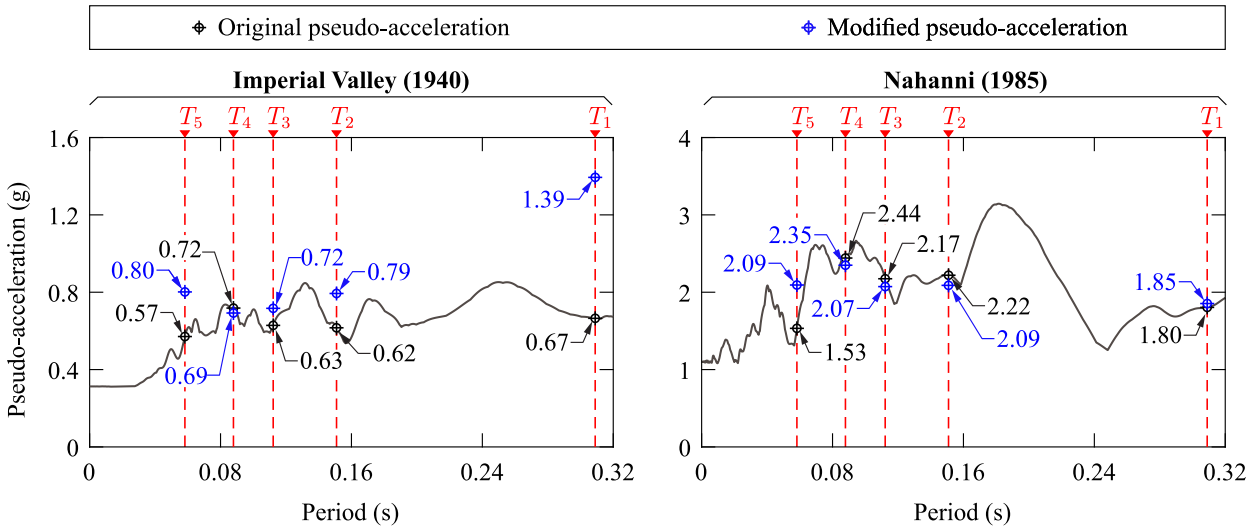

Figure 6.11 5%- damped pseudo-acceleration response spectra of the original ground motion and the modified ground motions of Pine Flat dam assuming water to be compressible in the reservoir.

absolute horizontal displacements obtained along the height of the upstream face of Pine Flat dam under the effects of the considered ground motions. It illustrates the relative horizontal displacement for each vibration mode of the dam using the proposed response spectrum analysis (RSA). The total maximum absolute relative horizontal displacements are also shown in the last columns titled *Total*. These total responses are obtained using two approaches: (i) a direct method consisting of the summation of the modal responses of horizontal relative displacements (i.e. algebraic values with signs obtained using time-history modal superposition analysis - THMSA) and then the computation of the maximum value of the resulting summed response, and (ii) the SRSS method consisting of summing the absolute values of the maximum horizontal relative displacements obtained for each mode using RSA. The results provided by the direct method are found to be identical to those of the reference solution. It is seen that the SRSS method yields larger values than the direct method at the dam

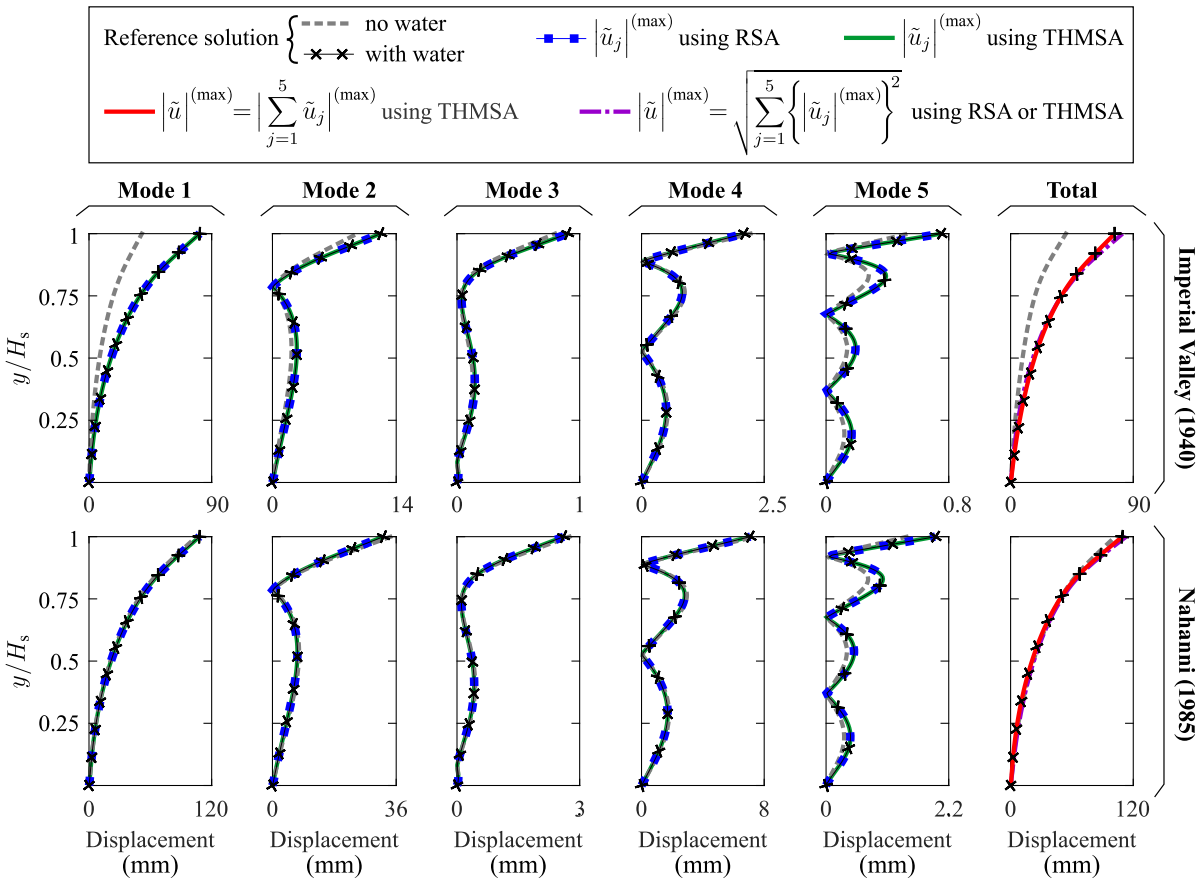

Figure 6.12 Absolute maximum displacements along the height of the upstream face of Pine Flat dam.

crest and slightly below. At lower heights, the total maximum responses obtained using the SRSS method are practically the same as the direct method or slightly smaller. The maximum absolute horizontal displacements of the dam with empty reservoirs, also shown in Figure 6.12, are found to be generally lower than those with the reservoir. It is seen that the hydrodynamic effects induced by the Nahanni (1985) ground motion on maximum horizontal displacements of the Pine Flat dam upstream face are negligible, a result that is consistent with the modified accelerations shown in Figure 6.10. The time-history relative displacements at any location of the dams can be obtained using the proposed method as described previously. Figure 6.13 shows the total time-history relative horizontal displacements at the crest of Pine Flat dam subjected Imperial Valley (1940) and Nahanni (1985) earthquakes. These results are identical to those obtained using the reference solution shown in the same figure. Figure 6.14 shows the maximum dynamic stresses σ_{xx} and σ_{zz} obtained using proposed methods of Pine flat dam subjected to the two earthquakes considered.

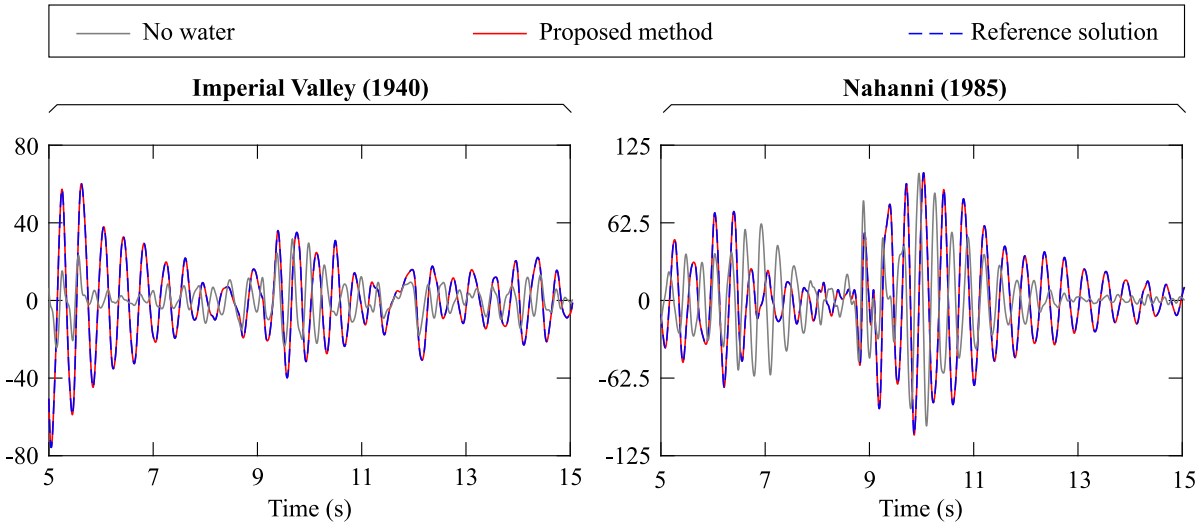

Figure 6.13 Time-histories of total relative horizontal displacements at the crest of Pine Flat dam.

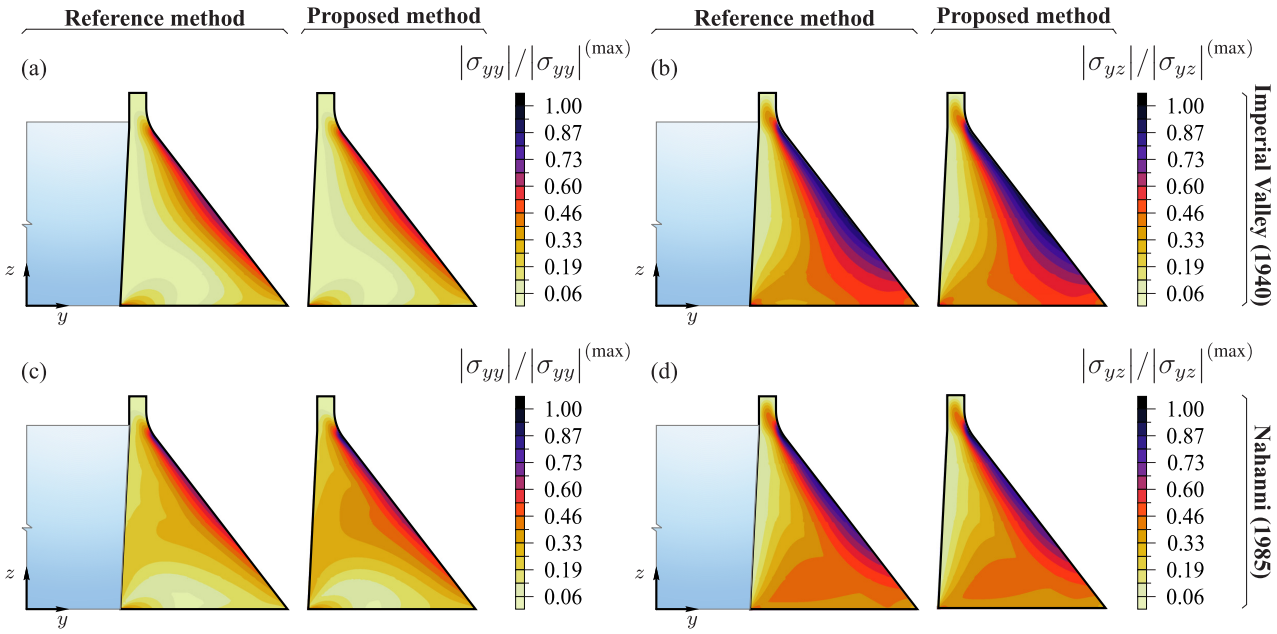

Figure 6.14 Maximum stresses σ_{yy} and σ_{xy} developing within Pine Flat dam subjected to the two earthquakes considered as obtained using proposed method: (a) and (b) Imperial Valley (1940) earthquake; (c) and (d) Nahanni (1985) earthquake.

6.2.3 Structure surrounded by water case study: San Bernardino intake tower

The reinforced concrete intake tower in Southern California, part of the California Aqueduct system, is chosen to further validate the application of the proposed method developed for axisymmetric structures surrounded by water. This tower stands approximately 190 feet (58 m) tall and has a cylindrical design with an outside diameter of 25 feet (7.6 m), as shown in Figure 6.15. The concrete properties assumed for the analysis include a modulus of elasticity of 4.5 million psi (31 GPa), a Poisson's ratio of 0.17, and a unit weight of 155 pounds per cubic foot (2480 kg/m^3). The tower is modeled using 20-node 3D-solid finite elements in ADINA [92]. For the fluid domain, the water is assumed to be non-viscous, irrotational, and compressible, with a density of $\rho_w = 1000$ kg/m^3 and a pressure wave velocity of $C_w = 1440$ m/s. The tower is subjected to three distinct ground accelerations,

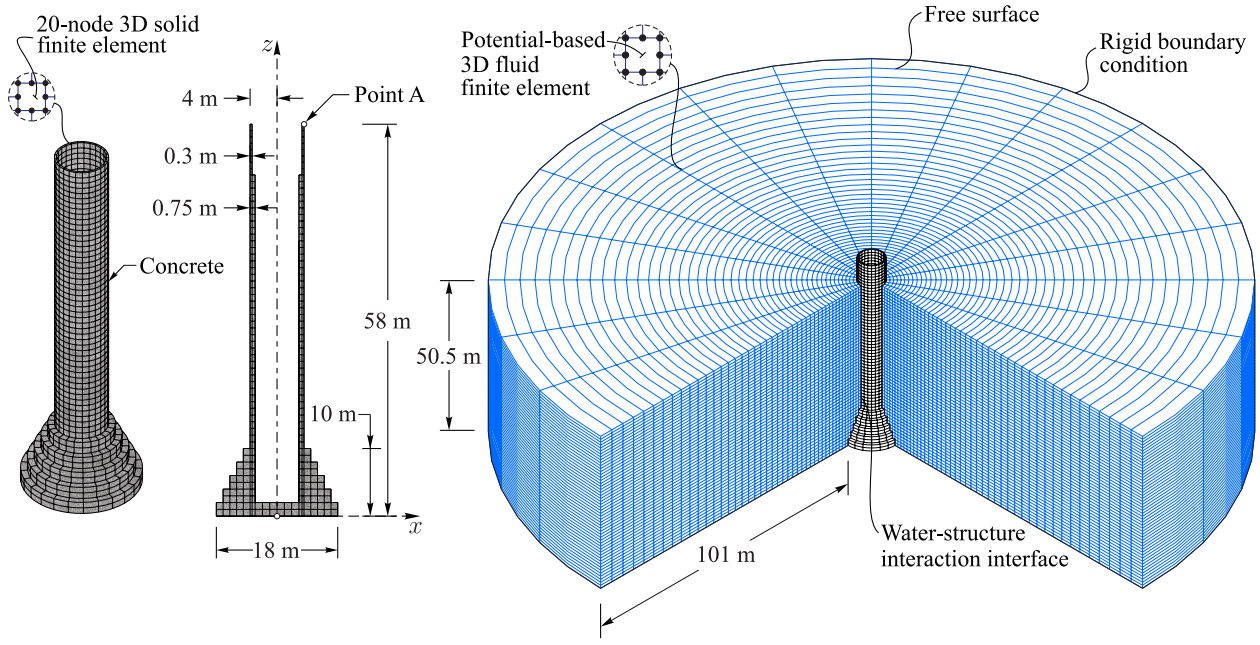

Figure 6.15 Dimensions and finite element meshes of San Bernardino intake tower.

each characterized by its frequency content and time signature: (i) the horizontal component of the Imperial Valley earthquake (1940) recorded at the El Centro station, (ii) the horizontal component of the Loma Prieta earthquake (1989) recorded at the Gilroy Array No. 2 station, and (iii) the horizontal component of the Nahanni earthquake (1985) recorded at the Iverson station. A constant 5% modal viscous damping ratio is applied to all the vibration modes of the tower with an empty reservoir, i.e., $\xi_j = 0.05$ for $j = 1$ to 5. Figure 6.16 illustrates the first six lateral modes as well as the corresponding vibration periods, i.e. T_1 to T_6 of the intake tower with empty reservoirs. These figures also show the effective modal masses,

i.e. $\Lambda_j^{(x)}$, $\Lambda_j^{(y)}$ and $\Lambda_j^{(z)}$, reflecting the relative importance of the contribution of each mode $j = 1 \ldots 6$ to the global seismic response of the tower.

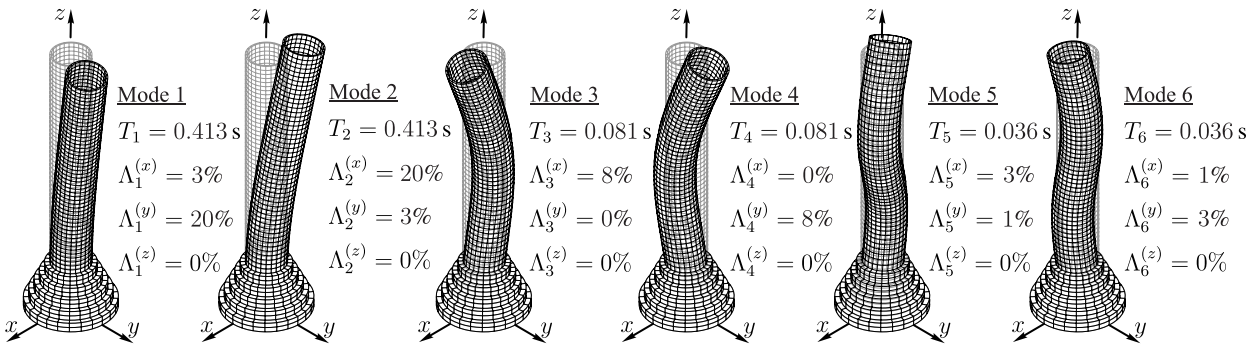

Figure 6.16 Finite element mode shapes and corresponding vibration periods of San Bernardino intake tower, as well as the modal mass participation factors.

The modified accelerograms for the three earthquakes are shown in Figure 6.17, considering both the compressible water assumption and the added mass formulation. For comparison, the original ground accelerations are also included in the figure. The differences between the two approaches for incorporating hydrodynamic effects are minimal, particularly in the fundamental mode, but become more pronounced in the higher modes. It is worth noting that the modified ground accelerations are presented for pairs of consecutive modes, with $a_{\text{g}}^{(1)}$ and $a_{\text{g}}^{(2)}$ displayed together in a single curve. This approach is necessitated by the unique characteristics of axisymmetric structures, where the modal analysis of a 3D axisymmetric model results in two consecutive modes that share the same natural frequency but have different modal participation factors and mode shapes.

The 5%-damped pseudo-acceleration response for the modified ground accelerations is then obtained for the six vibration periods T_1 to T_6, assuming the compressible water assumption and the added mass concept, and presented in Figure 6.11. These results are highlighted in blue. The pseudo-spectral accelerations of the original ground motions for the corresponding vibration periods are also shown, with values marked in black. It is observed that the acceleration demands for the fundamental mode (modes 1 and 2) of the San Bernardino intake tower increased by 141%, i.e. $(1.35 - 0.56)/0.56 \times 100$ when hydrodynamic effects are included using the compressible water assumption for the Imperial Valley (1940) earthquake. If hydrodynamic effects are included through the added mass formulation, the acceleration demands increased almost the same by 146%, i.e. $(1.38 - 0.56)/0.56 \times 100$. For the Loma Prieta (1989) earthquake, the acceleration demands decreased when hydrodynamic effects were included in the fundamental mode. For the compressible water assumption, the decrease is 13%, i.e.

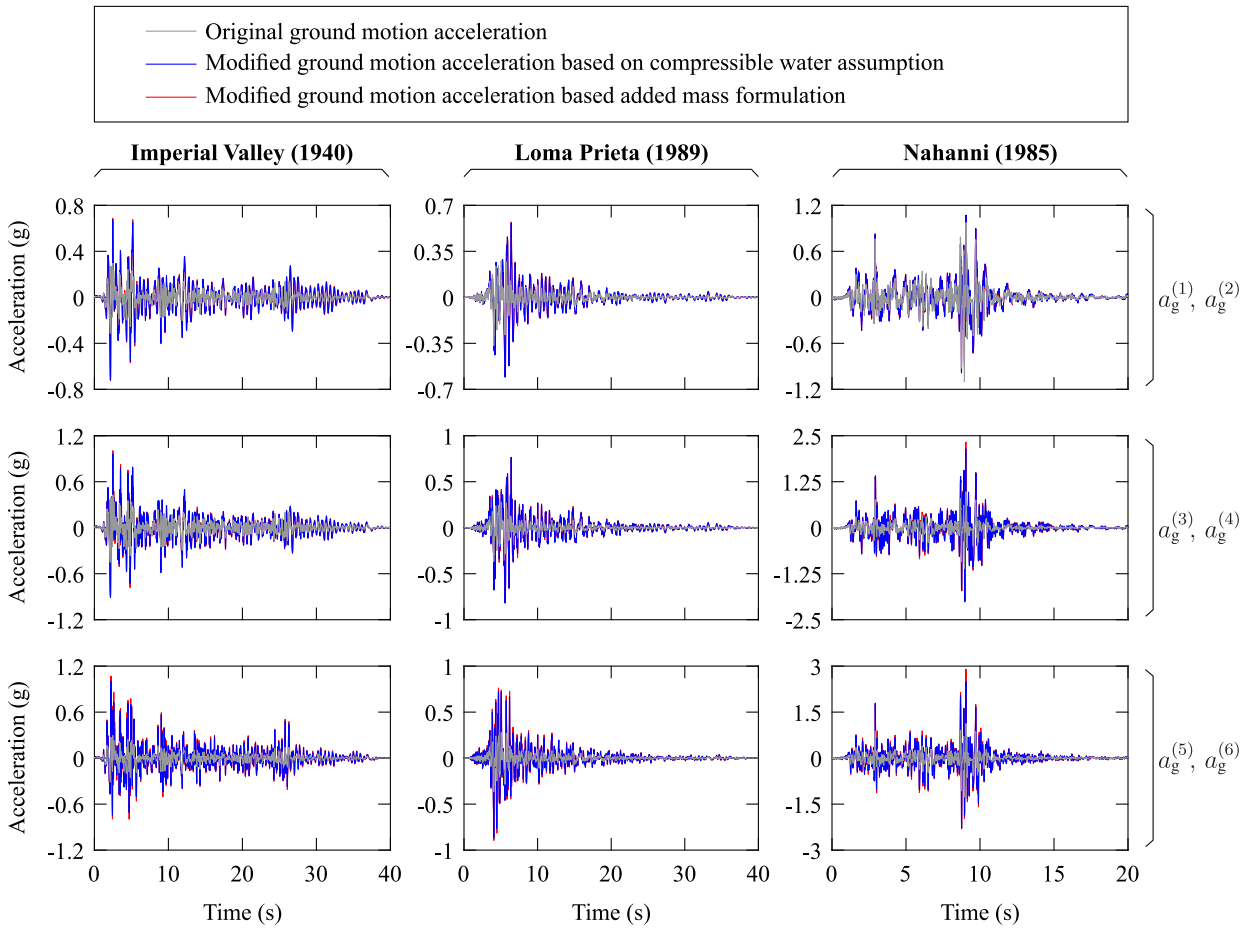

Figure 6.17 Original and modified ground accelerations $a_g^{(1)}$ to $a_g^{(6)}$ corresponding to the six mode shapes of San Bernardino intake tower, subjected to Imperial Valley (1940), Loma Prieta (1989), and Nahanni (1985) earthquakes considering compresssible water assumption and add added mass formulation..

$(1.34-1.17)/1.34\times 100$, and 14%, i.e. $(1.34-1.15)/1.34\times 100$ when hydrodynamic effects are included using the added mass formulation. By comparing Figures 6.11(a) and 6.11(b), particularly focusing on the fundamental modes, it is evident that the system incorporating hydrodynamic effects under the Imperial Valley (1940) earthquake exhibits nearly the same acceleration demands as the system without water under the Loma Prieta (1989) earthquake. This comparison clearly highlights the significant impact of dynamic reservoir effects and the frequency content of the original ground motion on the seismic response of the structure. For higher modes, similar observations can be made. For example, as shown in Figure 6.11(b) for the Loma Prieta (1989) earthquake, the increase in acceleration demand is nearly the same for both modes $3,4$ and modes $5,6$. For modes 3 and 4, the acceleration demands increased by 132%, i.e. $(1.01-0.44)/0.44\times 100$, when hydrodynamic effects were included using the com-

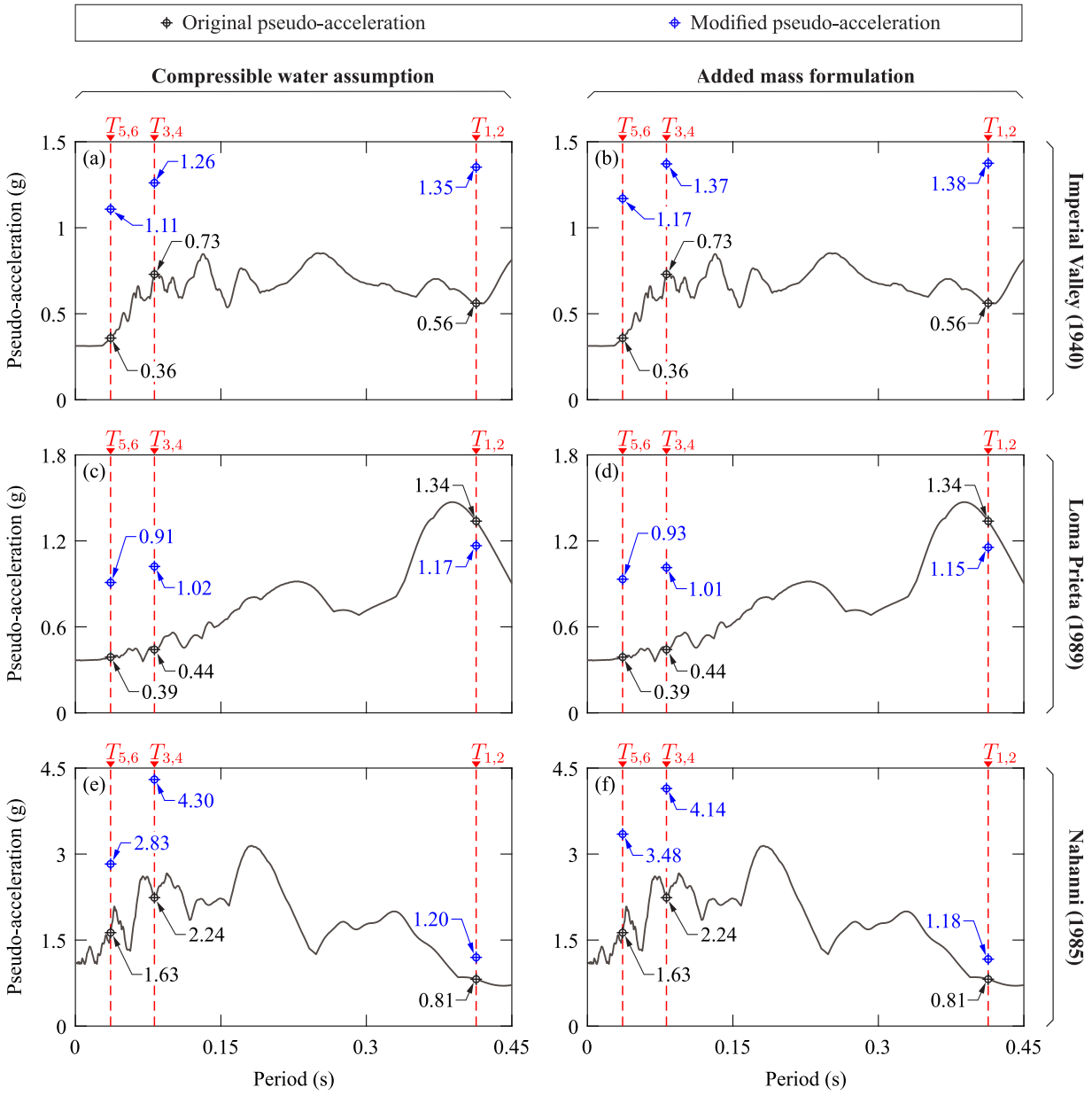

Figure 6.18 5%-damped pseudo-acceleration response spectra of the original ground motions and those of the modified ground motions corresponding to each of the selected six vibration modes assuming compressible water and added mass formulation.

pressible water assumption, and by 130%, i.e. $(1.02-0.44)/0.44\times 100$, when the added mass formulation was considered instead. Similarly, for modes 5 and 6, the acceleration demands increased by 133%, i.e. $(0.91-0.39)/0.39\times 100$, when hydrodynamic effects were included using the compressible water assumption, and by 138%, i.e. $(0.93-0.39)/0.39\times 100$, when the added mass formulation was considered instead. The time-history relative displacements at any location of the tower can be determined using the proposed method, as previously

described. Figure 6.19 illustrates the total time-history relative horizontal displacements at the top of the San Bernardino intake tower when subjected to the Imperial Valley (1940) and Loma Prieta (1989) earthquakes. These results are identical to those obtained from the reference solution, as shown in the same figure. For comparison, the response of the tower without water is also presented. As observed, the total relative horizontal displacement of the tower is higher when hydrodynamic effects are included for the Imperial Valley (1940) earthquake, while it is lower for the Loma Prieta (1989) earthquake. Figure 6.20 shows

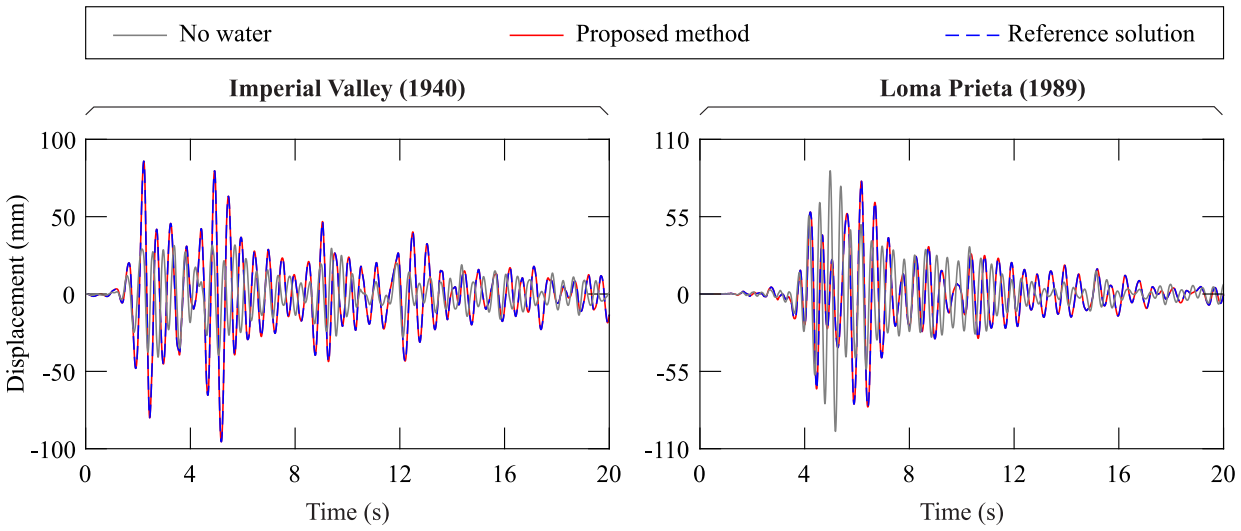

Figure 6.19 Time-histories of total relative horizontal displacements at top the top of San Bernardino intake tower including hydrodynamic effect considering Imperial Valley (1940) and Loma Prieta (1989) earthquakes obtained assuming compressible water in the reservoir.

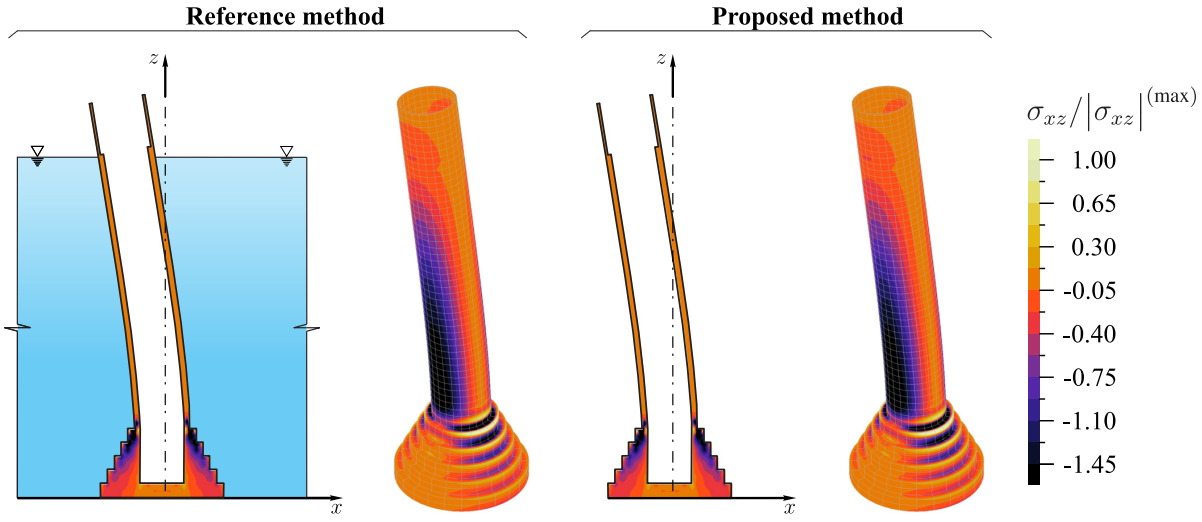

Figure 6.20 Maximum stresses σ_{xz} developing within San Bernardino intake tower subjected to Imperial Valley (1940) earthquake assuming compressible water.

of the normalized dynamic stresses σ_{xz} obtained using proposed methods of San Bernardino intake tower subjected to the Imperial Valley (1940) earthquake.

Figure 6.21 presents results of the maximum absolute horizontal displacements obtained along the height of the upstream face of San Bernardino intake tower under the effects of the considered ground motions. It illustrates the horizontal displacement for each vibration mode of the dam using the proposed response spectrum analysis (RSA). The total maximum absolute horizontal relative displacements are also shown in the last columns titled *Total*. These total responses are obtained using two approaches as mentioned before. The direct method's results match perfectly with the reference solution. It is observed that the Complete Quadratic Combination (CQC) method produces slightly higher values compared to the direct method, particularly at the top of the structure. As shown in Figure 6.21, the maximum absolute horizontal displacements of the tower without water are generally lower than those with the reservoir, except during the Loma Prieta (1989) earthquake. This finding aligns with the earlier discussion regarding the seismic acceleration demands induced by this record, as illustrated in Figure 6.11(b).

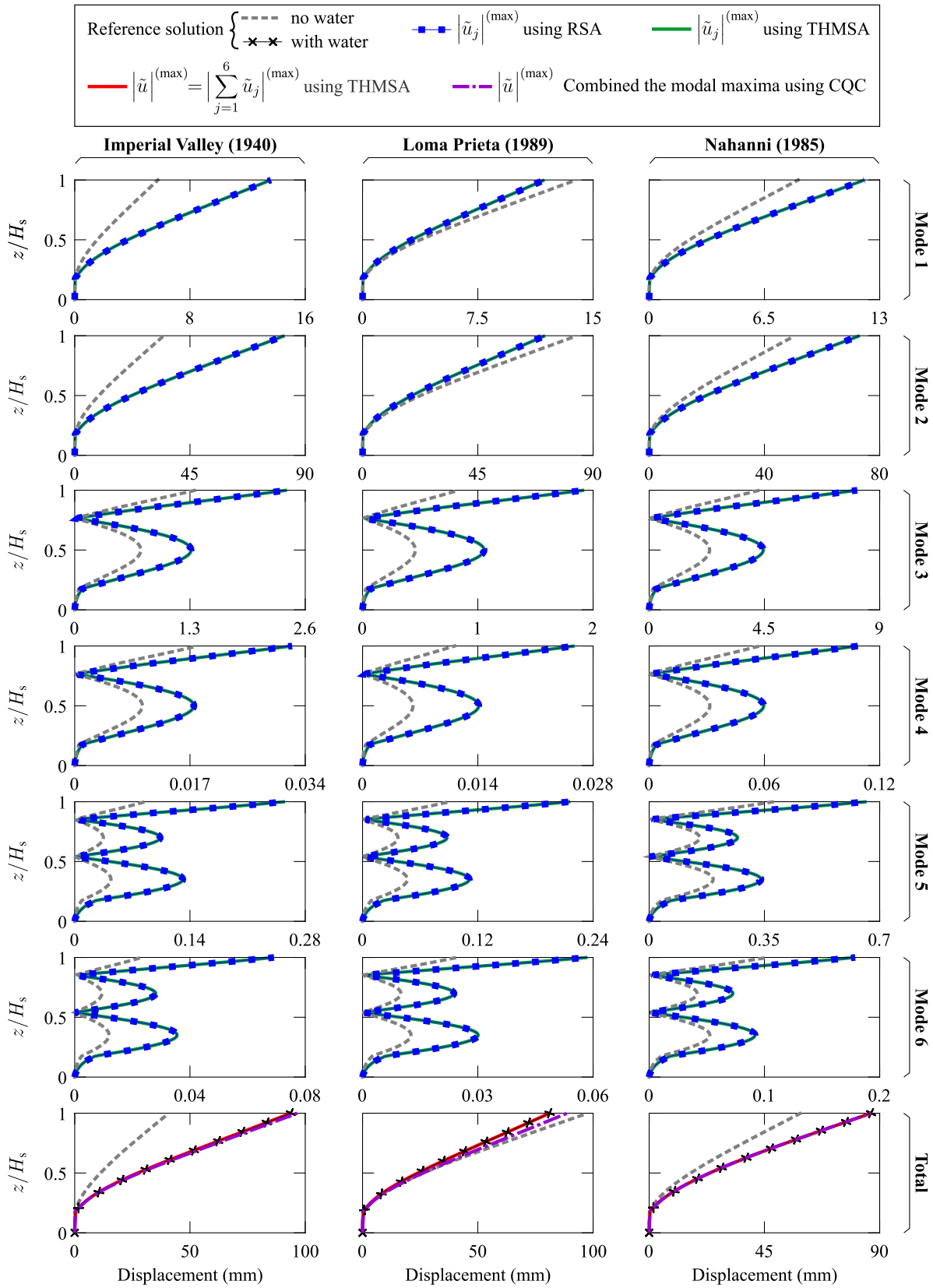

Figure 6.21 Absolute maximum relative displacements along the height of the face of San Bernardino intake tower determined for each vibration mode using modified ground accelerations $a_g^{(1)}$ to $a_g^{(6)}$ obtained assuming compressible water in the reservoir and then combined to obtain total response.

6.3 Application of the proposed method using general purpose structural analysis software

In this section, the application of the proposed method for performing seismic analysis of dam-reservoir systems and axisymmetric structures surrounded by water using general-purpose software is demonstrated. The analysis will be illustrated using dams D35 and D90 as examples of dam-reservoir systems, and the San Bernardino intake tower as a representative of axisymmetric structures surrounded by water. SAP2000 is selected as the example of general-purpose structural analysis software, but other standard software such as STAAD.Pro and SeismoStruct can also be used for this type of analysis. Both structure-water systems are subjected to the horizontal component of the Imperial Valley earthquake (1940), assuming compressible water in the reservoir. The modified ground acceleration for each structure-water system is prepared and defined in SAP2000, allowing for the inclusion of hydrodynamic effects in the analysis. The procedure for implementing the proposed method in SAP2000 involves the following steps:

Step 1. **Modeling**: Begin by creating finite element models of the structure in SAP2000. The structure's geometry, material properties, modal damping, and boundary conditions should be defined in this step.

Step 2. **Modal Analysis**: Perform a modal dynamic analysis to determine the dynamic properties of the structure, including natural frequencies, mode shapes, and modal participation factors. These parameters are essential for calculating the modified ground motion accelerations.

Step 3. **Ground Motion Definition**: Define the modified ground motions, $a_g^{(1)}$ to $a_g^{(j)}$, as time history functions within the software.

Step 4. **Load Cases Setup**: Set up modal analysis load cases for each mode (e.g. five modes) with appropriate frequency shifts to isolate the effects of each mode individually.

Step 5. **Time History Analysis**: Define five linear modal history load cases to execute time-history analyses corresponding to each modal analysis load case previously defined.

Step 6. **Load Combination**: Finally, combine the results from the linear modal history load cases to obtain the total time history response of the structures. This combined response reflects the cumulative effects of all considered modes under the modified ground motion inputs.

6.3.1 Dam-reservoir system

To illustrate the application of the proposed method using SAP2000 for seismic analysis of dam-reservoir systems, two gravity dam monoliths, D35 and D90, are selected as case studies. Dam D35, with a height of 35 m, impounds a reservoir with a water height of 32 m, while dam D90, standing 90 m tall, has a reservoir height of 86 m (Figure 6.1). For the analysis, these dams are subjected to the modified ground acceleration specific to each dam, generated under the Imperial Valley (1940) earthquake, with the assumption of compressible water in the reservoir. Figure 6.22 illustrates the first five modes of vibration for gravity dams D35 and D90 obtained from SAP2000. The modified ground accelerations for both dams were computed using these dynamic properties and are depicted in Figure 6.23. Figures 6.24

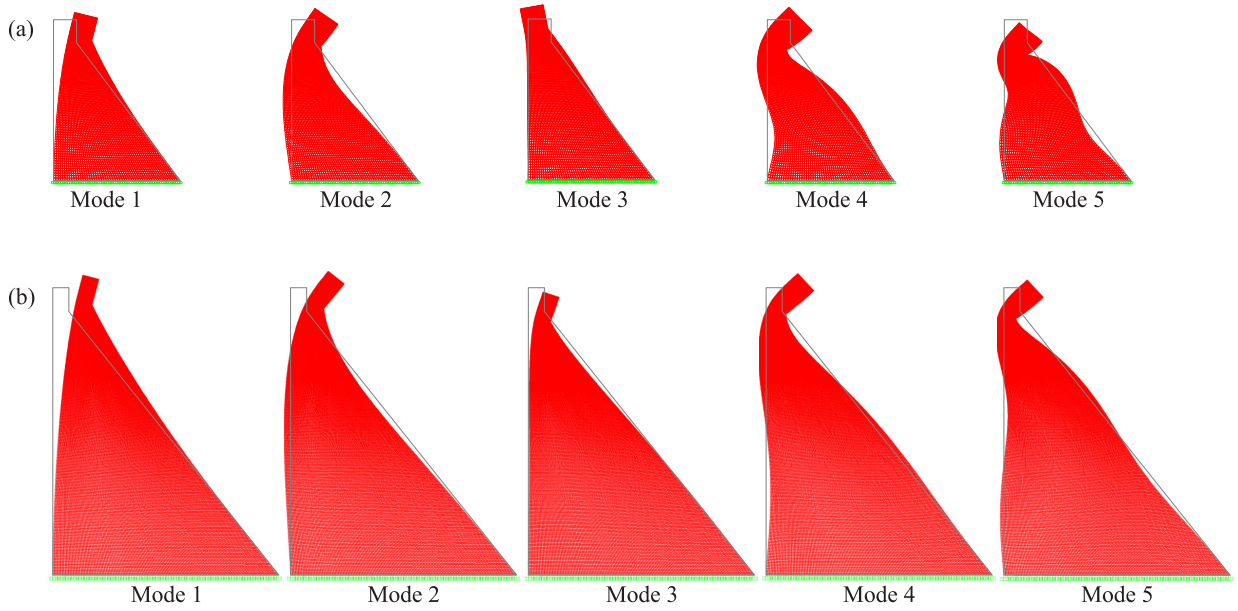

Figure 6.22 Five first mode shapes both gravity dam monoliths: (a) the 35 m height dam (D35); (b) the 90 m height dam (D90).

and 6.25 provide a detailed overview of the steps necessary to set up and perform a modal time history analysis of gravity dams, including the hydrodynamics effects, for dams D35 and D90, respectively. Figure 6.24 (a) presents the first 10 natural frequencies of the 35 m high dam (D35), with the first five modes highlighted in distinct colors, each considered in the analysis. The load case setup specifically for the fundamental mode of the dam is shown in Figure 6.24 (c). In this setup, the minimum and maximum number of modes are set to one, ensuring that only the fundamental mode is analyzed, with no frequency shifting required. As depicted in Figure 6.24 (d), the modified ground acceleration $a_g^{(1)}$ is applied as an acceleration time history, with a constant 5% viscous damping included in the analysis. The modified

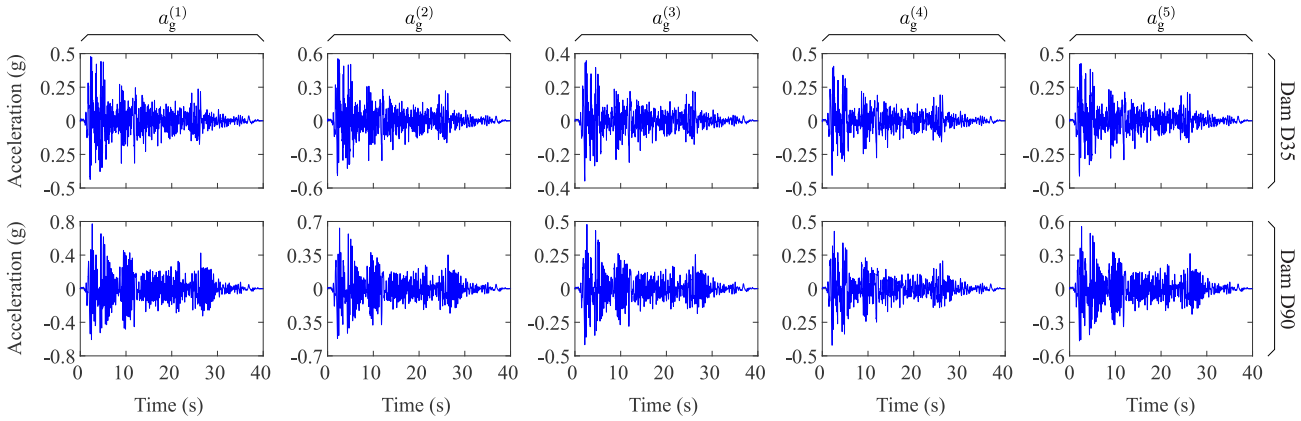

Figure 6.23 Modified ground motion accelerations $a_g^{(1)}$ to $a_g^{(5)}$ corresponding to the first five mode shapes of dams D35 and D90 both subjected to Imperial Valley (1940) earthquake and considering compressible water assumption.

ground accelerations are defined as time history functions, with Figures 6.24 (e), (h), (k), (n), and (q) showing the definitions of $a_g^{(1)}$ to $a_g^{(5)}$ for dam D35. Similarly, for higher modes, a load case setup with an appropriate frequency shift is implemented to isolate the effects of each mode, followed by a time history modal analysis that considers only the impact of the desired mode subjected to the modified ground acceleration. For instance, a frequency shift of 20 Hz is applied to the load case `MODAL-mode2` (mode 2) of dam D35, as illustrated in Figure 6.24 (f). This shift is applied to capture the first mode with a natural frequency greater than 20 Hz, which in this case is 25 Hz. Additionally, as shown in Figure 6.24 (o), a frequency shift of 60 Hz is necessary to accurately capture the natural frequency of mode 5, which is 66.2 Hz. The total time history response of the dam D35 is then obtained by combining the linear modal history load cases, as shown in Figure 6.24 (b).

For dam D90, the first five highlighted modes are presented in Figure 6.25 (a). The corresponding modal load cases are detailed in Figures 6.25 (c), (f), (i), (l), and (o), with an appropriate frequency shift applied to isolate the desired mode. For instance, a frequency shift of 16 Hz is applied to the load case `MODAL-mode4` (mode 4), as illustrated in Figure 6.25 (l). This shift ensures that the analysis captures the first mode with a natural frequency exceeding 16 Hz, which in this case is 16.47 Hz. Figures 6.25 (d), (g), (j), (m), and (p) depict the time history modal cases, incorporating a constant 5% modal damping and applying the modified ground accelerations $a_g^{(1)}$ through $a_g^{(5)}$, which are defined as time history functions shown in Figures 6.25 (e), (h), (k), (n), and (q). The total time history response of the dam is then obtained by combining the linear modal history load cases, as shown in Figure 6.25 (b).

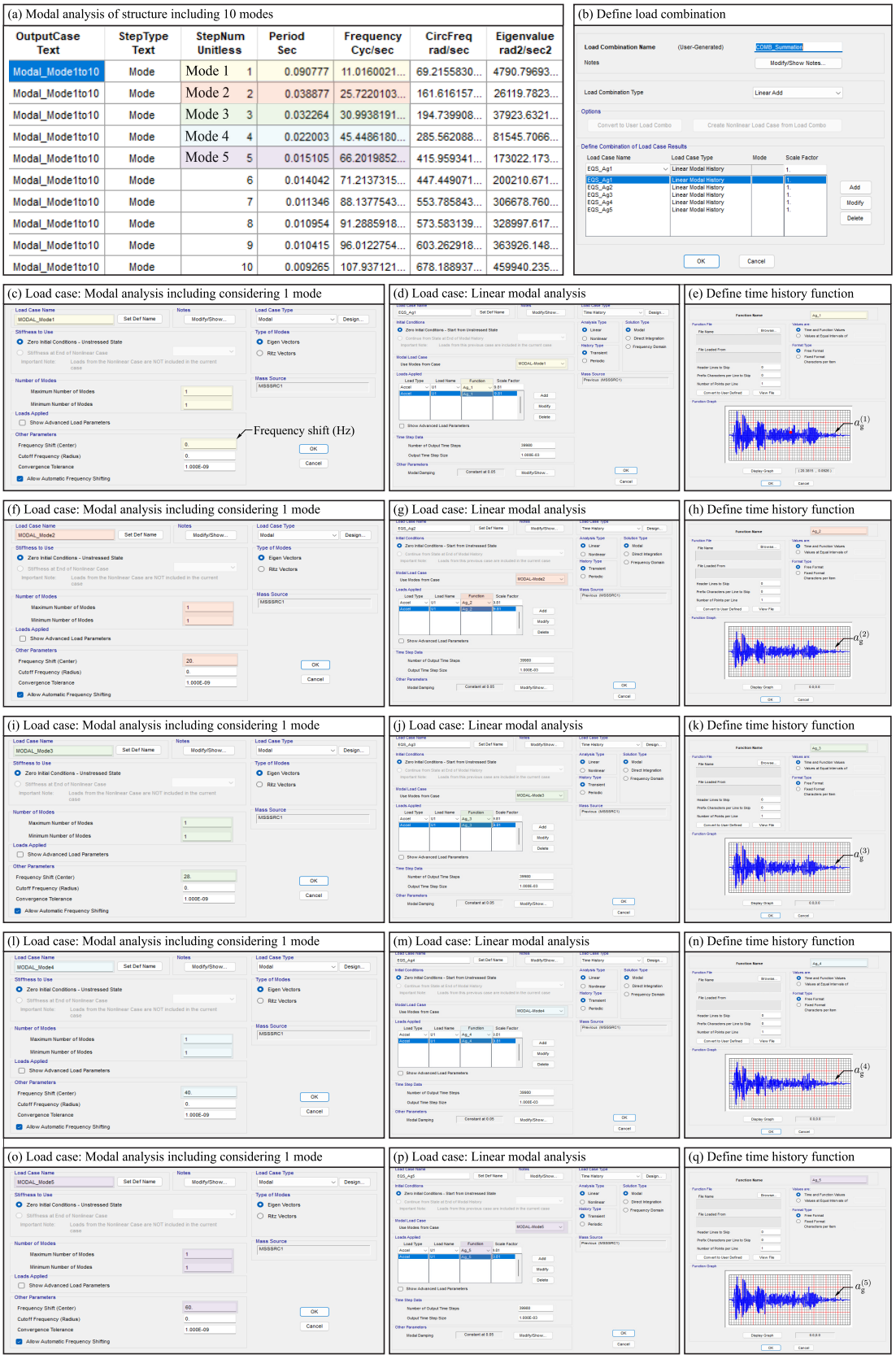

Figure 6.24 Steps for setting up and executing the modal time history analysis of dam D35 in SAP2000 including hydrodynamic effects.

(a) Modal analysis of structure including 10 modes

OutputCase Text	StepType Text	StepNum Unitless	Period Sec	Frequency Cyc/sec	CircFreq rad/sec	Eigenvalue rad2/sec2
Modal_Mode1to10	Mode	Mode 1 1	0.209676	4.76926655...	29.9661855...	897.972277...
Modal_Mode1to10	Mode	Mode 2 2	0.09862	10.1399077...	63.7109191...	4059.08121...
Modal_Mode1to10	Mode	Mode 3 3	0.077111	12.9683696...	81.4826698...	6639.42548...
Modal_Mode1to10	Mode	Mode 4 4	0.060702	16.4740522...	103.509522...	10714.2213...
Modal_Mode1to10	Mode	Mode 5 5	0.041374	24.1697816...	151.863216...	23062.4366...
Modal_Mode1to10	Mode	6	0.035011	28.5623272...	179.462395...	32206.7512...
Modal_Mode1to10	Mode	7	0.030215	33.0956598...	207.946163...	43241.6069...
Modal_Mode1to10	Mode	8	0.028072	35.6226087...	223.823451...	50096.9375...
Modal_Mode1to10	Mode	9	0.026262	38.0777124...	239.249323...	57240.2387...
Modal_Mode1to10	Mode	10	0.024207	41.3095157...	259.555342...	67368.9758...

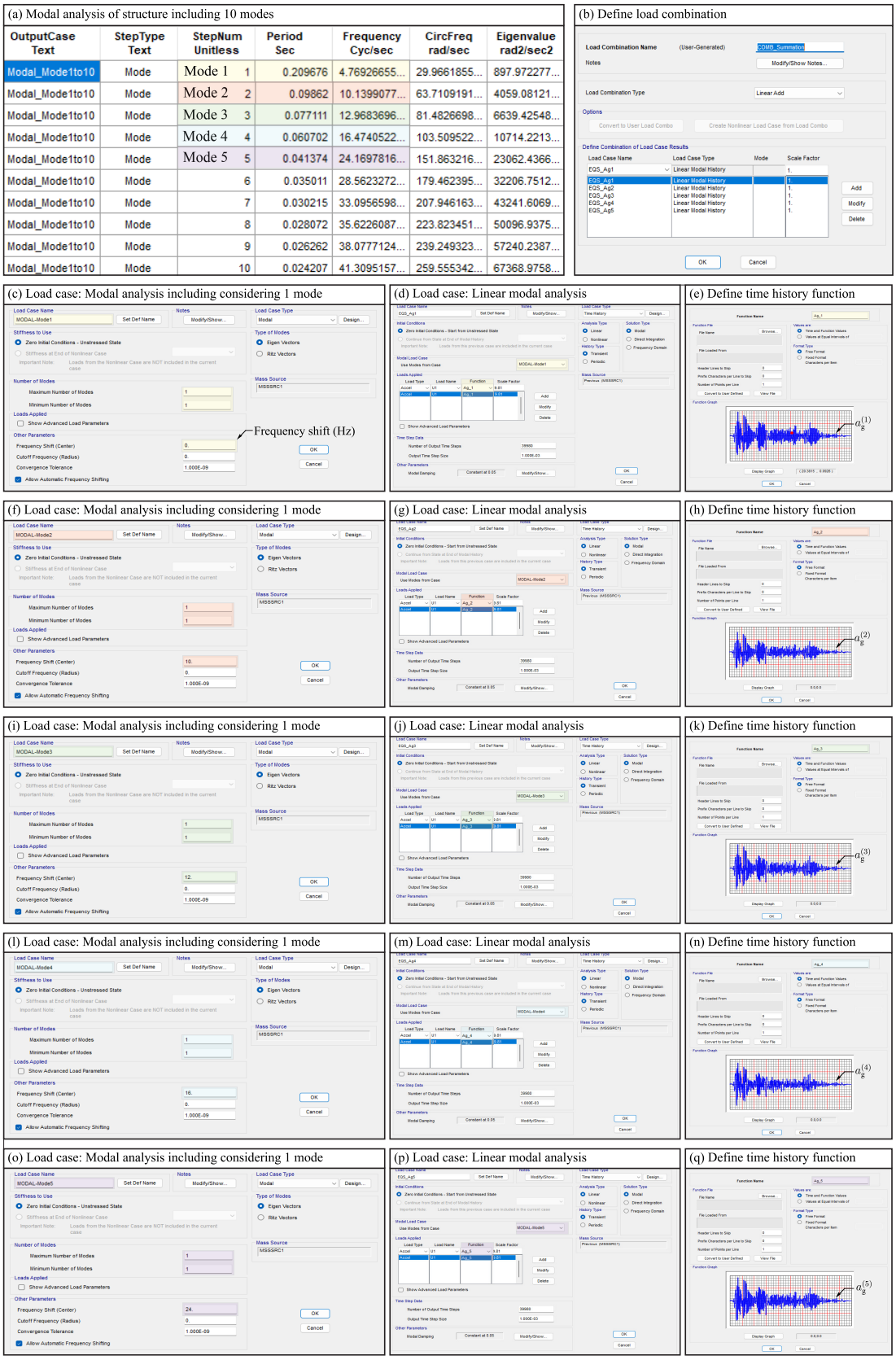

Figure 6.25 Steps for setting up and executing the modal time history analysis of dam D90 in SAP2000 including hydrodynamic effects.

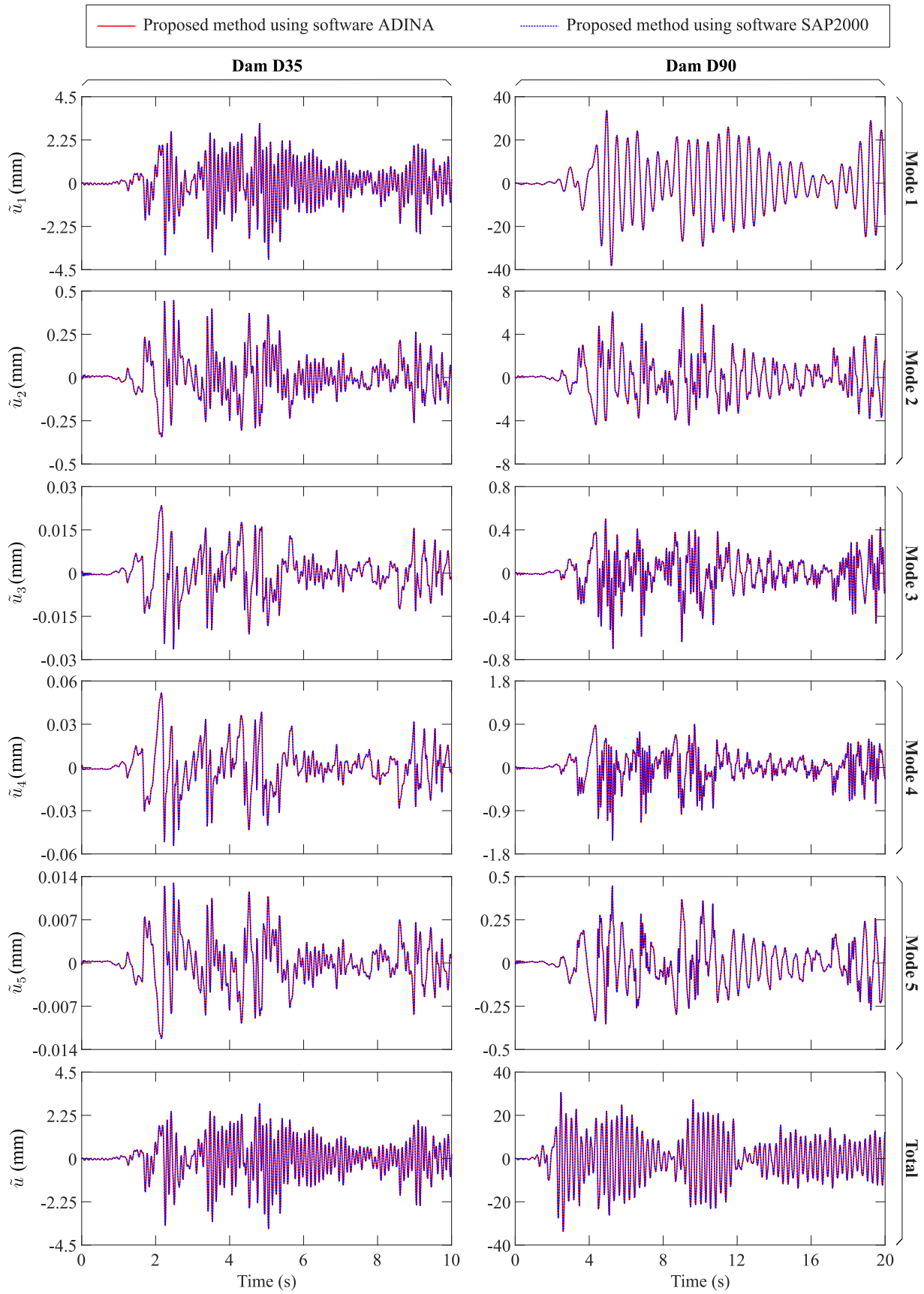

Figure 6.26 Time-history horizontal relative displacements (for the first 5 modes and the total) at the crest of dams D35 and D90 subjected to Imperial Valley (1940) earthquake obtained using to SAP2000 and ADINA.

Figure 6.26 presents the crest displacements of dams D35 and D90 under the effects of the modified ground motion accelerations $a_g^{(1)}$ to $a_g^{(5)}$ generated from the Imperial Valley (1940) earthquake. The red curves depict the response of the dams as calculated using the ADINA software, where the modified ground accelerations $a_g^{(1)}$ to $a_g^{(5)}$ were applied and then combined to obtain the total response. The blue curves represent the corresponding results obtained using SAP2000, following the same process. The figure demonstrates an excellent agreement between the results from SAP2000 and ADINA, with the curves are superposed.

Figure 6.27 compares the dynamic maximum stresses σ_{xx} and σ_{zz} within dam D90 subjected to the Imperial Valley (1940) earthquake, as obtained using the proposed methods in both ADINA and SAP2000 software. The results show excellent agreement, demonstrating that the stresses induced by the Imperial Valley earthquake are predominantly governed by the fundamental vibration mode. However, it is also notable that the contribution from the second mode is significant and should not be neglected. This example underscores the robustness and effectiveness of the proposed methodology, showing that it can be successfully implemented in standard structural analysis software such as SAP2000 in order to perform time history modal dynamic analyses of dam-reservoir system including hydrodynamic effects.

The results obtained from the proposed method using ADINA software already validated against a semi-analytical approach in Section 3, where hydrodynamic pressures analytically expressed and interacted with the vibrating dam modeled using finite element models [2, 26]. The semi-analytical approach were previously verified against coupled dam-reservoir solutions, namely by Bouaanani and Lu [2]. To further confirm the agreement between both types of solutions (coupled dam-reservoir solutions and the semi-analytical approach), additional analyses are performed where the water and the dam were modeled using potential-based fluid finite elements and solid plain strain finite elements, respectively, with interactions occurring through a fluid-structure interaction interface (Figure 6.28). These coupled models are built in ADINA, renowned for its capability to accurately model complex fluid-structure interaction problems, and used to obtain dam crest horizontal relative displacements, as well as the stresses within both dams subjected to Imperial Valley (1940) earthquake. Direct integration time-history dynamic analyses with Rayleigh damping (equivalent to modal viscous damping in modal analyses) are used.

The crest horizontal relative displacements are obtained and illustrated in Figure 6.29. The blue curve represents the results from the proposed method using ADINA or SAP2000. The green curve corresponds to the dam-reservoir system based on the analytical formulation, while the red curve represents the coupled dam-reservoir system using potential-based fluid

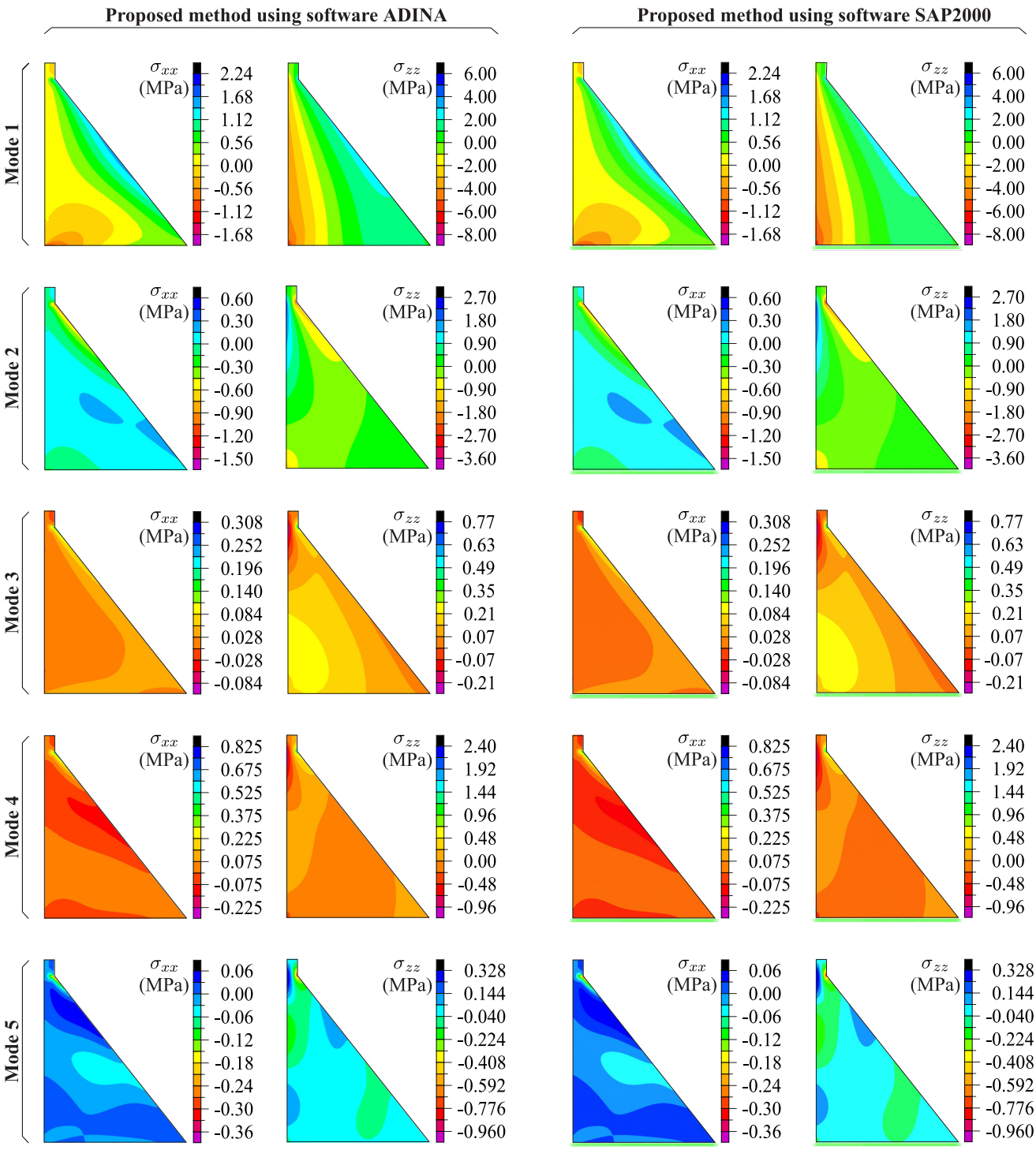

Figure 6.27 Maximum stresses σ_{xx} and σ_{zz} developing within dams D35 and D90 subjected to Imperial Valley (1940) earthquake.

elements. As can be seen, the agreement between these solutions is excellent. The very slight discrepancies between the coupled dam-reservoir finite element solutions and the semi-

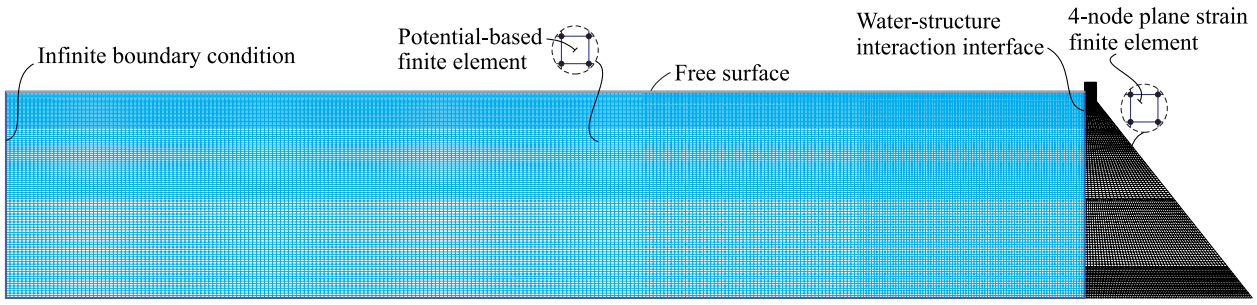

Figure 6.28 Coupled finite element dam-reservoir system.

analytical approach (proposed and reference methods, the results of which are superposed) are mainly due to issues related to finite element discretization of the reservoir, damping (modal vs Rayleigh), and boundary conditions (e.g. infinite elements at reservoir upstream vs mathematical expressions of hydrodynamic pressure). Details about these issues were discussed by Bouaanani and Lu [2].

Additionally, Figure 6.30 shows the distribution of maximum dynamic stresses σ_{xx} and σ_{zz} developed within dams D35 and D90 subjected to Imperial Valley (1940) earthquake, obtained using the proposed method and the coupled dam-reservoir solution. As can be seen again, the agreement between both approaches is excellent.

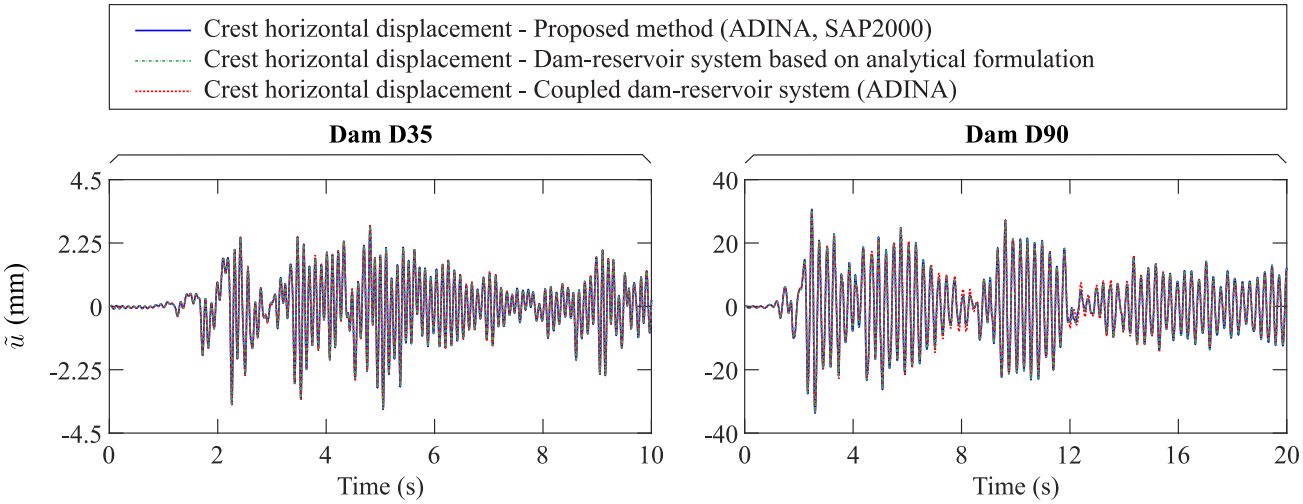

Figure 6.29 Time-history horizontal relative displacements at the crest of dams D35 and D90 subjected to Imperial Valley (1940) earthquake according to three different approaches: blue curve, proposed method using ADINA or SAP2000; green curve, dam-reservoir system based on analytical formulation; red curve, coupled dam-reservoir system using potential-based fluid elements.

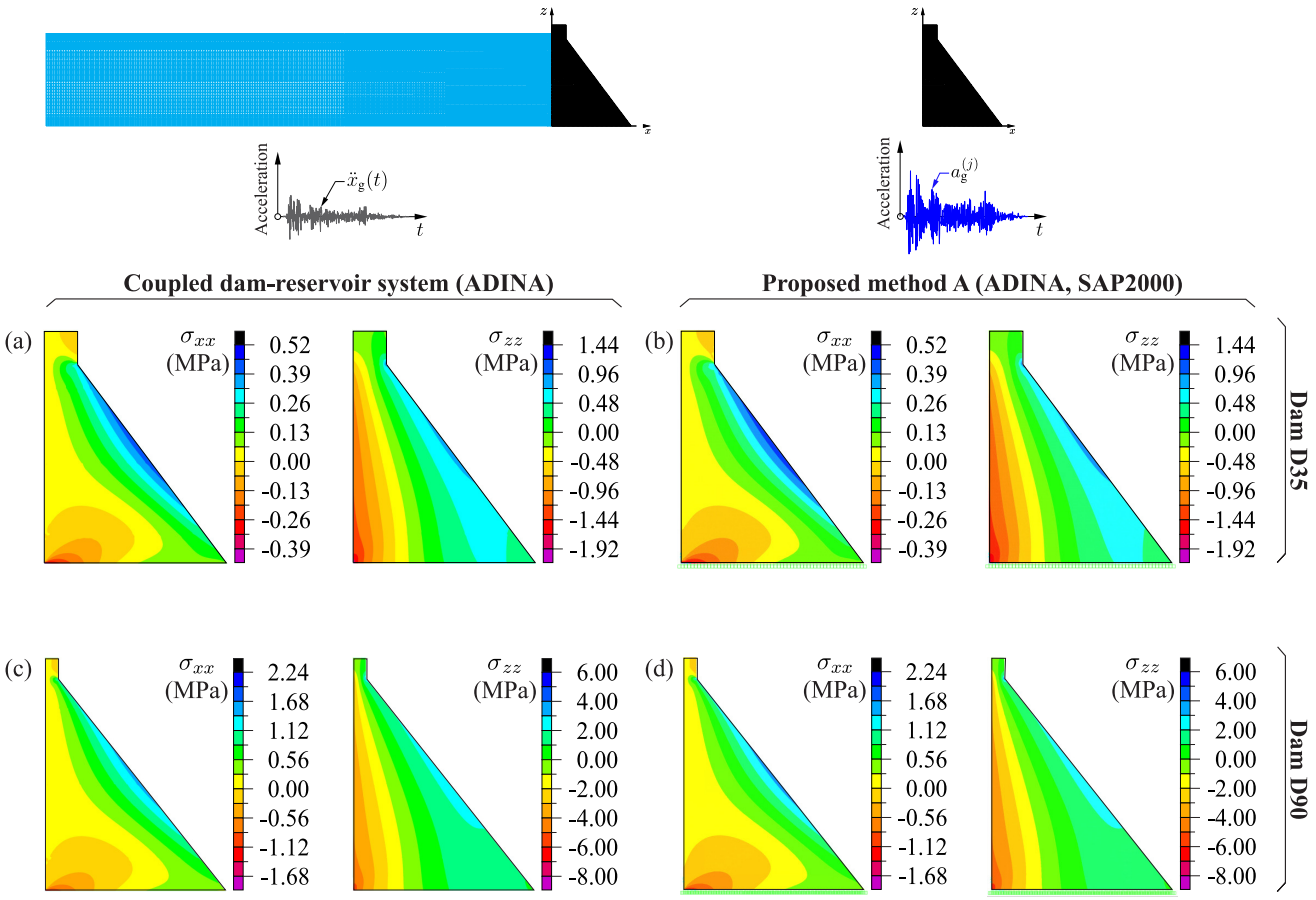

Figure 6.30 Maximum stresses σ_{xx} and σ_{zz} developing within dams D35 and D90 subjected to Imperial Valley (1940) earthquake: (a) and (c) coupled dam-reservoir system using potential-based fluid element; (b) and (d) proposed method using ADINA or SAP2000.

6.3.2 Axisymmetric structures surrounded by water

For the seismic analysis of axisymmetric structures like intake towers surrounded by water using SAP2000 based on the proposed methods, engineers can select either 3D beam elements or 3D solid elements, depending on the required level of detail and accuracy. Beam elements provide a simplified approach suitable for general structural behaviour analysis, while 3D solid elements offer a more detailed representation, capturing complex stress distributions and local effects, which are essential for rigorous assessments. Hydrodynamic effects are incorporated into the analysis by applying the modified ground motion acceleration. The unique characteristics of axisymmetric structures require special consideration for consecutive modes that share the same natural frequency but have different modal participation factors and mode shapes. In such cases, a single modified ground acceleration (e.g. $a_{\mathrm{g}}^{(1)}$) is applied to each pair of these modes (i.e. modes 1 and 2). The procedure for conducting a modal dynamic analysis of axisymmetric structures surrounded by water in SAP2000 involves creating the 3D model, performing a modal analysis to determine natural frequencies and mode shapes, defining the modified ground accelerations, setting up the load cases, and finally combining the time-history load cases to obtain the total structural response, including hydrodynamic effects. The San Bernardino intake tower, depicted in Figure 6.15, is analyzed using both beam and 3D solid elements under the Imperial Valley (1940) earthquake. The first six lateral modes of vibration are illustrated in Figure 6.31. Modified ground accelerations, generated using the dynamic properties of the structure, are shown in Figure 6.32.

Figure 6.34 presents a comprehensive guide to setting up and executing a modal time history analysis of axisymmetric structures surrounded by water. Six lateral modes are included in the analysis, with a constant modal viscous damping ratio of 5% applied to all vibration modes of the structure without water, i.e., $\xi_j = 0.05$ for $j = 1$ to 6. As illustrated in Figures 6.34 (c), (f), and (i), three modal load cases are defined, each with an appropriate frequency shift to isolate the desired modes. Notably, each modal load case captures two consecutive modes, with the maximum number of modes set to 2. This configuration ensures that the software accurately captures and utilizes these two consecutive modes for the analysis. For example, in Figure 6.34 (f), the load case `MODAL-mode3_4` is defined with a frequency shift of 10 Hz, allowing for the accurate capturing of modes 3 and 4, with a natural frequency of 12.31 Hz as shown in Figure 6.34 (a). This load case is then used for the time history analysis in load case `EQS_Ag3_4`, where the modified ground accelerations $a_{\mathrm{g}}^{(3)}$ and $a_{\mathrm{g}}^{(4)}$ are applied as input ground motions along the x-direction of the intake tower, as illustrated in Figure 6.34 (d). It is important to highlight that the modified ground accelerations for each pair of consecutive modes are identical, as depicted in Figure 6.32.

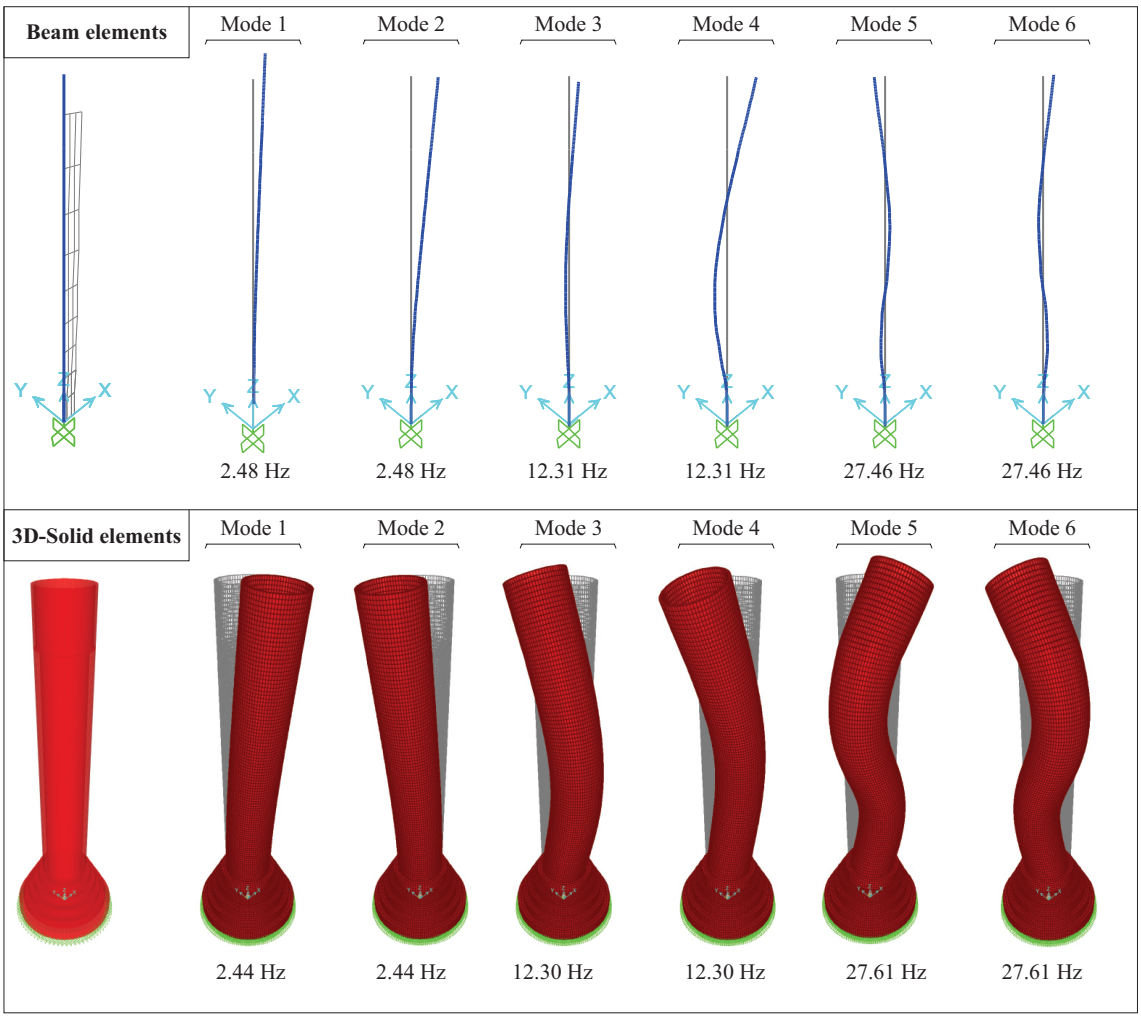

Figure 6.31 Six first lateral mode shapes of San Bernardino intake tower modeled using 3D beam elements and 3D-solid elements.

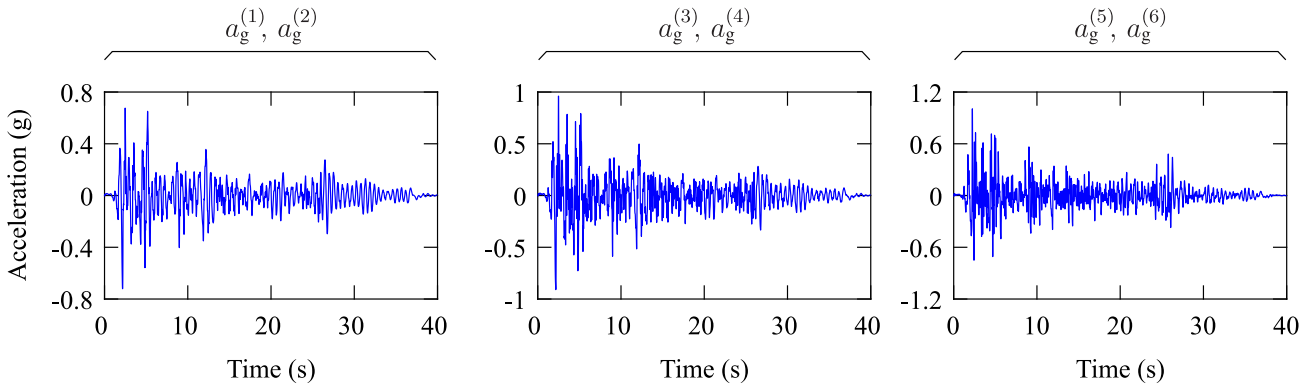

Figure 6.32 Modified ground motion accelerations $a_g^{(1)}$ to $a_g^{(6)}$ corresponding to the first six lateral mode shapes of San Bernardino intake tower subjected to Imperial Valley (1940) earthquake and considering compressible water assumption.

These modified ground accelerations are defined in the software as time history functions, as illustrated in Figures 6.34 (e), (h), and (k). The total time history response of the intake tower can be obtained by combining the linear modal history load cases, as shown in Figure 6.34 (b).

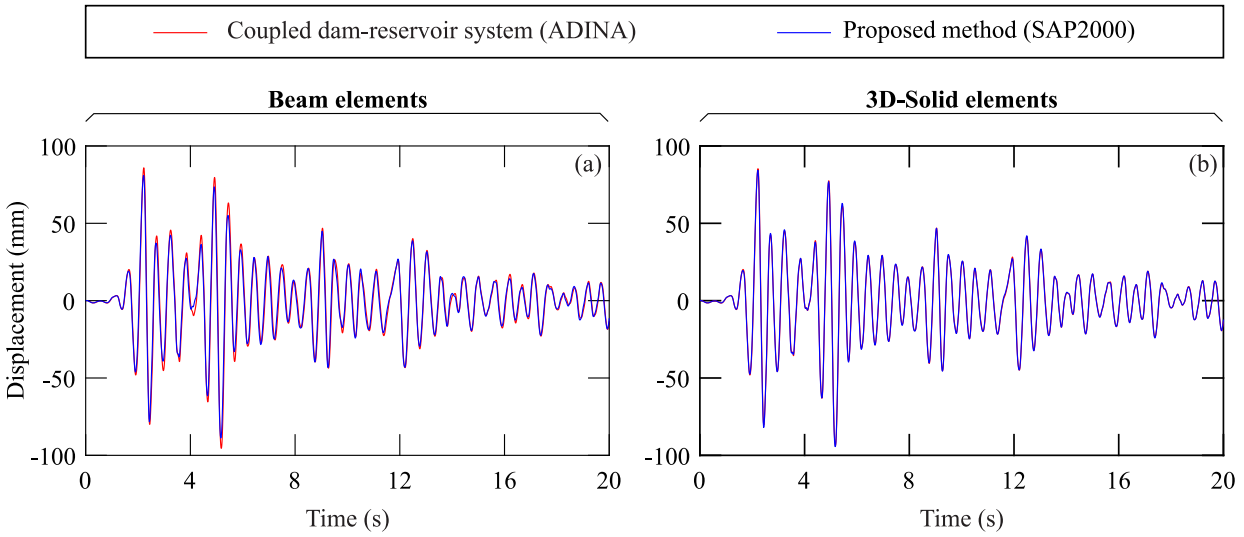

Figure 6.33 Time-history total relative horizontal displacements at the top of the San Bernardino intake tower subjected to the Imperial Valley (1940) earthquake, according to two different approaches: blue curves represent the proposed method using SAP2000 with beam and 3D-solid elements; red curves represent the coupled structure-water system using potential-based fluid elements modeled in ADINA software.

As shown in Figure 6.33 (a), the total relative horizontal displacements at the top of the San Bernardino intake tower are compared using the proposed method with beam elements in SAP2000 and the coupled structure-water model in ADINA. Similarly, Figure 6.33 (b) compares the results obtained using 3D-solid elements in SAP2000 with those from the coupled model. The comparison reveals excellent agreement between the methods, with only slight differences observed when beam elements are used in SAP2000. Despite these minor discrepancies, the proposed method with beam elements offers a significant advantage in terms of computational efficiency, completing the analysis in just 2 minutes compared to the 10 hours required for the coupled model. This demonstrates the effectiveness of the proposed method in delivering accurate results while significantly conserving computational resources. Additionally, when 3D-solid elements were used to model the San Bernardino intake tower, the analysis took 10 minutes to run, offering a much faster alternative to the coupled structure-water system. In comparison, the beam element approach is 300 times faster, and the 3D-solid element approach is 60 times faster, proving the method's efficiency.

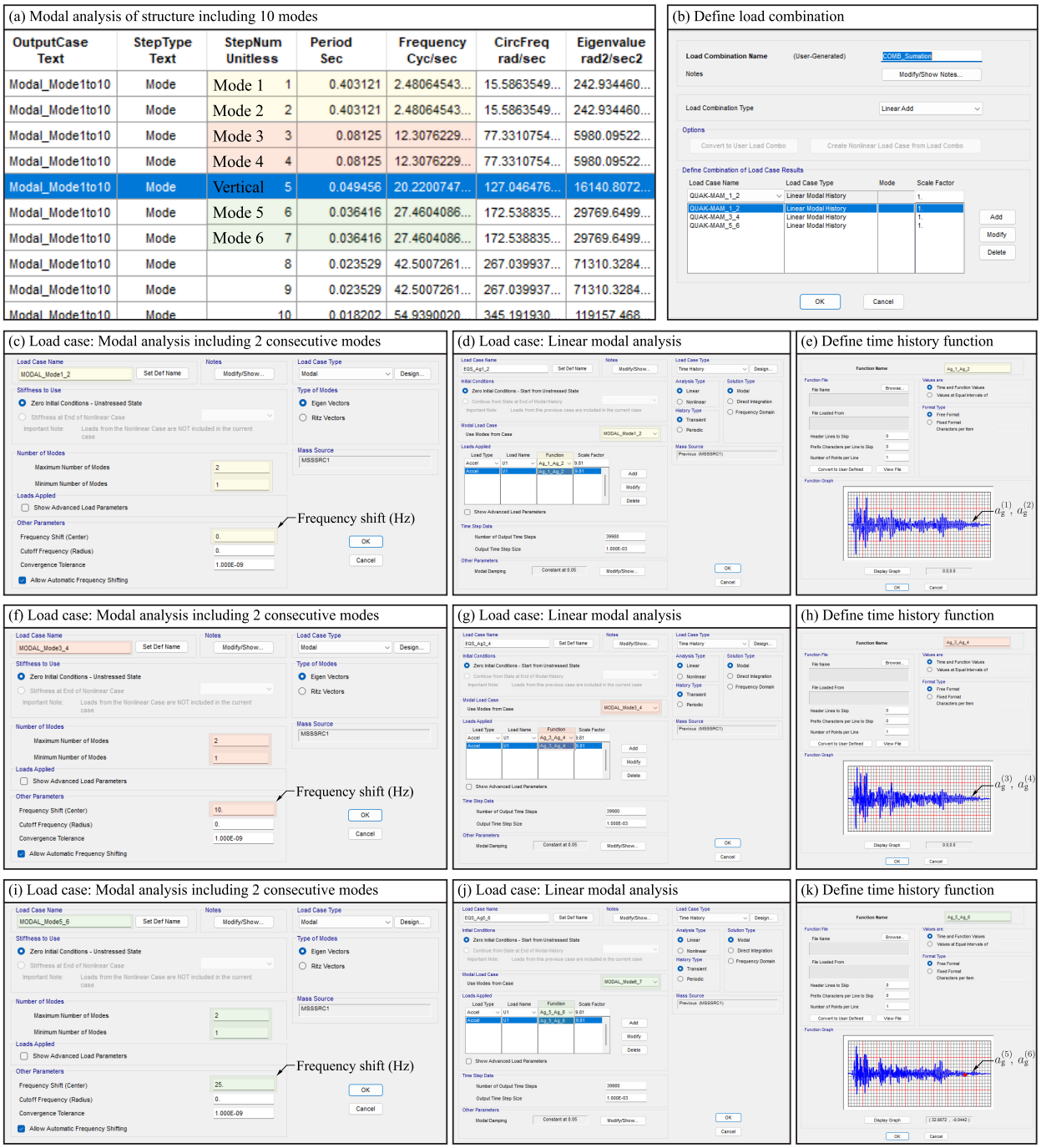

(a) Modal analysis of structure including 10 modes

OutputCase Text	StepType Text	StepNum Unitless	Period Sec	Frequency Cyc/sec	CircFreq rad/sec	Eigenvalue rad2/sec2
Modal_Mode1to10	Mode	Mode 1 1	0.403121	2.48064543...	15.5863549...	242.934460...
Modal_Mode1to10	Mode	Mode 2 2	0.403121	2.48064543...	15.5863549...	242.934460...
Modal_Mode1to10	Mode	Mode 3 3	0.08125	12.3076229...	77.3310754...	5980.09522...
Modal_Mode1to10	Mode	Mode 4 4	0.08125	12.3076229...	77.3310754...	5980.09522...
Modal_Mode1to10	Mode	Vertical 5	0.049456	20.2200747...	127.046476...	16140.8072...
Modal_Mode1to10	Mode	Mode 5 6	0.036416	27.4604086...	172.538835...	29769.6499...
Modal_Mode1to10	Mode	Mode 6 7	0.036416	27.4604086...	172.538835...	29769.6499...
Modal_Mode1to10	Mode	8	0.023529	42.5007261...	267.039937...	71310.3284...
Modal_Mode1to10	Mode	9	0.023529	42.5007261...	267.039937...	71310.3284...
Modal_Mode1to10	Mode	10	0.018202	54.9390020...	345.191930...	119157.468...

Figure 6.34 Procedural steps for setting up and executing the modal time history analysis of San Bernardino intake tower in SAP2000 including hydrodynamic effects: (a) natural frequencies highlighting the first six lateral modes; (b) combination of defined load cases; (c), (f), and (i) modal load cases with appropriate frequency shifts applied; (d), (g), and (j) linear modal history load cases; (e), (h), and (k) defining modified ground accelerations as time history functions.

6.4 Experimental consideration for shaking table test of water structure system

This section discusses the shaking table tests of structure-water systems and their appurtenant structures, with a focus on the rationale for selecting an axisymmetric structure surrounded by water as the primary structure. Additionally, it examines the reasoning behind this choice and provides a detailed discussion of the effects of low damping on the modified ground acceleration.

6.4.1 Shaking table test of axisymmetric structure surrounded by water

After selecting axisymmetric structures surrounded by water as the primary system on which the appurtenant structure, The next steps involved selecting the height of the specimen, section dimensions, material properties, and water levels. These parameters had to be chosen in such a way that the hydrodynamic effects would be significant and not negligible, as a system where these effects are minimal would not be suitable for the intended study. Another decision was made to avoid the potential impact of similitude laws on the input signal, particularly given the operational limitations of the shaking table. This led to the choice of not applying any similitude laws in the testing process. The goal of this approach was to preserve the integrity of the original signal, especially its frequency content, ensuring that the shaking table could accurately reproduce the necessary frequency range to cover the natural frequency of the selected testing specimen. The focus then set to select an axisymmetric structure with a low natural frequency, ideally within the range of structures such as offshore wind turbines or bridge piers, targeting a fundamental natural frequency of less than 10 Hz.

In this section, a detailed explanation of the selection process for the axisymmetric structure will be presented, highlighting the considerations and analyses that led to the final decision. This process ensured that the chosen structure would effectively demonstrate the interaction between hydrodynamic forces and seismic responses, making it a suitable candidate for the shaking table tests of structure-water system. The selection process involves three key considerations: (i) deciding whether the section should be solid or hollow, (ii) selecting the material for the axisymmetric structure, with potential options including steel and aluminum, while deliberately excluding concrete to avoid the complexities of casting, curing, and ensuring a crack-free specimen, and (iii) determining the appropriate height that provides sufficient flexibility while maintaining safety, particularly as very tall (slender) specimens can be challenging to control under seismic loading during experimental tests. It is crucial that the appurtenant structure fixed at the top remains secure, even during nonlinear behaviour. Each of these factors plays a significant role in the dynamic response of the system and must

be carefully evaluated.

The initial analysis focuses on comparing steel and aluminum as potential materials for a specimen with a height of 4.3 m, considering both circular hollow sections using HSS 127×9.5 and solid sections of the same diameter. The analysis includes performing a modal dynamic analysis to determine the dynamic properties of the specimen, emphasizing the effects of solid versus hollow sections, as well as the impact of the chosen material on the tower's dynamic characteristics. Additionally, the frequency response function (FRF) of relative horizontal acceleration at the top of the tower is compared under both dry (i.e. without water) and wet (i.e. with water surrounding the tower) conditions. This comparison aims to evaluate how the choice of material—steel or aluminum—and section type—solid or hollow—affects the seismic response of the axisymmetric tower when surrounded by water, highlighting the hydrodynamic effects in each scenario. Figure 6.35 depicts the axisymmetric structure mounted on the shaking table, alongside a person highlighting the specimen's dimensions relative to the size of the shaking table and the height of an average person.

The material properties used in this comparison for steel and aluminum include a density (ρ) of 7850 kg/m^3 for steel and 2700 kg/m^3 for aluminum. The Poisson's ratio (ν) was set to 0.3 for both materials, with a modulus of elasticity (E) of 200 GPa for steel and 69 GPa for aluminum. Table 6.3 summarizes the results of the modal dynamic analysis, providing the first six natural frequencies for the axisymmetric structure under different assumptions. The analysis considers both steel and aluminum materials, as well as hollow and solid sections. This comprehensive comparison highlights the influence of material selection and cross-sectional geometry on the dynamic properties of the structure. The table clearly shows that the

Table 6.3 First six natural frequencies of the axisymmetric structure using different section materials (steel vs. aluminum) and geometries (hollow vs solid)

Mode number	**Steel material**		**Aluminum material**	
	Hollow section	Solid section	Hollow section	Solid section
1	6.43 Hz	4.95 Hz	6.39 Hz	4.91 Hz
2	6.43 Hz	4.95 Hz	6.39 Hz	4.91 Hz
3	40.03 Hz	30.95 Hz	39.73 Hz	30.69 Hz
4	40.03 Hz	30.95 Hz	39.73 Hz	30.69 Hz
5	110.83 Hz	86.27 Hz	109.99 Hz	85.57 Hz
6	110.83 Hz	86.27 Hz	109.99 Hz	85.57 Hz

choice between steel and aluminum does not significantly affect the natural frequencies of the tower. This is due to the similar ratio of the modulus of elasticity to the density for both

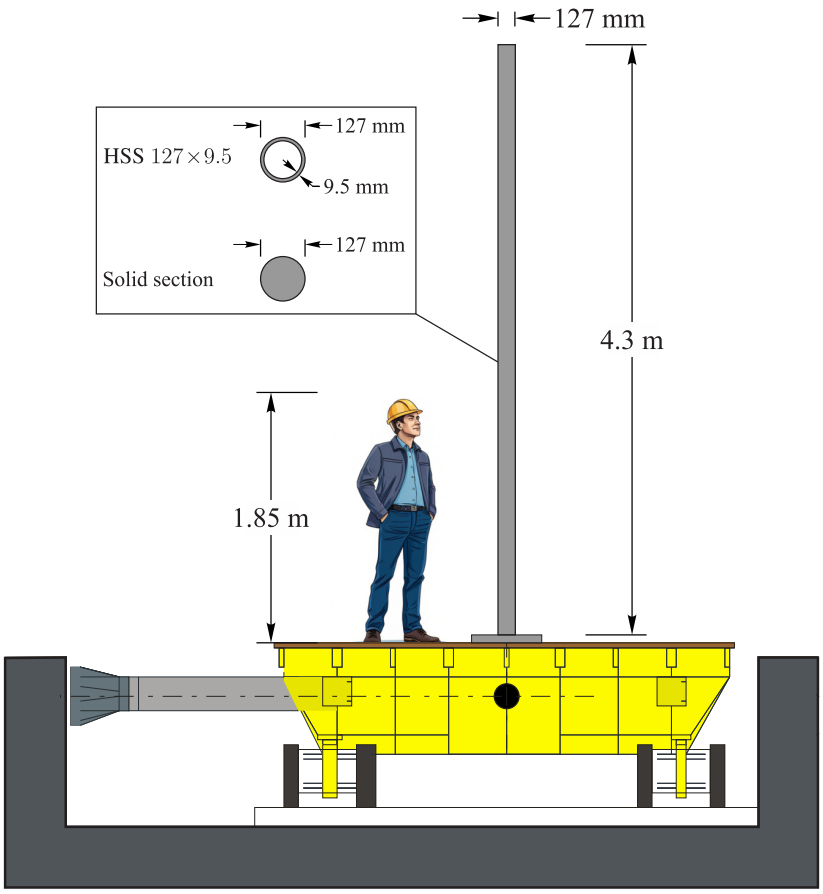

Figure 6.35 Dimensions of circular hollow sections using HSS 127 × 9.5 and solid sections of the same diameter mounted on the shaking table.

materials. It is important to note that the total mass of the steel structure is approximately 2.9 times greater than that of the aluminum structure, primarily due to the significantly higher density of steel.

The table also highlights the impact of section geometry on the natural frequencies of the tower. It is evident that using a solid section results in lower natural frequencies, indicating increased flexibility of the system. For instance, when steel is used for the tower, the fundamental natural frequency decreases by 23 %(from 6.43 Hz to 4.95 Hz) when a solid section is used instead of a hollow section. Similarly, for aluminum, the fundamental natural frequency decreases by 22.5 %, i.e. $(6.39 - 4.91)/6.39 \times 100$. This trend can be observed across higher modes; for example, in modes 5 and 6, the decrease is 22.1 % for both steel and aluminum when the solid section is used instead of the hollow section. These observations clearly indicate that a solid section increase the system's flexibility by approximately 20 to 30 %.

Figure 6.36 presents the frequency response function (FRF) of the horizontal acceleration at the top of the axisymmetric tower, comparing the effects of hollow and solid sections as well as steel and aluminum materials on the system's dynamic response, both with and without surrounding water. The analysis considers the hydrodynamic effects using compressible water assumption, with the water level the same as the height of the tower ($H_w = H_s$) and considering a constant 5 % modal viscous damping ratio. Although a 5% viscous damping ratio for aluminum material is higher than the actual value (which was measured and presented in Chapter 5), it is selected for illustrative purposes to ensure consistent comparisons.

This comparison highlights the influence of material choice and section geometry on the tower's seismic response, particularly when accounting for the hydrodynamic interactions with the surrounding water.

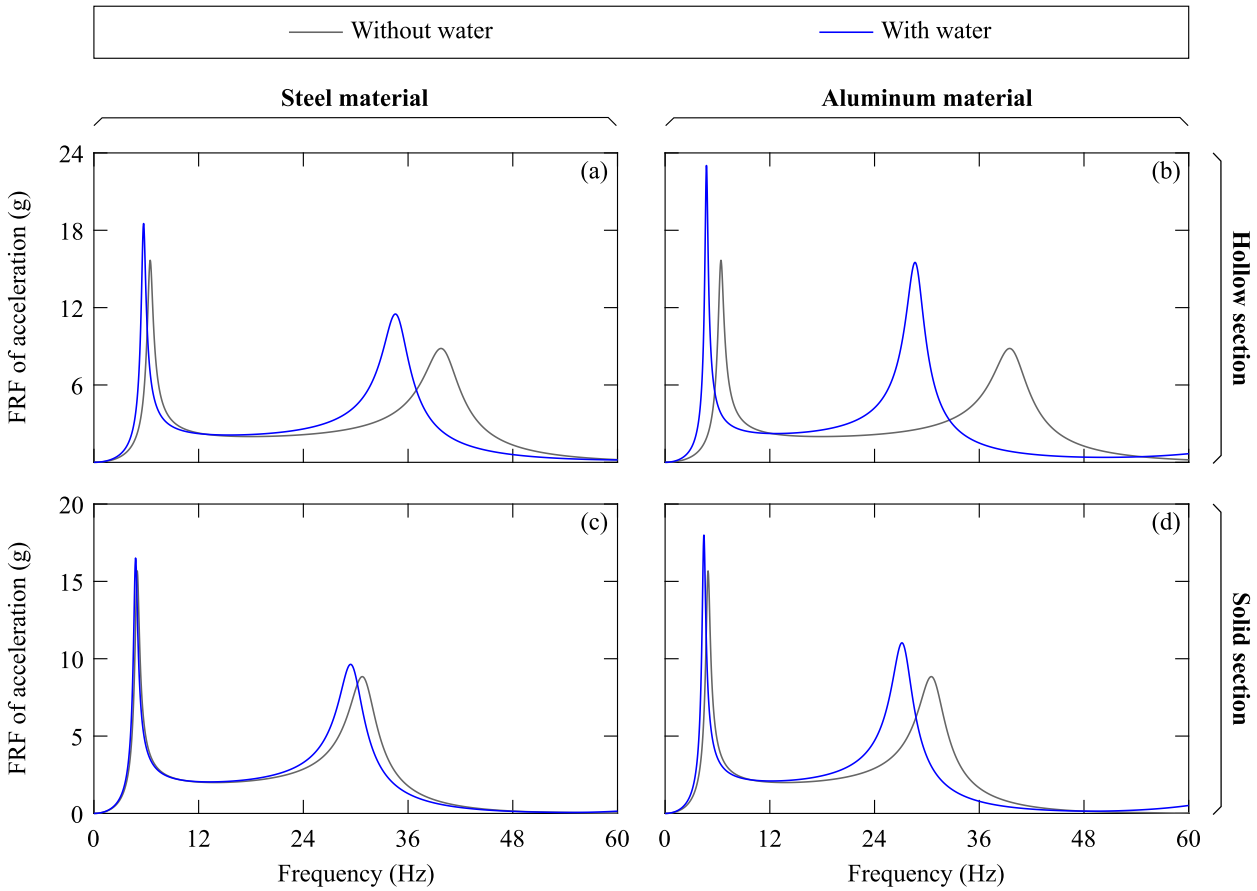

Figure 6.36 Frequency response function (FRF) of relative horizontal acceleration at the top of the axisymmetric tower, comparing the effects of hollow and solid sections and materials: (a) and (b) steel material; (c) and (d) aluminum material.

In this figure, the gray curves represent the response of the tower without surrounding water, while the blue curves show the response of the tower including hydrodynamic effects. It

is evident that, in all cases, the presence of water increases the flexibility of the system, leading to a shift in the natural frequency of the structure including hydrodynamic effects. By comparing Figures 6.36 (a) and (b), which represent the response of the tower with the same hollow section but different materials (steel and aluminum, respectively). It can be seen clearly that using aluminum instead of steel increase the hydrodynamic effects, as indicated by a more pronounced shift in the natural frequency to the left for the aluminum tower. This conclusion is further supported by the comparison of material effects for the solid section, as shown in Figures 6.36 (c) and (d), where the aluminum material again demonstrates a greater influence of hydrodynamic interactions. Considering both Figure 6.36 and Table 6.3, the optimal choice to maximize the impact of hydrodynamic pressures on the tower's response is an aluminum tower with a hollow section geometry. This combination not only provides the desired flexibility but also amplifies the influence of surrounding water, making it the most suitable configuration for the experimental study.

To determine the optimal height for the tower, four different heights were taken into account: 4.3 m, 3 m, 2 m, and 1.75 m. It is crucial to note that, as previously discussed, shorter heights are generally preferred for better safety control during shaking table tests. However, the selected height must also ensure that the tower's natural frequency remains within the target range (around 10 Hz) and that the hydrodynamic effects of the surrounding water have a significant impact on the tower's response.

Figure 6.37 compares the frequency response function (FRF) of horizontal acceleration at the top of axisymmetric towers with four different heights: 4.3 m, 3 m, 2 m, and 1.75 m. Each tower is modeled with a hollow HSS 127×9.5 cross-section, and aluminum is used as the material for all cases. The analysis evaluates the dynamic response of these towers, both with and without the inclusion of hydrodynamic effects, assuming compressible water with a level equal to the height of the tower ($H_{\mathrm{w}} = H_{\mathrm{s}}$) and considering a constant 5 % modal viscous damping ratio. In this figure, (a) represents the FRF for the 4.3 m height tower, with the gray curve showing the response for the dry system and the blue curve illustrating the response including hydrodynamic effects. Figure 6.37 (b) depicts the FRF for the 3 m height tower. Figures 6.37 (c) and (d) present the FRF for towers with heights of 2 m and 1.75 m, respectively. This comparison highlights how the height of the structure influences its dynamic response, particularly when hydrodynamic effects are considered.

Figure 6.38 schematically illustrates the specimens with varying heights mounted on the shaking table, alongside a typical person for comparison, offering a visual representation of the tower heights relative to an average person.

Based on the analysis and the results that is presented in Figure 6.37, it can be concluded that

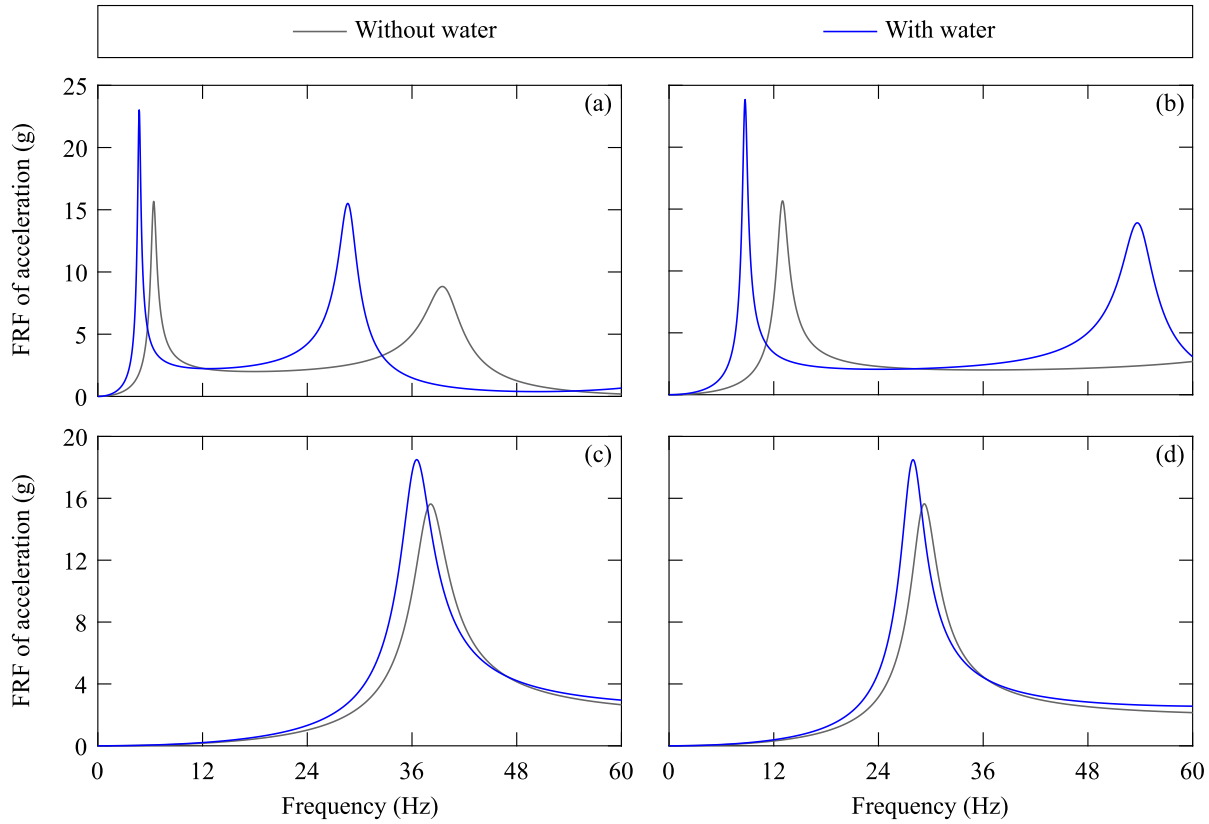

Figure 6.37 Frequency response function (FRF) of relative horizontal acceleration at the top of the axisymmetric tower, comparing the effects of different tower heights: (a) FRF for the 4.3 m tower; (b) FRF for the 3 m tower; (c) FRF for the 2 m tower; and (d) FRF for the 1.75 m tower.

the optimal choice for the height of the tower is 3 m. This height provides a balance between achieving a natural frequency within the desired range and ensuring that the hydrodynamic effects are sufficiently pronounced to affect the tower's response, while also maintaining safety and control during the shaking table test. The other reason for selecting a 3 m height as the final choice was the practical consideration of material availability. The standard length for HSS tubes in the market was 20 feet (around 6.95 m). By dividing this length in half, two identical 3 m specimens can be obtained. This not only ensures that a second specimen is readily available for repeat testing if needed but also results in significant cost savings. This practical advantage, combined with the optimal dynamic properties observed, confirmed the decision to proceed with the 3 m height for the tower. Considering the market availability at the time of scheduling the tests, several cross sections were evaluated. Table 6.4 summarizes the first six natural frequencies of the aluminum tower for each section analyzed. Figure 6.39 presents the FRF of the acceleration response at the top of the tower, comparing the dynamic behaviour across different geometric cross sections, assuming compressible water

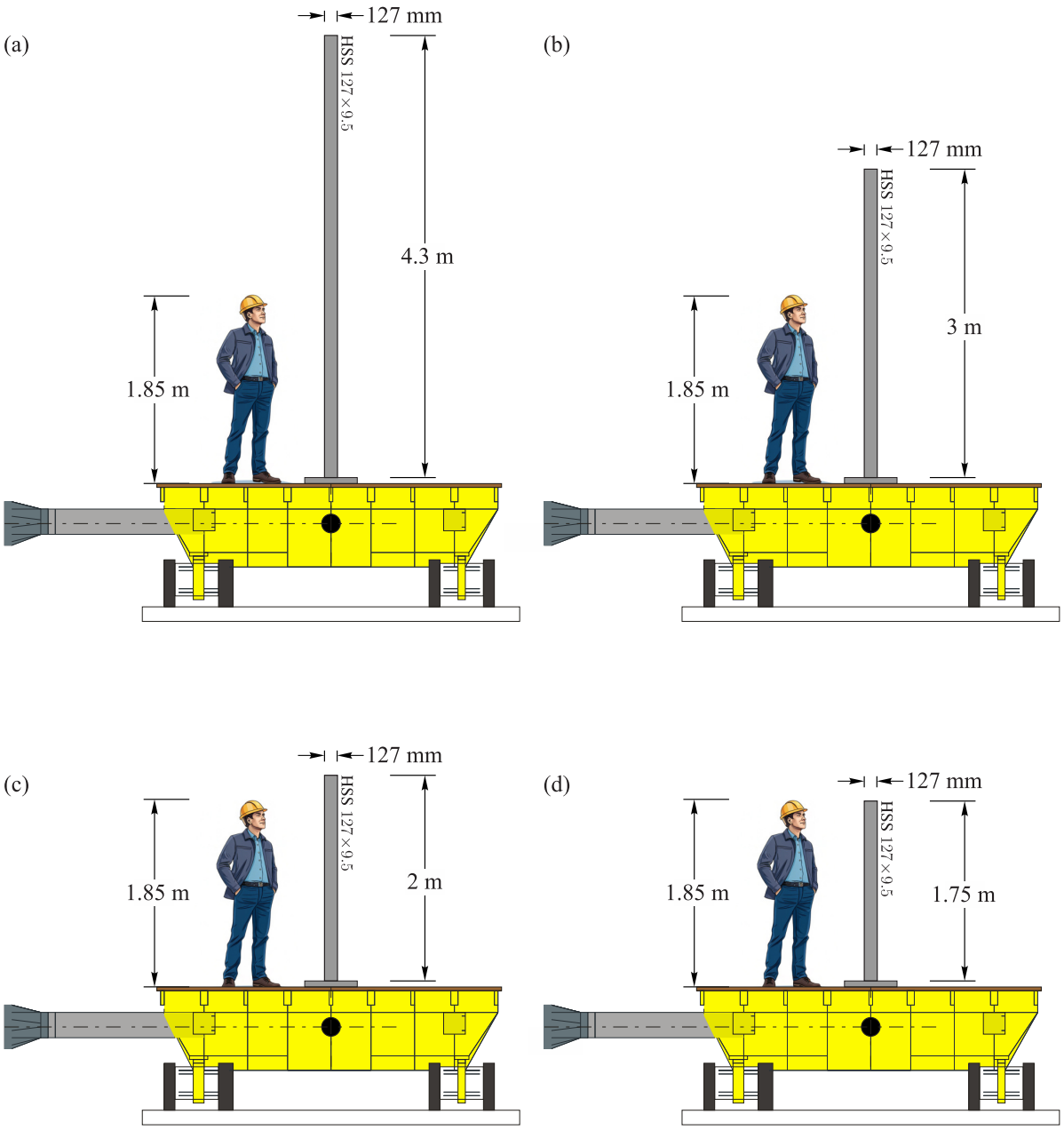

Figure 6.38 Dimensions of circular hollow sections using HSS 127 × 9.5 for towers of varying heights mounted on the shaking table: (a) 4.3 m; (b) 3 m; (c) 2 m; and (d) 1.75 m.

and applying a 5% viscous damping ratio for the structure. The impact of hydrodynamic effects is clearly depicted by the blue curves in this figure. Among the evaluated options, the HSS 76×6.4 section was selected as the optimal choice, providing dynamic properties within the desired range while effectively demonstrating the hydrodynamic effects on the response of the tower.

Table 6.4 First six natural frequencies of the aluminum material axisymmetric structure using different sections available in the market

Sections	**Natural frequencies (Hz)**					
	Mode 1	Mode 2	Mode 3	Mode 4	Mode 5	Mode 6
HSS 76×6.4	7.82	7.82	48.73	48.73	135.28	135.28
HSS 89×6.4	9.22	9.22	57.31	57.31	158.59	158.59
HSS 89×8.0	9.06	9.06	56.33	56.33	155.96	155.96
HSS 102×6.4	10.61	10.61	65.84	65.84	181.51	181.51
HSS 102×8.0	10.45	10.45	64.87	64.87	178.92	178.92
HSS 127×9.5	13.09	13.09	80.76	80.76	220.95	220.95

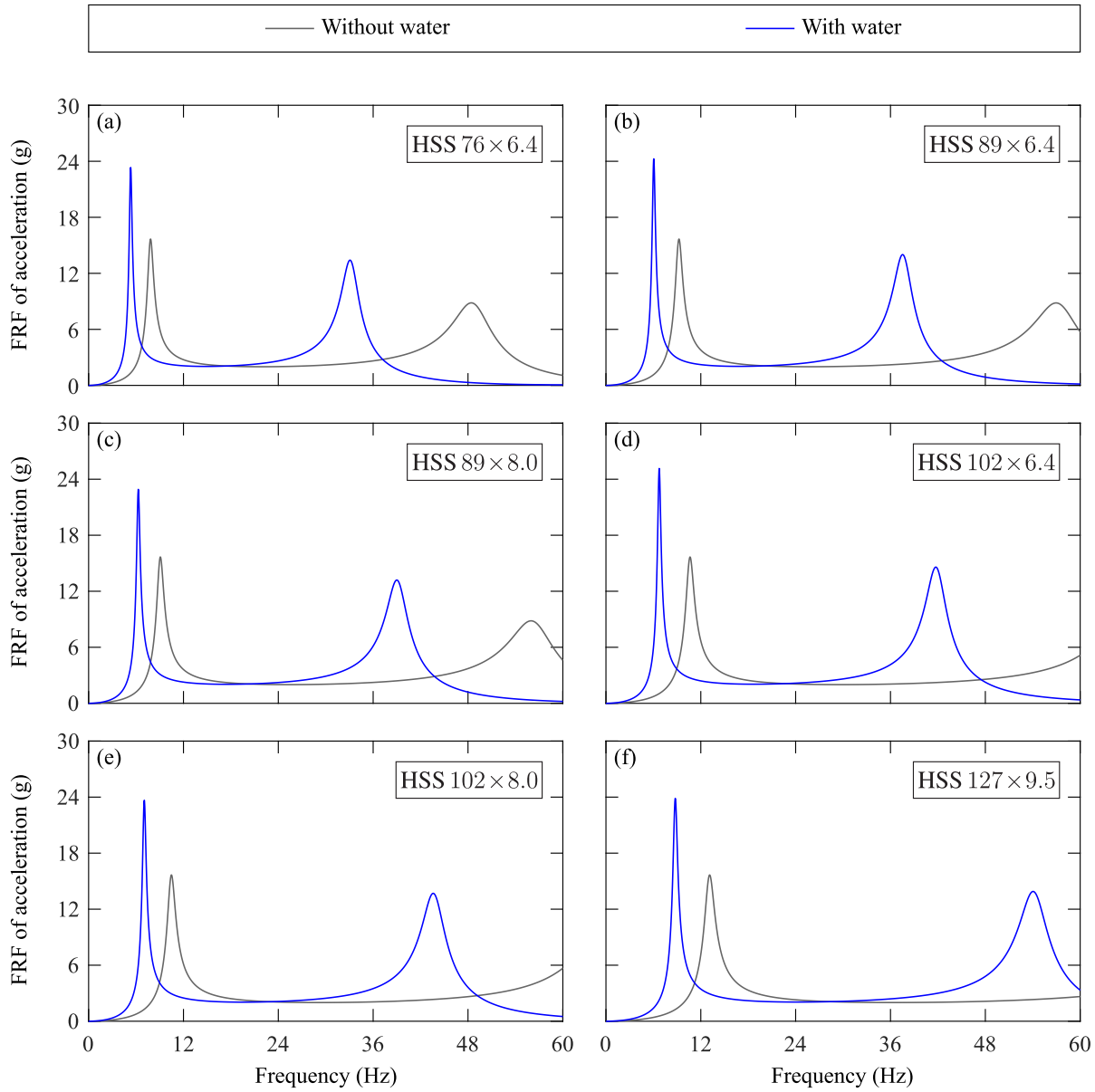

Figure 6.39 Frequency response function (FRF) of relative horizontal acceleration at the top of the axisymmetric tower, comparing the effects of different tower heights: (a) HSS 76×6.4; (b) HSS 89×6.4; (c) HSS 89×8.0; (d) HSS 102×6.4; (e) HSS 102×8.0; (f) HSS 127×9.5.

Figure 6.40 displays the final tower design, which was fabricated to serve as the experimental model representing an axisymmetric structure surrounded by water. Numerical analysis determined the fundamental frequency of the tower to be 7.82 Hz, a value that was later confirmed through experimental testing using pull-release tests and harmonic cyclic excitation. With a fundamental frequency below the 10, Hz, the tower is a suitable representation of a flexible structure-water system, comparable to offshore wind turbines, bridge piers, or intake towers in terms of dynamic flexibility.

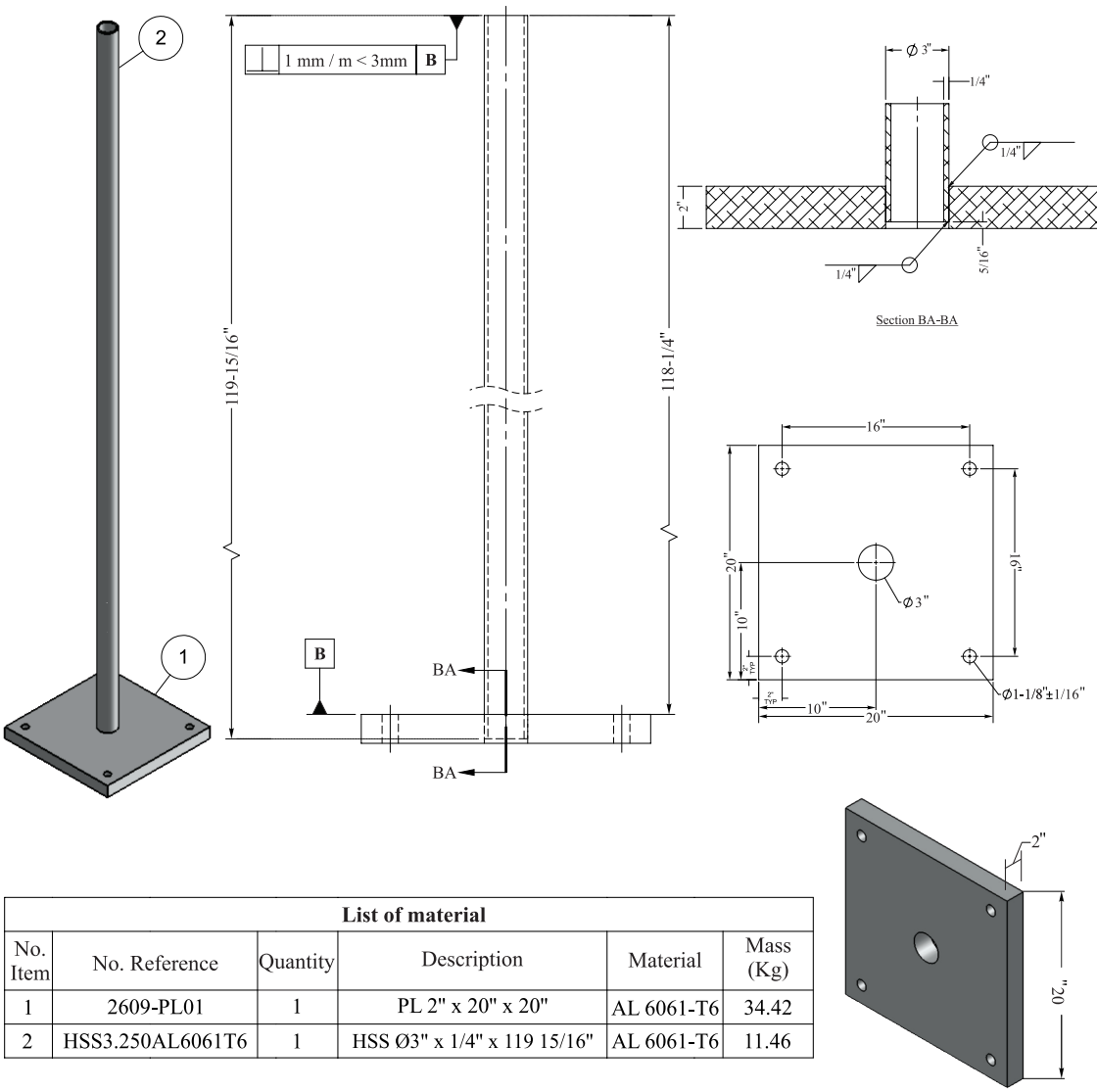

List of material					
No. Item	No. Reference	Quantity	Description	Material	Mass (Kg)
1	2609-PL01	1	PL 2" x 20" x 20"	AL 6061-T6	34.42
2	HSS3.250AL6061T6	1	HSS Ø3" x 1/4" x 119 15/16"	AL 6061-T6	11.46

Figure 6.40 Fabricated aluminum tower with HSS 76×6.4 cross section, including detailed views of the design features.

6.4.2 Experimental considerations for applying the proposed method for low-damping systems

Damping effect on modifed ground acceleration

During the experimental tests, it was found that the damping ratio of the aluminum tower, due to its material properties, was lower than anticipated (i.e. measured 0.25%). While this unexpectedly low damping presented challenges during the tests, it also provided a valuable opportunity to explore solutions by identifying and addressing potential issues that could arise, ultimately improving test outcomes and methodologies. Understanding these challenges is important for effectively implementing the modified ground acceleration method in shaking table tests of structure-water systems. This is particularly important when scaled models are used, as the similitude laws can result in reduced damping due to scaling factors. Accurately representing these low-damping characteristics and their effect on modified ground acceleration is essential for obtaining valid experimental results and for validating the proposed method under testing conditions.

Figure 6.41 illustrates the impact of damping on the FRFs of the acceleration at the top of the tower, as well as its effect on the modified ground motion acceleration. As the structural damping ratio decreases from 5% to 0.25%, the FRFs become sharper at the natural frequencies of the system, indicating more pronounced resonance peaks. This reduction in damping also affects the modified ground acceleration, as shown in the right column of this figure. It is worth mentioning that in this section Nahanni earthquake (1985) is used as original ground acceleration. A lower damping ratio leads to an increase in amplitude (or PGA) and introduces a harmonic-like pattern into the modified signal. This harmonic behaviour is due to the free vibration of the tower in water, which takes longer to dissipate in a low-damping system. As the damping decreases, this harmonic effect becomes more pronounced, as clearly seen in Figure 6.41 (h). This demonstrates that applying the modified ground motion acceleration to a dry structure can alter its free vibration characteristics, enabling it to accurately reflect the dynamic behaviour of a water-surrounded structure, highlighting the method's effectiveness even in low-damping conditions. Figures 6.41 (f) and (h) demonstrate that as damping decreases, the modified ground acceleration fails to align with the original ground acceleration at the initial condition (time equals zero). It should be noted that at initial time (i.e. $t = 0$), both the original and modified ground accelerations should start from zero. This misalignment shows a potential issue in the process of generating modified ground acceleration under low damping conditions.

To ensure the accurate generation of modified ground acceleration, a technique called zero

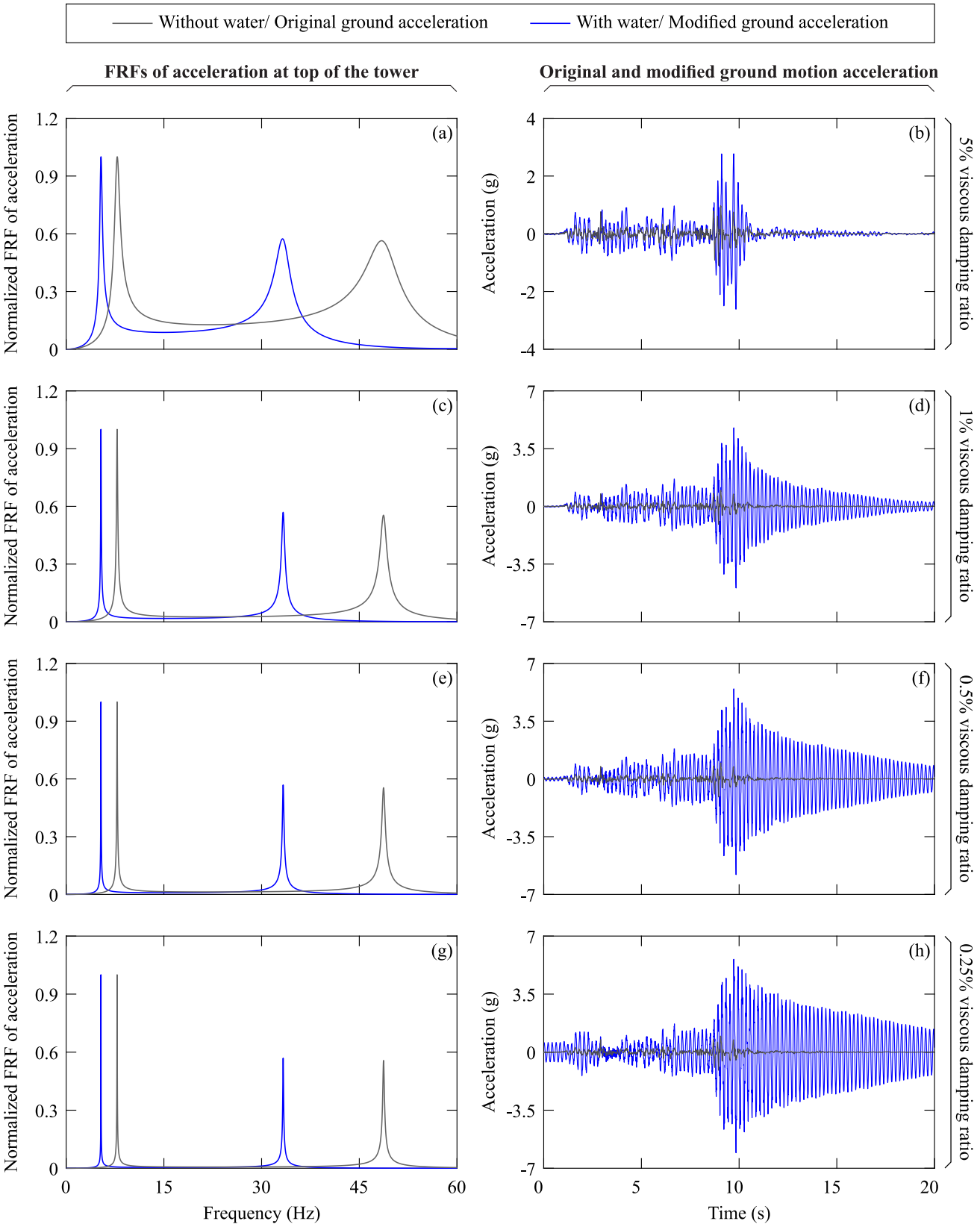

Figure 6.41 Damping effect on the FRF of acceleration at the top of the tower as well as on the modified ground motion acceleration.

padding is necessary. This technique involves adding zero values to the end of the ground acceleration data, and it serves two primary purposes. First, it enhances the efficiency of the Fast Fourier Transform (FFT) algorithm, particularly when processing signals with 2^{NEXP} data points, where NEXP represents the number of excitation frequencies. Second, zero padding improves frequency resolution, resulting in a more detailed representation of the frequency spectrum. In the EAGD84 program developed by Fenves and chopra [29], this process is referred to as the *quiet zone*, where N points of zero acceleration are automatically appended to the end of the ground acceleration records. By adding these zeros, the aliasing error inherent in the Discrete Fourier Transform (DFT) is reduced, leading to a more accurate representation of the frequency content.

For systems with low damping, zero padding becomes particularly crucial. In such cases, the free vibration response including hydrodynamic effects requires more time to damp out. Therefore, it required more time to get back to initial condition. To ensure that the modified ground acceleration follows the initial motion of the original ground acceleration, sufficient zero padding is required. Insufficient duration for zero padding, especially in low damping systems, can cause the modified ground acceleration to start with a false initial value, leading to inaccurate input acceleration. To generate the modified ground acceleration shown in Figure 6.41, zero padding equal in length to the original signal was applied. This extended the total duration of the signal to twice its original length, with the second half consisting of zero values (as detailed in Appendix B of Article 1). As illustrated in Figures 6.41 (b) and (d), this amount of zero padding is sufficient to produce accurate modified ground acceleration for systems with a structural damping ratio of not less than 1%. However, for low-damping systems, this padding length proves inadequate and can introduce errors. In such cases, extending the zero padding duration is required.

The same exercise is repeated by extending the signal length and adding zero values equal to four times the initial length of the original ground motion acceleration. Figure 6.42 compares the modified ground acceleration generated using two different lengths of zero padding: (i) zero padding equal to the initial length of the original signal, and (ii) zero padding four times the initial length of the original signal. As shown in Figure 6.42 (h) compared to (g), the modified ground acceleration generated using the four times lengthened signal aligns with the original ground acceleration at the initial time, clearly demonstrating that the extended duration is sufficient for effectively damping out the free vibration in a low-damping system.

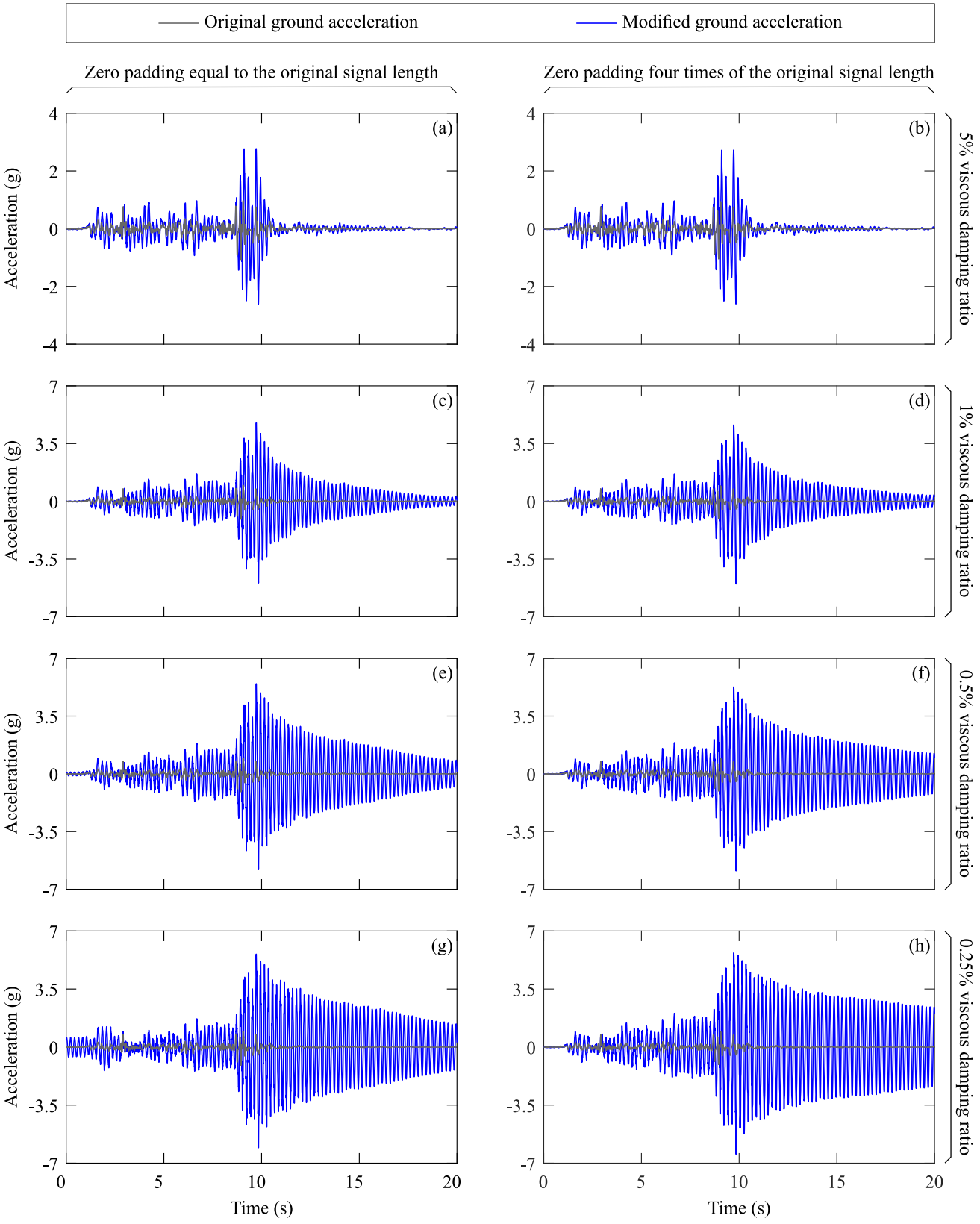

Figure 6.42 Effects of different zero padding lengths on modified ground acceleration: (a), (c), (e), and (g) zeros added with the same length as the original signal; (b), (d), (f), and (h) zeros added with four times the original signal length.

For the experimental tests, it is important to know how the low-damping system impacts the modified ground acceleration, particularly in understanding how the shaking table controller handles a combination of arbitrary signals, such as the Nahanni earthquake (1985), along with the harmonic-like component representing the free vibration of the tower, including hydrodynamic effects. To ensure the success of the test, it is vital to understand the mechanisms behind the operation of the shaking table. This guarantees that the modified ground acceleration is accurately replicated during the tests, meaning that the output signal (feedback) experienced by the specimen closely matches the input signal (command) defined for the shaking table.

6.5 Conclusion of discussion

This chapter presents a discussion on the proposed method, divided into numerical and experimental parts. In the numerical section, the focus was on the validation and applicability of the proposed method for seismic analysis of dam-reservoir systems and axisymmetric structures surrounded by water using modified ground acceleration method. This evaluation was conducted through a series of case studies, including detailed time-history and response spectra analyses and comparisons with classical solutions. Additionally, the applicability of the proposed method using general-purpose structural analysis software was addressed. In the experimental section, the discussion extends to the proposed shaking table tests of structure-water systems. The rationale for selecting an axisymmetric structure as the primary system was carefully examined, considering the experimental limitations. Based on these, the key conclusions can be summarized as follows

- The proposed method effectively modifies the frequency content of original ground motion acceleration by accounting for hydrodynamic effects, dynamic flexibility, and wave propagation within the reservoir. The method successfully captured the interaction between the dam and the reservoir, as evidenced by the close match with results from classical solutions across a wide range of forcing frequencies.

- Additional case studies, such as the seismic analysis of the Pine Flat dam and the San Bernardino intake tower, were carried out to further validate the proposed methods. Analyses under various earthquakes showed that the method effectively modified ground accelerations by incorporating hydrodynamic effects, proving its adaptability to different structural types and seismic conditions.

- The application of the proposed method for seismic analysis using general-purpose structural analysis software, specifically SAP2000, was also demonstrated. The method

was successfully applied using SAP2000 to two dam-reservoir systems and one axisymmetric structure, validating its accuracy and efficiency in providing solutions for complex fluid-structure interactions while significantly reducing analysis time.

- The process of selecting axisymmetric structures surrounded by water, as well as determining the optimal height, material, and section geometry to maximize hydrodynamic effects while maintaining safety, was carefully analyzed. This thorough evaluation led to the final configuration for shaking table tests of the structure-water system using modified ground motion acceleration.

CHAPTER 7 CONCLUSION AND RECOMMENDATIONS

This chapter summarizes the research project, discussing the major findings and conclusions drawn from the study. It also presents recommendations for further research and highlights the original contributions made in this work.

7.1 Conclusions

This Ph.D. study focused on developing practical numerical and experimental approaches for the dynamic analysis of structure-water systems, specifically gravity dam-reservoir systems, axisymmetric structures surrounded by water and their appurtenant structures. The flexibility of structures, coupled with the hydrodynamic effects during earthquake excitations, significantly complicates seismic analysis and evaluation of this type of structures. Accurate numerical analysis of structure-water systems often necessitates advanced approaches, either through robust analytical techniques or coupled finite element methods. These approaches demand specialized software with dynamic fluid-structure interaction capabilities and a high level of expertise to ensure reliable results. However, available simplified methods, rely on numerous approximations which may not be valid under all conditions. To address these limitations, the study developed simplified techniques that maintain accuracy while ensuring ease of implementation. The methods were specifically designed for two types of structure-water systems: gravity dam-reservoir systems and axisymmetric structures surrounded by water. The experimental part of this study focused on the seismic response of structure-water systems and their appurtenant structures, addressing the challenges posed by existing methodologies in incorporating structural flexibility and hydrodynamic effects during shaking table tests. As mentioned in the literature review section, three primary approaches exist for such tests: (i) using an underwater shaking table, which offers high accuracy but requires expensive facilities and poses safety challenges, particularly due to water leakage. Additionally, these facilities typically use water as the fluid medium, and any required changes in density due to similitude laws may violate the similitude laws. (ii) The second approach simplifies the problem by using added masses or a limited reservoir length to account for hydrodynamic effects during shaking table tests. However, due to the level of simplified assumptions, the results may lack the accuracy required for detailed seismic studies. (iii) The third approach involves completely ignoring hydrodynamic effects in the experimental test due to safety concerns and the complexity of incorporating such effects, potentially leading to incomplete or misleading conclusions.

This study proposed a novel methodology for shaking table tests of structure-water systems and their appurtenant structures using a system without water while incorporating hydrodynamic effects. The proposed method transfers these hydrodynamic effects into a modified version of the ground motion acceleration, which is then used as the input signal for the shaking table tests. This innovative approach allows for safe and feasible experiments on a standard shake table while accurately representing the hydrodynamic forces, thereby overcoming the limitations of available methods and ensuring the inclusion of hydrodynamic effects in shaking table tests.

The key contributions of this doctoral research can be summarized as follows:

- Development of a numerical method for time-history modal superposition and response spectrum analyses of gravity dam-reservoir systems. This method effectively incorporates earthquake-induced reservoir effects by modifying the original ground motion acceleration and its response spectrum, considering the desired vibration modes, including the flexibility of higher modes, and the overall response of the system.
- Extension of the modified ground acceleration method to other types of structure-water systems.
- Development of an innovative shaking table test of structure-water systems and their appurtenant structures using modified ground acceleration. This method enables the safe, practical, and accurate incorporation of hydrodynamic forces into shaking table tests, providing a more realistic assessment of seismic behaviour in these complex systems.

For each of these contributions, the following conclusions were highlighted:

7.1.1 Development of a numerical method for time-history modal superposition and response spectrum analyses of gravity dam-reservoir systems

This contribution, detailed in Chapter 3 and published as the article titled "*Response Spectrum and Modal Dynamic Analyses of Gravity Dams Using Ground Motion Accelerations Modified to Account for Hydrodynamic Effects*" in the Earthquake Spectra journal, presents a novel approach for seismic analyzing of gravity dam-reservoir systems. The key innovation lies in the incorporation of earthquake-induced reservoir effects into modified versions of the original ground motion acceleration and its response spectrum. These modified time-histories and spectral accelerations can be directly applied to the dam structure with an empty reservoir, effectively eliminating the need for specialized software to simulate fluid-structure inter-

action dynamics. Beyond the practical benefits, this approach allows for a detailed evaluation of the influence of individual vibration modes on the overall seismic response. This includes accurately assessing the coupled effects of structural flexibility and hydrodynamics, which are typically approximated by static correction methods in traditional analyses for higher modes. Additionally, the methodology utilizes analytical formulations of earthquake-induced hydrodynamic pressure in the reservoir, providing flexibility to consider either compressible or incompressible water, as well as the option to employ simplified Westergaard added-mass formulations representing hydrodynamic effects. This adaptability enables the investigation of how different water assumptions affect the acceleration demands on gravity dams, including hydrodynamic effects. The developed methods also offer an alternative to the traditional approach of implementing added masses at each node of the structure-water interface. Instead, the effects of these added masses are incorporated directly into the modified ground motion time-histories or spectral accelerations. Furthermore, a hydrodynamic modification factor was introduced, providing a means to evaluate the amplification or de-amplification of seismic acceleration demands due to earthquake-induced hydrodynamic effects. Finally, the results obtained using the proposed method were rigorously compared with those derived from finite element methods and advanced analytical approaches, utilizing two different gravity dam sections subjected to four distinct ground motion accelerations, each characterized by varying frequency content and time signatures. The proposed method demonstrated excellent agreement with the results from these more complex techniques, consistently achieving accurate results across different dam geometries and seismic event characteristics.

7.1.2 Extension of the modified ground acceleration method to other types of structure-water systems

As part of this Ph.D. study, one of the objectives was to conduct shaking table tests of appurtenant structures mounted on a structure-water system by proposing a new method to include hydrodynamic effects during shaking table using modified ground motion acceleration. The selected structure was an axisymmetric tower surrounded by water, designed so that it can be tested within the operational range of the shaking table. This latter study proposed a numerical method for time-history modal superposition and response spectrum analyses of axisymmetric structures surrounded by water. The technique accommodates both compressible and incompressible water assumptions to include hydrodynamic effects, as well as simplified added masses. In this study, two simplified methods—added mass based on radiation wave theory and Morison's added mass were employed to transfer hydrodynamic pressure into a modified version of the ground motion acceleration. This approach also enables the investigation of the impact of different water assumptions on the seismic re-

sponse of such structures for each vibration mode. The application of the proposed methods was demonstrated numerically through examples of three water-surrounded axisymmetric structures subjected to two earthquakes. The results obtained using the proposed method were rigorously compared with those derived from a coupled finite element method (FEM). The proposed method showed excellent agreement with these more complex FEMs, consistently delivering accurate results across different structure geometries and seismic event characteristics. Another advantage of the proposed technique is its ability to significantly reduce analysis time by eliminating the need for complex calculations in the fluid domain to generate hydrodynamic pressure at the structure-water interface at each time step. By removing the necessity for specialized software for fluid-structure interaction, the method simplifies the analysis process while still enabling a detailed evaluation of the structural response in specific vibration modes as well as the overall system response. This reduction in computational complexity makes the technique highly efficient and practical for real-world engineering applications, without compromising accuracy. The results of this study was published in the Ocean Engineering journal with the title of "*An Efficient Procedure for Modal Seismic Response Analysis of Axisymmetric Structures Surrounded by Water*" with further details provided in Chapter 4. It is worth mentioning that the result of application of proposed method developed for water-containing structures like storage tanks and navigation lock chambers is in press in the Journal of Engineering Structure, and will be published in coming weeks. However, this work is not included in this thesis.

7.1.3 Development of an innovative shaking table test of structure-water systems and their appurtenant structures using modified ground acceleration

This contribution involved the development of a novel methodology for conducting shaking table tests of structure-water systems and their appurtenant structures, incorporating hydrodynamic effects through the use of modified ground accelerations. The primary innovation of this methodology lies in its ability to integrate earthquake-induced hydrodynamic effects into modified versions of the original ground motion accelerations, effectively eliminating the need for the presence of water in the experimental setup. This approach addresses the significant challenges associated with underwater shaking table, which requires expensive facilities and poses safety risks due to water leakage and the potential distortion of similitude laws. Additionally, this method offers an alternative approach using the simplified added mass concept. While this concept is popular for its simplicity and safety benefits, it poses challenges in experimental setups, especially when it comes to evenly distributing the mass along the specimen's height and accounting for similitude laws. The proposed methodology overcomes these challenges by employing modified ground accelerations that account for the

added masses, thereby eliminating the need for physical added masses in the experimental setup. By using modified ground accelerations as input signals for shaking table tests, this approach allows for the safe, practical, and accurate inclusion of hydrodynamic forces, effectively overcoming the limitations of previous methods and ensuring the comprehensive incorporation of hydrodynamic effects in seismic analysis.

An axisymmetric structure surrounded by water was used as the primary structure-water system, selected due to operational limitations. An appurtenant structure with a notch was used as the appurtenant structure fixed at the top of the axisymmetric structure. Two different ground motion accelerations were employed as the original input in this study. To demonstrate the adaptability of the proposed method, three water levels were considered. Modified ground accelerations were generated based on both a compressible water assumption and Morison's added mass formulation, representing the influence of water on the dynamic response of the system. The shaking table tests were conducted through the following steps: (i) evaluating the dynamic properties of the specimen, including natural frequencies and damping ratios; (ii) building and calibrating a numerical model of the dry specimen using standard finite element software; (iii) generating modified ground accelerograms for the original earthquakes at different water levels, using various water assumptions such as compressible water and Morison's added mass formulation; (iv) employing different scaling factors to investigate both the linear and nonlinear responses of the appurtenant structure, while incorporating hydrodynamic effects; and (v) applying these modified accelerograms as input signals for the shaking table tests.

The experimental data obtained from these tests were compared with the results obtained using finite element models. The results underscored the substantial impact of the coupled hydrodynamic forces and structural flexibility on the seismic behaviour of both the primary structure and its appurtenant structure.

7.1.4 General conclusions

Developing the proposed methods and conducting the shaking table tests required careful selection of an appropriate structure-water system that effectively integrates the dynamic coupling of structural interaction with hydrodynamic effects while adhering to the operational constraints of the shaking table. This study involved extensive developments and discussions to ensure the validity of the proposed method. The discussion section (Chapter 6) provides a comprehensive and complementary validation of the proposed approach. The first part of the discussion focuses on further numerical validation by examining the influence of structural flexibility and hydrodynamic effects on the frequency content of the original ground

acceleration. The method was additionally validated through case studies, including the Pine Flat dam, representing a dam-reservoir system, and the San Bernardino intake tower, as an axisymmetric structure surrounded by water. The effectiveness of the method was demonstrated through its application in general-purpose structural analysis software, such as SAP2000, where it efficiently handled complex fluid-structure interactions while significantly reducing analysis time. In the experimental part of discussion, the method's effectiveness in conducting shaking table tests using modified ground acceleration was evaluated. The choice of axisymmetric structures surrounded by water over dam-reservoir systems as the primary structure for shaking table tests was explained. The discussion also highlighted the importance of selecting the appropriate height, material, and geometry of the specimen to optimize hydrodynamic effects and ensure safety during the operation of the shaking table. Additionally, a detailed discussion of the effects of low damping on the modified ground acceleration was provided.

7.2 Recommendations

Building on advancements in numerical modeling and experimental simulation of the seismic response of structure-water systems, this research has successfully developed numerical methods for various types of structure-water systems and proposed an innovative shaking table test for structure-water systems. These contributions pave the way for numerous opportunities in future research. The recommendations for future work are categorized into two primary areas: (i) numerical methods and (ii) experimental testing.

7.2.1 Numerical modeling

The methods developed in this thesis primarily address the fluid-structure interaction under horizontal acceleration. Given the existing analytical frameworks for vertical acceleration in the literature, future research could focus on incorporating vertical acceleration into the developed methods. This extension should not pose significant challenges, considering the progress already made.

The proposed methods can be extended to other types of structures, especially those where three-dimensional effects are critical, such as arch dam-reservoir systems. Applying the modified ground acceleration approach to these systems can offer significant advantages.

The methods developed during this doctoral thesis can all account for the effect of soil flexibility. However, by neglecting the mass of the soil, the inertial effect is ignored. This has the advantage of not requiring a deconvolution of the design earthquake but may introduce

an error in the dynamic behaviour of the structure. Additionally, the soil helps increase the overall damping of the system, so it is beneficial to consider it. Since the soil exhibits highly nonlinear behaviour, it would be interesting to study its impact on the behaviour.

Finally, applying the modified acceleration method to structure-water systems exhibiting nonlinear behaviour would be an interesting area of future research.

7.2.2 Experimental tests

For future experimental tests using shaking table, the proposed method could be applied to the seismic evaluation of appurtenant structures mounted on a dam-reservoir system using a shaking table capable of operating at a frequency range suitable for a scaled model dam. Exploring additional nonlinearities, such as sliding behavior in appurtenant structures, could further enhance the study's relevance and depth. Incorporating foundation flexibility effects into shaking table tests using modified ground acceleration, which accounts for both hydrodynamic and foundation flexibility, would also be a valuable direction for future work. This approach would allow for a more comprehensive exploration of the dynamic response of appurtenant structures mounted on the top of a dam-reservoir-foundation system. Developing a modified ground acceleration method that includes nonlinearity effects of the primary structures would also offer a valuable opportunity for the experimental seismic study of structure-water systems.

REFERENCES

[1] R. He and L. Pan, "Seismic responses and vibration control of offshore wind turbines considering hydrodynamic effects based on underwater shaking table tests," *Earthquake Engineering & Structural Dynamics*, vol. 53, no. 2, pp. 545–572, 2024.

[2] N. Bouaanani and F. Y. Lu, "Assessment of potential-based fluid finite elements for seismic analysis of dam–reservoir systems," *Computers & Structures*, vol. 87, no. 3-4, pp. 206–224, 2009.

[3] B. Miquel and N. Bouaanani, "Simplified evaluation of the vibration period and seismic response of gravity dam–water systems," *Engineering Structures*, vol. 32, no. 8, pp. 2488–2502, 2010.

[4] B. Miquel and N. Bouaanani, "Accounting for earthquake-induced dam-reservoir interaction using modified accelerograms," *Journal Of Structural Engineering*, vol. 139, no. 9, pp. 1608–1617, 2013.

[5] J. Guo, M. Zhao, P. Wang, and N. Zhang, "Comparative assessment of simplified methods for hydrodynamic force on cylinder under earthquakes," *Ocean Engineering*, vol. 234, p. 109219, 2021.

[6] K. Wei, N. Bouaanani, and W. Yuan, "Simplified methods for efficient seismic design and analysis of water-surrounded composite axisymmetric structures," *Ocean Engineering*, vol. 104, pp. 617–638, 2015.

[7] Q. Han, M. Li, Z. Wang, J. Sun, and M. Liu, "Strategy of scaled modeling for underwater shaking table tests on cylindrical marine structures under coupled earthquake and wave–current action: A review," *Earthquake Engineering And Resilience*, vol. 2, no. 3, pp. 263–281, 2023.

[8] Y. Ding, R. Ma, Y.-D. Shi, and Z.-X. Li, "Underwater shaking table tests on bridge pier under combined earthquake and wave-current action," *Marine Structures*, vol. 58, pp. 301–320, 2018.

[9] Z.-X. Li, K. Wu, Y. Shi, L. Ning, and D. Yang, "Experimental study on the interaction between water and cylindrical structure under earthquake action," *Ocean Engineering*, vol. 188, p. 106330, 2019.

[10] Y. Chen, X. Huang, K. Wu, and Z.-X. Li, "Experimental research on dynamic responses and hydrodynamic pressures of deep-water bridge piers under seismic and wave actions," *Engineering Structures*, vol. 313, p. 118276, 2024.

[11] R. W. N. A. Clough, "Shaking table research on concrete dam models," 1980.

[12] W. P. Donlon and J. F. Hall, "Shaking table study of concrete gravity dam monoliths," *Earthquake Engineering & Structural Dynamics*, vol. 20, no. 8, pp. 769–786, 1991.

[13] R. A. Mir and C. Taylor, "An experimental investigation into earthquake-induced failure of medium to low height concrete gravity dams," *Earthquake Engineering & Structural Dynamics*, vol. 24, no. 3, pp. 373–393, 1995.

[14] S. Mridha and D. Maity, "Experimental investigation on nonlinear dynamic response of concrete gravity dam-reservoir system," *Engineering Structures*, vol. 80, pp. 289–297, 2014.

[15] M. Wang, J. Chen, and W. Xiao, "Experimental and numerical comparative study on gravity dam-reservoir coupling system," *Ksce Journal Of Civil Engineering*, vol. 22, pp. 3980–3987, 2018.

[16] M. I. Ansari and P. Agarwal, "Rehabilitation technique for severely damaged concrete gravity dams," *Practice Periodical On Structural Design And Construction*, vol. 21, no. 3, p. 04016008, 2016.

[17] A. Aldemir, B. Binici, Y. Arici, O. Kurc, and E. Canbay, "Pseudo-dynamic testing of a concrete gravity dam," *Earthquake Engineering & Structural Dynamics*, vol. 44, no. 11, pp. 1747–1763, 2015.

[18] K. Wei, W. Yuan, and N. Bouaanani, "Experimental and numerical assessment of the three-dimensional modal dynamic response of bridge pile foundations submerged in water," *Journal Of Bridge Engineering*, vol. 18, no. 10, pp. 1032–1041, 2013.

[19] H. Zhang, C. Jiang, S. Liu, L. Zhang, C. Wang, and Y. Zhang, "Shaking-table tests of seismic responses of slender intake tower-hoist chamber systems," *Engineering Structures*, vol. 242, p. 112517, 2021.

[20] Polytechnique Montréal, "Laboratoire de structures - polytechnique montréal." `https://www.polymtl.ca/structures/laboratoire-de-structures`, 2024. Accessed: 2024-11-24.

[21] H. M. Westergaard, "Water pressures on dams during earthquakes," *Transactions Of The American Society Of Civil Engineers*, vol. 98, no. 2, pp. 418–433, 1933.

[22] A. K. Chopra, "Earthquake behavior of reservoir-dam systems," *Journal Of The Engineering Mechanics Division*, vol. 94, no. 6, pp. 1475–1500, 1968.

[23] P. Chakrabarti and A. K. Chopra, "Earthquake analysis of gravity dams including hydrodynamic interaction," *Earthquake Engineering & Structural Dynamics*, vol. 2, no. 2, pp. 143–160, 1973.

[24] S. S. Saini, P. Bettess, and O. Zienkiewicz, "Coupled hydrodynamic response of concrete gravity dams using finite and infinite elements," *Earthquake Engineering & Structural Dynamics*, vol. 6, no. 4, pp. 363–374, 1978.

[25] J. F. Hall and A. K. Chopra, "Hydrodynamic effects in the dynamic response of concrete gravity dams," *Earthquake Engineering & Structural Dynamics*, vol. 10, no. 2, pp. 333–345, 1982.

[26] G. L. Fenves and A. K. Chopra, *Earthquake analysis and response of concrete gravity dams*. University of California, Earthquake Engineering Research Center Berkeley, CA, 1984.

[27] G. Fenves and A. K. Chopra, "Earthquake analysis of concrete gravity dams including reservoir bottom absorption and dam-water-foundation rock interaction," *Earthquake Engineering & Structural Dynamics*, vol. 12, no. 5, pp. 663–680, 1984.

[28] P. L.-F. Liu and A. H.-D. Cheng, "Boundary solutions for fluid-structure interaction," *Journal Of Hydraulic Engineering*, vol. 110, no. 1, pp. 51–64, 1984.

[29] G. L. Fenves and A. K. Chopra, *Simplified analysis for earthquake resistant design of concrete gravity dams*. University of California, Earthquake Engineering Research Center Berkeley, CA, 1986.

[30] C.-S. Tsai and G. C. Lee, "Arch dam–fluid interactions: by fem–bem and substructure concept," *International Journal For Numerical Methods In Engineering*, vol. 24, no. 12, pp. 2367–2388, 1987.

[31] J. Humar and A. Jablonski, "Boundary element reservoir model for seismic analysis of gravity dams," *Earthquake Engineering & Structural Dynamics*, vol. 16, no. 8, pp. 1129–1156, 1988.

[32] O. Maeso, J. Aznarez, and J. Dominguez, "Three-dimensional models of reservoir sediment and effects on the seismic response of arch dams," *Earthquake Engineering & Structural Dynamics*, vol. 33, no. 10, pp. 1103–1123, 2004.

[33] Y. Ghanaat, R. C. Patev, and A. K. Chudgar, "Seismic fragility analysis of concrete gravity dams," in *Proceedings of the 15th world conference on earthquake engineering, Lisbon, Portugal*, pp. 24–28, 2012.

[34] A. Løkke and A. K. Chopra, "Response spectrum analysis of concrete gravity dams including dam-water-foundation interaction," *Journal Of Structural Engineering*, vol. 141, no. 8, p. 04014202, 2015.

[35] A. Løkke and A. K. Chopra, "Direct finite element method for nonlinear earthquake analysis of concrete dams: Simplification, modeling, and practical application," *Earthquake Engineering & Structural Dynamics*, vol. 48, no. 7, pp. 818–842, 2019.

[36] C. Bernier, R. Monteiro, and P. Paultre, "Using the conditional spectrum method for improved fragility assessment of concrete gravity dams in eastern canada," *Earthquake Spectra*, vol. 32, no. 3, pp. 1449–1468, 2016.

[37] V. Mircevska, M. Nastev, V. Hristovski, S. Malla, and M. Garevski, "Development and validation of the hdi matrix method for fluid–dam interaction," *Journal Of Computing In Civil Engineering*, vol. 31, no. 5, p. 04017035, 2017.

[38] I. D. Gupta and S. G. Joshi, "Response spectrum–based stochastic method for earthquake analysis of gravity dams," *Journal Of Engineering Mechanics*, vol. 143, no. 5, p. 04017007, 2017.

[39] M. A. Hariri-Ardebili and V. E. Saouma, "Random response spectrum analysis of gravity dam classes: simplified, practical, and fast approach," *Earthquake Spectra*, vol. 34, no. 2, pp. 941–975, 2018.

[40] R. Segura, C. Bernier, R. Monteiro, and P. Paultre, "On the seismic fragility assessment of concrete gravity dams in eastern canada," *Earthquake Spectra*, vol. 35, no. 1, pp. 211–231, 2019.

[41] N. Bouaanani and C. Perrault, "Practical formulas for frequency domain analysis of earthquake-induced dam-reservoir interaction," *Journal Of Engineering Mechanics*, vol. 136, no. 1, pp. 107–119, 2010.

[42] Q. Li and W. Yang, "An improved method of hydrodynamic pressure calculation for circular hollow piers in deep water under earthquake," *Ocean Engineering*, vol. 72, pp. 241–256, 2013.

[43] C.-g. Liu and G.-s. Sun, "Calculation and experiment for dynamic response of bridge in deep water under seismic excitation," *China Ocean Engineering*, vol. 28, no. 4, pp. 445–456, 2014.

[44] X. Y. Zheng, H. Li, W. Rong, and W. Li, "Joint earthquake and wave action on the monopile wind turbine foundation: An experimental study," *Marine Structures*, vol. 44, pp. 125–141, 2015.

[45] W. Yang, Q. Li, and H. Yeh, "Calculation method of hydrodynamic forces on circular piers during earthquakes," *Journal Of Bridge Engineering*, vol. 22, no. 11, p. 04017093, 2017.

[46] Z.-X. Li, Q. Zheng, K. Wu, and Y. Shi, "Seismic analysis and test facilities of deep-water bridges considering water–structure interaction: a state-of-the-art review," *Earthquake Engineering And Resilience*, vol. 1, no. 1, pp. 21–39, 2022.

[47] J. R. Morison, J. W. Johnson, and S. A. Schaaf, "The force exerted by surface waves on piles," *Journal Of Petroleum Technology*, vol. 2, pp. 149–154, 1950.

[48] J. Penzien and M. Kaul, "Response of offshore towers to strong motion earthquakes," *Earthquake Engineering & Structural Dynamics*, vol. 1, no. 1, pp. 55–68, 1972.

[49] G. Everstine, "A symmetric potential formulation for fluid-structure interaction," *Journal Of Sound And Vibration*, vol. 79, no. 1, pp. 157–160, 1981.

[50] L. G. Olson and K.-J. Bathe, "Analysis of fluid-structure interactions. a direct symmetric coupled formulation based on the fluid velocity potential," *Computers & Structures*, vol. 21, no. 1-2, pp. 21–32, 1985.

[51] B.-F. Chen, "Dynamic responses of coastal structures during earthquakes including sediment–sea–structure interaction," *Soil Dynamics And Earthquake Engineering*, vol. 20, no. 5-8, pp. 445–467, 2000.

[52] O. Czygan and O. Von Estorff, "Fluid-structure interaction by coupling bem and nonlinear fem," *Engineering Analysis With Boundary Elements*, vol. 26, no. 9, pp. 773–779, 2002.

[53] J.-F. Sigrist and S. Garreau, "Dynamic analysis of fluid–structure interaction problems with modal methods using pressure-based fluid finite elements," *Finite Elements In Analysis And Design*, vol. 43, no. 4, pp. 287–300, 2007.

[54] M. Millan, Y. Young, and J. Prevost, "Seismic response of intake towers including dam–tower interaction," *Earthquake Engineering & Structural Dynamics*, vol. 38, no. 3, pp. 307–329, 2009.

[55] J.-F. Lu and D.-S. Jeng, "Dynamic response of an offshore pile to pseudo-stoneley waves along the interface between a poroelastic seabed and seawater," *Soil Dynamics And Earthquake Engineering*, vol. 30, no. 4, pp. 184–201, 2010.

[56] L. Tao, H. Song, and S. Chakrabarti, "Scaled boundary fem solution of short-crested wave diffraction by a vertical cylinder," *Computer Methods In Applied Mechanics And Engineering*, vol. 197, no. 1-4, pp. 232–242, 2007.

[57] X.-N. Meng and Z.-J. Zou, "Wave interaction with a uniform porous cylinder of arbitrary shape," *Ocean Engineering*, vol. 44, pp. 90–99, 2012.

[58] J. Liu and G. Lin, "Numerical modelling of wave interaction with a concentric cylindrical system with an arc-shaped porous outer cylinder," *European Journal Of Mechanics-b/fluids*, vol. 37, pp. 59–71, 2013.

[59] L.-Y. Xu, C.-X. Song, F. Cai, W.-Y. Chen, Y.-Y. Xue, and G.-X. Chen, "An integrated model for offshore wind turbine monopile in porous seabed under multi-directional seismic excitations," *Ocean Engineering*, vol. 285, p. 115250, 2023.

[60] L. A. Padrón, S. Carbonari, F. Dezi, M. Morici, J. D. Bordón, and G. Leoni, "Seismic response of large offshore wind turbines on monopile foundations including dynamic soil–structure interaction," *Ocean Engineering*, vol. 257, p. 111653, 2022.

[61] A. Bigdeli, H. Akbari, M. Alembagheri, H. Haghgou, and M. Matinfar, "Influence of near-field ground motions and their equivalent pulses on nonlinear seismic response of intake-outlet towers and predicting based on artificial neural networks," in *Structures*, vol. 52, pp. 1051–1070, Elsevier, 2023.

[62] N. Li and Z.-X. Li, "Digital twins for the underwater shake table array facility," *Earthquake Engineering And Resilience*, vol. 1, no. 3, pp. 317–335, 2022.

[63] Z.-X. Li, Q. Zheng, J. Su, Y. Shi, and B. Zhao, "Underwater shaking table tests of a sea-crossing cable-stayed bridge under combined earthquake and wave action," *Ocean Engineering*, vol. 287, p. 115871, 2023.

[64] Z.-X. Li, K. Wu, Y. Shi, N. Li, and Y. Ding, "Coordinative similitude law considering fluid-structure interaction for underwater shaking table tests," *Earthquake Engineering & Structural Dynamics*, vol. 47, no. 11, pp. 2315–2332, 2018.

[65] R. Tinawi, P. Léger, M. Leclerc, and G. Cipolla, "Seismic safety of gravity dams: from shake table experiments to numerical analyses," *Journal Of Structural Engineering*, vol. 126, no. 4, pp. 518–529, 2000.

[66] J. Zhou, G. Lin, T. Zhu, A. Jefferson, and F. Williams, "Experimental investigations into seismic failure of high arch dams," *Journal Of Structural Engineering*, vol. 126, no. 8, pp. 926–935, 2000.

[67] A. Ghaemmaghami and M. Ghaemian, "Experimental seismic investigation of sefid-rud concrete buttress dam model on shaking table," *Earthquake Engineering & Structural Dynamics*, vol. 37, no. 5, pp. 809–823, 2008.

[68] P. J. Clough Ray W, *Dynamics of Structures*. New York: McGraw-Hill Book Company, 1975.

[69] ACB/CDA, "Dam safety guidelines," 2007.

[70] FEMA (Federal Emergency Management Agency), "Federal guidelines for dam safety," 2004.

[71] FERC (Federal Energy Regulatory Commission), "Engineering guidelines for evaluation of hydropower projects - chapter iii gravity dams," 1991. Report No. FERC 0119-2.

[72] Hydro-Québec, "Guide d'évaluation de la sécurité sismique des barrages," 2000.

[73] CSB (Comite Suisse des Barrages), "Methods of analysis for the prediction and the verification of dam behaviour," 2003.

[74] USBR (United States Bureau of Reclamation), "Design of small dams," 1987.

[75] J. Proulx and P. Paultre, "Experimental and numerical investigation of dam reservoir foundation interaction for a large gravity dam," *Canadian Journal Of Civil Engineering*, vol. 24, no. 1, pp. 90–105, 1997.

[76] F. Javanmardi, P. Léger, and R. Tinawi, "Seismic structural stability of concrete gravity dams considering transient uplift pressures in cracks," *Engineering Structures*, vol. 27, no. 4, pp. 616–628, 2005.

[77] C. L. Stefan, "Modèle constitutif hydromécanique tridimensionnelle pour l'analyse de stabilité des piliers d'évacuateur de crues," 2011.

[78] C. Christopoulos, P. Léger, and A. Filiatrault, "Sliding response of gravity dams including vertical seismic accelerations," *Earthquake Engineering And Engineering Vibration*, vol. 2, pp. 189–200, 2003.

[79] G. Fenves and L. M. Vargas-Loli, "Nonlinear dynamic analysis of fluid-structure systems," *Journal Of Engineering Mechanics*, vol. 114, no. 2, pp. 219–240, 1988.

[80] C. R. Noble, *Finite element techniques for realistically simulating the seismic response of concrete dams*. University of California, Davis, 2007.

[81] A. K. Chopra, "Hydrodynamic pressures on dams during earthquakes," *Journal Of The Engineering Mechanics Division*, vol. 93, no. 6, pp. 205–223, 1967.

[82] D. Maity and S. Bhattacharyya, "Time-domain analysis of infinite reservoir by finite element method using a novel far-boundary condition," *Finite Elements In Analysis And Design*, vol. 32, no. 2, pp. 85–96, 1999.

[83] N. Bouaanani, P. Paultre, and J. Proulx, "Two-dimensional modelling of ice cover effects for the dynamic analysis of concrete gravity dams," *Earthquake Engineering & Structural Dynamics*, vol. 31, no. 12, pp. 2083–2102, 2002.

[84] N. Bouaanani, P. Paultre, and J. Proulx, "Dynamic response of a concrete dam impounding an ice-covered reservoir: Part i. mathematical modelling," *Canadian Journal Of Civil Engineering*, vol. 31, no. 6, pp. 956–964, 2004.

[85] N. Bouaanani, P. Paultre, and J. Proulx, "Dynamic response of a concrete dam impounding an ice-covered reservoir: Part ii. parametric and numerical study," *Canadian Journal Of Civil Engineering*, vol. 31, no. 6, pp. 965–976, 2004.

[86] N. Bouaanani, P. Paultre, and J. Proulx, "A closed-form formulation for earthquake-induced hydrodynamic pressure on gravity dams," *Journal Of Sound And Vibration*, vol. 261, no. 3, pp. 573–582, 2003.

[87] N. Bouaanani and B. Miquel, "A new formulation and error analysis for vibrating dam–reservoir systems with upstream transmitting boundary conditions," *Journal Of Sound And Vibration*, vol. 329, no. 10, pp. 1924–1953, 2010.

[88] A. K. Chopra, *Earthquake engineering for concrete dams: analysis, design, and evaluation*. John wiley & sons, 2020.

[89] H. Lamb, *Hydrodynamics*. Dover Publications, Inc., 6th ed., 1945.

[90] A. Sommerfeld, *Partial differential equations in physics*. Academic press, 1949.

[91] O. Zienkiewicz, "Coupled vibrations of a structure submerged in a compressible fluid," in *Proc. of Symposium on Finite Element Techniques Held at the University of Stuttgart*, 1969.

[92] ADINA, "Theory and modeling guide, rep. no. ard 06–7.," *Watertown Ma*, 2022.

[93] N. Bouaanani and B. Miquel, "An error estimator for transmitting boundary conditions in fluid-structure interaction problems," *Wit Transactions On The Built Environment*, vol. 115, pp. 169–178, 2011.

[94] S. K. Sharan, "Finite element modeling of infinite reservoirs," *Journal Of Engineering Mechanics*, vol. 111, no. 12, pp. 1457–1469, 1985.

[95] S. K. Sharan, "A non-reflecting boundary in fluid-structure interaction," *Computers & Structures*, vol. 26, no. 5, pp. 841–846, 1987.

[96] S. K. Sharan, "Efficient finite element analysis of hydrodynamic pressure on dams," *Computers & Structures*, vol. 42, no. 5, pp. 713–723, 1992.

[97] I. Gogoi and D. Maity, "A non-reflecting boundary condition for the finite element modeling of infinite reservoir with layered sediment," *Advances In Water Resources*, vol. 29, no. 10, pp. 1515–1527, 2006.

[98] P. Léger and M. Boughoufalah, "Earthquake input mechanisms for time-domain analysis of dam—foundation systems," *Engineering Structures*, vol. 11, no. 1, pp. 37–46, 1989.

[99] J. Li, Y. Liu, Z. Li, and G. Lin, "Global method for nonlinear seismic analysis of embedded base-isolated nuclear island buildings in layered sites," in *Structures*, vol. 56, p. 105042, Elsevier, 2023.

[100] C. Corns, E. Schrader, and G. Tarbox, "Gravity dam design and analysis," in *Advanced Dam Engineering for Design, Construction, and Rehabilitation* (R. Jansen, ed.), ch. 16, Van Nostrand Reinhold, 1988.

[101] G. Fenves and A. K. Chopra, "Simplified earthquake analysis of concrete gravity dams," *Journal Of Structural Engineering*, vol. 113, no. 8, pp. 1688–1708, 1987.

[102] M. Leclerc, P. Léger, and R. Tinawi, "Computer aided stability analysis of gravity dams—cadam," *Advances In Engineering Software*, vol. 34, no. 7, pp. 403–420, 2003.

[103] M. Leclerc and P. Léger, "Computer aided analysis of concrete gravity dams, gated spillways and water intake structures - cadam3d user manual," 2017.

[104] M. Hatanaka, "Study on the earthquake-resistant design of gravity type dams," in *Proceedings of the second world conference on earthquake engineering*, vol. 3, pp. 2041–2059, 1960.

[105] S. Okamoto, *Introduction to earthquake engineering*. Steve Parish, 1984.

[106] S. R. Jafari and M. P. Khiavi, "Parametric study of the modal behavior of concrete gravity dam by using finite element method," *Civil Engineering Journal*, vol. 5, no. 12, pp. 2614–2625, 2019.

[107] H. Mohammadnezhad, M. Ghaemian, and A. Noorzad, "Seismic analysis of dam-foundation-reservoir system including the effects of foundation mass and radiation damping," *Earthquake Engineering And Engineering Vibration*, vol. 18, pp. 203–218, 2019.

[108] A. Aldemir, "Prediction equations for the fundamental period and mode shape of roller compacted concrete gravity dams considering three dimensional geometry effects," *Journal Of Earthquake Engineering*, vol. 25, no. 5, pp. 816–834, 2021.

[109] Y. Qu, D. Chen, L. Liu, E. T. Ooi, S. Eisenträger, and C. Song, "A direct time-domain procedure for the seismic analysis of dam–foundation–reservoir systems using the scaled boundary finite element method," *Computers And Geotechnics*, vol. 138, p. 104364, 2021.

[110] M. A. Hariri-Ardebili and F. Pourkamali-Anaraki, "An automated machine learning engine with inverse analysis for seismic design of dams," *Water*, vol. 14, no. 23, p. 3898, 2022.

[111] X. Guo, F. Dufour, and N. Humbert, "Modal analysis of an arch dam combining ambient vibration measurements, advanced fluid-element method and modified engineering approach," *Earthquake Engineering & Structural Dynamics*, vol. 51, no. 6, pp. 1321–1342, 2022.

[112] R. J. de Almeida Torres Filho, R. L. Segura, and P. Paultre, "Polynomial response surface-based transformation function for the performance improvement of low-fidelity

models for concrete gravity dams," *Probabilistic Engineering Mechanics*, vol. 74, p. 103544, 2023.

[113] A. Kita, A. Lupattelli, I. Venanzi, D. Salciarini, and F. Ubertini, "The role of seismic hazard modeling on the simplified structural assessment of an existing concrete gravity dam," in *Structures*, vol. 34, pp. 4560–4573, Elsevier, 2021.

[114] C.-Y. Liaw and A. K. Chopra, "Dynamics of towers surrounded by water," *Earthquake Engineering & Structural Dynamics*, vol. 3, no. 1, pp. 33–49, 1974.

[115] L. S. Jacobsen, "Impulsive hydrodynamics of fluid inside a cylindrical tank and of fluid surrounding a cylindrical pier," *Bulletin Of The Seismological Society Of America*, vol. 39, no. 3, pp. 189–204, 1949.

[116] H. Lamb, *Hydrodynamics*. The Cambridge University Press, 6 ed., 1932.

[117] P. Wang, M. Zhao, X. Du, J. Liu, and J. Chen, "Simplified evaluation of earthquake-induced hydrodynamic pressure on circular tapered cylinders surrounded by water," *Ocean Engineering*, vol. 164, pp. 105–113, 2018.

[118] R. T. McGoldrick, *Ship vibration*. US Government Printing Office, 1960.

[119] R. P. Han *et al.*, "A simple and accurate added mass model for hydrodynamic fluid—structure interaction analysis," *Journal Of The Franklin Institute*, vol. 333, no. 6, pp. 929–945, 1996.

[120] W. Yang and Q. Li, "A new added mass method for fluid-structure interaction analysis of deep-water bridge," *Ksce Journal Of Civil Engineering*, vol. 17, pp. 1413–1424, 2013.

[121] Y. Li, Z. Li, and Q. Wu, "Experiment and calculation method of the dynamic response of deep water bridge in earthquake," *Latin American Journal Of Solids And Structures*, vol. 14, no. 13, pp. 2518–2533, 2017.

[122] W. Yang and Q. Li, "The expanded morison equation considering inner and outer water hydrodynamic pressure of hollow piers," *Ocean Engineering*, vol. 69, pp. 79–87, 2013.

[123] T. Sarpkaya, "Forces on rough-walled circular cylinders," *Coastal Engineering Proceedings*, no. 15, pp. 134–134, 1976.

[124] H. GoTo and K. Toki, "Vibrational characteristics and aseismic design of sub-merged bridge piers," *Memoirs Of The Faculty Of Engineering, Kyoto University*, vol. 27, no. 1, pp. 17–30, 1965.

[125] L. Wei, Z. Tiehua, and L. Yong, "The effect of hydrodynamic drag force in morison equation on the seismic response of piles," *Sichuan Building Science*, vol. 4, pp. 163–168, 2007.

[126] Y. Yuan, W. Lai, J. Wang, and S. Hu, "The effects of hydrodynamic damping on seismic response of bridge piles," *World Earthquake Engineering*, vol. 21, no. 4, pp. 88–94, 2005.

[127] Q. Han, "Introduction to the national facility for earthquake engineering simulation," 2022.

[128] B. Bakhtin and V. Dumenko, "Seismic stability of a concrete gravity dam having a lightweight profile," *Power Technology And Engineering*, vol. 13, no. 5, pp. 445–450, 1979.

[129] D. W. Harris, N. Snorteland, T. Dolen, and F. Travers, "Shaking table 2-d models of a concrete gravity dam," *Earthquake Engineering & Structural Dynamics*, vol. 29, no. 6, pp. 769–787, 2000.

[130] S. K. Sharan, "Time-domain analysis of infinite fluid vibration," *International Journal For Numerical Methods In Engineering*, vol. 24, no. 5, pp. 945–958, 1987.

[131] J. Mays and L. Roehm, "Hydrodynamic pressure in a dam-reservoir system," *Computers & Structures*, vol. 40, no. 2, pp. 281–291, 1991.

[132] M. Hariri-Ardebili, S. Seyed-Kolbadi, V. Saouma, J. Salamon, and B. Rajagopalan, "Random finite element method for the seismic analysis of gravity dams," *Engineering Structures*, vol. 171, pp. 405–420, 2018.

[133] P. Paultre, *Dynamics of Structures*. John Wiley & Sons, 2013.

[134] V. Lotfi, J. M. Roesset, and J. L. Tassoulas, "A technique for the analysis of the response of dams to earthquakes," *Earthquake Engineering & Structural Dynamics*, vol. 15, no. 4, pp. 463–489, 1987.

[135] M. Çetin and Y. Mengi, "Transmitting boundary conditions suitable for analysis of dam-reservoir interaction and wave load problems," *Applied Mathematical Modelling*, vol. 27, no. 6, pp. 451–470, 2003.

[136] N. Bouaanani and S. Renaud, "Effects of fluid–structure interaction modeling assumptions on seismic floor acceleration demands within gravity dams," *Engineering Structures*, vol. 67, pp. 1–18, 2014.

[137] J. Salamon and J. Manie, "Numerical assessment of hydrodynamic loads induced during seismic interaction between reservoir and concrete dam," in *Proc., USSD Conf*, pp. 1–16, 2017.

[138] J. W. Cooley and J. W. Tukey, "An algorithm for the machine calculation of complex fourier series," *Mathematics Of Computation*, vol. 19, no. 90, pp. 297–301, 1965.

[139] G. D. Bergland, "A guided tour of the fast fourier transform," *Ieee Spectrum*, vol. 6, no. 7, pp. 41–52, 1969.

[140] E. O. Brigham, "The fast fourier transform prentice-hall," *Englewood Cliffs, Nj*, vol. 19742, 1974.

[141] R. N. Bracewell, *The Fourier Transform and Its Applications NY, McGraw-Hill*. 1986.

[142] R. E. Taylor and P. Duncan, "Fluid-induced inertia and damping in vibrating offshore structures," *Applied Ocean Research*, vol. 2, no. 1, pp. 3–12, 1980.

[143] A. N. Williams, "Earthquake response of submerged circular cylinder," *Ocean Engineering*, vol. 13, no. 6, pp. 569–585, 1986.

[144] Y. Tanaka and R. T. Hudspeth, "Restoring forces on vertical circular cylinders forced by earthquakes," *Earthquake Engineering & Structural Dynamics*, vol. 16, no. 1, pp. 99–119, 1988.

[145] M. Alembagheri, "Frequency domain analysis of submerged tower-dam dynamic interaction," *Soil Mechanics And Foundation Engineering*, vol. 54, pp. 264–275, 2017.

[146] P. Wang, M. Zhao, H. Li, and X. Du, "An accurate and efficient time-domain model for simulating water-cylinder dynamic interaction during earthquakes," *Engineering Structures*, vol. 166, pp. 263–273, 2018.

[147] J. Zhang, K. Wei, and S. Qin, "An efficient numerical model for hydrodynamic added mass of immersed column with arbitrary cross-section," *Ocean Engineering*, vol. 187, p. 106192, 2019.

[148] Z. Tian, F. Liu, L. Zhou, and C. Yuan, "Fluid-structure interaction analysis of offshore structures based on separation of transferred responses," *Ocean Engineering*, vol. 195, p. 106598, 2020.

[149] B. Sun, S. Zhang, W. Cui, M. Deng, and C. Wang, "Nonlinear dynamic response and damage analysis of hydraulic arched tunnels subjected to p waves with arbitrary incoming angles," *Computers And Geotechnics*, vol. 118, p. 103358, 2020.

[150] P. Wang, P. Long, M. Zhao, C. Zhang, and X. Du, "Analytical solution of earthquake-induced hydrodynamic pressure on arrays of circular cylinders considering high-order scattered waves," *Journal Of Engineering Mechanics*, vol. 147, no. 9, p. 04021051, 2021.

[151] H. Han, Y. Guo, and R. Huo, "Semi-analytical solution of transverse vibration of cylinders with non-circular cross-section partially submerged in water," *Journal Of Marine Science And Engineering*, vol. 11, no. 4, p. 872, 2023.

[152] Y. Huang, M. Zhao, P. Wang, X. Cheng, and X. Du, "Analytical solution of dynamic responses of offshore wind turbine supported by monopile under combined earthquake, wave and wind," *Ocean Engineering*, vol. 267, p. 113319, 2023.

[153] M. Greenhow and L. Yanbao, "Added masses for circular cylinders near or penetrating fluid boundaries—review, extension and application to water-entry,-exit and slamming," *Ocean Engineering*, vol. 14, no. 4, pp. 325–348, 1987.

[154] P. Wang, C. Zhang, X. Wang, M. Zhao, and X. Du, "An accurate and efficient time-domain numerical model for simulating water-axisymmetric structure subjected to horizontal earthquakes," *Marine Structures*, vol. 85, p. 103234, 2022.

[155] K. Wu, N. Li, and Z. Li, "An extended multiple-support response spectrum method incorporating fluid-structure interaction for seismic analysis of deep-water bridges," *Earthquake Engineering And Engineering Vibration*, vol. 22, no. 1, pp. 211–223, 2023.

[156] H. Jiang, B. Wang, X. Bai, C. Zeng, and H. Zhang, "Simplified expression of hydrodynamic pressure on deepwater cylindrical bridge piers during earthquakes," *Journal Of Bridge Engineering*, vol. 22, no. 6, p. 04017014, 2017.

[157] K. Wu, J. Ma, Y. Chen, X. Huang, L. Qi, and C. Li, "Study on the hydrodynamic added mass of rectangular pier under sine wave actions," in *Structures*, vol. 54, pp. 1371–1380, Elsevier, 2023.

[158] A. Goyal and A. K. Chopra, "Earthquake analysis of intake-outlet towers including tower-water-foundation-soil interaction," *Earthquake Engineering & Structural Dynamics*, vol. 18, no. 3, pp. 325–344, 1989.

[159] S. Bhattacharya, N. Nikitas, J. Garnsey, N. Alexander, J. Cox, D. Lombardi, D. M. Wood, and D. F. Nash, "Observed dynamic soil–structure interaction in scale testing of offshore wind turbine foundations," *Soil Dynamics And Earthquake Engineering*, vol. 54, pp. 47–60, 2013.

[160] G.-L. Lin, L.-Y. Lu, K.-T. Lei, K.-Y. Liu, Y.-Y. Ko, and S.-H. Ju, "Experimental study on seismic vibration control of an offshore wind turbine with tmd considering soil liquefaction effect," *Marine Structures*, vol. 77, p. 102961, 2021.

[161] Z. Zhou, D. Zhang, Y. Zhang, S. Gao, Y. Yue, and N. Li, "Real-time hybrid simulation for fluid-structure interaction: Structures under seismic and hydrodynamic forces," *Earthquake Engineering & Structural Dynamics*, vol. 52, no. 14, pp. 4602–4619, 2023.

[162] K. Wei, J. Zhang, and S. Qin, "Experimental and numerical assessment into frequency domain dynamic response of deep water rigid-frame bridge," *Journal Of Earthquake Engineering*, vol. 26, no. 1, pp. 307–330, 2022.

[163] X. Y. Zheng, H. Li, W. Rong, and W. Li, "Joint earthquake and wave action on the monopile wind turbine foundation: An experimental study," *Marine Structures*, vol. 44, pp. 125–141, 2015.

[164] C. Liu, S. Zhang, and E. Hao, "Joint earthquake, wave and current action on the pile group cable-stayed bridge tower foundation: an experimental study," *Applied Ocean Research*, vol. 63, pp. 157–169, 2017.

[165] G. Yun and C. Liu, "Shaking table tests on a deep-water high-pier whole bridge under joint earthquake, wave and current action," *Applied Ocean Research*, vol. 103, p. 102329, 2020.

[166] Y. Chen, X.-T. Yang, K. Wu, X. Huang, and Z.-X. Li, "Damage analysis of a reinforced concrete rigid-frame bridge under combined strong earthquake and wave action," *Ocean Engineering*, vol. 296, p. 116919, 2024.

[167] Y. Uchita, T. Shimpo, and V. Saouma, "Dynamic centrifuge tests of concrete dam," *Earthquake Engineering & Structural Dynamics*, vol. 34, no. 12, pp. 1467–1487, 2005.

[168] R. Mir and C. Taylor, "An investigation into the base sliding response of rigid concrete gravity dams to dynamic loading," *Earthquake Engineering & Structural Dynamics*, vol. 25, no. 1, pp. 79–98, 1996.

[169] H. B. Messtechnik, "Catman data acquisition software," 2000.

[170] N. Bouaanani, D. Goulmot, and B. Miquel, "Seismic response of asymmetric rectangular liquid-containing structures," *Journal Of Engineering Mechanics*, vol. 138, no. 10, pp. 1288–1297, 2012.

[171] R. Kouhdasti and N. Bouaanani, "Response spectrum and modal dynamic analyses of gravity dams using ground motion accelerations modified to account for hydrodynamic effects," *Earthquake Spectra*, 2024.

[172] R. Kouhdasti and N. Bouaanani, "An efficient procedure for modal seismic response analysis of axisymmetric structures surrounded by water," *Ocean Engineering*, vol. 304, p. 117771, 2024.

[173] T. M. Inc., "Matlab version: 9.13.0 (r2022b)," 2022.